NUREG/CP-0029
Vol. 2
CONF-820321/V2

Proceedings of the Fourth ASTM-EURATOM Symposium
on Reactor Dosimetry

RADIATION METROLOGY TECHNIQUES, DATA BASES, AND STANDARDIZATION

National Bureau of Standards
Gaithersburg, Maryland
March 22-26, 1982

Prepared for the U.S. Nuclear Regulatory Commission
Office of Nuclear Regulatory Research
Under Interagency Agreements DOE 40-551-75 and 40-552-75

Volume II

Printed in the United States of America. Available from
National Technical Information Service
U.S. Department of Commerce
5285 Port Royal Road, Springfield, Virginia 22161

Available from
GPO Sales Program
Division of Technical Information and Document Control
U.S. Nuclear Regulatory Commission
Washington, D.C. 20555

NUREG/CP-0029
Vol. 2
CONF-820321/V2
Dist. Category AN

Proceedings of the Fourth ASTM-EURATOM Symposium on Reactor Dosimetry

RADIATION METROLOGY TECHNIQUES, DATA BASES, AND STANDARDIZATION

Volume II

National Bureau of Standards
Gaithersburg, Maryland
March 22–26, 1982

Edited by

F. B. K. Kam

Manuscript Completed: May 1982
Date Published: July 1982

Prepared for the U.S. Nuclear Regulatory Commission
Office of Nuclear Regulatory Research
Under Interagency Agreements DOE 40-551-75 and 40-552-75
NRC FIN No. B0415

Sponsored by

ASTM, Subcommittee E10.05 on Nuclear Radiation Metrology
Joint Research Center of the Commission of the European Communities
U.S. Nuclear Regulatory Commission
U.S. Department of Energy, Office of Fusion Energy
U.S. Department of Energy, Office of Light Water Reactors
Electric Power Research Institute
National Bureau of Standards
International Atomic Energy Agency

prepared by

Oak Ridge National Laboratory
Oak Ridge, Tennessee 37830
operated by
Union Carbide Corporation
for the
U.S. Department of Energy
Contract No. W-7405-eng-26

CONTENTS OF VOLUME II

SESSION B.2: BENCHMARKS AND NUCLEAR DATA

SESSION B.3: FUSION-I

SESSION C.1: DAMAGE CORRELATION

SESSION C.2: NUCLEAR DATA NEEDS AND PROBLEMS

SESSION C.3: FUSSION-II

SESSION D.1: LIGHT WATER REACTORS-III

SESSION D.2: ADJUSTMENT CODES AND UNCERTAINTIES

SESSION HIGHLIGHTS

WORKSHOPS

Session B.2
Benchmarks and Nuclear Data

NBS ISNF and Cavity Fission U-235 Standard Neutron Fields

E. D. McGarry, G. P. Lamaze, C. M. Eisenhauer,
D. M. Gilliam, and F. J. Schima

National Bureau of Standards
Gaithersburg, Maryland

SUMMARY

A brief review and an update of the status has been given for the standard U-235 fission neutron field and the Intermediate-energy Standard Neutron Field (the ISNF) at the National Bureau of Standards. Recent improvements primarily deal with measurements and calculations done to better understand uncertainties. Two basic nuclear-data measurements are reported. The first, for an experiment in progress, is a 101 $\pm$ 3 mb U-235 spectrum-averaged cross section for the Ni-58(n,p)Co-58 reaction. The second is a final but prepublication value of 0.513 $\pm$ 1.8% for the Pu-240/U-235 fission rate ratio in the ISNF.

INTRODUCTION

This paper discusses two standard neutron fields developed and maintained at NBS, Gaithersburg, Maryland. The first is a U-235 fission neutron spectrum. It is frequently referred to as the Cavity Fission Source[1] because the neutron field is created by fissions in U-235 discs undergoing thermal neutron irradiation in a 30-cm diameter cavity in the thermal column of the NBS reactor. The second standard field is the Intermediate-energy Standard Neutron Field, referred to as the ISNF.[2] This field has most of its neutrons in the higher keV energy range, similar to spectra within a fast nuclear reactor. The ISNF also operates within the cavity in the thermal column.

The emphasis of the present paper is on work in progress to better understand these fields and to report briefly on results of several recent experiments.

It is first necessary to realize that the fluxes or fluences in the above mentioned fields are always measured with reference to two other fundamental types of neutron standards: the Cf-252 fission spectrum from spontaneously fissionable, nearly ideal point sources,[3] and source strengths measurements by comparison with an international radium-in-beryllium photo-neutron standard source in a manganeous-sulfate bath.[4] The Cf-252 sources provide the fundamental standard neutron fields. Based upon knowledge of the well-known Cf-252 neutron energy spectrum, a measured source strength, and a simple time and distance measurement, fluences in the near vicinity of these sources can be certified to nominally one percent accuracy. Such certification provides the means for calibrating instruments or other neutron sensors in terms of neutron flux units.[5] The calibrations, in turn, provide the means to accurately measure fluences in the Cavity Fission and ISNF neutron fields.

THE CAVITY FISSION U-235 NEUTRON FIELD

Fig. 1 shows the source-detector capsule in detail. It also depicts the capsule positioned, on the end of an aluminum rod, at the center of the cavity in the graphite thermal column. Two disks of U-235 metal (16 mm dia X 0.13 mm thick) are placed above and below a cylindrical cadmium box, which encloses the passive detectors for exposure. Fission neutron fluxes of $\sim 2 \times 10^{10}$ n/cm^{2}sec are obtained between the source disks at a separation distance of 1 cm. The neutron sensors, usually thin (< 0.254 mm thick) foils up to 12 mm in diameter, are held in the center of the cadmium pill box by an aluminum insert foil holder. This insert is item A in Fig. 2 which shows the flux gradient between the two fission disks as a function of distance from the bottom of the foil

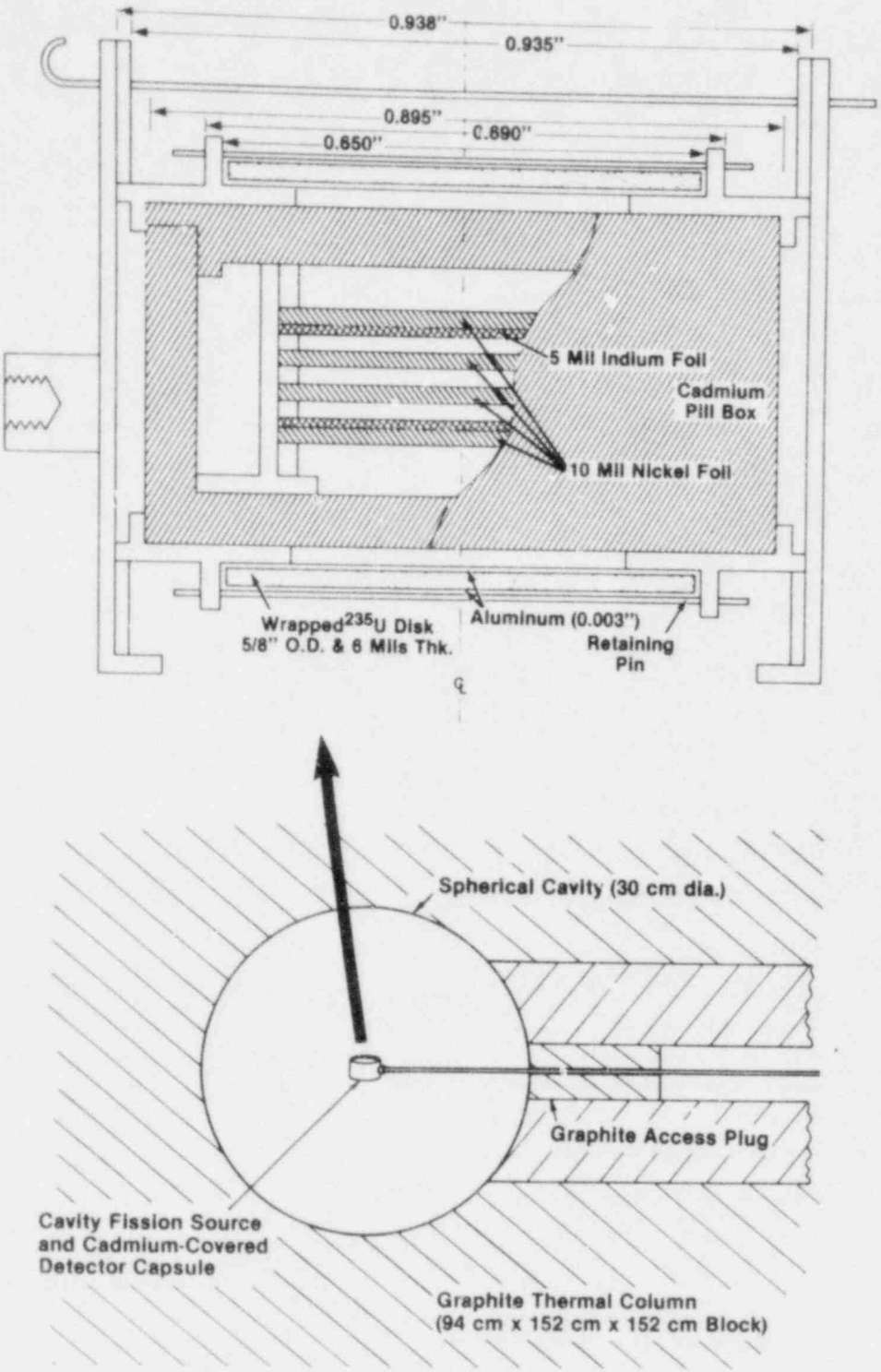

Fig. 1. U-235 Cavity Fission Source. Upper view: relative positions of neutron sensor foils, fission-disks and cadmium enclosure. Lower view: the upper assembly in the thermal column of the NBS reactor.

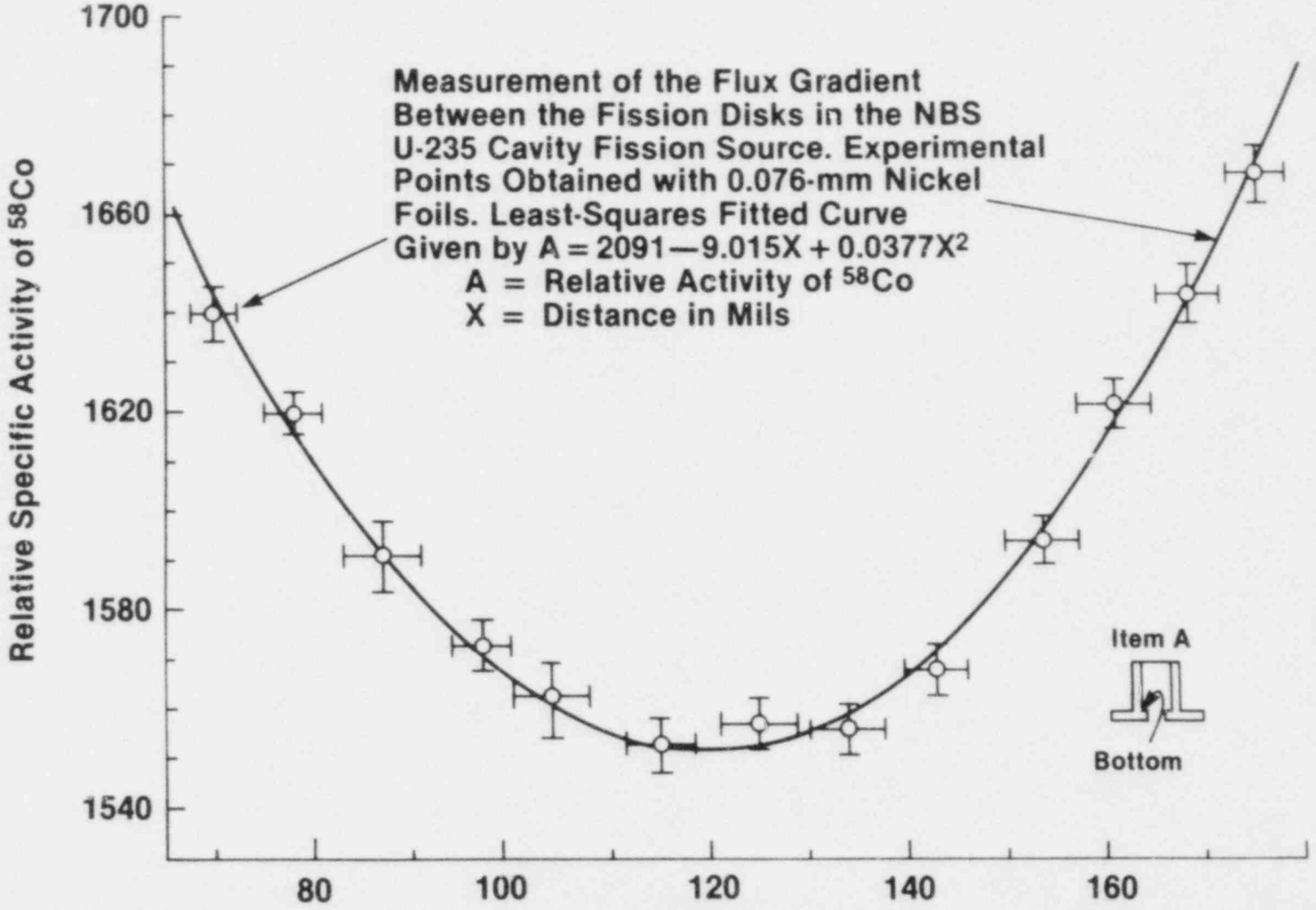

FIG. 2. **Distance in Mils (0.001 inches) from the Bottom (see Item A) of the Aluminum Foil Holder Insert.**

holder. The gradient was measured by simultaneously irradiating[13] nickel foils each 0.076 mm thick. The total mass of nickel involved is representative of a characteristic loading of three or four 0.25 mm foils and two 0.12 mm flux monitors, as shown in Fig. 1. This is important because the effects of scattering within this small irradiation volume must be addressed. Note also, the NBS cavity fission source is generally not used for non-threshold integral detectors when high accuracy is required.

Scattering in the Cavity Fission Source

Tables IA and IB summarized a significant effort on the part of the Monte Carlo Group, Los Alamos Scientific Laboratory to obtain scattering corrections by the Monte Carlo transport theory method. The Cavity Fission source contained the exact elements shown in Fig. 1. Table IA gives the contributions to flux perturbations because of the inscattering (as opposed to removal) of neutrons. The data in the table refer to calculations at the location of the bottom indium foil (see Fig. 1). Table IB combines the inscattering effects into inscatter contributions by material type and gives the total removal and the net flux perturbation effect, which is 4.09 percent. Because of inelastic scattering, predominatly in uranium and aluminum, there is an energy shift in the spectrum as shown in Fig. 3. As before, this is the spectrum at the bottom indium foil. By integrating the perturbed spectrum over cross sections of pertinent neutron sensor materials one can determine the effect on a particular isotopic reaction rate. Such effects may be negative or positive. For example, a negative result may be obtained whenever inelastic scattering decreases the neutron energy below the threshold of a reaction. Fig. 4 is an attempt to graphically represent the trend in the perturbation versus effective low-energy thresholds. The five data points (open circles) are, from left to right, for the reactions Np-237(n,f), In-115(n,n'), Ni-58(n,p), Al-27(n,α) and Cu-64(n,α).

Table IA. Monte Carlo Calculations of Neutron Scattering in the NBS U-235 Cavity Fission Source

(Results as Determined at the Bottom Indium Foil)

Part Name	$\left(\frac{\text{Flux Inscattered}}{\text{Free Field Flux}}\right)$	Fraction of Total (%)	Part Thickness (mm)
Top Cadmium Box	0.0145	13.61	0.97
Bottom Cadmium Box	0.0140	13.15	0.61
Foil Holder, Alum.	0.0137	12.86	0.56
Bottom Nickel Foil	0.0135	12.68	0.25
Bottom Indium Foil	0.0097	9.11	0.13
Bottom Source Disk	0.0097	9.11	0.15
Second Nickel Foil	0.0069	6.48	0.25
Top Source Disk	0.0064	6.01	0.13
Third Nickel Foil	0.0063	5.91	0.25
Top Nickel Foil	0.0040	3.76	0.25
Bottom Source Holder	0.0025	2.34	0.28
Top Source Holder	0.0021	1.97	0.28
Top Indium Foil	0.0016	1.50	0.13
Sides Cadium Box	0.0011	1.03	0.76
Aluminium on Source	0.0005	0.48	0.03
	Sum = 0.1065	*Sum = 100.0*	

Table IB. Breakdown of Monte Carlo Scattering and Removal Effects for Cavity Fission Source

Summary of Inscattering

Material	$\left(\frac{\text{Flux Inscattered}}{\text{Free Field Flux}}\right)$
Nickel	0.0307
Aluminium	0.0231
Cadmium	0.0296
U-235	0.0161
Indium	0.0113
Total Inscattering	0.1108
Total Removal	-0.0699
Net Effect	0.0409

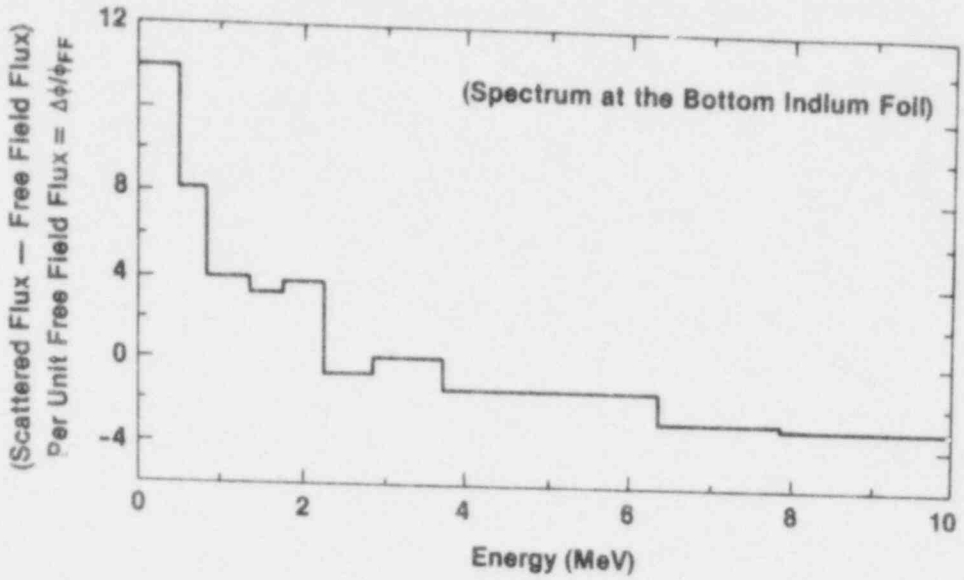

Fig. 3. Effects of Scattering on the Neutron Energy Spectrum in the NBS Cavity Fission Source

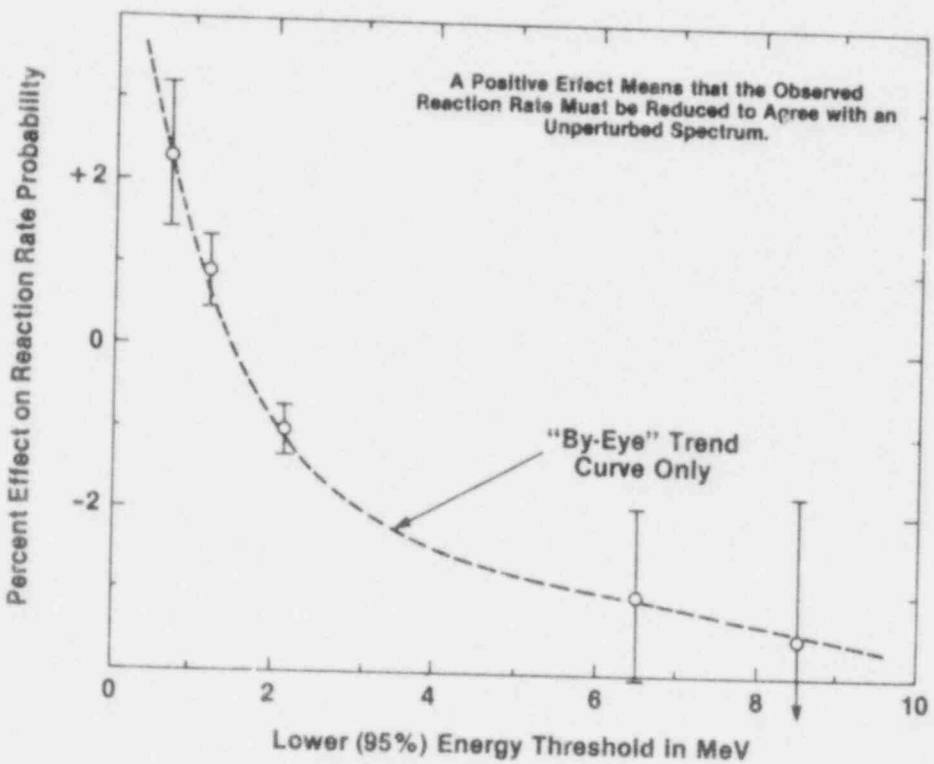

Fig. 4. Monte Carlo Estimates of Trends in Effects on Threshold-Type Nuclear Reactions Caused by Scattering in the Cavity Fission Source.

A Measurement of the Ni-58(n,p)Co-58 Integral Cross Section

Because of the frequent use of the Ni-58(n,p) reaction for materials dosimetry[6] and because of a possible discrepancy between calculated and measured values,[7] NBS is measuring the spectrum averaged cross section for U-235 fission spectrum. Brief details of the experiment are as follows:

1. Using the In-115(n,n')In-115* 4.5-hour half-life reaction, a germanium-lithium (GeLi) detector was calibrated in terms of its response to Cf-252 flux. The indium reaction is used because of its reasonably good sensitivity to a 2 X 10^9 n/sec Cf-252 source; also because the ratio of spectrum averaged cross sections in the Cf-252 and U-235 fields is nearly one (e.g., 1.05) and is believed known to one percent.
2. Nickel was irradiated in the cavity fission source to a fluence of 5 X 10^{15}n/cm^2. The In-115(n,n') reaction was used as the flux level monitor and a fission chamber monitored the reactor power level.
3. One of us (F. Schima) determined the absolute specific activity of the 70.78-day 810-KeV Co-58 activity in the nickel foil.
4. The U-235 fluence was determined from a time and the indium-115* activity as measured on the GeLi counter.
5. The ratio of the two results is the desired spectrum averaged cross section.

The results of the subject measurement are summarized in Table II. The necessary corrections and adjustments are indicated with the sources of uncertainty. The present value of 101 $\pm$ 3 mbarns is significantly less than the current best accepted experimental value of 108 $\pm$ 5 mbarns.[8] On the other hand, calculated values whose variation depends more on the choice of the form of the U-235 spectrum than particular cross section set, range from 100 to 105 mbarns. Investigation of Ni-58(n,p) cross section continues.

Table II. Results of ^{58}Ni (n, p) Cross Section Measurement

$\sigma_{U25}{}^{58}Ni\ (n, p) = 101 \pm 3$ mb

Summary of Uncertainties

Source	Contribution (%)
Source Strength of Cf	1.1
Cf Source to In Foil Distance	0.4
Statistics of In Activity Counting	0.5
σ_{Cf}/σ_{U25} of In (n, n')	1.0
Scattering Correction for In at Cf	0.8
Scattering Correction for In in Cavity	0.8
Total Uncertainty in Fluence	2.0
Efficiency of γ Counting of ^{58}Co	0.75
Statistics of γ Counting of ^{58}Co	0.17
Isotopic Abundance of ^{58}Ni	0.8
Flux Gradient in Cavity	0.4
Scattering Correction for Ni in Cavity	0.8
Total Uncertainty in σ	2.5%

THE INTERMEDIATE-ENERGY STANDARD NEUTRON FIELD

The important details of the ISNF are shown in the upper half of Fig. 5. There are eight U-235 disks mounted symmetrically in the thermal column cavity. They collectively produce about 6 X 10^{11}n/s (fission spectrum flux). In Fig. 5, the four disks not shown are directly behind those depicted. Light-weight aluminum structures hold the boron-10 sphere in the center of the cavity. The spectrum at the center of the ISNF is shown in the bottom half of the figure. The total fast flux in the central region is 7 X 10^{8} n/cm^{2}·s. The spectrum can be visualized as follows. Fissioning in the eight U-235 sources would produce a pure U-235 fission spectrum at the center of the cavity if it were not for the thermal neutrons driving the disks and moderated neutrons from the graphite. Scattering in the graphite produces a large spectral component below 1 MeV which further moderates to a near 1/E spectrum below 1 keV. The thermal and 1/E components can effectively be removed by a boron-10 spherical filter.

Because the system has, essentially, a one-dimensional spherical geometry and is composed of elements having well known cross sections, the spectrum[9] and its covariances[10] are well known from discrete ordinates calculations. Sensitivity studies and associated density and dimensional measurements have now stimulated a refinement of these calculations according to a slightly revised physical description of the ISNF (see Fig. 6). Fig. 5 lists the changes made for the latest calculations by LASL. Table III shows the effects of those changes. The top part of Table 3 summarizes the most significant changes. The lower portion of the Table lists absolute fluxes and spectrum averaged cross sections for a variety of calculational models for both the older, ISNF(1), and newer, ISNF(3), physical descriptions.

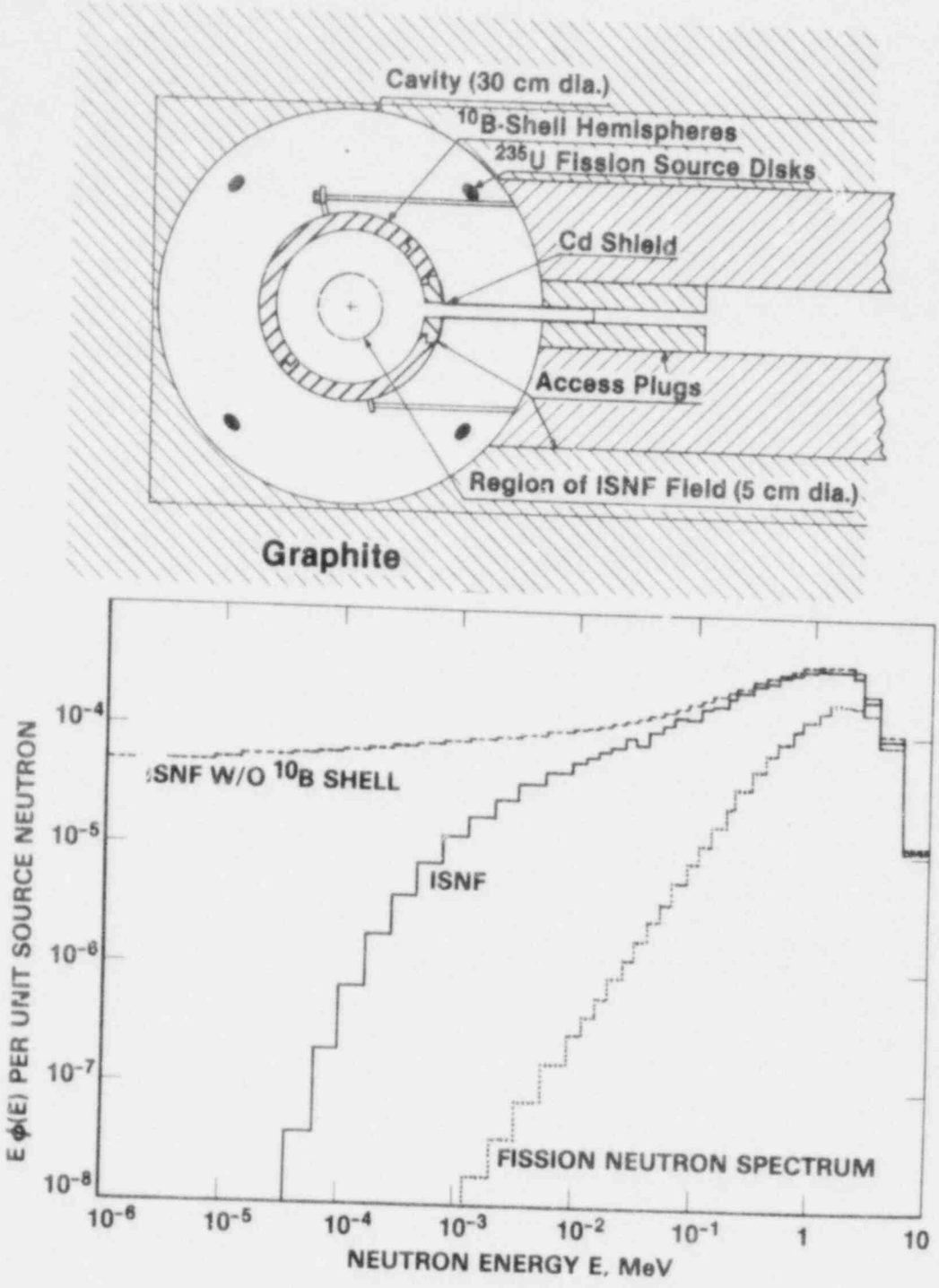

Fig. 5. **Upper view: The intermediate-energy Standard Neutron Field located within a 30-cm diameter cavity in the thermal column of the NBS reactor. Lower view: Comparison of the U-235 fission spectrum to the ISNF spectra with and without a boron-10 filter.**

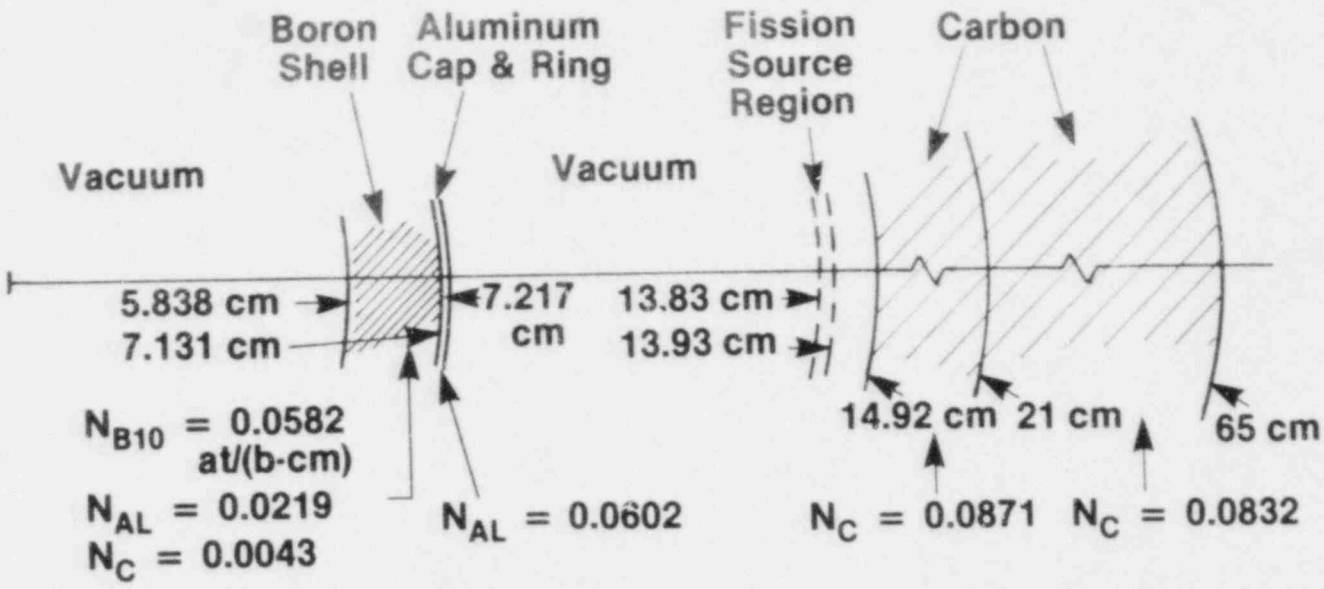

1. Changes in the Physical Parameters:
   - Two Percent Increase in the B-10 Density
   - Two-Zone Specification of the Graphite Reflector
   - Addition of 0.29% Hydrogen to the Graphite
   - Slight Increase in the Weight of the Aluminum Protective Shell
2. Changes in Calculations:
   - Cross Sections for Transport: From ENDF/B-IV to ENDF/B-V
   - Cross Sections for Dosimetry: From ENDF/B-IV to ENDF/B-V
   - Multigroup Specifications: 240 Group to 150 Group

FIG. 6. **Report of Changes in the Configuration of the NBS ISNF**

TABLE III.A. Effects of Changes in the ISNF Configuration

Parameter	Configurations		
	ISNF(1)	ISNF(3)	Ratio
Flux	0.001385	0.001362	0.983
U-235(n,f)	1.615	1.605	0.993
U-238(n,f)	0.1367	0.1392	1.018
Ni-58(n,p)	0.0366	0.0373	1.019
Al-27(n,α)	1.94E-04	1.98E-04	1.021

ISNF(1): Old (original) configuration; NBS U-235 fission spectrum
ISNF(3): New configuration; NBS U-235 fission spectrum

TABLE III.B. Inter-Comparison of LASL Calculations

		Spectrum Averaged Cross Section		
	Flux	$^{239}_{Pu}$	$^{235}_{U}$	$^{238}_{U}$
ISNF(1)-240-group EIV σ's EIV dosimetry	.001385	1.818	1.631	.1363
ISNF(1)-240-group EIV σ's EV dosimetry	.001385	1.823	1.616	.1367
ISNF(1)-70-group EIV σ's EV dosimetry	.001395	1.849	1.639	.1356
ISNF(1)-70-group EV σ's EV dosimetry	.001403	1.849	1.641	.1349
ISNF(3)-70-group EV σ's EV dosimetry	.001373	1.840	1.626	.1374
ISNF(3)-150-group EV σ's EV dosimetry	.001362	1.820	1.606	.1388

EIV and EV refer, respectively, to the Brookhaven managed ENDF/B-IV and -V cross section files.

PLUTONIUM-240 MEASUREMENTS IN THE ISNF

As for the ISNF Benchmark Field, we here report a new measurement of the Pu-240 fission cross section relative to that for U-235. Table IV gives the pertinent details, corrections made, basic experimental results and uncertainties, and finally a comparison of the derived experimental to calculated fission rate ratio for Pu-240(n,f)/ U-235(n,f). The result is 0.513 $\pm$ 1.8%(1σ uncertainty).

The experiment was conducted as follows:

1. The fissionable deposits on 0.127 cm-thick steel backings were irradiated back-to-back in the NBS dual fission chamber.
2. Although the ratio of Pu-240 to U-235 was desired, the experiment was performed relative to U-238 to avoid difficulties with the low energy response of U-235.
3. The irradiations were accomplished with the boron-10 shell in place and with and without the eight U-235 fission sources. The difference between the two types of irradiations experimentally compensates for:
   - 3.1 the effects of spontaneous fissions;
   - 3.2 thermal neutron leakage;
   - 3.3 response to reactor gamma rays and any unwanted fast neutron contamination;
   - 3.4 electronic background noise;
   - 3.5 a small neutron contribution which is thought to be due to (n,α) reactions producing alphas on boron-10, which in turn yield neutrons.

Note: Typical total backgrounds varied from 1.3 to 2.8 percent depending upon the isotope.

TABLE IV. PLUTONIUM-240 MEASUREMENT IN ISNF: MATERIALS AND SOME NECESSARY CORRECTIONS

Corrections for Fissionable Impurities

Pu-240 (Mass: 146.4 ± 0.8% micrograms)

Isotope	Percent	Principal Impurity	Present Correction
Pu-238	0.011		
Pu-239	0.673	Yes	
Pu-240	98.519		3.0%
Pu-241	0.429	Yes	
Pu-242	0.368		
Pu-244	0.001		
Am-241	0.170		

U-238 (Mass: 244.3 ± 1.0% micrograms)

U-238	99.939		
U-235	0.061	Yes	1.0%

Corrections for Fission Fragment Absorption

Pu-240	0.77%
U-238	1.27%

Corrections for Scattering in Backing and Chamber

Pu-240	0.35%
U-238	0.98%

EXPERIMENTAL RESULTS:

Fission Rate Ratio

$$\frac{F_{240}}{F_{238}} = \frac{N_{240}\,\sigma_{240}}{N_{238}\,\sigma_{238}} = 3.279 \pm 0.84\%$$

and

Cross Section Relative to U-238

$$\frac{\sigma_{240}}{\sigma_{238}} = 5.52 \pm 1.5\%$$

Cross Section Relative to U-235 (for Comparison to Calculated Value)

- Experimental

$$\frac{\sigma_{240}}{\sigma_{235}} = \frac{\left(\sigma_{240}/\sigma_{238}\right)}{\left(\sigma_{235}/\sigma_{238}\right)} = \frac{5.52}{10.76} = 0.513 \pm 1.8\%$$

- Calculated

$$\frac{\sigma_{240}}{\sigma_{235}} = \frac{0.8237}{1.602} = 0.514$$

The final table (Table V), is given to further explain our interest in the fission rate Pu-240/U-235 ratio rather than a direct comparison of the Pu-240/U-238 ratio. There is a long-standing, unexplained, five percent discrepancy in fission rate ratios relative to U-238. The data in Table V, where available, support this contention. The experimental uncertainties are on the order of 1.5 to 2.5 percent.

CONCLUDING REMARKS

Highlights of this paper are the new experimental results for the Ni-58(n,p) and the Pu-240(n,f) reactions. Both results demonstrate a need for further investigations.

The value of 101 $\pm$ 3 mb for the cross section of Ni-58(n,p) reaction in a standard, U-235, fission-neutron spectrum is significantly different than the long-standing value of 108 $\pm$ 5 mb measurement by Fabry.[11] Additional work is in progress to try and further reduce the uncertainty on our 101 mb value for the U-235 spectrum and we are performing a comparable experiment in the even better known Cf-252 spectrum. Furthermore, because our U-235 measurements are tied to the ratio of the In-115(n,n') reaction in the U-235 and Cf-252 fields, we are planning to investigate the indium measurements in these two spectra relative to the better known response of Np-237(n,f).

The experimentally determined Pu-240/U-235 fission rate ratio of 0.513 $\pm$ 1.8% for the ISNF fast reactor spectrum is in good agreement with the calculated result using ENDF/B-V cross sections.

TABLE V. COMMENTS ON THE CALCULATED-TO-EXPERIMENTAL RATIOS* FOR Pu-240 VERSUS U-235 AND U-238

Isotopic Ratio	Spectrum		
	ISNF	U-235	Cf-252
Pu-240 / U-238	1.058	---	1.043**
Pu-240 / U-235	1.002	---	0.994**
U-235 / U-238	1.056	1.068	1.052

* These are double ratios; that is, ratios of calculated-to-experimental values where each value represents a ratio of spectrum-averaged cross sections of the indicated isotopes.

** Both of these values expected to increase by approximately 0.5% when appropriate scattering corrections have been made to recent experimental data.

REFERENCES

1. J. A. Grundl, et al. "Compendium of Benchmark and Test Region Neutron Fields for Pressure Vessel Irradiation Surveillance," in LWR Pressure Vessel Irradiation Surveillance Dosimetry Quarterly Progress Report,* July-September 1980; NUREG/CR-0551 (December 1978).

2. C. M. Eisenhauer and J. A. Grundl, "Neutron Transport Calculations for the Intermediate-Energy Standard Neutron Field (ISNF) at the National Bureau of Standards," Proceedings International Symposium on Neutron Standards and Applications, NBS Special Publication 493, U.S. Dept. of Commerce, Washington, D.C. (March 1977).

3. J. A. Grundl, V. Spiegel, C. M. Eisenhauer, H. T. Heaton II, D. M. Gilliam, and J. Bigelow, "A Californium-252 Fission Spectrum Irradiation Facility for Neutron Reaction Rate Measurements," Nuc. Tech. 32, (March 1977).

4. R. H. Noyce, E. R. Mosburg, Jr., S. Garfinkel, and R. S. Caswell, "Absolute Calibration of the National Bureau of Standards Photoneutron Source. III Absorption in a Heavy Water Solution of Manganese Sulphate," J. Nucl. Energy A/B, 17, 313 (1963).

5. J. A. Grundl and C. M. Eisenhauer, "Fission Spectrum Neutrons for Cross Section Validation and Neutron Flux Transfer," Conf. on Nuclear Cross Sections and Technology, Washington, D.C.; NBS Special Publication 425, Vol. I, p. 250 (March 1975).

6. W. N. McElroy, et al., "LWR Pressure Vessel Surveillance Dosimetry Improvement Program 1979 Annual Report," NUREG/CR-1291, HEDL-SA 1949, Hanford Engineering Development Laboratory, Richland, WA (February 1980).*

7. A. Fabry, et al., "Review of Microscopic Integral Cross Section Data in Fundamental Reactor Dosimetry Benchmark Neutron Fields," Contribution to "Neutron Cross Sections for Reactor Dosimetry," Technical Report IAEA-208, Vol. I, review papers, p. 233 (IAEA, Vienna, 1978).

8. A. Fabry, (CEN/SCK, Mol, Belgium), J. A. Grundl and C. Eisenhauer, (NBS, USA); "Fundamental Integral Cross Section Measurements in the Thermal-Neutron-Induced Uranium-235 Fission Neutron Spectrum," Proceedings of a Conference on Nuclear Cross Sections and Technology, NBS Special PUblications 425, U.S. Dept. of Commerce, Washington, D.C., p. 254 (March 1975).

9. P. D. Soran, R. J. LaBauve, and D. C. George (LASL), and C. M. Eisenhauer (NBS), "Neutronic Analysis of the NBS Intermediate-Energy Standard Neutron Field (ISNF)," Trans. Am. Nucl. Soc. 32 (June 1979).

10. B. L. Broadhead, J. Wagschal, "The NBS Intermediate-Energy Standard Neutron Field (ISNF) Revisited," Trans. Am. Nucl. Soc. 33 (November 1979).

11. W. L. Zijp and J. H. Baard, "Nuclear Data Guide for Reactor Neutron Metrology. Part I: Activation Reactions (1979 Edition)"; Scientific Report of Commission of the European Communities, Nuclear Science & Technology, EUR 7164 EN, Luxembourg, Office of Official Publications of European Communities (1981).

*Available for purchase from the NRC/GPO Sales Program, U.S. Nuclear Regulatory Commission, Washington, D.C. 20555 or the National Technical Information Service, Springfield, VA 22161.

NEUTRON SPECTRUM INVESTIGATION IN THE REFERENCE SPECTRUM ΣΣ-ITN BY MEANS OF RECOIL PROTON SPHERICAL COUNTERS

D. Albert, W. Hansen, W. Vogel
Central Institute of Nuclear Research (ZfK), Academy of Sciences of the GDR, Rossendorf near Dresden, DDR-8051 Dresden, POB 19, German Democratic Republic
and
I. Gârlea, Chr. Miron, Cs. Roth
Institute of Nuclear Power Reactors (IRNE), State Committee of Nuclear Energy, Piteşti, POB 78, Socialist Republic of Roumania

ABSTRACT

In the fast neutron reference assembly ΣΣ-ITN neutron spectra measurements were carried out by means of the Rossendorf recoil proton counter spectrometer. Spherical proportional counters were applied. The energy range of 8...1400 keV was covered, containing about 85 % of the total lethargy flux.
The results have been compared with other experiments (carried out by Magurele and Karlsruhe groups), with calculations (ANISN, 100 groups, ENDF/B-III) and with the recommended ΣΣ-neutron spectrum. The agreement with the results of other experiments is rather good. The low energy limit could be decreased from about 20 keV - as reached up to now - to 10 keV. In the low energy region there are deviations from the recommended spectrum.

1. INTRODUCTION

Fast critical assemblies as well as internationally accepted reference configurations are necessary for the estimation, validation and adjustment of nuclear data which are used for calculations of fast breeder reactors and for reactor materials dosimetry.
In 1969, A. Fabry suggested a configuration[1] consisting of spherical shells of natural uranium metal and of B_4C which

should be placed in a cavity of the thermal column of a research reactor. The neutron spectrum in the centre is comparable to that in a fast breeder core. Since the nuclear data for the applied nuclides do not represent primary standards, it was designated as the secondary standard spectrum ΣΣ. But it could be calculated without difficulties (one-dimensional, homogeneous zones) and easily constructed in different laboratories. In 1970, it was constructed at Mol. Later on it was realized in different other laboratories, e.g. ΣΣ-ITN at Magurele near Bucharest in the Roumanian Institute of Nuclear Power Reactors IRNE.[2]

In 1973 ΣΣ was taken into consideration as a benchmark by the US Cross Section Evaluating Working Group CSEWG.[3] In 1976, ΣΣ was recognized as a reference system by the IAEA,[4] and a recommended spectrum was accepted.[5] The basic characterization of the reference spectrum ΣΣ was based on the experimental determination of the neutron spectrum and on a comparison with calculations. An international comparison was carried out at Mol with the participation of KFK Karlsruhe and RCN Petten groups, in which different methods of differential proton counter spectrometry were used.[6] In the range below 1 MeV the recoil proton counter spectrometry was applied. In the interval 30...100 keV significant deviations appeared, and below 30 keV it was impossible to obtain unambiguous experimental results.

In the ΣΣ-ITN recoil proton counter measurements were repeated;[7] 20 keV were reached as a low energy limit. In 1979, measurements were carried out by means of the Rossendorf recoil proton spectrometer[8,9] at Magurele. The aim of the measurements was to further decrease the low energy limit and to secure the reliability of the existing experimental results.

2. CONSTRUCTION OF THE ΣΣ-ITN AND MEASUREMENTS CARRIED OUT

The configuration of a spherical proportional counter within the ΣΣ-assembly is represented in fig. 1. The ΣΣ-assembly is situated within a cavity of 50 cm diameter inside the graphite thermal column of a research reactor of the WWR-S type at a distance of 1.5 m from the core boundary. The thickness of the uranium metal shell amounts to 5 cm, its outer diameter is 24.5 cm. The B_4C shell is

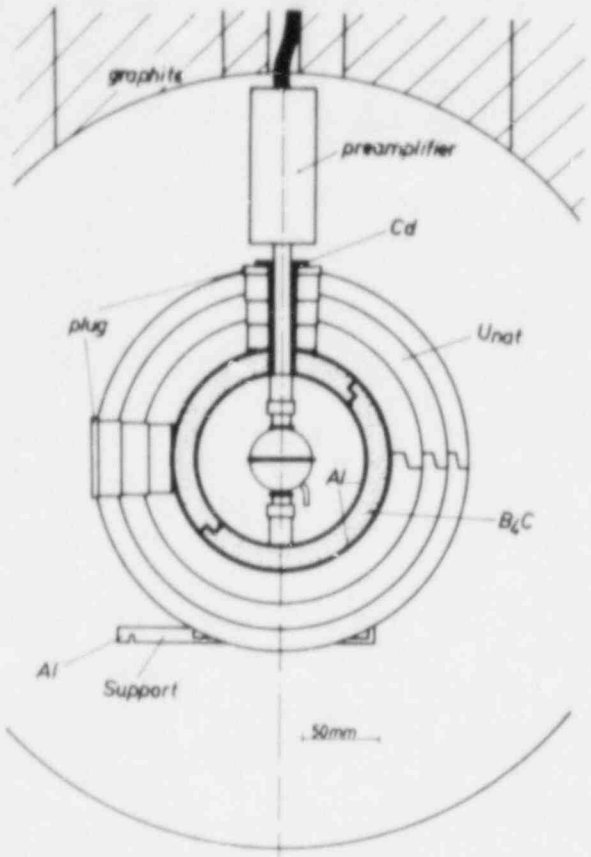

Fig. 1. Experimental arrangement of $\Sigma\Sigma$-ITN with a spherical recoil proton counter in the centre

1.5 cm thick; it is covered from both sides by 1 mm aluminium. As the $\Sigma\Sigma$-Mol and the $\Sigma\Sigma$-ITN assemblies should be identical, the B_4C vibrocompacted spherical shell was supplied from Belgium. Test measurements showed that $\Sigma\Sigma$-Mol and $\Sigma\Sigma$-ITN are identical, also with regard to the neutronic parameters.[2,7]

The Rossendorf Measurements in $\Sigma\Sigma$-ITN have been carried out using three different spherical counters, i.e. a counter with 100 kPa H_2 (counter of British origin SP9), a counter with 400 kPa H_2 (counter of British origin SP2-4) and a counter with 1 MPa H_2 (counter of Polish origin NOK 1043). As a power monitor, a BF_3 counter was placed in the outer part of the graphite column at a distance of 85 cm from the centre of the $\Sigma\Sigma$-ITN assembly.

In the $\Sigma\Sigma$-ITN the gamma background was comparatively high (about 1.5 uGy/s) so that the low energy limit of 1...2 keV usually attained in fast critical assemblies could not be reached here. But nevertheless the value of 10 keV is an improvement with respect to previous lower limits.

3. EVALUATION, RESULTS, COMPARISON AND DISCUSSION

The evaluation of the experimental data has been carried out using the codes SUBTRA and DIF-2.[9,10] In order to check the Rossendorf evaluation procedure our primary experimental data (multichannel spectra, results of energy

calibration) have been evaluated using the Magurele procedure (code SPEC 4)[11] as well. Within the usual error limits (± 10 % above 40 keV) agreement could be reached. Further details about the measurements and the evaluation are reported in ref. 12.

We take 100 group ANISN using ENDF/B-III data[7] as basis of calculation in order to compare different $\Sigma\Sigma$ spectrum experiments with calculations. We make use of the Karlsruhe measurements[6] and of the Magurele measurements.[7] All the results have been related to the Rossendorf results and have been normalized in energy regions (represented in ABBN groups)[13] as broad as possible: ANISN calculation in ABBN groups 6...11, Karlsruhe experiments in groups 6...9, Magurele measurements in groups 6...10. Deviations from Rossendorf experimental results are given in the table.

Table. Deviations from Rossendorf experimental results, given in percent

No. of ABBN-group i	$\frac{E_{Mag.}}{E_{Ross.}} - 1$	$\frac{E_{Karl.}}{E_{Ross.}} - 1$	$\frac{E_{recom.}}{E_{Ross.}} - 1$	$\frac{C_{ANISN}}{E_{Ross.}} - 1$
11	-	-	24.1	23.4
10	-6.6	-	22.2	55.6
9	-7.5	-5.1	0.5	16.2
8	-5.4	-8.3	-6.3	-3.1
7	6.8	4.0	-1.4	-1.6
6	1.5	3.6	-1.0	-14.0

It can be seen that all the experimental results agree quite well, especially below 800 keV. The calculation by ANISN and ENDF/B-III gives a systematically too soft spectrum, i.e. too few neutrons about 1 MeV and too many neutrons below 100 keV.

Possibly the deviations of the ANISN calculation from the Rossendorf results could be removed by a variation of the inelastic scattering matrix of ^{238}U in ENDF/B-III, so that the total inelastic scattering cross section will be decreased with decreasing energy. Concerning the influence of such variations see ref 14.

The Rossendorf experimental results have also been compared with the recommended $\Sigma\Sigma$ -spectrum[5], which has been normalized to the Rossendorf results in ABBN groups 6...11; see also the table and fig. 2. In the energy range 50...800 keV the agreement is rather good. In group No. 10 (21.5...46.5 keV) the recommended spectrum has been substantially decreased in comparison to ANISN, but it is still higher than the results obtained by Magurele and Rossendorf groups. In group No. 11 (10...21.5 keV) the recommended spectrum is higher than the Rossendorf results. The reason for this is that in group No. 11 only Belgian and Dutch measurements have been available until now,[5,6] which might be unreliable.

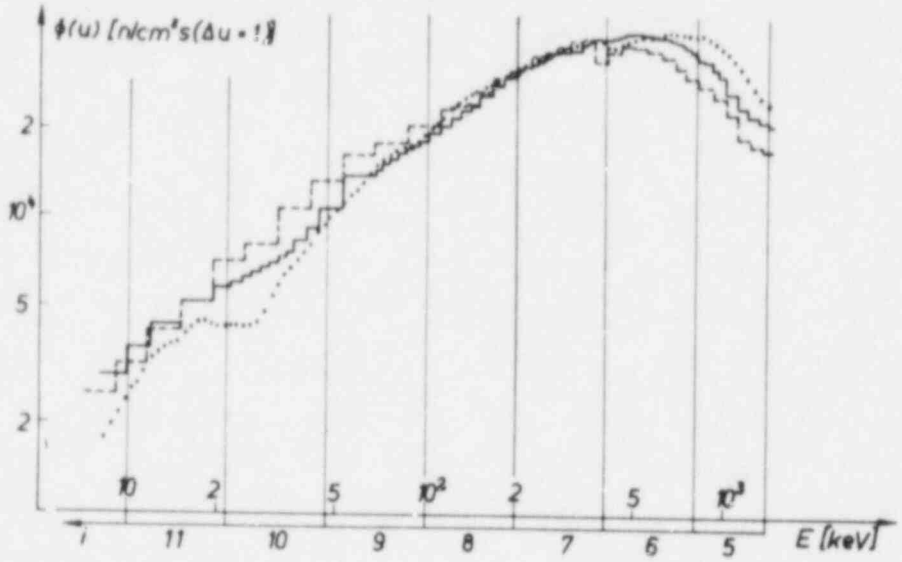

Fig. 2. Comparison of Rossendorf experimental results with recommended $\Sigma\Sigma$ spectrum and ANISN calculation.
... Experiment Rossendorf, ---- Recommended spectrum, - - - ANISN calculation

4. CONCLUSIONS

In the $\Sigma\Sigma$ -ITN assembly measurements by means of the Rossendorf recoil proton counter spectrometer have been carefully carried out and evaluated.

The low energy limit could be decreased from 20 keV to 10 keV. In the energy range (20...30) keV...800 keV the Rossendorf experimental results agree rather well with the results of measurements carried out earlier by Karlsruhe and Magurele groups. Furthermore, the recommended spectrum could be validated in the energy range 40...800 keV, but in the energy region 10...40 keV our results seem to be an improvement and should be taken into account.

There remains an unexplained deviation between the experimental results and the results of an ANISN-ENDF/B-III calculation which gives systematically too soft spectra. Here, uncertainties in the inelastic scattering matrix of ^{238}U could play a role.

REFERENCES

1. The Role of Standard Neutron Fields in Relation to Fast Reactor Spectrometry and Reactor Design, oral presentation by A. Fabry, collection of four technical documents sent to an IAEA working panel about Fast Reactor Spectrum Measurements and their Interpretation, Argonne, 10-13 November 1970.

2. I. Gârlea et al., Rev. Roum. Phys. 22 (1977) 627.

3. B.A. Magurno, O. Ozer, Trans. of American Nucl. Soc. 17 (1973) 528.

4. Conclusions and Recommendations of "IAEA Consultants' Meeting on Integral Cross Section Measurements in Standard Neutron Fields", Vienna, 15-19 November 1976, Report INDC(NDS)-81/L+M.

5. A. Fabry et al., Nuclear Technology 25, No. 2 (Febr. 1975), P. 349.

6. H. Bluhm et al., Intercomparison of Differential Neutron Spectrometry Techniques in the Mol-ΣΣ Fast Assembly, KFK 1658 - RCN 172 - BLG 471, 1972.

7. I.Gârlea, Contributii la Studiul Spectrului de Neutroni Rapizi in Domeniul 10 keV - 3 MeV, Doctor Thesis, Bucharest, 1979.

8. D. Albert et al., Kernenergie 21 (1978) 82.

9. D. Albert, W. Hansen, Kernenergie 20 (1977) 95.

10. W. Hansen, W. Vogel, Verbesserungen in der elektronischen Apparatur und der Auswertungsmethode zum Rossendorfer Rückstoßprotonen-Proportionalzählrohr-Spektrometer, Arbeitsbericht RPP-3/79, 1979.

11. P.W. Benjamin et al., The Analysis of Recoil Proton Spectra, AWRE 09/68, 1968.

12. D. Albert et al., Investigation of the Neutron Spectrum in the Reference Spectrum $\Sigma\Sigma$-ITN by means of Spherical Proton Recoil Counters, Arbeitsbericht RPP-16/80, July 1980.

13. L.P. Abagyan et al., Group Constants for Nuclear Reactor Calculations, Moscow 1964 (Russ.).

14. D. Albert et al., Otsenka sovremennykh dannykh po neuprugomu rasseyaniyu 238U putem integral'nykh eksperimentov vo vstavnoj reshetke iz prirodnogo urana SEG-II, prepared for the 5th All-Union Conference on Neutron Physics, Kiev, 15-19 September 1980.

CFRMF SPECTRUM UPDATE AND APPLICATION TO DOSIMETER CROSS-SECTION DATA TESTING*

R. A. Anderl, Y. D. Harker, D. A. Millsap,
J W Rogers and J. M. Ryskamp
EG&G Idaho, Inc.
Idaho National Engineering Laboratory
Idaho Falls, Idaho 83415 U.S.A.

ABSTRACT

The Coupled Fast Reactivity Measurements Facility (CFRMF) at the Idaho National Engineering Laboratory (INEL) is a Cross Section Evaluation Working Group (CSEWG) benchmark for data testing of dosimetry, fission-product and actinide cross sections important to fast-reactor technology. In this paper we present the results of our work in updating the CFRMF spectrum characterization and in applying CFRMF integral data to testing ENDF/B-V dosimeter cross sections. Updated characterization of the central neutron spectrum includes the results of neutronics calculations with ENDF/B-V nuclear data, the generation of a fine-group spectrum representation for integral data-testing applications, and a sensitivity and uncertainty analysis which provides a flux-spectrum covariance matrix related to uncertainties and correlations in the nuclear data used in a neutronics calculation. Our application of CFRMF integral data to cross section testing has included both conventional integral testing analyses and least-squares-adjustment analyses with the FERRET code. The conventional integral data-testing analysis, based on C/E ratios, indicates discrepancies outside the estimated integral test uncertainty for the $^{6}Li(n,He)$, $^{10}B(n,He)$, $^{47}Ti(n,p)$, $^{58}Fe(n,\gamma)$, $^{197}Au(n,\gamma)$ and $^{232}Th(n,\gamma)$ cross sections. The integral test uncertainty included contributions from the measured integral data and from the spectrum and cross sections used to obtain the calculated integral data. Within the uncertainty and correlation specifications for the input spectrum and dosimeter cross sections, the least-squares-adjustment analysis indicated a high degree of consistency between the measured integral data and the ENDF/B-V dosimeter cross sections for all reactions except $^{10}B(n,He)$.

* Work supported by the U.S. Department of Energy under DOE Contract No. DE-AC07-76ID01570.

1. INTRODUCTION

The Coupled Fast Reactivity Measurements Facility (CFRMF)[1,2], which is located at the Idaho National Engineering Laboratory (INEL), is a zoned-core critical assembly with a fast neutron spectrum zone in the center of an enriched ^{235}U, water moderated thermal driver. Approximately 95% of the neutrons in the central spectrum are between 4 keV and 4 MeV and the median and mean energies are 370 keV and 760 keV, respectively. The central neutron spectrum is a Cross-Section Evaluation Working Group (CSEWG) benchmark field.

Measurements of integral reaction rates in the CFRMF have been made and integral cross sections have been derived for fission-product, actinide and dosimetry class materials of importance to fast reactor technology. These integral data play an important role in the evaluation and testing of cross-section information for evaluated nuclear data files. The dosimetry integral data, measured as part of the Inter-Laboratory Reaction Rate Program[3], are of specific importance to dosimetry data development and testing for reactor fuels and materials which are key topics for this symposium.

The purpose of this paper is to present the results of our work in updating the CFRMF spectrum characterization and to demonstrate the application of CFRMF integral data to dosimeter cross-section data testing for ENDF/B-V. Characterization of the central neutron spectrum is discussed in section 2 of this paper. This discussion covers neutronics calculations, generation of a 620-group spectrum representation, and sensitivity and uncertainty analysis[4] for the CFRMF. The application of CFRMF integral measurements to cross-section data testing has included both conventional integral testing and least-squares adjustment analyses with the FERRET code[5]. A discussion of the conventional integral testing analysis is given in section 3. Section 4 presents preliminary results of the least-squares-analyses. Finally in Section 5 we present the conclusions of our work.

2. SPECTRUM CHARACTERIZATION

The CFRMF central neutron spectrum recommended for past data-testing analyses[6] has been specified to be that resulting from a transport calculation with ENDF/B-IV nuclear data. Generally, the measured spectra have not been used because they cover a limited range of the neutron energy spectrum. However, the measured spectra have provided a means to assess, at least qualitatively, the accuracy in the shape of the calculated spectrum over the applicable energy ranges. In view of the complexities involved with using a benchmark spectrum which is a composite of calculation and measurement, use of a calculated spectrum for data testing provides a consistent framework in which to evaluate different versions of ENDF/B. The major drawback

to this approach is that the spectrum shape is subject to change because the nuclear data used for the neutronics calculations vary from one version of ENDF/B to another. In principle, this is also true for measured spectra which rely on cross-section nuclear data in the analysis of the spectrometer response.

The present work does not deviate from the above philosophy in recommending calculated spectra for data-testing applications. In the following three subsections we present an overview of our work in updating the central neutron spectrum with respect to spectrum shape and uncertainty specification.

2.1 Neutronics Calculations

A series of transport calculations has been done which utilizes a limited set of ENDF/B-V nuclear data in selected regions of the nuclear model for the CFRMF. Wherever ENDF/B-V data were not used, ENDF/B-IV data were used. The primary purpose of the calculations was to investigate the changes in the central spectrum shape due to "ENDF/B-IV to ENDF/B-V" changes in the fission-spectrum shape representation and in the cross sections for ^{235}U, ^{238}U and ^{10}B.

A secondary outcome of these calculations was a suitable "Version-V" spectrum for data testing applications. The reasoning behind this is as follows. The isotopes ^{235}U, ^{238}U and ^{10}B are major consitituents of the uranium sleeve and boral which comprise the fast filter assembly[1]. As such their cross sections, along with the fission-spectrum shape for ^{235}U, are dominant factors in determining the shape of the neutron spectrum at the center of the facility (see sensitivity analysis, section 2.3). Although ^{11}B, aluminum, and stainless steel are also present in the filter assembly, their cross sections have a relatively minor effect on the central spectrum. In addition, the only isotopes in the thermal driver which have some impact on the central spectrum are hydrogen, oxygen and aluminum and their cross sections are essentially unchanged for ENDF/B-V. Finally, the ^{235}U and ^{238}U atom densities in the driver are relatively low and they affect primarily the source level at the driver-filter assembly boundary.

The calculational model used was a full core, 24 region, 193 mesh point, one dimensional cylindrical representation of the CFRMF reactor[6]. Microscopic shielded cross sections for the materials in each region of the computational model were generated with the SCRABL[7] and PHROG[8] codes using ENDF/B-IV and, as discussed above, ENDF/B-V nuclear data. Central flux spectra were obtained from eigenvalue calculations with SCAMP[9], a one dimensional P1 transport code, using an S-6 approximation. The calculations were made in 65 energy groups with 0.25 lethargy spacing from 1.125 eV to 10.0 MeV. SCAMP calculations were made for various combinations of input nuclear data, starting from ENDF/B-IV based nuclear data for all regions ("Version-IV" calculation) to utilizing ENDF/B-V nuclear data for ^{235}U, ^{238}U and ^{10}B

in the filter assembly and a Watt fission spectrum for all regions in which fission occurs ("Version-V" calculation). The calculations were made in a systematic manner so that the specific influence of the nuclear data changes could be noted.

Some of the results of these calculations are shown in Figures 1 and 2. The broad-group histogram plotted in Figure 1 is the relative flux per unit lethargy as generated by the "Version V" transport calculation. The fine-group histogram is discussed in subsection 2.2. In Figure 2 we illustrate the differences between the "Version-V" and "Version-IV" spectra by showing the ratio of the "Version-IV" to "Version-V" group fluxes. Both spectra were normalized to unit area before the ratio computation was made. Clearly, the ratio values indicate a general hardening of the spectrum in going from ENDF/B-IV to ENDF/B-V nuclear data. From an analysis of the transport calculations in which the input nuclear data from ENDF/B-IV were systematically substituted with ENDF/B-V data, we observed that the significant "Version-V" changes in the CFRMF spectrum (see Figure 2) could be attributed to the change in fission-spectrum representation (Maxwellian to Watt) and to the changes in the ^{238}U cross sections.

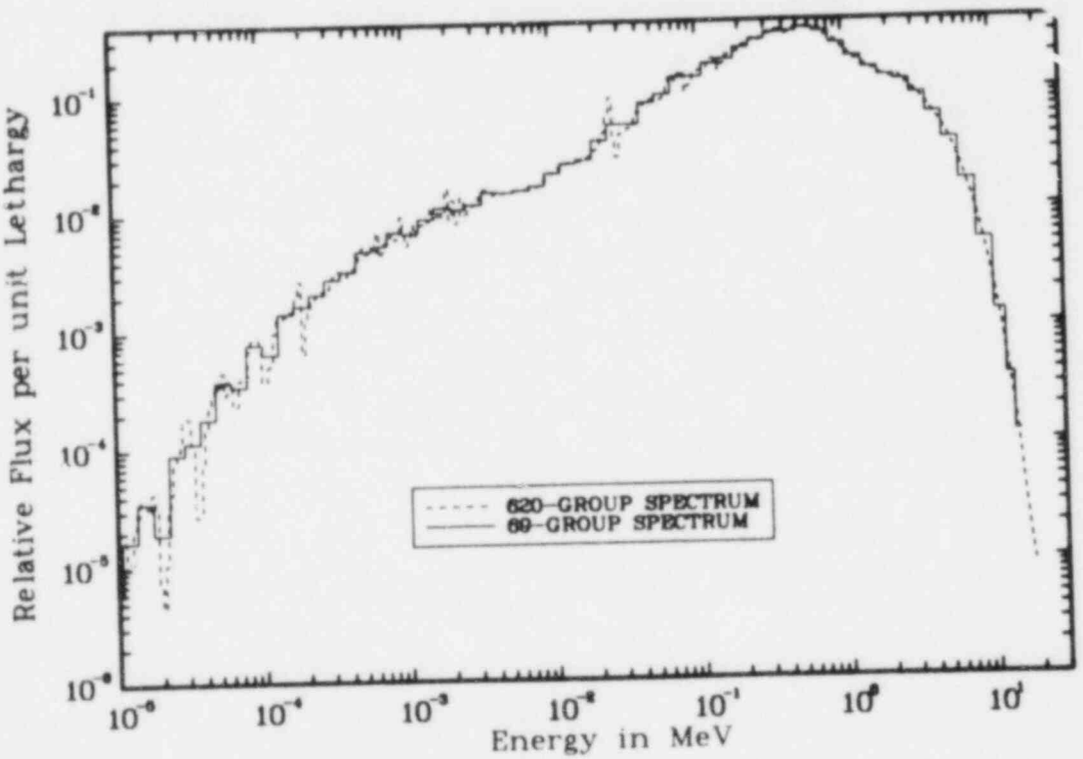

Figure 1. Comparison of 620-group and 69-group representations for the "Version-V" CFRMF central neutron spectrum.

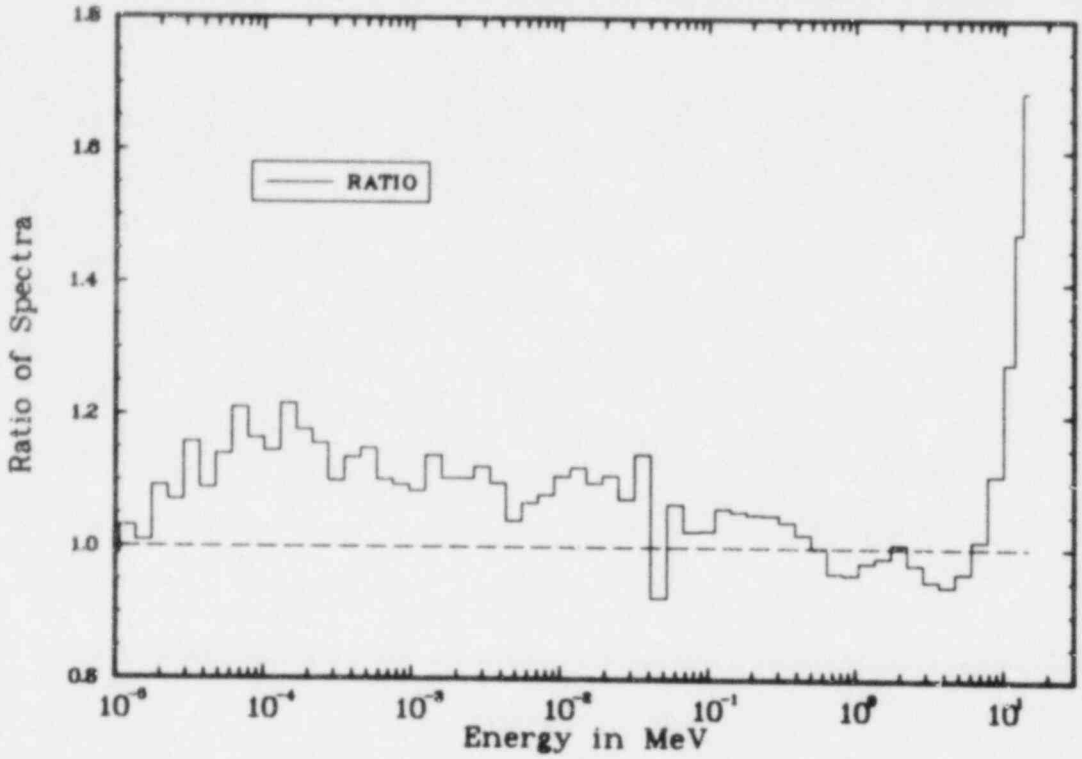

Figure 2. Ratio of group fluxes from transport calculation with ENDF/B-IV nuclear data to group fluxes from transport calculation with ENDF/B-V nuclear data.

The broad-group spectra (65-group) generated in the transport calculations with ENDF/B-IV and ENDF/B-V nuclear data were used as base data for subsequent data-testing applications. Prior to their use in the generation of the fine group spectra for integral data-testing applications (see section 3.), the spectra obtained from the transport calculations were extended from 10.0 MeV to 20.0 MeV using a Maxwellian fission function extrapolation for the "Version-IV" case and a Watt fission function extrapolation for the "Version-V" case.

2.2 Fine-Group Spectrum Representation

Conventional integral data testing requires the use of fine group representations (e.g., 620-group energy structure) of benchmark neutron field spectra. These representations are needed to derive accurate computations of spectrum-averaged cross sections. Discrepancies between measured and calculated spectrum-averaged cross-sections can, in some cases, be attributed to the use of incorrect weighting functions for cross-section collapsing computations or to inaccuracies, because of interpolation scheme deficiencies, in the fine-group spectrum representations[10,11].

The approach taken in the present work for the CFRMF entailed the merging of realistic fine-group spectral information from other neutronics calculations with the "base" broad-group spectrum from the transport calculation prior to generation of the 620-group spectrum using spline interpolation[10,11]. The sources of fine-group information used were a cell calculation for the CFRMF with the resonance theory code RABBLE[12] and a 100-group calculation made as part of the CFRMF sensitivity and uncertainty analysis. Output from the RABBLE calculation provided fine-group information from 1.0×10^{-6} MeV to 2.7×10^{-3} MeV. The 100-group calculation provided fine-structure information above 3.5×10^{-3} MeV. The merging approach used preserved the "broad-group" flux values between the energy bounds of each broad group. Spline interpolation was then used to generate a 620-group CFRMF spectrum from the merged spectrum. A comparison of the "Version-V" 620-group spectrum derived by this scheme to the broad-group spectrum generated from the transport calculation with ENDF/B-V nuclear data is shown in Figure 1.

2.3 Sensitivity and Uncertainty Analysis

Recently the AMPX[13] and FORSS[14] code systems were applied to a sensitivity and uncertainty analysis[4] for the CFRMF. The primary objective of this work was to determine, for the central neutron spectrum, a flux covariance matrix related to uncertainties and correlations in the nuclear data for the materials which comprise the facility. The reader is referred to Reference 4 for details of this work.

Approximately 2500 energy dependent sensitivity profiles were generated in the sensitivity analysis. Dominant sensitivities included those for ^{10}B capture, ^{238}U elastic and inelastic scattering, U-238 capture, H total, Fe total, ^{238}U χ and ν, and ^{235}U χ and ν.

A flux covariance matrix was generated by combining the sensitivity coefficients with cross-section and fission-spectrum covariances. The cross-section covariance matrices used were based on the covariance information as given in ENDF/B-V and as processed with the PUFF2[15] code. Uncertainties in the ^{238}U inelastic-scattering cross sections and in the ^{235}U fission spectrum were found to contribute most to the standard deviations in the central flux spectrum. The flux-spectrum covariance matrix contained strong correlations. This 26 x 26-group flux covariance matrix was used in the data testing and least-squares adjustment analyses discussed in sections 3 and 4.

3. INTEGRAL DATA TESTING

A conventional integral data testing analysis was done for those ENDF/B-V dosimeter reactions for which integral data have been measured in the CFRMF. References 11 and 16 provide a complete documentation for this integral testing study, in which the following topics were treated:

(1) compilation of up-to-date integral reaction-rate data measured as part of the ILRR program[3] and derivation of a consistent set of spectrum-averaged cross sections,
(2) characterization and specification of the CFRMF central neutron spectrum along the lines presented in section 2. of this paper,
(3) computation of spectrum-averaged cross sections using "Version-IV" and "Version-V" spectrum representations and dosimeter cross sections from ENDF/B-IV and ENDF/B-V,
(4) estimation of the spectrum and dosimeter cross-section uncertainty contributions to the uncertainty in each computed integral cross sections,
(5) comparison of calculated to measured integral cross sections and a consistency assessment of the integral test,
(6) characterization of the energy response for each dosimeter reaction in CFRMF, and
(7) an evaluation of sources of discrepancies for such integral data testing analyses.

A tabulation of up-to-date CFRMF integral data which was made in the above study is given here in column 2 of Table 1. These integral data correspond to a flux level in neutrons/cm^2-s of 7.94×10^{10} ($\pm$ 2.7%) for the HEDL-VI[3] irradiation. Spectrum-averaged cross sections are then computed as the integral reaction rate data divided by the flux.

Calculated spectrum-averaged cross sections were determined from computations with group-average quantities for the neutron spectra and the dosimeter cross sections as expressed in the 620-group energy structure. The 620-group CFRMF central neutron spectra were derived from transport calculations with ENDF/B-IV and ENDF/B-V nuclear data as discussed in section 2 of this paper. The 620-group averaged dosimeter cross sections were generated at Brookhaven National Laboratory for both ENDF/B-IV and ENDF/B-V data[17,18].

A comparison of the ratios of calculated to experimental integral data for ENDF/B-V dosimeter data and the "Version-V" spectrum is given in column 3 of Table 1. The values in parentheses are estimated percent errors in each calculated integral datum with the first value including only spectrum uncertainties and the second value including both spectrum and cross-section contributions. The spectrum uncertainty contribution was determined by utilizing the flux covariance matrix generated in the sensitivity and uncertainty analysis discussed in subsection 2.3. Dosimeter cross-section covariance matrices used in References 11 and 16 to estimate the cross-section contribution to the calculated integral datum uncertainty were generated from ENDF/B-V using the PUFF2 code[15]. The cross-section uncertainty contribution, as included in the second value in column 3 of Table 1 was generated using dosimeter covariance matrices as generated by F. Schmittroth[19] in an effort to improve on deficiencies in the ENDF/B-V dosimeter covariance files.

Table 1. Summary of Integral-Testing and FERRET Analyses for Dosimeter Reactions in CFRMF

Reaction	Measured Integral Reaction Rate[a] (rps/a) x 10^{15}	Ratio of Calculated-to-Experimental Integral Data	
		Unadjusted[b]	Adjusted[c]
^{6}Li(n,He)	74.82(1.1)	0.945 (3.3,3.9)	0.997(1.7)
^{10}B(n,He)	146.9(2.4)	0.864(3.5,3.7)	0.924(1.6)
^{27}Al(n,p)	0.06856(2.1)	1.087(8.7,11)	1.004(3.4)
^{27}Al(n,α)	0.01267(1.3)	0.991(9.1,11)	0.999(5.1)
^{45}Sc(n,γ)	1.841(1.9)	1.007(3.6,12)	1.002(2.6)
^{46}Ti(n,p)	0.2046(2.1)	0.952(8.8,12)	0.994(3.5)
^{47}Ti(n,p)	0.327(4.0)	1.287(3.5,12)	1.034(4.4)
^{48}Ti(n,p)	0.00540(2.1)	0.911(9.1,14)	0.996(5.1)
^{54}Fe(n,p)	1.368(1.1)	1.069(8.6,9.4)	1.001(2.9)
^{58}Fe(n,γ)	0.480(1.5)	1.093(3.6,8.1)	1.007(2.3)
^{59}Co(n,γ)	7.18(2.4)	0.937(4.0,6.6)	0.997(3.3)
^{58}Ni(n,p)	1.886(1.1)	1.019(8.5,11)	0.999(3.0)
^{63}Cu(n,γ)	3.44(5.5)	1.020(3.6,9.5)	1.020(4.9)
^{115}In(n,n')	4.02(2.8)	1.015(7.3,14)	0.998(3.8)
^{115}In(n,γ)	21.4(2.5)	1.014(3.4,5.0)	1.018(2.4)
^{197}Au(n,γ)	33.3(1.1)	0.905(3.6,5.4)	0.997(2.0)
^{232}Th(n,f)	1.56(4.4)	0.973(8.1,10)	0.971(4.2)
^{232}Th(n,γ)	23.00(2.2)	0.870(3.4,12)	0.995(3.0)
^{235}U(n,f)	122.1(1.4)	1.009(3.0,3.6)	1.014(1.6)
^{238}U(n,f)	5.96(1.9)	1.059(8.0,8.7)	1.000(3.0)
^{238}U(n,γ)	17.2(2.5)	1.001(3.4,5.7)	1.011(2.6)
^{237}Np(n,f)	43.5(1.9)	1.106(4.7,11)	1.003(2.8)
^{239}Pu(n,f)	142.3(1.6)	0.989(3.0,3.5)	1.006(1.7)
Reduced χ^2		16.6	.676

[a] Measured reaction rate corresponds to a flux level in n/cm^2-s of 7.94×10^{10} ($\pm$ 2.7%). Values in parentheses above are 1-sigma percent errors in measured integral data.

[b] Unadjusted Ratio: Calculated integral reaction rate is based on "Version-5" CFRMF spectrum and ENDF/B-5 dosimeter cross section. Values in parentheses are estimated percent errors in calculated integral data: first value includes only spectrum uncertainty contribution, second value includes both spectrum and cross-section contributions.

[c] Adjusted Ratio: Calculated integral reaction rate is based on using CFRMF spectrum and dosimeter cross sections as adjusted in FERRET analysis. Values in parentheses are errors computed from adjusted covariance matrices.

An assessment of the consistency between the measured integral data and the evaluated dosimeter cross sections can then be made by noting which C/E ratios indicate discrepancies outside the integral test uncertainty. If one defines the integral test uncertainty as the quadrature sum of the measurement error from column 2 of Table 1 and the spectrum and cross-section uncertain contributions (second error value in column 3), then the following assessment applies: the integral test discrepancies are between one and two times the integral test uncertainty for $^{6}Li(n,He)$, $^{58}Fe(n,\gamma)$, $^{197}Au(n,\gamma)$ and $^{232}Th(n,\gamma)$; the integral test discrepancies are approximately three times the integral test uncertainty for $^{10}B(n,He)$ and $^{47}Ti(n,p)$; consistency is achieved for all other reactions. Clearly large cross-section uncertainties mask a clear-cut assessment of consistency between measured integral data and the evaluated cross sections for several of the reactions. If one chooses to neglect the evaluated cross-section uncertainty contribution to the integral test uncertainty, the $^{27}Al(n,p)$, $^{59}Co(n,\gamma)$ and $^{237}Np(n,f)$ reactions should be added to the above list of reactions for which the measured integral data are inconsistent with the evaluated cross sections.

Discrepancies between measured and calculated integral data must be interpreted in light of the energy response of the specific reaction in the irradiation neutron spectrum. Such response plots have been generated [11,16] for all dosimeter reactions in the CFRMF spectrum. If a meaningful utilization of this conventional integral data testing analysis for cross-section evaluation purposes is to be made, it is important that that application be made in light of the response plots from References 11 and 16.

4. LEAST-SQUARES ADJUSTMENT ANALYSES

In an attempt to provide a more rigorous assessment of the consistency between the measured integral data and the ENDF/B-V dosimeter cross sections, least-squares adjustment analyses were made with the FERRET code [5]. In addition to this objective, these analyses provide a means of (1) quantitatively evaluating those specific regions of the dosimeter cross sections which should be re-evaluated and (2) refining the spectrum characterization for the CFRMF central neutron field. Preliminary results of these analyses, as reported here, included the following a priori data;

(1) the measured integral reaction rate data with associated uncertainties as specified in Table 1,
(2) 53-group representations of the CFRMF central neutron field and associated covariance matrices,
(3) 53-group representations of the dosimeter cross sections and associated covariance matrices.

Separate analyses were made in which the input spectrum used was based on ENDF/B-IV nuclear data and on ENDF/B-V nuclear data as discussed in section 2. The 53-group spectra were generated by collapsing the "Version-IV" and "Version-V" 620-group spectra specified in section 2. The spectrum covariance matrix used was derived from the flux covariance matrix generated in the sensitivity and uncertainty analysis described earlier. An interpolation program[19] was used to convert the 26 x 26-group covariance matrix into the 53-group energy structure used for the FERRET analyses. In addition to making adjustment analyses with this base spectrum covariance matrix, analyses were made in which additional normalization uncertainty was included in the covariance matrix specification.

Dosimeter cross sections in the 53-group energy structure were generated by collapsing the 620-group ENDF/B-V cross sections with the 620-group "Version-V" CFRMF spectrum. Covariance matrix specification for the dosimeters was accomplished in two ways: (1) processing the ENDF/B-V covariance files with the PUFF2 code[15] and (2) utilizing a 53-group covariance library generated by F. Schmittroth[19]. Most analyses were made with the Schmittroth covariance library.

Partial results of the least-squares-adjustment analysis utilizing all 23 measured integral data, the "Version-V" input spectrum, the spectrum covariance matrix which includes an additional 3% normalization uncertainty, and the Schmittroth covariance library are presented in Table 1 and in Figures 3 and 4. The fourth column of Table 1 tabulates the ratios of calculated-to-experimental integral data for which adjusted spectra and adjusted dosimeter cross sections were used to obtain the calculated integral data. Clearly, the least-squares adjustment analysis indicates a high degree of consistency between the measured integral data and the evaluated ENDF/B-V dosimeter cross sections within the uncertainty specification and correlation constraints for the input spectrum and cross sections. The $^{10}B(n,He)$ reaction is the only exception to this statement. This high degree of consistency is indicated by the reduced χ^2 of 0.676 for the adjusted integral data as compared to a reduced χ^2 of 16.6 for the unadjusted integral data. It should be emphasized that in the FERRET analysis, both group fluxes and group cross sections are adjusted to achieve consistency. For those cross sections with significant C/E discrepancies and relatively large a priori uncertainties, adjustments as large as 15% were made in group values.

Adjustments made to the input spectrum for the above analysis are illustrated in Figure 3. It can be observed that the least-squares analysis tends to soften the input spectrum somewhat. In fact, the shape of the plotted ratio of adjusted to unadjusted spectra is remarkably similar to the plot comparing the "Version-IV" and "Version-V" spectra in Figure 2. The reduction in the group wise uncertainties, especially between 10^{-1} and 10 MeV demonstrates how several dosimeter reactions with significant response in this energy range improve the spectrum specification.

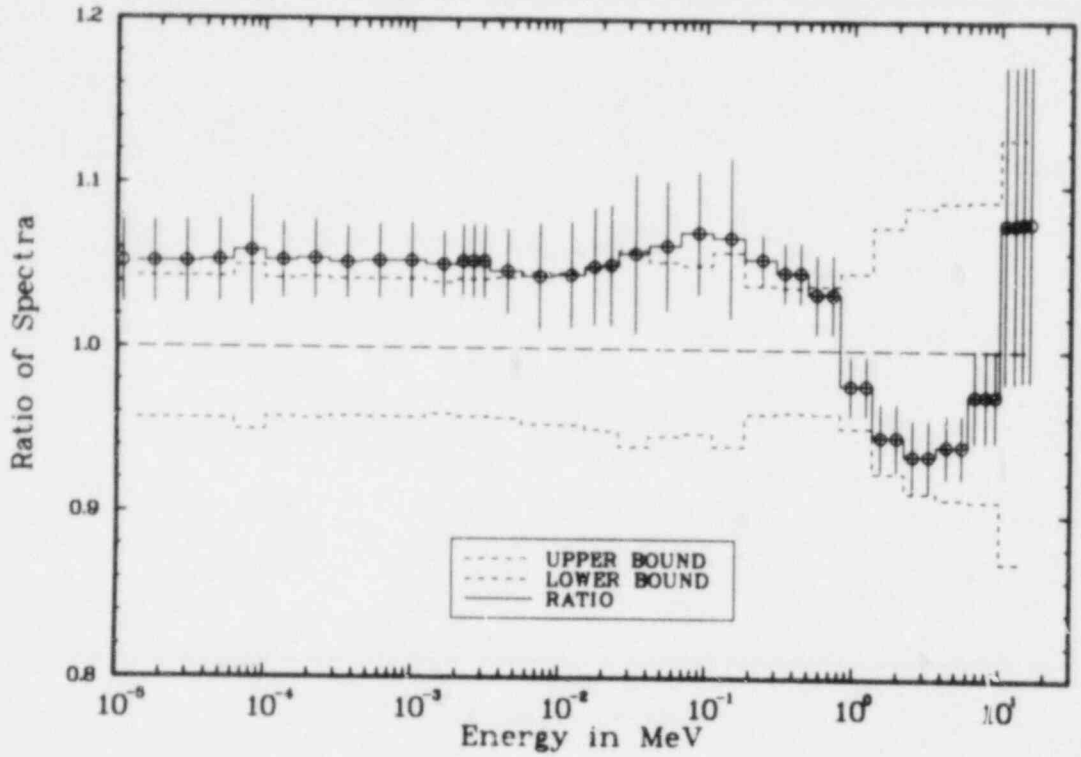

Figure 3. Ratio of adjusted-to-unadjusted group fluxes from FERRET analysis with "Version-5" input spectrum. Input spectrum uncertainties are indicated by the upper and lower bounds. Adjusted uncertainties are illustrated by vertical lines through the group mid-energy points.

As an example of the impact of the least-squares adjustment analysis on a somewhat poorly known dosimeter cross section, we show the adjustments for the $^{232}Th(n,\gamma)$ cross section. As noted from Table 1, prior to adjustment there was a significant discrepancy between the measured and calculated integral data. However, after adjustment there was no discrepancy. To achieve this consistency, a significant upward adjustment, as illustrated in Figure 4, was made in the capture cross section within the a priori uncertainty specification. This figure indicates both the energy range and the magnitude of the adjustments required to make future evaluations of the $^{232}Th(n,\gamma)$ cross section consistent with the CFRMF measured integral data.

5. CONCLUSIONS

Conventional integral data testing analyses, based on C/E ratios, reported here in Table 1 for ENDF/B-V dosimeter cross sections indicate discrepancies outside of the estimated integral test uncertainty for $^{6}Li(n,He)$, $^{10}B(n,He)$, $^{47}Ti(n,p)$, $^{58}Fe(n,\gamma)$, $^{197}Au(n,\gamma)$ and $^{232}Th(n,\gamma)$.

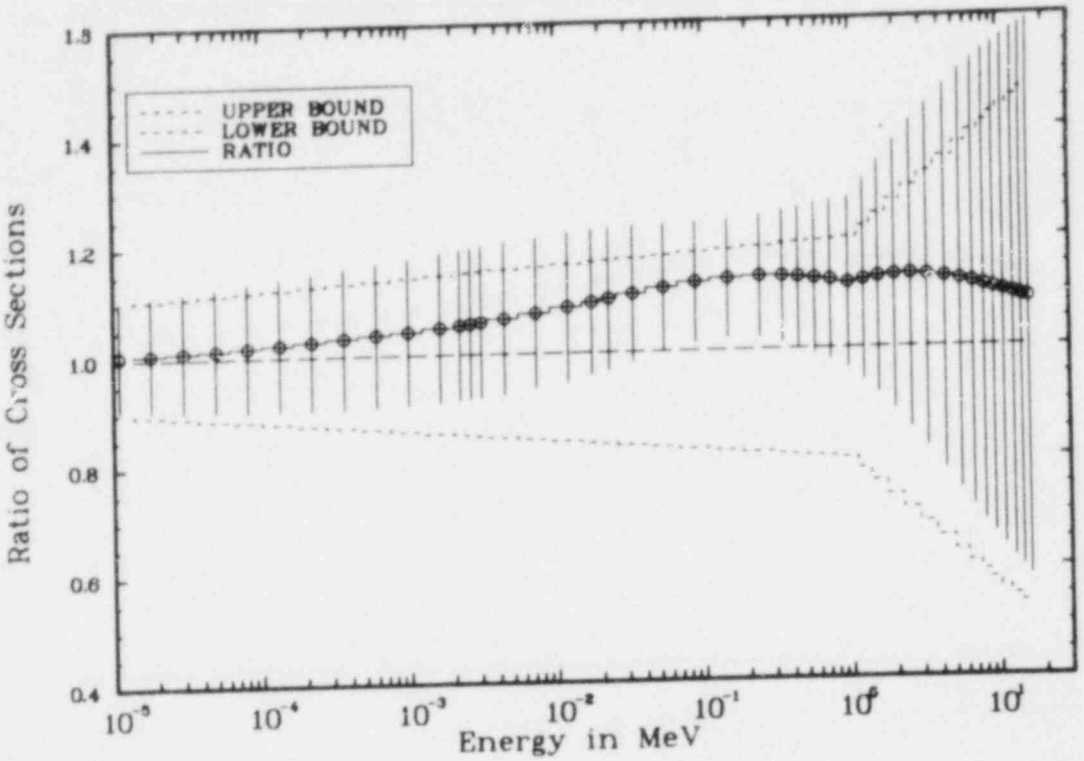

Figure 4. Ratio of adjusted-to-unadjusted $^{232}Th(n,\gamma)$ cross sections from FERRET analysis. Input cross-section uncertainties are indicated by upper and lower bounds. Adjusted uncertainties are illustrated by vertical lines through the group mid-energy points.

The integral test uncertainty includes contributions from the measured integral data and from the spectrum and cross sections used to obtain the calculated integral data.

Subsequent least-squares adjustment analyses with the FERRET code indicate a high degree of consistency can be achieved between the measured integral data and ENDF/B-V dosimeter cross sections for all reactions except $^{10}B(n,He)$. The flux and cross-section adjustments made to achieve consistency in this analysis are all within the input uncertainty specifications. It appears, however, that the a priori uncertainty specification is too tight for $^{10}B(n,He)$ in the keV to MeV region. As illustrated in this paper for the $^{232}Th(n,\gamma)$ reaction, this type of analysis provides a good tool to specify both the energy range and the magnitude of the adjustment required to make future evaluations of discrepant dosimeter cross sections consistent with the CFRMF measured integral data.

For the preliminary least-squares adjustment analyses reported here, the input "Version-V" spectrum was adjusted in such a way that the new spectrum is closer to the "Version-IV" representation than were the input data. Furthermore, in a least-squares analysis in

which the input spectrum was "Version-IV", little spectrum adjustment was required for cross-section adjustments comparable to those in the first analysis. We conclude that the present work provides not only a check on the ENDF/B-V dosimeter cross sections, but also a test of the ENDF/B-V nuclear data which have a significant influence on the calculated central spectrum, namely the ^{235}U fission spectrum representation and the inelastic scattering and capture cross sections for ^{238}U. The present study suggests possible problems with these nuclear data.

REFERENCES

1. J W Rogers, D. A. Millsap and Y. D. Harker, "CFRMF Neutron Field Flux Spectra Characterization," Nucl. Tech. 25, 330 (1975).

2. J W Rogers, D. A. Millsap and Y. D. Harker, "The Coupled Fast Reactivity Measurements Facility (CFRMF)," in Proc. of IAEA Consultants Meeting on Integral Cross-Section Measurements for Reactor Dosimetry, IAEA, Vienna, Austria, November 15-19, 1976, IAEA-208, Vol. II, 117 (1976).

3. W. N. McElroy and L. S. Kellogg, "Fuels and Materials Reactor Dosimeter Data Development and Testing," Nuc. Tech. 25, 180 (1975).

4. J. M. Ryskamp, R. A. Anderl, B. L. Broadhead, W. E. Ford III, J. L. Lucius, J. H. Marable, and J. J. Wagschal, "Sensitivity and Uncertainty Analysis of the CFRMF Central Flux Spectrum," accepted for publication in Nucl. Tech. (Oct., 1981).

5. F. Schmittroth, FERRET Data Analysis Code, USDOE Report HEDL-TME 79-40, Hanford Engineering Development Laboratory, (September 1979).

6. Y. D. Harker, J W. Rogers and D. A. Millsap, Fission-Product and Reactor Dosimetry Studies at Coupled Fast Reactivity Measurements Facility, USDOE Report TREE-1259, Idaho National Engineering Laboratory (1978).

7. Private communication from G. E. Putnam and D. Tomasko, EG&G Idaho Incorporated, (1978).

8. R. L. Curtis, F. J. Wheeler, G. L. Singer, and R. A. Grimesey, PHROG - A Fortran IV Program to Generate Fast Neutron Spectra and Average Multi-group Constants, IN-1435, Idaho Nuclear Corporation (April 1971).

9. Private communication from C. L. Beck, Idaho Nuclear Corporation (1968).

10. R. A. Anderl, INEL Integral Data-Testing Report for ENDF/B-V Fission Product and Actinide Cross Sections, USDOE Report EGG-PHYS-5406, Idaho National Engineering Laboratory (April 1980).

11. R. A. Anderl, D. A. Millsap, J W Rogers, Y. D. Harker, INEL Integral Data Testing Report for ENDF/B-V Dosimeter Cross Sections, USDOE Report EGG-PHYS-5608, Idaho National Engineering Laboratory (October 1981).

12. P. H. Kier and A. A. Robba, RABBLE, A Program for Computation of Resonance Absorption in Multiregion Reactor Cells, USAEC Report ANL-7326, Argonne National Laboratory (1967).

13. N. M. Green, W. E. Ford, III, et al., AMPX: A Modular Code System for Generating Coupled Neutron-Gamma Libraries from ENDF/B, USDOE Report ORNL/TM-3706, Oak Ridge National Laboratory (1976).

14. J. L. Lucius, C. R. Weisbin, J. H. Marable, J. D. Drischler, R. Q. Wright, and J. E. White, A User's Manual for the FORSS Sensitivity and Uncertainty Analysis Code System, USDOE Report, ORNL-5316, Oak Ridge National Laboratory (1977).

15. "PUFF2 Determination of Multigroup Covariance Matrices from ENDF/B-V Uncertainty Files," RSIC Computer Code Collection, PSR-157 (1980).

16. R. A. Anderl, D. A. Millsap, J W Rogers, Y. D. Harker, Addendum to Integral Data Testing Report for ENDF/B-V Dosimeter Cross Sections, USDOE Report EGG-PHYS-5668, Idaho National Engineering Laboratory (1982).

17. B. A. Magurno, editor, ENDF/B-IV Dosimetry File, Report BNL-NCS-50446/NEACRP-L-145/ENDF-216 (1973).

18. Private communication from B. A. Magurno, Brookhaven National Laboratory (1981).

19. Private communication from F. Schmittroth, Hanford Engineering Development Laboratory, (February 1982).

AVERAGE NEUTRON CROSS SECTIONS IN THE CF-252 BENCHMARK FIELD

W. Mannhart
Physikalisch-Technische Bundesanstalt (PTB),
3300 Braunschweig, FR Germany

ABSTRACT

Californium-252 spectrum-averaged cross sections were measured for the reactions Mg-24(n,p), Mn-55(n,2n),Co-59(n,p), Co-59(n,α), Co-59(n,2n), Ni-58(n,2n), Ni-58(n,np), Ni-60(n,p), Cu-63(n,α) and Zr-90(n,2n). The experimental results were compared with calculations based on ENDF/B-V data and other recent evaluations. Some of the results of this comparison were used as a test for the shape of the californium neutron spectrum above 8 MeV. In addition, the recent evaluation of a best set of spectrum-averaged cross sections has been expanded to 23 different reactions of importance in reactor dosimetry.

INTRODUCTION

Integral data, i.e. neutron cross sections averaged over simple and well-known neutron spectra, are of some use as additional information about energy-dependent cross section data. In the case of the neutron benchmark field of californium-252, a lot of experimental integral data is meanwhile available. However, in investigating the situation in more detail, one finds relatively often that our present knowledge of the integral value of a specific reaction is based only on a single experiment /1/. In such cases, there is an urgent need for additional experiments, particularly because, as the present work demonstrates, some of these data have to be regarded with caution.

The Cf-252 neutron spectrum is relatively well-established below 8 MeV neutron energy. At higher energies, the direct spectrum measurements show a large divergence, mainly due to intensity problems with the low number of neutrons at these energies. The present measurements of responses of integral detectors at high neutron energies give valuable additional information about the spectral shape of Cf-252 at high neutron energies.

Careful integral experiments in the Cf-252 neutron field can be done with relative uncertainties of the order of 2 %, whereas it is relatively seldom that the uncertainties of energy-dependent cross section measurements are better than 5 %. It is therefore of some advantage to include such integral data more extensively in future evaluations of energy-depen-

dent cross section data. At the last ASTM-EURATOM Symposium, an evaluation of a best set of integral Cf-252 data with regard to the data covariances was presented for these purposes. This evaluation has been expanded and updated. The result is given below.

EXPERIMENT

The irradiations were conducted at the PTB low-scattering outdoor irradiation facility /2/. Instead of the formerly applied combination of two californium sources, only a single source was used. The source was encapsulated in a double zircaloy cylinder with outer dimensions of 10 mm in diameter and 10 mm in height. The encapsulation was 1.5 mm thick. The neutron source strength was approximately 2.0×10^8 s^{-1} on July 1, 1981. Disk-shaped samples of high-purity metallic foils, 10 mm in diameter and between 0.125 and 0.25 mm thick, were used. Irradiations were performed with the sandwich method, i.e. each sample placed between two foils of either aluminium or nickel acting as neutron flux density monitors. The sandwich packets were almost touching the convex surface of the source cylinder. The neutron flux density at the position of the middle foil was of the order of 2.6×10^7 cm^{-2} s^{-1}. For a sandwich packet consisting of 0.25 mm thick foils, the neutron flux density gradient between the outer foils was 17 %. Control measurements gave a high reproducibility, i.e. the uncertainty of the neutron flux density at the position of the middle foil due to geometrical effects was 0.3 %.

An essential advantage of the sandwich method is a compensating effect in most corrections. Only the ratio of corrections of a similar order of magnitude influences the final results, and not the absolute magnitude of corrections for scattering and absorption effects in the source and the sample. The main corrections were perturbations of the neutron spectrum emerging from the californium source due to scattering and absorption processes in the source encapsulation, and absorption and scattering events in the sample. Besides weak absorption, inelastic scattering in the source encapsulation is mainly responsible for the perturbations of the neutron spectrum. The result of a first analysis is shown in Table 1. The ratio of the number of neutrons emerging from the source encapsulation to that of a pure californium spectrum is given as a function of the neutron energy. A more detailed analysis of these effects is in progress. Where sample and neutron monitor reactions have similar energy response ranges, the effect of spectrum perturbations becomes fully compensated. Experimentally determined ratio measurements of the reactions Ti-48(n,p) and Au-197(n,2n) relative to Ni-58(n,p)

Table 1 Perturbations of the Cf-252 neutron spectrum due to inelastic scattering and absorption processes in the source encapsulation

Neutron energy	Number of neutrons relative to a pure neutron spectrum
2 MeV	0.995
3 MeV	0.991
4-16 MeV	0.989
20 MeV	0.990

(where the energy response ranges of the former reactions (see Table 4) are at considerably higher neutron energies than for the Ni-58(n,p) reaction with a 90 % energy-response range between 2.1 and 8.0 MeV) showed no significant deviations due to spectrum perturbation effects, compared with the data of Table 1. The uncertainty component due to these effects is estimated at 0.5 %. Absorption (self-shielding) of neutrons in the sample is compensated due to the presence of a monitor foil in front of and behind the sample. The effect of elastically scattered neutrons in the sandwich packet, from the monitor foil to the sample foil and vice versa is not fully compensated. However, the net effect remains small and the uncertainty in neglecting such corrections is estimated at 0.7 %. Elastic scattering from the neutron source encapsulation and from the sample support structures does not have to be considered as it will automatically be taken into account in the response of the monitor foils.

Activities of irradiated samples were determined with a calibrated Ge(Li) detector with a volume of 130 cm^3 and a nominal efficiency of 28 %. The usual counting position for low activity sources was at a distance of 51 mm above the detector face. The detector calibration was done with a set of radioactive standard sources covering the gamma energy range between 0.1 and 1.8 MeV. Besides photopeak-efficiencies, total efficiencies were also determined in order to allow the necessary summing corrections for gamma sources emitting more than one gamma quantum. Dead-time corrections were applied but were in all cases of a negligible order of magnitude. In some cases activities which were too low required the counting in a second position only 12 mm distant from the detector. This position was calibrated in a way similar to the other one. Such radionuclides which gave summing corrections in this position which were too large (> 5 %) were measured relative to reference sources of the same radionuclide calibrated at a more distant position with sufficiently small summing corrections. Corrections were applied for the extended volume of the radioactive foil and for gamma absorption within the foils. With regard to all corrections, the relative uncertainty of the photopeak-efficiencies was 1.5 %. In the conversion of the measured counting rates into reaction rates, atomic-mass values, isotopic abundances and decay parameters were taken from Ref. 3.

Measured Average Cross Sections

The experimental results are summarized in Table 2. It must be mentioned that all present measurements are ratio measurements and not absolute ones. The Mg-24(n,p) reaction was measured relative to Al-27(n,α) and all other reactions relative to Ni-58(n,p). The data shown in Table 2 were normalized, based on absolute cross sections of 1.006 mb for Al-27(n,α) and 118 mb for Ni-58(n,p) determined earlier /2/. The uncertainties quoted correspond to a 1σ level and comprise counting statistics and all above-mentioned uncertainty contributions. Correlations have been taken into account. The uncertainty due to the normalization is not included. A detailed uncertainty analysis will be given at a later stage when the present data in the form of actual ratios will be added to the evaluation shown in the second part of this paper. Prior to this, additio-

nal measurements with a recent californium source (available within the next few months) of 20-fold source strength are planned to reduce some of the relatively large counting-statistical uncertainties.

Table 2 Experimentally determined spectrum-averaged cross sections (in mb) in the Cf-252 neutron field

REACTION	PRESENT WORK	OTHER EXPERIMENTS	
$^{24}Mg(n,p)^{24}Na$	2.01 ± 0.06	1.95 ± 0.12	/4/
$^{55}Mn(n,2n)^{54}Mn$	0.408 ± 0.009	0.58 ± 0.14	/5/
$^{59}Co(n,p)^{59}Fe$	1.66 ± 0.04	1.96 ± 0.10	/5/
$^{59}Co(n,\alpha)^{56}Mn$	0.208 ± 0.010	0.217 ± 0.015	/4/
		0.20 ± 0.01	/5/
		0.20 ± 0.01	/6/
$^{59}Co(n,2n)^{58}Co$	0.406 ± 0.010	0.57 ± 0.06	/5/
$^{58}Ni(n,2n)^{57}Ni$	$(1.01 \pm 0.12)\times10^{-2}$	-	
$^{58}Ni(n,np)^{57}Co$	0.412 ± 0.018	-	
$^{60}Ni(n,p)^{60}Co$	2.39 ± 0.13	-	
$^{63}Cu(n,\alpha)^{60}Co$	0.671 ± 0.018	0.709 ± 0.017	/7/
$^{90}Zr(n,2n)^{89}Zr$	0.221 ± 0.006	0.267 ± 0.015	/5/

Table 2 shows that for the reactions Ni-58(n,2n), Ni-58(n,np) and Ni-60(n,p) no previous experiments have been done. With the exception of the Co-59(n,α) reaction,only a single additional measurement is available for each remaining reaction. Good agreement has been found between the present data of Mg-24(n,p) and Co-59(n,α) and those measured by Kobayashi and Kimura /4/. The same is not true of the data measured by Deszö and Csikai /5/. Their data exceed those of the present experiment by about 20 % for the reactions Co-59(n,p) and Zr-90(n,2n) and by about 40 % for the reactions Mn-55(n,2n) and Co-59(n,2n). These discrepancies can only be resolved by additional future experiments. A very careful experiment has been done by Winkler et al. /7/ for the the reaction Cu-63(n,α). The uncertainty of 2.4 % quoted is similar to that of the present experiment. Neither experiment however, shows any overlap in the error bars. A remeasurement is planned to resolve the difference of 5.7 % between both experimental values.

Comparison with Calculations

In Table 3 the experimental results are compared with calculated average cross sections. In the calculations, $\sigma(E)$ data were taken from ENDF/B-V or from other recent evaluations /9-14/. For the californium neutron spectrum, two representations were chosen: the segment-adjusted NBS evaluation /8/ and a pure Maxwellian with a average energy of 2.13 MeV (temperature parameter T = 1.42 MeV). The calculated cross sections based on ENDF/B-V data and a pure Maxwellian can be compared with the calcu-

lations performed by Magurno /15/ and show complete agreement. For ENDF/B-V data and the segment-adjusted neutrum spectrum, calculations have been made by Nolthenius and Zijp /16/. Their results in some cases are between 1 % and 5 % lower than the present calculation. It is not at all clear if this divergence is due to the transformation of the original data to a specific group structure performed by the authors mentioned.

Table 3 Comparison between measured and calculated average cross sections (in mb)

Reaction	Experiment[a]	Calculation				Ref.
		ENDF/B-V		Other Evaluation		
		Seg.Adj.	Pure Maxw.	Seg.Adj.	Pure Maxw	
$^{24}Mg(n,p)$	2.01 ± 0.06			2.159	2.335	/9/
$^{27}Al(n,\alpha)$	1.006 ± 0.022	1.058	1.158	1.011	1.107	/10/
$^{48}Ti(n,p)$	0.42 ± 0.01	0.4092	0.4457			
$^{55}Mn(n,2n)$	0.408 ± 0.009	0.4458	0.5535			
$^{59}Co(n,p)$	1.68 ± 0.04			1.73	1.78	/11/
$^{59}Co(n,\alpha)$	0.208 ± 0.010	0.2162	0.2348			
$^{59}Co(n,2n)$	0.406 ± 0.010	0.4103	0.5118			
$^{58}Ni(n,2n)$	(1.01 ± 0.12)x10^{-2}	0.760x10^{-2}	0.997x10^{-2}	0.741x10^{-2}	0.973x10^{-2}	/13/
$^{60}Ni(n,p)$	2.39 ± 0.13	3.442	3.620			
$^{63}Cu(n,\alpha)$	0.671 ± 0.018	0.7577	0.8066	0.6761	0.7145	/14/
$^{90}Zr(n,2n)$	0.221 ± 0.006			0.2069	0.2690	/9/
$^{197}Au(n,2n)$	5.50 ± 0.14	5.646	6.550			

[a] Present work and Ref. /2/

The experimental value of Al-27(n,α) is more consistent with the recent evaluation of Vonach and co-workers /10/ than with ENDF/B-V. For the Co-59(n,p) reaction, the 90 % energy response range in the californium spectrum is between 3.6 MeV and 10.2 MeV, the energies corresponding to a response of 5 % and 95 %, respectively, of the total response. In the calculation of the average cross section, experimental σ(E) data from 2.6 MeV to 10 MeV were taken from Ref. /11/. The contribution to the average cross section from σ(E) data above 10 MeV is 5.4 %. For these energies, the data (labelled as data set III) were taken from Ref. /12/. The present experiment and the calculation agree within 3 %. The evaluation of the Ni-58(n,2n) cross section performed by Marcinkowski /13/ gives only slightly different results compared with ENDF/B-V. The ENDF/B-V data for Cu-63(n,α) overestimate the response in fission fields. The evaluation based on the data of Winkler et al. /14/ (see also Ref. /7/) fits the experimental result much better.

The Cf-252 Neutron Spectrum at High Energies

The reactions from Table 3 are again given in Table 4, ordered according to their energy response ranges. The ratio of the calculated average cross section relative to the experimental values is used as a test for the adequacy of the representation of the californium neutron spectrum at high neutron energies. This test compares two different spectral representations: a pure Maxwellian with an average energy of 2.13 MeV and the NBS evaluation /8/ indicating a deficit of neutrons compared to this pure Maxwellian at high neutron energies. Most C/E values allow a clear preference to be given to one of the two spectrum representations. For a few reactions, discrepancies between experiment and calculation have to be investigated. In the case of Ni-60(n,p), the experiment and the calculation disagree strongly.

Table 4 Ratio of the calculated to the experimental average cross section for two different spectral representations

Reaction	90 % Energy Response Range (in MeV)		C/E-Value		σ(E) -Data from	Spectral Form	
	from	to	Seg.Adj.	Pure Maxw. T=1.42 MeV		Seg.Adj.	Pure Maxw.
$^{63}Cu(n,\alpha)$	4.78	11.6	1.129	1.202	ENDF/B-V	+	(-)
			1.008	1.065	/14/		
$^{60}Ni(n,p)$	4.92	10.9	1.440	1.515	ENDF/B-V	?	?
$^{59}Co(n,\alpha)$	6.04	12.6	1.039	1.129	ENDF/B-V	+	-
$^{48}Ti(n,p)$	6.02	12.9	0.974	1.061	ENDF/B-V	+	(-)
$^{24}Mg(n,p)$	6.57	12.1	1.074	1.162	/9/	(+)	-
$^{27}Al(n,\alpha)$	6.60	12.5	1.052	1.151	ENDF/B-V	+	-
			1.005	1.100	/10/		
$^{197}Au(n,2n)$	8.91	14.2	1.027	1.191	ENDF/B-V	+	-
$^{55}Mn(n,2n)$	11.2	16.4	1.093	1.357	ENDF/B-V	(+)	-
$^{59}Co(n,2n)$	11.3	16.5	1.011	1.261	ENDF/B-V	+	-
$^{90}Zr(n,2n)$	12.8	17.5	0.936	1.217	/9/	(+)	-
$^{58}Ni(n,2n)$	13.1	18.0	0.752	0.987	ENDF/B-V	-	+
			0.738	0.973	/13/		

Due to the absence of data, the excitation function of ENDF/B-V between threshold and 6 MeV is based on model calculations, and above 6 MeV, it has been mainly determined by a single experiment. Up to 8 MeV, 65 % of the response in a californium spectrum is given. An error in the slope of the excitation function would have a relatively large influence on the calculated value of Table 3. Nevertheless, this reaction must be candidate for additional confirmative integral measurements. The reactions Mg-24(n,p), Mn-55(n,2n) and Zr-90(n,2n) show deviations of the C/E value from unity of the order of 10 %. Possible explanations of these deviations as far as the energy-dependent cross section data are concerned, will be briefly reviewed. The excitation function of Mg-24(n,p) between threshold and 10 MeV (83 % response in the californium spectrum) has been determined by only two experimental data sets and shows a distinct structure. The eva-

luation of Mn-55(n,2n) between reaction threshold and 13 MeV (53 % response) is based solely on model calculations. The first experimental data point for Zr-90(n,2n) is given at 13.4 MeV. Below this (22 % response), the evaluation is based on model calculations.

In the last two columns of Table 4, the spectral representation which appears to be more adequate is indicated. A positive sign defines a clear preference for a certain representation and a negative sign means the opposite. Terms in brackets signify that the statement is somewhat weaker. With the exception of Ni-58(n,2n) (and Ni-60(n,p)), the C/E values of all reactions indicate that the NBS evaluation of the neutron spectrum is more adequate than a pure Maxwellian in obtaining consistency between experimental and calculated integral data. A recent review of direct spectrum measurements of californium-252 /17/ shows strongly divergent data between 8 MeV and 15 MeV due to intensity problems. Above 15 MeV, no direct spectrum measurements are available. However, recent experiments in particular up to 15 MeV give some indication that the neutron spectrum can also be described by the pure Maxwellian at high energies. This fact is here alone confirmed by the result of the Ni-58(n,2n) reaction. In the light of this reaction, the problems in comparing integral experiments and calculations with the aim of deducing statements on the form of the neutron spectrum, will be briefly reviewed. First, the experimental value must be relatively accurate: (it is hoped that the present uncertainty of 12 % can be reduced in future experiments). Secondly, the calculated value depends strongly on the exactness of the slope of the excitation function near reaction threshold. For Ni-58(n,2n), for example, the energy range between threshold (12.4 MeV) and 2.3 MeV above it contributes half to the total response of this reaction in a californium neutron field. Unfortunately, energy-dependent cross section data near threshold have mostly large uncertainties (10 % for Ni-58(n,2n), for example) or must be approximated by model calculations in the case of missing data. On the other hand, the C/E values for high-threshold reactions are relatively sensitive where the form of the neutron spectrum is concerned (up to 30 % difference between the two spectral representations used here).

EVALUATION

The previous evaluation of Cf-252 spectrum-averaged cross sections comprised 17 reactions based on 31 data points /18/. The present evaluation, extends the set to 23 reactions and now includes 46 data points. The essential differences between both evaluations are as follows:

a) The data of Kobayashi and Kimura /4/ have been re-analysed with regard to their uncertainty components /19/ and have been added to the evaluation.

b) The recent experiment of the Cu-63(n,α) reaction by Winkler et. al /7/ has been included in the evaluation.

c) The covariance matrix of the NBS fission chamber measurements evaluated by Wagschal et al. /20/ has been corrected to its final version.

d) Two experimental data sets /21,22/ which mainly contributed to a certain inconsistency in the first evaluation have been modified as regards their weight in the evaluation.

The rules for generating the covariance matrices of experimental data and their application in evaluating a best set of data have been described in detail elsewhere /18,24/. It has been shown that an evaluation can be organized in such a way that a new data set can simply be added to a previously made calculation. This principle, for example, is valid for the recent data set of Ref. /19/, as these data in the form of ratios show no correlations to any of the data previously considered. However, the same principle cannot be applied to the experiment of Winkler et al. /7/, as this measurement is correlated with data already contained in the previous evaluation. The present evaluation has therefore been completely redone, this also being necessary to allow the correction of a few inconsistencies in the prior evaluation.

The data of Kobayashi and Kimura /4/ have been transformed back to the actual ratio measurements. The uncertainty analysis has been completely redone. Details can be found elsewhere /19/. The result is shown in Table 5.

Table 5 Measurements of Kobayashi and Kimura (from Ref. /19/)

Reaction ratio	Ratio	Rel.Std.Dev. %	Correlation matrix (x 100)
Mg-24(n,p)/In-115(n,n')	0.009651	4.24	100
Al-27(n,p)/Al-27(n,α)	4.797	3.73	-7 100
Al-27(n,p)/Al-27(n,α)	4.892	4.68	-6 23 100
Al-27(n,p)/Al-27(n,α)	4.936	5.58	-5 19 15 100
S -32(n,p)/Al-27(n,α)	72.95	3.75	2 8 19 5 100
S -32(n,p)/Al-27(n,α)	70.98	5.06	2 6 5 45 41 100
V -51(n,p)/Al-27(n,α)	0.7058	8.13	-8 15 6 5 2 2 100
Fe-54(n,p)/In-115(n,n')	0.4361	4.16	26 -4 -3 -2 3 2 -5 100
Fe-56(n,p)/In-115(n,n')	0.007166	4.02	27 -4 -3 -3 3 2 -5 31 100
Ni-58(n,p)/Al-27(n,α)	118.3	2.77	-10 16 30 11 32 8 10 -5 -6 100
Co-59(n,α)/Al-27(n,α)	0.2157	6.17	-4 18 5 5 6 4 10 -2 -1 9 100
Zn-64(n,p)/Al-27(n,α)	41.45	3.66	-2 28 8 6 9 7 13 0 0 13 17 100
In-113(n,n')/Al-27(n,α)	166.8	5.56	-10 10 8 44 3 44 8 -6 -6 14 6 6 100
In-113(n,n')/In-115(n,n')	0.8511	4.90	21 0 0 0 0 0 -1 16 16 -1 0 0 10 100
In-115(n,n')/Al-27(n,α)	198.9	4.39	-31 13 11 56 4 55 10 -25 -26 18 8 8 62 -15 100
Au-197(n,2n)/Al-27(n,α)	5.219	3.80	-15 32 11 10 5 4 21 -9 -9 20 21 28 15 -1 21 100

The uncertainties are essentially reduced compared with Ref. /4/. This is due to the compensating effects in ratio measurement and to the taking into account of correlations between the uncertainty components. The relatively low-valued positive or negative correlations shown in Table 5 are typical of strong compensation effects. For the NBS fission-chamber measurement, the values shown in Table 6 (Ref. 20) replace the older data of Table 2 of Ref. 18. In the analysis of the average cross section measurement of Cu-63(n,α) of Winkler et al. /7/, two uncertainty components were recognized which show full correlation with the NBS fission-chamber

Table 6 NBS-Fission-Chamber-Measurements (<σ> in mb) (from Ref./20/)

Reaction (-Ratio)	<σ> (-Ratio)	Rel Std.Dev. %	Correlation Matrix (x 100)			
U-235(n,f)	1205	2.10	100			
U-238/U-235	0.2644	1.06	40	100		
Np-237/U-235	1.105	2.00	-9	25	100	
Pu-239/U-235	1.500	1.33	-19	13	32	100

measurement: the component of 1.1 % for the source strength determination and that of 1 % for neutron scattering in the source encapsulation. Wagschal /23/ recently showed that the second term has to be reduced to 0.71 %, as this term also included scattering from sample support structures. This results in a relative covariance term (in %^{2}) of $1.1^2 + 0.71^2 = 1.71$ which must be added to the data of Table 7 of Ref. /18/.

In the previous evaluation /18/ we obtained a value of χ^2 per degree of freedom of 1.93. We took that into account by multiplying all standard deviations of the evaluated result with a factor of 1.39. This inconsistency was mainly attributed to the fission reaction measurement of Ref. 21 and Ref. 22. We discussed possible systematic errors in the data and tried to eliminate them by reducing the original data to ratios. Even this procedure was only a partial success. In the present evaluation, the reduction to ratios continues, but in addition, because of the impression that the uncertainties quoted seem to be underestimated, the uncertainties of the data of Adamov et al./22/ are enlarged by a factor of 1.5. The same has been done with the data of Ref. /21/ where all uncertainties (also those of the non-fission reactions) have been enlarged by the same factor. Here it should be remembered that the original uncertainty values had before been divided by a factor of 2 in order to reduce them from the 2σ level to the 1σ level. In both cases it has been assumed that the shape of the correlation matrix remains the same and that this enlargement does not influence the intercorrelations between different experiments. With this new weighting of the data of Ref. 21 and Ref. 22, the present evaluation resulted in a χ^2 value of 25.7 compared with the number of degrees of freedom of 25. The result of the present evaluation is shown in Table 7 and 8. It is believed that the new weighting is more realistic, as it concerns only the 11 data points which were in the past responsible for the inconsistency of the evaluation, instead of attributing the inconsistency to the whole evaluation.

Table 7 Cf-252 Averaged Cross Sections

Reaction	Previous Evaluation <σ> (mb)	Previous Evaluation Rel. Std.Dev. % [a]	Present Evaluation <σ> (mb)	Present Evaluation Rel. Std.Dev. % [b]
Mg-24(n,p)			1.898	4.2
Al-27(n,p)			4.825	3.2
Al-27(n,α)	1.019	2.4	1.004	1.9
S -32(n,p)			71.20	3.7
Ti-46(n,p)	14.17	2.6	13.92	2.1
Ti-47(n,p)	19.27	2.5	19.04	2.0
Ti-48(n,p)	0.4244	2.8	0.4202	2.2
V -51(n,p)			0.7094	8.0
Fe-54(n,p)	86.58	2.5	85.58	2.0
Fe-56(n,p)	1.468	2.8	1.446	2.1
Ni-58(n,p)	115.4	1.9	115.0	1.7
Co-59(n,α)			0.2165	6.2
Cu-63(n,α)			0.7089	2.3
Zn-64(n,p)	39.82	3.0	39.81	2.2
In-113(n,n')	162.5	2.7	160.8	2.0
In-115(n,γ)	126.0	3.5	124.6	2.6
In-115(n,n')	198.3	2.6	196.3	2.0
Au-197(n,γ)	77.20	2.7	76.17	2.0
Au-197(n,2n)	5.576	3.1	5.461	2.2
U -235(n,f)	1203	1.8	1208	1.4
Np-237(n,f)	1338	2.6	1339	2.0
U -238(n,f)	318.6	2.5	319.7	1.8
Pu-239(n,f)	1799	2.5	1803	1.5

a) Correlation matrix (see Ref. /18/)

b) Correlation matrix on Table 8

Table 8 Correlation Matrix of the Present Evaluation

Correlation Matrix (x 100)

Mg-24	100																						
Al-27	25	100																					
Al-27(α)	40	51	100																				
S -32	28	30	44	100																			
Ti-46	32	42	72	36	100																		
Ti-47	34	44	75	37	74	100																	
Ti-48	32	40	67	33	75	68	100																
V -51	6	16	19	3	16	17	16	100															
Fe-54	36	44	74	38	65	68	62	17	100														
Fe-56	35	42	72	37	63	66	59	16	69	100													
Ni-58	37	49	82	42	76	80	70	18	81	71	100												
Co-59(α)	12	20	26	15	21	22	20	10	22	21	24	100											
Cu-63(α)	3	4	7	4	6	6	6	2	6	6	11	2	100										
Zn-64	32	43	69	35	60	63	56	17	62	60	67	23	6	100									
In-113(n')	36	47	74	37	65	68	66	19	68	65	73	24	6	62	100								
In-115(γ)	29	36	58	29	51	54	52	15	53	52	57	19	5	49	71	100							
In-115(n')	40	48	76	38	67	70	70	19	70	68	75	24	7	63	87	69	100						
Au-197(γ)	36	46	74	36	65	67	64	19	68	65	73	24	6	62	86	69	86	100					
Au-197(2n)	33	45	69	33	59	63	59	20	63	60	67	24	6	58	78	61	78	84	100				
U -235(f)	5	6	11	6	9	10	8	2	9	9	16	3	25	9	9	7	10	9	9	100			
Np-237(f)	3	4	7	4	6	6	6	2	6	6	11	2	17	6	6	5	7	6	6	65	100		
U -238(f)	3	4	6	3	5	6	5	1	5	5	9	2	15	5	5	4	6	6	5	88	68	100	
Pu-239(f)	4	6	9	5	8	8	8	2	8	8	14	3	22	8	8	7	9	8	8	74	58	70	100

REFERENCES

/1/ W. Mannhart, Nucl. Sci. Eng. 77, 40 (1981)

/2/ W. Mannhart, W.G. Alberts, Nucl. Sci. Eng. 69, 333 (1979)

/3/ W.L. Zijp, J.H. Baard, Nuclear Data Guide for Reactor Neutron Metrology, Report ECN-70 (August 1979)

/4/ K. Kobayashi, I. Kimura, Proc. Third ASTM-EURATOM Symposium on Reactor Dosimetry, Ispra, October 1-5, 1979, EUR 6813, Vol. II, p. 1004 (1980)

/5/ Z. Dezsö, J. Csikai, Proc. IAEA Advisory Group Meeting Nuclear Data for Reactor Dosimetry, Vienna, November 13-17, 1978, INDC(NDS)-103/M, p. 176 (1979)
Z. Dezsö, J. Csikai, Proc. IV All Union Conf. Neutron Physics, Kiev, April 22-26, 1977, Vol. III, p. 32, Atomizdat, Moscow (1977)

/6/ G.J. Kirouac, H.M. Eiland, C.J. Slavik, Proc. Topl. Mtg. Irradiation Experimentation in Fast Reactors, Jackson Lake, Wyoming, September 10-12, 1973, CONF-730910, p. 412 (1973)

/7/ G. Winkler, V. Spiegel, C.M. Eisenhauer, D.L. Smith, Nucl. Sci. Eng. 78, 415 (1981)

/8/ J. Grundl, C. Eisenhauer, Techn. Doc. IAEA-208, Vol. I, p.53 (1978)

/9/ S. Tagesen, H. Vonach, B. Strohmaier, Physics Data Nr. 13-1 (1979)

/10/ S. Tagesen, H. Vonach, Physics Data Nr. 13-3 (1981)

/11/ D.L. Smith, J.W. Meadows, Nucl. Sci. Eng. 60, 187 (1976)
D.L. Smith J.W. Meadows, Report ANL/NDM-13 (June 1975)

/12/ G. Vasiliu, S. Mateescu, INDC(NDS)-103/M, p. 26 (1979)

/13/ A. Marchinkowski, INDC(NDS)-103/M, p. 40 (1979)

/14/ G. Winkler, D.L. Smith, J.W. Meadows, Nucl. Sci. Eng. 76, 30 (1980)
G. Winkler, priv. communication (January 1982)

/15/ B.A. Magurno, EUR 6813, Vol. II, p. 903 (1980)

/16/ H.J. Nolthenius, W.L. Zijp, Report ECN-103 (November 1981)

/17/ M.V. Blinov, Proc. IAEA Consult. Meeting on Neutron Source Properties, Debrecen, March 17-21, 1980, INDC(NDS)-114/GT, p. 79 (1980)

/18/ W. Mannhart, F.G. Perey, EUR 6813, Vol. II, p. 1016 (1980)

/19/ K. Kobayashi, I. Kimura, W. Mannhart, Measurement and Covariance Analysis of Californium-252 Spectrum Averaged Cross Sections, J. Nucl. Sci. Technology (to be published)

/20/ J.J. Wagschal, R.E. Maerker, D.M. Gilliam, EUR 6813, Vol.II, p. 683 (1980)

/21/ V. Spiegel, C.M. Eisenhauer, J.A. Grundl, G.C. Martin, Proc. 2nd ASTM-EURATOM Symposium on Reactor Dosimetry, Palo Alto, October 3-7, 1977, NUREG/CP-0004, Vol. 2, p. 959 (1978)

/22/ V.M. Adamov et al., Proc. Int. Spec. Symposium Neutron Standards and Applications, Washington, March 28-31, 1977, NBS Spec. Publ. 493, 313 (1977)

/23/ J.J. Wagschal, priv. communication (August 1981)

/24/ W. Mannhart, A Small Guide to Generating Covariances of Experimental Data, Report PTB-FMRB-81 (June 1981)

INTERCOMPARISON OF THE D_2O-MODERATED ^{252}Cf SOURCES AT THE N.B.S. AND AT THE SEFOR CALIBRATION CENTER

W. E. Brandon, C. O. Cogburn, R. R. Culp,
W. W. Sallee, J. G. Williams+
University of Arkansas
Fayetteville, AR 72701

C. M. Eisenhauer, J. A. Grundl, E. D. McGarry, R. B. Schwartz - N.B.S.

ABSTRACT

The D_2O-moderated ^{252}Cf source at the N.B.S. was developed as a calibration test source, whose spectrum simulates that found in the vicinity of light water reactors.[1] The D_2O/Cf-252 source is to be used for calibrating neutron personnel dosimeters and for LWR research. One of the requirements involved in the choice of a suitable reference source for this purpose is that a number of testing laboratories should be able to reproduce the source based on the N.B.S. model.

A source based upon the N.B.S. prototype, consisting of a 30 cm diameter spherical stainless steel tank covered with a cadmium shell, has been fabricated for use at the University of Arkansas SEFOR Calibration Center. The Arkansas source differs from the N.B.S. model in some small details, mainly concerning the method of loading the californium capsule into the central stem. In addition to minor differences between the sources used at SEFOR and at N.B.S., it was necessary to consider also the different irradiation cells in which the two sources are used, and to investigate the possible influence of wall-return neutrons on the spectra at the irradiation positions. Compatibility of measurement techniques is discussed, as well as the extent to which the desired reproducibility of the source spectrum has been achieved.

INTRODUCTION

The University of Arkansas calibration facility is located in the refueling cell of the decommissioned SEFOR fast reactor. The room, shown in Figure 1, has 1.2 m thick concrete walls, lined with 1.27 cm of steel. The principal dimensions of the room, neglecting a shelf and fuel transfer port at the top of the room, are: length 5.2 m, width 4.1 m, height 8.5 m. The D_2O moderated source is located 1.4 M above the floor.

+ Present Address: Imperial College, University of London.

EXPERIMENTAL METHOD

At NBS, measurements with the D_2O moderated source are made in the basement of the low-scatter room of the NBS Van de Graaff facility. This room has a concrete floor of 11.7 m length, and 11.0 m width, and concrete walls which extend to a "ceiling" height of 4.6 m. The "ceiling" is an aluminum grating which serves as the floor of the low-scatter room above. The source position is approximately 2 m above the floor.

In both facilities, measured instrument responses are corrected for the effects of wall-return neutrons by assuming that the total measured response can be expressed as:

$$C_T = \frac{C_o}{r^2} + \frac{C_A}{r} + C_{RR} \quad , \tag{1}$$

where r is the source-detector distance
C_o is the response to source neutrons at unit distance in a vacuum.
C_A is the response to neutrons scattered or removed in the air.
and C_{RR} is the response to neutrons reflected at least once from the walls of the room.

In calibration rooms with linear dimensions less than 10 m, the second term is small compared to the third term. This contribution is therefore estimated and subtracted from C_T:

$$C = C_T - \frac{C_A}{r} = \frac{C_o}{r^2} + C_{RR} \tag{2}$$

$$Cr^2 = C_o + C_{RR} r^2 \tag{3}$$

The form of this expression shows that a plot of the measured quantity Cr^2 against r^2 will give a straight line with C_o as the intercept and C_{RR} as the slope of the line. The intercept is the inferred response of the instrument at unit distance, corrected for air-scattering. The slope C_{RR} is the response to room-return neutrons.[2] Rearranging equation (3) gives:

$$Cr^2 = C_o\left(1 + \frac{C_{RR}}{C_o} r^2\right) \tag{4}$$

Figures 2 and 3 show plots of Cr^2 vs. r^2 from measurements with a 9-inch spherical remmeter in the NBS calibration room and in the SEFOR facility. Both sets of measurements were performed with the same instrument. An air-scattering correction of 1.3% per meter of air was made. The larger room-return response for the SEFOR facility (39.3% per m^2 vs. 7.5% per m^2 for NBS) is due to the smaller dimensions of the room.

In order to compare results in the two rooms, the free-field responses C_o should be expressed in units such as counts per mrem. If the room return corrections are made properly and the two source strengths are intercalibrated, the free-field values should be the same.

The dose equivalent rate H is given by

$$H = \frac{0.89 \times K \times Q}{4\pi r^2} \qquad (5)$$

where Q is the source emission rate
K is the fluence-to-dose equivalent conversion factor
and 0.89 accounts for absorption of thermal neutrons in the Cd shell of the D_2O sphere

For the NBS room:

$$H = \frac{0.89 \times 9.3 \times 10^{-6} \text{ (mrem cm}^2\text{)} \times 1.75 \times 10^9 \text{ s}^{-1}}{4\pi r^2 \text{ (m}^2\text{)} \times 10^4 \text{ cm}^2/\text{m}^2}$$

Therefore, the normalized free field value of C/H is

$$C/H = Cr^2/Hr^2 = \frac{301}{.115} = 2.6 \times 10^3 \text{ counts/mrem}$$

The ^{252}Cf source capsule used in the D_2O sphere for the SEFOR measurements has been calibrated at NBS using a $MnSO_4$ bath to establish its neutron emission rate within $\pm$ 1.3%. The emission rate at the time of the remmeter measurements was 4.19×10^9 n/s. This value gives:

$$H = \frac{0.89 \times 9.3 \times 10^{-6} \text{ (mrem cm}^2\text{)} \times 4.19 \times 10^9 \text{ s}^{-1}}{4\pi r^2 (\text{m}^2) \times 10^4 \text{ cm}^2/\text{m}^2}$$

$$H = 0.276 \text{ mrem/s}$$

The normalized C/H ratio for the measurements at SEFOR is

$$C/H = \frac{638}{0.276} = 2.3 \times 10^3 \text{ counts/mrem}$$

This value agrees well with the NBS results, considering that the measurements were made with an ordinary health physics instrument.

It is hoped that a further intercomparison of the two D_2O moderated sources can soon be made using an NBS dual-fission chamber. Other intercomparisons are planned.

REFERENCES

1. Schwartz, R. B. and Eisenhauer, C. M., "The Design and Construction of a D_2O-Moderated ^{252}Cf Source for Calibrating Neutron Personnel Dosimeters Used at Nuclear Power Reactors", NUREG/CR-1204, U.S. Nuclear Regulatory Commission, Washington (1980).

2. Eisenhauer, C. M. and Schwartz, R. B., "Analysis of Neutron Room Return Effects", Eighth DOE Workshop on Personnel Neutron Dosimetry, Louisville, KY (June 1981).

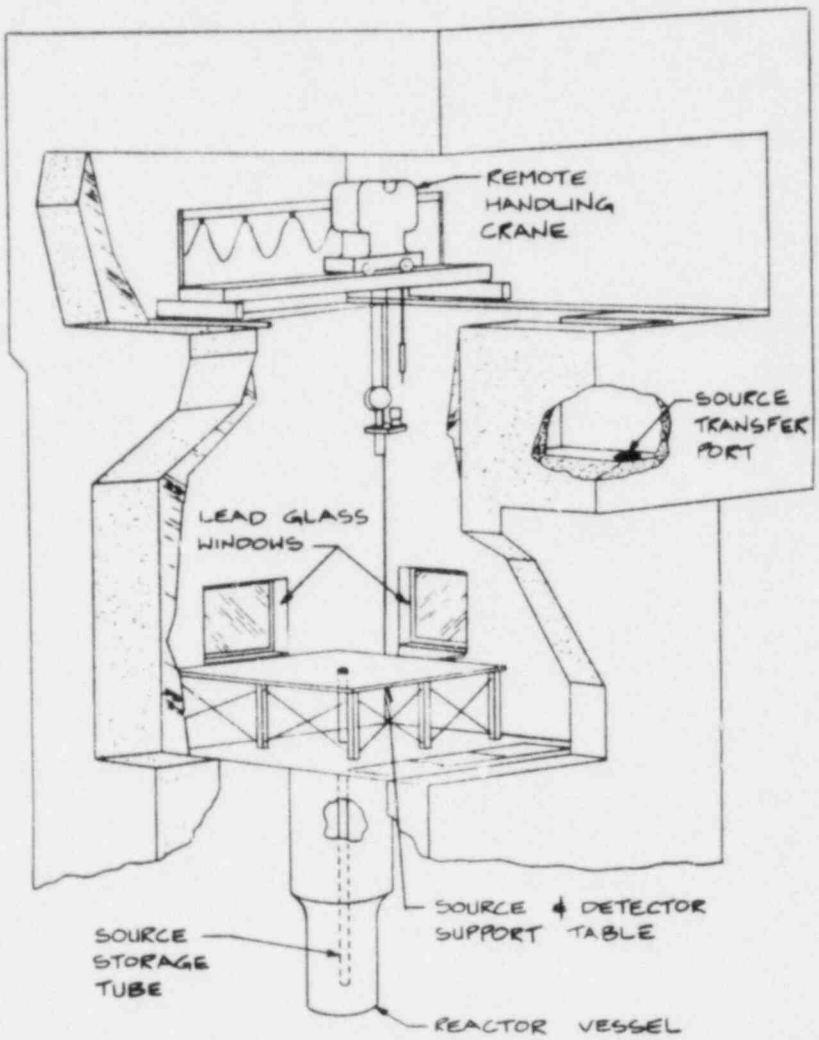

Figure 1 - The SEFOR Calibration Cell

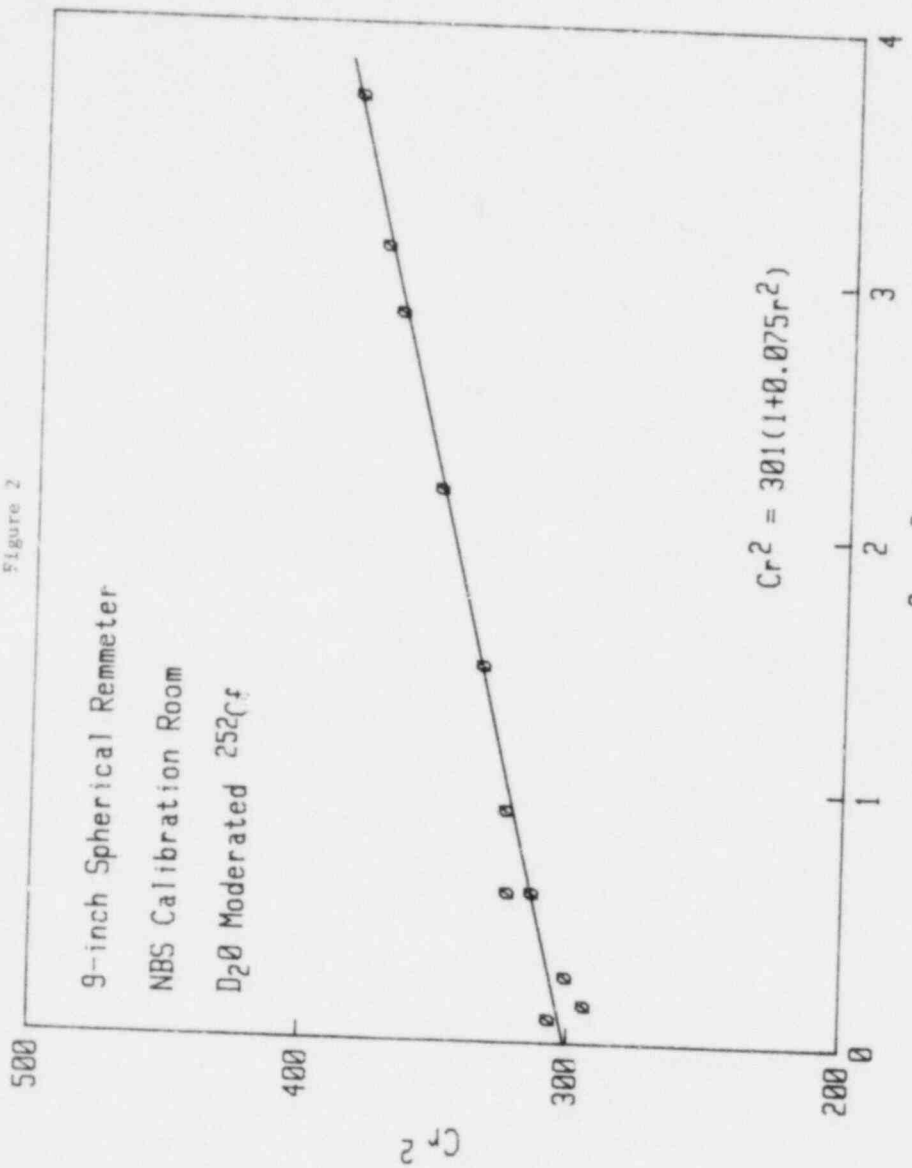
9-inch Spherical Remmeter
NBS Calibration Room
D_2O Moderated ^{252}Cf
$Cr^2 = 301(1+0.075r^2)$
r^2 (m^2)
C
500
400
300
200
0
1
2
3
4

Figure 2

Figure 3

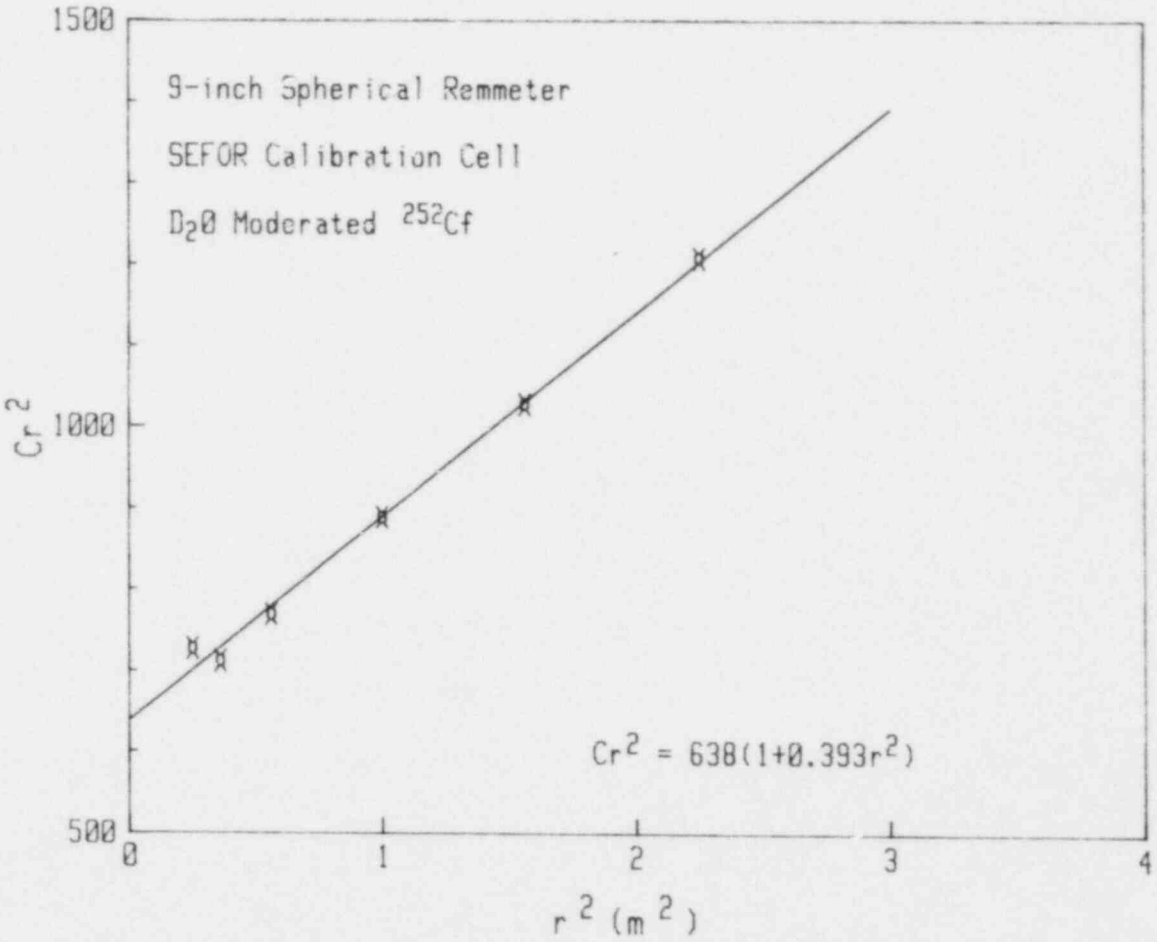
1500
1000
500
Cr 2
9-inch Spherical Remmeter
SEFOR Calibration Cell
D2Ø Moderated 252Cf
Cr2 = 638(1+Ø.393r2)
Ø
1
2
3
4
r 2 (m 2)

MULTIGROUP PROCESSING OF ENDF/B DOSIMETRY COVARIANCES

D. W. Muir, R. E. MacFarlane, and R. M. Boicourt
Los Alamos National Laboratory
Los Alamos, New Mexico, U.S.A.

ABSTRACT

The methodology of multigroup processing of ENDF/B dosimetry covariance (uncertainty) information is discussed, with specific references to the ERRORR covariance module of the NJOY nuclear data processing system. Also discussed is the recent application of ERRORR to the generation of a 137-group, 35-material covariance library for dosimetry applications, and a compact format for storing and transmitting fine-group covariance libraries is introduced.

THE ERRORR COVARIANCE PROCESSING MODULE

The NJOY nuclear data processing system[1] is used at Los Alamos and elsewhere to process data from ENDF/B into forms useful in various applications. A new version, NJOY (10/81), was released to the U. S. code centers in November, 1981. The particular module of NJOY used for preparing multigroup covariance matrices is called ERRORR. In addition, the module COVR is included in the NJOY system to plot and re-format multigroup covariance matrices produced by ERRORR. As with the other NJOY modules, ERRORR and COVR can be operated either as parts of the NJOY system or as stand-alone programs.

Basic Methodology of ERRORR

ERRORR is a flexible program which allows the user several choices in the particular method used to calculate covariances. The first method, the "pointwise" approach, is used when one has access to a data set containing resonance-reconstructed and linearized cross sections in the NJOY "point-ENDF," or PENDF format. The user can produce such a data set using the RECONR and BROADR modules of NJOY. This step is unnecessary for most dosimetry applications, because a PENDF tape containing all of the reactions on the ENDF/B-V dosimetry file, with all resonances reconstructed and Doppler broadened to 300 K, has been produced recently at Los Alamos and is available from the Los Alamos Nuclear Data Group. In order to keep the size of this data file down to a manageable

size (56 000 card images), a relatively coarse accuracy criterion (1% for non-fissile nuclides, 5% for fissiles) was employed in the resonance-reconstruction calculation.

In this mode of operation, the user can specify a group structure with complete flexibility (up to 620 user groups are allowed). The ERRORR module will determine the union of the user's energy grid and the ENDF/B evaluator's grid for the material of interest. The relationship between these three grids is illustrated in Fig. 1.

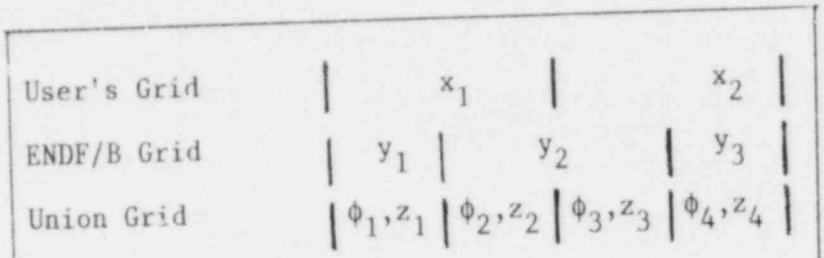

Fig. 1. Illustration of Energy Grid Relations

After forming the union grid, ERRORR integrates $\sigma(E)$ and the user-supplied weight function $\phi(E)$ to obtain the cross sections z_k and "fluxes" ϕ_k, multigrouped on the union grid. These, in turn, are used to calculate multigroup cross sections x_i on the user's grid according to

$$x_i = \frac{\sum_{k \varepsilon i} \phi_k z_k}{\sum_{k \varepsilon i} \phi_k} \quad . \tag{1}$$

In order to calculate the covariances of x_i, the methodology of ERRORR assumes that the $\phi(E)$ is free of uncertainty, so that the "propagation-of-errors" formula can be used,

$$\mathrm{cov}(x_i, x_j) = \sum_{\substack{k \varepsilon i \\ \ell \varepsilon j}} a_{ik} a_{j\ell} \, \mathrm{cov}(z_k, z_\ell) \tag{2}$$

where the "sensitivity coefficients" a_{ik} are the normalized group fluxes,

$$a_{ik} = \frac{\phi_k}{\sum_{k \varepsilon i} \phi_k} \tag{3}$$

The union-grid covariances $\mathrm{cov}(z_k, z_\ell)$ in Eq. (2) are formed from the numerical data in the ENDF/B covariance files by combining them, in the ENDF/B prescribed manner,[2,3] with the union-grid cross sections z_k.

The final step, if the user requests it, is to convert the absolute covariances, Eq. (2), to relative covariances,

$$\text{relcov}(x_i,x_j) = \frac{\text{cov}(x_i,x_j)}{x_i\, x_j} \quad . \tag{4}$$

Group Input Option

A slightly different calculational path is followed if one wishes to start from a multigroup cross section library rather than pointwise data. ERRORR will accept such multigroup cross section input, but only in the format produced by the NJOY group-averaging module GROUPR. Such a library contains both multigroup cross sections and group integrals of the weight function used to produce the cross sections.

In the multigroup input mode, the required union-grid cross sections and fluxes are obtained by collapsing (or expanding) the cross sections and fluxes on the input library. At present, no provision is made for replacing the library group fluxes with a set more appropriate for a given application. If a "library" group is subdivided by a union-group boundary, ERRORR assumes the cross section and weighting function are both energy-independent, in order to estimate ϕ_k and z_k above and below the point of subdivision. The remainder of the calculation proceeds as with pointwise input.

A 620-group (SAND-II) GROUPR output library has been produced recently for the ENDF/B-V dosimetry materials, using a constant weight function. This library is also available on request.

Recent Extensions

In some materials, and in certain energy regions, the cross section uncertainty is dominated by the uncertainty in resolved resonance parameters. One noteworthy example is $^{63}Cu(n,\gamma)^{64}Cu$ (ENDF/B-V Material 6435) in the energy range from 10 eV to 15.9 keV, where the entire cross-section uncertainty is represented by means of resonance-parameter uncertainties. The same is true of $^{237}Np(n,f)$ (ENDF/B-V Material 6337) from 0 to 10 eV.

Beginning with the (10/81) version of ERRORR, the resonance-parameter contribution to the uncertainty in infinite-dilution fission and capture cross sections is included automatically when cross section covariances are processed.

This contribution is obtained from the Breit-Wigner formula for the fission and capture areas of a resonance, A_f and A_γ. By differentiating this formula with respect to the resonance parameters, one obtains a set of sensitivities. With these sensitivities and the

covariance matrix of the parameters from ENDF/B, one can apply a propagation-of-errors formula, similar to Eq. (2), to obtain the covariances $cov(A_\gamma,A_\gamma)$, $cov(A_\gamma,A_f)$, and $cov(A_f,A_f)$. These results then are added to the ENDF-specified "long-range" cross section covariances.

The resonance contribution is properly weighted with the isotopic abundance and the ratio of the weight function at the resonance to the average weight in the group. It is assumed, however, that the area of a resonance lies entirely within the group which contains the resonance energy E_r. Because of this assumption, and because ENDF/B provides no correlations between parameters of different resonances, the calculated resonance-parameter contribution affects only the diagonal elements of the affected matrices.

With the implementation of this feature, the uncertainty in the capture cross section of ^{63}Cu, for example, computed for a group which contains the large 577-eV resonance is 3.0%, rather than zero, as in earlier ERRORR versions.

The (10/81) version of ERRORR also handles explicit cross-material covariances. The only explicit cross-material covariances appearing in ENDF/B-V pertain to fission $\bar{\nu}$ values, but there is a clear need for more information of this type in future versions of the Dosimetry File.

A third, more recent, extension of the program allows the processing of covariances in cases when one cross section is measured relative to a well-known "standard" cross section. In such a case, the evaluator may represent the uncertainty in the first cross section as being the sum of two components. The first component is described by an explicit statement of the uncertainty in the measured ratio, whereas the second component, due to uncertainty in the standard, is represented implicitly, with the details provided only in the ENDF/B evaluation for the standard reaction.

In the dosimetry file, this situation occurs for the $^{238}U(n,\gamma)$ reaction (ENDF/B Material 6398), which was measured relative to $^{10}B(n,\alpha)$ from 4 keV to 20 keV, and the $^{239}Pu(n,f)$ reaction (ENDF/B material 6399), which was measured relative to $^{235}U(n,f)$ from 0.2 to 15 MeV. When ERRORR was modified to include the uncertainty in the standard, there was little effect for $^{238}U(n,\gamma)$, but there was a noticeable increase in the uncertainty of $^{239}Pu(n,f)$, from about 2% to 4-5% in the MeV region. This ratio-to-standard capability is not implemented in the distributed version of ERRORR, but a set of code changes to accomplish this is available from the authors on request.

PRODUCTION OF FINE-GROUP COVARIANCE LIBRARIES

In the above discussion, it is assumed that ERRORR is being used to generate the needed covariances directly in the user's group structure, which is the normal use of the program.

However, one can also use ERRORR to generate a library in a fine-group structure, and then use auxiliary collapsing programs to produce coarse-group libraries later. Such auxiliary programs would duplicate the parts of ERRORR which perform the sums shown in Eqs. (1) and (2). However, such auxiliary programs could be much smaller than ERRORR because they need not deal with the considerable complexities of the ENDF/B-V covariance formats.

In order to study the feasibility of generating and using fine-group covariance libraries, we have used ERRORR to produce a 137-group covariance library (containing energy group boundaries, cross sections, relative standard deviations, and relative covariance matrices) containing all of the materials and reactions in the ENDF/B-V Dosimetry File (Tape 531). A 1/E weight function was used for group averaging.

The energy grid employed is the same for all reactions, and was constructed by forming the union of all energy grids used by evaluators in the covariance files of Tape 531. The resulting master grid is listed in Table I. For these 137-group calculations, the union grid is in all cases identical to the "user" grid, Fig. 1, because any ENDF energies found in a particular evaluation must match one of the "user" energies.

The choice of this group structure for an archival fine-group covariance library was made on the basis of minimizing the number of energy groups, subject to the constraint that information content of the ENDF/B covariance evaluations be preserved. The use of a coarser group structure would irreversibly average away at least some of the detailed correlation structure.

In addition, there is little economic incentive to go choose a coarser structure for the archival library. The computing time required to generate the 137-group 35-reaction library was rather modest, namely about 5 minutes of CDC-7600 central-processor time. This is only about 20% of the time required to produce the input resonance-reconstructed (PENDF) cross section set.

The library thus produced is, as expected, rather bulky. Even though the normal ERRORR output format suppresses zeros, the library contains over 38 000 card images. For this reason we have developed a new format for compact representation of covariance matrices which eventually will be an output option of the COVR module. The design of this format, called the "Boxer" format, proceeds from a simple fact: the ENDF/B-V covariance evaluations define certain rectangular regions (boxes) in energy space, over which the relative covariance is constant. (The ENDF/B format allowing a constant absolute covariance is rarely used, and is not used at all in the ENDF/B-V Dosimetry File). Thus one expects that an element of a multigroup relative covariance matrix derived from ENDF/B frequently will be identical either to the element before it in the same row, or to the element above it in the same column. Thus, the Boxer format allows a combination of "horizontal" and "vertical" repeat operations. Further details of the format are given in Appendix A.

The amount of data compression achieved by this format change is remarkable; from the original 38 000 card images the final library is reduced to less than 1000 card images. Of these 1000, only about 300 are needed for the covariance matrix data proper, with most of the remaining records containing cross section information. By way of comparison the covariance portion of the ENDF/B Dosimetry File itself occupies over 500 card images.

Table 1. RDC Library 137-Group Structure

Group Index	Lower Energy (eV)	Group Index	Lower Energy (eV)	Group Index	Lower Energy (eV)
1	1.00000E-05	47	2.30000E+05	93	4.10000E+06
2	2.53000E-02	48	2.50000E+05	94	4.50000E+06
3	3.00000E-02	49	3.00000E+05	95	5.00000E+06
4	9.00000E-02	50	3.03000E+05	96	5.50000E+06
5	2.50000E-01	51	3.40000E+05	97	5.75000E+06
6	6.25000E-01	52	3.50000E+05	98	6.00000E+06
7	1.00000E+00	53	4.00000E+05	99	6.25000E+06
8	1.80000E+00	54	4.50000E+05	100	6.40000E+06
9	3.00000E+00	55	5.00000E+05	101	7.00000E+06
10	5.00000E+00	56	5.30000E+05	102	7.50000E+06
11	1.00000E+01	57	5.50000E+05	103	8.00000E+06
12	1.50000E+01	58	6.00000E+05	104	8.50000E+06
13	2.00000E+01	59	6.30000E+05	105	9.00000E+06
14	4.00000E+01	60	6.50000E+05	106	9.28400E+06
15	5.00000E+01	61	7.50000E+05	107	9.50000E+06
16	8.00000E+01	62	8.00000E+05	108	1.00000E+07
17	1.55000E+02	63	8.25000E+05	109	1.00600E+07
18	2.00000E+02	64	8.30000E+05	110	1.04100E+07
19	3.00000E+02	65	8.50000E+05	111	1.05000E+07
20	4.00000E+02	66	9.00000E+05	112	1.06400E+07
21	5.00000E+02	67	9.50000E+05	113	1.06800E+07
22	6.00000E+02	68	1.00000E+06	114	1.10000E+07
23	1.00000E+03	69	1.02000E+06	115	1.15000E+07
24	2.00000E+03	70	1.05000E+06	116	1.16860E+07
25	3.00000E+03	71	1.20000E+06	117	1.20000E+07
26	4.00000E+03	72	1.40000E+06	118	1.24000E+07
27	4.80000E+03	73	1.60000E+06	119	1.24143E+07
28	7.00000E+03	74	1.61940E+06	120	1.25000E+07
29	8.00000E+03	75	1.74210E+06	121	1.30000E+07
30	1.00000E+04	76	1.89900E+06	122	1.31000E+07
31	1.59000E+04	77	2.00000E+06	123	1.35000E+07
32	2.00000E+04	78	2.07545E+06	124	1.40000E+07
33	2.30000E+04	79	2.20000E+06	125	1.42000E+07
34	2.50000E+04	80	2.40000E+06	126	1.45000E+07
35	3.00000E+04	81	2.50000E+06	127	1.50000E+07
36	4.00000E+04	82	2.60000E+06	128	1.55000E+07
37	5.00000E+04	83	2.80000E+06	129	1.60000E+07
38	6.00000E+04	84	2.96550E+06	130	1.65000E+07
39	6.76000E+04	85	3.00000E+06	131	1.70000E+07
40	8.00000E+04	86	3.10000E+06	132	1.75000E+07
41	9.00000E+04	87	3.24800E+06	133	1.80000E+07
42	1.00000E+05	88	3.27500E+06	134	1.85000E+07
43	1.30000E+05	89	3.30000E+06	135	1.90000E+07
44	1.50000E+05	90	3.50000E+06	136	1.92000E+07
45	1.84000E+05	91	3.70000E+06	137	1.96000E+07 - 2.00000E+07
46	2.00000E+05	92	4.00000E+06		

The 137-group library in Boxer format is called the RDC (Reactor Dosimetry Covariance) Library. The library and a short retrieval program, TRIEVR, which reads the library and reconstructs full 137 x 137 matrices, are available on request.

Because of the compactness of the library, the retrieval program runs very fast. For example, to search through to find the last reaction in the library and reconstruct the covariance matrix requires less than 2 seconds of CDC-7600 time. To reconstruct all 35 matrices and write them onto a binary disk file requires only 17 seconds of 7600 time. By adding collapse algorithms (see next section) to TRIEVR, one could avoid the cost of permanently storing the large output file.

Coarse-Group Collapse of the RDC Library

We next consider the subject of "collapsing" the RDC multigroup covariances to a relatively coarse user-defined energy grid. Typically one needs covariances on an energy grid which is not exactly a sub-set of the fine-group grid. Thus, we are back to a situation essentially identical to that shown earlier in Fig. 1, provided that the "ENDF/B Grid" is relabelled the "RDC Grid." While the ENDF grid in Fig. 1 referred to the (material-dependent) evaluator's grid, the RDC grid is a characteristic of the entire fine-group library, being the same for all materials. Thus the union grid is also the same for all materials, and it can be determined in advance of any collapse calculations. Also one can calculate in advance the union group fluxes ϕ_k, using any weighting function $\phi(E)$ of interest. Finally, the y_m values in Fig. 1 can be identified with the fine-group cross sections in the RDC Library.

It is convenient to re-cast Eq. (2) in terms of relative covariances,

$$\frac{\mathrm{cov}(x_i,x_j)}{x_i\ x_j} = \sum_{\substack{k\varepsilon i \\ \ell\varepsilon j}} f_{ik}\ f_{j\ell}\ \frac{\mathrm{cov}(z_k,z_\ell)}{z_k\ z_\ell} \tag{5}$$

where

$$f_{ik} = \frac{\phi_k\ z_k}{\sum\limits_{k\varepsilon i} \phi_k\ z_k} \tag{6}$$

is the fractional contribution to output group constant x_i from union group k.

The fact that the energy grid of the RDC Library includes all energy grids used in the ENDF/B-V dosimetry covariance files implies that the

relative covariance $\mathrm{cov}(z_k,z_\ell)/z_k\,z_\ell$ in Eq. (7) need not be reconstructed from ENDF/B; it is guaranteed to be exactly equal to one of the covariances $\mathrm{cov}(y_m,y_n)/y_m\,y_n$ in the RDC Library. It is only necessary to locate the RDC group m which contains union group k. This can be done, for example, by using a material-independent "pointer" array. For example, in the simple case shown in Fig. 1,

$$\frac{\mathrm{cov}(z_2,z_4)}{z_2\,z_4} = \frac{\mathrm{cov}(y_2,y_3)}{y_2\,y_3} \tag{7}$$

To complete the calculation of the coarse-group relative covariance, Eqs. (5) and (6), one needs only to evaluate the factors f_{ik}. If one has access only to the multigroup cross sections y_m, and not the underlying energy-dependent cross-section shape, one cannot proceed completely rigorously. However, because of the large number of groups in the RDC Library (see Table I), it is a good approximation to ignore the energy dependence here and simply set $z_k = y_m$, where RDC group m contains union group k.

REFERENCES

1. R. E. MacFarlane, D. W. Muir, and R. M. Boicourt, "The NJOY Nuclear Data Processing System, Vol. I: User's Manual," Los Alamos National Laboratory report LA-9303-M (1982).

2. F. G. Perey, "The Data Covariance Files for ENDF/B-V," Oak Ridge National Laboratory report ORNL/TM-5938 (ENDF-249) (1977).

3. R. Kinsey, "ENDF-102, Data Formats and Procedures for the Evaluated Nuclear Data Files, ENDF," Brookhaven National Laboratory report BNL-NCS-50496 (ENDF-102) 2nd. Ed. (ENDF/B-V) (1979)

APPENDIX A

The RDC Library (Boxer) Format

In the Boxer format, data is stored as a list of numerical data values (for example, relative covariances), together with a list of integers which control the loading of the data into the reconstructed array C(i,j). A negative integer, say -n, indicates that the next value in the data list is to be loaded into the next n j-values of C(i,j). A positive integer m means, for the next m j-values, simply carry down the value from the row above,

$$C(i,j) = C(i-1,j) \quad .$$

When the first row (i = 1) is being loaded, the row "above" is defined to be a row containing all zeroes.

In constructing the compressed data set, the choice between using the "repeat-new-value" method or the "carry-down" method is made dynamically on the basis of taking the longest possible "step." If m = n, the "carry-down" method is chosen, as it does not require an entry in the data list.

As an additional compression feature, one may indicate by a "flag" that the matrix C(i,j) is symmetric, hence only the upper right triangle is given explicitly in the compressed data library. These various aspects of the Boxer format are illustrated by a simple example in Fig. A-1. Here a, b, c, and d are arbitrary non-zero data values.

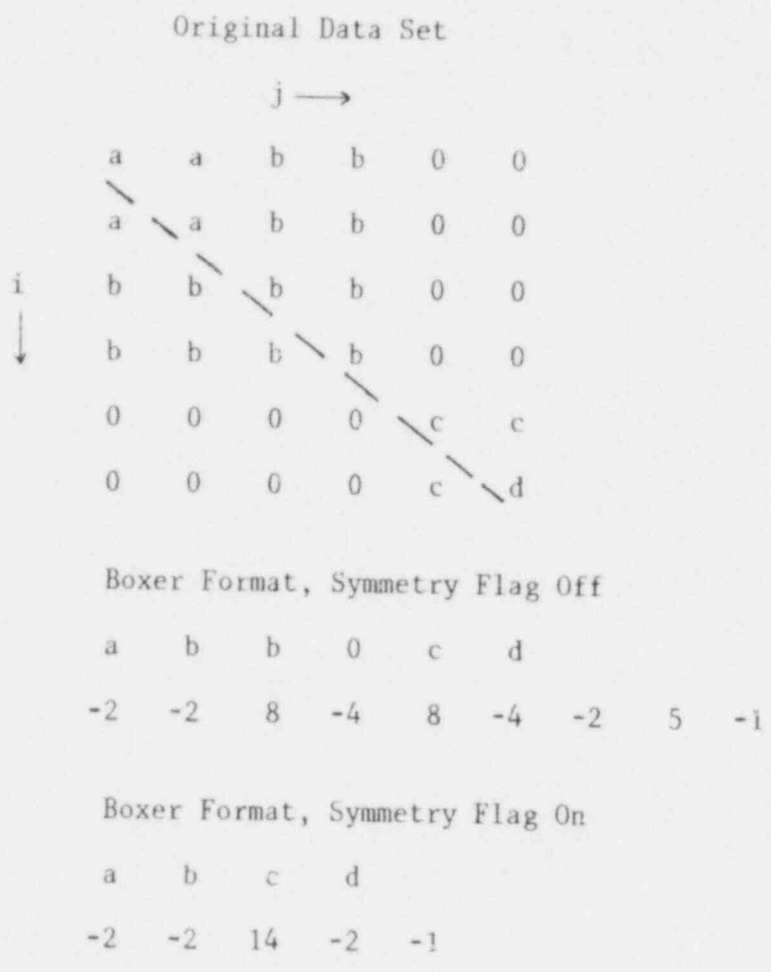

Fig. A-1. Illustration of Boxer Format

THE MOL CAVITY FISSION SPECTRUM STANDARD NEUTRON FIELD AND ITS APPLICATIONS

A. Fabry, G. Minsart, F. Cops and S. De Leeuw
SCK/CEN, Boeretang 200, B-2400 Mol, Belgium

SUMMARY

The uranium-235 fission spectrum standard neutron field in the one-meter diameter spherical cavity of the vertical thermal column of the Belgian BR1 reactor is being revisited. The work is still in progress. No bias in excess of 0.5 % has been found in previously published integral fission cross section ratio measurements and benchmark field referencing of passive and active dosimetry sensors except for high threshold reactions i.e. $\sim$ 3 % for $^{27}Al(n,\alpha)$. On another hand, significant advances in unravelling better all neutronic and gamma-ray features of the field do encompass :

1) the identification of the importance of low-energy ($\leq$ 3 eV) neutron upscattering effects on the cavity wall return reaction rates for non-threshold dosimetry sensors
2) considerably improved insight into assessing the space-energy perturbations caused by the structural cylindrical cadmium thimble into which the field is generated
3) the more detailed assessment of reactor core leakage background radiation fields.

It is confirmed in particular that the background response of threshold fission sensors is purely induced by gamma-rays, making integral checks of the relevant nuclear data possible. A novel approach to reactor gamma-ray dosimetry, spectroscopy and microcalorimetry standardization is proposed, using this facility. A novel Grazing-Angle Transmission Experiments (GATE) method is also suggested as further asset of the facility to test the adequacy of neutron angular scattering data; for a material as iron, these nuclear data are believed, on basis of the PCA reactor pressure vessel benchmark results, to be largely responsible for the remaining discrepancies and trends presently observed in reaction rate and neutron flux steel traverses.

Finally, the procurement of a removable pneumatic transfer system opens the facility to some fast neutron activation analysis, delayed-neutron and other calibration applications.

INTRODUCTION AND SCOPE

The standard neutron field under consideration is generated by means of a flexible uranium-235 source arrangment located at the center of spherical cavities [1][2] hollowed out of the BR1 reactor graphite thermal columns. It has been the subject of a number of cooperative ventures between various national and international groups (for instance references [2] to [8]). The same spherical cavities, of diameter 50 cm and 1 meter, are used also to generate, respectively the MOL-ΣΣ intermediate-energy reference neutron field [9] and the related natural uranium and iron shell material benchmarks [10][11].

The present paper is the progress report of a current in-depth experimental and theoretical study of the cylindrical source version(s) [4] of the uranium-235 fission spectrum standard neutron field in the one-meter spherical cavity. (Other source arrangments are in use [5]). The study has been promoted by various factors :

1) Request to document better correction and uncertainty sources in past integral cross section measurement [3][4][5] and benchmark-field referencing [12][13] work, including the calibration basis for absolute equivalent fission neutron fluxes[12]
2) Request to finalize the analysis of fission-spectrum average helium production cross section measurements for ^{10}B and ^{6}Li[14]
3) Desirability for exploratory investigations in support of some novel applications for the facility, such as the ones made possible by the recent procurement of a transportable, high speed pneumatic transfer system, or the ones suggested in the frame of programmatic activities in LWR neutron dosimetry, [15] in fusion plasma neutron diagnostics [16] and in gamma-ray dosimetry standardization [17].

In views of editorial and schedule limitations, the paper is written in a summary style, with many underlying details left for further scrutiny in a forthcoming technical publication.

GROSS FEATURES OF THE FACILITY AND OF THE FISSION NEUTRON SOURCES

The cylindrical source versions of the MOL cavity fission spectrum standard neutron field are schematized on figures 1 and 2. As may be seen from fig. 1 the facility offers great flexibility. Active and passive instruments, as well as the new pneumatic rabbit, can be inserted and extracted directly, even at a full reactor power

of 1 MW[a]. This is true also for the structural thimble, a 2 meter long co-extruded cadmium tube of 1 mm thickness and of diameter matching the inner diameter of the selected source shell (upper part of fig. 2). The source itself is furthermore removable for reactor background control measurements. The "Model II" source (fig. 2) has been applied most extensively thus far. Model I is reserved to special applications in which the contribution of graphite cavity wall-return neutrons (see below) has to be minimized [14] or had to be verified further [4]. This wall-return contribution is indeed proportional to the ratio between the source strength and the central equivalent fission neutron flux, i.e. considering the approximate values quoted on fig. 2 for these parameters, the wall return corrections are roughly 4.2 (respectively 8.5) times larger in model II (respectively model III) than in model I. The axial and radial unperturbed fast neutron flux gradients within the central zone of the sources are similar on the relative scale of the illustration (fig. 2 bottom). Model III thus offers the largest useful experimental volume combined to the most intense fast neutron flux. This model is being assembled at this time; it is intended at the novel applications to be briefly outlined - for which larger wall return neutron contributions to the central fast fluxes are not detrimental (in some instances, can be taken at advantage).

PRINCIPLES FOR ANALYSIS OF THE NEUTRON FIELD

It is most useful to decompose the standard radiation field with respect to the origin, space, angle and energy distribution of the nuclear particles "detectable" at any point within the cavity. Table 1 exemplifies such inventory of the central field for source model II in a gross three-neutron and one-gamma energy-group specification. Incorporated are footnotes and comments intended at providing general indications of the available detailed data less relevant to a survey.

Table I concepts can be translated to high accuracy into the following superposition equation for neutronic sensor integral reaction rate responses r(z) along the vertical axis of the source-thimble assembly :

$$r(z) = \left[\bar{\sigma}_{X25}\left(\frac{1}{4\pi\,\bar{z}^2}\right)\right] P_X(z)\, S_X + \left[r_W(o)\, g_W(z)\right] f_W(E_C)\, S_W + B(z) \quad [1]$$

where - $\bar{\sigma}_{X25}$: uranium-235 fission spectrum average cross section of considered sensor

(a) Occasional passive experiments at a power of 3.2 MW are possible [14].

- $\left(\frac{1}{4\pi \bar{z}^2}\right)$: unperturbed flux per unit total source strength for the considered source-sensor geometric arrangement; this is calculable exactly, in actual practice by means of an NBS-code, INTRAN [18]; $\bar{z}$ defines the "effective" source-sensor separation distance

- $P_\chi(z)$: virgin neutron field perturbation by the structural thimble (fig. 3)

- S_χ : virgin neutron field perturbation by the sensor(s)

- $r_W(o)$: central reaction rate induced by neutrons generated through virgin neutron collisions, energy degradation and backscattering from the graphite cavity walls (wall-return, fig. 4 and table 2)

- $g_W(z)$: relative space-variation of $r_W(o)$ (fig. 5, left)

- $f_W(E_C)$: effective cadmium cut-off dependency of $r_W(o)$ (fig. 5, right)

- S_W : wall return neutron field perturbation by the sensors

- $B(z)$: background responses, see all items referred to footnote (e) in table 1.

Equation [1] essentially expresses separability properties which are not mathematically exact but are very accurate approximations to the "physics" of most experiments in this standard.

In particular, the equation implicates that the three-dimensional geometry of fig. 1 can be analysed by superposition of one-dimensional spherical transport theory solutions to the cavity wall-return neutron "problem" and one-dimensional cylindrical or two-dimensional (R,Z) solutions to the thimble perturbation "problem".

As with any approximation, there are limitations to this "rosy" picture. On another hand, insofar as the S_W correction is small or does not involve excessive local heterogeneity, the wall-return and thimble effects can be handled by a more complete two-dimensional (R,Z) model.

At neutron energies above $\sim$ 3.5 MeV, wall return neutron fluxes are negligible. At energies below $\simeq$ 10 keV, the cavity wall return neutron field is spatially and angularly uniform, fig. 4 and reference [19]. The second property is fundamentally traceable to the neutron "memory loss" after numerous wall collisions and cavity crossings.

Both properties provide the basic justification for

1. accurate integral cross section measurements relevant to threshold reactor dosimetry and activation analysis
2. accurate fission flux absolute calibration relative to the $^{235}U(n,f)$ cross section
3. capability for accurate fission spectrum average cross section measurements of non-threshold reactions.

Fig. 6 and table 3 provide an illustration relative to 3, for $\frac{a}{z}$ rather complex experimental capsule arrangement [14]. Minimizing $\frac{a}{z}$ and enhancing S_W were two crucial aspects of the experiment design. Capsules containing ^{10}B and ^{6}LiF powders were exposed at the center of source Model I (fig. 6, upper part) as well as at off-centered locations, 30 cm above and below center. Table 3 presents a detailed example of the application of equation [1] to this experiment.

It has been noted from table 2 that neutron upscattering effects below ~ 3 eV are important, but do not necessarily affect as severely the actual reaction rates (table 3, footnote (d)). This point deserves a brief clarification.

The "Equivalent Wall-Return Epithermal Neutron Flux per Unit Lethargy" has been defined here as

$$\phi_{epi}^{eq.} = \frac{\int_{0.5\ eV}^{\infty} \phi_W(E)\ dE}{\int_{0.5\ eV}^{3.5\ MeV} \frac{dE}{E}} \qquad [2]$$

and the "Equivalent Wall-Return Resonance Integral" as

$$I_{eq.} = \frac{\int_{0.5\ eV}^{\infty} \phi_W(E)\ \sigma(E)\ dE}{\phi_{epi}^{eq.}} \qquad [3]$$

It is seen from table 2 that neutron upscattering effects produce a low-energy neutron spectrum much closier to the 1/E shape than when these effects are ignored. This also shifts the effective cadmium cut-off energy [20] to higher values, probably near 0.7 eV for 1/v-sensors. At this stage, our calculations of E_C have been based on the VITAMIN/C wall-return spectra and more exact values will thus have to be determined in future.

Figures 7 and 8 gather a number of recent absolute vertical traverse measurements in model II source, and the results of their

analysis by means of equation [1] are shown on figure 9. Negative coordinates on figures 7 and 8 point into the direction of the reactor core. The $^{237}Np(n,f)$ data close to the cavity upper edge are perturbed by a steel sleeve (fig. 10) of 6 mm thickness, extending all the way to the reactor top through the access hole, and used to suspend the iron and natural uranium shell benchmarks [10]. A second, identical plug is available and its steel sleeve is being removed at this time, to eliminate the undesirable degradation of the high-energy neutron wall-return spectrum near the access hole.

The valid C/E results for $^{237}Np(n,f)$ are consequently the open symbols on fig. 9, while the "agreement" displayed by the closed symbols is entirely fortuitous. The actual discrepancy of up to $\sim$ 30 % at the cavity bottom is believed traceable to exagerated forward-peaking of the cadmium elastic-scattering angular distribution in ENDF/B IV. A detailed discussion is beyond the scope of this paper. Let mention for clarity that the DOT (R,Z) calculations of this effect $P_\chi(z)$, fig. 3, have been performed by means of a biased quadrature with 210 angles (resolution of the order of 1°) and a P3 expansion. A reduction to 100 angles and half the mesh grid spacings does not affect $P_\chi(z)$, even although the $\sim$ 10 % agreement of the S210 results with INTRAN [18] calculations for the unperturbed (air) geometry is degraded significantly in the S100 case, with differences up to 50 % at z $\sim$ 40 cm. The influence of boundary conditions and convergence criterions has been examined also. It can be concluded that the discrete-ordinates solution for $P_\chi(z)$ is converged.(*)
A new type of benchmark experiments is being designed on basis of the present study and is illustrated by fig. 11.

GAMMA-RAY FIELD

Another by-product of this work is a proposal for reactor gamma-ray dosimetry and spectroscopy standardization, schematized on fig. 12.
It has been possible to assess that the $^{237}Np(n,f)$ and $^{238}U(n,f)$ responses on fig. 8 are pure photofission.
Integral photofission cross sections averaged over the cadmium prompt capture gamma-ray spectrum are being derived. The major difficulty at this time is the lack of gamma-ray metrology standardization. Model III source has been designed specifically for the novel applications proposed by figures 11 and 12.

(*) Except maybe relative to the scattering matrix expansion order at large values of z.

ACKNOWLEDGMENTS

The authors are indebted to Mr. J. Tissot for his support with many time-consuming calculations and to Mrs S. Andries, Mrs J. Vincent and J. Thijs for their excellent and expedient editorial help.

REFERENCES

[1] A. Fabry, P. Vandeplas, - Fast Reactor Physics I, 389, IAEA (1968).

[2] J.A. Grundl, C. Eisenhauer, "Benchmark Neutron Fields for Reactor Dosimetry", in IAEA Consultants' Meeting on Integral Cross Section Measurements in Standard Neutron Fields for Reactor Neutron Dosimetry, November 15-19 (1976).

[3] A. Fabry - Report BLG 465 (1972).

[4] A. Fabry, J.A. Grundl, C. Eisenhauer - NBS Spec. Publ. 425, I, 254 (1975).

[5] A. Fabry, K.H. Czock - Report IAEA/RL/27 (1974).

[6] A. Fabry, I. Girlea, "Quality control and calibration of miniature fission chambers by exposure to standard neutron fields. Application to the measurement of fundamental integral cross section ratios" ibid. 2.

[7] A. Fabry et al., "Review of Microscopic Integral Cross section Data in Fundamental Reactor Dosimetry Benchmark Neutron Fields", ibid. 2.

[8] A. Fabry, "Standard Integral Measurement Facilities", Proceedings of the International Specialists Symposium on Neutron Standards and Applications, held at the National Bureau of Standards, Gaithersburg, MD, March 28-31 (1977).

[9] A. Fabry, G. and S. De Leeuw - Nucl. Techn. 25, 349 (1975).

[10] G. De Leeuw-Gierts, S. De Leeuw, "Updated results for the MOL-ΣΣ benchmark and first results of the connected U_{nat} experiment", Fourth ASTM-EURATOM symposium on Reactor Dosimetry, held at the National Bureau of Standards, Gaithersburg, MD., March 22-26 (1982).

[11] G. and S. De Leeuw, "Neutron data of structural materials for fast reactors", Proceedings of a Specialists' Meeting, held at the Central Bureau of Nuclear Measurements, Geel, Belgium p. 93-104 (1977).

[12] W.N. McElroy, "LWR Pressure Vessel Surveillance Dosimetry Improvement Program : PCA Experiments and Blind Test", NUREG/CR-1861, HEDL-TME 80-87, R5 July (1981).

[13] E.D. McGarry, "NBS ISNF and Cavity Fission ^{235}U Standard Neutron Fields", Fourth ASTM-EURATOM Symposium on Reactor Dosimetry, held at the National Bureau of Standards, Gaithersburg, MD., March 22-26 (1982).

[14] B.M. Oliver, H. Farrar IV, E.P. Lippincott and A. Fabry, "Spectrum-Integrated Helium Generation Cross Sections for ^{6}Li and ^{10}B in the Sigma Sigma and Fission Cavity Standard Neutron Fields", Fourth ASTM-EURATOM Symposium on Reactor Dosimetry, held at the National Bureau of Standards, Gaithersbur, MD., March 22-26 (1982).

[15] A. Fabry et al., "Progress Report on the Belgian Contribution to the Improvement of LWR Pressure Vessel Steel Embrittlement Surveillance", Fourth ASTM-EURATOM Symposium on Reactor Dosimetry, held at the National Bureau of Standards, Gaithersburg, MD., March 22-26 (1982).

[16] G.N. Jarvis et al., "Development in Dosimetry Applied to Fusion Reactor", Fourth ASTM-EURATOM Symposium on Reactor Dosimetry, held at the National Bureau of Standards, Gaithersburg, MD., March 22-26 (1982).

[17] N. Maene et al., "Gamma Dosimetry and Calculations", Fourth ASTM-EURATOM Symposium on Reactor Dosimetry, held at the National Bureau of Standards, Gaithersburg, MD., March 22-26 (1982).

[18] C. Eisenhauer, National Bureau of Standards - Private Communication (1975).

[19] A. Fabry, J.D. Jenkins - "Trans. ANS 15, 940 (1972).

[20] S. Pearlstein and E.V. Weinstock - "Scattering and Self-shielding Corrections in Cadmium Filtered Gold, Indium and A/v Foil-Activation Measurements", Nucl. Sci. Eng. 29, 28-42 (1967).

Table 1. Components of the standard radiation field

Identification		Flux at 1 MW Reactor Power ($cm^{-2}sec^{-1}$)(a)	Present assessment method(s) and comments
Driver thermal neutron flux		1.0, +9	Experimental (gold foils, full axial traverses)
Source Fission Neutrons	*	2.0, +8(b)	Experimental Perturbed by structural thimble(c)
Wall return epithermal neutron flux (> 0.5 eV)	*	3.6, +6(b)	Transport theory and/or experiment. Effective cadmium cut-off energy is a consideration
Wall return subcadmium neutron flux (< 0.5 eV) (d)		3.6, +6(b)	Transport theory (S16P3 218 gr DLC43B, ENDF/B IV)
Reactor core leakage epithermal neutron flux(e) (> 0.5 eV)		~ 3.0, +4	Experimental (full axial traverses)
Reactor core leakage fast neutron flux(e)		≤ 1.0, +4	$^{32}S(n,p)$ equivalent fission flux measurement
Thermal neutrons transmitted through cadmium(e)		1.6, +3	$^{164}Dy(n,\gamma)$ activation measurement (full axial traverses); Cadmium ratio : 9.3 (1 mm Cd)
Gamma-ray flux(e)(f)	*	1.6, +8(f)	TLD measurements (full axial traverses). Enhanced to ~ 1.9, +8 by fission source. Calculated contribution from graphite walls : 5 %
Neutrino, Meson, Etc. ... flux		?	Unobserved

*Used or usable for practical applications or standardization work.

(a) At cavity center. (b) Model II source.

(c) Perturbation separable from gradient effects of fig. 2; corrections by 1 D or 2 D discrete-ordinates transport theory.

(d) Considered in terms of its possible enhancement effect on the prompt gamma-ray flux component. Effect found < 1.5 %.

(e) Lumped effect on sensors directly substractable by "background" measurements without the fission source.

(f) These 1975 TLD traverses may be precise, but not accurate by to-day methods. Ion chamber readings by the CEN/SCK Health Physics Group indicate $\bar{\alpha}_\gamma \sim 9.2, +7$.

Table 2. Calculated infinitely dilute epicadmium responses of selected dosimetry reactions in the central graphite wall-return neutron spectrum of the MOL one-meter cavity

Reaction	$r_W(o)$ (a)(b)(c)	Equivalent resonance integral (barns) (b)(d)	1/E resonance integral (barns) (d)(e)
$^{10}B(n,\alpha)$	1.817, -26 2.568	1085 1454	1722
$^{6}Li(n,\alpha)$	4.506, -27 6.733	269 381	423
$^{235}U(n,f)$	3.204, -27 4.096	191 232	281
$^{239}Pu(n,f)$	3.449, -27 4.600	206 260	303
$^{197}Au(n,\gamma)$	1.795, -26 1.725	1072 977	1566

(a) Reaction rate per nucleus and sec for a cadmium cut-off energy of 0.5 eV and using the ENDF/B V dosimetry file. Central source of unit strength (1 n/sec). Graphite density : 1.715 gr/cm^3 (8.60, -26 atoms/cm^3). Corresponding central epithermal neutron flux above 0.5 eV is 2.640, -4 and 2.783, -4 for the two calculations, footnote (b).

(b) Calculations are S16P3 one-dimensional spherical discrete-ordinates (ANISN); upper figures obtained with 171 gr VITAMIN/C and lower figures with 218 gr DLC43B cross sections (ENDF/B IV).

(c) Responses for threshold reactions also calculated but are orders of magnitude less; for instance, $r_W(o)$ = 7.975, -29 and 7.843, -29 for $^{237}Np(n,f)$, respectively using VITAMIN/C and DLC43B.

(d) See text. The ratio I/Ieq. is a measure of the epithermal wall-return neutron spectrum deviation from the 1/E shape (fig. 4).

(e) Cadmium cut-off energy of 0.5 eV and ENDF/B V dosimetry file.

Table 3. Typical application of the standard field superposition equation [1] : helium production cross section measurements [14]

Item (symbols of eq. [1])	$^{10}B(n,\alpha)$	$^{6}Li(n,\alpha)$
Virgin fission flux $\phi_f(o) = \frac{1}{4\pi \overline{z^2}}$ (a)	6.708, -2	
$\overline{\sigma}_{\chi 25}$ (ENDF/B V)	490.5, -27	454.7, -27
$r_{\chi 25}(o) = \phi_f(o)\overline{\sigma}_{\chi 25}$	3.290, -26	3.050, -26
$P_\chi(o)$	1.036	1.031
S_χ	1	1
$\phi_f(o)\overline{\sigma}_{\chi 25} P_\chi^o(o) S_\chi$	3.408, -26	3.145, -26
$r_W(o)\ f_W(0.53\ eV)$ (b)	1.763, -26	4.364, -27
g_W (30 cm)	1.003	1.003
S_W (c)	0.251	0.640
$r_W(o)\ f_W(0.53\ eV) S_W$	4.425, -27	2.792, -27
ϕ_f (30 cm) $\overline{\sigma}_{\chi 25} P_\chi$ (30 cm) S_χ	1.567, -28	1.445, -28
$B(o) \simeq B$ (30 cm)	4.25, -28	2.67, -28
PREDICTED REACTION RATE RATIO 30 cm OFF-CENTERED/CENTRAL	0.129 (d)	0.093 (d)

(a) For actual geometry of dosimetry capsules and source Model I.

(b) VITAMIN/C, E_C calculated by separate cylindrical ANISN run. Upscattering effects predicted by DLC43B result in a spectrum closier to 1/E and E_C increases then to an estimated value of $\sim$ 0.7 eV. The corresponding $r_W(o)\ f_W$ (0.7 eV) are 1.823, -26 and 4.799, -27 for $^{10}B(n,\alpha)$ and $^{6}Li(n,\alpha)$ respectively.

(c) 360° DOT (R,θ) S12P3 calculations, 31 groups.

(d) Correction for upscattering effects gives : $^{10}B(n,\alpha) = 0.132$, $^{6}Li(n,\alpha) = 0.100$.

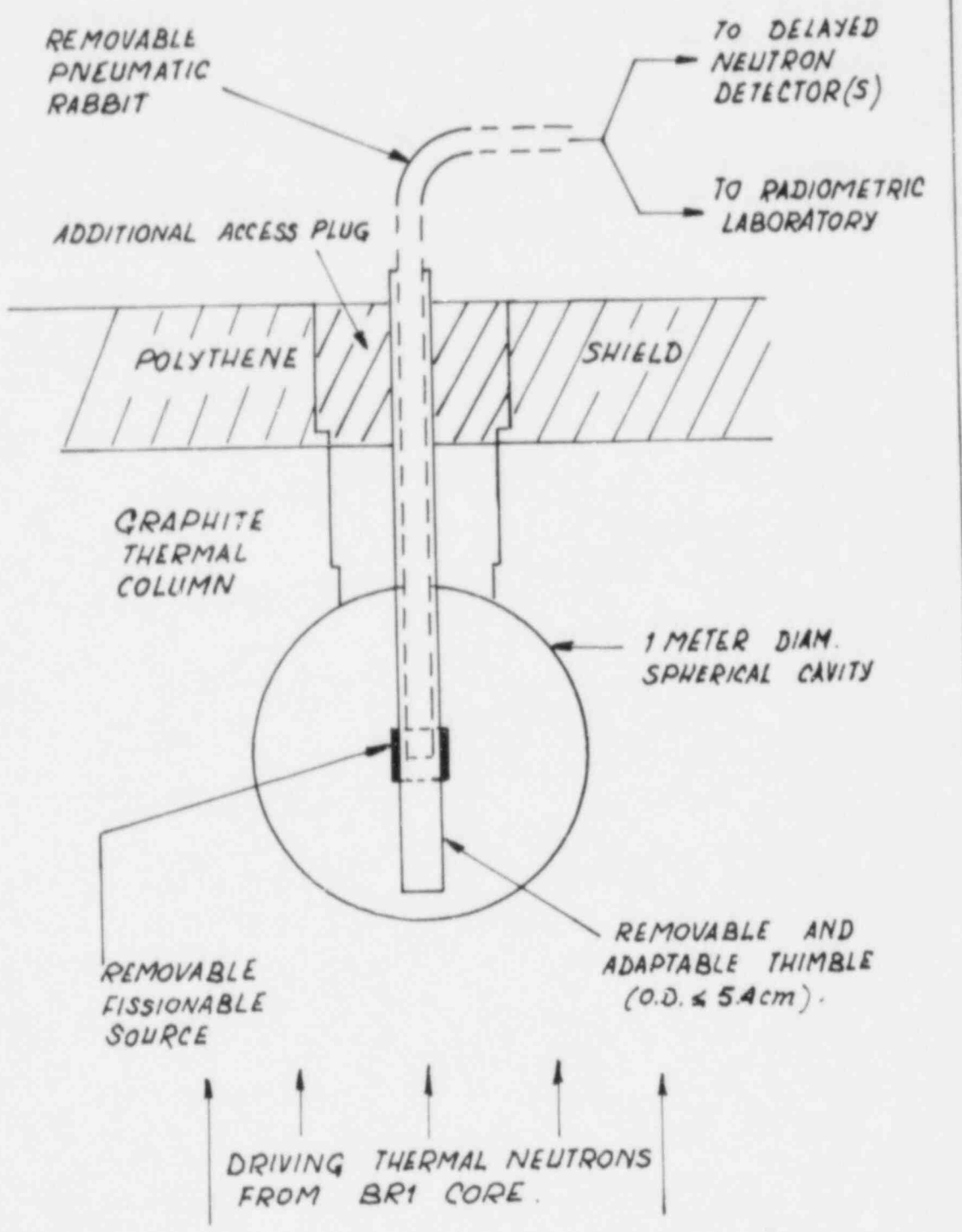

Fig. 1. Schematic Layout of the MOL Cavity Fission Spectrum Standard Neutron Field.

MODEL NUMBER	$2R_0$ (mm)	$2Z_0$ (mm)	ΔR (mm)	SOURCE (n/sec)*	CENTRAL FLUX ($cm^{-2}sec^{-1}$)*
I	10.0	68.0	0.1	5.0,+9	3.2,+8
II	33.0	77.0	0.1	1.3,+10	2.0,+8
III	52.5	79.5	0.4	1.0,+11	7.5,+8

* 1MW REACTOR POWER

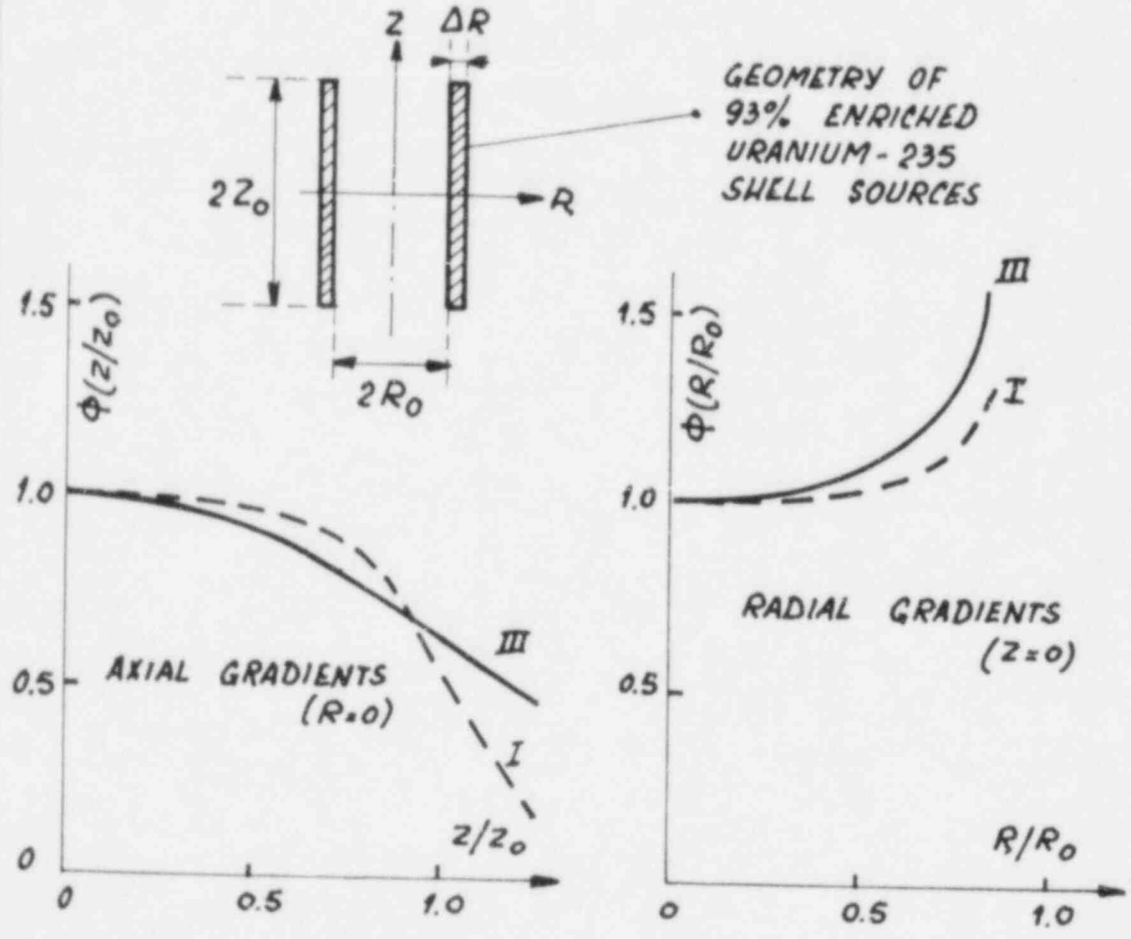

Fig. 2. Basic Parameters of the Available Neutron Sources.

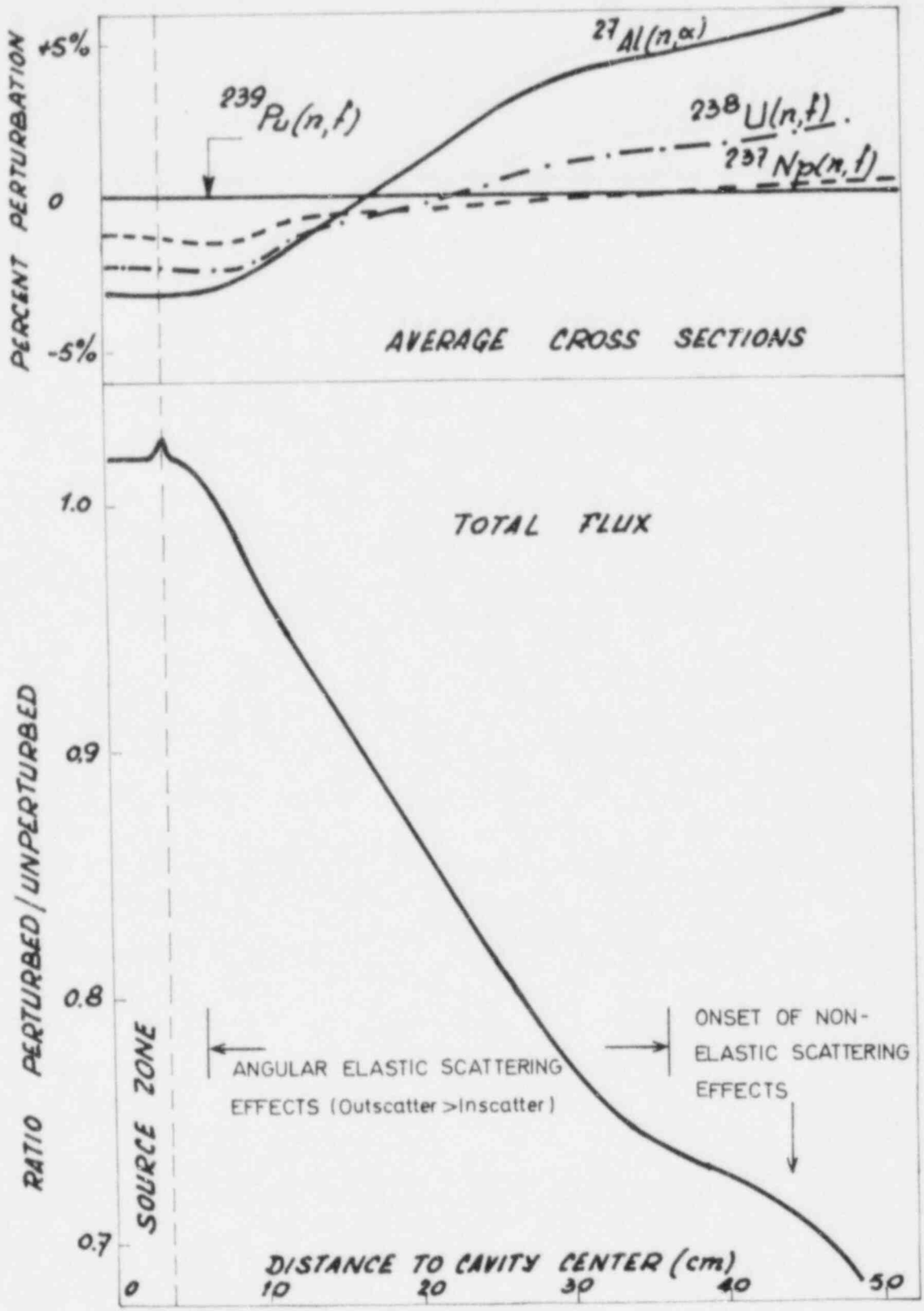

Fig. 3. Neutron Field Perturbation by Structural Cadmium Thimble.

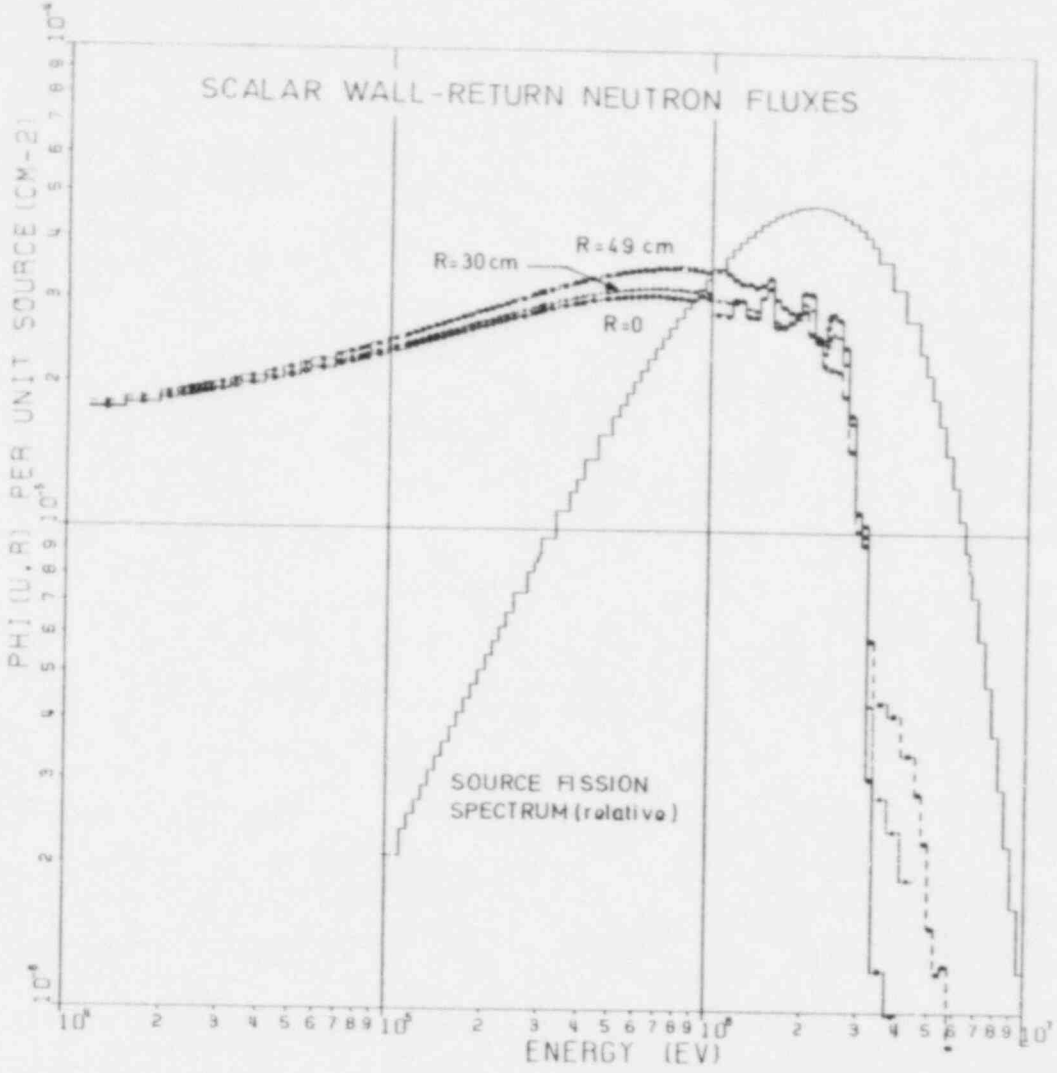

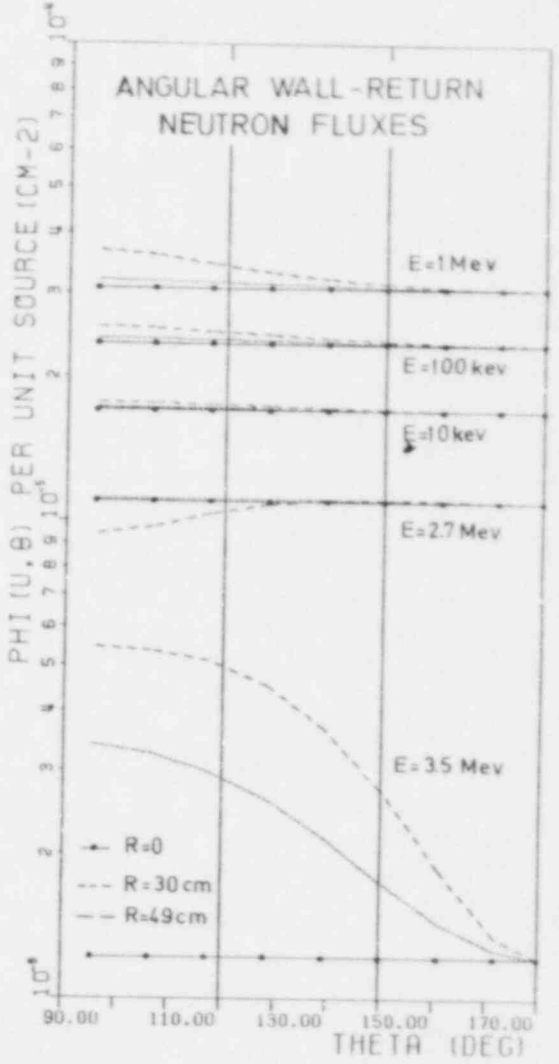

Fig. 4. One-dimensional S16P3 Calculation Results of Graphite Wall-Return Neutron Spectra in MOL one-meter Cavity Fission Spectrum Standard Neutron Field.

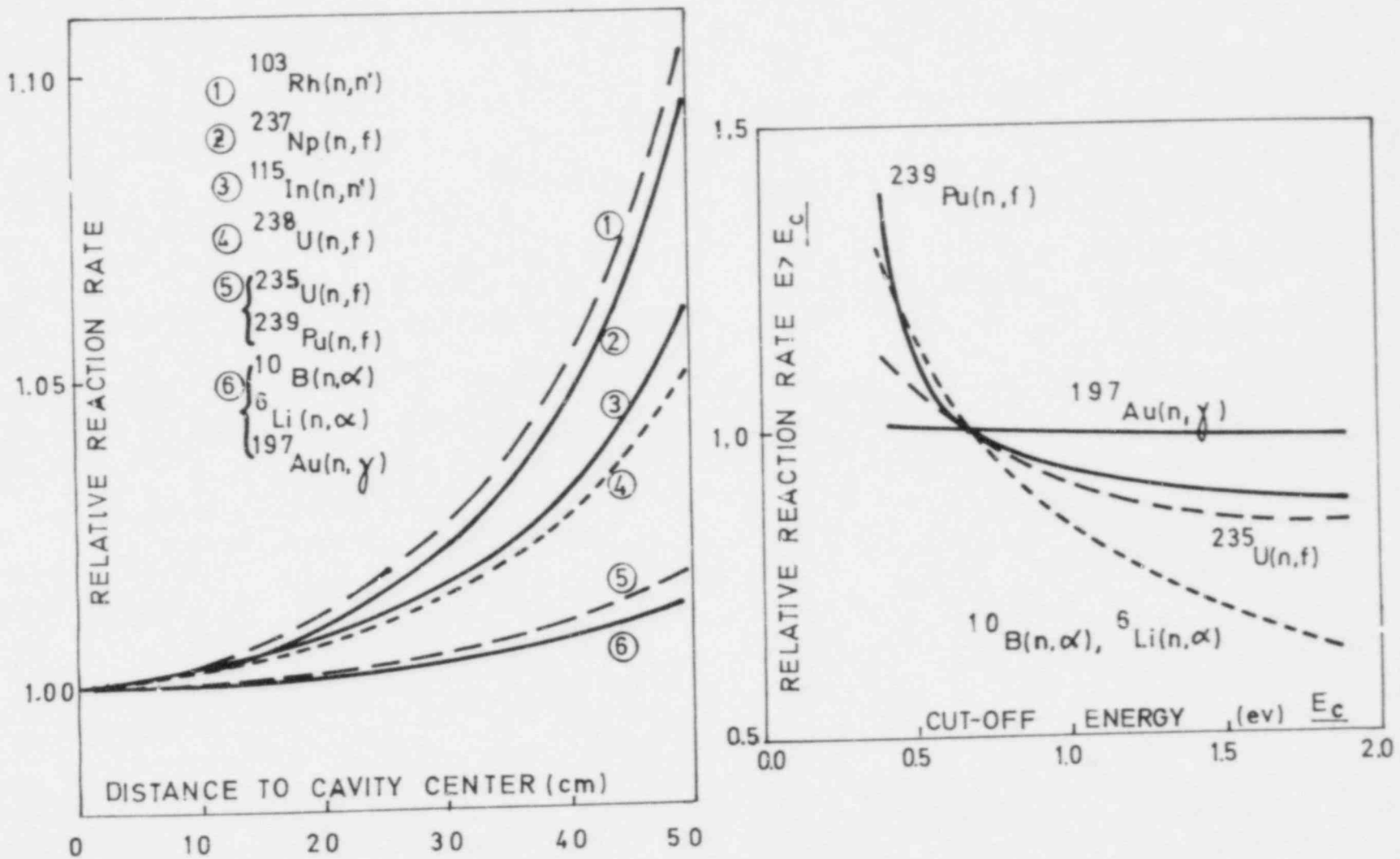

Fig. 5. Radial variation of Cavity Wall Return Neutronic Responses and Sensitivity to Cadmium cut-off Energy (No upscattering).

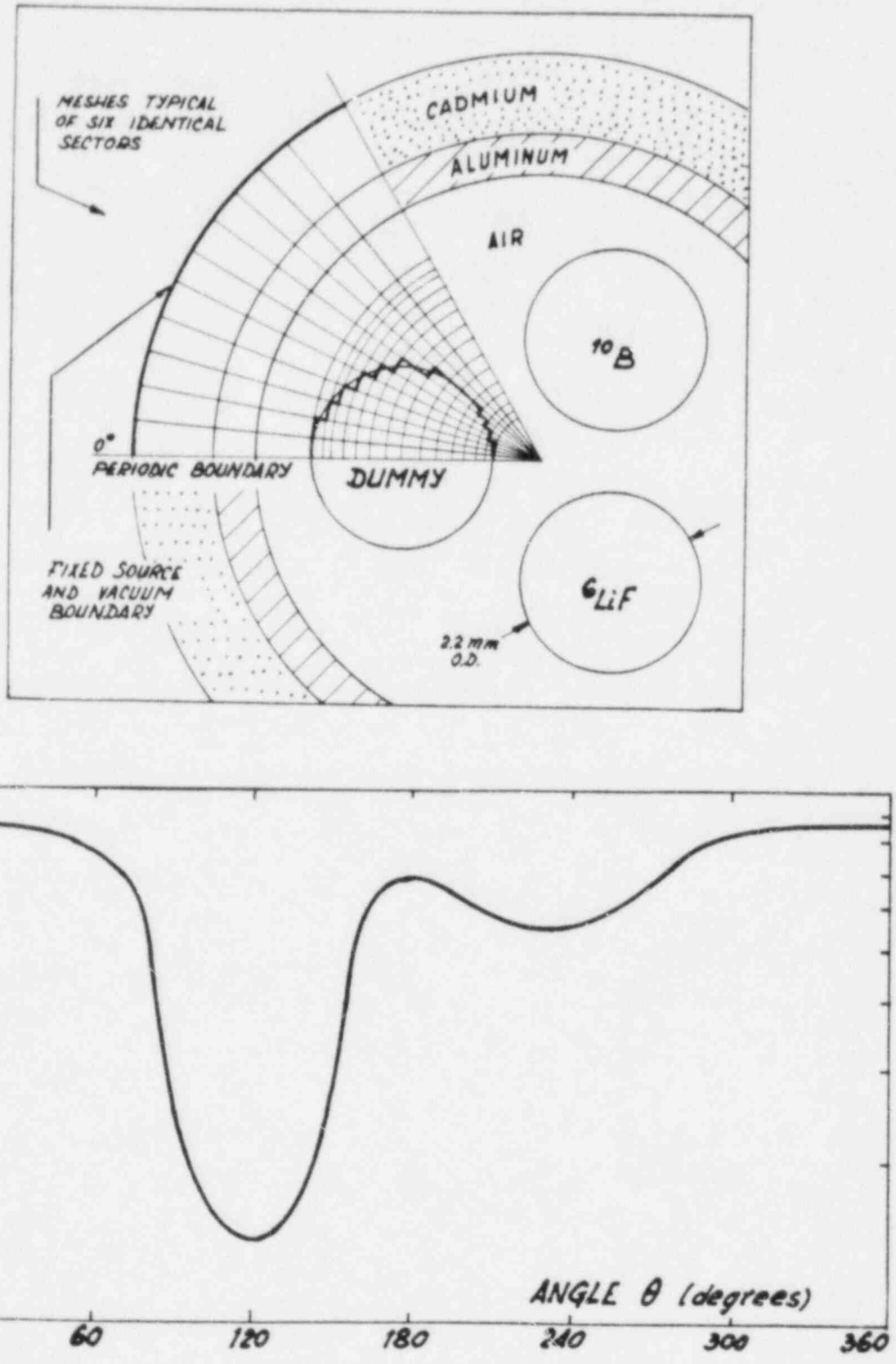

Fig. 6. Two-dimensional (R,θ) Modelling and S12P3 Calculation Results of the Circumferential $^{6}Li(n,\alpha)$ and $^{10}B(n,\alpha)$ Reaction Rate Perturbation along a Radius through the Centerline of the Experimental Capsules.

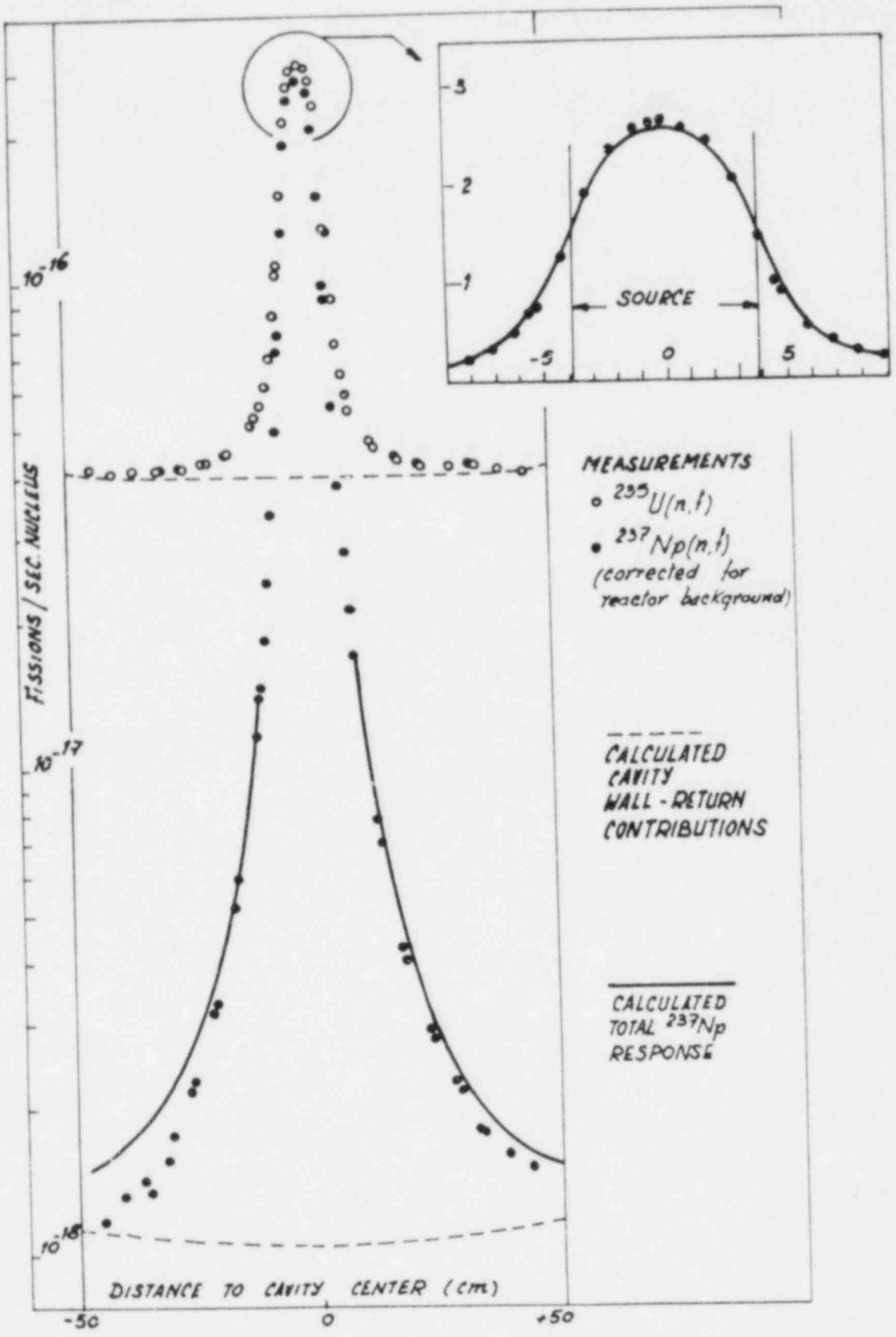

Fig. 7. Vertical Reaction-Rate Traverses in MOL one-meter Cavity Fission Spectrum Standard Neutron Field (Reactor background corrected, 1 MW Power and Model II Source).

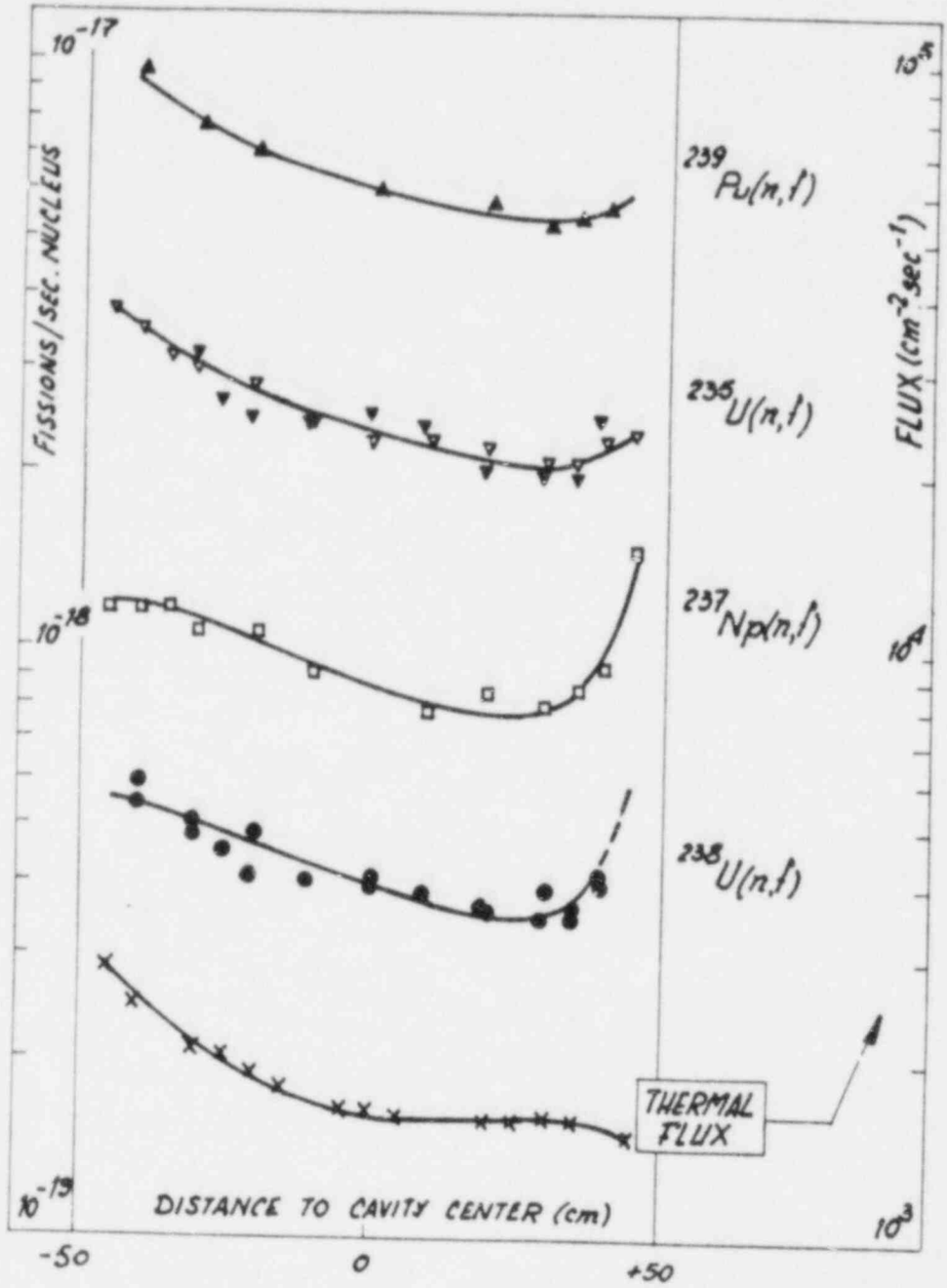

Fig. 8. Vertical Reaction-Rate and Thermal Neutron Flux Traverses in the Background Radiation Field of the MOL one-meter Cavity Model II Cadmium Thimble (No source, 1 MW Power).

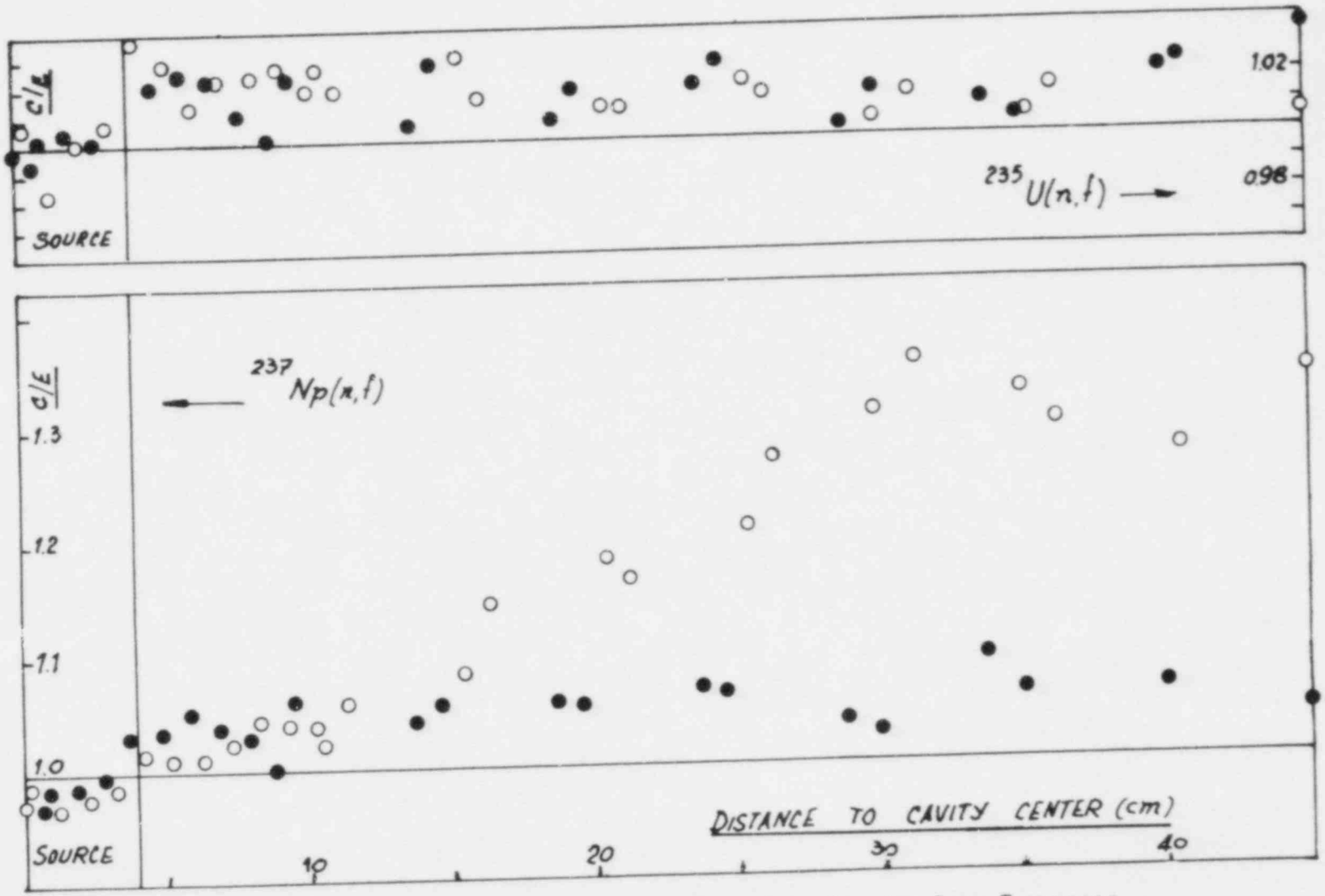

Fig. 9. Comparison between Calculated and Measured Absolute Fission Rate Traverses (Open symbols : From source towards reactor core. Full symbols : From source towards reactor top and shield).

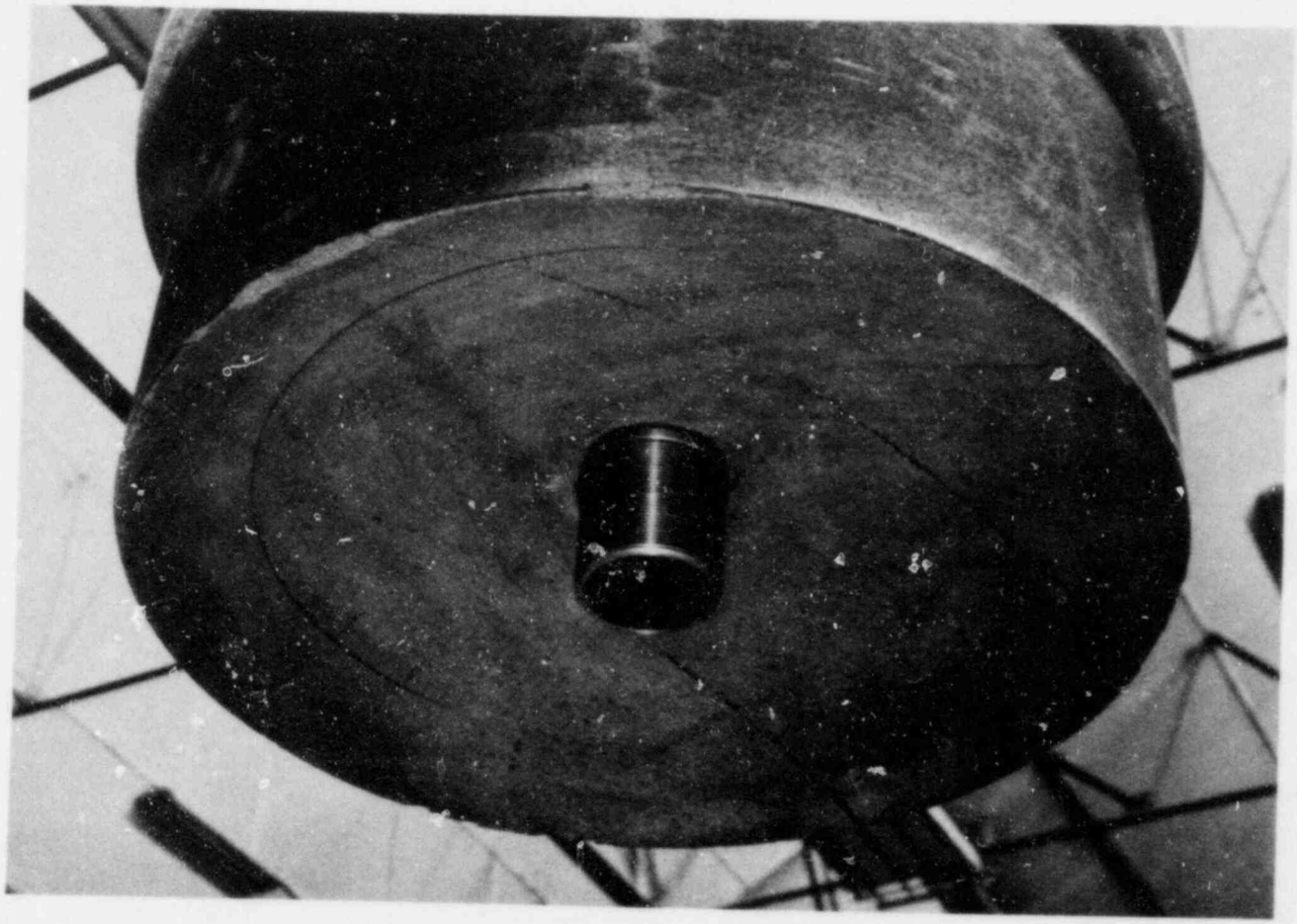

Fig. 10. Photograph of the steel sleeve perturbing high-energy wall-return neutron spectra at the upper edge of the experimental zone.

APPLICATION OF MOL-CAVITY RADIATION FIELD TO THE VALIDATION OF FAST-NEUTRON ELASTIC-SCATTERING ANGULAR DISTRIBUTIONS : GRAZING-ANGLE TRANSMISSION EXPERIMENTS "GATE"

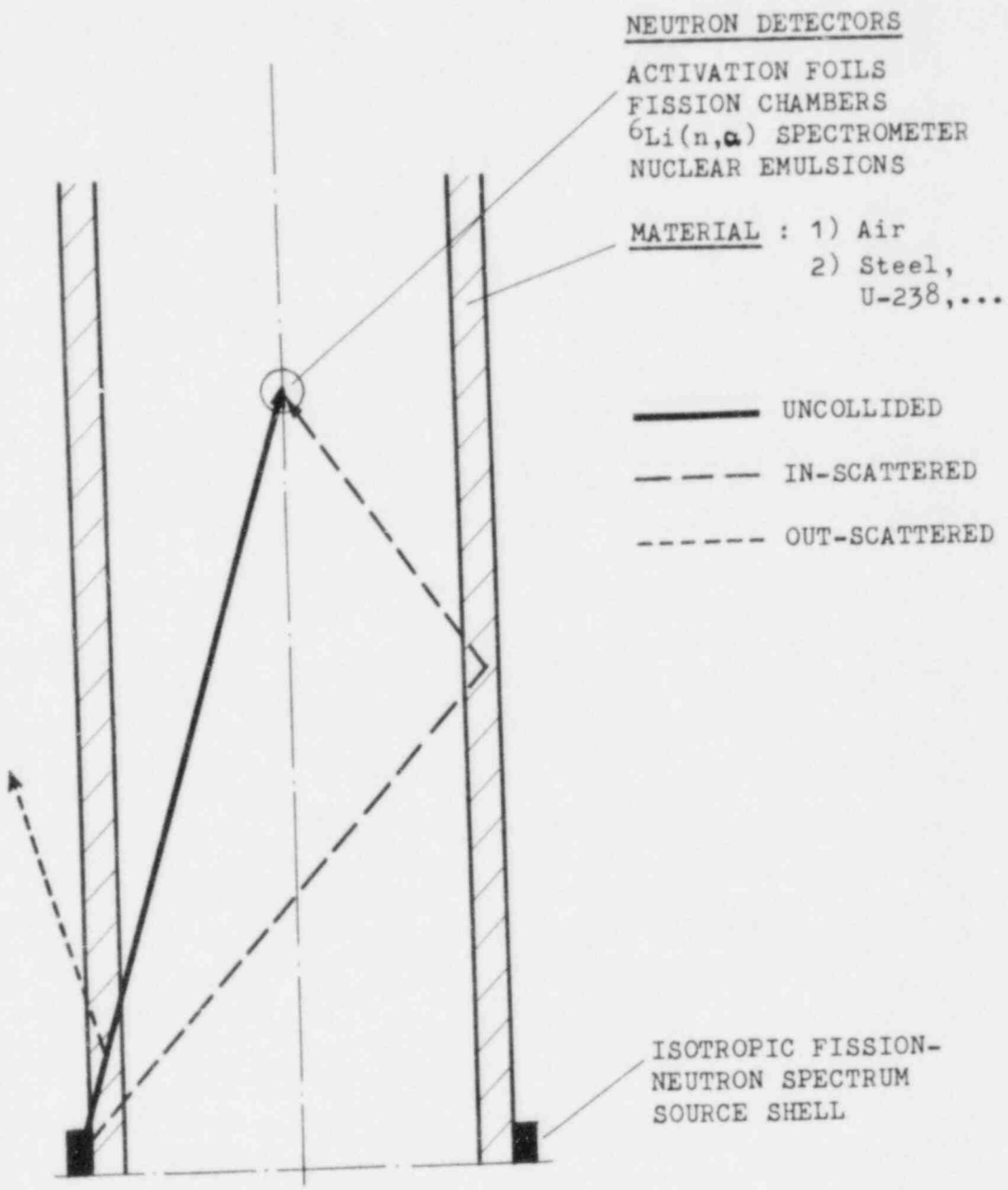

Fig. 11. Conceptual Illustration of a Two-Dimensional (R,Z) Experimental Geometry Complementary to the BETHE-BEYSTER-CARTER Spherical Shell Transmission Geometry of the MOL-ΣΣ Type Uranium and Iron Benchmark Fields.

APPLICATION OF MDL-CAVITY RADIATION FIELD TO NUCLEAR REACTOR GAMMA-RAY METROLOGY STANDARDIZATION

I. CONCEPT OF ISOTROPIC REACTOR GAMMA-RAY PRIMARY-STANDARD FIELD

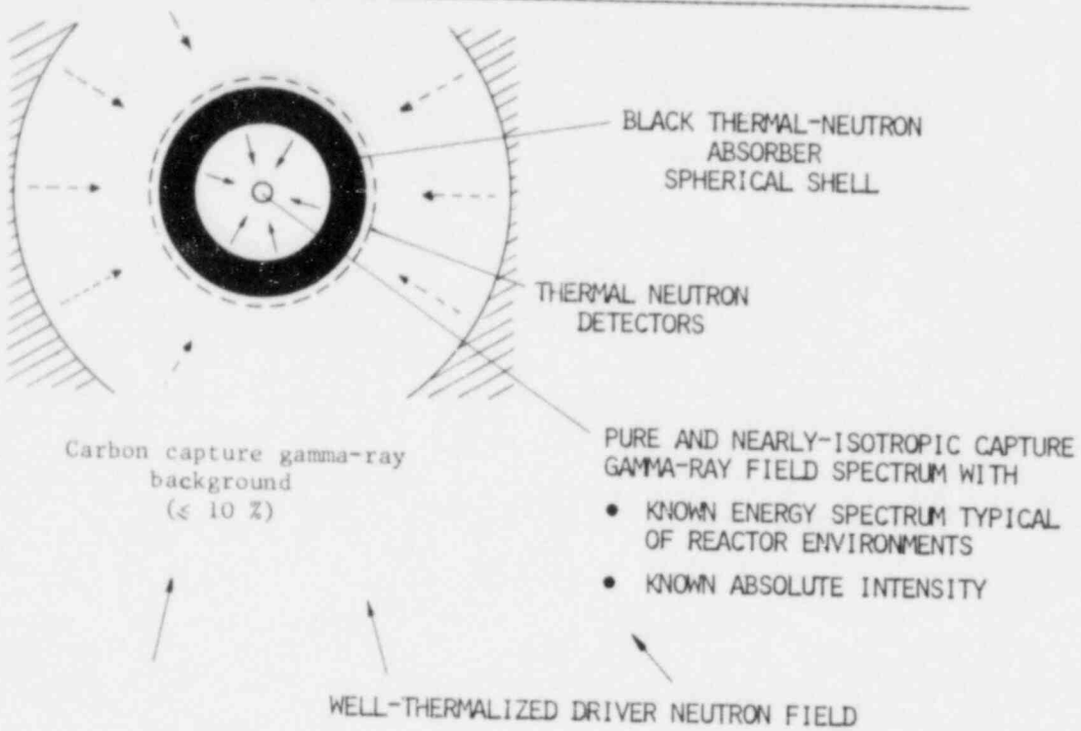

II. SECONDARY MIXED GAMMA-NEUTRON REFERENCE FIELDS

THE CYLINDRICAL-SOURCE FISSION-SPECTRUM NEUTRON FIELD CONCEPT OFFERS INEXPENSIVE AND ADEQUATE FLEXIBILITY TO GENERATE A VARIETY OF CONTROLABLE RADIATION ENVIRONMENTS

- FROM A NEARLY-INFINITE CYLINDER GEOMETRY VERSION OF I (AMENABLE TO γ-FLUX TRANSFER AND ELEMENTARY ANALYSIS)
- TO BENCHMARKS WITH VARIABLE (FAST/EPITHERMAL/THERMAL) NEUTRON TO-GAMMA FLUX RATIOS UNDER KNOWN SPECTRAL CONDITIONS

FIG. 12

SUPPLEMENTARY NEUTRON FLUX CALCULATIONS FOR THE ORNL POOL CRITICAL ASSEMBLY PRESSURE VESSEL FACILITY*

P. J. Maudlin
Los Alamos Scientific Laboratory
Los Alamos, New Mexico, USA
R. E. Maerker
Oak Ridge National Laboratory
Oak Ridge, Tennessee, USA

ABSTRACT

A three-dimensional Monte Carlo calculation using the MORSE code was performed to validate a procedure previously adopted in the ORNL discrete ordinate analysis of measurements made in the ORNL Pool Critical Assembly Pressure Vessel Facility. The results of these flux calculations agree, within statistical uncertainties of about 5%, with those obtained from a discrete ordinate analysis employing the same procedure. This study therefore concludes that the procedure for combining several one-and two-dimensional discrete ordinate calculations into a three-dimensional flux is sufficiently accurate that it does not account for the existing discrepancies observed between calculations and measurements in this facility.

INTRODUCTION

The Pool Critical Assembly Pressure Vessel Facility (PCA-PVF) was instituted to serve as a benchmark facility for validating calculational procedures in predicting neutron fluences in reactor pressure vessels for estimation of damage.[1] A description of the various calculations carried out for the PCA-PVF by an international group of analysts has been documented.[2,3] An underprediction (10 to 20%) seems to persist throughout a majority of the calculation-versus-experimental comparisons, and the source of this discrepancy is presently a point of speculation and controversy.

With one exception, all the analysts used one-and two-dimensional discrete ordinate transport methods and combined them in some way. The one exception used a continuous energy forward Monte Carlo method with importance sampling and biasing to perform a three dimensional calculation, but unfortunately the results had fairly large statistical uncertainties at times.[2,3]

*This work was sponsored by the Electric Power Research Institute under research project 1399-1, under Union Carbide Corporation contract W-7405-eng-26 with U.S. Department of Energy.

A tenable procedure first suggested by Combustion Engineering[2,3] and adopted by Oak Ridge[2-6] for scaling the discrete ordinate calculations may be summarized by the following flux synthesis equation:

$$\phi(x,y,z,E,\vec{\Omega}) \cong \phi(x,y,E,\vec{\Omega})\phi(y,z,E,\vec{\Omega})/\phi(y,E,\vec{\Omega}), \quad (1)$$

or, more conveniently,

$$\phi_{XYZ} \cong \phi_{XY}\,[\phi_{YZ}/\phi_{Y}] \quad (2)$$

where in the present application the accuracy of this approximation needs only to be evaluated at locations along the y-axis (i.e., for x=z=0 in Fig. 2 appearing in next section). Equation (2) states that a three-dimensional flux, ϕ_{XYZ}, can be constructed from two two-dimensional calculations, ϕ_{XY} and ϕ_{YZ}, and a one-dimensional calculation, ϕ_{Y}, by simply scaling the ϕ_{XY} calculation by a properly normalized z-correction term appearing in the brackets. The ϕ_{XY}, ϕ_{YZ}, and ϕ_{Y} calculations have geometry of infinite extent in the z-direction, x-direction and x,z-directions respectively. An inspection of Eq.(2) shows that the assumption underlying this particular flux synthesis is that the vertical (i.e.,z) flux profiles are the same for all x locations, i.e., the three-dimensional fluxes are separable in x and z.

In the PCA-PVF calculations, the source per unit height for the midplane XY calculation is normalized in such a way that when integrated over x, y, and z yields a value of unity (i.e., there is one fission neutron in the core). The effects of finite z essentially arise as a result of a source limited to the height of the core and with a measured cosine distribution peaking in the vicinity of the centerline. The normalization of the source distribution in z for the ϕ_{YZ} calculation relative to the source per unit height for the ϕ_{Y} calculation, with the ϕ_{XY} source the midplane source as described above, must be set equal to the ratio of the average to the midplane values as pictured in Fig. 1.

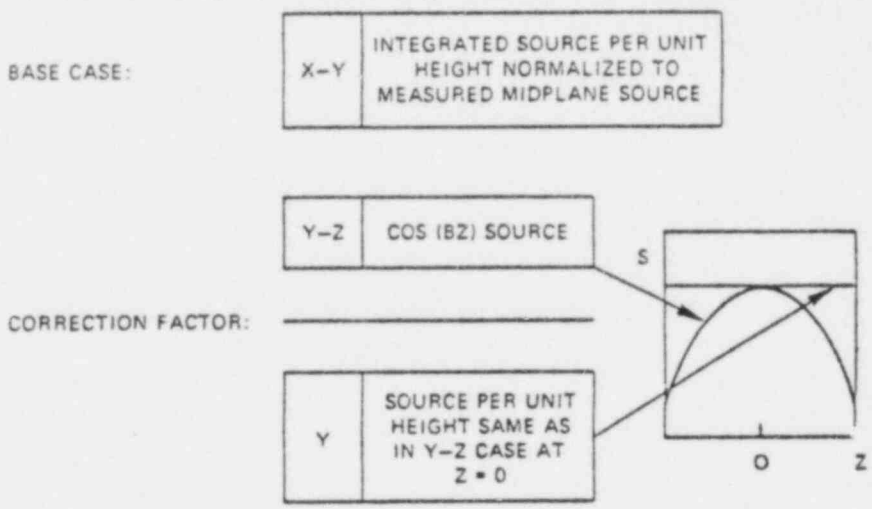

Fig. 1. Correcting Two-Dimensional Calculations for Finite Core Height and Measured Fission Density Distribution.

The object of this work is to evaluate the accuracy of Eq. (2) by calculating directly the three-dimensional flux ϕ_{XYZ} via a Monte Carlo transport code and to compare these results with the flux approximated by the right hand side of Eq. (2). For this purpose, the multigroup Monte Carlo code MORSE[7] was used to calculate ϕ_{XYZ} and the DOT-IV[8] discrete ordinates code was used to calculate ϕ_{XY}, ϕ_{YZ}, and ϕ_{Y}.

PHYSICAL DESCRIPTION OF THE PCA-PVF

The PCA-PVF was designed to simulate within intensity constraints the geometry and arrangement of materials that exist within a commercial pressurized water reactor pressure vessel. The geometry illustrated in Fig. 2 shows the locations of the PCA core, aluminum window (in analogy to the geometry of the Poolside Facility (PSF) in which high intensity measurements using the ORR were also performed), appropriate water gaps, and steel slabs representing the thermal shield and pressure vessel wall. This geometry is a slight simplification of the actual configuration, but should not compromise the present analysis. Values of 8.4 and 6.7 cm. respectively for the large water gap dimensions in Fig. 2 were used in this analysis. This "8/7 configuration" was chosen over the "12/13 configuration," which was more extensively measured, to reduce the statistical uncertainties in the MORSE calculations.

A reflective boundary condition exists on the left face of the core (i.e., the xz plane at y=0), and a vacuum boundary condition exists on the right face of the pressure vessel in Fig. 2 (i.e., the xz plane at y=66.7 cm). All remaining slab faces are reflected with water.

Seven neutron flux detectors designated D1 through D7, with coordinates as shown in Fig. 2, include all the locations along the y-axis where measurements were made along with the additional ones D2 and D4.

The spatial zones in Fig. 2 are identified by the cross-section medium numbers M1 through M8. In the pressure vessel there are three sets of cross sections, each weighted over a different region of the carbon steel with fluxes from a one-dimensional discrete ordinates calculation. Similarly, the two large water gaps have slightly different cross sections.

The fixed neutron source distribution has been documented,[2,3] and for the present purposes can be approximated as

$$S_{XYZ}(x,y,z) = S_{XY}(x,y) \cos(.0442z), \quad -30\text{cm} \leq z \leq 30\text{cm}, \tag{3}$$

where $S_{XY}(x,y)$ has quarter core symmetry and appears in Fig. 3. The average to centerline value for the z distribution in Eq. (3), which is the relative normalization of the ϕ_{YZ} to ϕ_{Y} calculations, becomes

ORNL-DWG 80-20107

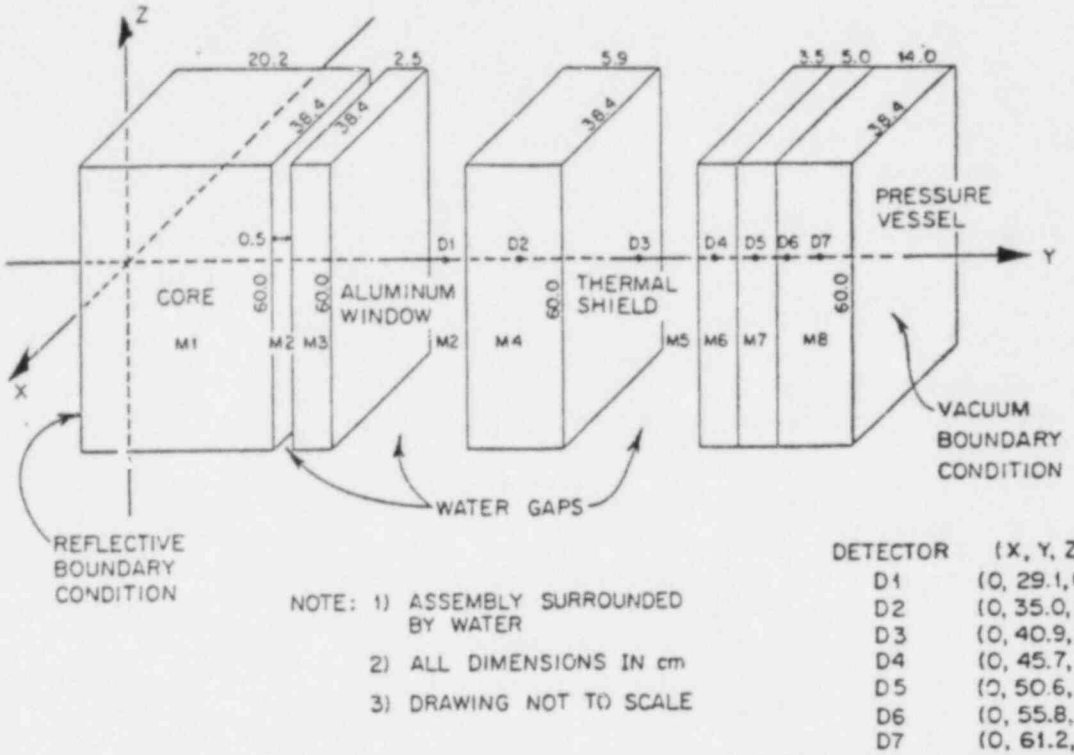

NOTE: 1) ASSEMBLY SURROUNDED BY WATER
2) ALL DIMENSIONS IN cm
3) DRAWING NOT TO SCALE

DETECTOR	(X, Y, Z)
D1	(0, 29.1, 0)
D2	(0, 35.0, 0)
D3	(0, 40.9, 0)
D4	(0, 45.7, 0)
D5	(0, 50.6, 0)
D6	(0, 55.8, 0)
D7	(0, 61.2, 0)

Fig. 2. Modeling Geometry for the Pool Critical Assembly Pressure Vessel Facility. For the 8/7 Configuration, the two Large Water Gaps are 8.4-and 6.7-cm. wide respectively.

ORNL-DWG 80-20106

x (cm)	y (cm) 0	1.3	2.2	3.1	4.0	5.1	6.2	7.0	7.8	8.8	9.4	10.3	11.2	12.1	13.2	14.3	15.1	15.9	16.7	17.5	18.4	19.3	20.2
18.8	1.79	1.82	1.82	1.82	1.69	1.69	1.69	1.69	1.69	1.69	1.49	1.49	1.49	1.32	1.32	1.12	1.12	1.12	1.12	0.99	0.99	0.99
17.7	1.79	1.82	1.82	1.82	1.69	1.69	1.69	1.69	1.69	1.69	1.49	1.49	1.49	1.32	1.32	1.12	1.12	1.12	1.12	0.99	0.99	0.99
16.6	1.70	1.70	1.70	1.67	1.59	1.59	1.55	1.55	1.55	1.55	1.37	1.37	1.37	1.22	1.22	1.05	1.05	1.05	1.05	0.96	0.96	0.96
15.1	1.70	1.70	1.70	1.67	1.59	1.59	1.55	1.55	1.55	1.55	1.37	1.37	1.37	1.22	1.22	1.05	1.05	1.05	1.05	0.96	0.96	0.96
14.3	1.87	1.87	1.87	1.87	1.86	1.86	1.91	1.91	1.91	1.91	1.69	1.69	1.69	1.48	1.48	1.16	1.16	1.16	1.16	1.11	1.11	1.11
12.1	0	0	0	0	0	0	0	0	0	0	0	0	0	0	0	0	0	0	0	0	0	0
11.0	2.66	2.74	2.74	2.74	2.80	2.80	0	0	0	0	0	2.19	2.19	1.69	1.69	1.35	1.35	1.35	1.35	1.24	1.24	1.24
8.9	2.66	2.91	2.91	2.91	3.07	3.07	0	0	0	0	0	2.38	2.38	1.79	1.79	1.42	1.42	1.42	1.42	1.29	1.29	1.29
6.5	2.96	3.07	3.07	3.07	3.26	3.26	0	0	0	0	0	2.50	2.50	1.94	1.94	1.50	1.50	1.50	1.50	1.39	1.39	1.39
4.4	0	0	0	0	0	0	0	0	0	0	0	0	0	0	0	0	0	0	0	0	0	0
3.3	2.50	2.53	2.53	2.53	2.51	2.51	2.58	2.58	2.58	2.58	2.21	2.21	2.21	1.94	1.94	1.57	1.57	1.57	1.57	1.46	1.46	1.46
1.2	2.54	2.57	2.57	2.57	2.40	2.40	2.32	2.32	2.32	2.32	2.03	2.03	2.03	1.85	1.85	1.56	1.56	1.56	1.56	1.41	1.41	1.41
0																							

Fig. 3. Quarter Core Midplane Fission Neutron Source Distribution in Units of 10^{-5} neutrons per second per $cm.^3$

$$\frac{\bar{S}_{YZ}}{S_Y} = \frac{\int_{-30}^{30} \cos(.0442z)dz}{\int_{-30}^{30} dz} = 0.7317. \qquad (4)$$

CALCULATIONAL DETAILS

An adequate comparison of the results from the two methods should not be strongly influenced by the particular cross section sets used, as long as they are the same in each method. Consequently, although the original discrete ordinate calculations employed 51 and 171 groups, these comparison calculations were performed with only 12 groups, the energy structure for which is shown in Table 1. Note that the energy range is sufficient to encompass all threshold reaction rates measured in the PCA-PVF. Details of the generation of this cross section library are described elsewhere.[4,9] Note also that the 12-group discrete ordinate calculations described here are not in any direct way connected with the 51-group DOT calculations used in the PCA-PVF analysis by ORNL.[2-6]

TABLE 1. NEUTRON GROUP STRUCTURE AND SOURCE ENERGY DISTRIBUTION

GROUP	UPPER ENERGY (eV)	SOURCE FRACTION[a]
1	1.9640E 07	5.5841E-04
2	1.1052E 07	4.7115E-03
3	8.1873E 06	2.0686E-02
4	6.0653E 06	8.1625E-02
5	4.0657E 06	1.0943E-01
6	3.0119E 06	6.6245E-02
7	2.5924E 06	9.4196E-02
8	2.1225E 06	7.1393E-02
9	1.8268E 06	9.1620E-02
10	1.4957E 06	8.3815E-02
11	1.2246E 06	1.0632E-01
12	9.0718E 05	1.0401E-01
	6.0810E 05	

[a]DERIVED FROM THE ENDF/B-V WATT THERMAL FISSION SPECTRUM FOR ^{235}U.

Although the calculation of the denominator in Eq. (2) is one-dimensional, the use of the two-dimensional code DOT to calculate ϕ_Y by inserting appropriate reflecting surfaces is preferable to the use of a one-dimensional code for this purpose because it preserves the same angular quadrature as is used in the calculation of the numerator ϕ_{YZ}.

The PCA-PVF problem features a large neutron source volume emitting neutrons which impinge upon essentially point detectors at locations D1 through D7 in Fig. 2. The penetration distance from the core to detector

D7 is of the order of 10 mean free paths for 2 MeV neutrons. Running MORSE in the forward mode with next flight statistical estimators is prohibitively expensive without the application of sophisticated biasing techniques. The use of boundary crossing or finite detector volume estimators reduces the expense substantially, but yields troublesome averaged fluxes rather than point fluxes. On the other hand, running MORSE in the adjoint mode not only permits the use of a track length estimator which scores over the entire core volume, but also avoids the singularity and associated poor statistics inherent in a point detector estimator. The disadvantage of using the adjoint mode is that a separate calculation is required for each detector location and, for reliable statistics, for each energy group as well. However, for the PCA-PVF problem the advantages of operating in the adjoint mode far outweigh the disadvantages. Hence, operating in the adjoint mode with only standard biasing techniques (i.e., Russian roulette, splitting, and pathlength stretching) was selected as the method for calculating the three-dimensional fluxes.

RESULTS

The units chosen for the fluxes (really fluences) presented in this section are neutrons per square centimeter per source neutron emitted from a cubic centimeter of the core. This particular normalization arises naturally from the Monte Carlo scoring procedure over the core volume as well as from treating the use of infinite dimensions in the DOT calculations. Multiplication of these results by the space-averaged neutron source density (in units of neutrons per second per cubic centimeter) would yield absolute fluxes.

Before Eq. (2) was tested, the presence of any possible bias in one method relative to the other was first investigated. Both MORSE and DOT were applied to identical one-dimensional and two-dimensional problems for several detectors. Table 2 shows a comparison of the total fluxes (group fluxes summed over all twelve groups) calculated with DOT (columns two through four) and with MORSE (columns five through seven). The uncertainties in the MORSE results represent one standard deviation, and are, of course, only themselves estimates. The comparisons shown in Table 2 are consistent with the fact that roughly 2/3 of the MORSE fluxes fall within one standard deviation of the DOT results. Although there is perhaps evidence of a small but unimportant bias, Table 2 serves to validate the equivalence of the two methods and provides confidence in the three-dimensional comparisons that follow.

TABLE 2. NEUTRON FLUX COMPARISONS BETWEEN DOT-IV AND ADJOINT MORSE CALCULATIONS FOR NEUTRONS ABOVE 0.6 MeV

DETECTOR	DOT-IV FLUXES[a]			ADJOINT MORSE FLUXES[a]		
	ϕ_{XY}	ϕ_{YZ}	ϕ_Y	ϕ_{XY}	ϕ_{YZ}	ϕ_Y
D1	0.775	0.804	0.827	0.786 ± 0.6%[b]	0.815 ± 0.8%[b]	0.947 ± 1.7%[b]
D2	0.414	0.435	0.522			
D3	9.40×10^{-2}	9.96×10^{-2}	0.124		9.96×10^{-2} ± 1.9%	0.124 ± 5.8%
D4	5.96×10^{-2}	6.51×10^{-2}	6.55×10^{-2}			
D5	3.86×10^{-2}	4.51×10^{-2}	5.70×10^{-2}	3.96×10^{-2} ± 3.0%	4.35×10^{-2} ± 3.7%	6.54×10^{-2} ± 5.2%
D6	2.15×10^{-2}	2.36×10^{-2}	3.38×10^{-2}	2.27×10^{-2} ± 4.6%		
D7	1.12×10^{-2}	1.23×10^{-2}	1.82×10^{-2}	1.16×10^{-2} ± 5.6%	1.38×10^{-2} ± 7.4%	2.19×10^{-2} ± 8.3%

[a]UNITS: NEUTRONS/cm^2/(SOURCE NEUTRON/cm^3) FOR ϕ_{XY} AND ϕ_Y, AND NEUTRONS/cm^2/(0.7317 SOURCE NEUTRONS/cm^3) FOR ϕ_{YZ}.
[b]UNCERTAINTIES ARE ONE σ.

In Table 3 MORSE calculated three-dimensional total fluxes are compared with the synthesized discrete ordinate values given by Eq. (2) for each detector. The relative disagreements between the two results (MORSE-DOT/DOT) are given in the last column, along with estimates of the standard deviations of the Monte Carlo results. As indicated by this column, the disagreement between the two methods is quite small - the largest being about 5%. Furthermore, these differences do not exhibit any particular trend as a function of detector location. It is true that there is evidence of a slight bias in the synthesized flux procedure (the MORSE results are slightly larger) but it is no greater than the small bias that can be ignored in the earlier comparisons in Table 2.

TABLE 3. THREE-DIMENSIONAL FLUX COMPARISONS FOR NEUTRONS ABOVE 0.6 MeV

DETECTOR	ADJOINT MORSE[a] ϕ_{XYZ}	DOT-IV CONSTRUCTION[a] $\phi_{XY}(\phi_{YZ}/\phi_Y)$	RELATIVE ERROR (%)
D1	0.682 ± 0.5%[b]	0.672	1.5 ± 0.5[b]
D2	0.346 ± 0.8%	0.345	0.3 ± 0.8
D3	7.77×10^{-2} ± 1.1%	7.55×10^{-2}	2.9 ± 1.1
D4	4.74×10^{-2} ± 1.3%	4.54×10^{-2}	4.4 ± 1.4
D5	2.85×10^{-2} ± 2.1%	2.81×10^{-2}	0.7 ± 2.1
D6	1.58×10^{-2} ± 3.4%	1.50×10^{-2}	5.3 ± 3.6
D7	7.53×10^{-3} ± 3.5%	7.57×10^{-3}	−0.5 ± 3.5

[a]UNITS: neutrons/cm^2/(source neutron/cm^3).
[b]UNCERTAINTIES ARE ONE σ.

Calculated one-and two-dimensional group fluxes using DOT are shown in Table 4 for detector D5 which corresponds to the "T/4" location. A summation over groups of these fluxes would yield the total flux values

for detector D5 in Table 2. The DOT fluxes from Table 4 are then combined using Eq. (2) to form the various group fluxes which are then com-

TABLE 4. DOT-IV NEUTRON GROUP FLUXES AT DETECTOR D5

ENERGY GROUP	DOT-IV FLUXES[a] ϕ_{XY}	ϕ_{YZ}	ϕ_{Y}
1	2.17×10^{-5}	2.23×10^{-5}	3.15×10^{-5}
2	1.41×10^{-4}	1.45×10^{-4}	2.10×10^{-4}
3	4.77×10^{-4}	4.95×10^{-4}	6.72×10^{-4}
4	1.31×10^{-3}	1.38×10^{-3}	1.83×10^{-3}
5	1.42×10^{-3}	1.51×10^{-3}	1.98×10^{-3}
6	1.37×10^{-3}	1.46×10^{-3}	1.93×10^{-3}
7	2.69×10^{-3}	2.87×10^{-3}	3.79×10^{-3}
8	1.99×10^{-3}	2.13×10^{-3}	2.82×10^{-3}
9	3.55×10^{-3}	3.81×10^{-3}	5.08×10^{-3}
10	3.82×10^{-3}	4.10×10^{-3}	5.47×10^{-3}
11	7.38×10^{-3}	7.98×10^{-3}	1.09×10^{-3}
12	1.44×10^{-2}	1.56×10^{-2}	2.21×10^{-2}

[a]UNITS: neutrons/cm^2/(SOURCE neutron/cm^3) FOR ϕ_{XY} AND ϕ_{Y}, AND neutrons/cm^2/(0.7317 SOURCE neutron/cm^3) FOR ϕ_{YZ}.

pared with the MORSE results in Table 5. (The summation over groups of the synthesized group fluxes appearing in Table 5 is the value 2.81×10^{-2} for detector D5 shown in Table 3). The synthesized group

TABLE 5. THREE-DIMENSIONAL GROUP FLUX COMPARISONS AT DETECTOR D5

ENERGY GROUP	ADJOINT MORSE[a] ϕ_{XYZ}	DOT-IV CONSTRUCTION[a] $\phi_{XY}(\phi_{YZ}/\phi_{Y})$	RELATIVE ERROR (%)
1	$1.56 \times 10^{-5} \pm 3.0\%$[b]	1.54×10^{-5}	1.3 ± 3.0[b]
2	$1.04 \times 10^{-4} \pm 1.9\%$	1.02×10^{-4}	2.0 ± 1.9
3	$3.62 \times 10^{-4} \pm 3.5\%$	3.51×10^{-4}	3.1 ± 3.6
4	$9.97 \times 10^{-4} \pm 2.9\%$	9.88×10^{-4}	0.9 ± 2.9
5	$1.07 \times 10^{-3} \pm 3.7\%$	1.08×10^{-3}	-0.9 ± 3.7
6	$9.83 \times 10^{-4} \pm 3.6\%$	1.04×10^{-3}	-5.5 ± 3.4
7	$1.99 \times 10^{-3} \pm 2.4\%$	2.04×10^{-3}	-2.4 ± 2.3
8	$1.44 \times 10^{-3} \pm 2.3\%$	1.50×10^{-3}	-4.0 ± 2.2
9	$2.79 \times 10^{-3} \pm 2.5\%$	2.66×10^{-3}	4.9 ± 2.6
10	$2.69 \times 10^{-3} \pm 2.3\%$	2.86×10^{-3}	-5.9 ± 2.2
11	$4.88 \times 10^{-3} \pm 2.4\%$	5.40×10^{-3}	-9.6 ± 2.2
12	$9.60 \times 10^{-3} \pm 2.2\%$	1.02×10^{-2}	-5.9 ± 2.1

[a]UNITS: neutrons/cm^2/(source neutron/cm^3).
[b]UNCERTAINTIES ARE ONE σ.

fluxes compare well with the MORSE fluxes for the first nine groups (E>1.5MeV), but there is an indication of a small disagreement outside of statistics for the synthesized group fluxes between 0.6 and 1.5 MeV. However, this latter disagreement is still probably due to statistical fluctuations since the total fluxes shown in Table 3 are in agreement when based on an earlier MORSE result.

CONCLUSIONS

Recalling that the object of this study was an evaluation of the accuracy of the flux synthesis method combining the results of three discrete ordinates calculations represented by Eq. (2), the investigations of the previous section clearly validate the use of this approximation over the PCA-PVF space and energy domain studied (i.e., over all y in the 8/7 configuration for x=z=0 and E>0.6 MeV). Based on this conclusion, use of Eq. (2) for somewhat less restrictive domains of x,y, and z and E is most likely justified. In particular, it should apply to the centerline threshold detectors in the 12/13 configuration.

It should further be noted that the combined three-dimensional aspects of the PCA-PVF geometry and source distribution apparently are separable and cancel out using the DOT synthesis of Eq. (2). Hence, the conjecture that any discrepancy between the PCA-PVF measurements and ORNL calculations is most likely due to the neglect of three-dimensional coupling effects, implied by Eq. (2), is shown to be unfounded by the results of this study. Apparently, the source of this discrepancy lies elsewhere.

REFERENCES

1. W. N. McElroy et. al., "LWR Pressure Vessel Surveillance Dosimetry Improvement Program," HEDL SA-1949, Proc. of NRC Seventh Water Reactor Safety Research Information Meeting in Gaithersburg, Maryland, Nov. 5-9, 1979.

2. F. W. Smallman, F. B. K. Kam, J. F. Eastham, and C. A. Baldwin, "Reactor Calculation 'Benchmark' PCA Blind Test Results," ORNL/NUREG/TM-428, Oak Ridge National Laboratory (1981).

3. W. N. McElroy, editor, "LWR Pressure Vessel Surveillance Dosimetry Improvement Program: PCA Experiments and Blind Test," NUREG/CR-1861 HEDL-TME 80-87, R5 Hanford Engineering Development Laboratory (1981).

4. R. E. Maerker, J. J. Wagschal, and B. L. Broadhead, "Development and Demonstration of an Advanced Methodology for LWR Dosimetry Applications," EPRI NP-2188 Project 1399-1 Interim Report (1981).

5. R. E. Maerker, "S_n Transport Calculations of the PCA Experiments with Some Estimated Uncertainties," Trans. Am. Nucl. Soc. 34, 628 (1980).

6. J. J. Wagschal, R. E. Maerker, and B. L. Broadhead, "LWR-PV Damage Estimate Methodology," Proceedings of the Conference 1980 Advances in Reactor Physics and Shielding, Sept. 14-17, Sun Valley, Idaho, pp. 612-624 (1980).

7. M. B. Emmett, "The MORSE Monte Carlo Radiation Transport Code System," ORNL-4972, Oak Ridge National Laboratory (1975).

8. W. A. Rhoades, D. B. Simpson, R. L. Childs, and W. W. Engle, "The DOT-IV Two Dimensional Discrete Ordinates Transport Code with Space-Dependent Mesh and Quadrature," ORNL/TM-6529, Oak Ridge National Laboratory (1979).

9. R. E. Maerker and P. J. Maudlin, "Supplementary Neutron Flux Calculations for the ORNL Pool Critical Assembly Pressure Vessel Facility," ORNL/TM-7602, Oak Ridge National Laboratory (1981).

A BENCHMARK EXPERIMENT FOR NEUTRON TRANSPORT IN IRON, CARBON STEEL AND SODIUM

J. Burian, B. Janský, M. Marek, J. Rataj, M. Tichý
Nuclear Research Institute,
Řež near Prague, Czechoslovakia

ABSTRACT

A description of an experiment providing the verification of the accuracy of the available neutron cross sections for use in transport calculations of the deep penetration of neutrons is presented. The neutron leakage spectra from a set of spheres having different diameters /20, 30, 50 cm for iron, 40, 60, 70 cm for carbon steel, 50, 100 cm for sodium/ with a ^{252}Cf neutron source in the sphere centre were measured. The set of spectrometers consisted of a stilben scintilator, a hydrogen proportional counter and Bonner balls. The calculation of the experiment was performed with the modified version of ANISN - JR code using the multigroup cross section libraries DLC 2 and EURLIB 4. The comparison of the calculations using the EURLIB 4 library with the experiment indicates a good agreement of results for all used materials.

INTRODUCTION

The sodium coolant which surrounds a fast reactor core and iron as a construction material constitute the major portion of the shield. Therefore it is essential that accurate experimental results be obtained to verify transport calculation of neutrons through sodium and iron. To test such calculations benchmark experiments for sodium and iron were carried out in the Nuclear Research Institute, Řež with collaboration of the FEI - Obninsk, USSR [1,2]. Comparisons of the calculated and experimental results for several spectrometers and integral detectors have been utilised to determine the accuracy of the transport calculations using two different cross-section data sets.

DESCRIPTION OF THE EXPERIMENT

A very precise information can be obtained from the experiments in the spherical geometry with a neutron point source in the centre of the sphere. A ^{252}Cf neutron source was used because of its relatively smooth and well-known spectrum of neutrons. The source had a stainless steel cover of the cylindrical shape 10 mm high and 4 mm in diameter, and its emission was about 10^9 neutrons per second.

Three sets of spheres from the following materials were investigated :

1. high purity iron - diameters 20, 30 and 50 cm
2. carbon steel /0.2 % C, 0.27 % Si and 0,5 % Mg/ - diameters 40, 60 and 70 cm
3. solid sodium filled in 1 cm thick spherical aluminium tank - diameters 50 and 100 cm.

The following methods for neutron spectra measurements were used :

1. a proton recoil spectrometer with a stilben scintilator for the energy range from 0.2 MeV to 15 MeV.
2. a proton recoil spectrometer with a cylindrical proportional hydrogene counter SNM-38 for the energy range from 20 keV to 700 keV.
3. a moderating spheres spectrometers /Bonner balls/ for the energy range from thermal to 10 MeV.

The spheres of iron or sodium were placed to the centre of the measuring room, the room-scattered background correction was made by means of a shadow cone.

CALCULATIONS

The calculations were performed using the modified Japanese version of the discrete ordinate transport code ANISN - JR[3]. To determine a suitable order of angular quadrature, an order of the scattering cross section expansion and the spatial mesh sizes, some tests were carried out which established a satisfactory mode of operation. The $S_{12}P_5$ approximation was found quite sufficient.

The ^{252}Cf neutron source was considered as the hollow sphere of diameter 0.8 cm. The source spectrum was approximated by the Maxwell distribution with an average energy E = 2.1 MeV/T = 1.4 MeV/ in the energy region 0.02 - 15 MeV.

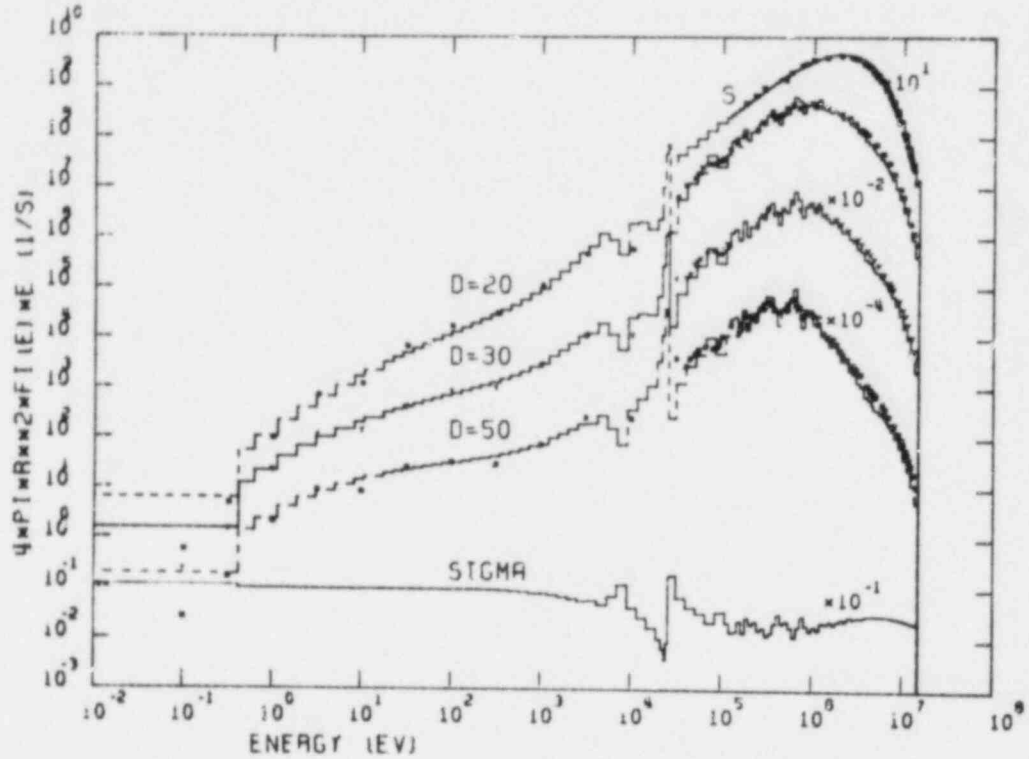

Fig. 1. Comparison of calculated and measured neutron spectra in the pure iron spheres - EURLIB 4 data set.

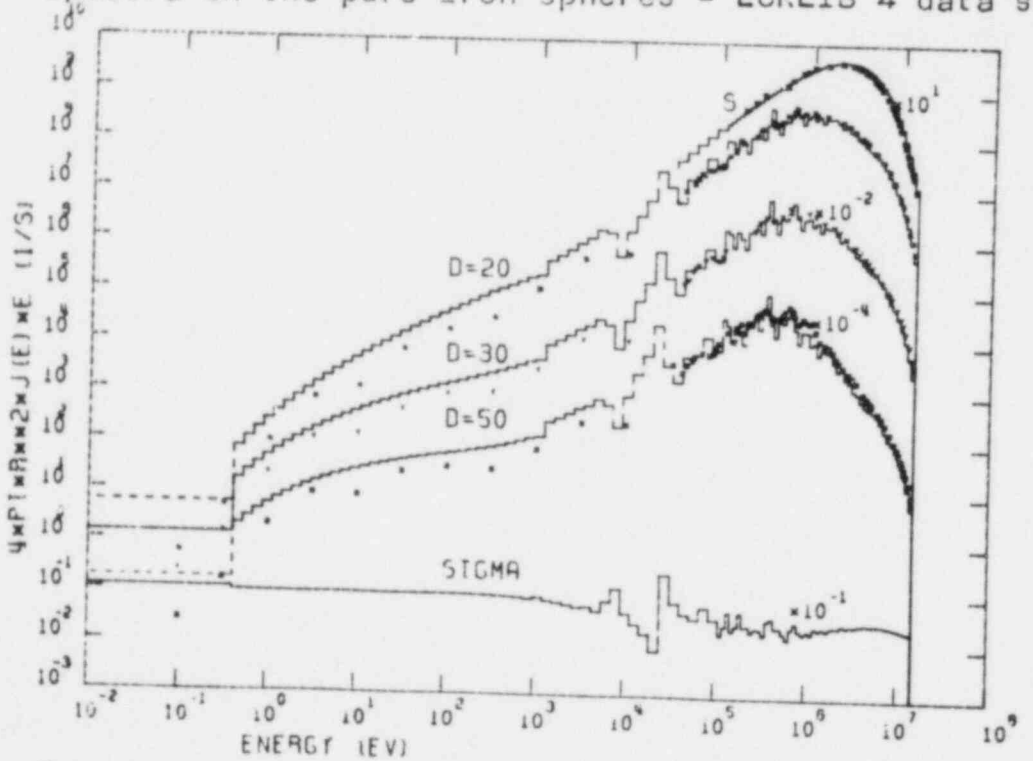

Fig. 2. Comparison of calculated and measured neutron spectra in the pure iron spheres - DLC 2 data set.

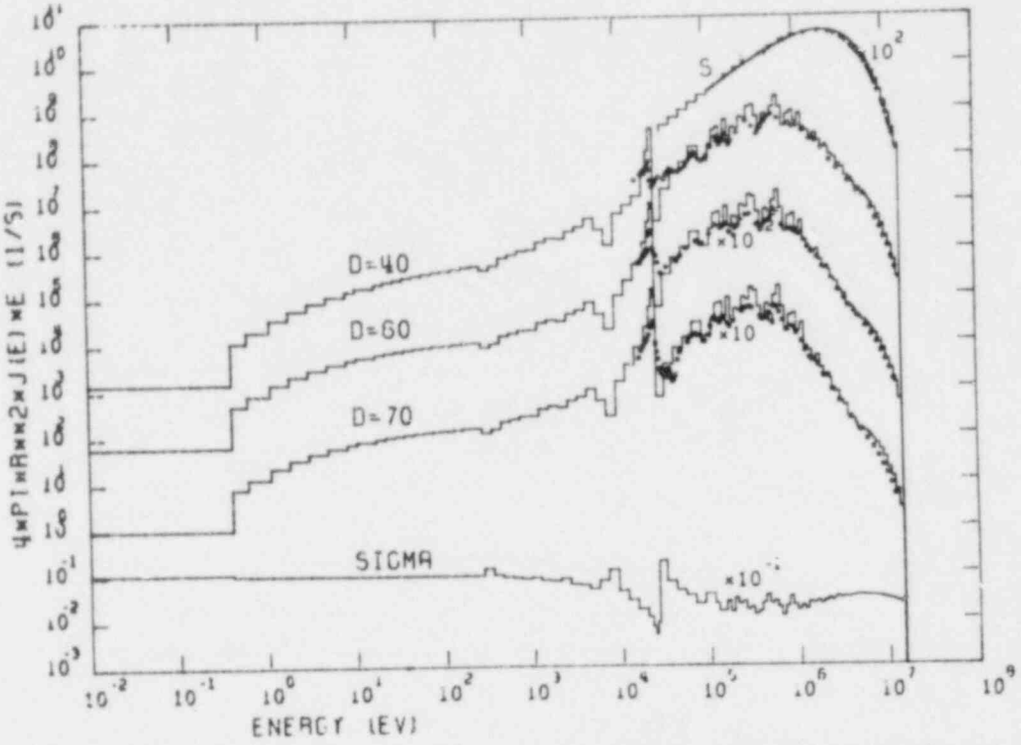

Fig. 3 . Comparison of calculated and measured neutron spectra in the steel spheres - EURLIB 4 data set.

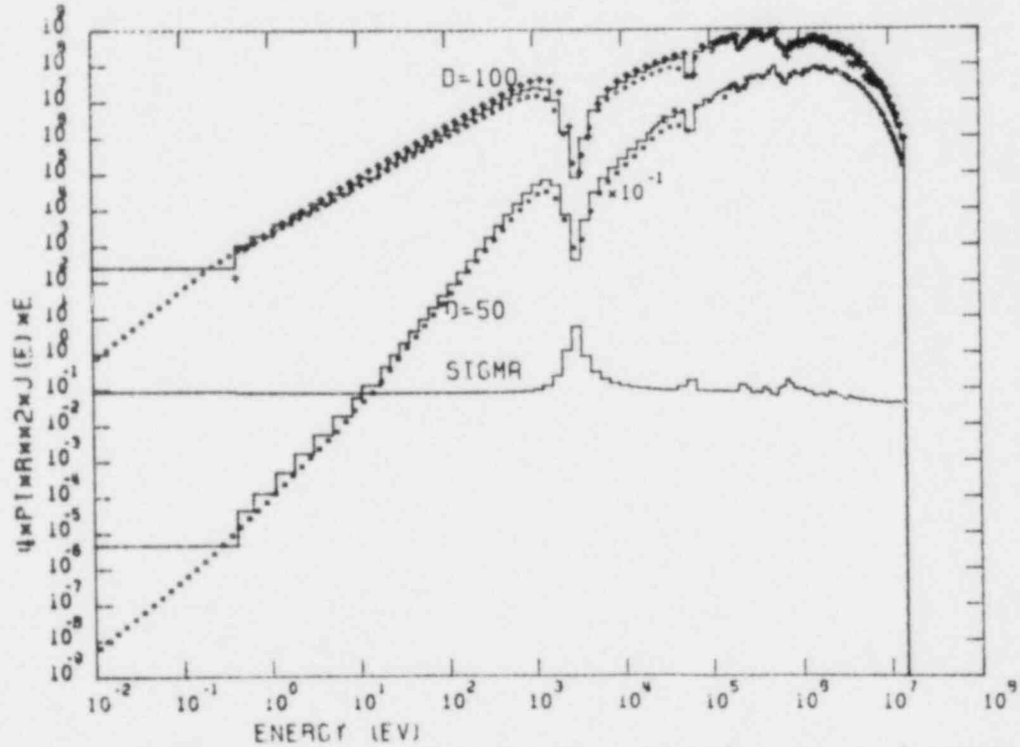

Fig.4. Comparison of calculated and measured neutron spectra in the sodium spheres.

The measured spectrum of this source is in good agreement with this distribution. Disagreement in the energy region 4 - 10 MeV /less then 10 %/ can be explained by the source spectrum changes due to neutron transport through the stainless steel capsule.

According to the theory comparing measured values in the position of a detector with the leakage spectrum from calculations[4], the error in the determination of the neutron flux in the detector distance 50 cm from the centre of the sphere would be 15 %. Neutron flux density for this geometry was therefore calculated in the position of a detector, the distance between the sphere surface and the detector was considered as vacuum.

The standard group cross section data of iron and sodium were used. The principal data set for iron was the 100-group library EURLIB 4[5] based on the ENDF/B IV data file. The calculation have also been performed with the 100-group library DLC 2[6] based on the ENDF/B III data set.

RESULTS

Fig.1. shows the results of the experiment compared with calculation for the library EURLIB 4 and Fe spheres. The results of calculation with the library DLC 2 compared with the experiment are shown in Fig.2. There are evident discrepancies observed below the energy 26 keV till thermal energy /calculated values overestimate measured ones/. Fig.3. presents results for the steel spheres. In this measurement attention was paid to the 26 keV energy region, the Bonner balls method was not used. Fig.4. shows the results for the sodium spheres. Additional calculation with the DLC 2 data library is marked by sign +.

REFERENCES

1. L. A. Trykov et al. , Transport of neutrons and gamma-rays through iron spheres, Report FEI - 943 /1979/.

2. L. A. Trykov et al. , Transport of neutrons and gamma-rays through sodium spheres, Report FEI - 1096 /1980/.

3. H. Werle et al., Messung und Berechnung der Neutronenleckage-Spektren von Eisenkugeln mit einer ^{252}Cf-Quelle im Zentrum, Report KFK 2219 /November 1975/.

4. RSIC RADHEAT Code Package CCC-300.

5. NEA - CPL Data Library EURLIB 4.

6. RSIC Data Library DLC 2.

ASTM STANDARD RECOMMENDED GUIDE ON APPLICATION OF ENDF/A CROSS SECTION AND UNCERTAINTY FILE: ESTABLISHMENT OF THE FILE

E. P. Lippincott and W. N. McElroy
Westinghouse Hanford Company
Hanford Engineering Development Laboratory
Richland, Washington, U.S.A.

ABSTRACT

A new ASTM Standard Recommended Guide is in preparation for application of an ENDF/A Cross Section and Uncertainty File for dosimetry and damage analysis. The file will consist of a standardized, self-consistent set of cross sections validated using measurements in benchmark spectra and cross sections and uncertainties will be in a convenient format for use with adjustment codes.

A new ASTM Standard Recommended Guide on "Application of ENDF/A Cross Section and Uncertainty File" is in preparation by ASTM Committee E10 on Nuclear Technology and Applications. This ASTM Standard is being prepared in support of the standardization of physics-dosimetry procedures and data needed for Light Water Reactor (LWR) power plant pressure vessel and support structure materials surveillance and test reactor development programs. However, the file will also be applicable for analysis of most fast reactor dosimetry and some fission neutron spectra. Later extension of the file to cover fusion applications such as neutron spectra from accelerator sources is possible. The main subject of this paper is the establishment of the "ENDF/A Cross Section and Uncertainty File."

The development of evaluated cross section files such as the "evaluated nuclear data file," ENDF/B, has occurred mainly to meet the needs of physics calculators. These files are tested by calculations of well-measured benchmark problems such as reactivity or critical mass measurements. Data in the files have then been re-evaluated where disagreements with the benchmark measurements indicate data to be deficient.

For cross sections of reactions used for dosimetry measurements it was found that a more specialized file was needed in order to contain the specific dosimetry reactions. For example, instead of an iron (n,p) cross section, the $^{54}Fe(n,p)^{54}Mn$ cross section is needed. Until the creation of the dosimetry file,[1] and later the ENDF gas production file,[2] the cross sections for many dosimetry reactions which are unimportant for neutron transport calculations, did not receive the proper attention by the evaluators.[3-5]

Furthermore, in neutron dosimetry and damage analysis work, standardized techniques and data must be established to characterize a diversity of irradiation environments.[6] The techniques must be implemented in such a manner that fuels and materials data from the different environments can be intercompared, and the environments are sufficiently characterized so that the fuels and materials data can be properly correlated, and then interpolated and extrapolated to different reactor design conditions. The need of such standardization is clear when the high cost of the replacement of fuels, materials, and components (including surveillance and irradiation tests) for light water reactor (LWR), fast breeder reactor (FBR), or magnetic fusion reactor (MFR) nuclear power systems are considered. Derived irradiation effects data, therefore, must have as much general applicability as possible to effect the highest benefit to cost ratio. For U.S. reactor programs key test irradiation facilities, adequately characterized and labeled as "Benchmarks", are being utilized for the validation and calibration of dosimetry, damage analysis, and the associated reactor analysis procedures and data. A provisional list of such benchmarks is given in Reference 6 as well as a discussion of goal accuracies. More recent information for LWRs is given in References 7, 8, and 9.

The need for a standardized approach is accentuated by the variety of dosimetry monitors and techniques used for the various applications. Consistency from one set of measurement conditions to another must obviously start with a consistent cross section file. To meet this need for LWR pressure vessel surveillance dosimetry, an ENDF/A cross section and uncertainty file is being established together with an ASTM Standard recommended guide for application of the file.[10] The file will be issued as ENDF/A because it may contain cross sections different than those on ENDF/B. (ENDF/B files are evaluated files officially approved by the Cross Section Evaluation Working Group (CSEWG) after suitable review and testing.) In addition, the ASTM ENDF/A file will contain damage cross sections [e.g. displacements per atom (dpa)] for steel, graphite, silicon, sapphire, quartz, etc. for which reaction mechanisms are only known theoretically and differential cross section measurements do not exist.

Differences with the ENDF/B dosimetry file will be created by the need for a standardized, self-consistent cross section set. At present, re-evaluations and testing of many dosimetry reactions have reduced discrepancies between the evaluations and integral data. Thus only a few cross sections need significant adjustment from the ENDF/B file to achieve self-consistency with benchmark integral data. In general, these cross sections are ones for reactions in energy regions in which present differential measurements are limited or non-existent and theoretical calculations have been used to fill the gap. An important example is the $^{58}Fe(n,\gamma)$ reaction. Table 1 shows the present status of cross sections measured in the ^{235}U thermal neutron induced fission spectrum compared with calculated values using the 620 point ENDF/B-V dosimetry file cross sections. It is seen that most reactions agree within about the quoted experimental error but discrepancies still exist with the reactions $^{47}Ti(n,p)$, $^{27}Al(n,p)$, $^{127}I(n,2n)$, and $^{55}Mn(n,2n)$.

In addition to the benchmark spectra which are well-defined, such as the ^{235}U fission spectrum, neutron spectra which are not determined by differential measurements or extensive calculations will also be used in the formation of the adjusted file. For example, five spectra from locations in the core and reflector of EBR-II will be included. Use of the EBR-II spectra will enable inclusion of measurements of long-lived or stable reaction products not accurately obtainable in low power facilities. These reactions can then be included in the adjustment procedure through their ratios to the other reactions in the EBR-II spectra. The relatively large number of reactions measured in the EBR-II spectra enables the neutron spectrum to be quite well determined by the integral data alone, even in the absence of other data.

Values of reaction rates in the selected spectra, together with starting cross sections (ENDF/B or other) and calculated multigroup fluxes for each spectrum will be entered in a least squares adjustment code. The code will require uncertainty estimates and correlations of all the above data. These "a priori" estimates will be tested by the code and inconsistencies recognized for further investigation. The code output will include an adjusted uncertainty correlation matrix which will contain extensive correlations between cross sections introduced by the integral relationships. The a priori uncertainty estimates neglect many of these correlations, which may be hidden in the differential data or cross section calculations, or introduced by the cross section evaluator. Use of the adjusted file approach with input of the highest accuracy integral data should enable construction of an uncertainty matrix containing accurate correlations (with neglected effects having little further significance).

It should be noted that creation of an adjusted file using the least squares method is quite different than application of "bias factors". Cross sections will be adjusted to give minimum deviations from evaluations and thus will be changed mostly in regions where sensitivity in the benchmark spectra is greatest. The resultant adjusted cross sections may be used as guidance for re-evaluations of the cross sections in the future.

By constructing the ASTM ENDF/A file for LWR pressure vessel dosimetry and damage analysis applications in this fashion, the file may not be suitable for all applications. Thus caution must be observed when extending its use beyond the limits within which the file has been tested. This is caused by the fact that cross section adjustments may be affected by data inconsistencies or effects not explicitly considered. An example of such an effect is ^{59}Co impurity in copper used as a dosimeter for the $^{63}Cu(n,\alpha)^{60}Co$ reaction. As little as 1 ppm ^{59}Co may cause a 20% effect in an environment containing thermal or low energy neutrons. Thus an effective copper cross section might contain a low energy part due to $^{59}Co(n,\gamma)^{60}Co$ that is specific for the source of the copper used. If the impurity effect is not correctly accounted for in the adjustment process (due to the limited number of spectra used), the adjusted cross sections will contain a bias but will be forced to give answers consistent with other monitors as long as application is only made to cases in which the measurements are biased. Other effects that could cause similar problems are photofission and burn-in, burn-out effects.[11]

An integral part of the ENDF/A file will be an uncertainty file which can be used by least squares adjustment codes such as FERRET[12] or STAYSL[13] to properly weight data used in neutron flux and spectrum determinations and provide a statistical evaluation of uncertainty in processed quantities such as fluence or dpa.[14,15] The use of a validated uncertainty file will provide the needed confidence to justify usage of the derived uncertainties for defining neutron induced materials property change exposure limits.[9]

In order to make the ENDF/A file easily usable by the adjustment codes,[14] it will be issued in a multigroup format with sufficient groups for most applications. Groups can be condensed for input to the codes. The uncertainties will be specified in the form of a covariance matrix and correlations between cross sections will be specified, either in the file or in the file documentation. Codes exist for collapsing or expanding covariance file data into any desired group structure.

It is expected that the use of the ENDF/A file will result in standardized analysis of LWR dosimetry and the subsequent derivation of exposure parameter values. It should therefore, find wide application to define uncertainties on a rigorous statistical basis, thereby enabling materials property exposure limits to be estabished in a consistent, scientifically justified manner. The use of such data files for international intercomparisons, such as REAL-80, can be expected to play an important part in meeting this goal.

References

1. B. A. Magurno and O. Ozer, "ENDF/B file for Dosimetry Applications," Nucl. Technol., 25, 376 (1975).

2. L. Stewart, et al., "Status of the ENDF/B Special Applications Files," Proceedings of the Second ASTM-EURATOM Symposium on Reactor Dosimetry, NUREG/CP-0004, pp.843-853, 1978.

3. W. N. McElroy and L. S. Kellogg, "Fuels and Materials Fast-Reactor Dosimetry Data Development and Testing", Nuclear Technology, 25, p. 180-223, February 1975.

4. A. Fabry, et al., "Review of Microscopic Integral Cross Section Data in Fundamental Reactor Dosimetry Benchmark Neutron Fields," Neutron Cross Sections for Reactor Dosimetry, IAEA-208, Vol. I, p. 233, 1978.

5. W. N. McElroy, et al., "Spectral Characterization of Combining Neutron Spectroscopy, Analytical Calculations, and Integral Measurements," Neutron Cross Sections for Reactor Dosimetry, IAEA-208, Vol. I, p. 147, 1978.

6. W. N. McElroy, et al., "Standardization of Dosimetry and Damage Analysis Work for U. S. LWR, FBR, and MFR Development Programs," Proc. of the Second ASTM-EURATOM Symposium on Reactor Dosimetry - Dosimetry Methods for Fuels, Cladding and Structural Materials, NUREG/CP-0004, Vol. I, p. 17, 1978 and HEDL-SA-1374, January 1978.

7. ASTM E706-81, "Standard Master Matrix for Light-Water Reactor Pressure Vessel Surveillance Standards," American Society for Testing and Materials, 1916 Race St., Philadelphia, PA, 19103, 1981.

8. W. N. McElroy, et al., "LWR Pressure Vessel Surveillance Dosimetry Improvement Program: PCA Experiments and Blind Tests," NUREG/CR-1861, HEDL-TME 80-87, Hanford Engineering Development Laboratory, Richland, WA, July 1981.

9. W. N. McElroy, et al., "Surveillance Dosimetry of Operating Power Plants," HEDL-SA 2546, Hanford Engineering Development Laboratory, Richland, WA, October 1981.

10. ASTM E706-81, "Standard Master Matrix for Light-Water Reactor Pressure Vessel Surveillance Standards, Section 5.3.2, Application of ENDF/A Cross Section and Uncertainty Files-IIB(E10.05)," American Society for Testing and Materials, 1916 Race St., Philadelphia, PA, 19103, 1981.

11. ASTM E706-81, "Standard Master Matrix for Light-Water Reactor Pressure Vessel Surveillance Standards, Section 5.3.3, Sensor Set Design and Irradiation for Reactor Surveillance-IIC(E10.05)," American Society for Testing and Materials, 1916 Race St., Philadelphia, PA, 19103, 1981.

12. F. A. Schmittroth, "FERRET Data Analysis Code," HEDL-TME 79-40, Hanford Engineering Development Laboratory, Richland, WA, 1979.

13. F. G. Perey, "Least-Squares Dosimetry Unfolding: The Program STAYSL," Oak Ridge National Laboratory, ORNL/TM-6062, 1977.

14. ASTM E706-81, "Standard Master Matrix for Light-Water Reactor Pressure Vessel Surveillance Standards, Section 5.3.1, Application of Neutron Spectrum Adjustment Methods-IIA(E10.05)," American Society for Testing and Materials, 1916 Race St., Philadelphia, PA, 19103, 1981.

15. J. J. Wagschal, R. E. Maerker, and B. L. Broadhead, "LWR-PV Damage Estimate Methodology," Transactions of the ANS Topical Meeting, 1980 Advances in Reactor Physics and Shielding, Sun Valley, ID, September 14-17, 1980.

TABLE 1

COMPARISON OF MEASURED AND CALCULATED CROSS SECTIONS
IN THE U-235 FISSION NEUTRON SPECTRUM

Reaction	Effective Threshold (MeV)	Measured Value (mb)(a)	Quoted Error in Measured Value %(a)	Calculated Value (mb)(b)	Calculated/ Measured
$^{115}In(n,\gamma)^{116m}In$		134.5	4.5	124.7	0.93
$^{197}Au(n,\gamma)^{198}Au$		83.5	6.0	78.3	0.94
$^{63}Cu(n,\gamma)^{64}Cu$		9.30	15.1	9.87	1.06
$^{235}U(n,f)$		1215	1.8	1236	1.02
$^{239}Pu(n,f)$		1826	3.0	1791	0.98
$^{237}Np(n,f)$	0.6	1340	4.0	1347	1.01
$^{115}In(n,n')^{115m}In$	1.2	191	3.7	179	0.94
$^{232}Th(n,f)$	1.4	81	6.7	75.0	0.93
$^{238}U(n,f)$	1.5	308	2.7	305	0.99
$^{47}Ti(n,p)^{47}Sc$	2.2	17.1	6.0	22.5	1.32
$^{58}Ni(n,p)^{58}Co$	2.8	109	5.5	105.0	0.96
$^{32}S(n,p)^{32}P$	2.9	66.8	5.5	70.5	1.06
$^{54}Fe(n,p)^{54}Mn$	3.1	83	6.5	81.0	0.98
$^{46}Ti(n,p)^{46}Sc$	3.9	11.5	7.0	11.2	0.97
$^{27}Al(n,p)^{27}Mg$	4.4	3.86	6.5	4.26	1.10
$^{56}Fe(n,p)^{56}Mn$	6.0	1.035	7.2	1.036	1.00
$^{59}Co(n,\alpha)^{56}Mn$	6.8	0.143	7.0	0.150	1.05
$^{63}Cu(n,\alpha)^{60}Co$	6.8	0.58	7.0	0.558	0.96
$^{27}Al(n,\alpha)^{24}Na$	7.2	0.708	7.0	0.719	1.02
$^{48}Ti(n,p)^{48}Sc$	7.6	0.269	7.0	0.282	1.05
$^{127}I(n,2n)^{126}I$	10.5	1.05	6.2	1.21	1.15
$^{55}Mn(n,2n)^{54}Mn$	11.6	0.244	6.1	0.201	0.82

(a) Taken from data updated by J. A. Grundl, March 1982, or Reference 4. Uncertainties are 1σ values.

(b) Using ENDF/B-V dosimetry file 620 point cross sections and the ENDF/B-V Watt form for the ^{235}U fission spectrum.

A BENCHMARK GAMMA-RAY SKYSHINE EXPERIMENT

R. R. Nason,* J. K. Shultis, and R. E. Faw
Kansas State University, Manhattan, Kansas 66506
and
C. E. Clifford†
Radiation Research Associates, Fort Worth, Texas 76107

ABSTRACT

A benchmark gamma-ray skyshine experiment is described in which ^{60}Co sources were either collimated into an upward 150-deg conical beam or shielded vertically by two different thicknesses of concrete. A NaI(Tl) spectrometer and a high pressure ion chamber were used to measure, respectively, the energy spectrum and the 4π-exposure rate of the air-reflected gamma photons up to 700 m from the source. Analyses of the data and comparison to DOT discrete ordinates calculations are presented.

I. INTRODUCTION

The ability to accurately predict exposure rates at large distances from a gamma radiation source of known intensity is becoming increasingly important as the control of radiation levels in and around nuclear facilities becomes more stringent. One component of exposure that is becoming of increasing concern in the design of nuclear installations is that of air-scattered photons, commonly referred to as "skyshine." Concern over the adequacy of various skyshine calculational methods has prompted a benchmark skyshine experiment with simplified geometry[1-3] to provide definitive data against which calculational methods may be tested and which may serve in their own right as useful design data.

In the benchmark skyshine experiment described here, a point ^{60}Co source was placed 2 m above grade on the axis of an annular concrete silo with walls sufficiently thick so that the radiation penetrating horizontally outward was negligible. Both energy spectra and total exposure rate measurements were made of the skyshine radiation field over a 700-m baseline (radially outward from the source) for three

*Present address: Sandia National Laboratories, Albuquerque, New Mexico 87185.

†Present address: Princeton University Plasma Physics Laboratory, Princeton, New Jersey 08540.

different source configurations: first with the source radiation collimated into a 150-deg upwardly directed conical beam and then with the sources shielded vertically by 21.0 and 42.8 cm of concrete. The experimental geometry is well modeled by two-dimensional cylindrical r-z geometry and, consequently, two-dimensional discrete ordinates calculations were performed and compared to the experimental results.

Details of this experiment, its subsequent analysis, and comparison with the two-dimensional transport calculations are presented in the following sections.

II. EXPERIMENTAL FACILITIES AND METHODS

The benchmark skyshine experiment described in this paper was performed at the 180-acre Kansas State University Nuclear Engineering Shielding Facility. The special facilities designed and constructed for this experiment and the experimental program are summarized below.

II.A. Skyshine Sources

To obtain skyshine radiation of sufficient intensity for accurate measurements with a large variation in experimental parameters, three ^{60}Co sources of strengths 10.3, 229, and 3800 Ci were used. These effective point source activities (corrected for self-absorption) were determined by cross calibration with a U.S. National Bureau of Standards reference ^{60}Co source and are estimated to be accurate to within 5%.

To define the skyshine source geometry, the irradiator cart assembly, which included the source casks, was placed on rails in a concrete silo with an approximately annular (actually dodecahedral) cross section (2.50-m i.d., 4.35-m o.d., 2.29-m height). The source casks could be moved easily so that each source when raised was 1.98 m above grade on the axis of the silo. For the unshielded skyshine measurements, 48 wedge-shaped, solid concrete blocks backed by lead blocks were placed around the top of the silo wall thereby forming the outer portion of a cone with a 150.5-deg angle whose projected apex coincided with the position of the exposed skyshine sources on the silo axis. In this manner, the ^{60}Co radiation was collimated into a well-defined upward 150.5-deg conical angle. For the shielded skyshine measurements, the collimator wedges were removed and two or four layers of stepped concrete roof slabs (1.22 x 3.66 x 0.11 m) were placed atop the silo thereby forming a concrete roof of thickness 21.0 $\pm$ 0.3 or 42.8 $\pm$ 0.5 cm (density of 2.13 $\pm$ 0.02 g/cm^3).

II.B. Gamma Spectrometer System

Gamma energy spectra of the skyshine radiation resulting from the bare/collimated and shielded sources were measured up to 700 m from the sources with a 4 x 5-in. Harshaw NaI(Tl) detector in conjunction with a Canberra 8180 multichannel analyzer. The NaI crystal was positioned 2.2 m above grade in a detector cavity with an associated shadow-shield collimator constructed on the rear of a 12-ton capacity flatbed trailer. The entire detector cavity/collimator assembly was surrounded by a minimum of 10 cm of lead, which in turn was shielded by 40 cm of concrete.

The spectrometer with its associated electronics was also mounted on the trailer to eliminate the need for long signal cables, and the entire detector assembly and spectrometer system were then enclosed in a single weather housing whose temperature control ensured the stability of the spectrometer response in all weather. With calibration sources, the spectrometer response was obtained for different photon energies. These response functions were later used to unfold the measured skyshine spectra and to calibrate the strength of the skyshine ^{60}Co sources.

II.C. Exposure Rate Measurements

In addition to the spectral measurements, a 25.4-cm-diameter spherical ion chamber[4,5] (Reuter-Stokes Area Monitor System, Model RS-111) was used to obtain 4π-skyshine exposure rates 1.0 m above grade over the 700-m source-to-detector range for all three source configurations. The 3.05-mm-thick steel shell of this ion chamber was filled with argon at 2.5 MPa (25 atm) and was protected from moisture and dust by a 2.4-mm-thick cubical aluminum housing. Calibration of this high pressure ion chamber (HPIC) in μR/h was verified using a point calibration source and a method proposed by Chilton.[6]

III. SPECTRAL RESULTS AND COMPARISONS

III.A. Results of Spectral Measurements

The energy spectra of the skyshine radiation measured with the collimated NaI spectrometer were corrected for background and then unfolded to obtain the energy spectra of the incident skyshine radiation. The SEGO code[7] was chosen to unfold the measured spectra. This particular method utilizes a set of idealized response functions which are constructed from measured spectra. The resulting unfolded spectrum then gives the actual incident photon energy distribution smoothed by the inherent energy resolution of the spectrometer.

In Fig. 1, the unfolded skyshine spectra are presented for the source collimated into an upward 150-deg conical beam. As can be observed, the spectral shape is relatively featureless and almost unchanged for the various source-to-detector distances. However, a slight variation is apparent in the lower energy portions of the spectra, especially for radial distances <300 m. This distortion is due primarily to in-silo scattering of the source photons, the result being that the upward collimated radiation field contained multiply scattered low energy photons as well as the desired uncollided photons. The magnitude of this effect is seen to decrease rapidly with distance as the lower energy, in-silo scattered photons are preferentially removed from the radiation field.

The unfolded and normalized skyshine spectra for the source shielded by 21.0 and 42.8 cm of concrete are presented in Figs. 2 and 3, respectively. Again these spectra are relatively featureless exhibiting a buildup of low energy, air-scattered photons and an exponential decrease with energy above the 75-keV maximum. As the shielding over the source increases, the skyshine spectra become increasingly shifted to lower energies as a consequence of the softer energy of the photons leaving the source silo and their smaller effective upward angle of collimation.

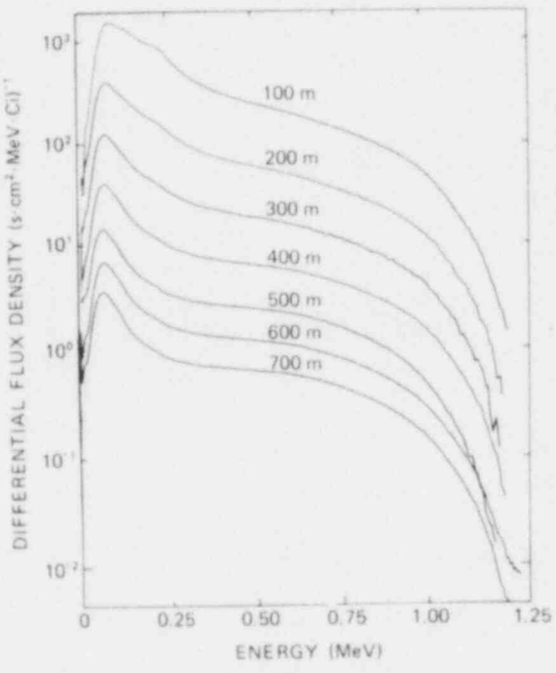

Fig. 1. Comparison of unfolded gamma-ray spectra obtained from the NaI spectrometer for the unshielded source configuration.

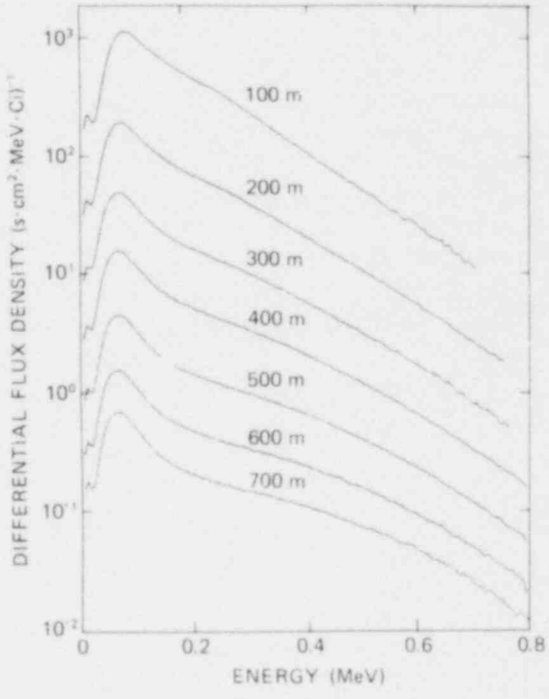

Fig. 2. Comparison of unfolded gamma-ray spectra obtained from the NaI spectrometer for the 21-cm-thick concrete shielded source configuration.

III.B. Comparison to Skyshine Calculations-Unshielded Configuration

Two sets of two-dimensional discrete ordinates calculations were performed with the DOT 3.5 code[8] for the unshielded skyshine experiment. The first, and most elaborate calculation, used a 39-group, P-5 cross-section library, and S-16 quadrature. All cross sections were prepared with the AMPX code system[9] from the ENDF/B-IV library.[10] To reduce the computational effort, a 10-group, P-3 library was utilized with S-12 quadrature in a second set of calculations. The 10-group structure was obtained by collapsing the 39 groups to 10 with a point-source, infinite-air weighting spectrum so that each group contributed approximately an equal amount to the total exposure rate.

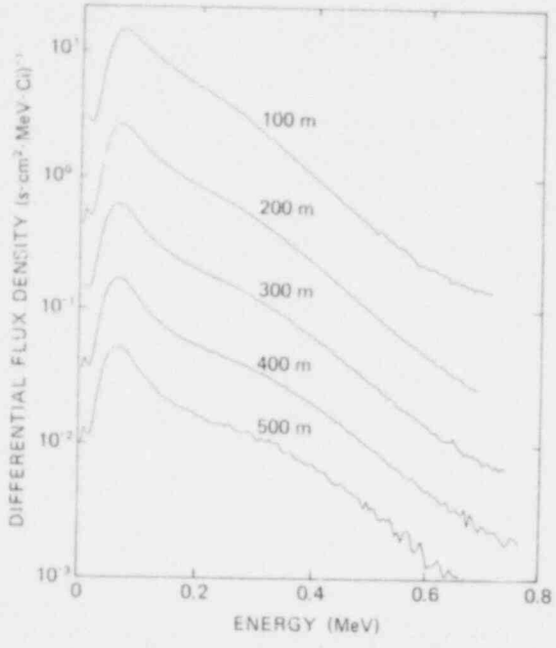

Fig. 3. Comparison of unfolded gamma-ray spectra obtained the NaI spectrometer for the 43-cm-thick concrete shielded source configuration.

Vacuum boundary conditions were used in the calculations except at r = 0 (silo axis) where a reflecting boundary condition was used. A first-collision source distribution (disregarding in-silo scattering effects) was used for both computational models. Finally, for the 39-group model a 0.2-m-thick ground from interface (z = 0) was used, while for the simpler 10-group model, the ground was replaced by an absorbing boundary.*

A comparison between the calculated and measured collimated skyshine spectra for the unshielded source configuration is shown in Fig. 4 for selected source-to-detector distances. To aid in the comparison, a Gaussian smoothing technique was applied to the 39-group fluxes. This smoothing procedure was not applied to the 10-group results because the energy bin widths employed in these calculations were larger than the resolution width of the spectrometer. As can be seen, the agreement between the experimental and 39-group results is very good in all cases. Because the in-silo scattering effect was not included in the DOT calculations, the 39-group results underpredict the low energy portion of the spectrum at 100 m. However, as mentioned earlier, the magnitude of this effect decreases rapidly with radial distance and is not observed in the 400- or 700-m comparisons.

---

* Resources did not permit 10-group calculations with a 0.2-m-thick ground interface.

The 10-group calculations agree with the measured spectra only between 0.4 and 0.8 MeV. At lower energies the spectrum is seriously underpredicted as a result of using only three groups for this energy region, while at higher energies the broad group structure is inadequate to describe the shallow angle photon scattering.

III.C. Comparison to Skyshine Calculations-Shielded Configurations

Calculations for the shielded source configurations were performed with the simpler 10-group model in two stages. First, the radiation penetrating the concrete shield over the source was calculated with the ANISN one-dimensional, discrete ordinates transport code.[11] The radiation calculated to penetrate the shield was then used as a source for the 10-group air skyshine calculation with DOT 3.5. The boundary conditions for the 10-group unshielded calculations were again used.

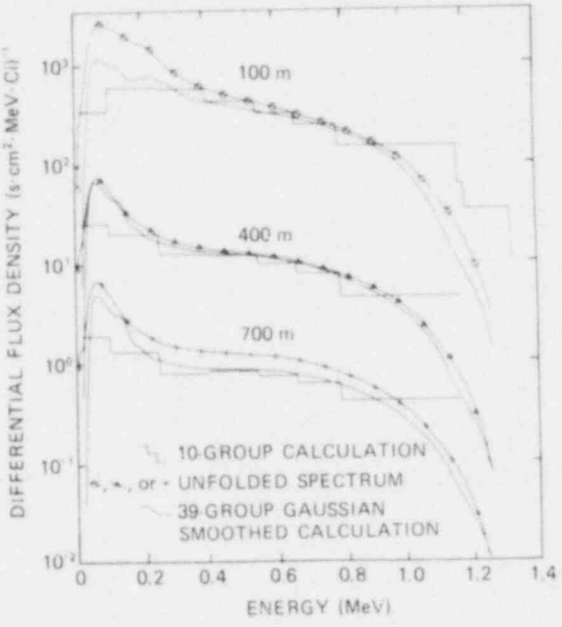

Fig. 4. Comparison of representative calculated and unmeasured spectra for the unshielded source configuration.

The comparison of the resulting calculated energy spectra to the measured spectra is shown in Figs. 5 and 6 for the two shielded configurations. Except for the high energy portion and the very lowest energy group, the agreement between the observed and calculated spectra is quite good especially in light of the simplifications used in the transport calculations.

IV. EXPOSURE RATES AND COMPARISONS

The second major objective of the skyshine experimental program was the measurement of the total skyshine exposure rate as a function of source-to-detector distance. Such integral measurements serve as additional benchmark data against which the results of various calculational schemes can be compared.

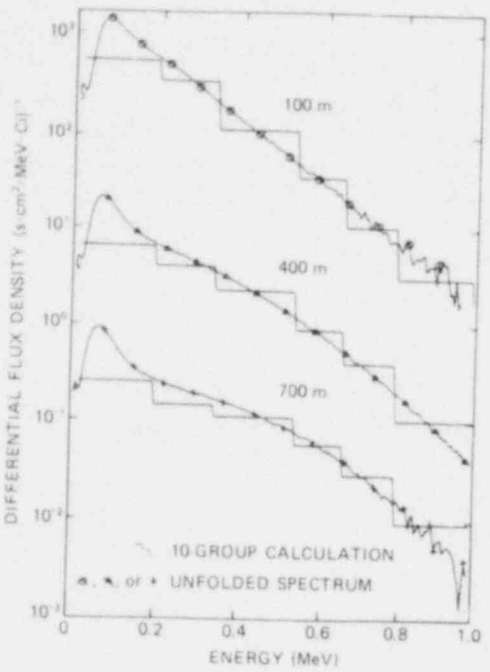

Fig. 5. Comparison of representative calculated and unfolded measured spectra for the 21-cm-thick concrete shielded source configuration.

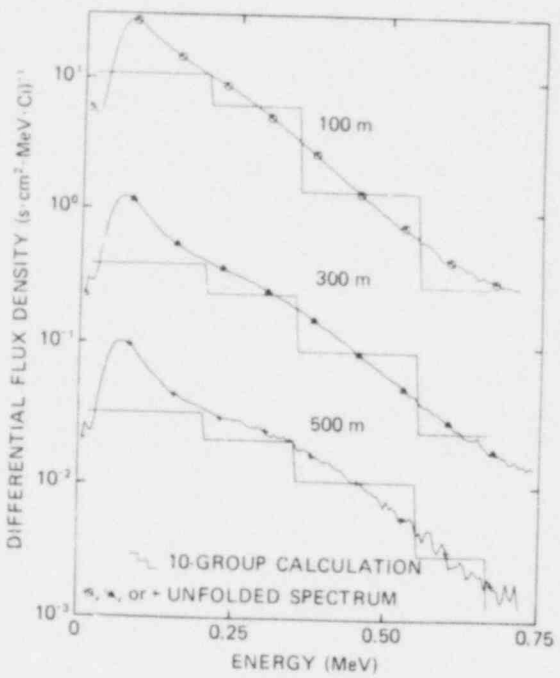

Fig. 6. Comparison of representative calculated and unfolded measured spectra for the 43-cm-thick concrete shielded source configuration.

IV.A. HPIC Measurements

The HPIC described in Sec. II.C was used to measure the 4π-exposure rate 1.0 m above grade over the 700-m measurement baseline for the three skyshine source configurations. In Tables I and II, the measured skyshine exposure rates, $\dot{X}_{meas}$, are given for the unshielded and the 42.8-cm shielded source configurations, respectively. The measured skyshine exposure rates for the 21.0-cm shielded source configuration are given in Reference 1. The air densities are corrected for temperature, pressure, and relative humidity, and the source-to-detector distances in mass units, ρr, are correct to within 2%.

TABLE I
Summary of Exposure Rate Measurements for Source Collimated to a Vertical Cone of 150.5 deg Full Angle

Distance, r (m)	Areal Density, ρr ($g \cdot cm^{-2}$)	Source (Ci)	Exposure Rate, $\dot{X}_{meas}$ ($\mu R \cdot h^{-1}$)	$\frac{r^2\dot{X}}{Ci}$ ($m^2 \cdot \mu R \cdot h^{-1} \cdot Ci^{-1}$)
50	5.72	10.39	281.0 ± 0.9	5.96(4)[a]
50	5.48	10.33	284.0 ± 0.9	6.06(4)
100	11.58	10.40	109.5 ± 1.4	9.28(4)
100	11.44	10.39	109.6 ± 0.8	9.29(4)
100	11.19	10.32	116.7 ± 0.8	9.96(4)
100	10.96	10.33	113.3 ± 0.7	9.66(4)
100	10.89	10.38	109.5 ± 0.6	9.29(4)
100	10.89	10.38	107.5 ± 3.0	9.12(4)
200	22.88	10.39	28.5 ± 0.6	9.79(4)
200	21.92	10.33	28.1 ± 0.4	9.70(4)
300	34.32	10.39	8.9 ± 0.4	6.95(4)
300	34.32	230.5	186.4 ± 0.6	6.56(4)
300	32.88	10.33	8.5 ± 0.4	6.68(4)
300	32.88	229.1	193.0 ± 0.9	6.84(4)
400	45.76	230.5	69.6 ± 0.7	4.39(4)
400	43.84	229.1	78.0 ± 0.4	4.95(4)
500	57.20	230.5	25.9 ± 0.5	2.57(4)
500	54.80	229.1	29.3 ± 0.6	2.92(4)
600	67.44	229.4	12.0 ± 0.6	1.72(4)
600	67.44	3809	210.7 ± 0.8	1.82(4)
600	65.76	3804	225.0 ± 0.4	1.95(4)
700	77.77	3811	101.7 ± 0.6	1.20(4)
700	76.72	3804	101.0 ± 0.9	1.19(4)

[a]Read as 5.96×10^4.

The HPIC used for this phase of the experiment was calibrated to display an exposure rate $\dot{X}_{meas}$ equal to the true exposure rate X for ^{60}Co gamma rays. However, the ratio of the HPIC response to the true exposure rate is not constant and, in general, depends on the energy of the incident radiation.[5] To compensate for this nonideal behavior, a correction factor $\bar{f}$ is defined as

$$\dot{X} = \bar{f}\dot{X}_{meas} , \qquad (1)$$

where $\bar{f}$ is the ratio of F_c, the instrument response (an ionization current) per unit exposure rate for ^{60}Co gamma photons, to $\bar{F}$, the instrument response per unit exposure rate for the gamma photon energy spectrum under consideration. The method for calculating $\bar{f}$ is given in Reference 1.

To correct the HPIC measurements for the nonideal energy response of the system, $\bar{f}$ values were calculated at 100-m intervals along the measurement baseline. The resulting values for the HPIC correction factors are given in Reference 1. Generally, the $\bar{f}$ values approach the ideal value of unity as the source-to-detector distance increases

TABLE II
Summary of Exposure Rate Measurements for Source Covered by 42.8-cm-thick Concrete of Density 2.13 g/cm^3

Distance, r (m)	Areal Density, ρr (g cm^{-2})	Source (Ci)	Exposure Rate, $\dot{X}_{meas}$ (μR·h^{-1})	$\frac{r^2\dot{X}}{Ci}$ (m^2·μR·h^{-1}·Ci^{-1})
30	3.380	226.5	94.7 ± 0.5	3.22(2)
30	3.378	226.6	93.0 ± 0.5	3.16(2)
30	3.343	226.6	93.4 ± 0.5	3.17(2)
50	5.653	226.5	49.6 ± 0.7	4.68(2)
50	5.611	226.6	50.3 ± 0.5	4.74(2)
50	5.572	226.6	50.6 ± 0.4	4.77(2)
70	7.971	226.5	27.8 ± 0.5	5.14(2)
70	7.828	226.6	28.0 ± 0.5	5.18(2)
70	7.772	226.6	26.4 ± 0.6	4.88(2)
100	11.42	226.5	14.8 ± 0.5	5.59(2)
100	11.18	226.6	14.7 ± 0.4	5.55(2)
100	11.10	226.6	15.4 ± 0.5	5.81(2)
150	17.20	3760	110.8 ± 0.6	5.76(2)
150	16.76	3762	109.0 ± 0.5	5.66(2)
150	16.65	3763	110.1 ± 0.6	5.71(2)
200	23.01	3760	49.7 ± 0.4	4.67(2)
200	22.35	3762	49.3 ± 0.5	4.63(2)
200	22.19	3763	50.2 ± 0.5	4.71(2)
300	34.61	3760	11.6 ± 0.5	2.52(2)
300	33.64	3762	11.9 ± 0.4	2.58(2)
300	33.29	3763	12.6 ± 0.4	2.74(2)
400	46.15	3760	3.3 ± 0.4	1.28(2)
400	44.83	3762	3.8 ± 0.5	1.47(2)
400	44.52	3763	4.1 ± 0.5	1.59(2)

because of the changing skyshine energy spectrum. The reason for this trend is seen from Figs. 1, 2, and 3. As the source-to-detector distance increases, the relative number of photons in the peak 70- to 200-keV portion of the skyshine spectra decreases. In this energy region, the HPIC overresponds thus forcing $\bar{f}$ to be less than unity and, hence, as the spectrum hardens with increasing distance, $\bar{f}$ can be expected to increase.

Knowing $\bar{f}$, the true skyshine exposure rates can be calculated from Eq. (1). The corrected 4π-exposure rates multiplied by the square of the source-to-detector distance r and normalized to unit source strength are also given in Tables I and II for the unshielded and the 42.8-cm shielded source configurations, respectively.

IV.B. Exposure Rates from NaI Measurements

As an independent verification of the HPIC measurements, an attempt was made to infer the 4π-exposure rates from the severely

collimated NaI spectral measurements. This method relies heavily on the DOT calculations in order to determine a geometry correction factor C defined as

$$C = \dot{X}(\text{collimated})/\dot{X}(4\pi) \ , \qquad (2)$$

where $\dot{X}$(collimated) is the DOT-calculated exposure rate due to photons in the collimation angle of the NaI detector and $\dot{X}(4\pi)$ is the DOT-calculated 4π-exposure rate. The resulting estimated geometry correction factors, having an average value of approximately 0.46, are given in Reference 1. With these correction factors, a 4π-exposure rate can be inferred from the NaI spectra. Inferred exposure rates are listed in Table III for the unshielded and the 42.8 cm shielded source configurations. The inferred exposure rate values for the 21.0 cm shielded source configuration are presented in Reference 1.

In Fig. 7, the HPIC-measured and NaI-inferred exposure rates are presented for all three source configurations. From this figure, it is seen that the independent NaI-based exposure rates are in remarkably good agreement with the HPIC results save for the values from 500 to 700 m for the 21-cm-thick shielded case. This close agreement between the inferred NaI results and the corrected HPIC measurements makes a clear argument for the accuracy of the experimental results.

IV.C. Comparison to the DOT Calculations

In Fig. 7 the 4π-exposure rate values calculated by DOT are plotted. It is seen that the simplified 10-group calculation tends to underpredict the corrected HPIC measurements by 10 to 15% at all locations for the unshielded source configuration. The 39-group calculation, which models more accurately the air-ground interface, yields 10 to 15% higher values than does the 10-group model and gives very close agreement (within a few percent) with the experimental data for radial distances >300 m. However, near the source silo, the 39-group model seriously underpredicts the skyshine exposure rate (20% low at 100 m). This underprediction is largely a consequence of the neglect in the 39-group calculation of the in-silo scattering component present in the skyshine source.

The nearly constant separation between the 10-group DOT results and the corrected HPIC values observed in the unshielded configuration is absent in the results for the 21-cm-thick rates. Although the DOT-calculated values underestimate the measured values for source-to-detector distances up to 400 m, the HPIC values are much lower than expected at the 500-, 600-, and 700-m locations. A possible explanation for this sudden decrease is due to the nonideal nature of the terrain at these particular measurement locations. Since the severely collimated NaI detector was not greatly influenced by the ground-scattered photons, it is felt that the NaI-inferred values give a better measure of the total skyshine radiation field for large distances in the shielded source configuration. If the NaI-inferred

TABLE III

Exposure Rates (4π) Inferred
NaI Detector Measurements

Source Configuration	ρr ($g \cdot cm^{-2}$)	$\frac{r^2 \dot{X}}{Ci}$ ($m^2 \cdot \mu R \cdot h^{-1} \cdot Ci^{-1}$)
Collimated upward (150.5 deg)	11.38	1.02(3)
	11.34	9.86(4)
	22.00	1.05(5)
	33.75	7.68(4)
	33.74	7.54(4)
	46.22	4.87(4)
	58.87	2.79(4)
	67.62	1.89(4)
	67.21	2.03(4)
	75.99	1.38(4)
Shielded by 42.8-cm-thick concrete (2.13 g/cm^3)	10.99	7.14(2)
	11.95	6.33(2)
	11.96	6.93(2)
	11.06	6.45(2)
	23.67	4.77(2)
	35.09	2.99(2)
	38.83	2.82(2)
	46.34	1.60(2)
	56.74	7.81(1)
	56.71	7.70(1)
	57.21	7.75(1)

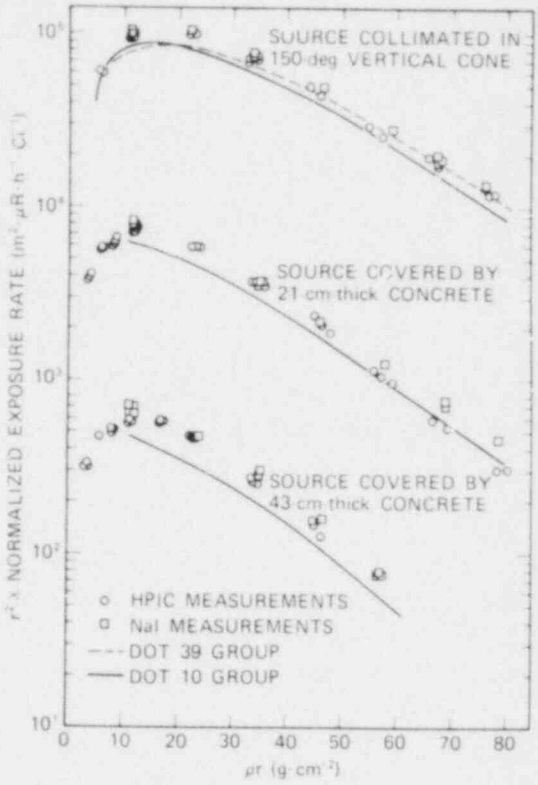

Fig. 7. Comparison of measured and calculated exposure rates.

values are used as the more accurate data for the far field exposure rates, the 10-group DOT results are observed to underpredict the measured values by 15 to 20% for all source-to-detector distances. Most of this underprediction is felt to result from the replacement of the air-ground interface by a perfect absorber in the 10-group DOT calculations.

Finally, it is observed that for the 42.8-cm-thick shielded source, the 10-group DOT values are ~20% lower than the measured values. Again, most of this underprediction can be accounted for by the simplified treatment of the air-ground interface in the DOT calculations.

V. CONCLUSIONS

The agreement between the unfolded NaI spectra and the DOT-calculated spectra was, in general, very good. Excellent results were obtained from the 39-group calculations both with regard to spectral

shape and normalization. However, the 10-group calculations were somewhat deficient in describing the spectral shape and as a consequence underpredicted the total exposure rate by ~20%. The excellent agreement between the ion chamber and scintillation detector results, which were independent determinations of the total exposure rate, lends credibility to the accuracy of the experimental measurements.

ACKNOWLEDGMENTS

The conception and sponsorship of this benchmark experiment was by the Study Committee on Air-Scattered Gamma Rays in Nuclear Facilities formed by the Japanese Nuclear Safety Research Association. The project was a joint effort by researchers at Radiation Research Associates and the Nuclear Engineering Department at Kansas State University. The authors express their appreciation to the many who contributed to the project. In particular, the efforts of M. Roseberry and W. Yoon are greatly appreciated.

REFERENCES

1. R. R. Nason, J. K. Shultis, R. E. Faw, and C. E. Clifford, "A Benchmark Gamma-Ray Skyshine Experiment," Nucl. Sci. Eng. 79, 404 (1981), copyright 1981 by the American Nuclear Society, La Grange Park, Illinois.

2. J. K. Shultis, C. E. Clifford, R. E. Faw, W. Y. Yoon, M. L. Roseberry, and R. R. Nason, "A Benchmark Gamma-Ray Skyshine Experiment: Measurements and Calculations," Trans. Am. Nucl. Soc. 28, 632 (1978).

3. M. L. Roseberry and J. K. Shultis, "Point Kernel Calculations of Skyshine Exposure Rates," Nucl. Sci. Eng. 80, 334 (1982).

4. "Operation Manual: RS-111 Area Monitor System," Reuter-Stokes Instruments, Inc., Cleveland, Ohio.

5. J. A. DeCampo, H. L. Beck, and P. D. Raft, High Pressure Argon Ion Chamber Systems for Measurement of Environmental Exposure Rates, U.S. AEC Health and Safety Laboratory Report HASL-260 (1972).

6. A. B. Chilton, "The Close-In Exposure Field From Point Isotropic Gamma-Ray Source Located at an Air-Ground Interface," Nucl. Sci. Eng. 27, 403 (1967).

7. M. H. Young and W. R. Burrus, "A Digital Filter for Unfolding Pulse Height Distributions," Nucl. Instr. Meth. 62, 82 (1968).

8. W. A. Rhoades and F. R. Mynatt, The DOT-3 Two-Dimensional, Discrete Ordinates Transport Code, Oak Ridge National Laboratory Report ORNL-TM-4280 (1973).

9. N. M. Green, J. L. Lucius, L. M. Petrie, W. E. Ford, J. E. White, and R. W. Wright, AMPX: A Modular Code System for Generating Coupled Multi-Group Neutron-Gamma Libraries from ENDF/B, Oak Ridge National Laboratory Report ORNL-TM-3706 (1976).

10. ENDF/B Summary Documentation, BNL-NCS-17541 (ENDF-201), 2nd ed. (ENDF/B-IV), D. Garber, Ed., available from the National Nuclear Data Center, Brookhaven National Laboratory, Upton, New York (1975).

11. Radiation Shielding Information Center Code Package CCC-254/ ANISN-ORNL, Multigroup One-Dimensional Discrete Ordinates Transport Code with Anisotropic Scattering, contributed by Oak Ridge National Laboratory.

COMPARISON OF MEASURED AND EVALUATED SPECTRUM-AVERAGED CROSS-SECTION DATA

W.L. Zijp, H.Ch. Rieffe, and H.J. Nolthenius,
Netherlands Energy Research Foundation ECN, Petten, The Netherlands

ABSTRACT

For several reference neutron spectra the measured spectrum-averaged cross-section values are compared with the spectrum-averaged cross-section values, derived from evaluated cross-section data files (ENDF/B-V reaction dosimetry file, and the DOSCROS81 library).

Apart from the discrepancy between these values themselves, we have also considered the consistency between the experimental and the evaluated cross-section values, taking into account the available information on the standard deviations in the averaged cross-section values. The standard deviations in the calculated cross-section values have been derived by taking into account the available information on the neutron spectrum in files 32 and 33 of the ENDF/B-V dosimetry file. For the ^{252}Cf spontaneous fission neutron spectrum it was possible to take into account also the covariance information for this spectrum.

INTRODUCTION

The information presented here is an updated version of earlier studies made at ECN on the same topic (see |Zij79|, |No81|). This comparison of measured and calculated spectrum-averaged cross-section values for reactor neutron metrology reactions compares experimental values (determined by means of the activation technique) with calculated values (derived from the evaluated cross-section library DOSCROS81 |Zij81b|, which is mainly based on the ENDF/B-V dosimetry file.

For the consideration of the so-called consistency between measured and evaluated spectrum-averaged cross-sections one needs to take into account the standard deviation in the experimental value, and the standard deviation in the calculated value (based in principle on the variance-covariance information for both the spectrum and the cross-section data). However, variance-covariance information of reference spectra is hardly available: only for the ^{252}Cf fission neutron spectrum this information has recently become available |Ma81|. Even the very recent IRDF-82 Benchmark Spectra Library presents the spectra without uncertainty information |Cu82|.

REFERENCE NEUTRON SPECTRA

In our consideration the following reference neutron flux density spectra have been considered.

1. The spontaneous fission neutron spectrum of ^{252}Cf. As representation of this spectrum we took the Maxwellian form with a mean energy of 2,13 MeV (see |Kn73|), with five continuous line segment corrections, as defined by J. Grundl et al., from the National Bureau of Standards |Gr77|.

2. The thermal neutron fission spectrum of ^{235}U. The spectrum is represented by a Maxwellian form with a mean energy of 1,97 MeV, again with five continuous line segment corrections as defined by J. Grundl et al. |Gr 77|.

3. The neutron spectrum in the Coupled Fast Reactivity Measurement Facility (CFRMF) at Idaho Falls, USA. The numerical data for the spectra were taken from Anderl |An82|.

4. The spectrum in the 10 per cent Enriched Uranium Cylindrical Critical Assembly (BIG-TEN). The numerical data were taken from the 30 group data, given in the review by Grundl and Eisenhauer |Gr78|.

5. The spectrum of the Coupled Thermal/Fast Uranium and Boron Carbide Spherical Assembly (SIGMA-SIGMA) at Mol, Belgium. The numerical representation of this spectrum is taken from a recent, unpublished communication by De Leeuw-Gierts |De82|.

6. The spectrum of the NISUS facility at London (similar to SIGMA-SIGMA). The 20 groups representation is taken from Williams et al. |Wi78|.

The work described here was nearly completely finished when the magnetic tape with the IRDF-82 data (see |Cu82|) arrived. Unfortunately we could not yet make a comparison between our spectrum representations and those on the IRDF-82.

MEASURED AVERAGE CROSS-SECTION VALUES

The measured activities and their uncertainties were taken from the most recent information sources, available to us.

1. For the ^{252}Cf spectrum: the review published by Mannhart |Ma81|, supplemented with the data published by Kobayashi et al. |Ko82|.

2. For the ^{235}U spectrum: the review published by Fabry |Fa78|, supplemented with data reported by Kobayashi |Ko80a| and |Ko80b|.

3. For the CFRMF spectrum: the recent communication by Anderl |An82|.

4 For the BIG-TEN spectrum: all values were taken from the review by Hansen et al. |Ha80|.

5. For the SIGMA-SIGMA spectrum: all values were taken from the review by Fabry |Fa78|.

6. For the NISUS facility: the data reported by Burholt |Bu79|.

CALCULATED AVERAGE CROSS-SECTION VALUES

For the reactions of interest we used the cross-section data as present in the DOSCROS81 library |Zij81| in a 640 groups structure of the SAND-II type |Mc67|. These data were derived from the ENDF/B dosimetry file and supplemented with data from INDL-V |Pr81|. In both cases the conversion from the ENDF/B format to the format of the DOSCROS81 library was performed with the program ENTOSAN |Ri81|.

We were able to take into account the covariance information available in the ENDF/B-V dosimetry files |Mag80|, not only with respect to the major region of unresolved resonances (file 33) |Va81|, but also with respect to the region with resolved resonance peaks (file 32). The covariance data in the calculated average cross-section values were derived by taking into account the correlations between the group cross-section values and in the case of the ^{252}Cf spectrum also the correlations between the group flux density values.

If one writes

$$\alpha_c = \langle \sigma_c \rangle = \sum_g \sigma_g(E).\phi_g(E).(\Delta E)_g \qquad (1)$$

then the general law for the propagation of uncertainties gives

$$\mathrm{var}(\alpha_c) = \sum_i \sum_j \left(\frac{\partial \alpha_c}{\partial \sigma_i}\right).\mathrm{cov}(\sigma_i,\sigma_j).\left(\frac{\partial \alpha_c}{\partial \sigma_j}\right) + \sum_i \sum_j \left(\frac{\partial \alpha_c}{\partial \phi_i}\right).\mathrm{cov}(\phi_i,\phi_j).\left(\frac{\partial \alpha_c}{\partial \phi_j}\right) \qquad (2)$$

Here it is assumed that the group cross-sections and the group fluence rates are uncorrelated.
The calculations of the variances and the standard deviations were performed using the 640 groups structure.

QUALITY OF DATA

In this comparison we considered the following aspects (see fig.1):

- The *imprecision*, defined as the statistical uncertainty, in terms of the standard deviation for both the measured and calculated average cross-section values. For reasons of easy comparison, values quoted are relative standard deviations, i.e. coefficients of variation, v.

In formula:

$$v_m = \frac{\sqrt{\text{var } \alpha_m}}{\alpha_m} \quad \text{and} \quad v_c = \frac{\sqrt{\text{var } \alpha_c}}{\alpha_c} \tag{3}$$

where α_m = measured average cross-section;
α_c = calculated average cross-section;
var α_m = variance of measured values;
var α_c = variance of calculated values.

- The *discrepancy*, defined as the relative difference Δ between measured and calculated average cross-section values.
In formula:

$$\Delta = \frac{\alpha_m - \alpha_c}{\alpha_c} . \tag{4}$$

- The *consistency*, generally defined as the chi-square value found with the formula

$$\chi^2 = \frac{(\alpha_m - \alpha_c)^2}{\text{var } \alpha_m + \text{var } \alpha_c} \tag{5}$$

In tables 1 to 6 a summary is presented of some main results obtained thus far in the study of uncertainties, discrepancies, and consistencies involved in reactor neutron metrology reactions. The following code is used to visualize the present situation in tables 7 and 8 for ^{252}Cf and CFRMF.

quality	symbol	uncertainty (in per cent)	discrepancy (in per cent)	consistency
very good	++	$0 < v \leq 2$	$0 < \Delta \leq 2$	$0 < \chi^2 < 1,5$
good	+	$2 < v \leq 4$	$2 < \Delta \leq 4$	$1,5 < \chi^2 < 3$
moderate	0	$4 < v \leq 6$	$4 < \Delta \leq 6$	$3 < \chi^2 < 4,5$
bad	-	$6 < v \leq 8$	$6 < \Delta \leq 8$	$4,5 < \chi^2 < 6$
very bad	--	$8 < v$	$8 < \Delta$	$6 < \chi^2$

SOME GENERAL CONCLUSIONS

. The standard deviations of the measured spectrum-averaged cross-sections are moderately good for most widely used neutron metrology reactions.

. The standard deviations of the calculated spectrum-averaged cross-sections are much larger than the standard deviations of the experimental values. This is an indication that the uncertainties in the ENDF/B-V dosimetry file may have been estimated somewhat too large.

. Large discrepancies between measured and calculated spectrum-averaged cross-sections are mainly observed for the category of (n,γ) and $(n,2n)$ reactions.

. For the ^{252}Cf spectrum and for the CFRMF spectrum many values of the χ^2-parameter for the consistency are classified as very good.

REFERENCES

|A177| W.G. Alberts, E. Günther, M. Matzke, and G. Rassl, Proc. First ASTM-Euratom Symposium on Reactor Dosimetry, Petten, September 22-26, 1975, Report EUR 5667 e/f, Part I, p. 131, (CEC-JRC, Ispra, 1977).

|An82| R.A. Anderl, D.A. Millsap, J.W. Rogers, Y.D. Harker, Addendum to integral data-testing report for ENDF/B-V dosimeter cross-sections, Report EGG-PHYS-5668 (EG&G, Idaho Falls, January 1982).

|Ba76| D.W. Barr and LASL Radiochemistry Group, Reaction Rate Measurements in BIG-10, LMFBR Reaction Rate and Dosimetry, 10th Progress Report, June 1974 through October 1975, Report HEDL-TME-75-130, pp. LASL 2-7 (Hanford Engineering Development Laboratory, August 1976).

|Bu76| M. Buczkö, Z.T. Bödy, J. Csikai, Z. Dezsö, S. Juhász, H.M. Al-Mundheri, and M. Varnagy, Average Cross Sections for ^{252}Cf Neutron Spectrum, Proc. International Symposium on Californium-252 Utilization, April 26-28, Paris (1976), Report CONF-760436, Vol. II, p. IV-19 (US-DOE, 1979).

|Bu79| G.D. Burholt, G.P. Dixon, and S. Ghanbar-Zadeh, Integral Cross-Section Measurements in the reference field NISUS, Proc. Advisory Group Meeting on Nuclear Data for Reactor Dosimetry, Vienna, 13-17 November 1978, Report INDC(NDS)-103/M, p. 157 (IAEA-NDS, Vienna, May 1979).

|Cu82| D.E. Cullen, N. Kocherov, and P.M. McLaughlin, The International Reactor Dosimetry File (IRDF-82), Report IAEA-NDS-41/R (IAEA, NDS, Vienna, January 1982).

|De77| Z. Dezsö and J. Csikai, Proc. IV All Union Conference on Neutron Physics, Kiev, USSR, April 22-26, 1977, Vol. III, p. 32 (Atomizdat, Moscow, 1977).

|De78| Z. Dezsö and J. Csikai, Proc. VIIth International Symposium on the Interactions of Fast Neutrons with Nuclei, Gaussey, November 21-25, 1977, Report ZfK-376 (Zentralinstitut für Kernforschung, Rossendorf, 1978).

|De82| S. Deleeuw-Gierts, Private Communication, February 1982.

|Fa78| A. Fabry et al., "Review of microscopic integral cross-section data in fundamental reactor dosimetry benchmark neutron fields", contribution to: Neutron cross-sections for reactor dosimetry, Technical report IAEA-208, Vol. 1, Review paper, p. 233 (IAEA, Vienna, 1978).

|Fa78a| H. Farrar IV, Integral (n,α) Cross-Sections by Helium Measurement, Interlaboratory Reaction Rate Program, 11th Progress Report, November 1975 through October 1976, Report HEDL-TME-77-34, Vol. I, pp. AI 1-14 (Hanford Engineering Development Laboratory, May 1978).

|Fa80| H. Farrar IV and B.M. Oliver, "Helium generation reaction rates for ^{6}Li and ^{10}B in benchmark facilities", contribution to Proc. Third ASTM-Euratom Symposium on Reactor Dosimetry, Ispra, 1-5 October 1979, H. Röttger, editor, Report EUR 6813, Vol. I (CEC-JRC, Ispra, 1980).

|Gi77| D.M. Gilliam, "Integral Measurement Results in Standard Fields", Proc. Intern. Specialists Symposium Neutron Standards and Applications, Gaithersburg, 28-31 March 1977, NBS Special Publication 492, p. 299 (National Bureau of Standards, Washington DC, 1977).

|Gi79| D.M. Gilliam, Personal Communications to G.E. Hansen (see |Ha80|).

|Gr77| J. Grundl and C. Eisenhauer, "Fission Rate Measurements for Materials Neutron Dosimetry in Reactor Environment", Proc. of the first ASTM-Euratom Symposium on Reactor Dosimetry, Petten, September 22-26, 1975, Report EUR-5667 e/f, Part I, p. 425 (CEC, Luxembourg, 1977).

|Gr78| J. Grundl and C. Eisenhauer, "Benchmark neutron fields for reactor dosimetry", Contribution to Neutron Cross Sections for Reactor Dosimetry, Proc. IAEA Consultants Meeting, Vienna, November 15-19, 1976. Report IAEA-208, Vol. I, p. 53 (IAEA, Vienna, 1978).

|Gr78a| R.C. Greenwood, R.G. Helmer, J.W. Rogers, R.J. Popek, R.R. Heinrich, N.D. Dudey, L.S. Kellogg, and W.H. Zimmer, "Radiometric Reaction Rate Measurements in CFRMF and BIG-10", Proc. 2nd ASTM-Euratom Symposium on Reactor Dosimetry, Palo Alto, October 3-7, 1977, Report NUREG/CP-0004, Vol. 3, p. 1207-1221 (1978).

|Ha80| G.E. Hansen, D.M. Gilliam, J.A. Grundl, "Dosimetry results for BIG-TEN and related benchmarks", Contribution to Proc. Third ASTM-Euratom Symposium on Reactor Dosimetry, Ispra, 1-5 October 1975, H. Röttger, editor, Report EUR 6813, Vol. II, p. 989 (CEC-JRC, Ispra, 1980).

|He76| H.T. Heaton II, D.M. Gilliam, V. Spiegel, C. Eisenhauer, and J. Grundl, Proc. NEANDC/NEACRP Specialists Meeting Fast Neutron Fission Cross Sections of U-235, U-238, and Pu-239, Argonne, June 28-30, 1976, Report ANL-76-90, CONF 760647 (1976), p. 333.

|Kn73| H.H. Knitter, A. Paulsen, H. Liskien, and M.M. Islam, "Measurements of the neutron energy spectrum of the spontaneous fission of ^{252}Cf", Atomkernenergie 22 (1973), no. 2, p. 84-86.

|Ko80a| K. Kobayashi, I. Kimura, "Fission Spectrum Averaged Cross Sections with Standard Neutron Fields", Proc. Third ASTM-Euratom Symposium on Reactor Dosimetry, Ispra, October 1-5, 1979. Report EUR 6813, Vol. II, p. 1004 (CEC-JRC, Ispra, 1980).

|Ko80b| K. Kobayashi, I. Kimura, "Measurement of the Average Cross Section for the $^{32}S(n,p)^{32}P$ Reaction with the Neutrons from the Spontaneous Fission of ^{252}Cf and the Thermal Neutron Fission of ^{235}U", Annu. Rep. Res. Reactor Inst. Kyoto Univ., Vol. 13 (1980), p. 1-10.

|Ko82| K. Kobayashi, I. Kimura, W. Mannhart, "Covariances in the Measurement of Californium 252 Spectrum Averaged Cross Sections", Journal of Nuclear Science and Technology (to be published).

|Ma79| W. Mannhart, W.G. Alberts, "Measurement and Calculation of Average Activation Cross Sections in the Spontaneous Fission Neutron Field of ^{252}Cf", Nuclear Science and Engineering 69 (1979), 333.

|Mag80| B.A. Magurno: "Status of data testing of ENDF/B-V reactor dosimetry file", Proc. Third ASTM-Euratom Symposium on Reactor Dosimetry, Ispra, Italy, October 1-5, 1979. Report EUR 6813 (CEC-JRC, Ispra, 1980).

|Man80| W. Mannhart and F.G. Perey, "Covariance matrices of ^{252}Cf spectrum averaged cross sections, Proc. Third ASTM-Euratom Symposium on Reactor Dosimetry, Ispra, Italy, October 1-5, 1979. Report EUR 6813 (CEC-JRC, Ispra, 1980).

|Ma81| W. Mannhart, "Progress in Integral Data and Their Accuracy: Average Neutron Cross Sections in the Californium-252 Benchmark Field", Nuclear Science and Engineering 77 (1981), p. 40-50.

|Mc67| W.N. McElroy et al., "A computer automated iteration method for neutron flux spectra determination by foil activation, SAND-II", Vol. I-IV, Report AFWL-TR-67-41 (Air Force Weapons Laboratory, New Mexico, September 1967).

|No81| H.J. Nolthenius, W.L. Zijp, "Consistency between data from the ENDF/B-V dosimetry file and corresponding experimental data for some fast neutron reference spectra", Report ECN-103 (Netherlands Energy Research Foundation ECN, Petten, November 1981).

|Pr81| V. Prongaev et al., "INDL/V. IAEA Nuclear Data Library for various neutron data evaluations in the ENDF/B-V format", Report IAEA-NDS-31 (IAEA - Nuclear Data Section, Vienna, July 1981).

|Ri81| H.Ch. Rieffe, H.J. Nolthenius, and W.L. Zijp, "ENTOSAN. A program for the calculation of fine group cross section values from ENDF/B data", Report ECN-93 (Netherlands Energy Research Foundation ECN, Petten, April 1981).

|Va80| N.J.C.M. Van der Borg et al., "Covariances of the data of the ENDF/B-V dosimetry file", ECN-80-091 (Netherlands Energy Research Foundation ECN, Petten, May 1980).

|Wi78| J.G. Williams and A.H.M.A. Hanna, Proc. Consultants' meeting, Vienna, 15-19 November 1976, Report IAEA-208, Vol. II, p.63-76, (IAEA, Vienna, 1978).

|Wi81| G. Winkler et al., "Measurement of the Average Activation Cross Section for the Reaction $^{63}Cu(n,\alpha)^{60}Co$ in the Spontaneous Fission Neutron Field of Californium-252", Nucl.Sci. and Eng. 78, (1981), 415.

|Zij79| W.L. Zijp, "On the consistency between integral and differential cross section data", Report ECN-56 (Netherlands Energy Research Foundation ECN, Petten, March 1979).

|Zij81| W.L. Zijp, H.J. Nolthenius, and H.Ch. Rieffe, "Cross-section library DOSCROS81 (in a 640 group structure of the SAND-II type)", Report ECN-111 (Netherlands Energy Research Foundation ECN, Petten, December 1981).

Table I. Cross-section data for the ^{252}Cf fission neutron spectrum. All cross section values are in units of millibarn ($10^{-31} m^2$). Standard deviations and discrepancies are expressed in per cent.

reaction	values			standard deviations		discrepancy $\frac{\langle\sigma_m\rangle - \langle\sigma_c\rangle}{\langle\sigma\rangle}$	consistency χ^2
	$\langle\sigma_m\rangle$*	ref.	$\langle\sigma_c\rangle$	$\langle\sigma_m\rangle$	$\langle\sigma_c\rangle$**		
^{19}F (n,2n) ^{18}F	0,0108	a)	0,01626	14,8	****	-33,58	11,668
^{23}Na(n,γ) ^{24}Na	0,335	a)	0,2709	4,48	12,9	23,66	2,841
^{24}Mg(n,p) ^{24}Na	1,94	b)	2,158	4,64	****	-10,10	5,865
^{27}Al(n,p) ^{27}Mg	4,891	b)	5,138	3,68	5,71	- 4,81	0,515
^{27}Al(n,α) ^{24}Na	1,006	c)	1,059	2,19	5,39	- 5,01	0,750
^{32}S (n,p) ^{32}P	72,5	b)	75,99	4,14	****	- 4,59	1,352
^{46}Ti(n,p) ^{46}Sc	13,8	c)	13,47	2,17	12,56	2,45	0,037
^{47}Ti(n,p) ^{47}Sc	18,9	c)	24,06	2,12	11,23	-21,45	3,569
^{48}Ti(n,p) ^{48}Sc	0,42	c)	0,409	2,38	10,25	2,69	0,065
^{51}V (n,γ) ^{52}V	2,8	a)	***	10,71	****	-	-
^{51}V (n,p) ^{51}Ti	0,713	b)	***	8,27	****	-	-
^{54}Fe(n,p)	85,1	a)	88,24	2,83	3,47	- 3,56	0,650
^{55}Mn(n,2n) ^{54}Mn	0,58	e)	0,4459	10,34	12,18	30,07	2,747
^{55}Mn(n,γ) ^{56}Mn	2,96	a)	2,793	7,09	****	5,98	0,633
^{56}Fe(n,p) ^{56}Mn	1,448	d)	1,414	2,90	4,41	2,41	0,204
^{58}Ni(n,p) ^{58}Co	118,0	d)	113,8	3,05	6,41	3,69	0,267
^{59}Co(n,γ) ^{60}Co	6,97	a)	6,026	4,88	13,25	15,67	1,183
^{59}Co(n,α) ^{56}Mn	0,218	b)	0,2162	6,42	4,23	0,833	0,012
^{59}Co(n,2n) ^{58}Co	0,57	f)	0,4104	10,53	10,17	38,89	4,766
^{59}Co(n,p) ^{59}Fe	1,96	a)	1,828	5,10	****	7,22	1,744
^{63}Cu(n,γ) ^{64}Cu	17,6	e)	9,642	7,95	19,01	82,54	11,91
^{63}Cu(n,α) ^{60}Cu	0,709	g)	0,7577	2,40	****	- 6,43	4,916
^{63}Cu(n,2n) ^{62}Cu	0,30	f)	0,1980	10,00	****	51,52	11,56
^{64}Zn(n,p) ^{64}Cu	40,0	d)	39,23	3,00	****	1,96	0,412
^{75}As(n,γ) ^{76}As	26,0	e)	44,12	6,15	****	-41,07	128,4
^{90}Zr(n,2n) ^{89}Zr	0,267	a)	***	5,62	****	-	-
^{92}Mo(n,p) ^{92}Nb	16,8	a)	***	4,17	****	-	-
^{93}Nb(n,2n) ^{92}Nb	0,88	a)	2,033	4,54	****	56,71	832,9
^{98}Mo(n,γ) ^{99}Mo	26,3	a)	27,56	4,94	****	- 4,572	0,941
^{100}Mo(n,γ) ^{101}Mo	14,85	a)	13,14	7,47	****	13,01	2,376
^{103}Rh(n,n') $^{103}Rh^m$	757	e)	712	4,35	****	6,32	1,867
^{113}In(n,n') $^{113}In^m$	162	d)	***	2,96	****	-	-
^{115}In(n,n') $^{115}In^m$	196,7	d)	181,9	2,95	10,9	8,14	0,513
^{115}In(n,γ) $^{116}In^m$	124,1	h)	121,2	2,90	4,29	2,39	0,210
^{181}Ta(n,γ) ^{182}Ta	119,9	a)	100,4	5,42	****	19,42	5,473
^{197}Au(n,γ) ^{198}Au	76,20	h)	76,30	2,36	8,38	- 0,131	0,00023
^{197}Au(n,2n) ^{198}Au	5,43	d)	5,647	2,95	****	- 3,84	0,302
^{199}Hg(n,n') $^{199}Hg^m$	168	e)	***	3,47	****	-	-
^{232}Th(n,f)	89,0	c)	78,06	10,11	5,09	14,02	1,237
^{235}U (n,f)	1205	i)	1236	2,24	1,95	- 2,51	0,734
^{238}U (n,f)	318,6	i)	313,5	2,50	1,10	1,63	0,345
^{237}Np(n,f)	1332	i)	1352	2,78	9,17	- 1,48	0,024
^{239}Pu(n,f)	1805	i)	1791	2,50	****	0,949	0,141

-cont.-

Table I (continued).

* This list of measured data is based on a review by Mannhart |Ma81|.
** Spectrum averaged cross-section uncertainties based on weighing spectrum with zero uncertainties.
*** Cross-section data not available on ENDF/B-V dosimetry file, and in DOSCROS81.
**** Uncertainty data not available in the ENDF/B-V dosimetry file.

a) Data from Dezsö |De77|.
b) Data from Kobayashi et al. |Ko82|.
c) Data from Alberts |Al77|.
d) Weighted average of data from Mannhart |Ma79| and Kobayashi et al. |Ko82|.
e) Data from Buczkö et al. |Bu76|.
f) Data from Dezsö |De78|.
g) Data from Winkler |Wi81|.
h) Data from Mannhart |Ma79|.
i) Data from Heaton et a'. |He76|.

Table 2. Cross-section data for the ^{235}U fission neutron spectrum. All cross-section values are in units of millibarn ($10^{-31} m^2$). Standard deviations and discrepancies are expressed in per cent.

reaction	values $\langle\sigma_m\rangle$	ref.	values $\langle\sigma_c\rangle$	standard deviations $\langle\sigma_m\rangle$	standard deviations $\langle\sigma_c\rangle$	discrepancy $\frac{\langle\sigma_m\rangle-\langle\sigma_c\rangle}{\langle\sigma_c\rangle}$	consistency χ^2
$^{24}Mg(n,p)\ ^{24}Na$	1,38	b)	1,455	5,07	**	- 5,155	1,149
$^{27}Al(n,p)\ ^{27}Mg$	3,65	b)	4,13	5,48	5,86	11,622	2,337
$^{27}Al(n,\alpha)\ ^{24}Na$	0,705	a)	0,694	5,67	5,65	1,59	0,039
$^{31}P\ (n,p)\ ^{31}Si$	33,5	b)	*	5,97		-	-
$^{32}S\ (n,p)\ ^{32}P$	64,6	b)	67,67	5,87	8,11	- 4,537	0,212
$^{46}Ti(n,p)\ ^{46}Sc$	11,8	a)	10,82	6,36	12,66	9,057	0,394
$^{47}Ti(n,p)\ ^{47}Sc$	19,0	a)	21,61	7,37	11,27	-12,078	0,863
$^{48}Ti(n,p)\ ^{48}Sc$	0,300	a)	0,2729	6,00	10,45	9,930	0,646
$^{52}Cr(n,p)\ ^{52}V$	1,06	b)	0,825	10,38	**	28,49	4,562
$^{54}Fe(n,p)\ ^{54}Mn$	78,1	b)	77,89	4,74	3,54	0,27	0,002
$^{55}Mn(n,2n)\ ^{54}Mn$	0,244	a)	0,2034	6,15	13,46	19,961	1,691
$^{56}Fe(n,p)\ ^{56}Mn$	1,025	b)	1,007	4,90	4,57	1,787	0,070
$^{58}Ni(n,2n)\ ^{57}Ni$	0,00577	a)	0,002966	5,38	10,94	94,538	39,0
$^{58}Ni(n,p)\ ^{58}Co$	108,5	a)	101,0	4,98	6,56	7,426	0,770
$^{59}Co(n,\alpha)\ ^{56}Mn$	0,143	a)	0,1450	6,99	4,38	- 1,379	0,029
$^{63}Cu(n,\gamma)\ ^{64}Cu$	9,30	a)	10,08	15,03	19,07	- 7,738	0,108
$^{63}Cu(n,\alpha)\ ^{60}Co$	0,500	a)	0,540	11,18	5,38	- 7,407	0,403
$^{93}Nb(n,n')\ ^{93}Nb^m$	122	b)	155,4	7,38	**	-21,493	13,760
$^{115}In(n,n')\ ^{115}In^m$	189	a)	173,5	4,23	11,0	8,934	0,561
$^{115}In(n,\gamma)\ ^{116}In^m$	134,5	a)	126,7	4,46	4,51	6,156	0,886
$^{127}I\ (n,2n)\ ^{126}I$	1,05	a)	1,189	6,19	17,21	-11,690	0,419
$^{197}Au(n,\gamma)\ ^{198}Au$	83,5	a)	81,01	5,99	8,06	3,074	0,092
$^{197}Au(n,2n)\ ^{196}Au$	3,00	b)	5,65	5,33	**	-46,9	274,7
$^{232}Th(n,f)$	81	a)	72,47	6,66	5,09	11,77	1,704
$^{235}U\ (n,f)$	1203	a)	1237	2,49	1,96	- 2,749	0,778
$^{238}U\ (n,f)$	305	a)	294,9	3,29	1,12	3,425	0,914
$^{237}Np(n,f)$	1312	a)	1323	3,81	9,33	- 0,831	0,007
$^{239}Pu(n,f)$	1811	a)	1787	3,32	**	1,343	0,159

* Reaction data not available in ENDF/B-V or in DOSCROS81.
**Uncertainty data not available in the ENDF/B-V dosimetry file.
a)Data from Fabry |Fa78|.
b)Data from Kobayashi |Ko80a| and |Ko80b|.

Table 3. Cross-section data for the CFRMF neutron spectrum. All cross-section values are in units of millibarn ($10^{-31}m^2$). Standard deviations and discrepancies are expressed in per cent.

reaction	values		standard deviations		discrepancy	consistency
	$\langle\sigma_m\rangle$*	$\langle\sigma_c\rangle$	$\langle\sigma_m\rangle$	$\langle\sigma_c\rangle$**	$\frac{\langle\sigma_m\rangle-\langle\sigma_c\rangle}{\langle\sigma_c\rangle}$	χ^2
$^{6}Li(n,\alpha)\ ^{3}H$	954,5	899,6	2,7	1,77	6,10	3,284
$^{10}B\ (n,\alpha)\ ^{7}Be$	1876	1618	2,8	1,43	15,94	20,204
$^{27}Al(n,p)\ ^{27}Mg$	0,863	0,930	3,4	5,88	- 7,20	1,166
$^{27}Al(n,\alpha)\ ^{24}Na$	0,1596	0,1564	3,0	5,66	2,05	0,101
$^{45}Sc(n,\gamma)\ ^{46}Sc$	23,2	23,78	3,3	25,01	- 2,44	0,009
$^{46}Ti(n,p)\ ^{46}Sc$	2,58	2,433	3,4	12,66	6,04	0,211
$^{47}Ti(n,p)\ ^{47}Sc$	4,12	5,251	4,8	11,27	-21,54	3,286
$^{48}Ti(n,p)\ ^{48}Sc$	0,0680	0,06127	3,4	10,46	10,99	0,976
$^{54}Fe(n,p)\ ^{54}Mn$	17,2	18,26	2,9	3,56	- 5,80	1,674
$^{58}Fe(n,\gamma)\ ^{59}Fe$	6,04	6,515	3,1	23,48	- 7,29	0,095
$^{59}Co(n,\gamma)\ ^{60}Co$	90,4	86,51	3,6	22,92	4,49	0,037
$^{58}Ni(n,p)\ ^{58}Co$	23,8	23,99	2,9	6,58	- 0,79	0,012
$^{63}Cu(n,\gamma)\ ^{64}Cu$	43,3	44,08	6,2	20,0	- 1,77	0,007
$^{115}In(n,n')^{115}In^{m}$	50,6	50,56	3,9	12,02	0,08	0,0004
$^{115}In(n,\gamma)^{116}In^{m}$	269	275,0	3,7	3,89	- 2,18	0,169
$^{197}Au(n,\gamma)^{198}Au$	419	382,9	2,9	3,61	9,43	3,848
$^{232}Th(n,f)$	19,6	18,91	5,2	5,10	3,65	0,242
$^{232}Th(n,\gamma)^{233}Th$	290	255,8	3,8	10,42	13,37	1,406
$^{235}U\ (n,f)$	1538	1558	3,1	2,11	- 1,28	0,119
$^{238}U\ (n,f)$	75,1	78,54	3,3	1,29	- 4,38	1,651
$^{238}U\ (n,\gamma)^{239}U$	217	217,8	3,7	1,66	- 0,37	0,008
$^{237}Np(n,f)$	548	594,8	3,3	9,63	- 7,87	0,607
$^{239}Pu(n,f)$	1792	1774	2,2		1,01	0,208

* Measured cross-section data taken from Anderl [An82].

** Spectrum averaged cross-section uncertainties based on weighing spectrum with zero uncertainties.

Table 4. Cross-section data for the BIG-TEN neutron spectrum. All cross-section values are in units of millibarn ($10^{-31} m^2$). Standard deviations and discrepancies are expressed in per cent.

reaction	values			standard deviations		discrepancy $\frac{\langle\sigma_m\rangle-\langle\sigma_c\rangle}{\langle\sigma_c\rangle}$	consistency χ^2
	$\langle\sigma_m\rangle$	ref.	$\langle\sigma_c\rangle$	$\langle\sigma_m\rangle$	$\langle\sigma_c\rangle$		
$^{6}Li(n,\alpha)\ ^{3}H$	966	a)	919,4	0,41	1,62	5,0	9,142
$^{10}B\ (n,\alpha)\ ^{7}Be$	1380	a)	1205	0,29	0,91	14,523	224,7
$^{27}Al(n,p)\ ^{27}Mg$	0,545	b)	0,6975	2,94	5,77	-21,86	12,39
$^{27}Al(n,\alpha)\ ^{24}Na$	0,107	a)	0,1383	2,80	5,55	-22,63	14,43
$^{45}Sc(n,\gamma)\ ^{46}Sc$	18,2	a)	19,0	1,65	25,86	- 4,21	0,026
$^{46}Ti(n,p)\ ^{46}Sc$	1,79	a)	1,818	1,68	12,62	- 1,54	0,015
$^{47}Ti(n,p)\ ^{47}Sc$	2,96	a)	3,667	3,72	11,26	-19,28	2,74
$^{48}Ti(n,p)\ ^{48}Sc$	0,049	a)	0,05353	2,04	10,37	- 8,46	0,645
$^{54}Fe(n,p)\ ^{54}Mn$	12,4	a)	12,75	3,22	3,51	- 2,745	0,341
$^{55}Mn(n,\gamma)\ ^{56}Mn$	7,4	b)	7,931	2,70		- 6,695	7,063
$^{56}Fe(n,p)\ ^{56}Mn$	0,128	b)	0,1888	3,91	4,49	-32,20	38,14
$^{58}Fe(n,\ )\ ^{59}Fe$	4,21	a)	3,537	2,61	17,05	19,03	1,205
$^{58}Ni(n,p)\ ^{58}Co$	16,9	a)	16,77	1,78	6,46	0,775	0,013
$^{59}Co(n,\gamma)\ ^{60}Co$	13,0	a)	12,66	1,54	24,80	2,64	0,012
$^{63}Cu(n,\gamma)\ ^{64}Cu$	22,5	a)	22,32	5,78	16,01	0,806	0,002
$^{113}In(n,\gamma)^{114}In$	583	b)	-	6,00	-	-	-
$^{115}In(n,\gamma)^{116}In^{m}$	200	b)	222,6	0,30	4,20	-10,15	5,82
$^{115}In(n,n')^{115}In^{m}$	37,2	a)	36,42	1,88	11,98	2,142	0,031
$^{197}Au(n,\gamma)^{198}Au$	230	a)	215,5	0,87	4,14	6,73	2,52
$^{197}Au(n,2n)^{196}Au$	0,49	b)	0,6609	10,20	-	-25,86	11,69
$^{233}U\ (n,f)$	2214	e)	2140	2,26	-	3,46	2,19
$^{235}U\ (n,f)$	1375	e)f)	1398	1,09	2,10	- 1,645	0,487
$^{237}Np(n,f)$	436	e)	495,1	1,83	9,62	-11,94	1,50
$^{238}U\ (n,\gamma)^{239}U$	151	a)	152,9	2,65	1,27	- 1,243	0,182
$^{238}U\ (n,f)$	51,3		55,28	1,36	1,35	- 7,20	15,18
$^{238}U\ (n,2n)^{237}U$	2,5	b)	-	4,00	-	-	-
$^{239}Pu(n,f)$	1647		1665	1,09	-	- 1,081	1,005

* All values taken from review by Hansen |Ha80|.
a) ILRR values based on data from Greenwood et al. |Gr78a|.
b) LASL values based on data from Barr et al. |Ba76|.
c) ILRR values based on data from Farrar IV |Fa78a| and |Fa80|.
d) ILRR values based on data from Gilliam |Gi79|.
e) ILRR values based on data from Gilliam |Gi77|.
f) Normalization value.

Table 5. Cross-section data for the ΣΣ fission neutron spectrum.

All cross section values are in units of millibarn ($10^{-31}m^2$).
Standard deviations and discrepancies are expressed in per cent.

reaction	values			standard deviations		discrepancy $\frac{\langle\sigma_m\rangle-\langle\sigma_c\rangle}{\langle\sigma_c\rangle}$	consistency χ^2
	$\langle\sigma_m\rangle$	$\langle\sigma_c\rangle$	ref.	$\langle\sigma_m\rangle$	$\langle\sigma_c\rangle$		
$^{27}Al(n,p)^{27}Mg$	0,983	1,038	a)	10,15	5,87	- 5,30	0,221
$^{27}Al(n,\alpha)^{24}Na$	0,153	0,174	a)	3,27	5,70	-12,1	3,57
$^{55}Mn(n,\gamma)^{56}Mn$	36,0	32,08	b)	5,56		12,2	3,84
$^{56}Fe(n,p)^{56}Mn$	0,260	0,251	a)	3,08	4,56	3,59	0,415
$^{58}Ni(n,p)^{58}Co$	26,5	26,8	a)	3,02	7,67	- 1,12	0,018
$^{63}Cu(n,\gamma)^{64}Cu$	36,2	37,19	b)	5,52	8,25	- 2,66	0,073
$^{115}In(n,n')^{115}In^m$	56,0	55,6	a)	2,50	12,16	0,719	0,003
$^{115}In(n,\gamma)^{116}In^m$	240,0	262,8	b)	3,75	3,72	- 8,88	2,94
$^{197}Au(n,\gamma)^{198}Au$	402	572,2	b)	2,49	3,68	-29,7	53,3
$^{235}U(n,f)$	1512	1537	b)	3,63	1,93	- 1,63	0,161
$^{238}U(n,f)$	84,8	87,18	a)	2,95	1,36	- 2,73	0,739
$^{238}U(n,\gamma)^{239}U$	174	217,2	b)	4,02	0,95	-19,9	35,1
$^{237}Np(n,f)$	586,5	629,6	b)	3,41	9,65	- 6,85	0,454
$^{239}Pu(n,f)$	1764	1795	b)	3,69	-1,73	- 1,73	0,171

a) Data from De Leeuw - Gierts |De 82|.
b) Data from Grundl and Eisenhauer |Gr78|.

Table 6. Cross-section data for the NISUS neutron spectrum. All cross-section values are in units of millibarn ($10^{-31}m^2$). Standard deviations and discrepancies are expressed in per cent.

reaction	values		standard deviations		discrepancy $\frac{\langle\sigma_m\rangle-\langle\sigma_c\rangle}{\langle\sigma_c\rangle}$	consistency χ^2
	$\langle\sigma_m\rangle$*	$\langle\sigma_c\rangle$	$\langle\sigma_m\rangle$	$\langle\sigma_c\rangle$		
^{10}B (n,α) ^{7}Be	1736	1489	6,22	0,87	16,59	5,158
^{24}Mg(n,p) ^{24}Na	0,345	0,3417	3,2	-	0,966	0,089
^{27}Al(n,p) ^{27}Mg	0,935	1,044	3	5,91	-10,441	2,586
^{27}Al(n,α) ^{24}Na	0,154	0,1624	2,6	5,47	- 5,17	0,743
^{56}Fe(n,p) ^{56}Mn	0,248	0,2451	2,4	4,55	1,183	0,053
^{58}Ni(n,p) ^{58}Co	25,5	27,66	2,35	6,62	- 7,81	1,257
^{64}Zn(n,p) ^{64}Cu	7,76	9,345	2,84	-	-16,96	51,73
^{103}Rh(n,n')$^{103}Rh^m$	300,8	313,1	3,96	-	- 3,928	1,066
^{115}In(n,γ)$^{116}In^m$	238	261,4	2,94	3,73	- 8,95	3,80
^{115}In(n,n')$^{115}In^m$	54,5	58,32	2,02	12,07	- 6,55	0,287
^{197}Au(n,γ)^{198}Au	391	326,2	2,56	3,75	19,865	16,81
^{235}U (n,f)	1506	1535	1,59	1,92	- 1,89	0,583
^{236}U (n,f)	181,3	-	1,38	-	-	-
^{237}Np(n,f)	580,6	648,6	1,02	9,59	-10,484	1,184
^{238}U (n,f)	85,0	91,04	1,29	1,26	- 6,634	14,49
^{239}Pu(n,f)	1770	1793	1,02	-	1,283	1,623

* Values taken from Burholt et al. [Bu79].

Table 7. Qualification of ^{252}Cf spectrum.

reaction	imprecision		discrepancy	consistency
	measured v_m	calculated v_c	Δ	χ^2
$^{19}F\ (n,2n)^{18}F$	--		--	--
$^{23}Na(n,\gamma)^{24}Na$	0	--	--	+
$^{24}Mg(n,p)^{24}Na$	0		--	-
$^{27}Al(n,p)^{27}Mg$	+	0	0	++
$^{27}Al(n,\alpha)^{24}Na$	+	0	0	++
$^{32}S\ (n,p)^{32}P$	0		0	++
$^{46}Ti(n,p)^{46}Sc$	+	--	+	++
$^{47}Ti(n,p)^{47}Sc$	+	--	--	0
$^{48}Ti(n,p)^{48}Sc$	+	--	+	++
$^{54}Fe(n,p)^{54}Mn$	+	+	+	++
$^{55}Mn(n,2n)^{54}Mn$	--	--	--	+
$^{55}Mn(n,\gamma)^{56}Mn$	-		0	++
$^{56}Fe(n,p)^{56}Mn$	+	0	+	++
$^{58}Ni(n,p)^{58}Co$	+	-	+	++
$^{59}Co(n,\gamma)^{60}Co$	0	--	--	++
$^{59}Co(n,\alpha)^{56}Mn$	-	0	++	++
$^{59}Co(n,2n)^{58}Co$	--	--	--	0
$^{59}Co(n,p)^{59}Fe$	0		-	+
$^{63}Cu(n,\gamma)^{64}Cu$	-	--	--	--
$^{63}Cu(n,\alpha)^{60}Co$	+		-	-
$^{63}Cu(n,2n)^{62}Cu$	--		--	--
$^{64}Zn(n,p)^{64}Cu$	+		+	++
$^{75}As(n,\gamma)^{76}As$	-	-	--	--
$^{93}Nb(n,2n)^{92}Nb$	0		--	--
$^{98}Mo(n,\gamma)^{99}Mo$	+		0	++
$^{100}Mo(n,\gamma)^{101}Mo$	+		--	+
$^{103}Rh(n,n')^{103}Rh^m$	0		-	+
$^{115}In(n,n')^{115}In^m$	+	--	--	++
$^{115}In(n,\gamma)^{116}In^m$	+	0	-	++
$^{181}Ta(n,\gamma)^{182}Ta$	0		--	-
$^{197}Au(n,\gamma)^{198}Au$	+	--	++	++
$^{197}Au(n,2n)^{196}Au$	+		+	+
$^{232}Th(n,f)$	--	0	--	++
$^{235}U\ (n,f)$	+	++	+	++
$^{238}U\ (n,f)$	+	++	++	++
$^{237}Np(n,f)$	+	--	++	++
$^{239}Pu(n,f)$	+		++	++

Table 8. Qualification for CFRM. spectrum.

reaction	imprecision		discrepancy	consistency
	$\langle\sigma_m\rangle$	$\langle\sigma_c\rangle$	Δ	χ^2
$^{6}Li(n,\alpha)^{3}H$	+	++	-	0
$^{10}B(n,\alpha)^{7}Be$	+	++	--	--
$^{27}Al(n,p)^{27}Mg$	+	0	-	++
$^{27}Al(n,\alpha)^{24}Na$	+	0	+	++
$^{45}Sc(n,\gamma)^{46}Sc$	+	--	+	++
$^{46}Ti(n,p)^{46}Sc$	+	--	-	++
$^{47}Ti(n,p)^{47}Sc$	0	--	--	0
$^{48}Ti(n,p)^{48}Sc$	+	--	--	++
$^{54}Fe(n,p)^{54}Mn$	+	+	0	+
$^{58}Fe(n,\gamma)$	+	--	+	++
$^{59}Co(n,\gamma)^{60}Co$	+	--	0	++
$^{58}Ni(n,p)^{58}Co$	-	-	++	++
$^{63}Cu(n,\gamma)^{64}Cu$	-	--	++	++
$^{115}In(n,n')^{115}In^{m}$	+	--	++	++
$^{115}In(n,\gamma)^{116}In^{m}$	+	+	+	++
$^{197}Au(n,\gamma)^{198}Au$	0	+	--	0
$^{232}Th(n,f)$	0	0	+	++
$^{232}Th(n,\gamma)$	+	--	--	++
$^{235}U(n,f)$	+	+	++	++
$^{238}U(n,f)$	+	++	+	+
$^{238}U(n,\gamma)$	+	++	++	++
$^{237}Np(n,f)$	+	--	--	++
$^{239}Pu(n,f)$	+		++	++

Table 9. Summary of discrepancies.

reaction	^{252}Cf	^{235}U	CFRMF	ΣΣ	NISUS	BIG-10
$^{6}Li(n,\alpha)^{3}H$			−			0
$^{10}B(n,\alpha)^{7}Be$			−−		−−	−−
$^{19}F(n,2n)^{18}F$	−−					
$^{23}Na(n,\gamma)^{24}Na$	−−					
$^{24}Mg(n,p)^{24}Na$	−−	0			++	
$^{27}Al(n,p)^{27}Mg$	0	−−	−	0	−−	−−
$^{27}Al(n,\alpha)^{24}Na$	0	++	+	−−	0	−−
$^{32}S(n,p)^{32}P$	0	0				
$^{45}Sc(n,\gamma)^{46}Sc$			+			0
$^{46}Ti(n,p)^{46}Sc$	+	−−	−			++
$^{47}Ti(n,p)^{47}Sc$	−−	−−	−−			−−
$^{48}Ti(n,p)^{48}Sc$	+	−−	−−			−−
$^{52}Cr(n,p)^{52}V$		−−				
$^{54}Fe(n,p)^{54}Mn$	+	++	0			+
$^{55}Fe(n,2n)^{54}Mn$	−−	−−				
$^{55}Mn(n,\gamma)^{56}Mn$	0			−−		−
$^{56}Fe(n,p)^{56}Mn$	+	++		+	++	−−
$^{58}Fe(n,\gamma)^{59}Fe$			−			−−
$^{58}Ni(n,2n)^{57}Ni$		−−				
$^{58}Ni(n,p)^{58}Co$	+	+	++	++	−	++
$^{59}Co(n,\gamma)^{60}Co$	−−		0			+
$^{59}Co(n,\alpha)^{56}Mn$	++	++				
$^{59}Co(n,2n)^{58}Co$	−−					
$^{59}Co(n,p)^{59}Fe$	−					
$^{63}Cu(n,\gamma)^{64}Cu$	−−	−	++	+		++
$^{63}Cu(n,\alpha)^{60}Co$	−	−				
$^{63}Cu(n,2n)^{62}Cu$	−−					
$^{64}Zn(n,p)^{64}Cu$	++				−−	
$^{75}As(n,\gamma)^{76}As$	−−					
$^{93}Nb(n,2n)^{92}Nb$	−−					
$^{93}Nb(n,n')^{93}Nb^{m}$		−−				
$^{98}Mo(n,\gamma)^{99}Mo$	0					
$^{100}Mo(n,\gamma)^{101}Mo$	−−					
$^{103}Rh(n,n')^{103}Rh^{m}$	−				+	
$^{115}In(n,n')^{115}In^{m}$	−−	−−	++	++	−	+
$^{115}In(n,\gamma)^{116}In^{m}$	+	−	+	−−	−−	−−
$^{127}I(n,2n)^{126}I$		−−				
$^{181}Ta(n,\gamma)^{182}Ta$	−−					
$^{197}Au(n,\gamma)^{198}Au$	++	+	−−	−−	−−	−
$^{197}Au(n,2n)^{196}Au$	+	−−				−−
$^{232}Th(n,f)^{233}Th$	−−	−−				
$^{232}Th(n,\gamma)$			+			
$^{233}U(n,f)$			−−			+
$^{235}U(n,f)$	+	+	++	++	++	++
$^{238}U(n,f)$	++	+	0	+	0	−
$^{238}U(n,\gamma)^{239}U$			++	−−		++
$^{237}Np(n,f)$	++	++	−	−	−−	−−
$^{239}Pu(n,f)$	++	++	++	++	++	++

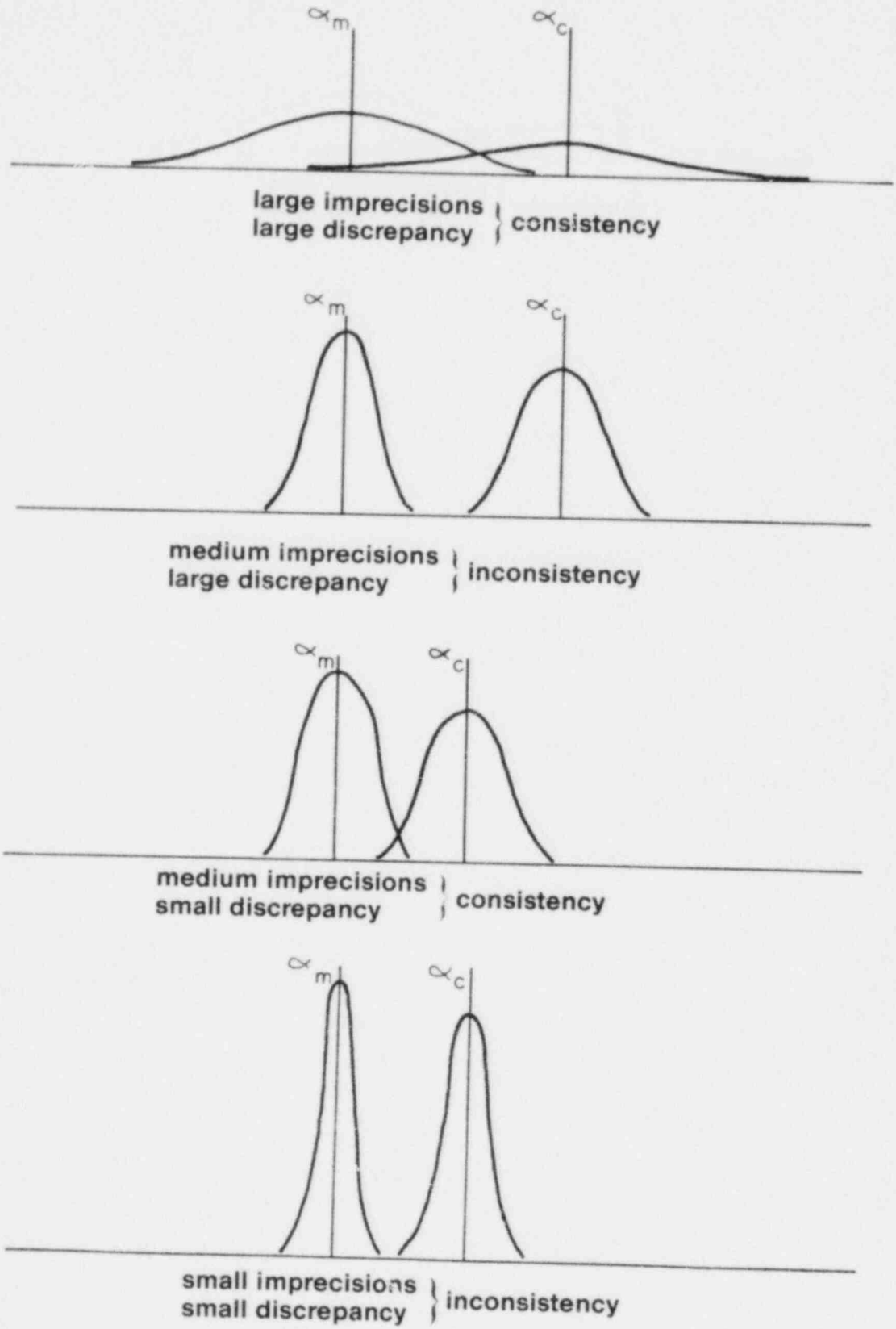

FIG. 1. RELATION BETWEEN IMPRECISION, DISCREPANCY, AND CONSISTENCY.

CHARACTERIZATION OF REACTOR NEUTRON SPECTRA AND MEASUREMENT AND EVALUATION OF RESONANCE INTEGRALS

A.Ahmad, S.M. Jefferies, T.D. Mac Mahon, J.G. Williams
University of London Reactor Centre, Ascot, Berks, U.K.,
and T.B. kyves,
National Physical Laboratory, Teddington, Middlesex, U.K.

ABSTRACT

The paper is concerned with the methods and data needed in the characterization of the thermal and epithermal neutron fluxes in reactor irradiation facilities. A convention is presented in which the neutron flux is represented by a Maxwellian thermal component and an epithermal component proportional to $E^{-(1+\alpha)}$. The nuclear data involved are the 2200 m/s cross-sections and the resonance integrals for activation of a variety of detector foils, and the decay scheme data for gamma-emission from the neutron capture products. Experimental activation data from three research reactors have been used in a consistency analysis to determine flux parameters for a total of nine irradiation positions, and to provide improved values for the nuclear data.

INTRODUCTION

In the characterization of thermal and epithermal neutron fields the assumption has often been made that the neutron flux distribution can be represented by a Maxwellian thermal component and an epithermal slowing down spectrum proportional to 1/E. The well known conventions of Westcott[1], Stoughton and Halperin[2], and Hogdahl[3] all make use of this assumption. In these conventions the reaction rate for a radiative capture reaction, in which the fast neutron contribution is negligible, depends on the effective thermal cross-section and on the resonance integral defined here as

$$I_o = \int_{E_{Cd}}^{\infty} \sigma(E)\, E^{-1} dE \qquad (1)$$

where E_{Cd} is the effective cut-off energy of a cadmium box, assumed here to be 0.55 eV for a 1 mm thick box[4].

The 1/E slowing down spectrum arises in systems in which the slowing down density is constant, which can only be expected in the absence of the effects of leakage and absorption. It has been shown by Williams[5] that in the case of energy independent buckling and

absorption cross section the flux per unit energy is approximately proportional to $1/E^{1+\alpha}$. Functions containing this type of deviation from the 1/E spectrum have also been proposed on empirical grounds by many authors[6-13].

In this paper an adaptation of the older flux conventions[1-3] is used in which the epithermal spectrum is assumed to be proportional to $1/E^{1+\alpha}$. The validity of this assumption is tested in a consistency analysis using reaction rates and cadmium ratios measured in three research reactors.

FLUX CONVENTION

We assume here that the flux can be represented by means of three empirical parameters. These are the conventional thermal flux Φ_{th}, defined to be the ratio of the thermal neutron induced reaction rate to the 2200 m/s cross-section of a 1/v detector, the epithermal flux parameter ϕ_e, equal to the flux per unit lnE at 1 eV, and α, the parameter describing the deviation from the 1/E spectrum. The thermal and epithermal flux densities, $F_{th}(E)$ and $F_e(E)$ respectively, are given by

$$F_{th}(E) = \Phi_{th} \left(\frac{4T}{\pi T_o}\right)^{\frac{1}{2}} \frac{E}{(kT)^2} \exp(-E/kT) \qquad (2)$$

$$F_e(E) = \phi_e E_1^{\alpha}/E^{1+\alpha}, \qquad \mu kT<E<\infty \qquad (3)$$

where T_o is the standard temperature of 293°K, E_1 is 1 eV, and μ is a number, assumed here equal to 5, specifying the cut-off energy of the epithermal flux. The temperature, T, of the Maxwellian distribution affects the reaction rates considered in this paper only slightly and is treated here as a known constant.

The reaction rate for a radiative capture reaction is given by[14]

$$A = g\sigma_o\{\Phi_{th} + \phi_e\left[f_1(\alpha) + \frac{W'}{g} + f_2(\alpha) + \left[\frac{E_1}{\bar{E}_r}\right]^{\alpha} \{\frac{I_o}{g\sigma_o} - f_2(o)\}\right]\} \qquad (4)$$

where g is the Westcott factor[15] accounting for the deviation of the cross-section from the 1/v law in the thermal region, σ_o is the 2200 m/s cross-section, W' is a correction, as tabulated by Ryves and Zieba[16], accounting for deviation of the cross-section from the 1/v law in the energy range μkT to E_{Cd}, and $\bar{E}_r$ is the effective resonance energy as defined and tabulated by Moens et al[17]. The functions $f_1(\alpha)$ and $f_2(\alpha)$ account for the epithermal activation of a 1/v detector and are defined as follows:

$$f_1(\alpha) = \int_{\mu kT}^{E_{Cd}} \frac{v_o}{v} \frac{E_1^{\alpha}}{E^{1+\alpha}} \, dE \qquad (5)$$

$$f_2(\alpha) = \int_{E_{Cd}}^{\infty} \frac{v_o}{v} \frac{E_1^{\alpha}}{E^{1+\alpha}} \, dE \qquad (6)$$

The saturated gamma-ray emission rate per unit mass of target element is given by

$$N_s = N_{Av} \, \eta \, A/g\sigma_o, \qquad (7)$$

where A is calculated using equation (4), N_{Av} is Avogadro's number and η is a compound nuclear data parameter defined by

$$\eta = \theta P_\gamma g\sigma_o M^{-1} \qquad (8)$$

where θ is the mole fraction of the target isotope, P_γ is the emission probability of the relevant gamma-ray and M is the element atomic mass.

SELF-SHIELDING FACTORS

In the previous section no account was taken of self-shielding. In neutron fluxes greater than $10^{15} m^{-2} s^{-1}$ it is usually possible to use foil detectors which are sufficiently dilute that any self-shielding effects are negligible. It is frequently necessary, however, to make measurements in much lower fluxes, for example in standard flux facilities. It is then necessary to use relatively thick foils in which self-shielding factors are important. The self-shielding factor, G, for a detector is defined[18] as the ratio of the experimental activation to the theoretically expected activation without self-shielding. It has been found convenient to consider separate self-shielding factors, G_{th} and G_r, for thermal and epithermal neutrons respectively.

The resonance, or epithermal self-shielding factor is usually the one which causes greatest difficulty. Although these factors have been studied perviously by several authors[19-23] there are still many detector materials for which the literature contains no precise data. Even when literature values are available it is not always evident how they should be applied, because of two conflicting definitions which are in use. For example, the experimental self-shielding factors, G_r, of Baumann[22] and of Jacks[23] should be used as factors premultiplying the resonance integral, I_o, defined in equation (1). Axton's[21] values, however, should premultiply a reduced resonance integral, I'_o, given by the normal resonance integral minus the 1/v contribution:

$$I'_o = I_o - g\sigma_o \, f_2(o) \, . \qquad (9)$$

We will denote this type of resonance self-shielding factor by G'_r.

In calculations of resonance self-shielding factors values have been published[19,20] which relate to individual resonances. If I'_i is taken to be the contribution to the reduced resonance integral of an individual resonance and G_i is the self-shielding factor relating to this resonance then one can calculate G'_r as follows:

$$G'_r = \sum_i I'_i G_i / \sum_i I'_i \quad , \tag{10}$$

where the summations are taken over all resonances.

Because of the lack of sufficient reliable self-shielding data for the materials used in this work, a Monte-Carlo code has been written to calculate them for plane foils and the results have been compared with the available experimental and theoretical values found in the literature already cited. The calculated self-shielding factor, G'_r, for ^{197}Au is shown in figure 1, where Axton's experimental values are also shown for comparison. The discrepancies are less than 2%. Similar agreement was found for ^{55}Mn and with Baumann's measured values for G_r. Comparison of our Monte-Carlo calculations of G_i with the calculations of Roe for ^{197}Au and of Selander for ^{55}Mn also showed agreement within 2%.

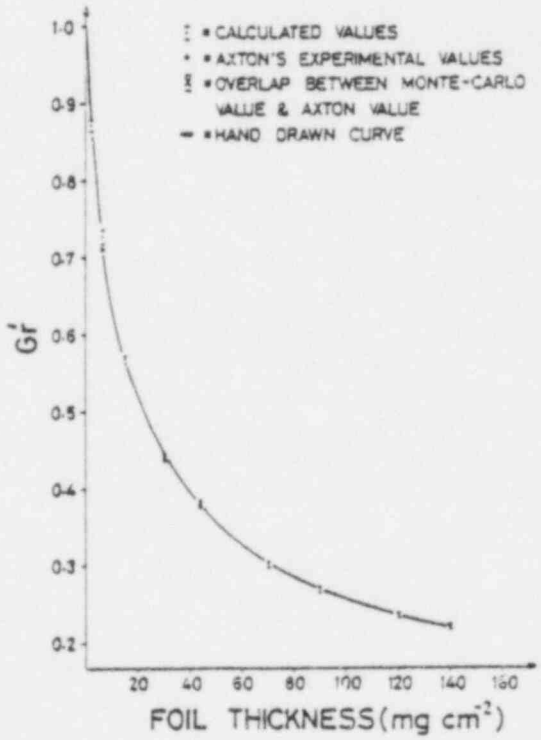

Fig. 1. Resonance self-shielding factor for ^{197}Au.

Because of the deviations from the 1/E spectrum already mentioned, it is necessary to consider the effect of these on the resonance self-shielding factors. In the cases considered so far no significant effect has been found for α values up to 0.2.

Detailed results of the Monte-Carlo calculations of resonance self-shielding and similar calculations of thermal self-shielding factors will be published elsewhere.

CONSISTENCY ANALYSIS

The model described by equations (4) and (7), together with analogous formulae for cadmium covered activities and cadmium ratios, has been tested by means of experimental data from Nakahara et al[24] and Bereznai. These consist of bare and cadmium covered activities and cadmium ratios from a total of nine irradiation positions in three research reactors. The measured quantities can be written as a vector $[E]$, with its associated variance-covariance matrix $[V_e]$, where non-diagonal terms arise because of correlated uncertainties in detector efficiency[26].

The data in $[E]$ are to be compared with the predictions of the model. These predictions, which form a vector $[C]$, depend on the parameters, $[P_o]$, used in the model, including both nuclear data and flux parameters. We need to find best estimates of these and their associated variance-covariance matrix. The method chosen to estimate $[P_o]$ was the generalised least-squares method in which we seek the values $[P_o]$ which minimize chi-squared:

$$\chi^2 = [P_1 - P_o]^T[V_p]^{-1}[P_1 - P_o] + [E - C]^T[V_e]^{-1}[E - C] \qquad (11)$$

in which the symbol T represents the transpose of a matrix and -1 the inverse. $[P_1]$ is a vector containing prior information about the parameters and $[V_p]$ is the variance-covariance matrix for $[P_1]$. Information on the data used in $[P_1]$ is given in the next section.

The iterative search procedure to find the values of $[P_o]$ which minimize chi-squared was carried out using the CERN library code MINUIT developed by James & Roos[25]. The code also supplies a variance-covariance matrix for the solution. The details are given by Ahmad[26].

INPUT DATA

Five items of nuclear data are needed to predict the measured gamma emission rates: η, $I_o/g\sigma_o$, $\bar{E}_r$, W'/g and the decay constant λ. The last three of these do not contribute significantly to the total uncertainty of the activities considered here, nor do the values of θ and M which appear in η, equation (8). All of these have therefore

been treated as known constants and the values were taken from the literature[17,16,27,28]. Uncertainties in P_γ, I_o and σ_o contribute significant uncertainties to the values of η and $I_o/g\sigma_o$. Values of P_γ and their standard deviations were taken from the Table of Isotopes[17]. I_o values were evaluated by one of the authors[26] using measured data from the compilation of Gryntakis and Kim[29]. Some measurements were excluded from the evaluation, either because no errors were given or because they were discrepant from the weighted mean of the remaining values by more than three standard deviations. Such scattered data are liable to arise when deviations from the 1/E spectrum are not taken into account in the measurements. σ_o values were either evaluated in a similar way or, in cases when no recent data were found, taken from BNL-325[30].

The resulting values of η and $I_o/g\sigma_o$ with their uncertainties form part of the prior information contributing to $[P_1]$ and $[V_p]$. The remaining values appearing in $[P_1]$ are initial estimates of the flux parameters ϕ_{th}, ϕ_e and α. Since these are poorly known the corresponding variances are taken to be very large and this ensures that the solution parameters $[P_o]$ are not influenced by them.

RESULTS

Before solution values $[P_o]$ from the minimization procedure can be accepted it is essential to consider the credibility of the model and the data. The minimum value of chi-squared as defined by equation (11) provides an appropriate test. Very high contributions to χ^2 were found for 9 out of the total of 130 measured activities and cadmium ratios. After omitting these the remaining 121 measurements were input together with 20 $I_o/g\sigma_o$ values, 14 η values and 25 flux parameters. The resulting value of chi-squared was 128 for 96 degrees of freedom, which just fails a two tailed chi-squared test at the 95% confidence level, which implies either a failure of the model, or that the input data variances have been underestimated by a small factor which can be estimated from the value of chi-squared per degree of freedom, in this case 1.33. This is a reasonable result and so the solution values $[P_o]$ have been accepted after applying this factor to the output variance-covariance matrix.

The flux parameters found for the nine irradiation positions are given in Table 1. In two positions only cadmium ratio data were available and that is the reason that only the ratios ϕ_{th}/ϕ_e, and not their absolute values, are given.

The solution values for the nuclear data parameters η and $I_o/g\sigma_o$ are given in Table 2 in which the input values are also shown. The last column of Table 2 shows the ratio of the input variances to the output ones. The reason that the output variances are larger than the input ones in a few cases is the factor 1.33 applied here only to the output variance-covariance matrix. Despite this the table shows that a substantial improvement in most of the data has resulted from the

Table 1. Solution Flux Parameters

Irradiation Positions	Flux Parameters		
	α	Φ_{th} ($cm^{-2}s^{-1}$)	ϕ_e ($cm^{-2}s^{-1}$)
1	0.046±0.019	(16.29±0.20)x10^{12}	(5.14±0.29)x10^{11}
2	0.053±0.019	(17.66±0.22)x10^{12}	(5.42±0.32)x10^{11}
3	0.053±0.020	(18.09±0.25)x10^{12}	(5.47±0.33)x10^{11}
4	0.067±0.019	(16.97±0.21)x10^{12}	(5.60±0.33)x10^{11}
5	0.065±0.020	(18.37±0.23)x10^{12}	(5.76±0.36)x10^{11}
6	0.065±0.020	(18.20±0.23)x10^{12}	(5.79±0.34)x10^{11}
7	0.024±0.014	(2.02±0.03)x10^{12}	(1.21±0.06)x10^{11}
8	0.074±0.030	Φ_{th}/ϕ_e = 30.57±3.38	
9	-0.054±0.026	Φ_{th}/ϕ_e = 22.05±1.96	

inclusion of the new information.

CONCLUSIONS

The results show that the model used provides an adequate and useful representation of the neutron flux in the irradiation positions studied. Application of the least-squares consistency has resulted in improved knowledge of the relevant nuclear data parameters and their errors. Space does not permit the inclusion here of the 59 x 59 covariance matrix of the solution parameters. This can be supplied by the authors and readers are advised that the covariance information must be used for any error calculation involving more than one of the parameters.

ACKNOWLEDGEMENTS

The authors thank Tomas Bereznai and the authors of reference 24 for providing the experimental data used here. We also thank Peter Gray for helpful discussions of statistical and computing problems.

REFERENCES

1. C.H. Westcott, J. Nucl. Energy 2, 59 (1955).
2. R.W. Stoughton and J. Halperin, Nucl. Sci. Eng. 6, 100 (1959).
3. O.T. Hogdahl, Radiochemical Methods of Analysis, IAEA Vienna 1, 23 (1965).
4. H. Goldstein, J.A. Harvey, J.S. Story and C.H. Westcott, Recommended definitions for Resonance Integral Cross Sections, EANDC-12 (1961).
5. M.M.R. Williams, The Slowing Down and Thermalization of Neutrons, North Holland, 1966.

Table 2. Input and Solution Nuclear Data

Parameter		Product Nuclide	Input P_1 (Errors %)	Output P_o (Errors %)	Relative Variances
η	keV 412	^{198}Au	0.4790(0.32)	0.4798(0.36)	0.76
	1173	^{60}Co	0.6355(1.20)	0.6293(0.93)	1.68
	1332		0.6355(1.20)	0.6310(0.94)	1.63
	604	^{134}Cs	0.2452(7.75)	0.2039(1.88)	24.8
	796		0.2147(7.80)	0.1786(1.87)	25.3
	222	^{182}Ta	0.9005×10^{-2}(7.2)	0.8802×10^{-2}(1.9)	14.3
	1189		0.1960×10^{-1}(6.7)	0.1920×10^{-1}(2.0)	11.8
	1221		0.3265×10^{-1}(6.7)	0.3149×10^{-1}(2.0)	12.7
	482	^{181}Hf	0.2013×10^{-1}(6.1)	0.2139×10^{-1}(1.2)	23.2
	889	^{46}Sc	0.5894(1.89)	0.5792(1.03)	3.52
	724	^{95}Zr	0.4081×10^{-4}(4.9)	0.4358×10^{-4}(1.7)	7.36
	756		0.5082×10^{-4}(4.8)	0.5349×10^{-4}(1.7)	7.17
	658	^{97}Zr	0.6903×10^{-5}(4.4)	0.7072×10^{-5}(3.6)	1.40
	744		0.6882×10^{-5}(4.4)	0.6685×10^{-5}(3.6)	1.54
$\frac{I_o}{g\sigma_o}$		^{198}Au	15.68(1.75)	15.69(1.94)	0.82
		^{60}Co	1.982(1.53)	1.979(1.66)	0.86
		^{134}Cs	13.62(8.96)	14.98(5.31)	2.35
		^{182}Ta	32.80(7.16)	32.41(3.38)	4.60
		^{181}Hf	2.442(6.55)	2.684(3.93)	2.31
		^{46}Sc	0.4426(6.01)	0.4473(5.53)	1.15
		^{95}Zr	6.654(18.0)	7.160(7.02)	5.69
		^{97}Zr	223.9(7.0)	240.1(6.0)	1.20
		^{140}La	1.308(5.43)	1.255(2.54)	4.94
		^{56}Mn	1.069(1.96)	1.048(1.99)	1.01
		^{51}Ti	0.6340(6.78)	0.6272(7.73)	0.79
		^{51}Cr	0.5470(6.95)	0.5678(6.56)	1.04
		^{52}V	0.5150(5.83)	0.4839(4.63)	1.79
		^{59}Fe	1.040(6.73)	1.000(7.02)	0.99
		^{75}Se	10.73(9.51)	11.45(7.81)	1.30
		^{86}Rb	19.51(12.3)	19.02(13.6)	0.84
		^{124}Sb	28.97(11.1)	30.90(7.73)	1.82
		^{131}Ba	24.55(37.6)	23.52(9.43)	17.0
		^{141}Ce	0.8420(9.38)	0.8238(6.75)	2.02
		^{160}Tb	15.69(11.3)	18.72(4.76)	3.96

η values are in barns $mole^{-1}$ for the gamma transitions identified by energies in keV.

6. J.W. Connoly, A. Rose and T. Wall, Integral Reaction Rates and Neutron Energy Spectra in Well Moderated Reactors, AAEC/TM191 (1963)
7. L.C. Schmid, J.H. Lauby, W.P. Stinson and V.O. Uotinen, Summary of Results of EBWR Critical Experiments, Phys. Res. Quart. Rept., HW-84608 (1965).
8. P. Schumann and D. Albert, Kernenergie, 8, 88 (1965).
9. K.W. Geiger and L. Van Der Zwan, Metrologia, 2, 1 (1966).
10. T.B. Ryves and E.B. Paul, J. Nucl. Energy, 22, 759 (1968).
11. T.B. Ryves, Metrologia, 5, 119 (1969).
12. T. Bereznai and T.D. Mac Mahon, J. Radioanal. Chem. 45, 423 (1978).
13. F. De Corte, L. Moens, A. Simonits, A. De Wispelaere and J. Hoste, J. Radioanal. Chem. 52, 295, (1979).
14. A. Ahmad, T.D. Mac Mahon, M. Macwani, M.J. Minski, J.G. Williams and T. Bereznai, Proceedings of 4th International Conference on Nuclear Methods in Environmental and Energy Research, CONF-800433, 1980.
15. C.H. Westcott, Effective Cross-Section Values for Well Moderated Thermal Reactor Spectra, AECL-1101 (1960).
16. T.B. Ryves and K.J. Zieba, J. Phys. A : Math. 7, 2318 (1974).
17. L. Moens, F. De Corte, A. Simonits, A. De Wispelaere and J. Hoste, J. Radioanal. Chem. 52, 295 (1979).
18. W.L. Zijp, "Intermediate Neutrons" in Neutron Fluence Measurements, Tech. Rept. 107, IAEA Vienna (1974).
19. G.M. Roe, The Absorption of Neutrons in Doppler Broadened Resonances, Rept. KAPL-1241 (1954).
20. W.N. Selander, Theoretical Evaluation of Self-Shielding Factors Due to Scattering Resonances in Foils, Rept. AECL-1077 (1960).
21. E.J. Axton, J. Nucl. Energy, Parts A/B, 17, 125 (1963).
22. N.P. Baumann, Resonance Integrals and Self-Shielding Factors for Detector Foils, Rept. DP-817 (1963).
23. C.M. Jacks, A Study of Thermal and Resonance Flux Detectors, Rept. DP-608 (1961).
24. H. Nakahara, M. Tsukada, A. Moriizumi, K. Horiuchi and Y. Murakami, Proceedings of 6th International Conference on Modern Trends in Activation Analysis, Toronto, (June 1981).
25. F. James and M. Roos, Computer Physics Communications, 10, 343 (1975).
26. A. Ahmad, Ph.D. Thesis, (February 1982).
27. C.M. Lederer and V.S. Shirley, Table of Isotopes, 7th Edition, John Wiley and Sons, 1978.
28. Chart of Nuclides, Kernforschungszentrum Karlsruhe, 1974.
29. E.M. Gryntakis and J.I. Kim, NEA Data Bank, ND1540, 1980.
30. S.F. Mughabghab and D.I. Garber, Neutron Cross-Sections BNL-325, 3rd Edition, Vol. 1, New York, 1973.

UPDATED RESULTS FOR THE MOL-ΣΣ BENCHMARK AND FIRST RESULTS OF THE CONNECTED U_{nat} EXPERIMENT

G. De Leeuw-Gierts, S. De Leeuw
SCK/CEN, Boeretang 200, B-2400 Mol, Belgium

MOL-ΣΣ BENCHMARK

The MOL-ΣΣ benchmark [1, 3] was recalculated by means of ANISN - VITAMIN/C (171 gr - S8P3), DTF IV - KEDAK 3 (208 gr - S8)* and ANISN - DLC43B/CSRL (218 gr - S8P3) [4]. The central experimental neutron spectrum was reevaluated by using the Li-6 spectral results of 1976 [5]. The evaluated spectrum is compared to the 171 gr ANISN and 208 gr DTF IV spectra in fig. 1. The experimental spectrum covering only the ~ 5 keV - 6 MeV energy range, the evaluated experimental spectrum was extrapolated, for the calculation of the average cross sections of the dosimetry detectors, with the ANISN - VITAMIN/C theoretical spectrum, normalized to the experiment between 9 keV and 5.8 MeV.

Between 5 and 5.8 MeV the average flux values of the theoretical and Li-6 data were taken, the difference in spectral shape here being rather important. The group fluxes of the final spectrum are reported in table 1.

The average cross sections of the reactions reported in table 2 were calculated by means of the ENDF/B V dosimetry file using the calculated spectra obtained from ANISN - VITAMIN/C, DTF IV - KEDAK 3 and ANISN - DLC43B (two different degrees of convergence) and for the evaluated spectrum.

To evaluate the sensitivity to the $^{115}In(n,n')^{115m}In$ cross section shape at the threshold, this average cross section was also calculated with the Helsinki evaluation [2]; the two values are given.

Table 3 gives the ratios of the theoretical average cross sections over the experimental ones. A systematic disagreement is observed between the data calculated with the evaluated spectrum and the experimental ones, only for the detectors with response below the lower limit of extrapolation i.e. $^{198}Au(n,\gamma)$, $^{235}U(n,f)$ and $^{239}Pu(n,f)$.
Because of the important role played by boron in this energy range, as is seen in fig. 2, it is difficult to conclude about the origin of this discrepancy.

*Diagonal transport calculation of scattering anisotropy.

The agreement between theory and experiment is worst for the DTF IV - KEDAK 3 results. The U_{nat} experiment will inform about the degree of importance of inaccuracies of the ^{238}U capture cross section in the discrepancies observed in the low energy range and clarify the reasons for the differences between the experimental and theoretical spectral shape between 10 keV and 6 MeV.

U_{nat} EXPERIMENT

The U_{nat} experiment was set-up to test the ^{238}U group cross sections as used for reactor calculations. Three natural uranium spherical shell configurations are used of thickness 1 cm, 6 cm and 11 cm respectively. They are located in a 1 m diameter cavity hollowed in the vertical thermal column of BR1 [6].

The central theoretical spectra, calculated by means of ANISN - VITAMIN/C, are shown in fig. 3. To eliminate, in first approximation, the dependence on the detector cross sections,ratios of the spectra are considered. Fig. 4 compares the 1 cm/6 cm and 6 cm/11 cm ratios, calculated with ANISN - VITAMIN/C and DTF IV - KEDAK 3 respectively.

Fig. 5 shows the Li-6 results in the 6 cm and 11 cm shells obtained up to now, fig. 6 the ratios in a 40 energy group structure for the Li-6 and theoretical spectra.
To compare to the In foil measurements already performed, the average cross sections for this reaction were calculated in the energy range covered by the Li-6 technique, i.e. 10 keV - 10 MeV, using the theoretical and Li-spectra (table 4). In table 5 the theoretical fluxes (normalized to the thermal neutron flux, 30 cm deep in the graphite) the experimental $^{115}In(n,n')^{115m}In$ and Li-6 fluxes are compared in the same energy range.
From these figures we can conclude that in absolute shape the Li-6 spectra agree best with the ANISN - VITAMIN/C spectra, while for the ratios a slightly better agreement with DTF IV - KEDAK 3 is observed.

No explanation is yet found for the structures appearing in the Li-6 spectra between 100 keV and 1 MeV. An insert showing part of the spectra, deduced from the E_t response of each detector, is added to highlight these structures.

The neutron flux ratio - 6 cm U_{nat}/11 cm U_{nat} - between 10 keV and 10 MeV lies between the flux ratios deduced from the In reaction rate measurements, using the average cross sections calculated with ANISN and DTF IV respectively.

The 1 cm/6 cm (U_{nat}) In flux ratio is respectively 8 % and 4 % lower than the flux ratios calculated by means of ANISN and DTF IV, while the 6 cm/11 cm In flux ratio is respectively 7 % and 12 % higher.

On completion of the experiment a better assess of the $^{6}Li(n,\alpha)t$ cross section, between 1 and 2 MeV, and an improvement of the $^{115}In(n,n')^{115m}In$ cross section shape in the vicinity of the threshold will be possible.

The data still needed to reach these three experimental goals are : the interpretation of the (n,p) spectrum measurements in the 11 cm shell, the achievement and interpretation of the Li-6 spectrum up to 10 MeV in the 1 cm shell and the irradiation of the dosimetry detectors as used in MOL-ΣΣ.

REFERENCES

[1] A. Fabry, G. De Leeuw-Gierts, S. De Leeuw, Nucl. Techn. 25, 349 (1975).

[2] See table 1.

[3] H. Bluhm et al., KFK 1658, RCN 172, BLG 471 (1972).

[4] G. Minsart, BLG Annual Report 1981, to be published.

[5] G. De Leeuw et al., BLG 520, pp 1-14, 1-15 (1976).

[6] G. and S. De Leeuw, "Neutron data of structural materials for fast reactors," Proceedings of a Specialists' Meeting, held at the Central Bureau of Nuclear Measurements, Geel, Belgium, p. 93-104 (1977).

ACKNOWLEDGMENTS

The authors wish to thank Messrs F. Cops and D. Langela for their valuable assistance in the measurements and their interpretation respectively and Mrs Andries for her skillful and fast editing work.

Table 1. Evaluated experimental neutron spectrum, extrapolated above 5.5 MeV and below 9 keV with the theoretical 171 gr ANISN - VITAMIN/C spectrum

E_n in keV - Group fluxes

0.17333E+05	0.16487E+05	0.15683E+05	0.14918E+05	0.14550E+05	0.14191E+05
0.13840E+05	0.13499E+05	0.12840E+05	0.12214E+05	0.11618E+05	0.11052E+05
0.10513E+05	0.10000E+05	0.95123E+04	0.90484E+04	0.86071E+04	0.81873E+04
0.77880E+04	0.74082E+04	0.70469E+04	0.67032E+04	0.65924E+04	0.63763E+04
0.60653E+04	0.57695E+04	0.54881E+04	0.52205E+04	0.49659E+04	0.47237E+04
0.44933E+04	0.40657E+04	0.36788E+04	0.33287E+04	0.31664E+04	0.30119E+04
0.28650E+04	0.27253E+04	0.25924E+04	0.24660E+04	0.23852E+04	0.23653E+04
0.23457E+04	0.23069E+04	0.22313E+04	0.21225E+04	0.20190E+04	0.19205E+04
0.18268E+04	0.17377E+04	0.16530E+04	0.15724E+04	0.14957E+04	0.14227E+04
0.13534E+04	0.12873E+04	0.12246E+04	0.11648E+04	0.11080E+04	0.10026E+04
0.96164E+03	0.90718E+03	0.86294E+03	0.82085E+03	0.78082E+03	0.7427 E+03
0.70651E+03	0.67206E+03	0.63928E+03	0.60810E+03	0.57844E+03	0.55023E+03
0.52340E+03	0.49787E+03	0.45049E+03	0.40762E+03	0.38774E+03	0.36883E+03
0.33373E+03	0.30197E+03	0.29850E+03	0.29720E+03	0.29452E+03	0.28725E+03
0.27324E+03	0.24724E+03	0.23518E+03	0.22371E+03	0.21280E+03	0.20242E+03
0.19255E+03	0.18316E+03	0.17422E+03	0.16573E+03	0.15764E+03	0.14996E+03
0.14264E+03	0.13569E+03	0.12907E+03	0.12277E+03	0.11679E+03	0.11109E+03
0.98037E+02	0.86517E+02	0.82500E+02	0.79500E+02	0.72000E+02	0.67379E+02
0.56562E+02	0.52475E+02	0.46309E+02	0.40868E+02	0.34307E+02	0.31828E+02
0.28500E+02	0.27000E+02	0.26058E+02	0.24788E+02	0.24176E+02	0.23579E+02
0.21875E+02	0.19305E+02	0.15034E+02	0.11709E+02	0.91188E+01	0.71017E+01
0.55308E+01	0.43074E+01	0.37074E+01	0.33546E+01	0.30354E+01	0.27465E+01
0.26126E+01	0.24852E+01	0.22487E+01	0.20347E+01	0.15846E+01	0.12341E+01
0.96112E+00	0.74852E+00	0.58295E+00	0.45400E+00	0.35358E+00	0.27536E+00
0.21445E+00	0.16702E+00	0.13007E+00	0.10130E+00	0.78893E-01	0.61442E-01
0.47851E-01	0.37267E-01	0.29023E-01	0.22603E-01	0.17603E-01	0.13710E-01
0.10677E-01	0.83153E-02	0.64760E-02	0.50435E-02	0.39279E-02	0.30590E-02
0.23824E-02	0.18554E-02	0.14450E-02	0.11254E-02	0.87642E-03	0.68256E-03
0.53156E-03	0.41399E-03	0.10000E-03	0.10000E-07		
0.79416E-05	0.15087E-04	0.25540E-04	0.20833E-04	0.26667E-04	0.34762E-04
0.44708E-04	0.13528E-03	0.20785E-03	0.32073E-03	0.48519E-03	0.71369E-03
0.10262E-02	0.14205E-02	0.19510E-02	0.26194E-02	0.34355E-02	0.43400E-02
0.55562E-02	0.70632E-02	0.87187E-02	0.32870E-02	0.71818E-02	0.12355E-01
0.14839E-01	0.17424E-01	0.19926E-01	0.22695E-01	0.25674E-01	0.29041E-01
0.60594E-01	0.80617E-01	0.91281E-01	0.49454E-01	0.53080E-01	0.56535E-01
0.59570E-01	0.61736E-01	0.61705E-01	0.40581E-01	0.10390E-01	0.10487E-01
0.21697E-01	0.45712E-01	0.70831E-01	0.69744E-01	0.69823E-01	0.74976E-01
0.76362E-01	0.76272E-01	0.76335E-01	0.75194E-01	0.74379E-01	0.75887E-01
0.79351E-01	0.83072E-01	0.87642E-01	0.91734E-01	0.20116E+00	0.98259E-01
0.14576E+00	0.13168E+00	0.13453E+00	0.13875E+00	0.14640E+00	0.15286E+00
0.15266E+00	0.15846E+00	0.16000E+00	0.16218E+00	0.16428E+00	0.16508E+00
0.16517E+00	0.32788E+00	0.32051E+00	0.15859E+00	0.15759E+00	0.30427E+00
0.29163E+00	0.33526E-01	0.12658E-01	0.26264E-01	0.72404E-01	0.14410E+00
0.27867E+00	0.13338E+00	0.13029E+00	0.11280E+00	0.12527E+00	0.12177E+00
0.11769E+00	0.11311E+00	0.10825E+00	0.10394E+00	0.99170E-01	0.94841E-01
0.91305E-01	0.88602E-01	0.85755E-01	0.82505E-01	0.79805E-01	0.18713E+00
0.17010E+00	0.61590E-01	0.46768E-01	0.11935E+00	0.74655E-01	0.19309E+00
0.72555E-01	0.10913E+00	0.92358E-01	0.11141E+00	0.42427E-01	0.58944E-01
0.27698E-01	0.17833E-01	0.24629E-01	0.12110E-01	0.11964E-01	0.34961E-01
0.55558E-01	0.10092E+00	0.75955E-01	0.60844E-01	0.47483E-01	0.39225E-01
0.34080E-01	0.17952E-01	0.12180E-01	0.10259E-01	0.96767E-02	0.43542E-02
0.76350E-02	0.74488E-02	0.96994E-02	0.26609E-01	0.18446E-01	0.19449E-01
0.17708E-01	0.14154E-01	0.12849E-01	0.10316E-01	0.10053E-01	0.72955E-02
0.95575E-02	0.59299E-02	0.19896E-02	0.50428E-02	0.25786E-02	0.24753E-02
0.71039E-03	0.12294E-02	0.88786E-03	0.25618E-03	0.58062E-03	0.36482E-03
0.16452E-03	0.10123E-04	0.15315E-04	0.33045E-04	0.18039E-04	0.91791E-05
0.33213E-05	0.11360E-05	0.28491E-06	0.64842E-07	0.16751E-07	0.61873E-08
0.36030E-08	0.57868E-08	0.73596E-09			

Table 2. Average cross sections (mb) in MOL-II

Reaction	Experimental results [1]	ENDF/B 5 Dosimetry file				
		Theoretical results				Evaluated experimental spectrum [4]
		171 gr ANISN - VITAMIN/C	218 gr ANISN - DLC43B/CSRL [3]		208 gr DTF IV - KEDAK 3	
$^{197}Au(n,\gamma)^{198}Au$	402	455	427	444	429	463
$^{235}U(n,f)$	1512	1613	1587	1605	1582	1620
$^{239}Pu(n,f)$	1764	1843	1827	1838	1860	1842
$^{103}Rh(n,n')^{103m}Rh$	281	304	304	299	349	292
$^{237}Np(n,f)$	586.5	621	624	614	705	598
$^{238}U(n,f)$	84.8	88.5	88.1	85.9	106.3	83.1
$^{115}In(n,n')^{115m}In$	56	56.3	55.7	54.4	67.3	52.9 57.1 [2]
$^{232}Th(n,f)$	20.35	21.3	21.2	20.6	25.5	20.1
$^{58}Ni(n,p)^{58}Co$	26.5	26.4	25.95	25.2	32.1	25.7
$^{27}Al(n,p)^{27}Mg$	0.983	0.985	1.01	0.976	1.145	0.993
$^{56}Fe(n,p)^{56}Mn$	0.260	0.234			0.250	0.239
$^{27}Al(n,\alpha)^{24}Na$	0.153 (J.G.Williams) 0.171 (A. Fabry)	0.163			0.161	0.166

[1] A. Fabry et al., Neutron cross sections for Reactor Dosimetry, p. 233, Vol. I, IAEA-208 (1978).

[2] A. Fabry et al., "$^{115}In(n,n')^{115m}In$ cross section evaluation", Nuclear Data for Reactors, p. 535, Vol. II, IAEA (1970).

[3] Improved convergence.

[4] Experimental evaluated spectrum, extrapolated below 9 keV and above 5.5 MeV with the theoretical 171 gr ANISN-VITAMIN/C spectrum (normalization based on equal areas between 9 keV and 5.8 MeV).

Table 3. Calculated/measured average cross sections in MOL-ΣΣ

Reaction	ANISN-VITAMIN/C Exp.	ANISN-DLC43B/CSRL [3] Exp.	DTF IV-KEDAK 3 Exp.	Exp. eval. spectrum Exp.
$^{197}Au(n,\gamma)^{198}Au$	1.132	1.105	1.067	1.152
$^{235}U(n,f)$	1.067	1.061	1.046	1.071
$^{239}Pu(n,f)$	1.045	1.042	1.054	1.044
$^{103}Rh(n,n')^{103m}Rh$	1.082	1.063	1.241	1.039
$^{237}Np(n,f)$	1.059	1.047	1.203	1.020
$^{238}U(n,f)$	1.044	1.012	1.253	0.980
$^{115}In(n,n')^{115m}In$	1.005 1.085 [2]	0.97	1.201	0.945 1.020 [2]
$^{232}Th(n,f)$	1.047	1.013	1.254	0.988
$^{58}Ni(n,p)^{58}Co$	0.996	0.951	1.211	0.970
$^{27}Al(n,p)^{27}Mg$	1.002	0.993	1.165	1.010
$^{56}Fe(n,p)^{56}Mn$	0.900	1.204	0.962	0.919
$^{27}Al(n,\alpha)^{24}Na$	1.065 (J.G.Williams) 0.953 (A. Fabry)		1.052 0.942	1.085 0.971

Table 4. Comparison of the $\bar{\sigma}_{calc.}$ (mb) for $^{115}In(n,n')^{115m}In$ over the neutron energy range covered by the $^{6}Li(n,\alpha)t$ technique i.e. from 10 keV to 10 MeV

Configuration	ANISN - VITAMIN/C			DTF IV - KEDAK 3		^{6}Li spectrum	
	ENDF/B 5 dosimetry file	Helsinki evaluation [2]	ENDF/B 5 / Helsinki	ENDF/B 5	Helsinki	Helsinki	ANISN / DTF IV ENDF/B 5
1 cm U_{nat}	110.0	119.2	0.92	114.7	124.1		0.96
6 cm U_{nat}	51.0	57.6	0.885	58.0	65.1	57.5	0.88
11 cm U_{nat}	29.5	34.4	0.86	35.5	41.0	36.6	0.83

Table 5. Comparison of theoretical and experimental In(n,n') and $^{6}Li(n,\alpha)t$ fluxes between 10 keV and 10 MeV

Configuration	$k_1\phi$(n/cm^{2}s) theor.		$k_2\phi_{In}$(n/cm^{2}s) ENDF/B 5		^{6}Li spectra	Exp./Theor. ANISN	Exp./Theor. DTF IV
	ANISN-VITAMIN/C	DTF IV-KEDAK 3	$\bar{\sigma}_{In}$ from ANISN	$\bar{\sigma}_{In}$ from DTF IV			
1 cm U_{nat}	1097	1102	707	679		0.644	0.616
6 cm U_{nat}	2303	2234	1615	1428		0.701	0.639
11 cm U_{nat}	2375	2283	1554	1302		0.654	0.570
$\frac{1}{6}$ cm U_{nat}	0.476	0.493	0.438	0.475		0.92	0.96
$\frac{6}{11}$ cm U_{nat}	0.970	0.978	1.039	1.097	1.068	1.071	1.12

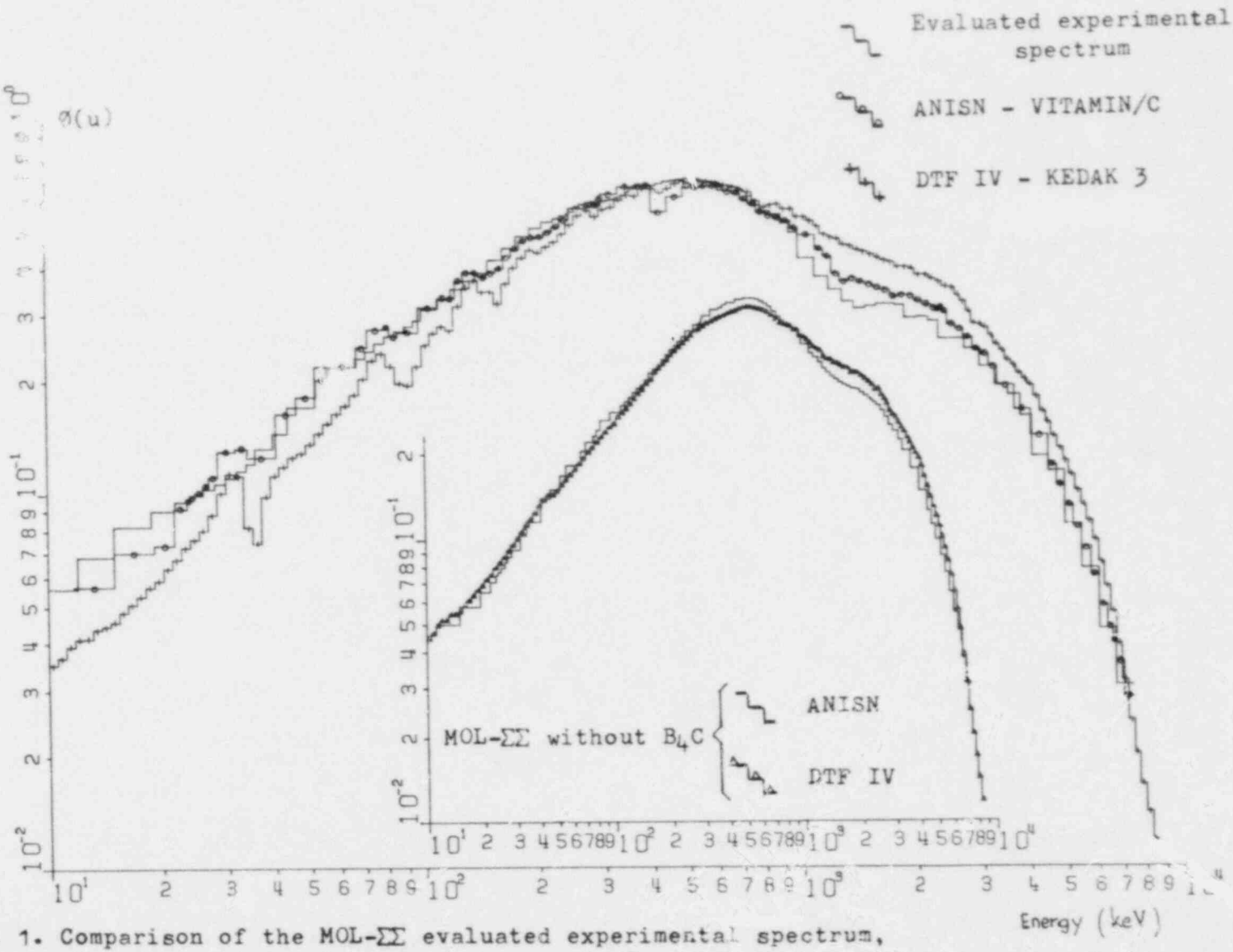

Fig. 1. Comparison of the MOL-ΣΣ evaluated experimental spectrum, the 171 gr ANISN - VITAMIN/C and the 208 gr DTF IV - KEDAK 3 theoretical spectra. Insert : Theoretical spectra of MOL-ΣΣ without the inner B_4C shell.

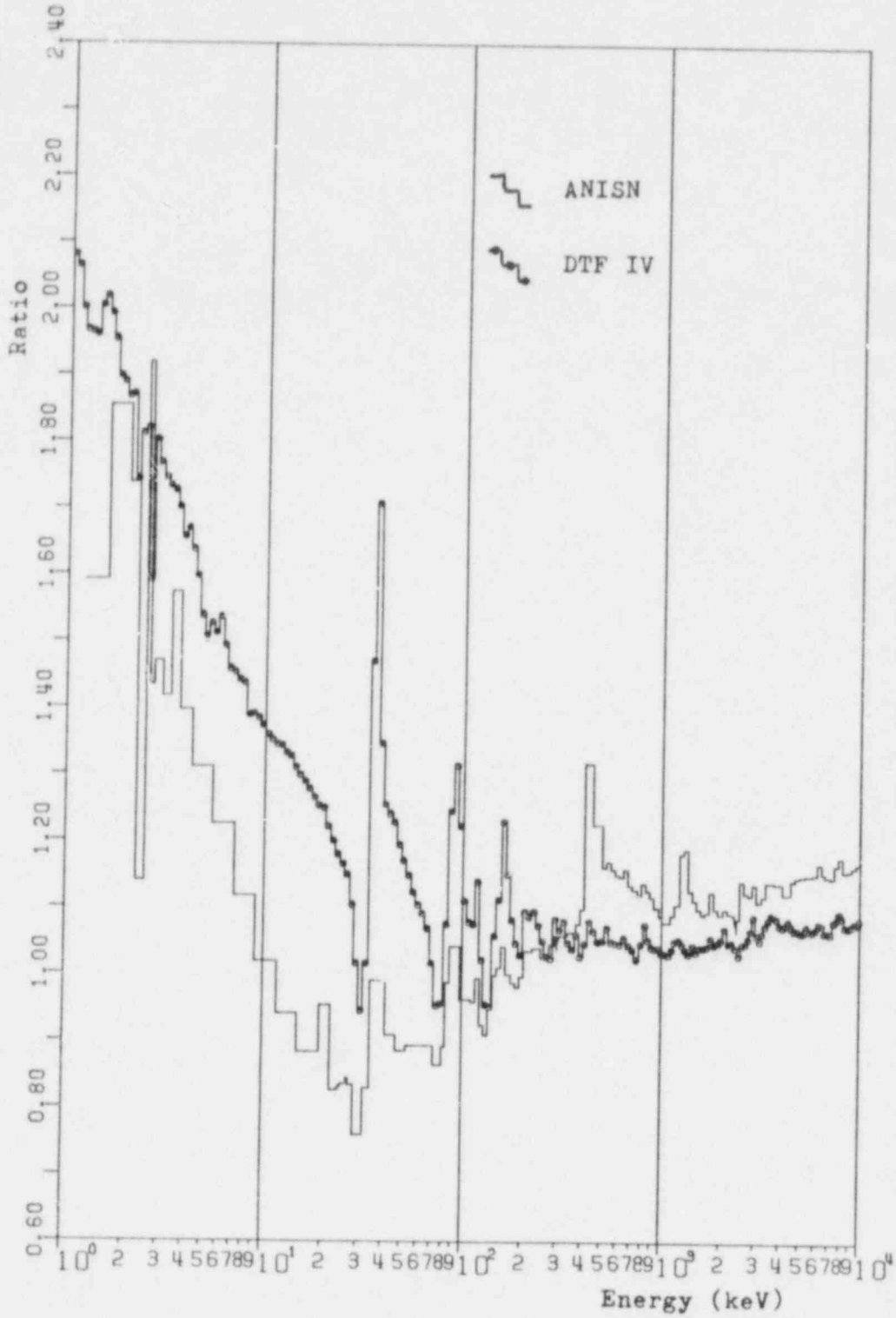

Fig. 2. Comparison of the ratios of the ANISN and DTF IV spectra calculated for MOL-ΣΣ without and with the B_4C shell.

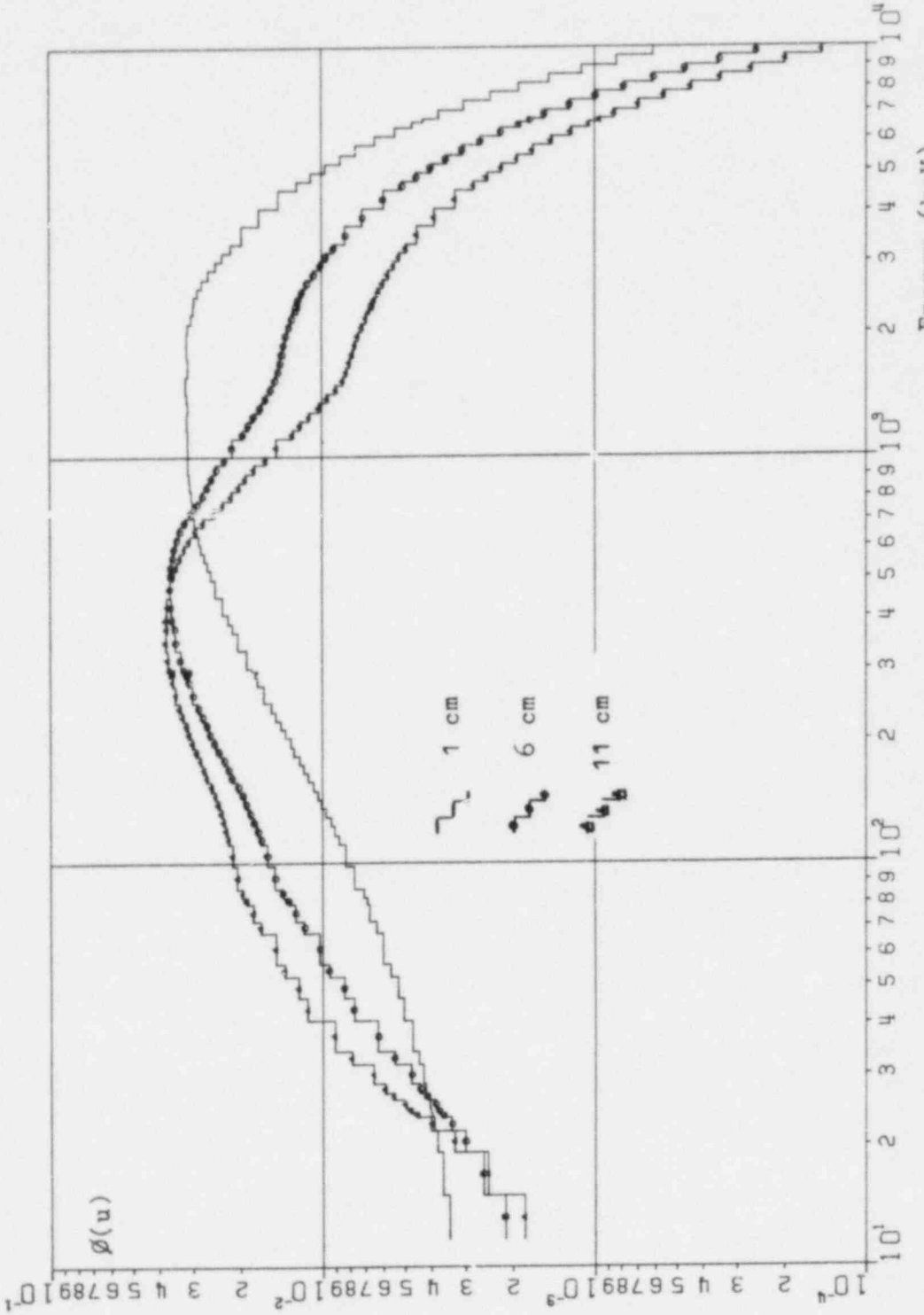

Fig. 3. Theoretical ANISN - VITAMIN/C central neutron spectra of the 1, 6 and 11 cm thick U_{nat} configurations.

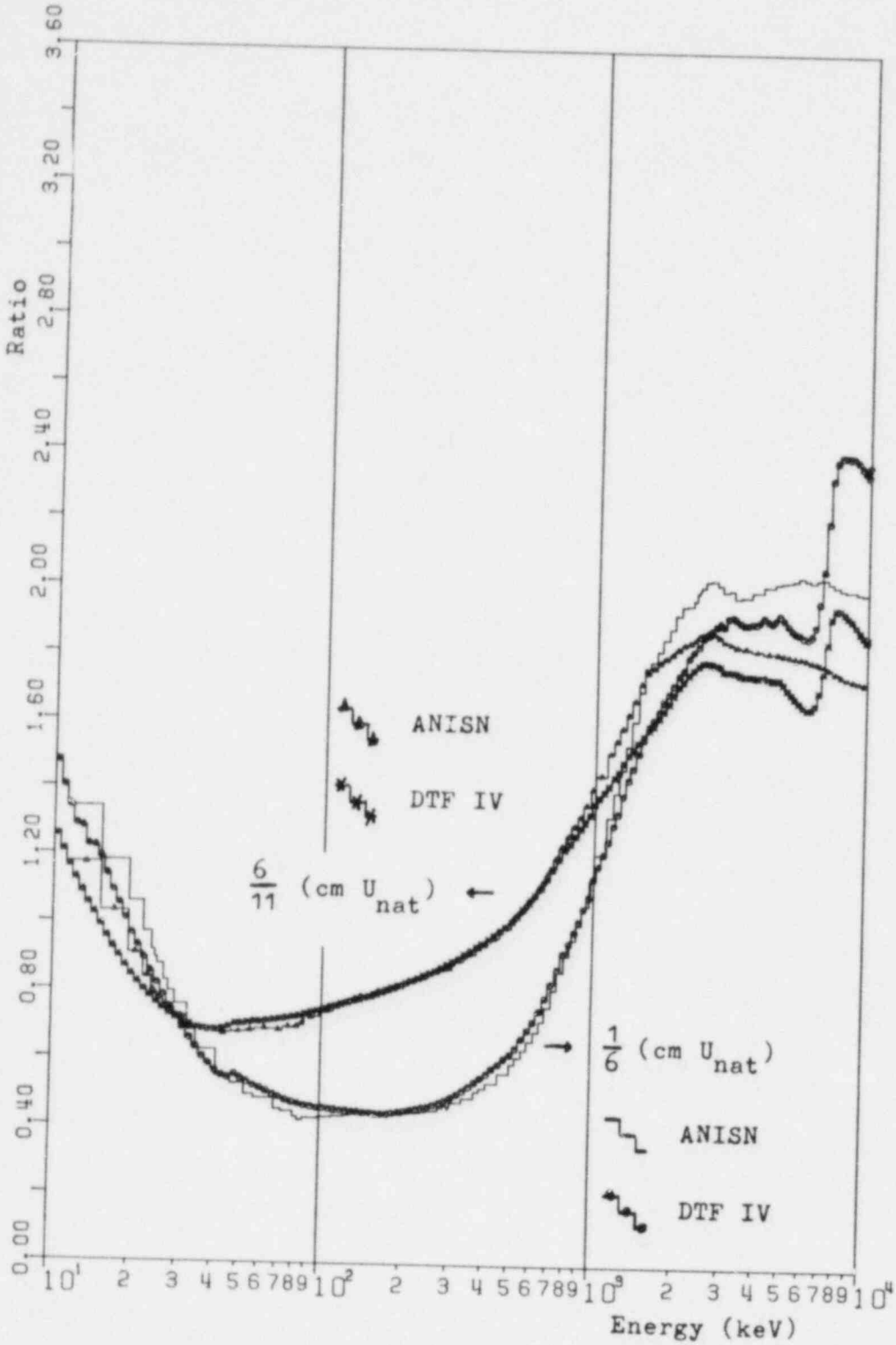

Fig. 4. Comparison of the ANISN - VITAMIN/C and DTF IV - KEDAK 3 spectral ratios for the 1/6 cm U_{nat} and 6/11 cm U_{nat} configurations.

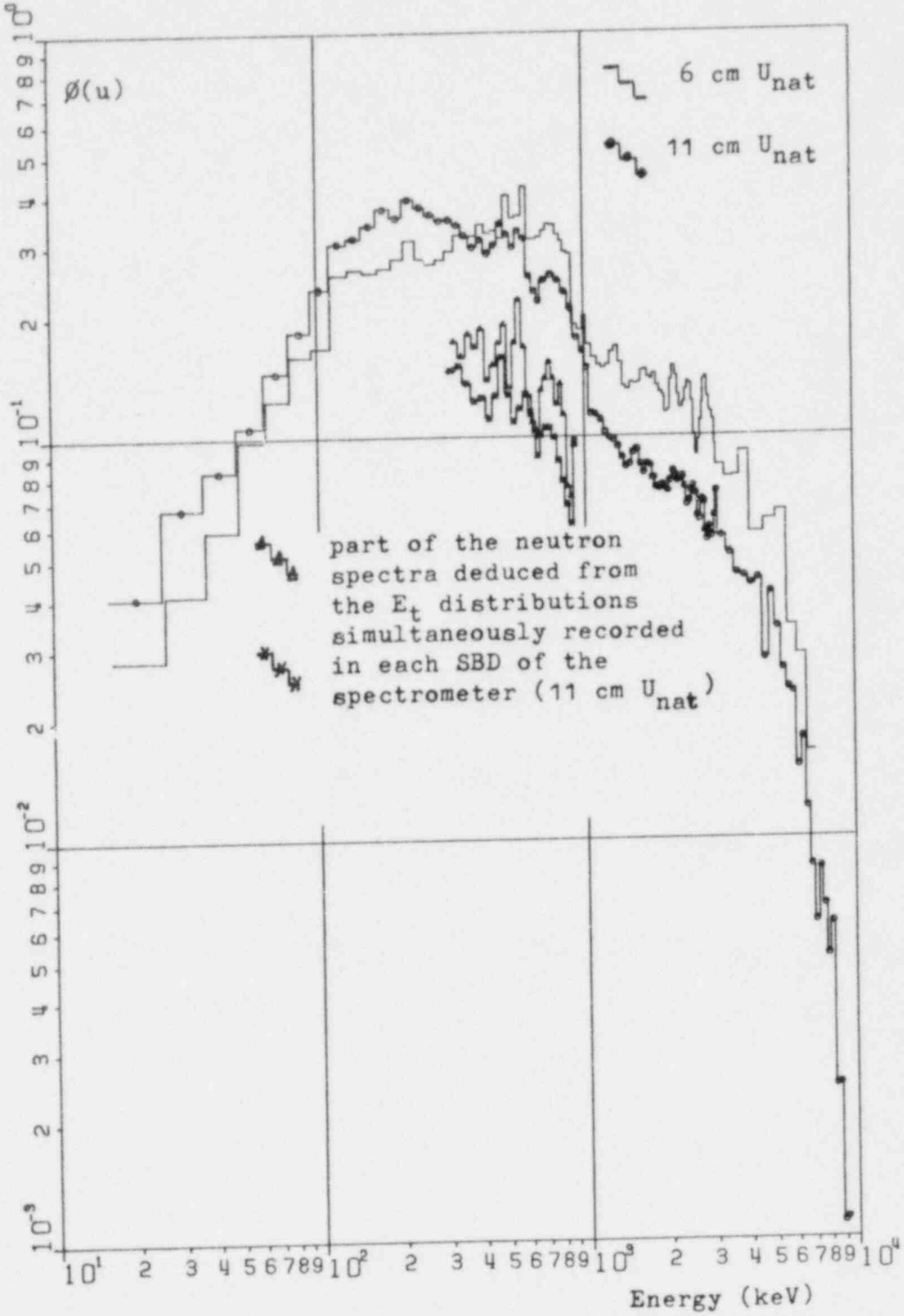

Fig. 5. Experimental Li-6 spectra in the center of the 6 and 11 cm U_{nat} configurations.

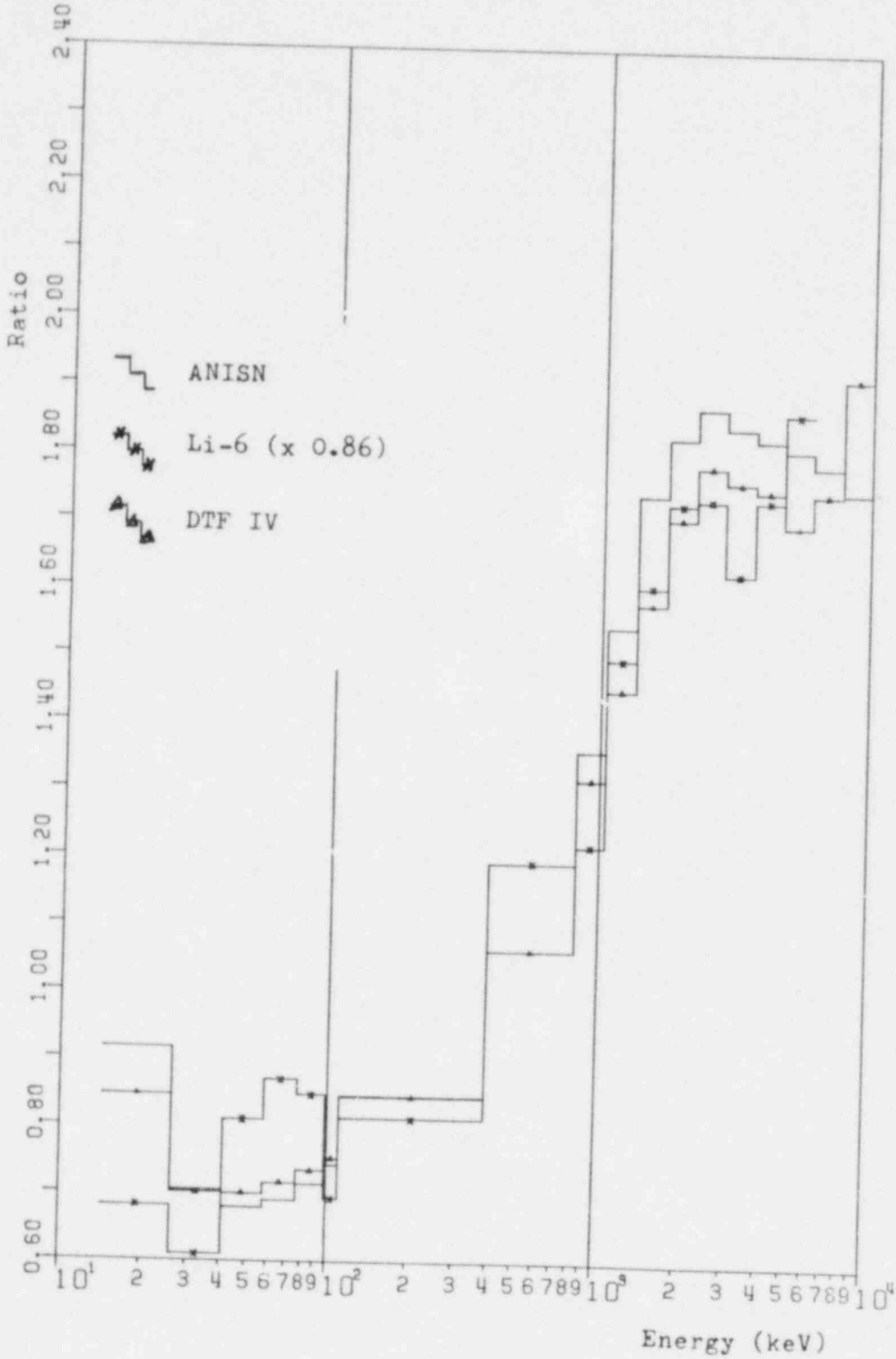

Fig. 6. Comparison in the ORNL energy group structure of the 6 cm/11 cm U_{nat} spectral ratios deduced from the ^{6}Li experiment, the ANISN and DTF IV calculations.

Session B.3
Fusion-I

PROPOSED NEUTRON DIAGNOSTIC SYSTEMS FOR JET

O. N. Jarvis, M. T. Swinhoe and P. Dixon
A.E.R.E., Harwell, Oxfordshire, OX11 ORA, U.K.

ABSTRACT

The neutron diagnostics systems currently proposed for installation on the Joint European Torus (JET) are described in this paper. These systems include a time-resolved neutron yield monitor (using fission counters), a time-integrated neutron yield monitor (employing activation techniques), two multi-collimator detector arrays for measuring neutron emission profiles and a variety of high-resolution neutron spectrometers for measurement of the energies of neutrons emitted from deuterium and deuterium/tritium plasmas.

INTRODUCTION

It is hoped that with the two tokamaks being assembled, the Joint European Torus (JET) in the U.K. and the Tokamak Fusion Test Reactor (TFTR) in the U.S., it will prove possible to demonstrate the scientific feasibility of fusion power from magnetic confinement reactors. The single parameter which most succinctly summarizes the state of progress towards this goal is the power multiplication factor, Q, which is the ratio of the total energy output from fusion reactions to the energy input to the device. The energy output is related to the number of fusion neutrons produced. It follows that a measurement of the total number of neutrons emitted from the plasma is of the greatest importance. But it is not sufficient just to count neutrons leaving the device; it is also necessary to identify the neutrons as being produced in D-D or D-T fusion reactions.

Whilst it is easy to establish the role of neutron measurements as an arbiter of success, as above, it should be appreciated also that the implicated techniques can be used to good account in the determination of plasma conditions, a contribution of more immediate significance. This aspect is particularly relevant for the new generation of tokamaks for which the neutron measurements will be all the more valuable because other, more conventional, diagnostic techniques will experience difficulties due to increasing plasma opacity and damage to instrumentation by neutron and gamma radiation.

The present paper contains a non-technical description of the comprehensive range of neutron diagnostics systems at present proposed for JET by our group at Harwell (U.K.) and by other groups at

Studsvik, Stockholm and Gothenberg in Sweden and at Mol in Belgium. At the time of writing only the Time Resolved Neutron Yield System has been approved by JET and is in the construction stage. The other systems are in the design stage and may be changed substantially before construction begins; indeed, there is no guarantee that all will be implemented. In particular, the plans for the 14 MeV spectrometer are still in the formative stage.

BACKGROUND INFORMATION

There are several processes which give rise to neutron production within the vacuum vessel of a tokamak. Neutrons, being uncharged, easily escape from the vessel and may be used for diagnostic purposes. However, in the case of JET (see fig. 1), the surrounding structure is massive and much of the energy and spatial information content will be lost unless the plasma volume is viewed through relatively thin vacuum windows.

The first neutron producing process to be encountered will be that associated with high-energy ($\lesssim$ 70 MeV) runaway electrons which appear at low plasma densities. These electrons will usually terminate their careers by striking a plasma limiter, thus giving rise to bremsstrahlung emission and hence inducing photoneutron emission from the limiter. Neutrons can also be produced directly from the deuterium ions by electron dissociation. These photoneutrons constitute an undesirable background for the more important neutron production processes.

At moderate plasma densities and temperatures the neutron production rates, assuming thermodynamic equilibrium, are proportional to the product $n^2 \langle\sigma v\rangle$ where n is the plasma density and $\langle\sigma v\rangle$ is proportional[1] to $T^{-2/3} \exp(-A\ T^{-1/3})$ with T the plasma temperature. The neutron production rates therefore afford a very sensitive determination of ion temperature (provided n is known). However, the production rate is very sensitive to departures of the ion energy distributions from Maxwellian so this approach must be used with care.

A more reliable measurement is obtainable through a study of the spread in kinetic energies of the thermonuclear neutrons. It can be shown[2] that these neutrons have an energy distribution which is approximately Gaussian with a fwhm of $82.5\sqrt{T}$ for DD plasma, and $198\sqrt{T}$ for DT plasma, where T is the plasma temperature in keV. Measurement of this broadening requires an instrumental energy resolution of the order of 3% for few keV plasmas.

Neutral beam injection, with injected powers of at least 10 MW, will constitute a major source of additional plasma heating. A D^o beam injected into a deuterium or tritium plasma will produce neutrons by beam-beam and beam-plasma collisions with an intensity an order of magnitude above that expected from a 5 keV deuterium plasma in thermodynamic

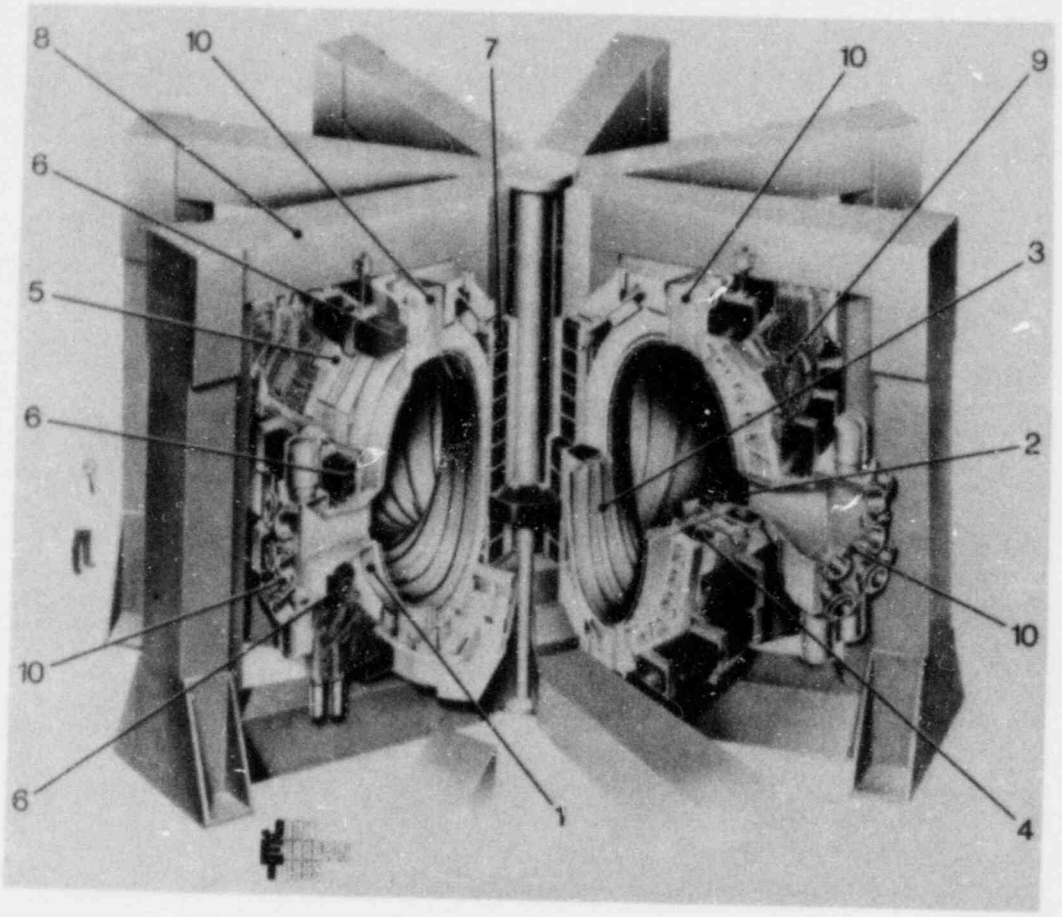

Fig. 1. The JET apparatus

1. Vacuum vessel (double walled)
2. Material limiter defining the outer plasma edge
3. Poloidal protective shields to prevent the plasma touching the vessel
4. Toroidal field magnet of 32 D-shaped coils
5. Mechanical structure
6. Outer poloidal field coils
7. Inner poloidal field coils (primary or magnetising windings)
8. Iron magnetic circuit (core and eight return sections
9. Water and electrical connections for the toroidal field coils
10. Vertical and radial ports in the vacuum vessel.

equilibrium. Also, there will be a considerable shift in energy of the beam-plasma neutrons as well as an enhanced broadening. Careful measurements of the beam-plasma neutron energy spectra should therefore provide valuable information concerning the fast ion distribution. Additional heating by r.f. methods is also planned for JET.

ENVIRONMENTAL PROBLEMS

Whilst the instrumentation proposed (Table 1) for neutron diagnostics is very familiar in the context of particle accelerators and reactors, as used for nuclear physics research, it should be appreciated that most of

Table 1. Proposed Neutron Diagnostics Systems

1. Time-Resolved Neutron Yield Monitor	- Six fission counters
2. Time-Integrated Neutron Yield Monitor	- Foil activation using gamma counting techniques. Delayed Neutron counting (proposed by the group at Mol).
3. Neutron Yield Spatial Profile Monitor	- Multichannel collimators to measure radial and vertical profiles.
4. 2.5 MeV Spectrometer	- ^{3}He ionization chamber and a proton-recoil counter. Time-of-flight measurement of scattered neutrons (proposed by the groups at Stockholm and Studsvik).
5. 14 MeV Spectrometer	- Proton-recoil with magnetic transport. Associated-particle time-of-flight measurement (proposed by groups at Stockholm and Gothenberg).

these techniques have not before been applied at an experimental plasma fusion facility. This new environment poses a number of problems (Table 2), none of which are individually serious but, taken together, they demand careful design, considerable circumspection and result in a much greater expenditure than would at first sight be expected.

Table 2. Environmental Problems

. Height above floor level (6m)
. Torus Hall temperature (up to 38°C)
. Time-varying magnetic fields (up to 150 gauss in the vicinity of some detectors)
. Unknown level of e.m. interference
. Vibration
. Pulsed operation (typical duty cycle - 10 sec plasma discharge every 10 min.)
. Wide dynamic range of neutron yields (10^8 to 10^{20} neutrons/discharge)
. Massive structure of JET scatters neutrons
. High neutron and gamma radiation backgrounds
. Spatially extended neutron source
. Radiation damage inhibits use of electronics in Torus Hall
. Remote handling capability needed
. Penetrations into Diagnostic Hall need comprehensively shielding

THE NEUTRON DIAGNOSTIC SYSTEMS

The five systems will be described in turn, concentrating mainly on any unusual features they might possess. A possible layout for these systems is illustrated in Fig. 2. The actual allocation of space for the neutron diagnostics has yet to be agreed; the problem of their disposition would be immediately apparent if the many other systems were also to be represented on the figure.

Neutron Yield Measurements (Time-Resolved)

The essential feature of a time-resolved neutron yield monitor is an ability to respond linearly to the rate of production of neutrons from JET during the discharge period, with an operational range covering 12 decades. Because the required efficiency is not very high it is acceptable to utilize fission counters. These provide large output signals which can be clipped hard so as to obtain a high countrate capability.

Two types of fission chamber are to be employed. The more sensitive contains 0.5g of ^{235}U and is surrounded with a 5 cm thickness of polyethylene moderator, giving a response of about 0.1 counts per $n.cm^{-2}$. The less sensitive chamber contains 0.5g of ^{238}U and no moderator: its response will be about 0.1×10^{-3} counts per $n.cm^{-2}$. The ^{235}U counter has a response which is engineered to be flat between 0.1 and 20 MeV; the ^{238}U counter has a threshold at about 1.5 MeV. These counters will be employed both in pulse-counting and current modes, depending on the neutron flux. Together, they will enable the neutron emission to be

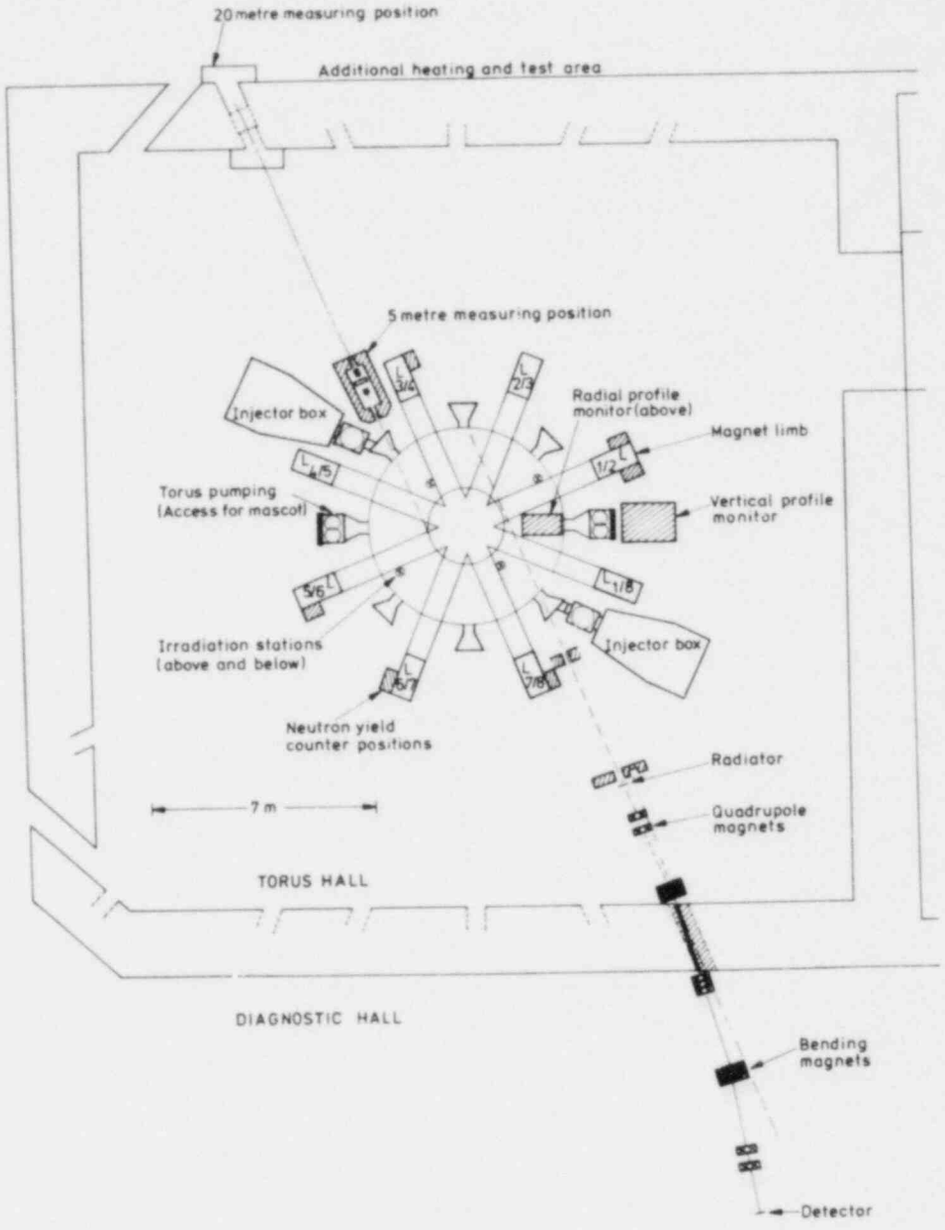

FIG.2. TORUS HALL SCHEMATIC, SHOWING POSSIBLE LOCATIONS FOR THE NEUTRON DIAGNOSTICS

monitored from 10^9 n/sec to 10^{21} n/sec.

Lead shielding is specified for both counters to reduce their responses to bremsstrahlung radiation arising during minor disruptions and to gamma radiation when the counters are operated in current mode.

Three pairs of fission counters are to be provided, positioned on the vertical magnet limbs at the horizontal mid-plane of the torus. By suitably distributing the counter positions in azimuth around the torus it should be possible to minimize (or identify) distortions caused by localized emission hot-spots.

The most significant technical problem connected with these counters is the need to operate them without the benefit of preamplifiers, which would be vulnerable to radiation damage (up to 100 Mrad total). Instead, the signals (~ 20 μV fast pulses and d.c. currents down to 100 na) will be transmitted along 100m coaxial cables to the diagnostic hall: superscreened cables[3] will be used to reduce the electromagnetic interference (from what can be expected to be a very noisy environment) to an acceptable level.

Neutron Yield Measurements (Time-Integrated)

The technique of Multi-Foil Activation analysis (MFA) is well established as a means for determining neutron fluences and energy spectra. The proposed activation system is complementary to the fission counters in that it gives only the time-integrated neutron yield, and the method is totally insensitive to some of the problems besetting the fission counters (magnetic fields, radiation damage, vibration, electrical interference) as the counting takes place at a remote station during the quiet periods between discharges. Most important, the measurements can be made absolute with high accuracy (~ 5%) because the eight irradiation positions are located within the bulk of the structure of the torus so that corrections for neutron attenuation are negligible and the backscattering is small and calculable.

To exploit the capabilities of the activation method it will be necessary to install a pneumatically operated transport system to move polyethylene capsules rapidly from a hopper to any specified irradiation position and from there to any of the remote stations for analysis. Three types of detector are proposed (Ge diode, NaI scintillator and Delayed Neutron Counting equipment), all duplicated. Also, a number of delay stations are required to hold irradiated capsules awaiting analysis. A transport system utilizing a 20-position carousel is proposed for this application.

The choice of activation reactions poses some difficulty because, on JET, we would ideally like to analyse irradiated samples from all eight irradiation stations following each 10-second discharge, with only 10 minutes permitted for counting the decay emissions.

Unfortunately, there are rather few reactions available which have reaction threshold energies suitable for use with D-D neutrons (i.e. thresholds between 1 and 2.5 MeV) which also offer the necessary sensitivity as these generally involve radioactive decay half-lives of the order of hours, if not days. The situation for 14 MeV neutrons is much better. The most sensitive of the reactions involves gross gamma-counting of short-lived radiations from fission foils. The foils used in gamma analysis must be allowed to cool for appreciable periods before they can be used again: this implies a need for a large inventory of foils and capsules. Alternatively, routine irradiation and analysis can be based on the technique of counting the delayed neutrons emitted from irradiated fission foils as advocated by the team from Mol. The longest half-life for delayed neutron emission is about 100 seconds and the overall sensitivity of the method is quite high (comparable with that for gross gamma-counting); it may prove possible to recycle the same foil for use in successive discharges, a very desirable operational simplification.

The Profile Monitor

The profile measuring system is intended to sample the intensity of neutron emission, as a function of position, from a vertical section of plasma. The measurements should give useful information (in the form of a neutron emission contour plot) on the behaviour of the plasma during MHD fluctuations and, more generally, on the shape of the plasma (which is non-circular). The device is intended to operate from low temperature DD operation (10^{15} n/shot) up to the highest temperature DT operation (10^{20} n/shot) with a spatial resolution of about 10 cm, to cover a spatial intensity variation of a factor of 100 and, at high yields, to offer a temporal resolution of a few milliseconds.

The equipment consists of two multicollimator assemblies positioned at one of the pumping port sectors, the horizontal profile device being supported on the magnet limbs and the vertical profile device being supported on a strong support tower. The entire profile monitoring equipment is designed for operation in the active phase so that a full remote handling capability is essential.

A number of design problems have been encountered with the profile monitor. First, the shielding has to be sufficiently thick that the background flux of neutrons entering through the sides is small compared with that entering via the collimators. Second, the physical separation between collimator channels must be sufficient to reduce the cross-talk to an acceptable level. Third, the plasma must be viewed through a thin window ($\leq$ 6 mm Inconel) otherwise the image of the plasma will be blurred by neutron scattering, much as a rainbow is blurred by viewing through a sheet of frosted glass. Fourth, the neutrons from the plasma must be observed against a background of lower energy neutrons back-scattered from the structural material lying in the field of view of the collimators. Finally, the neutrons must be distinguished against a background of gamma radiation.

For D-D operation a NE213 scintillator/photomultiplier combination offers the necessary efficiency, energy resolution (~10%) and n-γ discrimination properties. For D-T operation a much reduced efficiency is needed and the energy resolution requirement can be relaxed. A promising detector has been investigated by Chrien and Strachan[4]; it is a scintillator made from a mixture of LiF and ZnO which utilizes the $^{7}Li(n,n'\alpha)t$ threshold reaction and, like the Hornyak button, is insensitive to gamma radiation.

2.5 MeV Spectrometers

The most stringent objective that can reasonably be set for the spectrometers is that of making several determinations of the plasma ion temperature at 2 to 3 keV (and $n = 3 \times 10^{13}$ ions cm^{-3}) in a single 10-second discharge. To achieve this, an instrumental resolution of better than 4% is needed and the efficiency must be such that between 100 and 1000 counts are accumulated in the useful portion of the energy spectrum. Of course, both efficiency and resolution requirements can be relaxed when the ion temperature rises.

It is most unlikely that any single spectrometer can be constructed which will perform acceptably over the entire range of plasma conditions of interest. It is, therefore, necessary to pursue several approaches in the expectation that conditions will be favourable for at least one of them at all times.

Four spectrometers have been identified as being suitable for use with deuterium plasmas:

(i) the ^{3}He ionization chamber, which combines excellent energy resolution (2% at 2.5 MeV) with sufficiently high efficiency for it to be exploited on tokamak devices[5];

(ii) a thin-radiator "in-line" proton-recoil device, in which the silicon diode detector is positioned to detect forward-scattered protons but must also suffer the transmission of the unscattered neutron beam;

(iii) the thick-target NE213 scintillator, offering poor energy resolution (~ 10%) but very high efficiency and therefore useful for detecting the 0.5% of 14 MeV neutrons emitted from secondary t-d reactions in the deuterium plasma;

(iv) a time-of-flight spectrometer as proposed by Elevant[6]; it is based on the detection of double-scattering events in two NE213 scintillators, offers efficiency similar to that of the ^{3}He chamber but requires very good shielding from background neutrons.

Of these, the ^{3}He ionization chamber and the NE213 scintillator do not demand the angle of incidence of the neutrons to be defined by

collimation, the "in-line" proton-recoil device requires only modest collimation (± 8°) whilst the time-of-flight approach needs tight collimation (± 0.5°). This varying permissiveness in the degree of collimation is seen to be illusory when the further specification is added that the desired spatial resolution at the plasma should be no more than 10 cm.

The present intention is to house the first three spectrometers (listed above) inside a moveable shield/collimator assembly positioned against one of the horizontal diagnostic ports and viewing the plasma tangentially. This is the 5 metre position. These detectors share the properties of being of modest dimensions and of not being unduly sensitive to background neutrons. The shielding assembly is being designed for operation with deuterium plasmas only and the spectrometers it contains will only be operated for relatively low neutron yields. Thus, it will be of a very simple design and - since it is not required for use in the active phase - need not be fully prepared with remote handling attributes.

The time-of-flight spectrometer as proposed by the team from Sweden requires a detector separation of up to 3 metres. As it is fairly efficient, but must be provided with a spacious low background environment, it appears sensible to locate it outside the biological shield wall, from which position it can view the plasma through two collimators - the first in the moveable shield assembly and the second in the biological shield wall. Even at this large distance (20 metres) the time-of-flight equipment should come into operation for plasma temperatures as low as 4 keV and even lower temperatures when beam-heating is used. For high neutron yields from deuterium plasmas a second ^{3}He ionization chamber will join the time-of-flight spectrometer at the 20m station.

14 MeV Spectrometers

The obvious approach to high-resolution spectrometry with 14 MeV neutrons is the conventional "scattering-geometry" proton-recoil arrangement, in which knock-on protons from a thin-radiator are detected in silicon diodes set at a sufficiently large angle (> 10°) to the incident neutron direction that incident neutrons do not pass through the detector. The solid angle subtended by the detector at the radiator must be kept small if an overall energy resolution of 2% is to be achieved, with the result that the detection efficiency of the spectrometer is very low. Even allowing for the likelihood that tritium operation will not be embarked upon until an ion temperature in a deuterium-only plasma in excess of 5 keV has been attained, the requirement of obtaining several good spectra in a single discharge demands that the plasma to spectrometer separation should be kept as short as possible. The original proposal was therefore to house the proton-recoil spectrometer within a massive (100 tonne) but moveable shield unit, provided with full remote handling capabilities and positioned

inside the torus hall as close to one of the diagnostic ports as possible.

The approach described above has the obvious disadvantage of being inconvenient and expensive. Consequently, much thought has been given to the design of a more efficient spectrometer which can be located further from the plasma with the biological shield wall providing at least the major portion of the required shielding against background neutrons. This is precisely the reasoning applied for 2.5 MeV spectrometry for high plasma temperatures. Of course, with this approach the radiation levels in the diagnostic hall will be much greater for a deuterium-tritium plasma than for a deuterium-only plasma and a substantial secondary shield wall surrounding the spectrometer in the diagnostic hall will be essential.

Three ideas for high-efficiency 14 MeV spectrometers are being investigated. The first possibility is to take advantage of the nuclear reaction induced by high-energy neutrons in a silicon diode. The $^{28}Si(n,\alpha_0)^{25}Mg$ reaction[7] leading to the ground state in ^{25}Mg has a 14 MeV cross-section of about 15 mb and offers an instrumental resolution of slightly less than 1%. Unfortunately, the method has a number of disadvantages and has never yet been applied to a directly comparable problem. Also radiation damage is such that this method is unsuitable for routine use and must be reserved for special investigations where the best possible energy resolution is needed.

The second technique, being studied in Sweden, is the associated-particle time-of-flight method. This is a thin-radiator proton-recoil spectrometer in which the solid angle subtended by the proton detector at the radiator is permitted to be relatively large. If nothing else were to be done, the energy resolution would be poorer than 10%. However, by recording the time-of-arrival of the scattered neutron in a suitably placed detector relative to the proton arrival time it is possible (since the proton energy is measured accurately) to deduce the energy of the scattered neutron and to obtain, by summation, that of the incident neutron. This method promises good energy resolution (~ 2%) with an efficiency not much less than that of the "in-line" proton-recoil method. Unfortunately, if the spectrometer is located in the diagnostic hall there will remain the problem of building a substantial shield wall around the instrument to protect personnel in that area from the transmitted neutrons.

Finally, consideration is also being given to the design of an "in-line" proton-recoil technique in which magnetic elements are used to transport the recoil protons to a detector positioned well away from the transmitted neutron flux. Several arrangements are possible, of which the one illustrated in Fig. 2 is the most favoured at present because the detector is located conveniently within the diagnostic hall, yet there is no direct view from the diagnostic hall of the torus - so that the radiation leakage into the diagnostic hall should be small. The particular problem of this approach is that the magnetic transport system

must be achromatic over an energy band of ± 5% (at least) centred on 14 MeV.

ACKNOWLEDGEMENTS

The plans for neutron diagnostics at JET outlined above include proposals from the Harwell (U.K.) team, from the group at Mol (A. Fabry and colleagues) concerned especially with delayed-neutron counting and from the groups in Studsvik, Stockholm and Gothenberg (T. Elevant, J. Lorenzen and colleagues) concerned with exploiting the Time-of-Flight approach. The design work has been greatly influenced by the work done at Princeton, both in practice on PLT and in planning for TFTR, and also from discussions with members of the JET diagnostics team, in particular with P. Stott and G. Sadler.

This work was carried out under contracts B-EH-394, JBO/9006, JB1/0132 and JB1/9001 with the JET Joint Undertaking.

REFERENCES

1. D. L. Book, "NRL Plasma Formulary", 1978 (revised).

2. H. Brysk, "Fusion neutron energies and spectra", Plasma Physics 15 (1973) 611.

3. E. P. Fowler, "Superscreened cables", The Radio and Electronic Engineer 49 (1979) 38.

4. R. E. Chrien and J. D. Strachan, "Selective fast neutron detector", Rev. Sci. Instrum. 51 (1980) 1638.

5. J. D. Strachan et al, "Measurement of the neutron spectra from beam-heated PLT plasmas", Nature 279 (1979) 626.

6. T. Elevant, "A neutron spectrometer suitable for diagnostics of extended fusion plasmas", Nuclear Instruments and Methods 185 (1981) 313.

7. D. W. Mingay, J. P. F. Sellschop and P. H. Johnson, "Neutron induced reactions in silicon semiconductor detectors", Nucl. Instr. and Methods 94 (71) 497.

NEUTRON FLUX AND SPECTRAL MEASUREMENTS TO CHARACTERIZE IRRADIATION FACILITIES FOR FUSION MATERIALS STUDIES

L. R. Greenwood
Argonne National Laboratory
Argonne, Illinois, U.S.A.

ABSTRACT

Neutron dosimetry measurements are described to characterize fusion irradiation facilities including fission reactors and particle accelerators. Multiple activation measurements are used to adjust the flux-spectrum. All sources of uncertainty are considered and correlations are assigned resulting in a covariance matrix for the adjusted flux-spectrum which can be used to propagate errors in damage parameters. Nuclear cross-sections have been tested and the results are summarized.Deficiencies in nuclear data and procedures are discussed.Examples are shown for the High Flux Isotopes Reactor at ORNL, spallation-type Intense Pulsed Neutron Source at ANL, and 14 MeV Rotating Target Neutron Source II at LLNL.

INTRODUCTION

Fusion reactors are expected to produce very high fluxes ($\sim 10^{15}$ n/s) of fast neutrons capable of causing severe damage in materials due to the displacement of atoms, gas generation, and nuclear transmutation. Since fusion reactors are not available for materials testing, this work is being conducted at a variety of irradiation facilities. Unfortunately, no one, single facility duplicates expected fusion neutron energy spectra and flux levels. Hence, several distinctly different types of neutron sources must be used. Fission reactors produce high neutron fluxes, although the neutron energy is low resulting in slow atomic displacement rates and little gas generation. However, nickel-bearing materials, such as stainless steel, can be studied thanks to the high thermal cross-sections leading to helium production. The 14-MeV neutron generators produce fusion-energy neutrons; however, the fluxes available ($\sim 10^{13}$ n/s) are quite low compared to fusion reactors. Broad-spectrum accelerator sources using the Be(d,n) or spallation reactions can also be used to produce comparable levels of fast neutrons; however, the energy spectra extend to 40-50 MeV, somewhat complicating the picture.

In order to make sense out of the materials studies now underway at these neutron facilities, we must be able to routinely measure the neutron fluences and energy spectra and to calculate the resultant atomic displacements, gas production, and transmutation. Preliminary studies[1] support the belief that these basic exposure parameters can be used to correlate materials effects between facilities and eventually to predict materials behavior in fusion reactor environments.

We have developed techniques to measure neutron fluxes and energy spectra at all of the existing materials facilities, primarily using the multiple-foil activation method.[2] Dosimetry materials are now routinely included with all fusion materials irradiations. Following irradiation, gamma spectroscopy is usually employed to determine activation rates which are then used to adjust neutron flux-spectra with the STAYSL computer code.[3] All uncertainties and data correlations are explicitly considered so that errors can be specified for all measured and calculated exposure parameters. Our calculation of damage rates is presented in the following paper at this symposium. We have also worked closely with Rockwell International to measure helium production cross-sections for dosimetry as well as gas production; this work is presented in a joint paper at this symposium. The neutron flux-spectral measurement technique will be illustrated for several facilities in the remainder of this paper.

Nuclear Data and Uncertainties

The success of our technique to measure neutron flux-spectra depends quite heavily on our knowledge of neutron activation cross-sections. Many of the cross-sections can be obtained from ENDF/B-V[4] supplemented above 20 MeV with measurements at LANL,[5] extrapolated where necessary to 50 MeV.[6] Integral testing has been performed, especially for the high-energy neutron data used at particle accelerators.[7,8] The results of these tests, summarized in Table 1, along with similar integral testing in fission benchmark fields, demonstrates that the nuclear data base is adequate for most routine dosimetry, although more data is needed, especially above 14 MeV. In fission reactors, several reaction cross-sections are found to be discrepant, such as $^{47}Ti(n,p)$, $^{60}Ni(n,p)$, and $^{58}Ni(n,2n)$. For accelerators, multiple (n,xn) reactions are needed to cover the energy region above 28 MeV, where no measurements currently exist. Specific requests have been made to WRENDA to cover these needs.

Uncertainties and covariances are assigned to all cross-sections used to adjust the neutron energy spectrum. A least-squares procedure is used to minimize χ^2 by constructing a covariance matrix for the input flux spectrum, integral activity measurements, and activation cross-sections. Uncertainties in the starting spectrum are usually the largest (30-100%) since this data is not generally available from neutronics calculations. Activity errors are usually quite small (1-5%) and contribute little to the uncertainty in the flux spectrum. Cross-section uncertainties are typically 5-30%; however, correlations are very poorly known either between energy groups or between different reactions.

Table 1. Results of Integral Cross Section Testing

Differential cross sections from ENDF/B-V, unless noted.
Estimated cross section errors are listed in percent.

Reaction	ORR[a]	RTNS II[b]	Be(d,n)[c]	
	Mixed-Spectrum	0°, 14.9 MeV	14-16 MeV	40 MeV
$^{27}Al(n,\alpha)^{24}Na$	+2	+6	+6	-1
$^{45}Sc(n,2n)^{44m}Sc$[d]	-	-3	-15	+3
$Ti(n,x)^{46}Sc$	-1	+9	-1	+24
$Ti(n,x)^{47}Sc$	+25	-28	+6	-56
$^{48}Ti(n,p)^{48}Sc$	-2	-8	-1	+4
$Fe(n,x)^{54}Mn$	-3	-2	-3	+4
$^{54}Fe(n,\alpha)^{51}Cr$[d]	-17	+3	+1	-20
$^{56}Fe(n,p)^{56}Mn$	-	-	-2	-4
$^{55}Mn(n,2n)^{54}Mn$	-2	-7	-	-
$^{59}Co(n,p)^{59}Fe$[d]	-	+26	-4	+5
$^{59}Co(n,2n)^{58}Co$	-	+2	+6	-3
$^{59}Co(n,\alpha)^{56}Mn$	-	-	-2	-5
$^{58}Ni(n,p)^{58}Co$	-3	+12	-3	+3
$^{58}Ni(n,2n)^{57}Ni$	-	-12	+1	+14
$^{60}Ni(n,p)^{60}Co$	+13	-22	-2	+3
$^{63}Cu(n,\alpha)^{60}Co$	-4	-4	-	-
$Zr(n,xn)^{89}Zr$[d]	+7	-6	+9	-1
$^{93}Nb(n,2n)^{92m}Nb$[d]	-4	(+6)[b]	+6	+7
$^{107}Ag(n,2n)^{106m}Ag$[d]	-	+8	-	-
$^{169}Tm(n,2n)^{168}Tm$[d]	-	+5	-	+10
$^{169}Tm(n,3n)^{167}Tm$[d]	-	-	-	-8
$^{197}Au(n,2n)^{196}Au$[d]	-1	-2	-8	+1
$^{197}Au(n,3n)^{195}Au$[d]	-	-	-	+12
$^{197}Au(n,4n)^{194}Au$[d]	-	-	-	+1
$^{115}In(n,n')^{115m}In$	-	-	-2	-2
$^{235}U(n,f)$	-1	-	+8	+1
$^{238}U(n,f)$	-2	-	+4	-1
$^{238}U(n,2n)^{237}U$[d]	-	-	+1	-11

[a] Spectrum from neutronics calculation; values relative.

[b] T(d,n) source; values normalized to $^{93}Nb(n,2n)$, 463 mb ± 7%.

[c] See References 7 and 8.

[d] Cross section not in ENDF; see Reference 6.

There are a number of special problems which have not yet been addressed which can significantly affect uncertainty data. The most important one is that codes are not yet available to assign group uncertainties and covariances in the resonance region, although such computer codes should be available shortly. Uncertainties also cannot be assigned at present to a variety of corrections including neutron self-shielding, burnups, cadmium or other covers, and flux-spectral gradients. Although geometric self-shielding corrections are included with the cross-sections prior to spectral adjustment to minimize uncertainties. For accelerators, gradients may be incredibly steep, resulting in some additional uncertainty in the comparison of reaction rates at different locations. Finally, variations in the irradiation history can introduce relative errors between reactions with different half-lives. Work is clearly needed to develop more rigorous procedures for assigning such uncertainties. Nevertheless, these uncertainties are generally quite small compared to uncertainties in the trial flux spectrum and cross-sections.

At present, a number of educated guesses are unavoidable in the spectral unfolding process, especially concerning uncertainties and covariances. However, it should be pointed out the very fact that we are now including such data represents a major advance in the technique. Of course, data will improve slowly as new measurements are made, although sensitivity studies are also badly needed to help understand the meaning of some of our approximations. It should also be remembered that fine details in the flux-spectrum are rarely of interest to damage experiments and their effects are usually unimportant in defining neutron fluences or displacement damage rates.

Neutron Flux and Spectral Measurements

Activation dosimetry has been used to measure the neutron flux spectrum in most facilities currently in use for fusion materials studies. Fission reactors include the Oak Ridge Research Reactor (ORR) and High Flux Isotopes Reactor (HFIR), both at Oak Ridge National Laboratory; the Experimental Breeder Reactor II (EBR II) at Argonne National Laboratory (Idaho); the Omega West Reactor (OWR) at Los Alamos National Laboratory; the High Flux Beam Reactor (HFBR) at Brookhaven National Laboratory; and the FRM reactor at the Technical University of Munich, Germany. Measurements have also been made in a variety of other reactors at national laboratories and universities. The principal accelerator source measurements have been made at the 14-MeV Rotating Target Neutron Source II (RTNS II) at Lawrence Livermore Laboratory;[9] the Be(d,n) cyclotron source at the University of California at Davis (UCD);[10] and the spallation-type Intense Pulsed Neutron Source (IPNS) at Argonne National Laboratory.[11]

Figure 1 gives a general overview of these irradiation facilities in terms of weekly displacements per atom (DPA) and helium production in iron. The line labeled fusion starts at a wall loading of 1 MW/m^2. FMIT stands for the planned Li(d,n) Fusion Materials Irradiation Test Facility

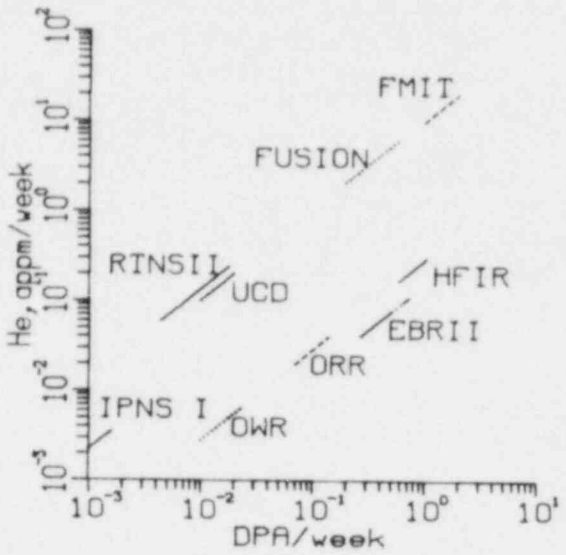

Fig.1. Comparison of Weekly DPA and He Production Rates in Iron for Various Irradiation Facilities (see text).

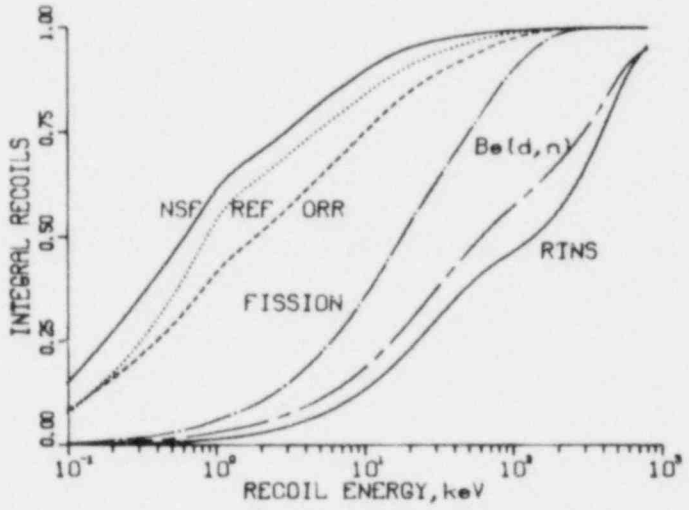

Fig. 2. Integral Recoil Fractions in Nickel for Various Neutron Sources. The Neutron-Scattering and Radiation Effects Facilities of the IPNS are Compared to the Oak Ridge Reactor, a Fission Spectrum, a Be(d,n) Source, and RTNS.

Unfortunately, construction of this facility is now uncertain. Fission reactors can produce high DPA rates; however, helium production is low except in nickel-bearing alloys where thermal helium production is significant. Accelerators do produce the right mix of DPA and helium; however, the rates are quite low in present facilities.

Figure 2 shows integral recoil curves in nickel for various irradiation facilities. Clearly, spectral differences are very important and neutron fluence is somewhat meaningless when comparing damage produced at different sources.

Figures 3 and 4 compare measured spectra at three of these irradiation facilities. The dotted and dashed lines represent one standard deviation uncertainties in individual flux groups. However, these values are quite misleading since the output fluxes are highly correlated. The entire spectrum cannot be moved to either extreme; instead, an increase in one part of the spectrum (e.g., thermal) can only be accomplished by a simultaneous decrease in some other part of the spectrum (e.g., epithermal). Actually, the output uncertainty matrix is a 10,000-element array which must be used to properly calculate uncertainties in integral fluxes or damage parameters. Due to strong anti-correlations in broad flux groups, these integral uncertainties are typically only 10-15%. This should not be surprising since our activation measurements are also integral measurements which are known to 2-5%.

The HFIR spectrum in Figure 3 is typical of a measurement in a mixed-spectrum reactor and is similar to ORR and OWR. The particular data shown was obtained during an actual materials irradiation for the fusion program (CTR32) lasting 124 days. It is important to note that results can be easily obtained under these restrictive conditions with only a limited number (10) of activation measurements. Much better spectral measurements can of course be made during short irradiations where we can use cadmium or gadolinium covers, fissionable materials, and reactions with short half-lives. In the best cases, 35-40 reactions can be measured. Such a measurement has been made for ORR and this data was used in the REAL-80 exercise. (See the paper by C. Ertek reporting the status of REAL-80 also at this symposium.) Two problems are the most significant in fission reactor measurements. First, there is a shortage of activation reactions with very long-lived reaction products. Some materials irradiations in ORR are expected to last 5-6 years. Hence more nuclear data is needed. However, we are also developing stable product dosimetry techniques and have already integrated helium measurements jointly with Rockwell International (see paper by D. Kneff also at this symposium). The other difficulty countered in reactor dosimetry is the lack of sensitivity in the 1-500 keV energy range. Reactions such as $^{93}Nb(n,n')^{93}Nb(16y)$ would help in this energy region; however, it will always be necessary to place some reliance on calculations in this energy region.

The IPNS spectra shown in Figure 3 are typical of a spallation source. The spectra extend upwards to 500 MeV, the energy of the proton

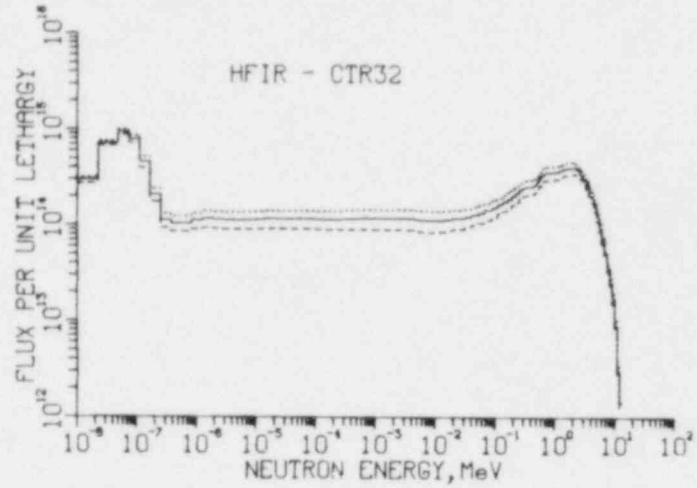

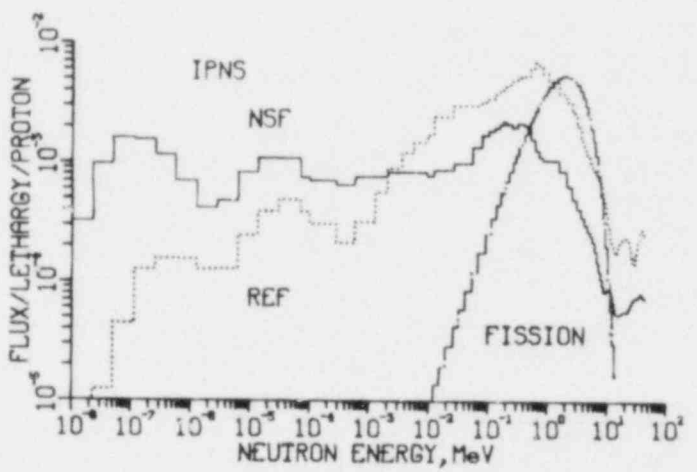

Fig. 3. Measured Neutron Spectra for the HFIR Reactor at ORNL and the IPNS Spallation Neutron Source at ANL. The Dotted and Dashed Lines Show One Standard Deviation Errors; However, Group-to-group Correlations are Very Strong. The Neutron Scattering Facility (NSF) at IPNS has a Be-c Moderator Resulting in a Softer Spectrum than at the Radiation Effects Facility (REF) With a Pb Moderator.

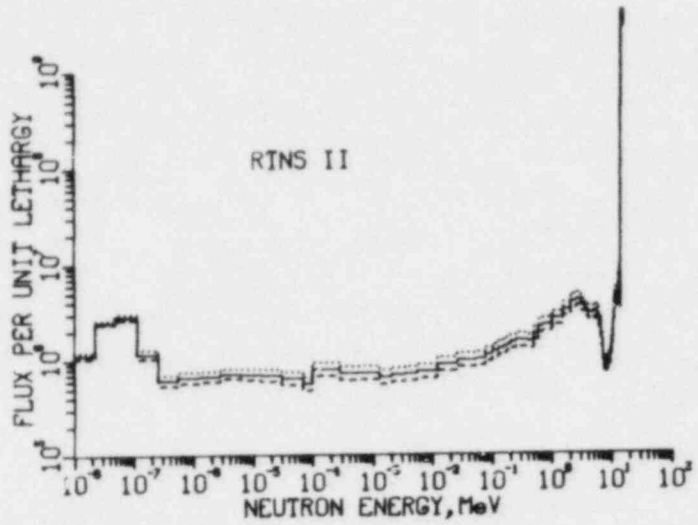

Fig. 4. Measured Neutron Spectrum at the RTNS II d-t Neutron Source at LLL at a Distance of 30 cm on the 0° Beam Axis. The 14.9 MeV Spike is from the Source and All Lower Energy Neutrons are Due to Scattering from the Walls. The Room Return Energy Spectrum is Constant Throughout the Target Room.

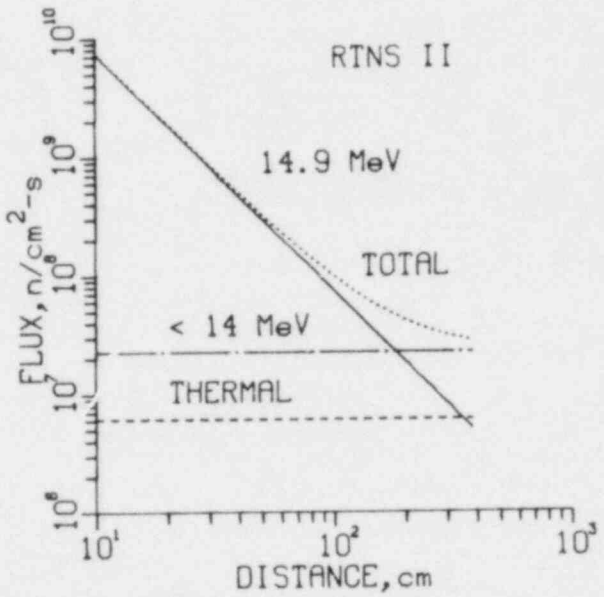

Fig. 5. Neutron Flux Maps for the RTNS II d-t Source at LLL. The 14.9 MeV Spike Decreases as the Distance Squared Whereas the Room Return Flux is Isotropic. The Room Return Flux is Insignificant (<1%) at Distances Less Than 18 cm.

beam; however, our activation cross-section files only extend to 44 MeV and there are no known cross-section measurements above 28 MeV. Multiple (n,xn) reactions should be measured in the 20-50 MeV energy range. Above this energy, spallation reactions could be used, as demonstrated recently by Routti and Sandberg.[12] However, less than 1% of displacement damage in materials is caused by neutrons above 30 MeV, so the weak, high-energy tail of the spectrum is not very important. Actually, the spectrum is rather low-energy and vaguely resembles that of a fast breeder reactor like EBR II. Studies are now in progress to define the weak gamma and proton fluxes at IPNS since these contribute to total ionization doses in insulators. The IPNS now has a fully operational cryogenic facility for damage studies.[11]

Extensive measurements have been made at RTNS II in collaboration with Lawrence Livermore Laboratory and Rockwell International. Helium generation samples were irradiated near the source and numerous radiometric samples were irradiated at distances of 5, 15, 30, 120, and 380 cm from the source. Cross-section measurements are summarized in Table 1. The $^{58}Ni(n,p)$ and (n,2n) reactions are especially troubling since the ratio indicates a 24 % relative error in the ENDF/B-V dosimetry data. Figure 4 shows a spectrum obtained at 30 cm. Figure 5 shows that the room return neutrons are isotropic in the target room. The spectra were calculated by C. Logan[13] and adjusted slightly with 17 reactions. The total room return neutron flux (<14 MeV) is only 3.1% at 30 cm from the source increasing to 32% at 120 cm and 83% at the backwall. (In fact, the room return flux is isotropic and the 14 MeV flux decreases as the distance is squared.) At distances closer than 30 cm from the source, the room return flux cannot be observed (<1% of total) except in the thermal reactions. The RTNS II spectrum shown in Figure 4 is especially interesting since it resembles the spectrum expected at the first wall of a fusion reactor. The steady state flux at 100 cm is about 10^8 n/cm^2-s resulting in about 10^{13} n/cm^2 in a week. This fluence level is comparable to that expected in some experiments at the TFTR fusion reactor under construction at Princeton. By placing moderator materials closer to RTNS II it is clear that return neutrons could be increased to generate higher fusion-like flux-spectra for fusion materials studies.

The above examples demonstrate that neutron sources can be adequately characterized for materials studies. Neutron fluences and damage parameters can generally be measured to relative accuracies of 10-15% for an irradiation, although it should be pointed out that uncertainties in displacement and transmutation cross-sections are at least this large resulting in absolute errors of 15-20% for calculated damage parameters. Improvements are needed in the nuclear data base to reduce these uncertainties. The success of these measurements of neutron exposure parameters can only be determined by future attempts to correlate various materials properties between the diverse neutron facilities.

REFERENCES

1. R. R. Vanderwoort, E. L. Raymond, and C. J. Echer,Radiation Effects 45, 191 (1980).

2. L. R. Greenwood, Review of Source Characterization for Fusion Materials Irradiation, BNL-NCS-51245, p. 75 (1980).

3. F. G. Perey, "Least-Squares Dosimetry Unfolding: The Program STAYSL," ORNL-TM-6062 (1977); modified by L. Greenwood (1979).

4. Evaluated Nuclear Data File, Part B, Version V, National Neutron Cross-Section Center, Brookhaven National Laboratory (1979).

5. B. P. Bayhurst, J. S. Gilmore, R. J. Prestwood, J. B. Wilhelmy, N. Jarmie, B. H. Erkkila, and R. A. Hardekopf, Phys. Rev. C12, 451 (1975).

6. L. R. Greenwood, "Extrapolated Neutron Activation Cross-Sections for Dosimetry to 44 MeV," ANL-FPP/TM-115 (1979).

7. L. R. Greenwood, R. R. Heinrich, R. J. Kennerley, and R. Medrzychowski, Nucl. Technol. 41, 109 (1978).

8. L. R. Greenwood, R. R. Heinrich, M. J. Saltmarsh, and C. B. Fulmer, Nucl. Sci. Eng. 72, 175 (1979).

9. D. W. Kneff, B. M. Oliver, M. M. Nakata, and H. Farrar IV, Experimental Helium Generation Cross-Sections for Fast Neutrons, to be published in Jour. Nucl. Mater.

10. D. W. Kneff, H. Farrar IV, L. R. Greenwood, and M. W. Guinan, "Characterization of the Be(d,n) Neutron Field by Passive Dosimetry Techniques," BNL-NCS-51245, p. 113 (1980).

11. M. A. Kirk, R. C. Birtcher, T. P. Blewitt, L. R. Greenwood, R. J. Popek, and R. R. Heinrich, Jour. Nucl. Mater. 96, 37 (1981).

12. J. T. Routti and J. V. Sandberg, Commputer Physics Communications 21, 119 (1980).

13. C. Logan, Lawrence Livermore Laboratory, private communication, (1981).

DISPLACEMENT DAMAGE CALCULATIONS USING ENDF/B-V CROSS SECTIONS INCLUDING THERMAL CAPTURE AND BETA DECAY EFFECTS*

R. K. Smither and L. R. Greenwood
Argonne National Laboratory
Argonne, Illinois, U.S.A.

ABSTRACT

Materials irradiations at reactors and accelerators require accurate knowledge of neutron exposure parameters in order to correlate property changes between facilities and to predict materials performance in future fission or fusion environments. Presently, the most reliable exposure index is the number of atoms displaced from their lattice sites or displacements-per-atom since this removes the dependence on the neutron energy spectrum. Displacement damage cross sections have been calculated to 20 MeV for 23 elements of interest to the U.S. Fusion Materials Program using ENDF/B-V recommended cross sections and the DISCS[1] computer code. Six elements (Cu, Ni, Cr, Fe, Nb, and Au) have also been extended to 50 MeV for Be or Li(d,n) accelerator studies. All significant reaction channels have been included. Thermal neutron capture reactions and beta decay are also included using a newly developed model. Primary recoil atom energy distributions are provided independently for each channel, allowing the experimenter to vary the energy required to cause a nuclear displacement. All data files have been sent to the Magnetic Fusion Energy Computer Center at Lawrence Livermore Laboratory. The SPECTER computer code has been provided so that experimenters need only specify a neutron spectrum. The code will then calculate spectrum-averaged damage energy, displacements, gas production, recoil atom distributions, and nuclear cross sections. Examples are presented for spectra of interest to fusion materials studies.

---

*Work performed under the auspices of the U.S. Department of Energy.

INTRODUCTION

The purpose of the program at Argonne is to characterize irradiation environments in facilities of interest to the Office of Fusion Energy (DOE). This requires the measurement of the neutron flux as a function of neutron energy at reactors and accelerators over the full range of neutron energies from thermal to 50 MeV. These neutron energy spectra are then used to calculate displacement damage, transmutation rates, and gas production at the different irradiation test facilities. This data is needed to correlate the results of material damage effects studies from the different laboratories and to extrapolate the results to fusion reactor environments. The neutron spectral and flux measurements are made by the multiple-foil activation technique using Ge(Li) gamma-ray analysis.

NEUTRON SPECTRUM AND DISPLACEMENT CROSS SECTION CALCULATIONS

A least-squares elaborate computer program (STAYSL) is used to combine neutron reaction rate information obtained from dosimetry experiments with the known cross sections for these reactions from the ENDF/B-V files and an approximate spectral shape for the neutron source to generate a neutron spectrum appropriate for the source during the materials damage effects experiments.[2] This neutron spectrum is then used in conjunction with the cross sections for neutron reactions in the ENDF/B-V files to calculate the primary displacement rates, primary recoil energy spectra, transmutation rates, gas production , and other damage rates in 31 different elements associated with fusion reactor studies.

The calculations consider the following reaction:

(a) (n,n)
(b) (n,n') + [(n,n'p) + (n,n'α), etc.]
(c) (n,2n) + [(n,3n) + (n,2np) + (n,2nα), etc.]
(d) (n,p) + [(n,d) + (n,t)]
(e) (n,α) + [n,3He]
(f) (n,γ)

where the first reaction is the only one calculated in detail. The cross sections of the reaction in the brackets are summed and treated as additional cross section for the first reaction. The calculation of displacement damage resulting from the (n,γ) process assumes that all the gamma-rays are emitted separately in time and lead to separate recoil events. Up until now no effort was made to account for the momentum of the captured neutron or any of the effects from multiple gamma-ray cascades where more than one gamma-ray is emitted before the nucleus slows down appreciable through interactions with the host matrix. Also, no

calculation is made for the displacement damage caused by recoils follow ß-decay that often follows neutron capture or by recoils from gamma-ray emission following the ß-decay.

NEW CALCULATIONS

Displacement damage from recoil events generated by neutron capture are usually only important when there is a large thermal neutron flux present at the test site. This is, however, the case for some test facilities so a detailed analysis was made of the (n,γ) and ß-decay processes to evaluate the need for additions to the present damage codes. Our treatment includes the effects of the momentum of the captured neutron, the γ-ray recoil momentum, angular correlation between the neutron momentum and the subsequent gamma emission, the γ-γ angular correlations, lifetimes of the intermediate states, beta-neutrino angular correlations, and ß-γ angular correlations.

Primary Recoil Energy Spectrum from the (n,γ) Reaction

The (n,γ) reaction recoil process is shown in Fig. 1 where a neutron with energy E_n is captured by a nucleus with At. wt. = A. The recoiling atom, At. wt. = A+1, then emits sequential gamma-rays with energies, $E_{\gamma 1}$, $E_{\gamma 2}$, etc.

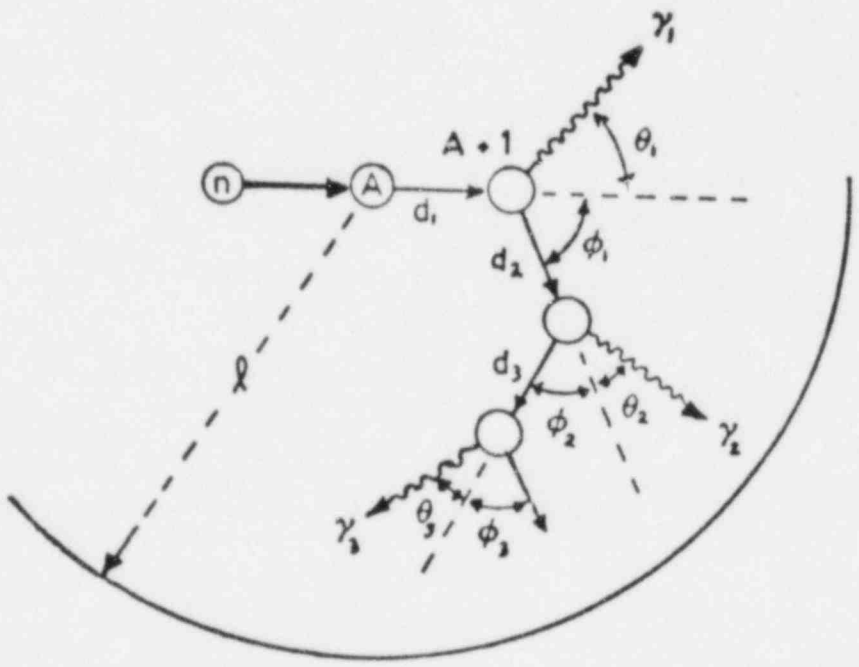

Fig. 1. Schematic of an (n,γ) Recoil Event with the Emission of 3 γ-rays.

The recoil energy, $E_r(n)$, after neutron-capture is given by equation (1)

$$E_r(n) = \frac{E_n}{A+1} \tag{1}$$

After the emission of the first γ-ray the recoil energy is given by equation (2)

$$E_r(n) = \frac{1}{2(A+1)mc^2}\,[E_{\gamma 1}^2 + 2E_n mc^2 - 2E_{\gamma 1}(2E_n mc^2)^{1/2}\cos\theta_1] \tag{2}$$

where θ_1, is the angle between the momentum vector of the captured neutron and direction of emission of the γ-ray and m is atomic mass unit. After the emission of the second γ-ray $E_r(n)$ is given by equation (3) (for isotopic γ-emission) where [ ] is the bracket in equation (2)

$$E_r(n) = \frac{1}{2(A+1)mc^2}\left\{[\ ] + E_{\gamma 2}^2 - 2E_{\gamma 2}[\ ]^{1/2}\cos\theta_2\right\} \tag{3}$$

and θ_2 is the angle between the direction of emission of the second gamma-ray and the previous recoil momentum vector. If, E_n, the energy of the captured neutron is too small to have any appreciable effect (thermal neutron captive) then equation (3) reduces to equation (4)

$$E_r(n) = \frac{[E_{\gamma 1}^2 + E_{\gamma 2}^2 - 2E_{\gamma 1}E_{\gamma 2}\cos\theta_2]}{2(A+1)mc^2} \tag{4}$$

where θ_2 is now the angle between direction of emission of the second γ-ray and the recoil momentum vector of the recoiling atom which is 180° from the direction of emission of the first γ-ray. The form of equation (4) is identical to equation (2) and both events lead to a distribution of recoil energies that has a very simple spectral shape. For the 2-gamma cascade case the maximum recoil energy is given by equation (5)

$$E_r(\max) = \frac{(E_{\gamma 1} + E_{\gamma 2})^2}{2mc^2\ (A+1)} \tag{5}$$

and the minimum recoil energy is given by equation (6).

$$E_r(\min) = \frac{(E_{\gamma 1} - E_{\gamma 2})^2}{2mc^2\ (A+1)} \tag{6}$$

What is of special interest is that the number of recoils per unit recoil energy between these limits is a constant, (see Fig. 2b). The average value for $E_r(n)$ in equation (4) is given by equation (7).

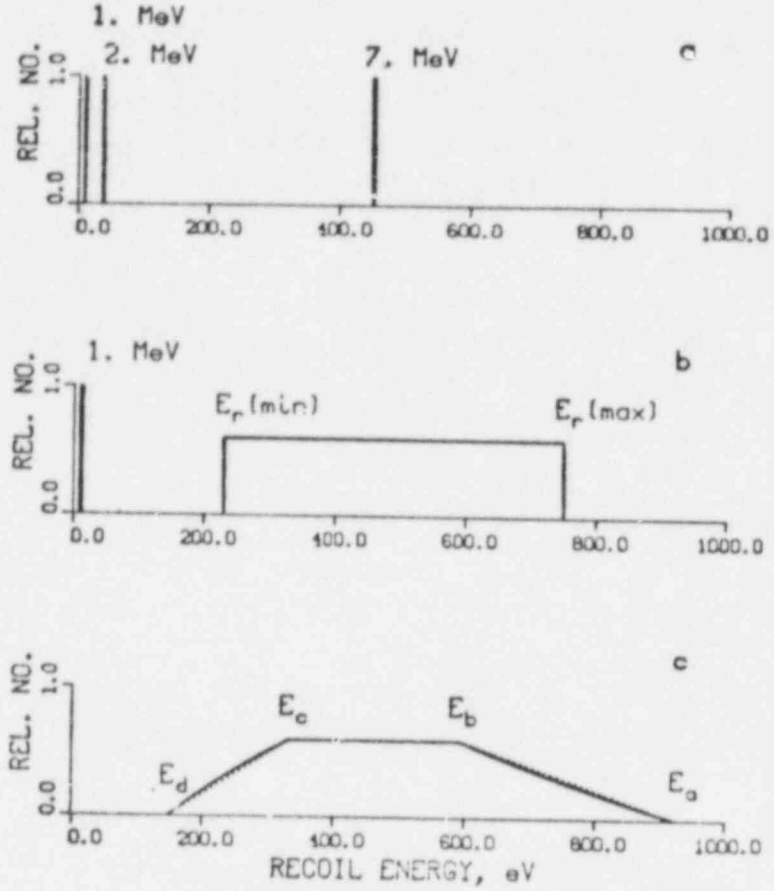

Fig. 2. (a) Recoil Energy Spectrum for Three Gamma Rays (7 MeV, 2 MeV, and 1 MeV) Considered as Separate Events in the $^{57}Fe(n,\gamma)^{58}Fe$ Reaction. (b) The Recoil Energy Spectrum for a Two Step Cascade (E_γ = 7 MeV and 2 MeV) which has a Rectangular Shape Followed by a One Step Cascade (E_γ = 1 MeV) which Generated the Spike at 9.3 ev. (c) The Recoil Energy Spectrum of a Three Step Cascade (E_γ = 7 MeV, 2 Me , and 1 MeV) which Results in a Near Trapezoidal Shape Dis ribution. $E_r(ev) = 9.255\ E_\gamma^2\ (Mev)^2$. The Dashed Lines Indicate the Trapezoidal Approximation to the Triple Cascade Case (c).

$$\overline{E_r(n)} = \frac{E_{\gamma 1}^2 + E_{\gamma 2}^2}{2mc^2\ (A+1)} \qquad (7)$$

This expression is identical to that for the sum of the recoil energies for the two gamma-rays calculated as separate recoil events using equation (1). Thus the value of $\overline{E_r(n)}$ is insensitive to the lifetime of the intermediate state. The value calculated from equation (1) is also the average recoil energy per recoil event, $\overline{E_r(r.e.)}$, if the lifetime of the intermediate state is shorter than the stopping time (the time for the

recoiling atom to lose 63% of its recoil energy). If the lifetime is long compared to the stopping time then the two recoils are two separate events and the average recoil energy per recoil event is one-half the value of the average recoil energy per neutron capture. It is important to maintain the distinction between the average recoil energy per neutron capture, $\overline{E_r(n)}$, and the average recoil energy per recoil event, $\overline{E_r(r.e.)}$ because the later can be much smaller than the former for (n,γ) events with a high multiplicity of gamma-rays.

If the gamma cascade consists of three gamma-rays and the lifetimes of the intermediate states are short then there is only one recoil event per neutron capture. In this case $E_r(n)$ is given by equation (8),

$$E_r(n) = \frac{1}{2(A+1)mc^2}\left[\left\{\right\} + E_{\gamma 3}^2 - 2E_{\gamma 3}\left\{\right\}^{1/2}\cos\theta_3\right] \qquad (8)$$

where $\left\{\right\}$ is the similar bracket in equation (3). If E_n is small (thermal neutron capture) then the recoil energy spectra has a nearly trapezoidal shape as is seen in Fig. 2c. The upper limit of the recoil spectrum, E_a, can be very much more energetic then the recoil energy of any of the gamma-rays when they are considered as individual events (see Fig. 2a). The break points in the recoil energy distribution (Fig. 2c), E_a, E_b, E_c, and E_d are given by equations (9-12), respectively:

$$E_a = (E_{\gamma 1} + E_{\gamma 2} + E_{\gamma 3})^2/2(A+1)mc^2 \qquad (9)$$

$$E_b = (E_{\gamma 1} + E_{\gamma 2} - E_{\gamma 3})/2(A+1)mc^2 \qquad (10)$$

$$E_c = (E_{\gamma 1} - E_{\gamma 2} + E_{\gamma 3})/2(A+1)mc^2 \qquad (11)$$

$$E_d = (E_{\gamma 1} - E_{\gamma 2} - E_{\gamma 3})/2(A+1)mc^2 \qquad (12)$$

where $E_{\gamma 1} \geq (E_{\gamma 2} + E_{\gamma 3})$ and $E_{\gamma 1} \geq E_{\gamma 2} \geq E_{\gamma 3}$. The actual shape of the curve (solid line in Fig. 2c) is given by equation (13) between E_a and E_b

$$I(\text{rel.}) = \frac{(E_{\gamma 1} + E_{\gamma 2} + E_{\gamma 3}) - [E_r\ (mc^2)(A+1)]^{1/2}}{8\ E_{\gamma 1}E_{\gamma 2}E_{\gamma 3}} \qquad (13)$$

and by equation (14) between E_c and E_d.

$$I(\text{rel.}) = \frac{[E_r\ (mc^2)(A+1)]^{1/2} - (E_{\gamma 1} - E_{\gamma 2} - E_{\gamma 3})}{8\ E_{\gamma 1}E_{\gamma 2}E_{\gamma 3}} \qquad (14)$$

The value of I(rel.) is constant between E_c and E_d with a value given by equation (15).

$$I(\text{rel.}) = \frac{1}{4\ E_{\gamma 1}E_{\gamma 2}} \qquad (15)$$

A somewhat more complicated shape occurs for the $E_r(n)$ spectrum when $E_{\gamma 1} \leq (E_{\gamma 2} + E_{\gamma 3})$ but a similar analysis is possible. In the triple cascade case, the average recoil energy per neutron capture, including the neutron momentum, is given by equation (16).

$$\overline{E_r(n)} = \frac{1}{2(A+1)mc^2}\left\{2E_n mc^2 + E_{\gamma 1}^2 + E_{\gamma 2}^2 + E_{\gamma 3}^2\right\} \qquad (16)$$

The generalized form for a cascade of x gamma-rays is given by equation (17).

$$\overline{E_r(n)} = \frac{1}{2(A+1)mc^2}\left\{2E_n \cdot mc^2 + E_{\gamma 1}^2 + E_{\gamma 2}^2 + \ldots . E_{\gamma x}^2\right\} \qquad (17)$$

As noted above this is just the sum of the recoil energies considering each step of the reaction as a separate recoil event.

The energy distribution of triple cascade recoil events, $E_r(n)$, for the short half-life case can be approximated by a trapezoid as discussed above with break points given by equations (9-12) (see Fig. 2c). In most cases this is a quite good approximation and the value of $\overline{E_r(n)}$ calculated from this distribution agrees with the exact calculation, equation (17) to within a few percent.

The recoil spectrum of the $^{57}Fe(n,\gamma)^{58}Fe$ reaction was calculated in detail taking into account all the known information about the level scheme, gamma decay pattern observed following neutron capture, and the lifetimes of the low-lying states.[3] Recoil energy spectra were calculated separately for the single gamma recoil events, the double gamma recoil events and the triple gamma recoil events, see Fig. 3a, 3b, and 3c, respectively. The sum of these spectra is shown in Fig. 4a. It is quite different from the recoil spectrum (Fig. 4b) that is calculated assuming that each gamma ray leads to a separate recoil event. These two different spectral distributions will predict different amounts of displacement damage if as in the Lindhard model the fractions of the recoil energy that goes into displacement damage varies with recoil energy. It will also be different if the damage process has a low energy cutoff. For the Fe case these two effects tend to cancel each other and the average energy contributing to displacement when calculated for the spectrum in Fig. 4a and 4b with the Lindhard model differ by only a few percent.

The above analysis has assumed that the γ-rays were emitted isotropically. The effect of an angular correlation between the γ-rays was

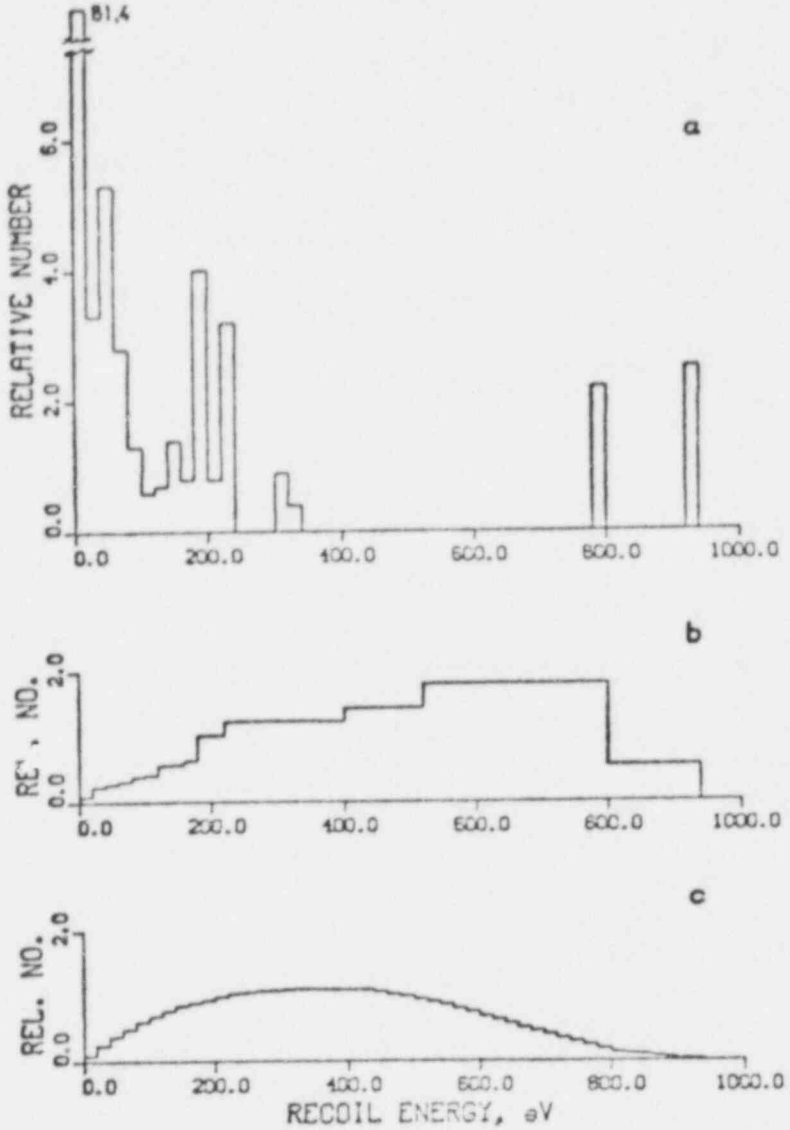

Fig. 3. Recoil Energy Spectra for $^{57}Fe(n,\gamma)^{58}Fe$ for Cascade Case Where (a) is the Spectrum for Single Gamma Events, (b) Two Step Cascades, and (c) Three Step Cascades.

examined and found to have only a small effect on the spectral shape of the recoil distribution and virtually none on the value of $E_r(n)$. This is because the γ-γ angular correlation contains only even Legendre polynomials, which are symmetric with respect to $\theta = 90°$, and thus for every case where these is increased alignment of the two momentum vectors there is a corresponding case where the momentum vectors oppose each other. The distortions to the spectral shapes are also quite small because most of the strong angular correlations are between low energy gamma rays that depopulate the low-lying states and thus correspond to single recoil

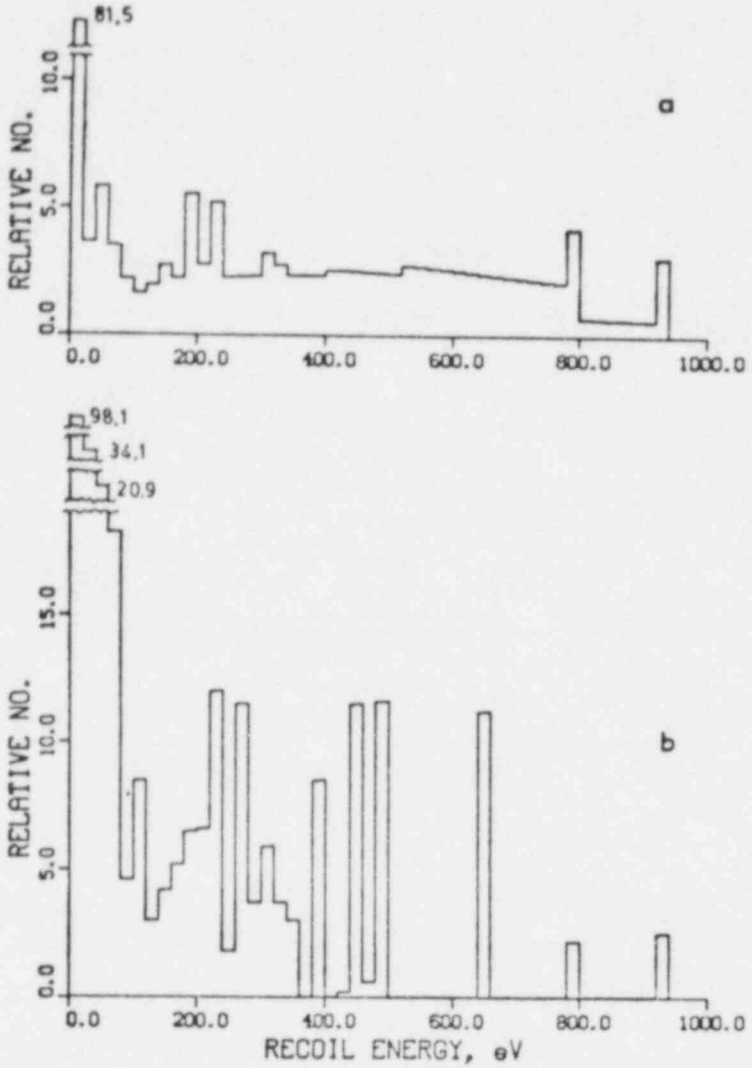

Fig. 4. Recoil Energy Spectra for the $^{57}Fe(n,\gamma)^{58}Fe$ Reaction Where (a) is the Sum of Calculated Cascade Spectra for the Single Events and the Two Step Cascade and the Three Step Cascades, Shown in Figures 2a, 2b, and 2c, Respectively, and Spectrum (b) is the Recoil Spectrum When All Gamma Rays are Treated as Individual Recoil Events.

events (because of the long lifetimes of these low-lying states) that do not interact with other recoil events. Even the small effects that do occur for individual cascades tend to wash out when the recoil energy spectra from many cascades are added together.

In summary, the approximation presently used in our damage calculations where $\overline{E_r(n)}$, the average recoil energy per neutron capture is calculated from the weighted average of the recoil energies assuming each γ-ray produces its own recoil event is a good one and needs only the additions of the neutron recoil term, equation (1) to be complete,

even when the lifetimes of the intermediate states are short. The more complex model must be used to obtain the right spectral shape for the primary recoil spectrum but even these dramatic spectral changes result in only small changes in displacement damage when current models (like the Lindhard model) are used.

Primary Recoil Energy Spectra from β-Decay

Quite frequently the (n,γ) reaction is followed by the β-decay of the product nucleus (A+1). If the endpoint energy, E_o, of the β-decay is a few MeV or more, there will usually be (depending on the mass of the product nucleus) enough recoil momentum from the β-decay (β + ν) to displace the daughter nucleus (A+1, Z±1). The recoil energy of the daughter nucleus is a function of both the β-decay and the neutrino energy, and it is necessary to take into account the appropriate angular correlation between the β and the neutrino in the recoil calculations. This angular correlation is different for different classes of β-decay and can materially affect the average value of the $\overline{E_r(\beta+\nu)}$. The recoil energy $\overline{E_r(\beta+\nu)}$ is given by equation (18).

$$E_r(\beta+\nu) = \frac{F(\theta)}{2(A+1)mc^2}\left\{E_e(E_e + 2m_ec^2) + (E_o - E_e)^2 + 2[E_e(E_e + 2m_ec^2)]^{1/2}\,(E_o - E_e)\cos\theta\right\} \qquad (18)$$

where E_e is the electron energy, E_o is the endpoint energy, $(E_o - E)$ is the neutrino energy, θ is the angle between the neutrino and the electron, m_e is the mass of the electron,[7] "m" is the mass of one atomic mass unit and $F(\theta)$ is the appropriate weighting factor that takes into account the angular correlation between the electron and the neutrino. It is convenient to parameterize these expressions in terms of the endpoint energy, E_o. If we use the normalized energy parameters $a = E_e/E_o$ and $b = m_ec^2/E_o$ then equation (18) becomes equation (19)

$$E_r(\beta+\nu) = \frac{E_o^2\,F(\theta)}{2(A+1)mc^2}\left\{a(a+b) + (1-a)^2 + [a(a+b)]^{1/2}(1-a)\cos\theta\right\} \qquad (19)$$

where $F(\theta)$ is given by equation (20)

$$F(\theta) = (a+b)^2(1-a)^2\,(1 + C\,\beta\cos\theta)(2\pi\sin\theta)\,F_s(\beta) \qquad (20)$$

and $F_s(\beta)$ is a slowly varying function of β ($\beta = v_e/c$) and is approximately equal to one in most cases. The coefficient C depends on the character of the β-decay process, allowed (Gamow-Teller), scaler, polar vector (Fermi), etc. Figure 5 shows the recoil spectrum for the β-decay of ^{28}Al [E_o = 2.871 MeV, axial vector (Gamow-Teller)]. In this case, "C", the coefficient in the angular correlation between the neutrino and

the electron, is equal to -1/3. The average value of the recoil energy in this case is approximately 61% of the maximum value of $E_r(\beta + \nu)$ which occurs when the electron energy equals the endpoint energy ($E_e = E_o$). The β-decay of ^{28}Al to ^{28}Si is followed by the emission of a 1.8 MeV γ-ray. The lifetime of the intermediate state is 0.5×10^{-12} sec; which is the same order of magnitude as the slowing down time so some of the γ-rays will be emitted before the daughter comes to rest. This will complicate the calculation of the recoil spectrum but for the calculation of the average recoil energy per β-decay or per neutron capture the two recoil energies can be treated as separate recoil events as discussed above.

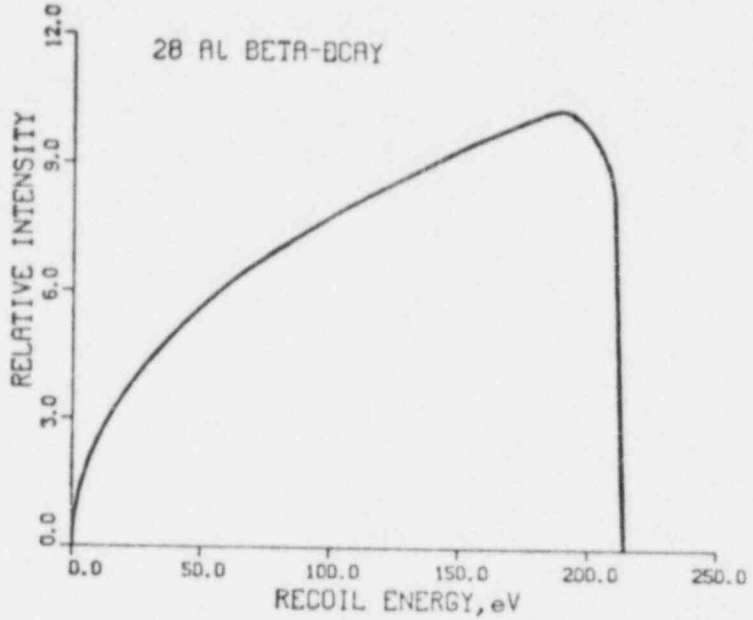

Fig. 5. Recoil Spectrum for the ^{28}Al β-Decay to ^{28}Si. The Recoil Momentum of the Following Gamma Ray Transition in ^{28}Si is not Included in This Spectrum.

MODIFICATION OF THE DISPLACEMENT CODE

Based on the above discussion one can see that the present method for calculating the average recoil energy per neutron capture can be easily modified to include the effects of the momentum of the captured neutron and the subsequent β-decay and γ-ray emission. If more than one endpoint energy, E_o, is involved in the β-decay process they can be treated separately and then summed as a weighted average just as one did with the γ-decays following the (n,γ) reaction. The total average recoil energy per neutron capture is then just the sum from the different decays.

$$\overline{E_r(n)}(\text{total}) = \overline{E_r(n)}(n,\gamma) + \overline{E_r(n)}(\beta\text{-decay} + \gamma\text{'s}) \qquad (19)$$

Table 1 summarized the (n,γ) and β-decay results for 25 fusion-related materials where $\overline{E_r}(\gamma)$ is the average recoil energy per gamma-ray (using an appropriate low energy cutoff), $\overline{E_r}(n)$ is the average recoil energy per neutron capture and $\overline{E_r}(\beta)$ is the average value per β-decay. The parentheses are used to indicate recoils where the β-decay lifetime is longer than one year. The detailed spectral distribution of recoil events for a particular material following β-decay will have to be calculated separately and added to the detail calculation for the (n,γ) process.

Table 1. Recoil Energies from (n,γ) and β-Decay

Element	(n,γ) Recoil Energy (ev)			β-Decay Recoil Energy (ev)		
	Max.	$\overline{E_r}(\gamma)$	$\overline{E_r}(n)$	Max.	$\overline{E_r}(\beta)$	$\overline{E_r}(n)$
Be	2494.	1188.	1912.	47.	(42.)	(42.)
C	939.	683.	891.	7.	(5.)	(>.1)
N	3945.	1050.	2309.	4011.	2370.	2.
O	546.	183.	365.	742.	539.	1.
F	1168.	496.	822.	1517.	722.	722.
Na	1086.	297.	566.	795.	200.	200.
Mg	2544.	279.	745.	186.	101.	5.
Al	1148.	506.	640.	499.	190.	190.
Si	1950.	334.	730.	65.	46.	1.
P	1057.	268.	550.	78.	63.	63.
Cl	1098.	325.	639.	413.	16.	16.
K	1335.	209.	413.	205.	171.	9.
Ca	1514.	206.	468.	412.	224.	4.
Ti	1508.	367.	481.	72.	50.	0.1
V	1259.	360.	426.	203.	105.	105.
Cr	906.	515.	670.	92.	8.	1.
Mn	507.	281.	385.	167.	82.	82.
Fe	917.	404.	473.	42.	18.	0.2
Co	502.	264.	362.	89.	(63.)	(63.)
Ni	973.	530.	592.	56.	35.	0.1
Cn	526.	383.	413.	79.	20.	20.
Zr	436.	112.	162.	34.	11.	0.5
Nb	297.	102.	126.	36.	18.	0.1
Mo	469.	132.	119.	76.	21.	0.2
Ag	302.	107.	136.	55.	31.	31.
Ta	108.	102.	3.	14.	6.	5.
W	160.	115.	14.	9.	4.	2.
Au	114.	71.	68.	6.	4.	4.
Pb	140.	140.	140.	3.	3.	<.1

REFERENCES

1. G. R. Odette and D. R. Dorian, Nucl. Technol. 29, 346 (1976).

2. L. R. Greenwood, Neutron Flux and Spectral Measurements to Characterize Irradiation Facilities for Fusion Materials Studies, see preceeding paper in these proceedings.

3. H. Schmidt, W. Michaelis, and U. Fanger, Nuc. Phys. A136, 122 (1969); U. Fanger, W. Michaelis, H. Schmidt, and H. Ottmar, Nuc. Phys. A128, 641 (1969).

Session C.1
Damage Correlation

REVIEW OF IAEA SPECIALISTS' MEETING ON IRRADIATION EMBRITTLEMENT AND SURVEILLANCE OF REACTOR PRESSURE COMPONENTS VIENNA, AUSTRIA 19-21 OCTOBER 1981

L. E. Steele
Naval Research Laboratory
Washington, DC, USA

ABSTRACT

A meeting of specialists on irradiation embrittlement of reactor pressure vessel steels under sponsorship of the International Atomic Energy Agency (IAEA) provided a forum for full discussion of this critical topic as well as the basis for defining recommended future research and engineering studies. The author, who served as chairman, was obligated to all provide to participant a summary with conclusions and recommendations on major topics discussed. This paper encompasses the chairman's report but reflects as faithfully as possible the concensus of participants though clearly the chairman's view is evident in many areas. It is hoped that ideas generated will be useful to those concerned with defining the neutron radiation environment as well as to the international specialists who attended the Vienna conference.

SUMMARY

As in the two preceding meetings of specialists in this subject area which were held in May 1976 in Plzen, Czechoslovakia and in February 1979 in Vienna, *the underlying theme was the understanding of radiation embrittlement of light water reactor pressure vessels so as to aid in assuring their structural integrity*. The sponsoring organization within the IAEA, the Working Group on Reliability of Reactor Pressure Components has assured a serial approach to the subject though the specific meeting emphasis has been determined by events or new knowledge occurring in the intervening three years. The emphasis in the current meeting while aimed toward surveillance data from operating reactors exhibited a number of papers influenced both directly and indirectly by the Three Mile Island accident in the USA. This influence arose from new rules and added concerns (whether real or imagined) following that event.

The Three Mile Island event, while a background shadow, was not a direct topic of the conference but the rules or codes growing out of this event clearly influenced the content of many papers. However, several papers reflected research programmes and direct approaches to reactor vessel surveillance and reports thereon where were begun before the TMI-2 event.

The meeting programme was organized to provide an introductory overview session highlighting the status of the subject studies in the three major light water reactor producing countries, France, the Federal Republic of Germany, and the United States. This session contained a special paper on neutron dosimetry as well. The remaining two sessions emphasized respectively irradiation effects studies and annealing as well as radiation embrittlement surveillance results.

Papers from Czechoslovakia, France, the Federal Republic of Germany, Hungary, United Kingdom, and United States provided results on irradiation effects and annealing or techniques for analysis thereof while papers from Austria, Finland and the United States provided results of surveillance programmes or advice on surveillance approaches including preferred specimens and analysis of groups of capsules to test data trends previously considered and developed for code or rule making. One paper from the United States brought limit trends to be offered for public comments before issue as a regulatory guide revision. This is the well known Regulatory Guide No. 1.99 revised last in 1977. Another United States paper brought a detailed review of surveillance data aimed toward the goal of explaining the reality or fallacy of the much discussed saturation which was a highlight issue at the 1979 specialists' meeting.

The papers presented and the related specific and general discussion emphasized and elucidated crucial aspects of national programmes to assess the influence of radiation on the engineering integrity of reactor systems, the best approaches for simulating in research programmes the fracture potential of reactor steels, the advances occurring in neutron dosimetry and, in a limited way, national regulatory rules for assuring vessel integrity as well as a series of papers dealing with surveillance approaches, surveillance results and alternatives for assessing failure potential. Full and free discussion followed each paper or discussion time was provided at the end of the session. In addition, a highly active general discussion comprised the final session. This was arranged in three parts: (1) a review of significant or influential national or international events (primarily technical ones influencing the subject since 1979), (2) highlights of formal and informal papers presented, and (3) from (1) and (2), recommendations agreed upon. The following summarizes the latter two areas by first citing and describing the key subject and then addressing the recommendations growing from a consensus of the attendees through open discussion.

CONCLUSIONS AND RECOMMENDATIONS

The most significant observations and related recommendations of the body of specialists are outlined by major subject areas.

Activities to Support Dissemination of Knowledge by IAEA

The open review of national research programmes and those to assure structural integrity in spite of radiation damage plus the full discussion offered by the specialists meeting under IAEA auspices indicates an opportunity to meet the Agency goals of encouraging research toward advancing the safe and peaceful use of nuclear power and the dissemination of needed information especially to the so-called lesser developed nations. To this end the following recommendations were adopted:

Recommendations

(a) Retain and continue support of the Co-crdinated Research Programme which has (1) sought verification of the technology used in irradiation effects studies and (2) evaluated the benefits of revised specifications for advanced steel for new vessel construction.

(b) Continue the series of specialists' meetings on a triennial basis. (More often if circumstances dictate).

(c) Provide an objective statement of results obtained and precautions taken to assure safety of currently operating reactors and improve further the operating safety through application of knowledge from research results presented in forums offered by (a) and (b). Develop this report for popular publication.

(d) Update the volume commissioned and published by the IAEA in 1975 entitled "Neutron Irradiation Embrittlement of Reactor Pressure Vessel Steels," TRS 163.

(e) Commission consultants' meetings, specialists' meetings and special publications on the subject as requirements dictate.

(f) Collaborate to assure optimum information exchange and minimal duplication of effort with other international bodies, such as the OECD/NEA group on Neutron Dosimetry and the CSNI/NEA group on data base development (steel composition, weld properties, irradiation effects etc.), the International committee on Cyclic Crack Growth. Consider incorporation of The Metal Properties Council data base in IAEA computer data system. These efforts are important to assure meeting general goals mentioned in the introductory paragraphs.

Radiation Embrittlement

Pertinent papers and discussion elucidated new observations particularly regarding the influence of selected component elements, correlation of fracture data from traditional Charpy-V-notch, advanced linear elastic and elasto-plastic approaches (the latter not standardized), the influence of the particular nuclear environment (flux, fluence, spectrum effects), the effects of temperature and the mechanisms of radiation damage.

Recommendations

(a) While the principal concern of the 1979 meeting was the so-called saturation effect, this has been refuted through comparison of results from a large number of surveillance capsules in the United States and has been replaced by a concern for an influence of nickel above certain composition levels. Future studies require fuller analysis of steels for this potentially deleterious element, a better knowledge of its influence both in the presence and absence of copper, and a statistical and phenomenological base formation for defining its effects.

(b) The possible influence of other factors such as time, temperature and applied stress along with composition should be studied to differentiate particular effects of radiation and so advance the understanding of the condition in an individual plant.

(c) In spite of significant fundamental studies conducted in the past there is a need for carefully executed, systematically designed fundamental studies for mechanistic definition. Such studies must be carefully integrated with available knowledge and with the engineering oriented studies completed or now underway.

(d) Some hope was offered for a non-destructive indicator of radiation embrittlement based on fundamental understanding thereof. Such studies should be conducted in close collaboration with those described above.

(e) Fundamental studies of the mechanisms of thermal annealing correction require the same degree of dedicated study cited for radiation embrittlement.

(f) Compare and correlate data from research reactors and from surveillance programs to evaluate any discrepancy between results which might be attributable to the difference in environment. If significant differences are noted seek an explanation. (It is to the advantage of all concerned to be able to use data from both accelerated and typical operating environments as the former are cheaper in time and permit multiple parametric evaluation not readily possible near the wall of an operating reactor).

Annealing to Correct Radiation Embrittlement

Several investigators described results of annealing studies, that is, experiments to evaluate the potential for heating an embrittled vessel to restore all or a portion of its useful life. Results were remarkably similar among the several investigators with general agreement that the shelf level restoration is more readily accomplished than correction of the transition temperature.

This tends to support the contention of several investigators that different physical mechanisms control the two phenomena. Further, for complete recovery a temperature of more than 400°C is required and it was agreed that this should be the principal consideration for future studies or engineering applications analysis.

The concept of pressurized thermal shock or "re-pressurization during emergency core cooling" after an accident is the principal driving force behind studies of annealing as the transition temperature or RT_{NDT} must be lower than would otherwise be required if this phenomenon could not occur. (See Sect. 5 for related discussion of measures to be taken to assure adequate vessel toughness at all times and studies underway to provide such assurance).

The following recommendations were considered and approved by the specialists:

Recommendations

(a) Continue annealing studies with emphasis on the higher (400°C) temperature regime but do not omit lower temperatures as these may be of value for restoration of ductile "shelf" toughness in systems where this is the limiting factor.

(b) If temperatures above this range are used, assess the potential effects of thermal aging along with embrittlement and annealing.

(c) As cited in (e) above, investigate fundamental phenomena for annealing along with other such studies.

(d) Seek data from annealing of surveillance specimens, preferrably from a reference steel which has been irradiated in both accelerated and surveillance (near wall) positions.

Surveillance

This topic, one of the intended principal themes of the meeting, did not comprise as much of the formal program as was the original intent. Nevertheless, it loomed large in the discussion as the five directly related papers engendered discussion covering the whole spectrum of topics covered by this report. It was evident from the results presented that

some older reactors having pressure vessels constructed before the revelation of serious composition effects on embrittlement are showing, through surveillance results, significant embrittlement.

Fortunately new surveillance data will be growing rapidly in the near future. For example, ongoing surveillance is expected to produce an additional 90 capsules from French reactors over the remainder of this decade. Such data are essential to an updated assessment of radiation embrittlement in operating reactors. Further, comparative analysis of data from a number of United States reactor surveillance capsules provided the conclusion that the "saturation effect" was more likely a phenomenon involving synergistic responses of steels to irradiation effects where copper and nickel contribute in a complementary way to exaggerate the embrittlement picture. In addition, surveillance data are becoming predominant in decisions related to the individual plant and its operation relative to the embrittlement state and provide the principal data base for development of radiation embrittlement trends.

The following conclusions and recommendations grew out of the papers and discussion of surveillance.

Recommendations

(a) Surveillance programs are essential to the understanding of the embrittlement state of a specific reactor vessel. The data therefrom complemented by accelerrated irradiation of the same steels where possible will provide the reactor owner a "running" view of the vessel condition. Consequently it requires the best possible analytical effort.

(b) Analysis of capsules in existing surveillance programs requires most careful analysis to assure that it is representative of the plant as constructed.

(c) Regarding new or complementary surveillance programs (add-on or coordinated parallel efforts in sister reactors) these should:

  (1) Contain truly representative materials
  (2) Be located to well represent the level of irradiation expected on the wall
  (3) Be constituted to optimize chances for good neutron dosimetry and fracture toughness measures of the vessel
  (4) Contribute to a data base of related data for future analysis of embrittlement trends.

Analysis of Fracture Potential of Vessel Steels

The thrust of the introductory overview papers as well as most of the specialty papers was toward presenting new data on or programs or proposals for establishing the critical knowledge required to assess the failure potential of irradiated (and unirradiated) steels. As most

of the available data from materials testing or operating reactors (surveillance) are based on the Charpy V-notch test or small related versions designed for quantitative assessment of fracture toughness, many questions remain regarding their direct applicability to large vessels or similar heavy walled structures in nuclear plants. In spite of these uncertainties however, because these are the only specimens available from vessel surveillance, correlative techniques to larger specimens and then to structures must form the basis for future safety analyses of irradiated structures. Projections made by the introductory papers and others which provided data on linear elastic fracture mechanics of irradiated steels provided the directions for future emphasis.

In relation to this topic, several recommendations were reviewed and adopted by the convened specialists. These included the following:

Recommendations

(a) New data presented recognized the generally conservative position of the widely used American Society of Mechanical Engineers (ASME) Boiler and Pressure Vessel Code, Appendix G which shows the relationship between steel toughness and temperature. This refers to the commonly used reference K_{IR} curve. Concerning this curve, its placement and shape after irradiation, there remains uncertainty along with the choice of the preferred tests for its validation. Clarification of these uncertainties were cited as a crucial need. For perspective, the original curve was designed using both linear elastic fracture mechanics (LEFM), K_{Ic}, and so-called crack arrest, K_{Ia} neither of which was considered standard at the time of first publication. The need for standarization of both was a strong recommendation. The K_{Ic} test has recently been standardized in the United States by the ASTM but K_{Ia} remains to be standardized as do the much discussed procedures for elastic-plastic fracture (EPFM).

(b) Strong support was evident for a unified experimental fracture method for both LEFM and EPFM based on a single specimen. Inherent to this discussion was the understanding that the acceptable specimen implies a smaller specimen for irradiation studies than might otherwise be used but at the same time recognizes that smaller specimens may be essential because of space limits and maybe acceptable because of radiation induced embrittlement.

(c) Beyond the move to a more unified specimen there is the critical need for acceptable procedures for their use and interpretation. This was evident in the repeated use of data called J_{Ic}, J-R curve, tearing modulus or tearing instability value without the unification essential through methodology and analytical standarization. This need was probably the most often repeated recommendation of the meeting. The reason for this lies in the fact that such data may provide the only basis for verifying the continued licenseability of a plant which contains a vessel that is shown to be sensitive to radiation embrittlement.

(d) Building on a, b, and c there was agreement that, based on irradiation effects data, (from research and surveillance programs) and the clear statement in the overview papers of a potential for a condition of "pressurized thermal shock," the IWG must support efforts to evaluate vessel condition and minimize radiation damage in any way possible as well as to extend the analytical procedures from specimens to structures. Inherent to such analyses are the need to assure a conservative yet valid interpretation of data from small specimens for prediction of the performance of the structure. It was clearly noted that this can be accomplished only by correlation of small irradiated specimens with larger irradiated specimens and thence to the irradiated vessel. Further, factors which may influence the predictions arising therefore such as, effects of size, dynamic versus static loading, effects of toughness gradient, etc, were considered and identified as being most important to the ultimate projection of vessel condition and, hence, its propensity for structural integrity or, in more popular terms, its safety or projected safety.

(e) A most important factor in the analysis of fracture potential and, thus, of vessel safety, is the clarification of the meaning of low shelf toughness as most often described by low Charpy V-notch values but as well by low K_{Ic} and J_{Ic} values. Low toughness on the shelf was considered by the specialists to be both a critical factor in many reactors and thus of high importance to structural integrity or safety but also a phenomenon based on a different defect mechanism or mechanisms than the very commonly defined, ΔT, or increase in transition temperature. Therefore this phenomenon should be studied as such and possibly to be treated as a separate structural phenomenon.

(f) For some reactors exhibiting significant radiation embrittlement based on early surveillance capsule results special steps are being considered to minimize the potential effects. These include special consideration of (1) the fracture toughness projections using best available computations or measurements where possible, (2) adjustment of the vessel wall exposure by modification of the outer region of the core in some cases replacing fuel with dummy stainless steel elements to absorb neutrons and minimize vessel exposure, (3) consideration of heating the emergency core cooling (ECC) water to minimize thermal shock in the event of ECC activation and, (4) evaluation of the potential for annealing the vessel to correct the embrittlement. These steps along with the improvements in fracture analysis cited above were endorsed to avoid the circumstance of projected severe embrittlement near the end-of-life in some systems.

Neutron Environmental Analysis

Besides the invited overview on measuring the neutron environmental much of the discussion and each of the papers reporting irradiation

embrittlement or surveillance results. The overview paper described advances of recent years and current and future activities to better define the neutron environment through the full vessel wall and in direct comparison with measured mechanical properties in a so-called "Benchmark Facility." Recommendations drawn from the discussions include the following:

Recommendations

(a) Support the goals and the activities of sister international groups which are seeking improved dosimetry damage function analysis for the specific purposes of those concerned with effects of neutrons in pressure boundary steels. This includes endorsement of the "CAPRICE" committee activities and joint conference plans with the OECD/NEA groups.

(b) Actively support national and international standardization activities such as the extensive efforts of ASTM in directly related standards developed in connection with research efforts and organized to systematically advance:

(1) The accuracy of pertinent nuclear constants.
(2) The methodology of activation or related techniques for long-term dosimetry
(3) Specific support of surveillance studies.
(4) Analytical efforts for defining damage functions for steel damage in the specific environment of the light water reactors.
(5) Definition of the environment in the most appropriate units, n/cm^2, DPA, n/m^2 or other with the appropriate energy limit cut-off.
(6) Techniques for accurate projection of damaging environment from surveillance capsule to vessel wall or appropriate thickness location in the vessel.

Acknowledgements

The scope of the preceding recommendations is such that all participants endorsed the importance of the IAEA support through all possible avenues but especially through those activities cited under (1) above. The enormity of the questions of public safety and of the size of investments in nuclear power were such as to focus further support on the questions discussed above. The pertinent IAEA leaders endorsed the work of the conference as well as the need for continued support of research cited by the specialists. The support of the national representatives as well as the IAEA representatives made possible a most successful meeting and a statement of recommendations which should be most helpful to all investigators. Special thanks are owed to Mr. A. Sinev, IAEA Scientific Secretary for his many efforts toward the conduct of a successful meeting.

INVESTIGATION ON THE DEPENDENCE OF RPV STEEL EMBRITTLEMENT ON IRRADIATION TEMPERATURE AND NEUTRON EXPOSURE

J. Ahlf, D. Bellmann, F.J. Schmitt, W. Spalthoff
GKSS-Forschungszentrum Geesthacht GmbH
Institut für Werkstofftechnologie
West Germany

ABSTRACT

Three steel heats with copper contents of 0.04, 0.15 and 0.25 % respectively have been irradiated at 255 °C, 285 °C and 310 °C to 1.7 x 10^{19} cm^{-2}(E>1MeV). A dependence of the ductile-to-brittle transition temperature shift ΔTT on the irradiation temperature T_B was found. The slope of the ΔTT vs T_B curves increases strongly with copper content.

Irradiations of ASTM A533 gr B cl 1 steel from HSST plate 03 have been performed under a variety of neutron exposure as regards fluence Øt, spectrum and flux density Ø. The exponent b in the relation ΔTT ∿ $(Øt)^b$ is 0.65, which is a little larger than the 0.5 of Reg. Guide 1.99. Spectrum and flux density effects were smaller than to be discerned from the scatter band of ΔTT in the ranges covered by this investigation.

INTRODUCTION

The quickly growing number of transition temperature shift measurements - mainly from surveillance programs - is (statistically) analysed with respect to the established or supposed influencing parameters
- chemical composition [1,2,3]
- neutron exposure (fluence [1,3] or other exposure units [4])
- flux density [5]
- irradiation temperature.[6]

The trend lines resulting from these analyses have in most cases rather large scatter bands, because the data are often derived from irradiations in which the conditions differed in more than one parameter, not to speak of differences in the applied methods.

We have evaluated a number of ΔTT-measurements from four steels of different chemical composition which have been irradiated at different temperatures in the same neutron environment and - on the other hand - at (nearly) the same temperature in different neutron environments as regards spectrum, flux density and fluence, and we have looked for the

influence of these parameters on ΔTT separately.

The analysis is limited by the accuracy of ΔTT-measurement. According to our experience the 41 J transition temperature determined by standard practice has to be assigned with a standard deviation of 3...7 K, in some cases up to 10 K. The standard deviation of ΔTT is of the same order. Therefore effects on ΔTT smaller than about 5...8 K fall into the error band and can hardly be detected.

EXPERIMENTAL PROCEDURE AND RESULTS

Steels investigated

Four steels have been investigated, the chemical composition and heat treatment of which are listed in tables 1 and 2.

Table 1: chemical composition in weight %

No.	designation	C	Si	Mn	P	S	Ni	Cr	Mo	Cu	Al	C.R.[a]
1	base material 20MnMoNi55	0,18	0,28	1,29	0,007	0,0078	0,73	0,04	0,46	0,04	0,022	0,152
2	weld material (20MnMoNi55)	0,07	0,24	1,21	0,015	0,011	0,79	0,04	0,49	0,15	0,010	0,430
3	weld material (22NiMoCr37)	0,08	0,18	1,75	0,013	0,008	1,01	0,40	0,64	0,25	-	0,845
4	base material A533 B cl 1 (HSST plate 03)	0,20	0,25	1,26	0,011	0,018	0,56	0,10	0,45	0,12	0,034	0,375

[a] chemistry relation according to Varsik and Byrne[2]

Table 2: heat treatment

No.	designation	heat treatment
1	base material 20MnMoNi55	8h/870..910°C/water + 10½h/635...660°C/air
2	weld material (20MnMoNi55)	10h/550°C + 10h/610°C
3	weld material (22NiMoCr37)	29h/550°C + 11h/600°C
4	base material A533 B cl 1 (HSST plate 03)	see Ref. 7

Irradiation experiments

Irradiation experiments have been performed in various different neutron environments:

pos. A : in reflector positions of FRG-2, a 15 MW swimming-pool reactor, in small magazine rigs [6,8].

pos. B : behind stainless steel gamma shields (60 mm thick) in border positions of FRG-2 in small magazine rigs [6].

pos. C : behind stainless steel gamma shields (60 mm thick) in border positions of FRG-2 in large volume rigs [9]
pos. D : in a surveillance capsule position of KKS, a 600 MWe PWR
Pos. E : in an irradiation position near the core of VAK, a 16 MWe BWR[10].
Whereas the irradiation temperature in position A, B and C was measured continously by thermocouples, for positions C and D it could only be estimated from the cooling water temperature and heat flux calculations (melting monitors gave no unambiguous results).

Dosimetry

Neutron exposure has been determined from Fe54(n,p)Mn54 and Ni58(n,p)Co58 reactions on the basis of neutron spectra from two-dimensional transport calculations with DOT using the EURLIB library with 31 groups > 1MeV.[11] The dosimetry cross sections were taken from ENDF/B V.

Table 3: cross section for the monitor reactions and dpa

Position	σ(Fe54, E>1MeV) [mbarn]	σ(Ni58, E>1MeV) [mbarn]	σ(dpa) [barn]
A	72 ... 83	97 ... 110	1440 ... 1480
B	85	--	1650
C	47 ... 56	64 ... 77	1800 ... 2140
D	96	--	1610
E	82	--	1520

The cross sections for neutrons with E > 1MeV for the monitor reactions and the dpa cross sections for the different irradiation positions are listed in table 3.

The cross sections are defined as follows:

$$\sigma(E > 1\text{MeV}) = \frac{\int_0^\infty \sigma(E)\Phi(E)dE}{\int_{1\text{MeV}}^\infty \Phi(E)dE} \qquad (1)$$

$$\sigma(\text{dpa}) = \frac{\int_0^\infty \sigma_d(E)\Phi(E)dE}{\int_{1\text{MeV}}^\infty \Phi(E)dE} = \frac{\text{dpa}}{\int_{1\text{MeV}}^\infty \Phi(E)dE} \qquad (2)$$

$\sigma_d(E)$: displacement cross section for iron according to ASTM E693-79[12].

Mechanical Testing

Charpy tests were performed with a 300 J impact testing machine installed in a lead cell and operating automatically. The same machine was used to test the unirradiated specimens.

The impact energy versus testing temperature curves were approximated by the Gaussian integral. The 41 J transition temperature was taken from the fitted curves.

The experimental results are collected in table 4. In some cases the exposure values (fluence and / or dpa) differ from earlier publications because of reevaluation on the basis of improved spectrum calculations. Where the irradiation temperature deviated from the reference temperature of 285 °C, the 41 J transition temperature shift was corrected (s. next section). For steel 4 also the 41 J shift normalized to a fluence of 2×10^{19} cm^{-2} is included in table 4.

Table 4: experimental results

steel	irr.pos.	fluence E>1MeV [10^{19}cm^{-2}]	flux density E>1MeV [10^{11}cm^{-2}s^{-1}]	dpa [%]	irr.temp. [°C]	ΔTT(41J) [K]	ΔTT(41J) corr.[a] [K]	ΔTT(41J) norm.[b] [K]
1	B	1,7	32	2,9	286	16		
	A	1,8	295	5,4	285	22		
	B	1,7	32	2,9	318	11		
	B	1,7	32	2,9	256	48		
	C	2,9	49	5,3	289	31	33	
	C	7,1	54	13	280	65	56	
2	B	1,7	32	2,8	286	40		
	A	3,5	280	5,1	285	40		
	B	1,7	32	2,8	310	34		
	B	1,7	32	2,8	255	55		
	C	2,8	48	5,1	286	49		
	C	7,3	55	13	279	56	81	
3	B	1,8	34	3,0	286	136		
	B	1,8	34	3,0	311	78		
	B	1,8	34	3,0	253	207		
4	A	0,55	244	0,8	287	21		42,2
	A	2,1	163	3,0	286	43		
	A	9,4	143	13	284	118		38,4
	D	2,3	8	3,7	282	42		41,4
	C	2,6	45	4,8	287	45		
	C	6,9	52	13	277	120	113	
	E	2,4	29	3,5	285	63		56,1

[a] corrected to an irradiation temperature of 285 °C

[b] normalized to a fluence of 2×10^{19} cm^{-2} (E>1MeV)

DISCUSSION

Dependence of ΔTT on irradiation temperature

Fig. 1 shows the transition temperature shift ΔTT versus irradiation temperature T_B for steels 1, 2 and 3 in the range from 255 °C to 310 °C for the same neutron exposure (as regards fluence, flux density and spectrum). The results show that the influence of irradiation temperature has to be considered even for small differences in irradiation temperature. The slope of the curve ΔTT vs T_B for steel 3 is

$$\frac{\Delta(\Delta TT)}{\Delta T_B} = 2.2$$

The shapes of the curves ΔTT vs. T_B suggest that the annealing mechanisms for the three steels might be different because of the diffe-

rent chemical composition. On the other hand van Asbroeck[13] has proposed to correlate the data by only one equation, namely

$$\Delta TT = 2.25 \times (\%Cu)^{0.2} \times (\%Ni)^{3.92} \times (350\ ^{\circ}C - T_B) \times (\phi t)^{0.423} \qquad (3)$$

ϕt : fluence of fast neutrons, $E > 1MeV [10^{19}\ cm^{-2}]$

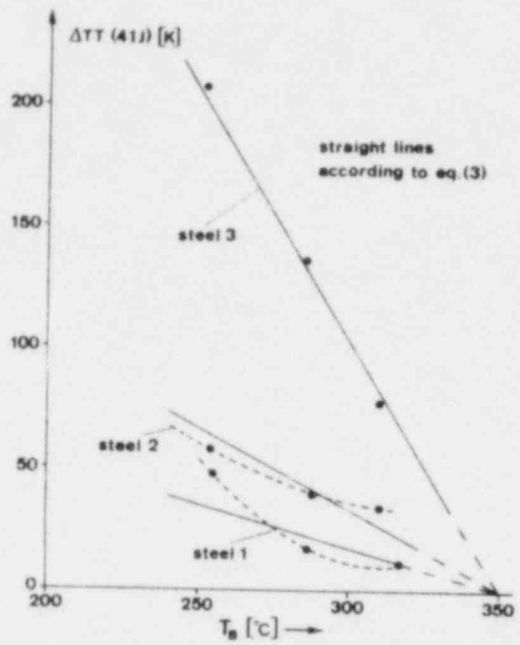

Fig. 1: Transition Temperature Shift versus Irradiation Temp.

His fitted lines are drawn into figure 1. Of course more data from steels with different chemical composition are necessary to validate this correlation.

A more detailed description of this part of the investigation was given recently [6].

Dependence of ΔTT on neutron exposure

Fluence

The results for steels 1, 2 and 4 for T_B in the range 280...290 °C, and slightly outside this range, but then corrected to 285 °C on the basis of the preceeding section, have been plotted in the usual log ΔTT vs. log Ø manner together with the corresponding Reg. Guide curves [1] and the curves recently proposed by Randall [2] in figures 2, 3 and 4. In figure 4 also results from other investigators [14] are included as far as they fall into the same T_B-range. This figure seems to show that the scatter is mainly due to different methods of evaluation rather than to different neutron spectra.

The results for each individual steel have been fitted to

$$\Delta TT = a\ (\phi t)^b \qquad (4)$$

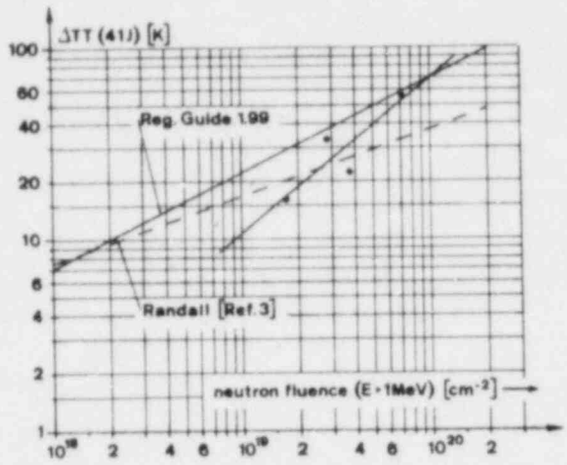

Fig. 2: Transition Temperature Shift of Steel 1 versus Neutron Fluence

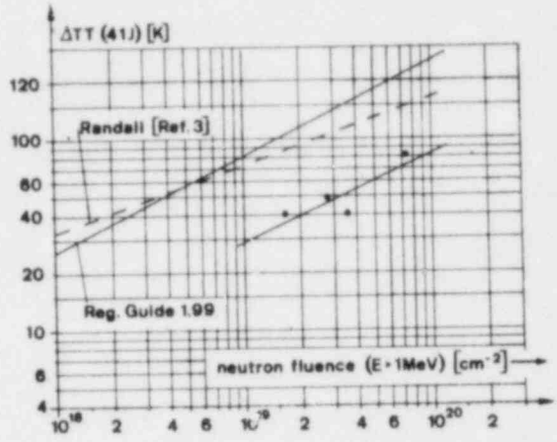

Fig. 3: Transition Temperature Shift of Steel 2 versus Neutron Fluence

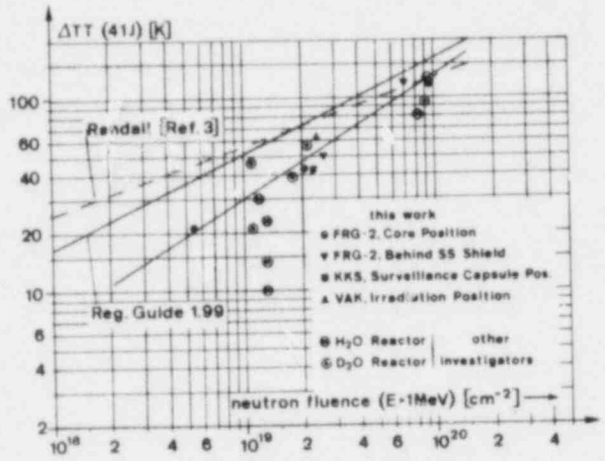

Fig. 4: Transition Temperature Shift of Steel 4 versus Neutron Fluence

Table 5: fluence and dpa exponents for steels 1, 2 and 4

steel	C.R.[a]	wt% Ni	b[b]	b*[c]
1	0,152	0,73	0,87	0,81
2	0,430	0,79	0,56	0,53
4	0,375	0,56	0,65	0,67

[a] chemistry relation according to Varsik and Byrne[2]

[b] exponent of fluence in eq. (4)

[c] exponent of dpa in eq. (5)

The Øt-exponents b are given in table 5 along with the Ni-content and the chemistry relation. No clear trend can be discerned from these few data.

Spectrum

In figure 5a measured ΔTT-values are plotted against ΔTT-values calculated from the fitting correlations according to equation (4). The standard deviation of 7.5 K is not larger than that of the ΔTT-determination itself as stated in the introduction, though the experimental ΔTT-values originate from irradiations in significantly different spectra. This supports the earlier statement of Steele that "little reason for con-

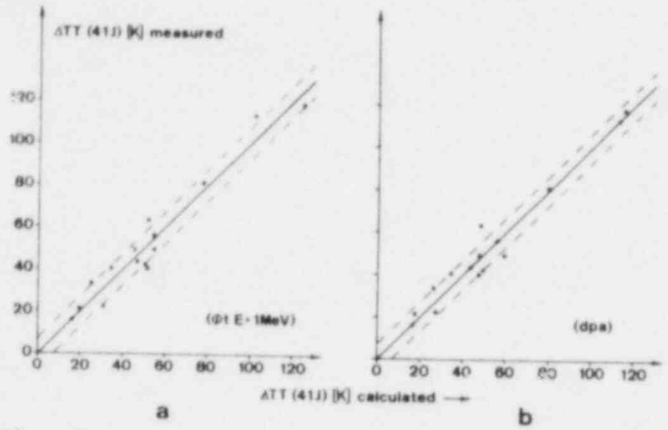

Fig. 5: Transition Temperature Shift Correlated with (a) Neutron Fluence, E>1MeV (b) dpa

cern is apparent where only light-water-moderated reactors are involved" [15], even if the spectra are rather heavily deformed as in our case by a gamma shield. Nevertheless also a fit according to

$$\Delta TT = a^* (dpa)^{b^*} \qquad (5)$$

was attempted b^* is also included in table 5. In this case the standard deviation of the fit in figure 5b is 6.4 K, which is slightly but not significantly less than that for the correlation with Øt.

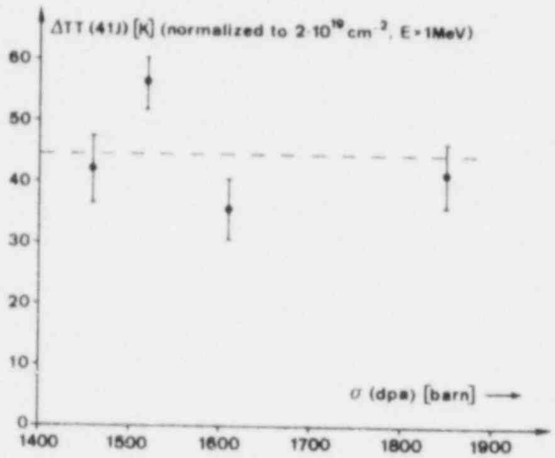

Fig. 6: Transition Temperature Shift of Steel 4 versus dpa Cross Section

In figure 6 the ΔTT-values for steel 4 determined in different spectra and normalized to 2×10^{19} cm^{-2} (only data points with fluences near 2×10^{19} cm^{-2} are taken into account) are plotted against σ(dpa). An upward trend, as it would be expected when dpa were a more appropriate exposure unit than Øt, cannot be discerned.

Flux Density

As the irradiation experiments on steel 4 cover a wide range of flux density $\dot{\emptyset}$ we have looked for a staturation effect. Figure 7 shows ΔTT, normalized to 2×10^{19} cm^{-2}, versus flux density together with a trend line calculated according to a first order defect annihilation model [16]. The data do not show a saturation effect in the flux density range ($\sim 10^{12}$...2×10^{13} cm^{-2}s^{-1}) covered by our investigation. More data at lower flux density are desirable. The results from other investigators [14] also shown in figure 7 merely extend the scatter band.

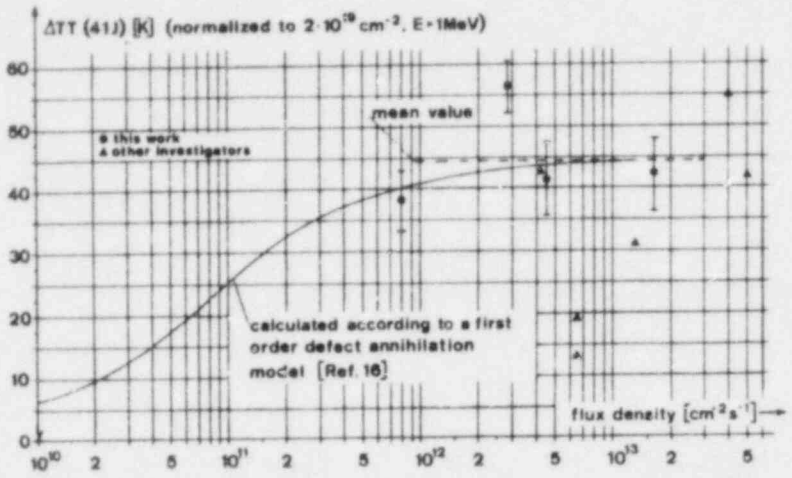

Fig. 7: Transition Temperature Shift of Steel 4 versus Flux Density

CONCLUSIONS

- Irradiation temperature must seriously be considered when evaluating RPV steel radiation embrittlement, as changes of ΔTT of more than 2 K for an irradiation temperature change of 1K may arise in steels with high copper content at 2 x 10^{19} cm^{-2}.

- The exposure exponent in the $\Delta TT \sim (\emptyset)^b$ relation should be determined for individual steel heats whenever possible to find out its dependence on chemical composition.

- Effects of neutron spectrum and flux density are small in the ranges covered by this investigation and fall into the scatter band of ΔTT determination.

REFERENCES

1. U.S. Nuclear Regulatory Comission, Regulatory Guide 1.99, Effects of Residual Elements on Predicted Radiation Damage to Reactor Vessel Materials (April, 1977).

2. J.D. Varsik and S.T. Byrne, " An empirical Evaluation of the Irradiation Sensitivity of Reactor Pressure Vessel Materials ", Proc. of ASTM Ninth Int. Symp. on the Effects of Radiation on Structural Materials, July 10-12, 1978, Richland.

3. P.N. Randall and C.Z. Serpan, " The Status of Trend Curves and Surveillance Results in U.S. NRC Regulatory Activities ", IAEA Spec. Meeting on Irradiation Embrittlement and Surveillance of Reactor Components, Oct. 19-21, 1981, Vienna.

4. G.R. Odette, " Neutron Exposure Dependence of the Embrittlement of Reactor Pressure Vessel Steels: Correlation Models and Parameters ", Proc. of an IAEA Techn. Committee Meeting, (CAPRICE 79), Sept. 24 - 27, 1979, Jülich.

5. S.E. Yanichko and J.N. Chirigos, " Observation of a Steady State Effect Limiting Radiation Damage in Reactor Vessel Steels ", Nuclear Eng. and Design 56, 297 (1980).

6. J. Ahlf and F.J. Schmitt, " Investigation on the Dependence of Transition Temperature Shift on Irradiation Temperature ", IAEA Spec. Meeting on Irradiation Embrittlement and Surveillance of Reactor Components, Oct. 19-21, 1981, Vienna.

7. C.E. Childress, Manual for ASTM A-533 Grade B Class 1 Steel (HSST Plate 03)Provided to the International Atomic Energy Agency.U.S.-Report ORNL-TM-3193 (March, 1971).

8. J. Ahlf, F.J. Schmitt, W. Spalthoff, " Irradiation Embrittlement of ASTM A-533 B Pressure Vessel Steel ", Co-ordinated Research Programme on Analysis of the Behaviour of Advanced Reactor Pressure Vessel Steels under Neutron Irradiation. IAEA-Report, IWG RRPC-78/1, p. 8 (October, 1977).

9. J. Ahlf, D. Bellmann, H. Dittmer and H. Martens, An Irradiation Capsule for Reactor Pressure Vessel Steel with a Large Specimen Volume, German Report GKSS 81/E/42, (September, 1981).

10. J. Föhl, Ch. Leitz, D. Anders, " Radiation Experiments in the Testing Nuclear Power Plant VAK ", IAEA Spec. Meeting on Irradiation Embrittlement and Surveillance of Reactor Components, Oct. 19-21, 1981, Vienna.

11. D. Bellmann, J. Ahlf, P. Wille, G. Prillinger, " Neutron Dosimetry in Irradiation Capsules for Large RPV Steel Specimens ", Fourth ASTM-EURATOM Symposium on Reactor Dosimetry, March 22-26, 1982, Gaithersburg.

12. ASTM E 693-79, Standard Practice for Characterizing Neutron Exposures in Ferritic Steels in Terms of Displacements per Atom.

13. P. van Asbroeck, private communication.

14. Co-ordinated Research Programme on Irradiation Embrittlement of Pressure Vessel Steels, Report IAEA-176 (1975).

15. L.E. Steele, " Neutron Irradiation of Reactor Pressure Vessel Steels " Nuclear Safety, 17, 327 (1976).

16. J. Ahlf, D. Bellmann and W. Spalthoff, " Investigation on the Influence of Flux Density on RPV Steel Embrittlement ", Proc. of the Third ASTM-EURATOM Symp. on Reactor Dosimetry, October 1-5, 1979, Ispra, Report EUR 6813.

"STANDARDS FOR MATERIALS BEHAVIOUR UNDER NEUTRON IRRADIATION"

P. D. Hedgecock* and J. S. Perrin**

ABSTRACT

A background to the American Society for Testing and Materials (ASTM) involvement with the development of standards for materials behaviour under neutron irradiation is given. Current practices for the surveillance of light-water reactor (LWR) pressure vessels steels are briefly described. Improvements in the standards for the basic parametric measurements have been identified and new standards are being developed which will lead to better empirical relationships between material behaviour and the variables of neutron fluence and energy, irradiation temperature, dose rate, alloy composition and welding technique. A need is cited for the development of verifiable mechanistic models which will permit more rapid development of damage - tolerant materials and welding process, as well as increased accuracy for predicting damage in older materials.

INTRODUCTION

The American Society for Testing and Materials (ASTM) is an international society, based in the USA, which manages development of standards. ASTM was founded in 1898, with emphasis in early years on standards primarily related to testing methods and materials. The society now covers a much broader area, and has grown to a size of 30,000 members in over 137 committees.

ASTM is defined in the following manner: 'ASTM is a management system for the development of voluntary full consensus standards. It provides a legal, administrative and publications forum within which producers, users, and those representing the general interest can meet on a common ground to write standards which will best meet the needs of all concerned' (1). The scope of ASTM is as follows: 'The American Society for Testing and Materials is a non-profit corporation formed for the development of standards on characteristics and performances of materials, products, systems, and services, and the promotion of related knowledge' (1).

*P. D. Hedgecock - Chairman, ASTM Subcommittee E-10.02. NUTECH Engineers, Inc., San Jose, California, USA

**J. S. Perrin - Vice Chairman, ASTM Committee E-10. Fracture Control Corporation, Goleta, California, USA

The standards developed through ASTM are of a number of types. These are:

1. Standard definitions which create a common language for a given area of knowledge.

2. Standard recommended practices which suggest accepted procedures for performing a given task.

3. Standard measurement of tests which prescribe ways of making a given measurement.

4. Standard classification which set up categories in which objects or concepts may be grouped.

5. Standard specifications which define boundaries or limits on the characteristics of a material, product, system, or service.

The individual committees are organized into the following groups of committees:

1. Ferrous Metals

2. Nonferrous Metals

3. Cementitious, Ceramic, Concrete and Masonry Materials

4. Miscellaneous Materials (paint, rubber, textiles, etc.)

5. Miscellaneous Subjects (nuclear, testing and analysis methods, etc.)

6. Materials for Specific Applications

7. Corrosion, Deterioration, and Degradation of Materials

The major publication is the ASTM Annual Book of Standards (2). This currently consists of 48 volumes. Changes and additions are made annually to each book, with the complete set being therefore reissued each year. Two periodicals, ASTM Standardization News and ASTM Journal of Testing and Evaluation, are published. ASTM also publishes a substantial number of special technical publications, which are often the proceedings of major technical symposia. For example, a recent nuclear special technical publication is Effects of Radiation on Materials, which is the proceedings of the Tenth International Symposium held in this area by ASTM Committee E-10 on Nuclear Technology and Applications.

A large number of standards developed by ASTM are in the area of nuclear technology, with many of these pertaining to the effects of nuclear radiation on structural materials in reactor power systems. Many of these are in Part 45 of the Annual Book of ASTM Standards (3). A majority of the standards are developed by the members of ASTM Committee E-10 on Nuclear Technology and Applications.

The Committee E-10 scope is "to promote the advancement of nuclear science and technology and the safe application of nuclear energy in all forms by:

1. Standardizing measurement techniques and specifications for radiation effects and dosimetry including materials response, instrumentation response, and fuel burnup;

2. Standardizing the nomenclature and definitions used in or relating to testing methods or instruments in support of nuclear industry;

3. Maintaining a broad expertise in application of nuclear science and technology, especially the measurement of radiation effects from environments of nuclear reactor, particle accelerators, indigenous space, spacecraft, and radioisotopes;

4. Maintaining a broad expertise in the applications of radioisotopes;

5. Sponsoring scientific and technical symposia and publications in our fields of specialisation;

6. Performing liaison with related ASTM committees and other technical societies and organizations, both national and international;

7. Advising other technical committees of the society in our fields of expertise."

As previously described by Steele (4), Committee E-10 on Nuclear Technology and Applications consists of a number of subcommittees. The two subcommittees which are most active in developing standards pertaining to irradiation of materials in power reactors are Subcommittee E-10.02 on Behaviour and Use of Metallic Materials in Nuclear Systems and Subcommittee E-10.05 on Nuclear Radiation Metrology.

SURVEILLANCE OF REACTOR PRESSURE VESSEL MATERIALS

Current Practice

A practical example of the development and evaluation of a standard

which contributes strongly to the structural integrity of a nuclear reactor is ASTM E-185 on "Surveillance Tests for Nuclear Reactor Vessels (5)". The tests in this standard pertain to the series of surveillance capsules contained in most commercial power reactors. These capsules provide a means to monitor and determine the effect of neutron radiation on the pressure vessel. Most capsules contain mechanical property specimens, neutron dosimeters, and thermal monitors. During the lifetime of a plant, capsules are periodically removed. They are then sent to a hot cell laboratory for examination and evaluation.

The scope of ASTM E-185 includes 'procedures for irradiating and testing mechanical test specimens for the purpose of monitoring and evaluating at periodic intervals, the radiation-induced changes occurring in the mechanical properties of the reactor vessel steels of light water-cooled nuclear power reactors'. One main area of recommendations in the standard relates to the design of a surveillance program for a reactor; this includes both the capsule design and the subsequent irradiation. This area of ASTM-185 is utilized by the reactor vendor who prepares the capsules for each reactor being constructed. It covers selection of the material used in the program (including specific vessel plates and base/weld/heat-affected zone areas), material characterization (chemical composition and fabrication history), selection of mechanical property specimens, thermal monitors, neutron dosimeters, and placement of capsules in a reactor.

A second area of recommendations in ASTM-185 is that of the post-irradiation examination of the specimens in the capsules. This area of the standard guides the reactor owner and the hot cell laboratory performing the capsule examination and covers the recommended schedule for removal of capsules, the examination and evaluation of Charpy V-notch impact and other mechanical property specimens, the neutron dosimetry, and the reporting of the results of the examination.

The various phases of a surveillance capsule examination program are covered by a number of individual ASTM standards used in conjunction with ASTM E-185. Figure 1 shows how some of these standards are integrated into the overall program.

New Standards-- Committee E-10 published a standard, E-706 Master Matrix for LWR Pressure Vessel Surveillance Standards (6) in which the interrelationship of the standards for determining pressure vessel material behaviour is clearly defined as shown in Figure 2. The matrix approach to the identification of standards needs has been aggressively implemented within Committee E-10.

E-185 was written before the matrix approach to identification of standards needs was adopted. In the areas of neutron dosimetry and thermal monitoring the quidance provided in E-185 must be expanded to the provision of new standards as noted in Figure 2. These needs were exemplified in the Subcommittee E-10.02 and E-10.05 efforts to develop a correlation between the shift in nil-ductility transition temperature (ΔNDTT) with neutron fluence for certain pressure vessel steels and

associated weldments. The Metal Properties Council, Subcommittee 6 has published the results of their treatment of a data base base which includes data from power reactors and experimental reactors up until November 1977 (7). When the data is treated using statistical regression analysis it is possible to roughly separate out the effects of elements such as copper on the irradiation-induced changes measured using the Charpy test; however, a large standard deviation exists in the plotted data. The ability to accurately predict trends and to more readily separate out influencing variables is thus compromised. New data will be of much greater value if the uncertainties in measurements of neutron fluence and irradiation temperature history can be reduced.

Action is already being taken within Committee E-10 to improve the standards. Improved techniques in fluence determination are being incorporated into new standards within Subcommittee E-10.05. A survey of thermal monitoring techniques has been performed and the basis for development of a new standard is being examined with Subcommittee E-10.02. More extensive information upon changes in mechanical behaviour of irradiated materials which has been acquired is being studied within Subcommittee E-10.02. A Task Group has been created to study the use of miniature test specimens, such as impact and tensile specimens which can be incorporated into irradiation surveillance capsules. Standards will be produced as deemed necessary.

Needs for Mechanistic Models-- The prediction of changes in structural material behaviour for design purposes has been hampered not only by the uncertainties associated with the acquisition of data within experimental and power reactors but by the lack of mechanistic models which accurately describe damage resulting from the accumulated fluence of neutrons of varying energy levels. In light water reactors the energies associated with measurable damage are those above 1MeV. It has been known for many years that lower energy neutrons also provide some damage contribution. Furthermore, the effect of the temperature at which a material is irradiated is known to be of great importance but a quantitative relationship is imprecise and is empirically based. The effect of minor elements such as copper, nickel, phosphorus, sulphur and silicon in the chemical composition of pressure vessel steels is similarly imprecisely known.

While experimental practices are improved by the uniform application of new standards related to dosimetry and thermal monitoring, the effects of neutron spectral energy distribution, dose rate, irradiation temperature, alloying elements and welding techniques are still empirically determined. Alloy selection and design application would benefit from a mechanistic understanding, especially for the future development of fast breeder and fusion reactors. Furthermore, this improved understanding would permit more accurate predictions for current operating plants, and avoid overly conservative assumptions. A significant basis of research into basic damage mechanisms already exists but an accelerated effort is required if more damage-tolerant materials and welding techniques are to be quickly developed.

Conclusion-- A significant number of standards related to the determination of material behaviour under neutron irradiation have been developed within the scope of ASTM Committee E-10 activities. The monitoring of damage accumulated by light water reactor pressure vessel steels has been conducted using these standards over the last decade of reactor operation. Using power reactor and experimental reactor data, relationshps between neutron fluence and the extent of damage have been established. Prediction curves have been derived from these data but the precision associated with data points needs the improvement which can arise from the employment of new and more rigorous standards. The resultant improvement in the quality of new data will permit greater understanding of the empirical relationships between damage and the variables of neutron fluence and energy, irradiation temperature, dose rate, alloy composition and welding techniques.

An improved empirical understanding of the effects of variables on irradiation induced damage will be of practical benefit in predicting damage precisely and developing more damage-resistant steels. Associated with the use of new standards, however, is a great need to pursue fundamental studies which will result in verifiable mechanistic models.

Throughout the process of standards development the voluntary consensus activities of ASTM Committee E-10, its Subcommittees and Task Groupgs in association with bodies such as the Metal Properties Council and the Electric Power Research Institute are an essential part of reliable nuclear power generation.

REFERENCES

1. ASTM Brochure, ASTM and Voluntary Consensus Standards, ASTM, Philadelphia, PA.

2. Annual Book of ASTM Standards, ASTM, Philadelphia, PA., 1981.

3. Annual Book of ASTM Standards, Part 45, Nuclear Standards, ASTM, Philadelphia, Pa., 1981.

4. Steele, L. E., 'The Role of the American Society for Testing and Materials (ASTM) in Providing Standards to Support Reliability Technology for Nuclear Power Plants,' Proceedings of the IAEA Symposium on Reliability Problems of Reactor Pressure Components, Vienna, Austria, October 10-13, 1977.

5. ASTM E-185-79 (1979). 'Standard Recommended Practice for Surveillance Tests for Nuclear Reactor Vessels,' Annual Book of ASTM Standards, Part 45, ASTM, Philadelphia, PA., pp. 873-881, 1981.

6. ASTM E-706-81 (1981). 'Master Matrix of Procedures for Irradiation Surveillance Dosimetry of Pressure Vessels of Light Water Reactors,' Annual Book of ASTM Standards, Part 45, ASTM, Philadelphia , PA., pp.1228-1253, 1981.

7. 'Prediction of Shift in the Brittle-Ductile Transition Temperature of LWR Pressure Vessel Materials,' Metal Properties Council, Subcommittee 6, June 1980.

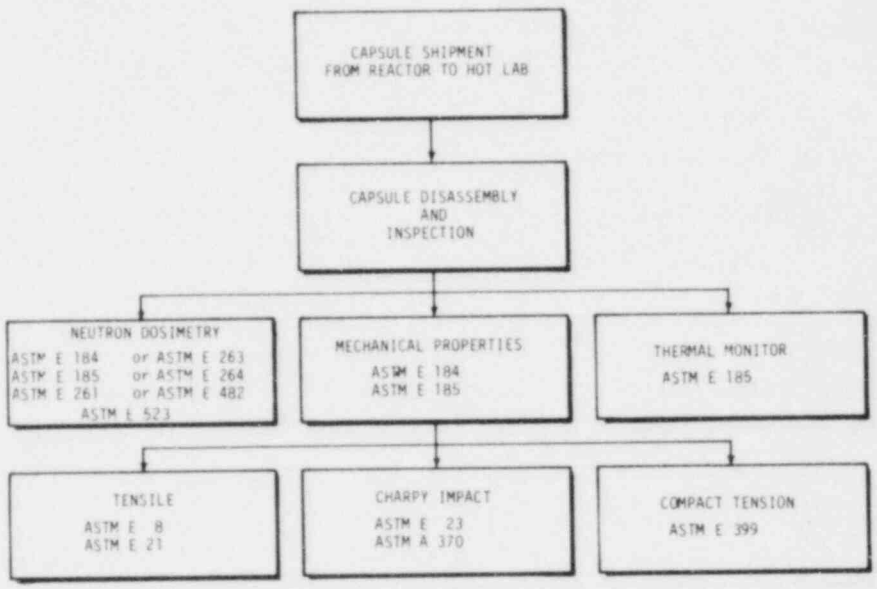

Figure 1. Summary of Some of the ASTM Standards Used in a Pressure Vessel Surveillance Capsule Program

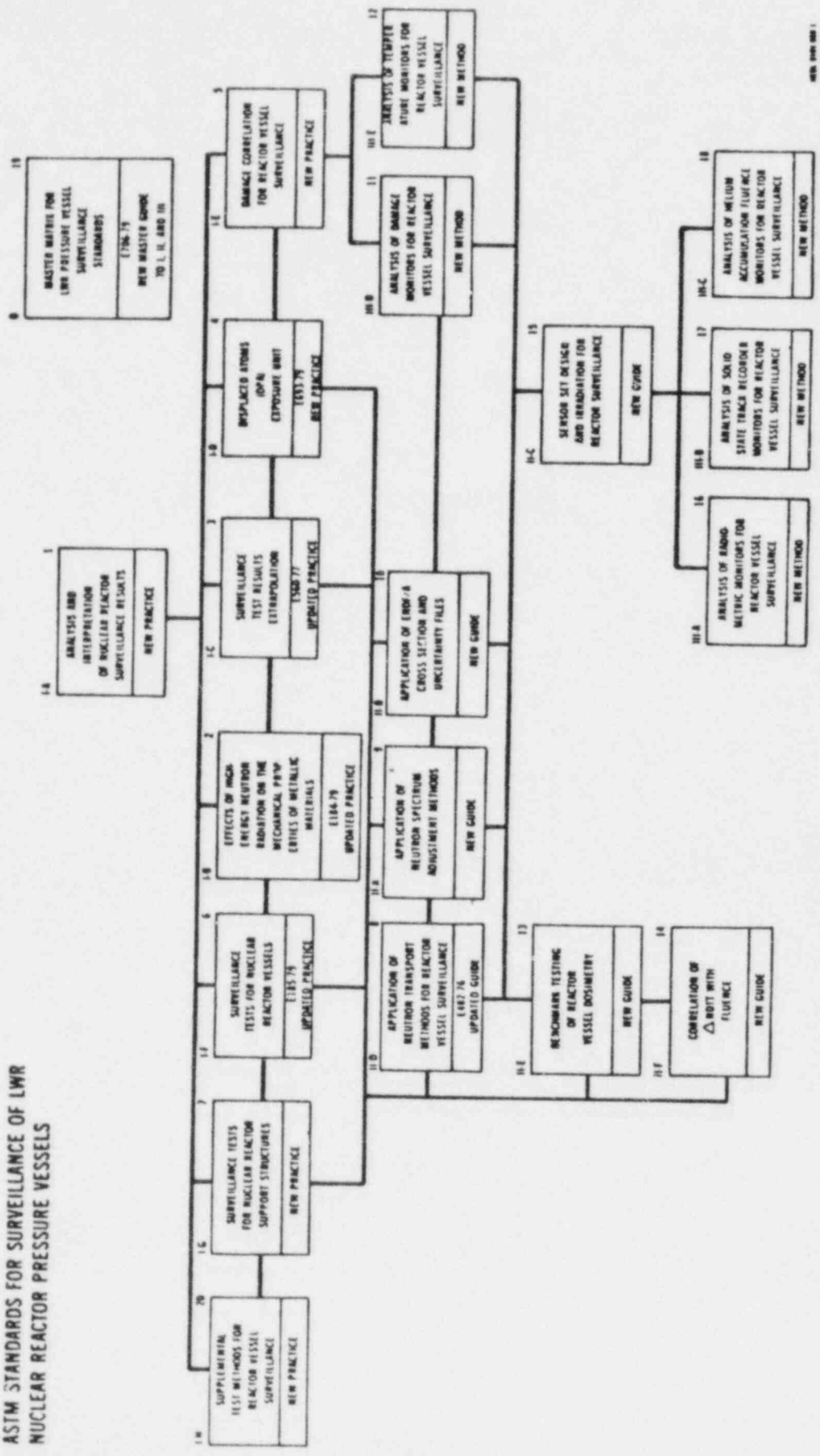

Figure 2
ASTM STANDARDS FOR SURVEILLANCE OF LWR
NUCLEAR REACTOR PRESSURE VESSELS

INFLUENCE DES NEUTRONS THERMIQUES SUR LA FRAGILISATION DE L'ACIER DE PEAU D'ETANCHEITE DES REACTEURS A HAUTE TEMPERATURE (H.T.R.)

A. Alberman, Services des Piles de Saclay
P. Pépin, Département d'Etudes Mécaniques et Thermiques
P. Soulat, Département de Technologie

C.E.N./Saclay, 91191 Gif Sur Yvette, France

RESUME

Un acier ferritique A 537, représentatif de la peau d'étanchéité des R.H.T., a été irradié dans le réflecteur du réacteur à eau lourde EL.3. Le rapport élevé de neutrons thermiques / rapides a permis de mettre en évidence un effet de fragilisation. L'analyse du décalage de température de transition montre que le dommage induit par un neutron thermique est inférieur à 1/100 de celui induit par un neutron rapide.

SUMMARY

An A 537 ferritic steel worthing for HTR vessel liner steel has been irradiated in the EL.3 heavy water reactor. Intense thermal/fast neutrons ratio has shown embrittlement effect. Transition temperature shift curves indicate relative damage effectiveness below 1/100.

INTRODUCTION

La peau d'étanchéité de la cavité coeur des réacteurs à haute température est réalisée à l'aide de tôles en acier ferritique. Cet acier est soumis à un spectre neutronique $\emptyset^{th}/\emptyset r \sim 1\ 000$ (extérieur réflecteur en graphite).

Sur la base d'un modèle de section efficace de déplacements atomiques (d.p.a), le calcul de la variation de température fragile/ductile montre que l'influence du flux thermique est plus importante que celle du flux rapide.

En effet, en utilisant, selon la recommandation EURATOM [1], le flux de fission équivalent fer (ou, pour simplifier, le flux fer) :

$$D^r(\text{dpa/s}) = 835.10^{-24} \cdot \emptyset_{fer}$$

tandis que dans le domaine thermique par capture (n,γ) :

$$D^{th}\ (dpa/s) = 13.10^{-24} \cdot \emptyset^{th}$$

Cette dernière valeur est calculée à partir de l'énergie de recul du noyau de fer :

$$E\ (n,\gamma) = 516\ eV$$

L'efficacité théorique relative en dommages (D^{th} / D^{r}) est donc de 1,5 %.

Deux irradiations de durées différentes, comprenant chacune 12 éprouvettes CHARPY V nues et 12 éprouvettes sous écran cadmium, ont été réalisées à EL.3. La première correspond aux fluences reçues par l'acier en fin de vie du réacteur ; la deuxième est destinée à la confrontation avec un modèle théorique.

CARACTERISTIQUES DE L'IRRADIATION

Nature de l'acier

Acier A 537 Lukens de composition :

	C %	Mn %	P %	S %	Cu %	Si %	Ni %	Cr %	Mo %
Analyse requise sur coulée	0,24 max	0,70 1,35	0,035 max	0,040 max	0,35 max	0,15 0,50	0,25 max	0,25 max	0,08 max
Analyse coulée	0,20	1,32	0,005	0,022	0,26	0,26	0,21	0,14	0,05

On remarquera la teneur en Cu qui, bien que conforme aux spécifications d'un tel acier, est très élevée.

En général, pour les matériaux soumis à l'irradiation, on préfère limiter cette teneur à < 0,10 %.

La température de l'acier est restée inférieure à 60°C au cours des irradiations (température maxi de la peau d'étanchéité).

Dosimétrie des emplacements d'irradiation

Les deux emplacements d'irradiation ont été choisis pour leurs caractéristiques neutroniques voisines. Deux maquettes comportant un chargement d'acier équivalent ont été réalisées pour la dosimétrie. Les résultats de dosimétrie sont indiqués dans le tableau 1. Les fluences de dommages sont déduites des dosimétries GAMIN [2]. Des dosimètres au tungstène avaient été rajoutés pour leur étalonnage en fonction du flux thermique. Les autres détecteurs utilisés pour l'irradiation ont été :

$\emptyset^{th}$: cobalt

$\emptyset^{r}$: nickel, cuivre.

Tableau 1 - Caractéristiques des irradiations à EL.3

Emplacement	DS 8	DS 9
Début d'irradiation	9.02.77	29.12.76
Fin d'irradiation	23.05.77	30.03.79
Nombre J.E.P.P.	79	596
$\emptyset^{th}$ (hors écran Cd)	$1,8.10^{13}$ n.cm^{-2}s^{-1}	$2,2.10^{13}$ n.cm^{-2}s^{-1}
$\emptyset_{Ni}$ maxi	$2,0.10^{10}$ n.cm^{-2}s^{-1}	$2,0.10^{10}$ n.cm^{-2}s^{-1}
$\emptyset^{th} / \emptyset_{Ni}$	900	1 100
Réponse GAMIN : r	5,78	6,78
$\emptyset_G / \emptyset_{Ni}$	2,89	3,39
Indices de spectre :		
$\emptyset_{fer} / \emptyset_{Ni}$	1,81	2,02
$\emptyset > 1$ MeV / $\emptyset_{Ni}$	0,47	0,47
$\emptyset^{th} / \emptyset > 1$ MeV	1 900	2 300

RESULTATS DE L'IRRADIATION

Le décalage de la température de transition mesurée est indiqué sur la figure 1 pour les 2 irradiations DS 8 et DS 9. Tous les résultats expérimentaux (ΔTT, expansion latérale) avec les fluences rapides et thermiques sont donnés sur le tableau 2. La consommation du cadmium en DS 9 explique une fluence thermique élevée. On constate ainsi un effet important de fragilisation dû aussi bien aux neutrons rapides que thermiques selon le cas (avec et sans écran cadmium).

Tableau 2 - Résultats des essais de résilience

Irradiation	Flux de dommage Φ fer n/cm²	Flux thermique Φ th n/cm²	θ transition en résilience °C	θ transition Exp latérale °C	ΔTT en résilience °C	ΔTT Exp. latérale °C	Valeur palier ductile Joules	ΔK du palier %
Témoin			-66	-55			52	0
DS8 avec cadmium	$2,8 . 10^{17}$	$9 . 10^{17}$	-42	-42	24	13	53	0
DS8 sans cadmium	$3,2 . 10^{17}$	$1,84 . 10^{20}$	-17	-3	49	52	51	0
DS9 avec cadmium	$1,8 . 10^{18}$	$1 . 10^{20}$	+6	+10	72	65	53	0
DS9 sans cadmium	$1,9 . 10^{18}$	$11,8 . 10^{20}$	+56	+94	122	149	43	17

INTERPRETATION

Equation d'évolution de la température de transition

En corrélant les effets d'irradiation, selon une loi en $(\text{fluence})^{1/2}$, on peut écrire :

$$\Delta TT = K \, (\Phi_{éq})^{1/2} \qquad (1)$$

en introduisant une fluence équivalente :

$$\Phi_{éq} = \Phi_{fer} + Y \, \Phi^{th}$$

(Y représentant la contribution relative des "dommages thermiques").

On montre que l'équation (1), pour les quatre résultats d'irradiation du tableau 2, est vérifiée à mieux que 4 % pour :

$$\Delta TT = 145 \left[\Phi_{fer} \times 10^{-19} + 4,5 . 10^{-3} \cdot \Phi^{th} \times 10^{-19} \right]^{1/2} \qquad (2)$$

La courbe analytique de l'équation (2) est donnée sur la figure 2 avec les points expérimentaux.

Effet des neutrons thermiques

L'influence des neutrons thermiques est un peu plus faible que celle prévue par le modèle théorique mais reste du même ordre de grandeur (v. Introduction), soit 0,5 % environ.

L'analyse des dommages, à partir de l'équation (2), montre ainsi que pour les irradiations d'un acier de peau d'étanchéité dans un spectre où

$$\phi^{th} / \phi^{r} \approx 1\,000$$

plus de 70 % de la fragilisation est causée par les neutrons thermiques, ce qui montre l'intérêt de l'expérience.

REFERENCES

[1] J.P. Genthon, B.W. Hasenclever, ...
Recommandations sur les mesures des irradiations reçues par les matériaux de structure de piles
EUR 5274 (1975)

[2] A. Alberman, C. Morin, ...
Dosimétrie de dommages dans le réflecteur d'EL.3
CEA.CONF.4171 (1978)

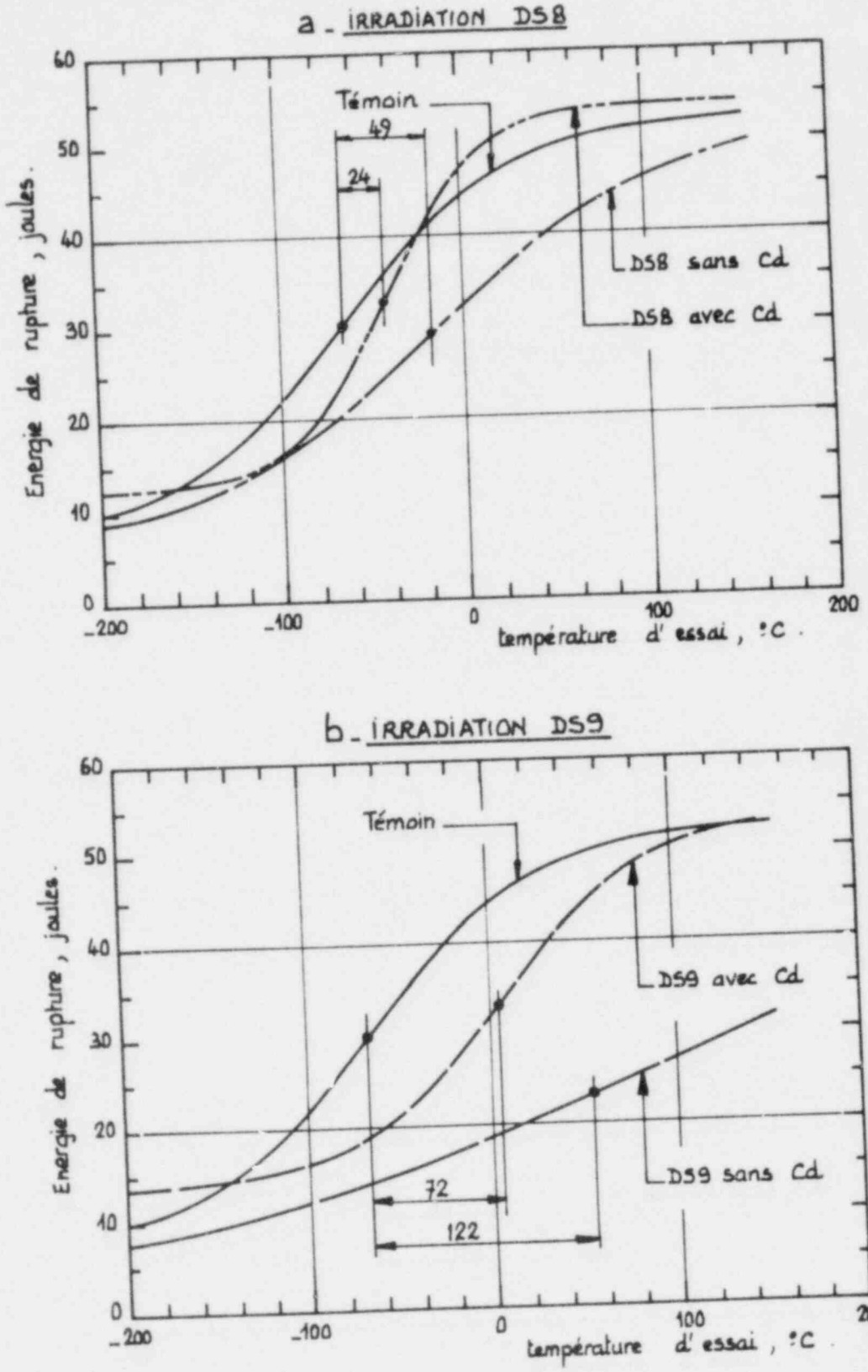

FIG.1 - DÉCALAGE DE LA TEMPÉRATURE DE TRANSITION DE L'ACIER A 537.

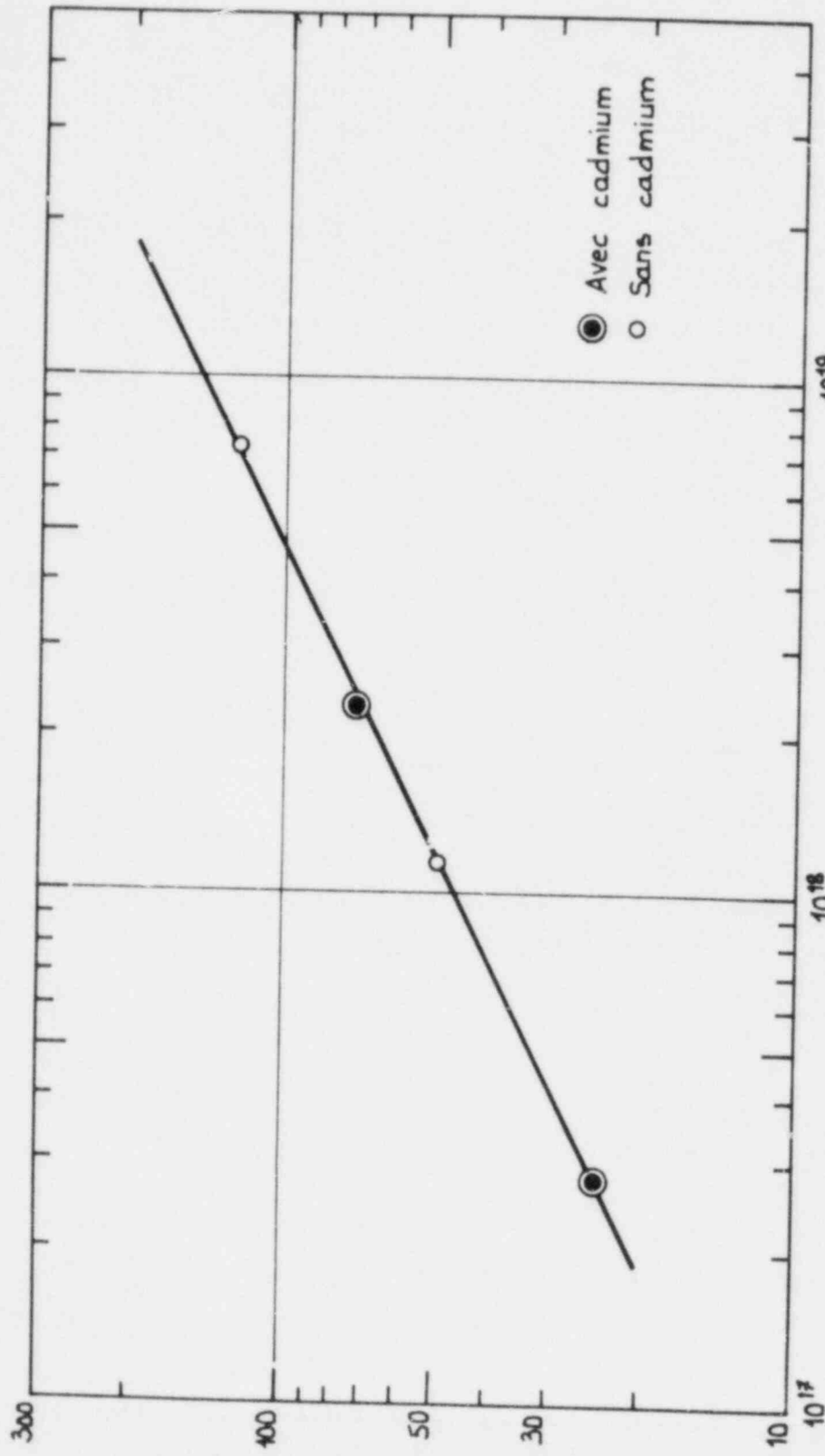

FIG. 2 - INFLUENCE DES NEUTRONS RAPIDES ET THERMIQUES SUR UN ACIER A537 IRRADIÉ À 60 °C -

CARACTERISATION D'EMPLACEMENTS D'IRRADIATION EN SPECTRES NEUTRONIQUES ET EN DOMMAGES

P. Mas, R. Perdreau
Centre d'Etudes Nucléaires de Grenoble, Service des Piles

CHARACTERIZATION OF IN-REACTOR POSITIONS FOR NEUTRON SPECTRA AND RADIATION DAMAGE DETERMINATION

ABSTRACT

This report describes the general method of neutron spectra and radiation damage determination which is used at "Centre d'Etudes Nucléaires de Grenoble - Service des Piles (CEA-FRANCE)".

The application of these methods -two dimensions neutron transport calculation, measurements by threshold and fissile detectors, radiation damage in steel and tungsten-, in very different neutron spectra, gives results best than 15 %.

INTRODUCTION

L'étude des dommages causés aux matériaux de structure des réacteurs revêt une grande importance technologique. La vitesse d'altération des matériaux soumis aux rayonnements conditionne la sûreté et l'économie des réacteurs de puissance.

Dans les réacteurs d'essai de matériaux, on cherche à réaliser des conditions d'irradiation analogues à celles rencontrées dans les réacteurs de puissance, ou bien à relier entre elles ces conditions d'irradiation par l'intermédiaire des formules théoriques d'endommagement. Ceci nécessite la connaissance du spectre des neutrons.

GENERALITES

Les modèles théoriques d'endommagement s'expriment par la réponse d'une fonction dans le spectre énergétique des neutrons qui doit être connu surtout dans le domaine de haute énergie, responsable des dommages : 0.1 MeV - 10 MeV.

La méthode adoptée au Service des Piles de Grenoble pour caractériser les emplacements est de calculer les spectres à l'aide d'un code de neutronique (DOT 3.5) dans chaque dispositif d'irradiation. La validité de la méthode peut être testée par divers moyens :

1. Comparaison des indices mesurés et calculés
2. Comparaison des effets d'endommagement calculés et mesurés lorsque la mesure d'endommagement est possible.

3. Reconstitution du spectre (méthode SAND.2) à partir d'un nombre suffisant de détecteurs à seuil.

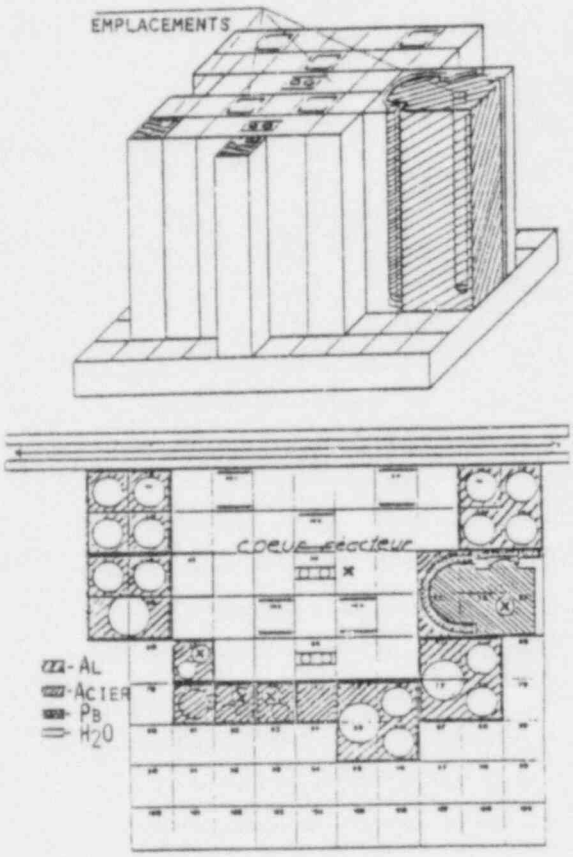

Fig. 1. Emplacements d'irradiation dans Mélusine et leurs environnements.

On présente ici des résultats d'étude de trois emplacements types du réacteur Mélusine, recouvrant les spectres rencontrés lors des irradiations d'essai dans un réacteur de type piscine :

- emplacement interne au coeur du réacteur
- emplacement en 1ère rangée
- emplacement spécial au sein d'un bloc d'acier alimenté en neutrons par une face latérale du coeur.

A cause des réactions inélastiques sur le fer, le spectre est enrichi entre 0.1. MeV et 1 MeV et présente des analogies avec ceux régnant au voisinage des cuves des réacteurs de puissance.

Chaque emplacement est destiné à recevoir une capsule reproduisant des conditions physico-chimiques particulières.

Les irradiations d'étude de spectre ont été effectuées dans de telles capsules.

COMPARAISON DES INDICES CALCULES ET MESURES

Les indices pour une réaction x sont considérés par rapport au Nickel (réaction $^{58}Ni(n,p)\ ^{58}Co$) selon :

$$\rho_{x/Ni} \equiv \frac{A_x}{\bar{\sigma}_x} \Big/ \frac{A_{Ni}}{\bar{\sigma}_{Ni}} \qquad (1)$$

$$A_x \text{ activation} = \int_0^\infty \sigma_x \Psi \ dE \qquad (2)$$

$\bar{\sigma}_x$, section efficace calculée sur un spectre de Cranberg.
A chaque valeur $\rho_{x/Ni}$ calculée dans un spectre $\Psi(E)$ avec une fonction $\sigma(E)$ est associée une valeur expérimentale déduite des mesures d'activité et des grandeurs $\sigma_{exp,x}$.

Mesures

Nous avons utilisé 8 réactions à seuil sur des dosimètres par activation ou fissiles. Les sections efficaces utilisées pour le traitement des dosimètres sont répertoriées dans le tableau I. Les détecteurs fissiles ont été traités par leur activité en ^{140}La. Les incertitudes globales sur de telles mesures peuvent atteindre 10 %.[1]

Les résultats montrent la forte sensibilité de l'indice du Neptunium au spectre de l'emplacement spécial, ceci souligne l'importance de ce dosimètre pour la surveillance des cuves de P.W.R.

Tableau I. Indices par rapport au Nickel

REACTION		^{237}Np	^{115}In	^{238}U	^{54}Fe	^{46}Sc	^{63}Cu	^{27}Al
σ_{exp}		1.312 b	189 mb	305 mb	79.7 mb	11.8 mb	0.5 mb	0.705 mb
$\bar{\sigma}$		1.336	169.7	299.5	77.03	0.95	0.5	0.629
COEUR	MES.	1.28	1.14	1.27	0.98	0.9	1.07	0.9
	CALC.	1.31	1.14	1.11	0.98	0.94	0.93	0.93
1er RANG	MES.	1.3	1.06	1.09	0.99	0.87	0.98	0.89
	CALC.	1.32	1.14	1.11	0.98	0.94	0.98	1.
SPECIAL	MES.	2.97	1.6	1.67	0.92	0.8	0.99	0.86
	CALC.	3.13	1.79	1.52	0.91	0.8	0.83	0.84

σ_{exp} : publiée en référence 2.
$\bar{\sigma}$: moyennée sur un spectre de Cranberg.

Calculs

Les structures d'irradiation sont approximées à deux dimensions, en général sur le quart du réacteur, pour être traitées à l'aide du code DOT 3.5. en coordonnées (X, Y).

Les sections efficaces des matériaux sont préparées par des calculs de condensation ANISN sur des systèmes à une dimension, appropriés pour représenter le spectre de la structure globale. Ces sections efficaces proviennent de ENDF/BIII. Les options choisies dans DOT sont :

- calcul de type source
- discrétisation énergétique à 26 groupes appropriés aux domaines de sensibilité des dosimètres et aux résonances du fer autour de 27 keV
- discrétisation angulaire S 12.

Les taux de réaction attendus sur les dosimètres sont calculés avec les flux solutions et les sections efficaces ENDF/BIV ou BV (cuivre). Les indices calculés sont donnés dans le tableau 1. Les spectres obtenus sont montrés en figure 2.

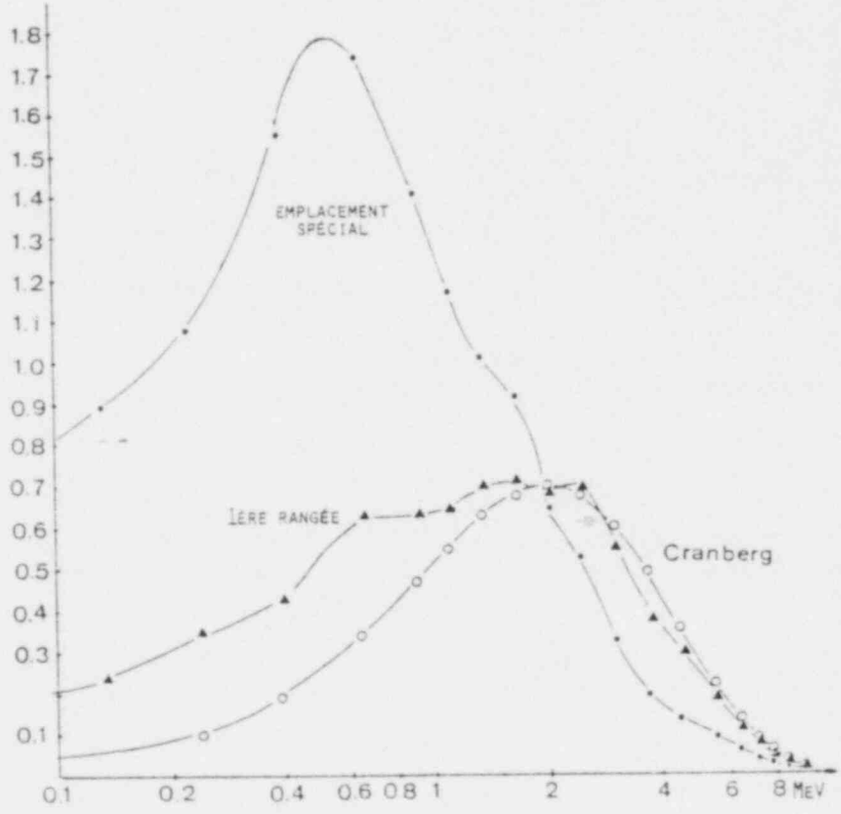

Figure 2. Spectres calculés $\Phi_{>1\ MeV} = 1$.

Comparaison

Sur l'ensemble des résultats, on observe une bonne cohérence entre les mesures et les calculs. Cependant, les mesures ne reproduisent pas complètement les fortes augmentations d'indices calculées dans l'emplacement spécial pour les détecteurs à seuil bas. Les indices des réactions à seuil élevé indiquent que l'emplacement en première rangée a un spectre voisin de celui dans le coeur à énergie élevée.

ANALYSE D'ENDOMMAGEMENTS

Endommagement de l'acier[3]

Deux lots d'éprouvettes CHARPY ont été irradiés en première rangée et dans l'emplacement spécial.

Les conditions d'irradiation étaient fixées de façon à augmenter au maximum les effets d'endommagement :

Acier A 508 - classe 3 à forte teneur en cuivre conditionné à 235° C.

Les irradiations étaient monitorées par des dosimètres de Fe et Cu. Le déplacement de la courbe de transition ductile fragile des éprouvettes traduit la fragilisation causée par les défauts créés dans le fer. Les déplacements mesurés ΔTT sont donnés dans le tableau 2. Les quantités de dommages d.p.a.[4] et zones probables p.a.[5] sont obtenues à partir des taux de réaction calculés recalés par les dosimètres de fer. Ces fluences de dommages caractérisent chaque emplacement mieux que $\phi > 1$ MeV.

Tableau 2. Effet des irradiations dans Mélusine

FLUENCES / EMPLACEMENTS	ϕ_{Fe} (79,7 mb) 10^{18} n.cm^{-2}	ϕ(> 1 MeV) 10^{18} n.cm^{-2}	ϕ(> 0,1 MeV) 10^{18} n.cm^{-2}	d.p.a. (fer)	zones probables par atome	ΔTT
1ère RANGEE	9.35	7.6	16.3	$1.025\ 10^{-2}$	$1.16\ 10^{-4}$	82,5° C
EMPLACEMENT SPECIAL	5.9	9.1	39.2	$1.57\ 10^{-2}$	$1.96\ 10^{-4}$	119° C
SPECIAL/STANDARD		1.2	2.41	1.532	1.682	1.425

Endommagement du tungstène

L'effet d'endommagement mesuré est la variation relative de résistivité d'un filament de tungstène.[6] Cette variation $\Delta R/R$ est proportionnelle à l'énergie déposée par les neutrons rapides dans le filament. Pour le modèle de dosimètre utilisé, la formule d'étalonnage est :

$$\Delta R/R = \frac{10^5 \; 0.101 \; 10^{-24}}{0.247} \; (\rho_{W/Ni}) \; \Phi \qquad (3)$$

Φ est la fluence mesurée par les dosimètres de Nickel associés au dosimètres de dommages :

$$\rho_{W/Ni} = \frac{\int E_W \Psi}{\overline{E_W}} \Big/ \frac{\int \sigma_{Ni} \; \Psi}{\sigma_{Ni}} \qquad (4)$$

Alors $(\rho_{W/Ni})\Phi$ est une mesure de l'énergie déposée $\int E_W(E)\Psi(E)dE$. Deux irradiations ont été effectuées dans les emplacements -spécial et 1ère rangée-.

La comparaison de cette valeur attendue avec la valeur $\Delta R/R$ effectivement mesurée donne des indications sur la validité du spectre calculé dans le domaine de sensibilité, c'est-à-dire au-dessus de 0.1 MeV. Les résultats sont dans le tableau 3.

Tableau 3. Endommagement du tungstène

Emplacement	$\rho_{W/Ni}$	Φ n.cm^{-2}	$\Delta R/R$ attendu	$\Delta R/R$ mesuré
1ère rangée	1.3	$2.99 \; 10^{16}$	$0.159 \; 10^{-2}$	$0.163 \; 10^{-2}$
Spécial	3.14	$1.3 \; 10^{16}$	$0.166 \; 10^{-2}$	$0.145 \; 10^{-2}$

Dans l'emplacement de 1ère rangée, l'accord est excellent ; dans l'emplacement spécial, l'indice calculé apparaît 15 % trop fort.

Reconstitution du spectre

A partir d'un lot d'activités mesurées et d'un flux d'essai, SAND 2 construit un flux compatible avec ces activités. Nous utilisons en flux d'essai Ψ(DOT) et les activités des 8 réactions ; on adjoint une 9ème réaction en considérant, à partir de la formule (3), une activité tungstène :

$$\int E_W(E) \; \Psi(E) \; dE = (\overline{E}_W/\overline{\sigma}_{Ni}) \; . \; 0.247 \; 10^{-5}(\Delta R/R)$$

On peut considérer cette activité produite par une réaction à bas seuil, du fait de la contribution des neutrons de basse énergie à l'endommagement.

Sur la figure 3, sont portées les quantités Ψ(SAND 2) / Ψ(DOT). Elles traduisent les corrections à apporter à Ψ(DOT) pour assurer la compatibilité avec les mesures.

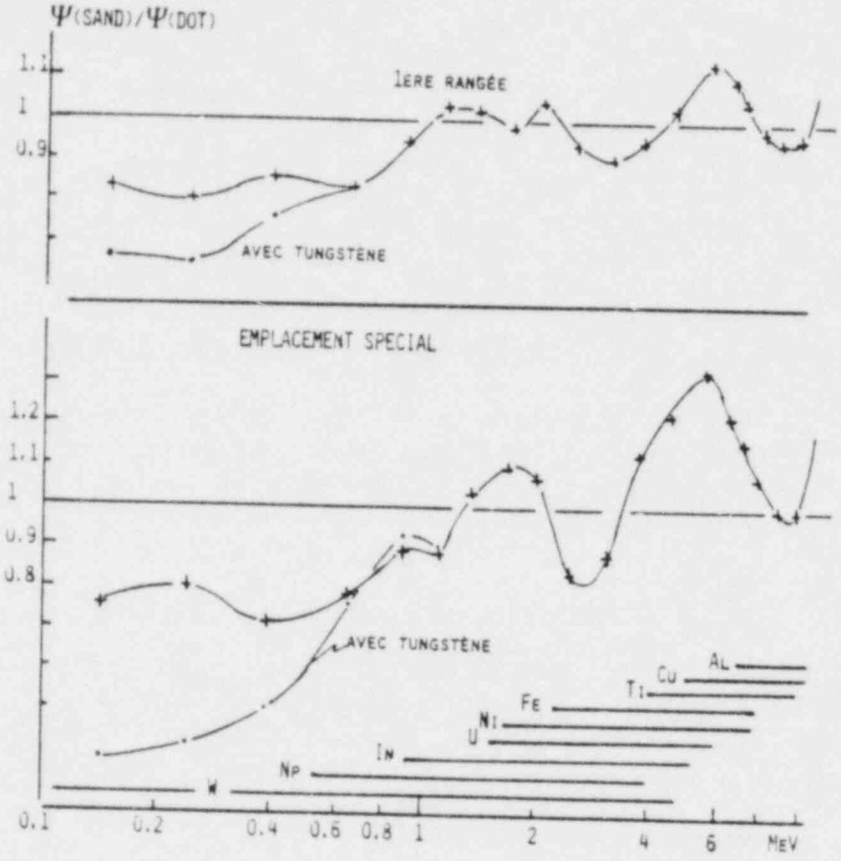

Figure 3. Comparaison des spectres calculés et mesurés.

A partir du domaine de sensibilité du Neptunium, les corrections peuvent atteindre 30 % dans l'emplacement spécial. Au-dessous, la réaction tungstène demande un flux nettement plus faible que Ψ(DOT). Ceci indique que DOT surestime ce domaine. Cette situation peut résulter de l'élargissement de la discrétisation en énergie par rapport au domaine des énergies élevées.

CONCLUSION

Les méthodes mises en oeuvre au Service des Piles du Centre d'Etudes Nucléaires de Grenoble pour caractériser des emplacements d'irradiation en spectre et en dommage peuvent être considérées comme qualifiées. En effet, l'exploration de spectres très différents par le calcul, les détecteurs à seuil et fissiles et les réponses obtenues dans l'acier et le tungstène ne diffèrent pas plus de 15 % au maximum, avec les modèles de dommages couramment utilisés.

Les améliorations à venir porteront sur une meilleure connaissance des données nucléaires, tant pour les détecteurs que pour celles nécessitées par les calculs neutroniques et passeront par la prise en compte des méthodes à matrice de covariance dans la déconvolution des spectres neutroniques à partir des détecteurs.

REFERENCES

1. P. Marcone, Caractérisation d'emplacements d'irradiation en réacteurs d'essais au moyen de détecteurs fissiles et de détecteurs de dommages, Thèse présentée à l'Université Scientifique et Médicale de Grenoble (octobre 1980).

2. W. L. Zyp and J. H. Baard, Nuclear data guide for reactor neutron metrology, EUR 7164 Parts I and II (1979).

3. P. Tran Dai, Influence du spectre des neutrons sur la fragilisatio des aciers de cuves de réacteurs, Note CEA-N 2077 (janvier 1979).

4. M. Lott, J. P. Genthon, F. Gervoise, P. Mas, J.C. Mougnot, Nguyen Van Doan, Sections efficaces de création de dommages, IAEA-SM-170/65.

5. A. Alberman, J. M. Cerles, M. Destot, J.P. Genthon, Fonction de dommages pour les propriétés mécaniques des aciers - Application aux réacteurs EL 3 - OSIRIS - TRITON, 1st ASTM EURATOM Symposium PETTEN (septembre 1975).

6. A. Alberman, J.P. Genthon, L. Larivière, P. Léger, L. Salon, M. Thierry, M. Cance, Le dosimètre de dommages miniaturisé au tungstène 3rd ASTM EURATOM Symposium ISPRA (octobre 1979).

oOo

EVALUATION AND UNCERTAINTY ESTIMATES OF CHARPY IMPACT DATA*

F. W. Stallmann

Mathematics Department
The Univeristy of Tennessee
Knoxville, Tennessee 37916

and

Oak Ridge National Laboratory
Oak Ridge, Tennessee 37830

ABSTRACT

Shifts in transition temperature and upper-shelf energy from Charpy tests are used to determine the extent of radiation embrittlement in steels. In order to determine these parameters reliably and to obtain uncertainty estimates, curve fitting procedures need to be used. The hyperbolic tangent or similar models have been proposed to fit the temperature-impact-energy curve. These models are not based on the actual fracture mechanics and are indeed poorly suited in many applications. The results may be falsified by forcing an inflexible curve through too many data points. The nonlinearity of the fit poses additional problems.

In this paper, a simple linear fit is proposed. By eliminating data which are irrelevant for the determination of a given parameter, better reliability and accuracy can be achieved. Additional input parameters like fluence and irradiation temperature can be included. This is important if there is a large variation of fluence and temperature in different test specimens. The method has been tested with Charpy specimens from the NRC-HSST experiments.

INTRODUCTION

Shift in transition temperature and upper-shelf energy from Charpy tests are used to determine the extent of radiation embrit[illegible] in steels and to construct trend curves in order to predict the safe op[illegible]ng limits of reactor pressure vessels over the lifetime of the reactor. These parameters are obtained from temperature-impact-energy curves which summarize

*Research sponsored by the Division of Reactor Safety Research, U.S. Nuclear Regulatory Commission under Interagency Agreement DOE 40-551-75 with the U.S. Department of Energy under contract W-7405-eng-26 with the Union Carbide Corporation.

the results of Charpy tests under varying test temperatures. Eyeball fitting is at present the most widely used procedure for obtaining these curves. This method contains a large measure of arbitrariness and is not suited to determine uncertainty bounds for the test results. It has therefore been suggested to apply least squares fitting procedures which allow a complete uncertainty analysis of the test data. Such an analysis is particularly important if the number of test specimen is relatively small as it is the case in pressure vessel surveillance capsules and in most materials irradiation experiments. One such method has been developed by the author and is published in Ref. 1. This paper gives a brief description of the procedure and a typical application.

DESCRIPTION OF THE METHOD

Each Charpy test is characterized by a number of test parameters. Impact energy and test temperature are the most important ones; in addition there are lateral expansion, fibrosity, irradiation fluence and temperature, and chemical composition, e.g. copper content. A set of k parameters may be selected for the analysis, x_{ij} being the value of the i-th parameter for the j-th experiment. These parameter values are considered random variables, normally distributed with known variances σ_{ij}. The parameters are fitted to a linear model

$$C_0 + \sum_{i=1}^{k} C_i \bar{x}_{ij} = 0, \; j = 1, 2, \ldots n \quad . \tag{1}$$

The coefficients are determined through a procedure which minimizes the differences between the measured values x_{ij} and the adjusted values $\bar{x}_{ij}$ in the sense of minimum χ^2, i.e.

$$\chi^2 = \sum_{i=1}^{k} \sum_{j=1}^{n} (x_{ij} - \bar{x}_{ij})^2 / \sigma^2_{ij} \rightarrow \min \quad . \tag{2}$$

There are no dependent and independent variables as in the conventional least squares curve fitting procedures. Instead there is an arbritrary scale factor which permits to fix one of the coeffients, say c_k, to

$$c_k = 1 \quad . \tag{3}$$

The other coefficients are themselves random variables whose variances and covariances can be determined by standard statistical methods.[2]

The test parameters $\bar{x}_{ij}$ cannot always be expected to fit adequately a linear model (1) but there are usually not enough data available to distinguish between the simple linear model and a more complex nonlinear

one. Indeed any linear model is valid locally, that is for a range of parameter values which is sufficiently restricted. Most importantly, data from the upper shelf region should be separated from data obtained in the transition zone since the determination of upper shelf energy should not influence the determination of the 30 ft-lb or 50 ft-lb transition temperature and vice versa.

Instead of restricting the parameter values a nonlinear transformation may be applied to fit a wider range of different conditions. Empirical trend curves can be tested in this manner.

NUMERICAL EXAMPLE

The method was applied to a series of weldments which had been irradiated in the second and third series of the BSR-HSST metallurgical experiments.[3] The Charpy specimen in these experiments received widely differing amount of fluence (between 4 and 12 · 10^{18} n/cm^2 ϕ > 1.0 MeV), irradiation temperature (500° - 600°F), and had different chemical composition (0.2% - 0.4% copper content). In each group with the same chemical composition there was also a set of unirradiated control specimen.

The specimen were grouped into sets with similar irradiation conditions and chemical composition. However the number of specimen in each group was usually too small to determine reliably the transition temperature and upper shelf energy. Next specimen with the same chemical composition but different irradiation conditions were combined. The common temperature-impact-energy curve for one set is shown in Fig. 1. This graph contains not only the linear approximations in the transition and the upper shelf region but also their 1 σ uncertainties, both for irradiated and control specimen. The calculation gives also the coefficients for the dependency of the transition temperature on fluence unirradiation temperature together with their standard deviations. The values for the 63W series were

30 ft-lb transition temperature = 184°F ± 19°

irradiation temperature coefficient = -0.54 ± 0.44 (°F transition temperature per °F irradiation temperature)

fluence coefficient = 8.6 ± 8.1 (°F transition temperature per 10^{18} n/cm^2 > 1.0 MeV)

The temperature and fluence coefficients have reasonable values but the large variances render them not statistically significant. By combining all irradiated specimens one obtains

irradiation temperature coefficient = -0.78 ± 0.09

fluence coefficient = 14.9 ± 1.7

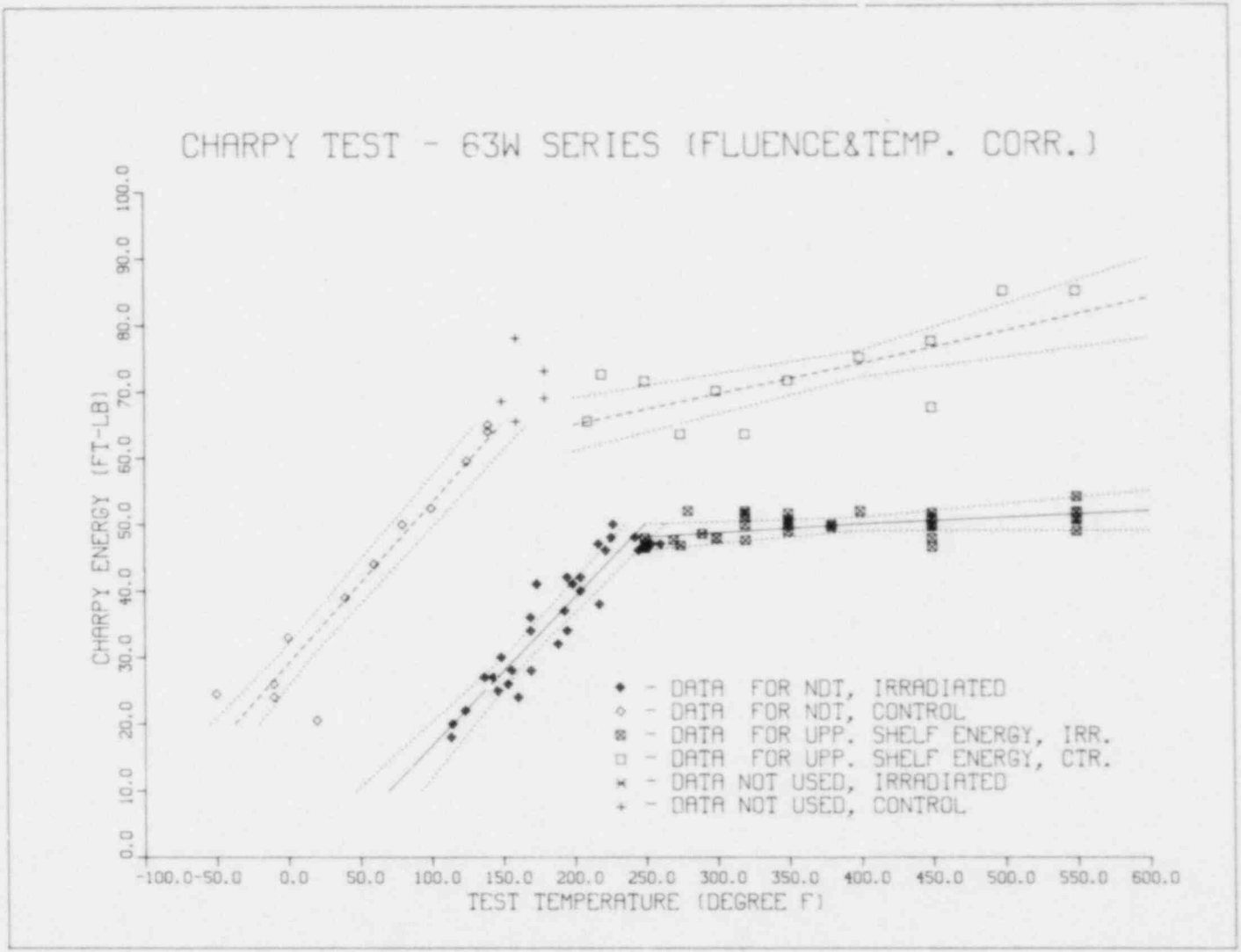

Fig. 1. This graph represents the Charpy test results of the 63W series of weldments. The transition and upper shelf regions are fitted to straight lines. The upper and lower broken lines are the 1σ uncertainty bounds. The open symbols on top represent unirradiated controls.

copper coefficient = 77.7 ± 6.6 (°F transition temperature per 0.1% copper content)

These values are certainly significant.

The linear model implied in these coefficients differs from the customary 0.5 or 0.3 power model for the relation between fluence and shift of transition temperature. Work is in progress to modify the present computer code to accept the corresponding non-linear transformation of the test parameters. The basic algorithm remains the same.

CONCLUSION

A statistical analysis of charpy test data is necessary to obtain reliable uncertainty bounds for the determination of transition temperature and upper shelf energy. A generalized linear least squares fitting method can be an effective tool for the determination of these parameters and their variances. It can also be used to determine the dependency of these parameters on irradiation conditions and chemical compositions. Modifications of the existing computer code are in progress in order to investigate non-linear models.

REFERENCES

1. F. W. Stallmann, Curve Fitting and Uncertainty Analysis of Charpy Impact Data, ORNL/TM-8081 (1981).

2. F. W. Stallmann, Theory and Pranxio of General Adjustment and Model Fitting Procedures, ORNL/TM-7896 (1981).

3. R. G. Berggren, Charpy Toughness of Irradiated High Copper Welds, Presentation to the Ninth Water Reactor Safety Research Information Meeting (Oct. 29, 1981).

COMPARISON AND LIMITATION OF UNCERTAINTIES IN SURVEILLANCE AND LIFETIME PREDICTION OF LWR PRESSURE VESSELS

For the CAPRICE Planning Meeting at
the 4th ASTM-EURATOM Symposium on Reactor Dosimetry

prepared* by W. Schneider
ZBB, Kernforschungsanlage Jülich, Germany F. R.

ABSTRACT

Uncertainty and variation statements to the mentioned task, as available from the CAPRICE 79 meeting and from other recent sources, are reviewed. While it has been agreed at CAPRICE 79 that there is need for a further reduction in the contributions to the lifetime assessment uncertainty, no guideline about the quantification of uncertainty limits has been given.
Therefore it is suggested to prepare a report resulting in quantified uncertainty limits for the above mentioned lifetime prediction. After that report will have appeared, the necessity of further studies for an adequate reduction of the overall lifetime uncertainty limits should be discussed, in relation to the uncertainty limits to be required. For this discussion, it is suggested to convene a second CAPRICE meeting

INTRODUCTION

For demonstrating the influence of uncertainties and the importance of the consistency of test results from LWR pressure vessel steel irradiations, we have to realize the use of correlation curves for the predetermination of the material properties shift which is induced by fast neutron irradiation; we relate to Fig. 1 and 2 (from /I, 439/). For the conduction of surveillance tests in this frame one is referred to ASTM Standard E 185 /III/. If the damage of the material is exceeding the predicted value, the correlation is the basis for a new estimation of the material state for the pressure vessel End-of-Life.

* using mainly parts from the presentation "Accuracy and Consistency in Irradiation Tests of LWR Pressure Vessel Steels" at /VII/

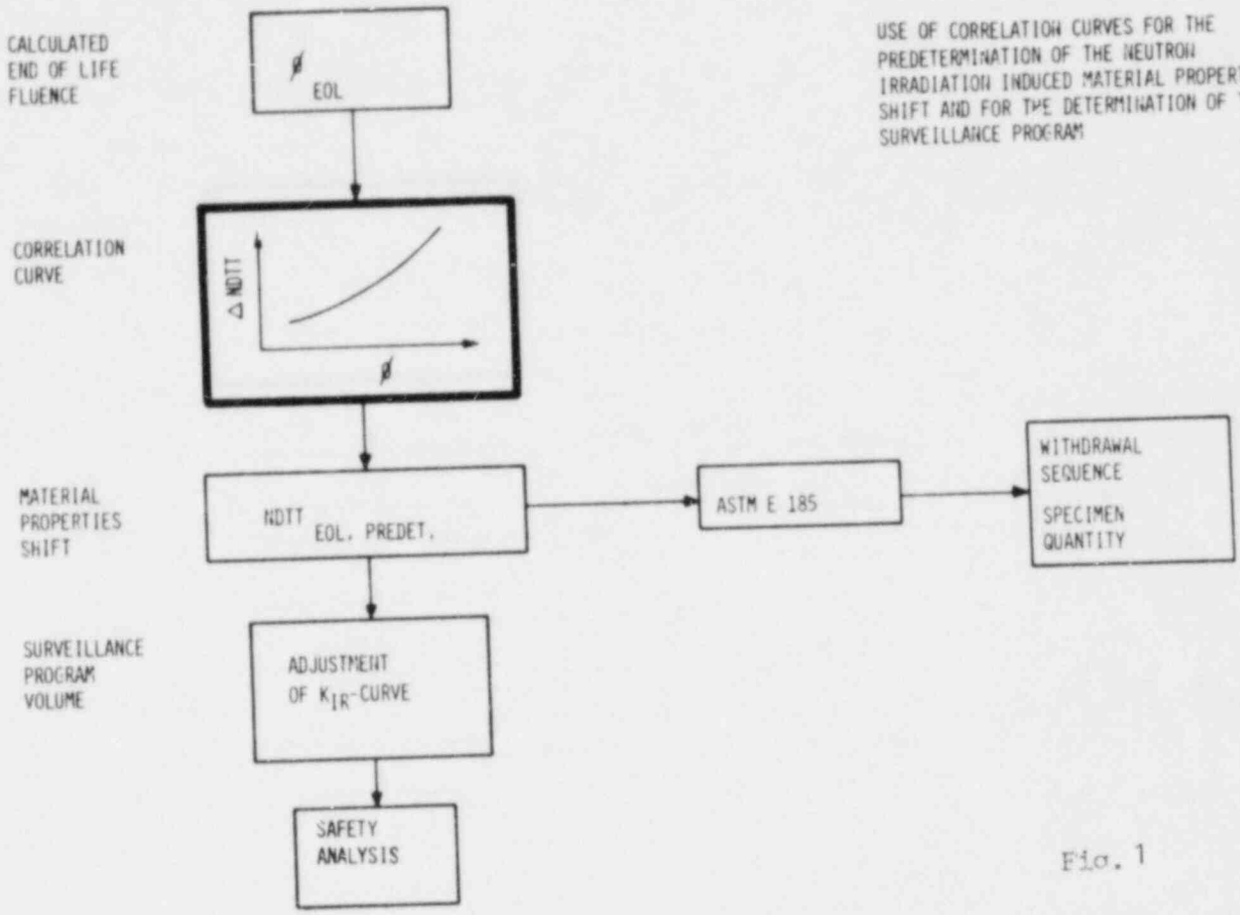

USE OF CORRELATION CURVES FOR THE PREDETERMINATION OF THE NEUTRON IRRADIATION INDUCED MATERIAL PROPERTIES SHIFT AND FOR THE DETERMINATION OF THE SURVEILLANCE PROGRAM

Fig. 1

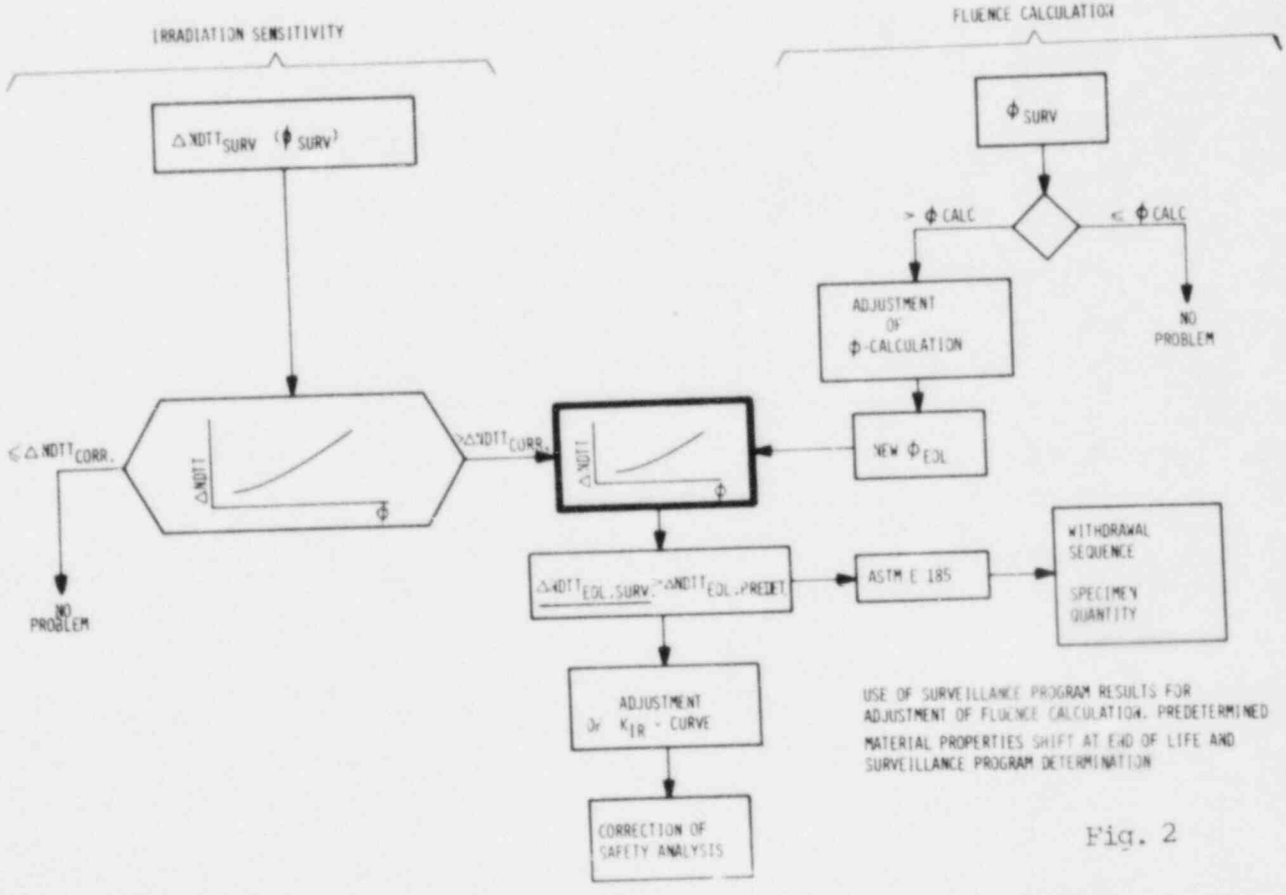

USE OF SURVEILLANCE PROGRAM RESULTS FOR ADJUSTMENT OF FLUENCE CALCULATION, PREDETERMINED MATERIAL PROPERTIES SHIFT AT END OF LIFE AND SURVEILLANCE PROGRAM DETERMINATION

Fig. 2

The correlation curves require consistent experimental points if they claim to be generally valid. Uncertainties appear in these curves on the material side as well as on the side of the irradiation environment characterization, i.e., they combine to probability windows. An ex mple of this for one correlation point is given in Fig. 3 rom /I,439/), using /1/ /V,1123/ surveillance irradiation results, estimates of fluence uncertainties and different error bounds.

In our example in Fig. 3, the window frame has two directions of extension, standing for uncertainties belonging to the material behaviour and to the irradiation environment characterization, resp. It does not make much sense to discuss on such a probability window if we do not know principally how large we have to adopt the extension relation of its sides, and even what its complete composition is. E. g., let us assume tentatively that (in a manner different from that displayed in Fig. 3) one side of the window would be much more extended than the other one: Then in consequence of the correlation between both sides of the window, the more extended uncertainty would counterfeit the possibility of the presence of an error also on the other side of the window. If we want to overcome the poor status of knowledge of the uncertainties in our problem here, then we have to investigate the composition and the extension of that probability window more in detail.

Aiming at questions like these, the IAEA Technical Committee Meeting CAPRICE (1979) /I/ was held. Its theme has been the discussion and comparison of all relevant uncertainties which may occur in the determination of the behaviour of that reactor structural material under neutron irradiation.

Before entering the discussion of the results from CAPRICE 79 meeting, I want to recollect the principal types of uncertainty contributions to both sides of the probability window, i.e., to the axes of the correlation curve.

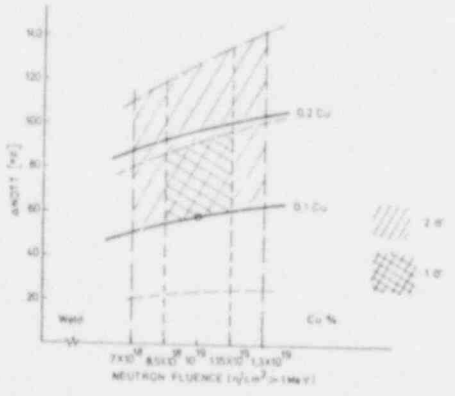

Fig. 3. Probability window for correlation point.

TYPES AND STATEMENTS ON UNCERTAINTIES (FROM CAPRICE 79 AND ELSEWHERE)

Uncertainties in calculations of the neutron radiation field /II,448//II,1275//III-E706//IV,147//V,1093/ can stem mainly from the neutron spectrum calculating procedure, from the location dependence including flux perturbation, and from time-dependent variations of the reactor power-to-local neutron flux density relation.

On the other hand, in monitoring the irradiation fluence by neutron detectors, uncertainties arise mainly by disturbing detector reactions, in the reaction cross-section averaged over the neutron spectrum in the irradiation position, and again in the time-dependent power-to-flux density variations. Furthermore one expects to have a better correlation in representing the neutron exposure by the number of displaced atoms in the material (in our case: steel) instead by the neutron fluence /I,310//V,1123//VI-A,B//2/. In Table 1 is presented the common neutron exposure evaluation by measurements, with uncertainty contributions roughly to be expected for the constituents of the reported formulae; we are referring particularly to the following assessments and considerations: /I,130//I,210//I,271//I,310//II,164//II,334//II,493/ /II,623//II,1275//1II-E261ff//III-E482//III-E706//IV,233/ /V,1123//VII, L.R. Greenwood on Neutron Flux and Spectral Measurements/. For the "flux density conversion factor from reference to test field" we may expect about 25 to 50% 1σ uncertainty incl.the perturbation by the surveillance capsule material (i.e., for the lead factor), according to /IV,1093/. For the conversion factor from "fluence" to "number of displaced atoms" uncertainty guess values according to /II,448/ /III-E693//VII, L.R. Greenwood on Displacement Damage Calculations//VII, R.L. Simons on Correlation/ have been assumed.

The main origins of the uncertainties in the material state determination are shown in Table 2 (according to /3/). As prominent examples of a lack of correspondence between compared results can be mentioned the manufacturing history depending influence of a ±30 K transition temperature variation of specimens taken from different locations in a steel plate /4/; and an error of ±15 K in irradiation temperature determination /5/: in both cases an error in the fluence and so in the test exposure or lifetime determination will result, s. Fig. 4/V,285/. To the lack of correspondence cf also /6/.

Table 1

NEUTRON EXPOSURE DETERMINATION

by

Fluence Measurement $$\Phi^I(T) = \frac{R^I}{\sigma^J} \cdot T \cdot \frac{f^{J \to I} \cdot H(T)}{K^I}$$

DPA Evaluation $$N_D^I(T) = \Phi^I(T) \cdot f_D^I$$

with:

I Irradiation Test Field Characterization Index

J Reference Field Characterization Index

D Damage Field

Constituents		Uncertainty /1σ/rel.,ca.
T	Irradiation Time	(neg.)
R	Detector Reaction Rate (incl. photoreactions)	1-5 ($\lesssim$50) %
σ^J	Reference Field Averaged Reaction Cross Section	2-10 %
$f^{J \to I}$	(Flux Density) Conversion Factor from Reference to Test Field	$\lesssim$20 %
H	Irradiation Time Correction (for Flux Density/Mean Reactor Power)	10-20 %
K	Flux Perturbation Correction	$\lesssim$10 %
f_D^I	Conversion Factor from Fluence to Number of Displaced Atoms in the Test Field	10-30 %

Table 2.

ORIGINS OF UNCERTAINTIES IN THE MATERIAL STATE DETERMINATION:

1. Materials property variation from chemical composition and from manufacturing history

2. Influence of (pre- and post-irradiation) material testing

3. Unsufficient physical correlation of the test results (e.g., of different provenance)

Reviewing the single reports on uncertainties made at the CAPRICE 79 meeting /I/, on the materials side there has been found that more detailed evaluation is necessary because of the complexity of data. The need for applying standard procedures for the material selection as well as for the evaluation and for a comprehensive documentation has been stressed /I,4/. The problem in focus beside the usual variability of material properties and test procedures is the establishment of a measure for the accuracy needed applying safety analysis. Furtheron the importance of the single influences to the correlation of irradiation induced damage with neutron exposure is to investigate. The use of correlation mean curves is suggested, demanding an increased level in accuracy and documentation.
Under the uncertainties connected to the characterization of the irradiation environment, the lack of knowledge appeared more obvious in the results of calculations and in the technical conditions (local flux densities, temperatures) than in the methods of neutron metrology where the considerations show that a satisfyingly low uncertainty seems to be achievable.
A present-day review of the understanding - i.e., the status and the aims - of the main uncertainties in the pressure vessel surveillance and lifetime assessment is given in Table 3.
A more detailed review of the uncertainty statements made in /I/ the reader may find in /3/. In /II,164/ it has been shown how errors and uncertainties may combine in a very puzzling manner in the pressure vessel surveillance and lifetime prediction.

INFERENCES FROM CAPRICE 79 AND ELSEWHERE

The central issue of the CAPRICE 79 meeting has been the following: If the overall uncertainty in the life-time assessment needs further reduction then, to attain this, some specific individual uncertainties should be found out which promise to act on the overall uncertainty prominently in the sense of a reduction. In special areas - like for neutron damage cross-sections /VII, Summary Report/ - some progress has been made in the meantime toward a standardization.
Beyond that, it has been the more or less common opinion that the uncertainties connected to the lifetime assessment as looked at should further be more thoroughly estimated and reduced /I,140//I,210//I,271//I,439//II,397/. Current efforts are aimed at improvements in accuracy on the materials side as well as on the irradiation environmental side. The results of these efforts can take effect only in a probabilistic concept. Equally the estimation of the effect and of the accuracy possible or necessary will need correlation mean curves. The curves could easily be determined, if enough

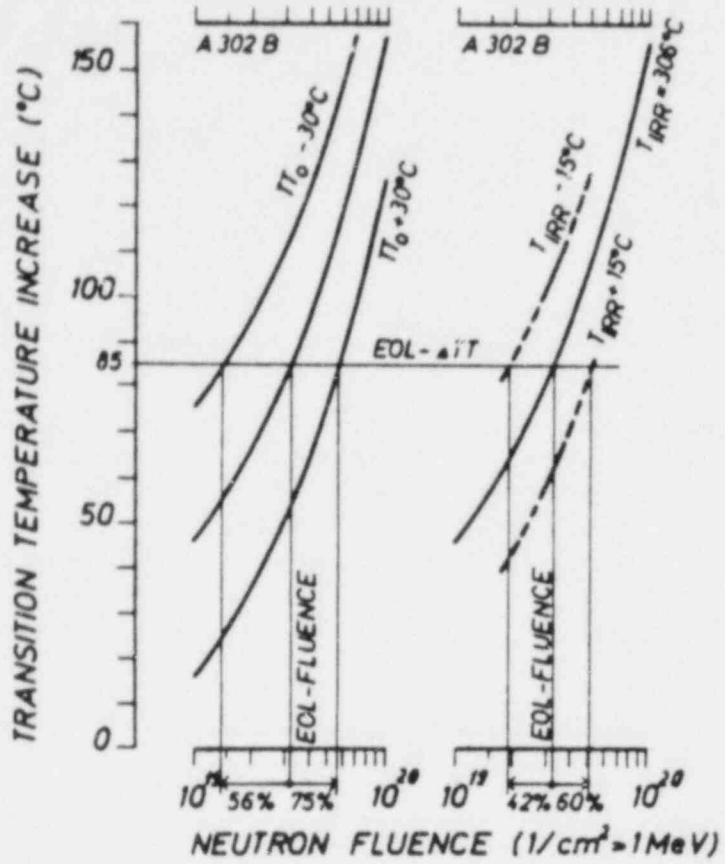

- LACKING CORRESPONDENCE OF THE COMPARED IRRADIATED AND UNIRRADIATED MATERIAL STATES IN THE UNIRRADIATED CONDITION (LEFT HAND FIGURE):

  INFLUENCE DEMONSTRATED ON THE BASIS OF A 30°C-TRANSITION TEMPERATURE DECREASE FROM THE MIDDLE TO THE OUTER EDGES OVER THE WIDTH OF THE PLATE, AS MEASURED ON HSST-PLATE 03 (CENTRAL AREA 1/4 THICKNESS)/

- ERROR IN THE DETERMINATION OF THE IRRADIATION TEMPERATURE (RIGHT HAND FIGURE):

  INFLUENCE DEMONSTRATED ON THE BASIS OF A ±15°C IRRADIATION TEMPERATURE ERROR, USING A GRADIENT OF 1.4°C TRANSITION TEMPERATURE SHIFT DECREASE PER 1°C IRRADIATION TEMPERATURE INCREASE

- ERROR IN THE DETERMINATION OF FLUENCE:

  THE RELATIVE FLUENCE ERROR IS CAUSING AN DIRECTLY EQUIVALENT RELATIVE IRRADIATION TIME ERROR

Fig. 4

Table 3: STATUS AND AIMS FOR UNCERTAINTIES
as a compilation of main consistuents of the overall uncertainty in pressure vessel lifetime assessment. Since partly from different origin, the figures given here must not combine to each other

1σ Uncertainty for the	Main Sources	Obtained until now		Desirable and possible		
		% value	Reference	% value	Remarks	References
Metallurgical variables	Chemical composition, microstructure	±45..90	/I,271/ *	±20..30		/III-E706/
Steel Irradiation temperature	Applied measuring and interpolating methods	±20..40	" *	≤±10..30		"
Irradiation exposure parameters	Lacking correction or normalization, resp.	±20..40	" *	±10..15	for neutron metrology	" /I,210/***
Overall for Transition Temperature Shifts (ΔTT)	Composed by uncertainties like above	±60..160	/II,164/ **	±15..25		/II,164/

* cf. also: /I,298//II,164//III-E706/
** " " : /VII, M. Brumovsky e. a./
*** " " : /II,164/

irradiation results favourably from surveillance irradiations and sufficient in accuracy and documentation would be available.

It should be said clearly and distinctly to which extent uncertainty limits should be required, i.e., what amount of uncertainties from a pragmatic standpoint should be even tolerated without accepting a too big safety margin which in turn would lead to a too big sacrifice of lifetime of the reactor component. As far as we know, until now there does not exist a unique figure marking such an uncertainty limit requirement.
To the single values of the wanted uncertainty reduction (as in Table 3) there is to say that arguments for just this extent of reduction has not been given what indeed would be difficult because such a requirement as mentioned above must be seen in the context of the overall uncertainty with respect to the tolerable safety margin.

Therefore we feel that at first a comprehensive uncertainty limit requirement in the mentioned pragmatic sense should be stated for a task like considered here.

SUGGESTED FURTHER STEPS

After the CAPRICE 79 meeting it was the general opinion to have a follow-up meeting again on an international scale /I,474/ /II,386/. While it has been agreed at CAPRICE 79 that there is need for reduction in the uncertainties in the lifetime assessment for pressure vessel steels, no guide-line about the quantification of uncertainty limits has been given. So it is not possible to state whether the existing uncertainties are within or are not within uncertainty limits. The quantification of uncertainty limits from the background of safety analysis which appears to be the only applicable measure should be part of the future task of the CAPRICE evaluation. This should result in a reasonable estimation of the efforts necessary to reduce particular uncertainty constituents further.

Therefore, as a first step it is recommended to prepare a report resulting in a quantification of uncertainty limits which should be required for the lifetime prediction for LWR pressure vessels.
After that, as a second step it should be considered to discuss the necessity of a study for a possible further reduction of the constituents of that uncertainty, in relation to the uncertainty limits to be required. For this discussion, a second CAPRICE meeting should be convened. Since

the first CAPRICE meeting (1979) /I/ has focused mainly on the uncertainties in the material state and in the test irradiation results, a second CAPRICE meeting should be with priority devoted to a comprehensive discussion of the uncertainty in the lifetime predetermination of the pressure vessel steel itself.

CLOSING REMARK

In the CAPRICE Planning Meeting to be held at the Fourth ASTM-Euratom Symposium on Reactor Dosimetry, Washington, D.C., 1982, there should be discussed whether a conclusion can be reached on the further procedure with respect to our problem (following to the suggestions as given above, or to other ones). If such a conclusion can be reached, it should specifically be agreed how (in which order, and in which time scale) the further steps should be initiated, and who would cooperate in such a task.

REFERENCES

PROCEEDINGS AND COMPILATIONS

/I/ CAPRICE 79 -
Correlation Accuracy in Pressure Vessel Steel as Reactor Component Investigation of Change of Material Properties with Exposure Data.
Proc. IAEA Technical Committee Meeting, Jülich, Germany F.R., 24-27 September 1979,
Editor W. Schneider. JÜL-Conf-37 (1980)

/II/ Proc. 3rd ASTM-Euratom Symposium on Reactor Dosimetry
Ispra, Italy, 1-5 October 1979
Vols. 1, 2. EUR 6813 (1980)

/III/ 1981 Annual Book of ASTM Standards,
American Society for Testing and Materials,
Philadelphia, Pa, USA

/IV/ Neutron Cross Sections for Reactor Dosimetry,
Vols. 1, 2. IAEA-208 (1978)

/V/ Proc. 2nd ASTM-Euratom Symposium on Reactor Dosimetry Palo Alto, Ca., USA, 3-7 October 1977, Vols. 1 to 3, NUREG/CP-0004

/VI-A/ IAEA Specialists' Meetings on Radiation Damage Units in Graphite and Ferritic and Austenitic Steel. Seattle, WA, USA, 3o October - 1 November 1972, Nucl. Eng. Design 33 (1975), No. 1

/VI-B/ IAEA Specialists' Meeting on Radiation Damage Units, Harwell, UK, 2-4 November 1976

/VII/ IAEA Advisory Group Meeting on Nuclear Data for Radiation Damage Assessment and Related Safety Aspects, Vienna, 12-16 Oct. 1981, (Summary Report edited by N. Kocherov: INDC(NDS)-128/GR)

INDIVIDUAL PAPERS

Papers taken from these Proceedings and Compilations (as /I/, e.g.,) are quoted in the text as /I, page No. in I/, e.g., other papers as listed below with single consecutive numbers /1/ff.

/1/ J.N. Kass, et al., Radiation Effects in BWR Pressure Vessel Steels. NEDO-21708, 77 NED 168 (1977)

/2/ A. Alberman, J.P. Genthon, et al., Introduction of Neutron Metrology for Reactor Radiation Damage. EUR 6182 (1978)

/3/ G. Nagel, W. Schneider, Discussion of Uncertainty Statements after CAPRICE 79 Meeting. IAEA Specialists Meeting on Realiability Engineering and Lifetime Assessment of Primary System Components, Vienna, 1-3 Dec. 1980

/4/ D.A. Canonico, Transition Temperature Considerations for Thick-Wall Steel Nuclear Pressure Vessels, Nucl. Eng. Design 17, 149-160 (1971)

/5/ H. Dorner, E. Sommer, Theoretische Grundlagen des Bruchverhaltens. 1. MPA-Seminar, Stuttgart, Germany F.R. (1975)

/6/ G. Nagel, Effect and Possibilities of Irradiation Results Error Correction (demonstrated on the results of the IAEA Co-ordinated Programme). 9th ASTM Symposium on Effects of Radiation on Structural Materials, Richland, WA, USA, 11-13 July, 1978

Session C.2
Nuclear Data Needs and Problems

HIGHLIGHTS FROM THE IAEA ADVISORY GROUP MEETING ON NUCLEAR DATA FOR RADIATION DAMAGE ASSESSMENT AND RELATED SAFETY ASPECTS

Vienna, 12 - 16 October 1981

N.P. Kocherov
IAEA Nuclear Data Section, Vienna, Austria

ABSTRACT

The IAEA Advisory Group Meeting on Nuclear Data for Radiation Damage and Related Safety Aspects was held in Vienna on 12 - 16 October 1981. The participants discussed the status of nuclear data, required for characterization of reactor environment by activation and damage detector techniques; uncertainties in the data and their representation in the form of covariance matrices; status of displacement cross sections and models for calculation of radiation damage in materials; data required for calculation of gas production and transmutation; correlations between microscopic damage calculations and macroscopic property changes in irradiated materials. Uncertainties in such correlations and their effect on life-time predictions for reactor structural components were also considered. First results of the REAL-80 international exercise were reported.

The IAEA Advisory Group Meeting on Nuclear Data for Radiation Damage and Related Safety Aspects was held in Vienna on 12 - 16 October 1981. The meeting was attended by 34 participants from 15 countries and two international organizations and consisted of six sessions and three workshops. 31 papers were presented and three more papers were distributed during the meeting. All of these papers as well as the conclusions and recommendations of the meeting are planned to be published soon in the IAEA Technical Document Series.

The main objectives of the meeting were to review the requirements for and the status of nuclear data needed for radiation damage estimates in reactor structural materials and related reactor safety aspects, and to develop recommendations to the Nuclear Data Section of the IAEA for its future activities in this field.

Approximately one half of the papers were devoted to the characterization of the radiation environment in fission and fusion reactors by means of activation and damage detectors.

E.P. Lippincott (USA) reported on the development of a recommended guide on the application of the ENDF/A dosimetry and damage cross section and uncertainty file to radiation damage computations and described the contents of this future file in some detail.

The present status of neutron cross-section covariance files was discussed in a paper by W. Mannhart (FRG). The emphasis was placed on the influence of relative cross-section measurements on future evaluations and also on rules for transforming covariance matrices from one neutron energy group structure to another.

The problem of optimization of the set of activation detectors was considered in a paper by A. Cesana et al. (Italy). The authors drew attention to the fact that subthreshold fission of ^{241}Am and ^{237}Np could be utilized with benefit to increase the accuracy of unfolded neutron spectra in certain environments.

Some experimental results on neutron dosimetry measurements with the ^{93}Nb (n,n') reaction were described in a paper by K. Sakurai (Japan) (not presented at the meeting), and the results of integral measurements for several dosimetry reactions in the ^{235}U fission neutron field were reported by M. Najzer (Yugoslavia).

The results of calculations of neutron reaction cross sections for ^{52}Cr, ^{55}Mn, ^{56}Fe and $^{58,60}Ni$ were reported by M. Uhl (Austria) for the neutron energy range up to 30 MeV. Comparison with available experimental data was also made.

The status of displacement cross-section sets, currently available for the use by the community was reviewed by P. Stiller (Switzerland). Careful comparison of various data sets was presented and the reasons for differences between some of them were clearly defined. Several examples when these differences have a significant impact on final results of the d.p.a. calculations were identified. L. Greenwood (USA) reported on the results of displacement damage calculations on the basis of ENDF/B-V and compared them to similar results based on ENDF/B-IV library data. The differences were found to be within 10 %. It was shown that the treatment of some processes (e.g. (n, gamma) reactions, beta-decay and some others) needs improvement to raise the accuracy of calculation of their contribution to material damage and to enable proper error assignments.

Three papers were devoted to correlations between the results of microscopic damage calculations and macroscopic property changes in irradiated materials. R. Simons (USA) reviewed the status in this field and came to the conclusion that for most materials of importance the present data files are adequate for correlating irradiation effects in materials for neutron energies up to 15 MeV. The greatest correlation problem at present lies not in the estimation of the number of primary knock-on atoms, but in material property measurements, irradiation temperature determination and in modelling of residual damage (so-called (T) function).

W. Schneider (FRG) reviewed the results of the 1979 Juelich CAPRICE meeting and subsequent developments and came to the conclusion that an authoritative quantification of uncertainty limits for crucial metallurgical and dosimetry data should be made from the point-of-view of safety analysis and service life predictions for reactor components. The need for further standardization in reactor environment characterization techniques was stressed and the suggestion made to create an international status report (and later a guidebook) on techniques of performing lifetime predetermination and surveillance of reactor pressure vessels.

W. Zijp (Netherlands) presented an analysis of first results of the REAL-80 project. It was noted that the shapes of output neutron spectra show considerable spread and also that the predicted displacement rates in steel show more convergence (7.5 % and 2.5 % variations in ORR and YAYOI), than the predicted activation rates in nickel (25 % and 10 % variations for ORR and YAYOI). The final results of this exercise will be discussed in greater detail at this Symposium in a paper by W. Zijp et al.

Discussions of the presented material were organized during three workshops (W) on nuclear data for environment characterization (W.1), on the status of displacement cross-sections and damage correlations (W.2), and on the evaluation of REAL-80 exercise results (W.3).

A number of recommendations by these working groups to the IAEA were approved at the final session of the meeting. One of the most important recommendations of the meeting was to develop a new Reactor Radiation Damage Nuclear Data File of an international reference status within the next three years. This file should incorporate the ENDF/A file which is now under preparation in the USA and should be complemented by European evaluations. The list of proposed additions to the ENDF/A file and other details can be found in "Conclusions and recommendations of the IAEA Advisory Group meeting on Nuclear Data for Radiation Damage Assessment and Related Safety Aspects" which are published in the report INDC(NDS)-128/GR.

EXPERIENCE IN USING THE COVARIANCES OF SOME ENDF/B-V DOSIMETRY CROSS SECTIONS: PROPOSED IMPROVEMENTS AND ADDITION OF CROSS-REACTION COVARIANCES*

C. Y. Fu and D. M. Hetrick
Oak Ridge National Laboratory
Oak Ridge, Tennessee USA

ABSTRACT

Recent ratio data, with carefully evaluated covariances, were combined with eleven of the ENDF/B-V dosimetry cross sections using the generalized least-squares method. The purpose was to improve these evaluated cross sections and covariances, as well as to generate values for the cross-reaction covariances. The results represent improved cross sections as well as realistic and usable covariances. The latter are necessary for meaningful integral-differential comparisons and for spectrum unfolding.

INTRODUCTION

Simultaneous evaluation of cross sections is required where ratio data exist. Because ratio measurements do not require absolute neutron flux determination, which is usually the largest source of uncertainties, correct use of ratio data would establish the relative magnitudes of various cross sections quite well. High-precision absolute data for one reaction would improve the absolute magnitudes of all other cross sections connected by high-precision ratios. In a previous paper,[1] we considered three reactions: $^{32}S(n,p)$, $^{56}Fe(n,p)$, and $^{65}Cu(n,2n)$. Previously available evaluations of cross sections and covariances, such as those from the ENDF/B-V dosimetry file,[2] were used as part of the input. These were combined with several data sets, including new absolute and relative data, by the least-squares technique. The resulting evaluations had not only updated cross sections and covariances, but also cross-reaction covariances.

In this paper, we increase the number of reactions and expand the data base. Certain problems were encountered, but not unexpectedly. These problems were traced to three areas of deficiencies in the covariances of the ENDF/B-V evaluations. First, some of the ratios calculated from the preliminary output evaluations lie outside the interval defined

*Research sponsored by EPRI and the Division of Basic Energy Sciences of the U.S. Department of Energy under contract W-7405-eng-26 with the Union Carbide Corporation.

by the ratio data and the ratios calculated from the ENDF/B-V evaluations. These results, though theoretically possible, suggest unrealistically large correlations in some of the input evaluations. Second, an unduly large energy range of full correlation enhances propagation of discrepancies. For example, the input evaluations for $^{46}Ti(n,p)$ and $^{235}U(n,f)$ both have a fully correlated range from 4 to 10 MeV, so that a local discrepancy between ratio data and evaluations near 4 MeV propagates all the way up to 10 MeV. Third, changes in evaluated cross-section values larger than one standard deviation are present in most energy ranges. This implies that uncertainty estimates are generally too small in the ENDF/B-V evaluations and possibly in the ratio data too. For example, the output $^{63}Cu(n,\alpha)$ cross sections from 8 to 11 MeV changed from the input by up to five standard deviations (up to 50%). Such large changes, if due to an oversight in one evaluation, would adversely affect other output values through the ratio data and through the cross-reaction correlations. These problems are explained in detail, and the proposed remedies described.

GENERALIZED LEAST-SQUARES

The use of generalized least-squares technique in nuclear data work has been widely discussed and demonstrated. A rather detailed review has been prepared by Peelle.[3] We summarize the solution to the minimization of least squares for the present application following the notations of Perey.[4]

Let the vector T stand for a set of input evaluations of the cross sections with the covariance matrix M. T and M define a set of joint normal probability density functions. Let the vector R be a set of new data, related to some of these cross sections, with the covariance matrix V. R and V also define a set of joint normal probability density functions. R and T are assumed to be uncorrelated. After combining R and T, the output evaluation T' and M' are given by:

$$T' = T + A(N+V)^{-1}(R-R_T) \tag{1}$$

$$M' = M - A(N+V)^{-1}A^t \tag{2}$$

where $A = MG^t$, $N = GA$, and the superscript t denotes the transpose. R_T is the vector containing calculated values for R from T. G, the sensitivity matrix, is the matrix of partial derivatives of the elements of R_T with respect to the elements of T. The χ^2 value is given by

$$\chi^2 = (R-R_T)^t(N+V)^{-1}(R-R_T) \tag{3}$$

A more useful value is χ^2 per degree of freedom (χ^2/F). The number of degrees of freedom, F, is the number of independent input data elements less the number of output data elements, and in the present case is equal to the dimension of R. Note that this χ^2 value does not depend on T' or M'.

INITIAL INPUT DATA

The dosimetry reactions and the input ratio data are summarized in Table 1. Except for $^{63}Cu(n,2n)$, all input evaluations were taken from the ENDF/B-V dosimetry file.[2] The $^{63}Cu(n,2n)$ reaction is not included in the file but is a widely used standard for cross-section measurements. The input evaluation for this reaction was taken from Tagesen et al.[5]

The ratio data were taken from those measured in four laboratories: Geel[6] - ratios with respect to $^{56}Fe(n,p)$; NPL (National Physical Laboratory of Great Britain)[7] - ratios to $^{56}Fe(n,p)$; Chalk River[8-11] - ratios to $^{32}S(n,p)$; and ANL[12-16] - ratios to $^{235}U(n,f)$ below 4 MeV and to $^{238}U(n,f)$ above 4 MeV. In addition to the ratios, some high-precision absolute cross sections for $^{56}Fe(n,p)$ from NPL were also included. The data from each laboratory were measured with the same equipment and reduced with the same techniques, therefore strongly correlated among the reactions. The method used to derive the covariances from the available documents has been given previously.[1] Some of the older Chalk River measurements were included simply because sufficient experimental information is available to permit a credible derivation of covariances. Few older measurements have such qualification.

It can be seen in Table 1 that data from different laboratories are indirectly correlated, resulting in cross correlations among all reactions in the output evaluations.

The desire to cross-correlate all reactions resulted in a minor problem. Some of the input ratio data had been used as absolute cross sections in the ENDF/B-V evaluations, thus violating the requirement that R and T be independent. However, omitting these ratios would leave large gaps in some energy regions. Moreover, these ratios had not been previously used as ratios and the covariances and cross-reaction covariances among these ratios had never been generated and used. In the latter sense, these input ratios could be considered as "new" in the present situation. Although it is desirable to start from original data sets so that R and T are truly independent, the large effort required does not at the present appear worthwhile.

Much more severe problems than the above were encountered. These problems have been outlined in the introduction. In Table 2, we show some of the ratios (Column 4) calculated from the resulting evaluations that lie outside the interval defined by the ratio data (Column 3) and the ratios (Column 2) calculated from the ENDF/B-V evaluations. These peculiar results can be best understood with a simplified but realistic example. In Fig. 1, T and R both have data at E_1 and at E_2. The standard deviations are all 10%. The correlation coefficients in the covariance matrices M and V are denoted by ρ_t and ρ_r. The four small figures show results for a fixed ρ_t and a variable ρ_r.

The case for $\rho_t = 1$ is what frequently is found in the covariances of the ENDF/B-V evaluations; namely, the values of two neighboring

Table 1. Summary of Input Ratio Data
(Denominators are circled.)

Reaction/Lab	Geel[a]	NPL[b]	Chalk River[c]	ANL[d]
$^{27}Al(n,\alpha)$			X	
$^{32}S(n,p)$			(X)	
$^{46}Ti(n,p)$				X
$^{54}Fe(n,p)$	X			X
$^{56}Fe(n,p)$	(X)	(X)	X	X
$^{58}Ni(n,p)$				X
$^{63}Cu(n,\alpha)$				X
$^{63}Cu(n,2n)$		X		
$^{65}Cu(n,2n)$		X	X	
$^{235}U(n,f)$				(X)
$^{238}U(n,f)$				(X)

[a]Ref. 6.

[b]Ref. 7.

[c]Refs. 8-11.

[d]Refs. 12-16.

Table 2. Comparison of Some Input and Output Ratios to $^{238}U(n,f)$ at 10 MeV

Reaction	Input Ratio		Output Ratio	
	ENDF/B-V	Data[a]	Initial	Revised
$^{46}Ti(n,p)$	0.257	0.239 ± 0.029	0.230	0.251
$^{54}Fe(n,p)$	0.495	0.461 ± 0.027	0.430	0.474
$^{56}Fe(n,p)$	0.072	0.064 ± 0.004	0.063	0.067
$^{58}Ni(n,p)$	0.601	0.587 ± 0.035	0.543	0.590

[a]From Smith and Meadows (ref. 12).

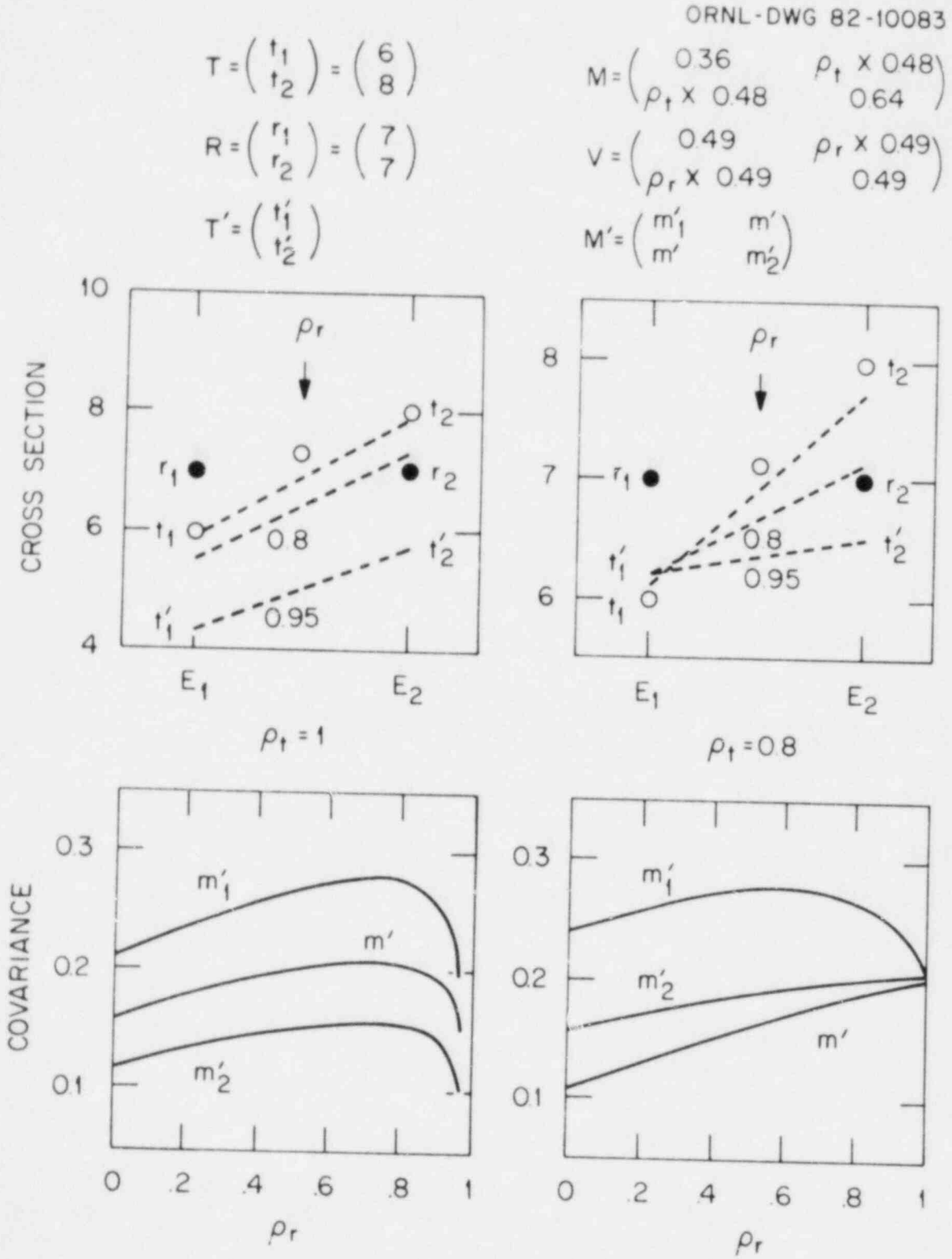

Fig. 1. An example of combining two uncorrelated cross-section sets shown as T and R. Each set is correlated. The covariance matrices are shown as M for T and V for R. The combined cross sections and covariance matrix are T' and M'.

cross-section entries are indicated to be fully correlated. In this case, t_1' is always smaller than t_1 and r_1, regardless of the value of ρ_r. Shape compromise is impossible. Strong correlation is always present in the result since $m' \sim (m_1' m_2')^{1/2}$ for all ρ_r. In short, full correlation in T will not permit even a slight shape adjustment. The covariance matrix of T must be revised to be less than fully-correlated unless the shape really is perfectly known.

The case for $\rho_t = 0.8$ is more acceptable. Shape compromises are now possible. For example, for $\rho_r = 0$, the correlation coefficient in the result is 0.587, in between the two input values. However, t_2' goes outside the (t_2, r_2) interval if $\rho_r > 0.86$. The shape difference between the two sets of data and the correlation of uncertainties in each set are in conflict if both are large. How large is large? We do not know. But when a result is outside the interval between the two input data sets, these input data should be checked carefully.

The ratios shown in the last column of Table 2 were obtained using the revised input described below.

REVISED INPUT DATA

ENDF/B-V Covariances

A segment of the ^{46}Ti(n,p) correlation matrix in ENDF/B-V is shown in the top part of Table 3. The matrix has been multiplied by 100. Two features of this matrix, which are typical of others used here, are apparent. The matrix is made of fully-correlated submatrices, each having several energy entries. There is a discontinuity in the correlation coefficients across the boundary of the submatrices. These features should be understood as resulting from subjective evaluation and/or economical file representation. We therefore felt free to remove these fully-correlated submatrices and reduce the discontinuity. The 100's in each fully-correlated submatrix were replaced by (C+P)/2 where C is the average correlation coefficient in the neighboring off-diagonal submatrices and P is a parameter taken to be 80 in the present case. The revised correlation matrix is shown in the middle part of Table 3. Note that the reduction in the correlation coefficients would result in a reduction in the uncertainty of the energy-integrated cross section, which appears undesirable. A better procedure, suggested by Peeile,[17] might be to increase the standard deviations simultaneously such that the uncertainty in the energy-integrated cross section is preserved. The final result is shown in the bottom of Table 3. Elements of the correlation matrix that fall within ±2 have been combined to reduce the dimension of the output matrix for economical reasons. A special combination of formats[18] was used to avoid having fully-correlated submatrices in the output.

If this revision of the ENDF/B-V correlation matrices was not made, the output correlation matrix in Table 3 would still contain

Table 3. A Segment of the $^{46}Ti(n,p)$ Covariance Matrix in Input (ENDF/B-V), Revised Input, and Output

E (MeV)	STD (%)	Correlation Matrix (x 100)						
7	12.8	100						Input
8	12.8	100	100					
9	12.8	100	100	100				
10	14.1	55	55	55	100			
11	14.1	55	55	55	100	100		
12	14.1	55	55	55	100	100	100	
7	12.8	100						Revised Input
8	12.8	67	100					
9	12.8	67	67	100				
10	14.1	55	55	55	100			
11	14.1	55	55	55	67	100		
12	14.1	55	55	55	67	67	100	
7	5.6	100						Output
8	5.7	25	100					
9	5.7	17	19	100				
10	7.0	17	19	19	100			
11	7.0	13	14	14	32	100		
12	10.7	13	14	14	32	32	100	

fully-correlated submatrices as in the input. After the input correlation matrix has been changed to be less than fully correlated, localized adjustments in uncertainties and correlations are possible, thus reducing the long-range impact of a local discrepancy. The implication of this revision is particularly significant for the ENDF/B-V ^{46}Ti(n,p) and ^{238}U(n,f) evaluations in which a fully-correlated range extends from 4 to 10 MeV.

This revision of the ENDF/B-V correlation matrices is mainly responsible for obtaining the ratios shown in the last column of Table 2, although they were obtained with further revisions of the input data discussed below.

Traceable Discrepancies

Some traceable discrepancies between the input evaluations and the input data were removed. One area is near thresholds of the (n,p) and (n,α) reactions where cross sections are so small that even large adjustments have little consequences in broad-spectrum applications. However, when ratios are used, problems do arise. For example, a measured value of ^{54}Fe(n,p)/^{235}U(n,f) ratio[12] at 2 MeV has an uncertainty of 10%, but the discrepancy between this value and the one from ENDF/B-V is 75%. Removing this single datum resulted in a change of 16% in the ^{54}Fe(n,p) cross section at 2 MeV and 3% change in ^{235}U(n,f). While the 16% change in ^{54}Fe at 2 MeV is practically unimportant, the 3% change in ^{235}U at 2 MeV is unacceptably large. Several such ratios have been removed, not because they are wrong but because we do not know how to use them correctly.

Another area of obvious discrepancy is in the ^{63}Cu(n,α) cross sections from 8 to 10 MeV. In this energy range, the measured ^{63}Cu(n,α)/^{238}U(n,f) ratios[13] differ from the ones calculated from ENDF/B-V by up to 60%. We subsequently decided that the uncertainties assumed in the evaluation for ^{63}Cu are too small. However, enlarging these uncertainties resulted in a large step in the ^{63}Cu cross sections at 10 MeV because the ratio data are below 10 MeV. To avoid this large step, we replaced the ENDF/B-V values by a previously calculated cross-section curve[19] from 7.7 to 13.2 MeV which is normalized to the ENDF/B-V value at 7.7 MeV. Since this curve is in better agreement with that indicated by the ratio data, the large step at 10 MeV is much reduced. Apparently the decision to change the ENDF/B-V cross sections was influenced by the new ratio data. Thus the requirement that R and T be independent was again violated, but with a good reason.

Untraceable Discrepancies

There are small and subtle discrepancies that cannot be easily ascertained. An indication of such discrepancies may be found in the value of χ^2/F. The final covariances may be multiplied by this value to reflect the fact that a reduction in uncertainties after combining two discrepant data sets is unwarranted. Two methods may be used to

compute the χ^2/F value and to multiply it to the final covariances. One is to apply a single χ^2/F value to all results uniformly at the end. The other is to combine the data sets from each laboratory sequentially and apply the χ^2/F weighting for each step sequentially. The two methods are not equivalent and neither is theoretically rigorous. The second method has the advantage of selectivity in weighting different reactions and was chosen for the present case. The χ^2/F values as computed and applied sequentially are: 1.38 for the NPL data, 1.32 for Chalk River, 1.02 for Geel, and 1.01 for ANL. One may see from Table 1 that only the covariances of the $^{56}Fe(n,p)$ cross sections have been multiplied by all four χ^2/F values.

RESULTS

In addition to the 11 reactions listed in Table 1, the ENDF/B-V $^{115}In(n,n')$ cross sections were updated with new data[20] which are uncorrelated with the other reaction cross sections. For the 11 correlated reactions, the adjusted cross sections vary mostly from 1 to 7%. The auto-correlation averaged approximately 50% and the cross-correlation 20%. The $^{54}Fe(n,p)$, $^{56}Fe(n,p)$, $^{63}Cu(n,\alpha)$, and $^{63,65}Cu(n,2n)$ cross sections are much improved with recent high-quality data.[6,7,13] The results are given in the ENDF/B-V formats[18] and are available on request. In the updated covariances, no two cross sections in any neighboring energy entries are fully correlated, a drastic difference from ENDF/B-V. This work also resulted in an improved version of the GLUCS code.[21] Maerker has found the present results generally superior to ENDF/B-V in providing more consistent C/E values in the PCA and PSF experiments.[22]

CONCLUSION AND RECOMMENDATIONS

This work represents a large-scale application of the generalized least-squares technique for data combination. It results in 12 updated dosimetry cross sections with credible covariances and cross-reaction covariances. The new data base will be useful for incorporating future data. Addition of three more reactions, $^{27}Al(n,p)$ and $^{47,48}Ti(n,p)$, to the new data base is in progress. Incorporation of the ENDF/B-VI $^{235}U(n,f)$ standard cross sections, when available, is planned.

As pointed out, several problems existed but did not hurt the results too badly. Some examples are: weak dependence of R and T, need to reduce the correlation coefficients in the fully-correlated submatrices, and selection of methods in applying the χ^2/F weighting. Continued efforts in these areas are needed.

Covariance information implying full correlation over an extended energy range should be avoided unless it correctly represents the available information.

ACKNOWLEDGEMENT

The authors are grateful to F. G. Perey, R. W. Peelle, J. K. Dickens, N. M. Larson, and R. E. Maerker for assistance in various phases of this work.

REFERENCES

1. C. Y. Fu, D. M. Hetrick, and F. G. Perey, "Simultaneous Evaluation of $^{32}S(n,p)$, $^{56}Fe(n,p)$, $^{65}Cu(n,2n)$ Cross Sections," p. 63 in Proc. Conf. Nuclear Cross Sections for Technology, eds. J. L. Fowler, C. H. Johnson, and C. D. Bowman, NBS-SP-594 (1979).

2. ENDF/B-V Dosimetry File, available from National Nuclear Data Center, Brookhaven National Laboratory.

3. R. W. Peelle, "Uncertainty in the Nuclear Data Used for Reactor Calculations," in Procedures for Evaluating Uncertainties in Estimated Reactor Performance Parameters, to be published in Adv. Nucl. Sci. and Technology, Plenum Press, ed. Martin Becker.

4. F. G. Perey, "Covariance Matrices of Experimental Data," p. 104 in Proc. Int. Conf. Neutron Physics and Nuclear Data for Reactors and Other Applied Purposes, Harwell, England, 1978.

5. S. Tagesen, H. Vonach, and B. Strohmaier, Physics Data 13, 1 (1979).

6. T. B. Ryves, P. Polkowski, and K. J. Zieba, Metrologia 14, 127 (1978).

7. A. Paulsen, R. Widera, F. Arnotte, and H. Liskien, Nucl. Sci. Eng. 72, 113 (1979).

8. D. C. Santry and J. P. Butler, Can. J. Phys. 42, 1030 (1964).

9. D. C. Santry and J. P. Butler, Can. J. Phys. 44, 1183 (1966).

10. D. C. Santry and J. P. Butler, Can. J. Phys. 41, 123 (1963).

11. J. P. Butler and D. C. Santry, Can. J. Phys. 41, 372 (1963).

12. D. L. Smith and J. W. Meadows, Nucl. Sci. Eng. 58, 314 (1975).

13. G. Winkler, D. L. Smith, and J. W. Meadows, Nucl. Sci. Eng. 76, 30 (1980).

14. D. L. Smith and J. W. Meadows, Cross Sections for (n,p) Reactions on ^{27}Al, $^{46,47,48}Ti$, $^{54,56}Fe$, ^{58}Ni, ^{59}Co, and ^{64}Zn from Near Threshold to 10 MeV, Argonne National Laboratory Report ANL/NDM-10 (1975).

15. D. L. Smith and J. W. Meadows, Response of Several Threshold Reactions in Reference Fission Neutron Fields, Argonne National Laboratory Report ANL/NDM-13 (1975).

16. D. L. Smith, Remarks Concerning the Accurate Measurement of Differential Cross Sections for Threshold Reactions Used in Fast-Neutron Dosimetry for Fission Reactors, Argonne National Laboratory Report ANL/NDM-23 (1976).

17. R. W. Peelle, Oak Ridge National Laboratory, private communication (1981).

18. R. W. Kinsey, Data Formats and Procedures for the Evaluated Nuclear Data File, ENDF, Brookhaven National Laboratory Report BNL-NCS-50496, ENDF-102 (1979).

19. C. Y. Fu and F. G. Perey, Nucl. Matr. 61, 153 (1976).

20. H. Liskien, F. Arnotte, R. Widera, and A. Paulsen, Nucl. Sci. Eng. 67, 334 (1978).

21. D. M. Hetrick and C. Y. Fu, GLUCS: A Generalized Least-Squares Program for Updating Cross-Section Evaluations with Correlated Data Sets, Oak Ridge National Laboratory Report ORNL/TM-7341 ENDF-303 (1980).

22. R. E. Maerker, Oak Ridge National Laboratory, private communication (1981).

SPECTRUM-INTEGRATED HELIUM GENERATION CROSS SECTIONS FOR ^{6}Li AND ^{10}B IN THE SIGMA SIGMA AND FISSION CAVITY STANDARD NEUTRON FIELDS

B. M. Oliver and Harry Farrar IV
Rockwell International Corporation
Canoga Park, California 91304, USA

and

E. P. Lippincott
Hanford Engineering Development Laboratory
Westinghouse Hanford Company
Richland, Washington 99352, USA

and

A. Fabry
CEN/SCK Laboratories
B2400 Mol, Belgium

ABSTRACT

The spectrum-integrated helium generation cross sections for ^{6}Li and ^{10}B have been determined for the Sigma Sigma and Fission Cavity standard neutron fields of the BR1 reactor at the CEN/SCK Laboratories, Mol, Belgium. The cross sections were obtained from helium concentrations measured in numerous small crystalline samples of natural boron, enriched ^{10}B, and enriched ^{6}LiF by precise high-sensitivity mass spectrometry. The measured helium concentrations have been corrected for such factors as neutron self-shielding, flux depression, and flux gradients. The determined cross sections are compared with values calculated from the ENDF/B-V cross section file using theoretical and evaluated spectra for the two facilities. The results of these comparisons are similar to those previously obtained for ^{6}Li and ^{10}B in BIG-10 and CFRMF, and indicate discrepancies between the measured and calculated cross sections. Obtaining acceptable consistency will require changes to the neutron spectrum in Sigma Sigma and to one or both isotope cross sections.

INTRODUCTION

Background

The Interlaboratory Reaction Rate (ILRR) program was established to meet the neutron dosimetry requirements for obtaining accurate fluence and spectral data in future breeder reactors. The goal was to reduce uncertainties associated with measured fission and nonfission neutron dosimetry reactions. The program has included cooperative irradiations in several low-power breeder reactor benchmark fields and in EBR-II and other LMFBR environments. The low-power reactors included the Coupled Fast Reactivity Measurements Facility (CFRMF) at the Idaho Nuclear Engineering Laboratory (INEL),[1] the 10% enriched U-235 critical assembly BIG-10 at the Los Alamos National Laboratory (LANL),[2] and the Sigma Sigma and Fission Cavity fields of the BR1 reactor at the CEN/SCK Laboratories in Mol, Belgium.[3] The particular reactions studied were $^{6}Li(n,He)$ and $^{10}B(n,He)$. These reactions have very extensively characterized cross sections, particularly at energies below ~0.1 MeV. Comparisons of the measured and calculated helium generation data for ^{6}Li and ^{10}B in the BIG-10 and CFRMF irradiations have been reported previously.[4] Those results indicated that even though the ^{6}Li and ^{10}B cross sections are considered well known, adjustments to one or both are required to obtain consistency in breeder-type neutron spectra.

Overview of HAFM Method

Helium accumulation neutron dosimetry involves the irradiation of small samples of various materials, each with its own energy-dependent helium generation cross section. The resulting generated helium is then measured using specialized high-sensitivity mass spectrometric techniques.[5] The total neutron fluence can then be obtained by dividing the measured helium concentration by the appropriate spectrum-integrated helium generation cross section. Usually, the sensor material, known as a helium accumulation fluence monitor (HAFM), is encapsulated in a miniature capsule. In principal, the method is equivalent to the well-established radiometric multiple foil method. The fact that the irradiation product, helium, is stable makes the HAFM technique attractive for long-term irradiations. Further, the HAFM method is entirely compatible with other dosimetry techniques, including radiometric foils[6] and solid-state track recorders,[7] and existing spectral adjustment codes.[8,9]

IRRADIATION DETAILS

Sigma Sigma

The secondary intermediate energy standard neutron field, Sigma Sigma ($\Sigma\Sigma$), is a thermal-fast coupled spherical source assembly located within a 50-cm-diameter spherical cavity in the horizontal graphite

thermal column of the BR1 reactor.[3] The spherical source shell consists of a natural uranium shell, 24.5 cm OD and 5 cm thick. Inside the uranium, there is a 1.5-cm-thick inner shell of natural boron carbide. The 11-cm inner diameter defines the limits of the actual irradiation volume. With this configuration, the outer portion of the uranium shell acts as a thermal-to-fast neutron converter. The resulting fast neutrons are then degraded in energy by inelastic scattering in the interior portion of the uranium shell and by elastic collisions in the boron carbide. The boron preferentially removes the low-energy neutrons, resulting in a final "shaped" neutron energy distribution that is particularly useful for fast reactor dosimetry experiments. Flux gradient measurements in Sigma Sigma indicate a maximum anisotropy in the central region (±3 cm) of ≤4%.[3]

Twenty-one bare and encapsulated crystals of natural boron, enriched boron (93% ^{10}B) and ^{6}LiF (99.1% ^{6}Li) were irradiated for ~103 hours in the Sigma Sigma facility. The arrangement of the various capsules, bare crystals, and empty capsules is shown in Fig. 1. Empty capsules were included in order to measure any helium production from the capsules themselves, although negligible amounts were expected.

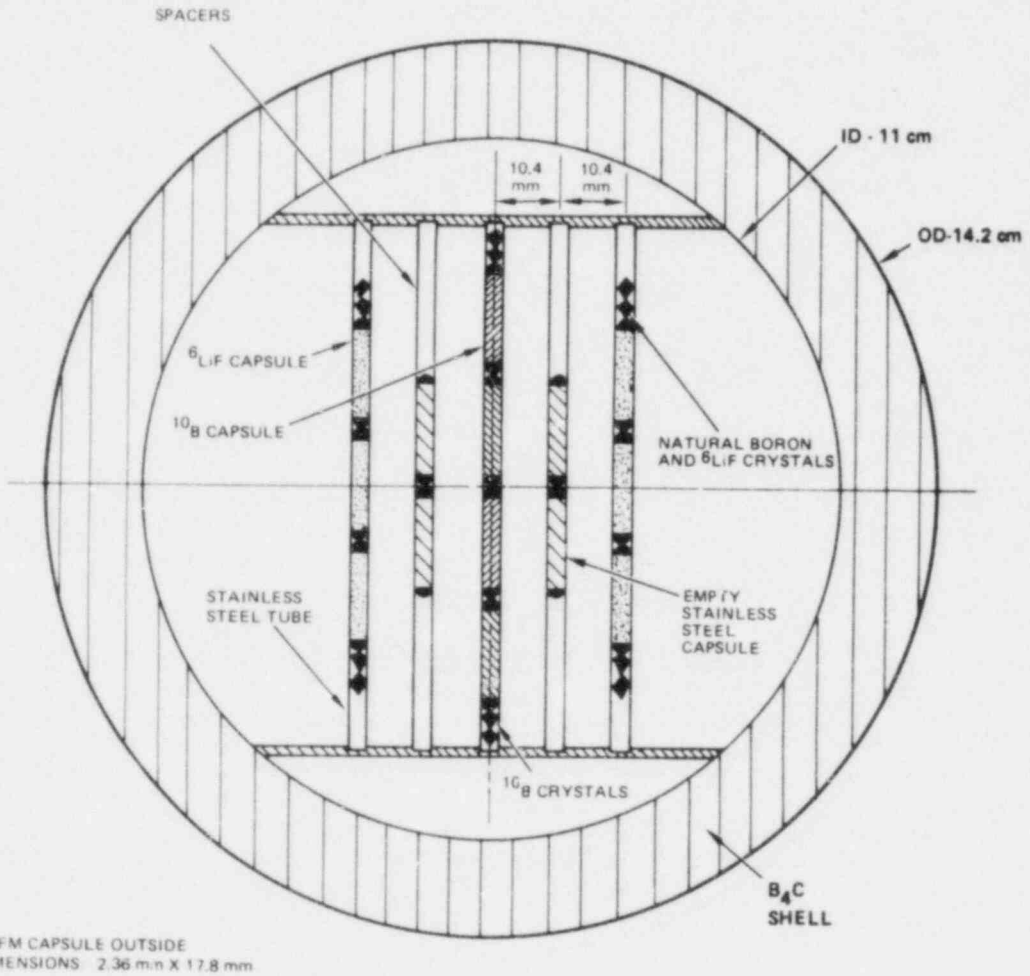

Fig. 1. Configuration of HAFMs in Sigma Sigma

The HAFM capsules used for the Sigma Sigma irradiation were manufactured from thin-wall (0.076 mm), 2.36-mm-OD, Type 304 stainless steel tubing. The finished length of each capsule (after electron beam welding of each end) was ~17.8 mm. Each capsule was stamped on one end with an identifying letter (A-Z) to aid in post-irradiation recovery. These capsules were considerably larger than any HAFM capsules used previously, in order to compensate for the very low flux levels in the irradiation. The mass content of ^{10}B and ^{6}LiF in each capsule ranged from 60 to 70 mg as compared to ~5 mg for the HAFM capsules used in CFRMF and BIG-10,[4] and ~0.2 mg for power reactor HAFMs.[5]

The particular loading arrangement shown in Fig. 1 was chosen because it approximated a series of infinite ^{10}B and ^{6}Li cylinders, and maximized the distance between adjacent samples, thus optimizing the accuracy in the self-shielding, flux depression, and cross-shielding corrections. The irradiation assembly was located in a plane perpendicular to the thermal column axis. In this plane, flux spectrum gradients display radial symmetry around the assembly center, and axial flux gradients are minimized. Two multiple foil packs each containing ~1.3-cm-diameter foils of Fe, Ni, In, and Au were attached at the center of the assembly, one each on the front and rear faces. The foils were oriented parallel to the plane of the assembly.

Fission Cavity

A separate 1-meter spherical cavity, situated in the vertical graphite column of BR1, was used to produce a fission neutron spectrum at the same time as the Sigma Sigma irradiation. The HAFM capsules irradiated in this experiment were identical to those used in Sigma Sigma. The experimental geometry, shown in Fig. 2, is similar to that used previously by Fabry et al.[10] Twenty-four bare and encapsulated crystals of natural boron, and enriched boron and ^{6}LiF were irradiated along with some empty capsules and some Fe, Ni, In, and Au radiometric foils. Three packages were made using small aluminum cylindrical boxes (8 mm OD, 46 mm long) at three locations (+30 cm, 0, -30 cm) inside a 1-meter-long cadmium tube (10 mm OD, 8 mm ID). The central 6.8-cm section of this tube was wrapped with a 0.1-mm-thick enriched uranium (93% ^{235}U) foil, providing the cylindrical "fission cavity" source. With this arrangement, the HAFMs in the central region of the cadmium tube were exposed to a fission neutron spectrum. The cadmium tube shielded the HAFMs from the incident thermal neutrons coming from the graphite column. Placement of the HAFMs near the top and bottom of the cadmium tube provided a means for measuring the additional ^{4}He generation in the boron and lithium from the small epithermal wall-return neutron flux that was not absorbed by the cadmium tube. Thus, by subtracting this epithermal helium contribution from the helium concentrations measured in the central region, the responses of ^{10}B and ^{6}Li for a pure fission spectrum were obtained.

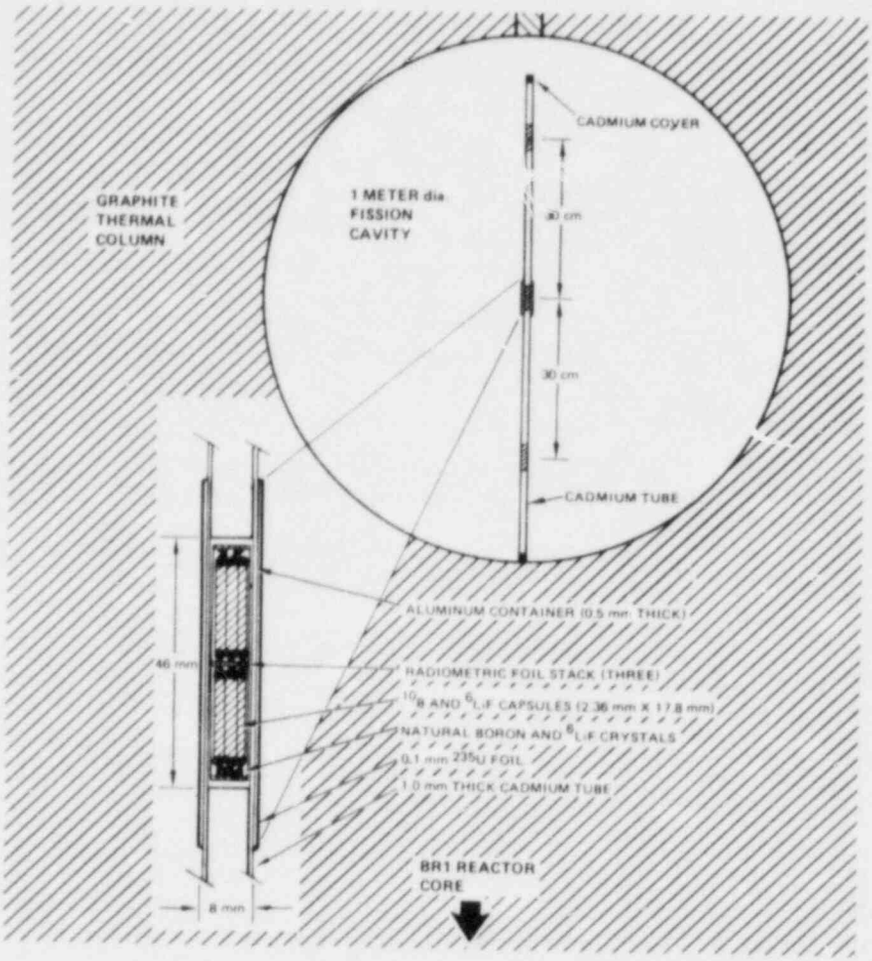

Fig. 2. Configuration of HAFMs in the BR1 Fission Cavity

EXPERIMENTAL RESULTS

Helium Generation Measurements

The results of the helium analyses for the Sigma Sigma and Fission Cavity irradiations are summarized in Tables 1 and 2. Listed in each table are the various boron and lithium sample types and configurations, and the number of each included in the two irradiations. The mean measured helium concentrations listed in each table are the mean values obtained from the independent measurements of samples from each different sample type. Much of the observed variability in the measured helium concentrations between different samples of each isotope is because these data are uncorrected for neutron perturbations such as self-shielding, flux depression, and flux gradients. Corrections for these neutron perturbations significantly reduced the data variability, as discussed below.

Table 1. Measured Helium Concentrations from Sigma Sigma

Material	Isotopic Enrichment (%)	Sample Form	Number Analyzed	^{4}He Concentration[a] (appb) Mean[b] Measured	Mean[c] Corrected	Final Mean[d]
^{10}B	19.8	Crystals	4	1.514 (9)	1.571 (31)	1.575 (37)
	93.0	Crystals	4	1.449 (20)	1.588 (41)	
	93.0	Capsules	4	1.433 (16)	1.570 (41)	
^{6}LiF	99.1	Crystals	4	0.8435 (44)	0.871 (12)	0.870 (11)
	99.1	Capsules	5	0.8512 (18)	0.870 (10)	

[a] Helium concentrations in atomic parts per billion (10^{-9} atom fraction) with respect to ^{6}Li or ^{10}B.
[b] Mean of measured values. Numbers in parentheses indicate measurement reproducibility (1σ).
[c] Weighted mean of measured values after correction for neutron perturbations (see text). Numbers in parentheses indicate the total estimated uncertainty (random plus systematic).
[d] Final weighted mean corrected helium concentrations for ^{10}B and ^{6}Li, and total estimated uncertainty (1σ).

Neutron Perturbations

In both Tables 1 and 2, the measured helium concentrations have been corrected for various neutron perturbations to enable intercomparison of the measured helium concentrations for the various sample types included in Sigma Sigma and the Fission Cavity, and to enable comparison with calculated values. These perturbations include neutron self-shielding and flux depression, neutron flux gradients over the irradiation assemblies, and assembly scattering.

For these particular calculations, the neutron self-shielding and surface flux depression in the various samples were computed using a SAND-II adjusted spectrum for Sigma Sigma, and a Maxwellian fission spectrum for the Fission Cavity. Cross sections for ^{6}Li and ^{10}B were taken from the ENDF/B-IV file.[11] The use of ENDF/B-IV cross sections and the Maxwellian spectrum rather than ENDF/B-V data and the Watt fission spectrum used in later calculations was done for convenience. The small differences introduce negligible uncertainty to the final results because the corrections being calculated were themselves small. The computations were based on first-flight transport theory approximations.[12] For small self-shielding, the corrections are insensitive to sample surface area-to-volume ratio. Thus, for each bare (unencapsulated) boron and ^{6}LiF crystal, a spherical sample of equal mass could be assumed. In the case of the ^{10}B and ^{6}LiF HAFM capsules, however, the modified approach used for the earlier BIG-10 and CFRMF irradiations[4] was applied here. Basically, this approach

Table 2. Measured Helium Concentrations from the Fission Cavity

Material	Isotopic Enrichment (%)	Sample Form	Cavity Location[a]	Number Analyzed	^{4}He Concentration[b] (appb) Mean[c] Measured	Mean[d] Corrected	Final Mean[e]
^{10}B	93.0	Capsule	Center	2	0.2477 (49)	0.2092 (43)	
			+30 cm	2	0.0313 (4)		0.209 (6)
			-30 cm	2	0.0301 (4)		
	19.8	Crystal	Center	2	0.303 (20)	0.209 (32)	
			+30 cm	2	0.105 (7)		
			-30 cm	2	0.061 (11)		
^{6}LiF	99.1	Capsule	Center	2	0.2176 (66)	0.1876 (46)	
			+30 cm	2	0.0217 (15)		0.185 (5)
			-30 cm	2	0.0237 (19)		
	99.1	Crystal	Center	2	0.206 (7)	0.182 (5)	
			+30 cm	2	0.017 (1)		
			-30 cm	2	0.015 (2)		

[a] Irradiation position in 1-meter-long tube.
[b] Helium concentration in atomic parts per billion (10^{-9} atom fraction) with respect to ^{6}Li or ^{10}B.
[c] Mean of measured values. Numbers in parentheses indicate measurement reproducibility (1σ).
[d] Weighted mean of measured values after correction for wall return background (average of corrected data from ±30-cm locations) and neutron perturbations (see text). Numbers in parentheses indicate the total estimated uncertainty (random plus systematic).
[e] Final weighted mean helium concentrations at the center locations for ^{10}B and ^{6}Li, and total estimated uncertainty (1σ).

consists of a compromise between the two limiting cases of: (1) assuming a fine-grain crystalline powder of reduced effective density uniformly distributed over the full inside diameter of the capsule, and (2) assuming a solid cylindrical crystal of ^{10}B or ^{6}LiF of reduced radius. Self-shielding and flux depression corrections were calculated to be from 1.1 to 9.0% in Sigma Sigma and from 0.2 to 1.0% for the Fission Cavity, depending on the sample type and size. A conservative estimate of the uncertainty is ±20% of the correction values.

Neutron flux gradients and effects of assembly scattering and other neutron perturbations in both facilities were calculated using transport theory codes. Additional details of these calculations, for the Fission Cavity irradiation, are given in Ref. 13. Flux gradients, calculated with respect to the physical "center" of each facility, ranged up to ~2.5% and ~4% in Sigma Sigma and the Fission Cavity, respectively. Assembly scattering corrections were determined to be negligible in Sigma Sigma. For

the Fission Cavity, fission neutron scattering from the structural cadmium tube resulted in corrections to the ^{6}Li and ^{10}B helium generation of 3.1 and 3.6%, respectively. Uncertainties in the flux gradient and assembly scattering corrections were estimated to be negligible (<0.2%) except for an 0.8% uncertainty in the radial fission flux gradient in the Fission Cavity. Neutron perturbations from the HAFM samples and aluminum structure in the Fission Cavity were determined to be negligibly small and essentially identical for all the sensors, including the nickel radiometric foils used for flux normalization.

Alpha recoil corrections were not required for the present data, because: (1) the boron and lithium capsules included in Sigma Sigma and the Fission Cavity were vaporized in the mass spectrometer as a unit, and (2) the bare (unencapsulated) crystals included in both irradiations were etched prior to analysis. Helium generation in the capsule material itself was determined to be negligible from analyses of irradiated empty capsules. Unirradiated samples of the various boron and LiF material lots were also analyzed to verify negligible initial helium contamination.

Final Corrected Helium Concentrations

Weighted mean helium concentrations, corrected for the various neutron perturbations discussed above, are listed in the last two columns of Tables 1 and 2. The uncertainties indicated in parentheses are the total estimated random-plus-systematic uncertainties for each mean value, combined in quadrature. Absolute uncertainty in the helium generation measurements is estimated to be 0.7%.

The data presented in Table 1 for the Sigma Sigma irradiation are straightforward. The Fission Cavity data in Table 2, however, require some additional explanation. Specifically, the mean helium concentrations listed in Column 7 for the central location have been obtained by first subtracting the measured wall-return contribution to the helium generation. This contribution was obtained from the mean ^{10}B or ^{6}Li data at the ±30-cm locations outside the central fission source (Column 6). An ~3% correction to account for the epithermal wall-return spectral gradients, and helium generation from the central fission source, was applied to these data prior to averaging. Following subtraction of the mean wall-return contribution, the helium generation data from the samples inside the fission source were corrected for fission neutron self-shielding, and flux gradients relative to the center of the cylindrical fission source.

Transport theory calculations were performed for comparison with the measured wall-return background helium contribution. These calculations, using ENDF/B-V ^{6}Li and ^{10}B cross sections, resulted in theoretical contributions of 9.3% and 12.9% for the ^{6}Li and ^{10}B HAFM capsules, respectively.[13] These values compare very favorably with the measured 10.4 ± 1.8% and 12.4 ± 0.9% values obtained from the data in Table 2 for the ±30-cm capsules, indicating that this background correction is well understood. Therefore, uncertainty in this correction should not significantly affect the final results.

Examination of the data in Tables 1 and 2 indicates the excellent internal consistency in the corrected helium concentration data. For Sigma Sigma, the average standard deviation for the three groups of boron and two groups of ^{6}LiF samples is only ~0.4%, even though different amounts and configurations of ^{10}B and ^{6}LiF were involved. This is very close to the 0.5% reproducibility of the helium mass spectrometer system, and substantiates the low uncertainties in the various neutron corrections applied to each group. For the Fission Cavity data, the mean standard deviation for the two groups of boron and ^{6}LiF samples is ~1%. This uncertainty is somewhat higher than that obtained for Sigma Sigma because the helium concentrations were significantly lower ($<<10^{-9}$ atom fraction) in these samples.

Reaction Cross Sections

Measured and calculated spectrum-averaged helium generation cross sections for ^{6}Li and ^{10}B in Sigma Sigma and the Fission Cavity are shown in Table 3. The measured cross sections were obtained from the mean helium generation data in Tables 1 and 2 using total neutron fluences of 9.29 x 10^{14} n/cm^2 and 3.86 x 10^{14} n/cm^2 for Sigma Sigma and the Fission Cavity, respectively. For ^{6}Li(n,He), corrections of 5 mb and 23 mb in Sigma Sigma and the Fission Cavity, respectively, have been applied to the data to account for the helium generation from ^{19}F. These corrections were calculated using the ENDF/B-V ^{19}F(n,He) cross section and the derived neutron spectra, as discussed below.

Table 3. Comparison of Measured and Calculated Spectrum-Averaged Helium Generation Cross Sections for ^{6}Li and ^{10}B

Reaction	Facility	Experimental σ (mb)[a]	Calculated[b] σ (mb)	Calculated-to-Experimental
^{10}B(n,He)	Sigma Sigma	1695 (71)	1492	0.88
^{6}Li(n,He)		931 (35)	869	0.93
^{10}B/^{6}Li		1.82 (2)	1.72	0.95
^{10}B(n,He)	Fission Cavity	541 (24)	491	0.91
^{6}Li(n,He)		456 (20)	455	1.00
^{10}B/^{6}Li		1.19 (2)	1.08	0.91

[a]Measured cross section (mb) obtained from the data in Tables 1 and 2 and the total neutron fluence in each facility (see text). For the ^{6}LiF sensor materials, subtractions of 5 mb and 23 mb have been applied to account for ^{19}F helium generation in Sigma Sigma and the Fission Cavity, respectively. Numbers in parentheses indicate the total estimated 1σ uncertainty (random plus systematic).

[b]Calculated spectrum-averaged cross section (mb) using theoretical and adjusted spectra and the ENDF/B-V cross section file (see text).

The neutron fluences used in the calculations were obtained from absolute measured $^{58}Ni(n,p)^{58}Co$ reaction rates in the two facilities. For these calculations, spectrum-averaged cross sections[14] of 26.5 mb and 108.5 mb were assumed for this reaction in Sigma Sigma and the Fission Cavity, respectively. Additional reaction rate data from the indium foils could not be used due to power-level variations in BR1 during the irradiation and the relatively short half-life of the $^{115}In(n,n')^{115m}In$ reaction. Reaction rate data from the Fe and Au foils require further analysis. It is anticipated that when these additional dosimetry data are included in the analyses, the absolute neutron fluences will be better defined. Uncertainties in the presently adopted fluences are conservatively estimated to be ±3.5%.

The values for the calculated cross sections in Table 3 were determined using a 136-group calculated neutron spectrum for Sigma Sigma, and the ENDF/B-V Watt ^{235}U fission spectrum for the Fission Cavity, both in conjunction with the ENDF/B-V dosimetry cross section file. The calculations provide no theoretical estimate of the uncertainty in the calculated spectral shape in Sigma Sigma, or in the microscopic cross sections. Thus, no uncertainties were estimated for the calculated spectrum-integrated cross sections presented here. It is planned, however, in future work, to use the Sigma Sigma and Fission Cavity data in conjunction with the FERRET code,[15] both to estimate the uncertainty in the calculated neutron spectra and cross sections, and to determine probable sources of any discrepancies.

DISCUSSION

The results from Table 3 are compared in Table 4 with calculated-to-experimental (C/E) ratios determined earlier[4] in two other benchmark facilities, CFRMF and BIG-10. The actual C/E ratios shown in Table 4 for CFRMF and BIG-10 are values recently reevaluated by Anderl et al.[16,17] using ENDF/B-V cross section data. Uncertainties in the C/E ratios are given only for CFRMF because uncertainties in the calculated values for the other spectra are not presently available. The uncertainty quoted for the $^{10}B/^{6}Li$ ratio in CFRMF was obtained by combining the individual uncertainties in quadrature, and thus this uncertainty represents an upper limit.

Comparison of the data in Table 4 shows that the Sigma Sigma C/E ratios, and to a lesser extent the Fission Cavity ratios, are very similar to those determined earlier for CFRMF and BIG-10. Specifically, the ^{10}B and ^{6}Li calculated cross sections are significantly lower than their measured values. The exception to this is the measured ^{6}Li cross section in the fission spectrum, where calculations and measurements agree.

Table 4. Comparison of C/E Ratios in Four Neutron Spectra

Reaction	Calculated-to-Experimental Ratios			
	Sigma Sigma	Fission Cavity	CFRMF	BIG-10
$^{10}B(n,He)$	0.88	0.91	0.86 ± 0.03	0.85
$^{6}Li(n,He)$	0.93	1.00	0.95 ± 0.04	0.90
$^{10}B/^{6}Li$	0.95	0.91	0.91 ± 0.05	0.94

The reevaluation of the CFRMF spectrum by Anderl et al. was conducted in part to test numerous ENDF/B-V dosimeter cross sections. The work included both conventional integral data testing and least-squares-adjustment using the FERRET code.[8] The conventional integral testing indicated discrepancies between the measured and calculated cross sections for several reactions, including $^{6}Li(n,He)$ and $^{10}B(n,He)$. In the case of the latter two reactions, it can be seen from Table 4 that the discrepancies were outside the estimated integral test uncertainties. Least-squares-adjustment, using the FERRET code, however, resulted in a high degree of consistency within the presently estimated uncertainty limits for the ENDF/B-V cross sections and CFRMF spectrum, for all the integral data (including ^{6}Li), with the exception of ^{10}B. In view of the similarity of the results in Table 4, and the similarity of the neutron spectra of Sigma Sigma, CFRMF, and BIG-10, we expect that consistency is also attainable for ^{6}Li in Sigma Sigma and BIG-10, but that difficulties will remain with the ^{10}B results.

In an extension of the work of Anderl, preliminary calculations by R. E. Schenter (HEDL) indicate that consistency can also be obtained for ^{10}B if less stringent uncertainty limits are applied to the ^{10}B cross section above ~0.1 MeV. Further, qualitative consideration of the Fission Cavity results in Table 4, along with the ^{10}B results in the Sigma Sigma, CFRMF, and BIG-10 neutron spectra, suggests that the ENDF/B-V ^{10}B cross section is too low between ~0.1 and 2 MeV and perhaps too high at higher energies. If the uncertainties in the ^{10}B cross section values are in fact underestimated in these energy ranges, and increased uncertainty values can be justified, a simultaneous least-squares-adjustment in all four benchmark spectra may yield a consistent cross section value.

An examination of the ^{10}B-to-^{6}Li cross section ratios in Table 4 shows that the C/E values of 0.95 and 0.91 for Sigma Sigma and the Fission Cavity are also comparable with values observed earlier in CFRMF and BIG-10. In this case, however, it is important to note that the ratio of these two reactions is sensitive only to changes in the isotopic cross section and/or the spectrum shape, and not to changes in the absolute neutron fluence. In addition, systematic sources of uncertainty, particularly in the neutron self-shielding corrections, cancel out to a large extent in the ratio. Thus, the estimated uncertainty of these results is significantly lower

than the uncertainty in the individual measured cross sections. The fact that the cross section ratios, for both irradiations, are also different from their calculated values, is further evidence that changes in the ^{6}Li and ^{10}B (n,He) cross sections, and in the adjusted spectra for BIG-10, CFRMF, and Sigma Sigma are required to obtain acceptable consistency.

In summary, the results of the two irradiations indicate that mass spectrometric measurements of helium generated in irradiated ^{6}Li and ^{10}B samples can yield accurate and consistent reaction rate information. The present data, however, in agreement with the earlier BIG-10 and CFRMF results, indicate that discrepancies remain in the evaluated cross sections, and calculated or measured neutron spectra. The discrepancies in the case of boron are outside the estimated uncertainties. Resolution of these discrepancies will require adjustment of the neutron spectra and changes to one or both isotope cross sections.

ACKNOWLEDGEMENTS

The authors wish to acknowledge contributions to this work by M. M. Nakata and J. F. Johnson of Rockwell International and by R. E. Schenter of HEDL. We also wish to express our thanks to J. W. Lewellen and P. B. Hemmig of the U.S. Department of Energy for their continued interest and support of this work. This work was supported under DOE Contracts DE-AT03-81SF11561 at Rockwell International and DE-AC14-76FF02170 at Westinghouse Hanford Company.

REFERENCES

1. JW Rogers, D. A. Millsap, and Y. D. Harker, "CFRMF Neutron Field Spectral Characterization," Nucl. Technol. 25, 330 (1975).

2. E. J. Dowdy, E. J. Lozito, and E. A. Plassman, "The Central Neutron Spectrum of the Fast Critical Assembly BIG-TEN," Nucl. Technol. 25, 381 (1975).

3. A. Fabry, G. DeLeeuw, and S. DeLeeuw, "The Secondary Intermediate Energy Standard Neutron Field at the Mol-ΣΣ Facility," Nucl. Technol. 25, 349 (1975).

4. H. Farrar IV, B. M. Oliver, and E. P. Lippincott, "Helium Generation Reaction Rates for ^{6}Li and ^{10}B in Benchmark Facilities," Proc. 3rd ASTM-EURATOM Symposium on Reactor Dosimetry, Ispra, Italy, October 1-5, 1979, EUR 6813 EN-FR, Vol. 1, p. 552 (1980).

5. H. Farrar IV and E. P. Lippincott, "Helium Production Cross Section of Boron for Fast-Reactor Neutron Spectra," Nucl. Technol. 25, 305 (1975).

6. W. N. McElroy and L. S. Kellogg, "Fuels and Materials Fast-Reactor Dosimetry Data Development and Testing," Nucl. Technol. 25, 180 (1975).

7. J. H. Roberts and R. Gold, "SSTR and Emulsion Technology and Their Applications for FBR, LWR and MFER Programs," Proc. 2nd ASTM-EURATOM Symposium on Reactor Dosimetry, NUREG/CP-0004, Palo Alto, California, October 3-7, 1977, Vol. 2, p. 739 (1978).

8. F. A. Schmittroth, "FERRET Data Analysis Code," Hanford Engineering Development Laboratory Report HEDL-TME 79-40 (September 1979), published in part in Nucl. Sci. Eng. 72, 19 (1979).

9. F. G. Perey, "Least Squares Dosimetry Unfolding: The Program STAY'SL," Oak Ridge National Laboratory Report ORNL-TM-6062 (1977).

10. A. Fabry, J. A. Grundl, and C. Eisenhauer, "Fundamental Integral Cross Section Ratio Measurements in the Thermal-Neutron-Induced-Uranium-235 Fission Neutron Spectrum," Nuclear Cross Sections and Technology, NBS-425, Vol. 1 (October 1975).

11. B. A. Magurno, ed., "ENDF/B-IV Dosimetry File," Brookhaven National Laboratory Report BNL-NCS-50446, p. 1 (April 1975).

12. K. M. Case, F. de Hoffman, and G. Placzek, "Introduction to the Theory of Neutron Diffusion," Los Alamos Scientific Laboratory, Los Alamos, New Mexico, Vol. 1 (June 1953).

13. A. Fabry, G. Minsart, F. Cops, and S. DeLeeuw, "The MOL Cavity Fission Spectrum Standard Neutron Field and its Applications," Proc. 4th ASTM-EURATOM Symposium on Reactor Dosimetry, National Bureau of Standards, Gaithersburg, Maryland, March 22-26, 1982.

14. A. Fabry, W. N. McElroy, L. S. Kellogg, E. P. Lippincott, J. A. Grundl, D. M. Gilliam, and G. E. Hansen, "A Review of Microscopic Integral Cross Section Data in Fundamental Reactor Dosimetry Benchmark Neutron Fields," IAEA-208, p. 233 (1978).

15. E. P. Lippincott and W. N. McElroy, "ASTM Standard Recommended Guide on Application of ENDF/A Cross Section and Uncertainty File: Establishment of the File," Proc. 4th ASTM-EURATOM Symposium on Reactor Dosimetry, National Bureau of Standards, Gaithersburg, Maryland, March 22-26, 1982.

16. R. A. Anderl, Y. D. Harker, D. A. Millsap, JW Rogers, and J. M. Ryskamp, "CFRMF Spectrum Update and Application to Dosimeter Cross-Section Data Testing," Proc. 4th ASTM-EURATOM Symposium on Reactor Dosimetry, National Bureau of Standards, Gaithersburg, Maryland, March 22-26, 1982.

17. R. A. Anderl, D. A. Millsap, JW Rogers, and Y. D. Harker, "Addendum to Integral Data-Testing Report for ENDF/B-V Dosimetry Cross Sections," EG&G Idaho Report EGG-PHYS-5668 (January 1982).

RE-EVALUATION OF THE DOSIMETRY FOR REACTOR PRESSURE VESSEL SURVEILLANCE CAPSULES

R. L. Simons, L. S. Kellogg, E. P. Lippincott,
W. N. McElroy, and D. L. Oberg*

Westinghouse Hanford Company
Richland, Washington, USA

ABSTRACT

Revised fluences and displacements per atom (dpa) and their uncertainties were determined after re-evaluating the neutron dosimeters from forty-one pressurized water reactor (PWR) surveillance capsules. The goals of this Hanford Engineering Development Laboratory (HEDL) Reactor Dosimetry Center work are (1) to apply and test new ASTM recommended physics-dosimetry analysis methods and data being developed for LWR power plant surveillance and (2) to provide improved neutron exposure values for reactor pressure vessel steel metallurgical data bases; particularily for the changes in nil ductility transition temperature (ΔNDTT) and upper shelf energy. Uncertainties in the FERRET-SAND adjustment Code derived neutron exposure values range from 10-34%. The ratio of the new to the old exposure values for fluence greater than 1 MeV varied from a low of 0.79 to a high of 2.11, with an average value of 1.30. The fission reactions for ^{238}U and ^{237}Np were found to be instrumental in producing low uncertainties in the exposure values (10-15%) whereas with their absence the uncertainty increased to 25-34%. Corrections for fissile impurity atoms in the ^{238}U dosimeters were found to be as high as 29% in some cases. Other sources of corrections such as surveillance capsule perturbations and photo fission reactions have been considered.

INTRODUCTION

The Light Water Reactor Pressure Vessel Surveillance Dosimetry Improvement Program was established by the NRC in order to improve and standardize the neutron dosimetry analysis, damage correlation, and reactor analysis procedures and data used to predict the condition of light water reactor (LWR) pressure vessels.[1,2] As part of this program a number of new ASTM standards have or will be written for LWR power plant surveillance.[3] Before these standards can be routinely

*Presently with Sigma Research Corp. Richland, Washington, USA

applied,the recommended procedures and data must be benchmark tested with actual test and power reactor derived physics-dosimetry and metallurgical data.[1-8] In addition to the Materials Property Council (MPC) data base,[4] NRC has supported the development of the MATSURV[9] and EPRI has supported the development of its own computerized data base.[10,11]

Over the period in which the physics-dosimetry for the various LWR power reactor surveillance capsules were analyzed for these and other data bases, the auxiliary parameters such as cross sections, decay constants, neutron spectra, etc. used by vendors and service laboratories have differed but have progressively improved.[2] For example, originally the fission spectrum was used to determine spectrum averaged cross sections. Over a period of years, the use of one- and two-dimensional neutron transport theory calculations were adopted in an effort to improve the physics-dosimetry analysis.[5-7] Further, the more recent evaluations of the physics-dosimetry have included consideration of the capsule perturbation to the flux.[1-3,5,7]. Current correlations of the irradiation effects data on shift in ΔNDTT and upper shelf, for example, have not considered these variations in the analysis of the physics-dosimetry.[4] Thus, unnecessary errors are currently included in most correlations of irradiation effects data using existing surveillance data bases. Consequently, the present analytical effort involves re-evaluating the physics-dosmetry for all discharged surveillance capsules from operating power plants in order to place all damge exposure values on a common basis.

This report gives results of the reanalysis of dosimetry from 41 LWR surveillance capsules using the HEDL Reactor Dosimetry Center FERRET-SAND adjustment code procedures and data which were first benchmark tested using differential and integral data from the "PCA Experiments and Blind Test."[5] This reanalyses has been a joint effort involving HEDL, NBS, Westinghouse, Babcock & Wilcox, Combustion Engineering, General Electric, South West Research Institute, Battelle Memorial Institute, EPRI and its contractors, and select US Utilities. The work is being accomplished in support of the preparation of the new series of ASTM Committee E10 standards for Light Water Reactor Pressure Vessel Surveillance.[3] The information will be documented in a much more complete form in a special Nuclear Regulatory Commission loose leaf document to facilitate future additions of new and updating of existing physics-dosimetry data. These data are urgently needed for 1) verification of the accuracy of LWR power plant final safety analysis reports (FSAR) current and end-of-life projections of changes in the fracture toughness and embrittlement condition of the pressure vessel steel and 2) the establishment of improved trend curves of the shifts in the initial reference nil-ductility temperature and upper shelf energy versus fluence (or dpa) derived from test reactor and power reactor surveillance programs. The ASTM E706-81 Master Matrix Standard, Reference 3, provides more detailed information on the status of the preparation of the new ASTM Physics-Dosimetry-Metallurgy related standards.

ANALYSIS PROCEDURE

The basic analysis method used in this work is the adjustment of the a priori calculated neutron spectrum by a generalized least squares analysis method using measured reaction rates. The FERRET computer code[12] is used in this work. The SAND II code[13] has been used primarily to process data that was input to the FERRET code.[5] The main focus of the present analysis efforts is aimed at determining the correct reaction rates and their uncertainties. This involves evaluation of the power time history, corrections for dosimeter position, corrections for competing reactions due to impurities, and the initiation of necessary HEDL and NBS overchecks on measured reaction rates and isotopic mass assay of dosimeters.[2] As a result of the "PCA Experiments and Blind Test" studies, the limiting accuracy of the FERRET-SAND (or any other such code system) derived values of exposure parameters (flux-fluence greater than 1 MeV and dpa) is estimated to be in the range of ±5% to 15% (1σ).[5]

The effective time at full power and the extrapolation of reaction rates at time of shut down to the reaction rates at full power were determined from the power history for each reactor and the TIMWH computer code.[14] The decay constants currently used by the HEDL Reactor Dosimetry Center were used in this analysis.[15] Saturated reaction rates reported in the surveillance reports and the rates found in this work differed at most by 1-2%. This was generally attributed to slight differences in the decay constants used. The power time history analysis assumes a constant flux level per megawatt of power. For most capsules, this is a fair assumption. However, in some cases reaction rate variations of 10-20% were noted due to differences in fuel loading for each fuel cycle. In these circumstances long half lived dosimeters integrate over the irradiation period to give the average effective flux level while short half lived dosimeters are sensitive to the flux level at the end of the irradiation.

Nuclear cross section and fission yield data used in this work were based on the ENDF/B-V data file.[16-17] The cross section covariance files were based on the ENDF/B-V data for most cross sections.[19] However, some are due to recent HEDL evaluations.

Significant geometry corrections were necessary in the Westinghouse and Babcock and Wilcox (B&W) capsules in order to determine the reaction rate at the center of the surveillance capsule. For Westinghouse plants these corrections were in the 5 to 15% range. No corrections were necessary for the fission foils which were located at the capsule center. Westinghouse transport calculations show that there is about a 10% variation in flux from the top to the bottom of the capsule. This could introduce a maximum bias in the fluence for any particular metallurgical specimen of about ±5%. The determination of the charpy transition temperature shift is not expected to be sensitive to this level of flux difference. For B&W plants the front and rear dosimeters were logrithmically averaged to account for flux gradients. This value was then linearly averaged with the side dosimeters.

Corrections for impurity fissile atoms were found to be significant in some cases. In all cases, cadmium covers were used to reduce competing reactions. Babcock and Wilcox indicate <375 appm ^{235}U impurity in their ^{238}U dosimeters. For vessel wall capsules this amounts to <3.4% correction for ^{235}U fission. Exact corrections are probably on the order of 1-3% which is of marginal consequences. The Westinghouse ^{238}U dosimeters have 300-350 appm ^{235}U. This level of impurity in the accelerated capsules requires about a 9% correction for ^{235}U fission. For Combustion Engineering ^{238}U dosimeters the impurity level is about 300 appm. This requires about a 7% correction for both wall capsules and accelerated surveillance capsules. The exact correction for each surveillance capsule would require knowledge of the exact impurity level for each dosimeter. Preliminary results of HEDL over checks on the purity and/or isotopic content of a number of the Point Beach 2 Capsule R dosimeters are discussed in Reference 2. Good agreement was found between HEDL and ORNL results for the ^{238}U dosimetry material.

Burn-in of ^{239}Pu in the high fluence accelerated surveillance locations was found to be important. For low fluxes ($<10^{13}$ n/cm^{2}sec, E >0 MeV) and irradiation times on the order of a year or longer the ^{239}Pu fission rate contribution can be approximated by

$$R_{239} = 0.5 \cdot S \cdot \sigma_8 \cdot \sigma_9 \cdot \phi^2 t$$

where S is a neutron self shielding factor which is dependent on the size and density of the dosimeter, σ_8 is the infinitely dilute spectrum averaged cross section for the $^{238}U(n,\gamma)^{239}U$ reaction, σ_9 is the spectrum averaged cross section for the $^{239}Pu(n,f)$ F.P reaction (both in cadmium covers), ϕ is the total neutron flux (E >0 MeV), and t is the effective irradiation time at full power. Figure 1 shows the measured ^{238}U fission rate as a function of fluence (E >1 MeV) for eight Westinghouse surveillance capsules from similar two loop plants. The dashed curve is the calculated fission rate with Pu buildup and 320 appm ^{235}U for operation at full power, with S set equal to 1.0. The similarity of the slope of the calculated and measured data is apparent. The lower two points are from the R. E. Ginna plant. Even through the slope is about 1/2 that for the other capsules, the two Ginna data points extrapolate back to a common initial fission rate of about 4.5 x 10^{-14}fps/nucl. At least a part of the explanation for the lower slope is neutron self shielding in the ^{238}U dosimeter. A calculated estimate of the actual value of S has yet to be obtained. Precise self shielding corrections for ^{238}U dosimeters, however, may be difficult to obtain due to the fact that the density and geometry of individual dosimeters may not be well known. Since the low energy spectrum is nearly proportioned to 1/E, the ^{239}Pu build up is approximately the same for all spectra. Thus the relative ^{239}Pu correction to the measure fission rate in a ^{238}U dosimeter is most sensitive to the relative number of fissions from the ^{238}U. For example the ^{238}U fission cross section in a two loop Westinghouse plant is $\sim$ 30 mb compared to $\sim$ 46 mb in a four loop plant thus the two loop plant requires a larger correction then the four loop plant. No explanation is obvious for the high fission rate datum point at low fluence which is obtained for the Point Beach Unit 2 capsule V. Seven of the eight measured fission rates extrapolate back to an initial fission rate (corrected for ^{235}U) in good agreement with the calculated value of 4.4 x 10^{-14}fps/nucl.

Other corrections which have not been made yet but may be important are for photo fission and variation in the flux per megawatt from differences in cycle to cycle fuel loadings. The photo fission correction was estimated by Anderson of Westinghouse to be <3% for the Point Beach 2 capsule R and similar capsules*. For Westinghouse capsule locations this would be a marginally important correction. Flux level variation would only be important when mixing the use of short- and long- half-lived dosimeter reactions. The long half lived dosimeters give an average flux value while the short half lived ones give an end of cycle flux value. One possible method of experimentally reconciling this problem is to analyse various half lived fission products in the fission reaction dosimeters to see if they all give the same fission rates.

The reaction rate uncertainties were generally set at 10% for a specific capsule. In some cases, larger uncertainties were assigned to account for anamoulous reaction rate values.

Given the corrected reaction rates at full power the a priori neutron spectrum is adjusted with the FERRET-SAND analysis codes. In simple terms, the FERRET code minimizes the variance in reaction rates, logarithms of group fluxes and cross sections using a generalized least squares approach. The FERRET code is run with 53 energy groups. Correction factors for spectrum weighting of the cross section were determined from 620 group cross sections and spectra using the SAND code.

The uncertainty assigned to the relative a priori fluxes was 50% (1σ). This may be overly conservative in some cases where a smaller relative uncertainty in group fluxes may be justified. The normalization uncertainty was set high (100%) so that the dosimeters would have complete freedom to determine the correct normalization. Short range correlation between energy groups extended over three energy groups. This primarily is used as a smoothing technique. Additional discussion of the FERRET-SAND code procedures and data is presented elsewhere.[2,5,12]

RESULTS

The desired exposure parameters resulting from this analysis are the traditional fluence (E > 1 MeV) and the new ASTM recommended displacements per atom (dpa) in iron[20] and their uncertainties. Additional information obtained from the analysis are the neutron spectrum and its uncertainties in each energy group. An example of such information is shown in Figures 2a and 2b. Generally speaking adjustments in the spectrum shape were modest and are limited to the energy range where significant dosimeter responses occured. Figure 2b shows the group fractional

*At present, there is no direct experimental method to determine photofission correction factors; however, Gold et.al., have recently proposed a method which has yet to be tested.(18)

uncertainties. It is noted that the energy ranges with significant response (generally 0.5 - 10 MeV, around ~130 eV and <0.4 eV) show a reduction in uncertainty while low response ranges reflect the assigned uncertainty in the a prior i spectrum shape.

Table 1 summarizes the pertinent data obtained from the reevaluation of dosimeters from 41 PWR surveillance capsules. When the ^{238}U fission rate was used to determine the exposure it was corrected for an assumed 320 appm ^{235}U content and ^{239}Pu buildup assuming a 0.7 self shielding factor. For this reason, these exposure values differ from previous values (including Reference 2). In addition, correction by Norris of SWRI to the ^{54}Fe (n,p)^{54}Mn reaction rate for some plants and improved neutron spectra are the cause for other differences. Several generalizations can be made from this table. Nearly all the ratios of new fluence (E >1 MeV) to original fluence (E >1 MeV) are greater than one. The average ratio is 1.30. The extreme variations range from 0.79 to 2.11. The uncertainties for both fluence and dpa range from about 10-34%, (1σ). The ^{237}Np and ^{238}U fission reactions were instrumental in determining low uncertainties for the exposure values. When both ^{237}Np and ^{238}U were used the uncertainties were in the 10-15% range. Whereas without these reactions the uncertainty were generally in the 25-34% range. When only a ^{238}U dosimeter was included, the uncertainties were in the intermediate range of 15-22%. This illustrates the importance of obtaining accurate fission rate data so as to minimize exposure uncertainties. The spectrum averaged displacement cross sections for neutrons (E >1 MeV) (i.e., dpa/ϕt new) show only a small average deviation (±7%) from the average value of $1.63 \times 10^{-21} cm^2$. References 2 and 3 provide more detailed information on the expected change in dpa/ϕt versus distance from the core through the pressure vessel wall of PWRs. This indicates that the present surveillance capsules spectra are all very similar from a damage correlation view point. More important however, may be the fact that the displacement rates vary by nearly a factor of forty, which may be most significant when flux level effects are considered.

The quality of reaction rates and their assigned uncertainties from a specific surveillance capsule can be verified by comparing them with the reaction rates from other capsules discharged from reactors with the same generic design. In consultation with Anderson of Westinghouse and Whitmarsh of B&W, capsules from three generic reactor designs were studied: a two loop and four loop Westinghouse PWR and a four loop Babcock and Wilcox PWR. A number of advantages from this method of analysis were realized:

- Uncertainties assigned to reaction rates were verified and anomolous reaction rates were easily identified.
- Average reaction rates for a number of capsules showed improved agreement with calculated values for the same generic plant design.
- Trends in the data were identified such as burn-in of ^{239}Pu in the ^{238}U dosimeter.

- Variation in the flux/megawatt between fuel cycles were identified as in the case with Oconee Unit 1 Capsule E.

Table 2 shows a summary of reaction rates relative to the average value for eight Westinghouse two-loop plants at a power level of 1520 MWT. Only two of fifty-one dosimeter reaction rates show a substantial deviation from the average (R. E. Ginna Capsule R ^{54}Fe (n,p) and R. E. Ginna Capsule V $^{237}Np(n,f)$). A few other reaction rates show approximately a 2σ deviation. All the threshold reactions show less than a 10% one standard deviation variation. The ^{238}U reaction rates were corrected for fissile impurities. The standard deviation for the average ^{238}U reaction rate without the Point Beach Capsule V value is about 3%. A comparison with calculated reaction rates for the generic capsule show good agreement. The 10% discrepancy of the ^{58}Ni results may be due to the coarse power time history histograms used and the short half life of ^{58}Co. The calculated flux (E >1 MeV) is 1.48×10^{11} n/cm^{2}sec which is in good agreement with the FERRET adjusted value of 1.44×10^{11} n/cm^{2}sec. The uncertainty in the adjusted value is 11% (1σ).

Similar results (Table 3) were found for the Westinghouse four loop plants at a power level of 3565 MWT. A relatively larger number of discrepant reaction rates are in this group. Otherwise the conclusions are similar. The calculated flux (E >1 MeV) is 8.64×10^{11} n/cm^{2}sec compared to the adjusted value of 8.89×10^{11} n/cm^{2}sec. The average of the plant specific fluxes is 9.3×10^{11} n/cm^{2}sec. The difference is, primarily, due to not using fission dosimeter results in a number of cases.

Results for the four loop B&W plants at a power level of 2568 MWT are shown in Table 4. A discrepancy in the Oconee 1F fission rate data stands out prominently. A large variation in the cadmium ratio values for these plants was observed. This may be due to problems with the dosimetry set cadmium shielding. The Oconee Unit 1 capsule E results show a consistently high ratio relative to the average. This is apparently due to differences in the fuel loading pattern between fuel cycle one and cycle two.

DISCUSSION

It is of interest to study the historical and projected trend of changes and uncertainties in neutron exposure parameter values for surveillance capsules. Figure 3 shows the ratio of new/old fluences (E > 1 MeV) as a function of the date the original fluence was reported. It is clear that there is less scatter in recent years as the analysis methods and our understanding of the neutron environment has improved.(1-8) This provides an experimentally derived overview of the state-of-the art accuracy of past and present day analysis techniques and data. Most but not all analyses of the past three years have approached the upper bound limiting accuracy (±15%) established by the "PCA Experiments and Blind test" studies.(5) Figure 2 in Reference 2, which gives state-of-the art estimates of accuracy capabilities is qualitatively very similar.

It is important to note that the intense effort put forth over the last few years by the participants of the LWR PV Surveillance Dosimetry Improvement program in completing (1) the "PCA Experiments and Blind Test" studies and (2) the intercalibration of the laboratories measuring the reaction rates has provided the technological data base which was needed for the verification and certification of the accuracy of derived exposure parameter values. As a result of this multi-laboratory program and the preparation of the new ASTM LWR Surveillance Standards, it is expected that future dosimetry analyses by service and vendor labratories should be near or within the ±15% upper bound limiting accuracy.

In this analysis a number of improved practices for the dosimetry analyses were tested. It will be recommended through the ASTM standards that such practices be applied and results be documented in future surveillance reports. These include:

- Tabulate or reference all pertinent parameters used in the analysis for cross comparison with other laboratories, and where possible, use ASTM recommendations which incorporate ENDF and IRDF data.[3,16,17,19-25] For example, all nuclear data (cross sections and fission yields) should come from ENDF/B-V and the IAEA International Reactor Dosimetry File (IRDF).[23,24]

- Report measured detector activities corrected to reactor shutdown. A number of reports give only fluence, time, and cross section. The reported reaction rates are the key reference measured data needed to derive adjusted values of exposure parameters and uncertainties.

- Tabulate the reactor, and if possible the surveillance capsule, power (flux) time history, in for example, a coarse time histogram such as average power per month. Everyone uses the power history data. It should be recorded as part of the data used in the analysis. Normally such a tabulation would entail only a few extra pages which could be taken directly from a computer output.

- Count multiple fission products of various half lives. This was found to be particularly useful to roughly assess the accuracy of the fission rate data and provide information on flux/MW variation during the irradiation.

- Report detector mass assay and purity information, particularly for fission sensors.

- Depict accurately the orientation and location of the dosimeters in the capsule relative to the direction to the core.

- Use advanced radiometric (RM), solid track recorders (SSTR), helium accumulation fluence monitors (HAFM), and damage monitors (DM): such as Nb for RMs, ^{238}U, ^{237}Np, ^{232}Th, ^{235}U for SSTR's;

$Cu(n,\alpha)$ and $Fe(n,\alpha)$ for HAFMs; and iron and sapphire disks for DMs (see the Reference 3 recommended ASTM Standard Methods for discussions of the RM, SSTR, HAFM, and DM methods).

Additional recommended practices are discussed in Reference 2 and the new ASTM E706 (IA) Standard on Analysis and Interpretation of Nuclear Reactor Surveillance Results.[25]

CONCLUSIONS

The revised fluence values in this work were found to average about 30% higher than originally reported fluences. The accuracy of the new exposure values is strongly influenced by the use of the ^{237}Np and ^{238}U fission dosimeters. With these dosimeters the fluence uncertainty was generally found to be in the range 10-15% (1σ) while in the cases without these dosimeters the uncertainty approximately doubled. Buildup of ^{239}Pu was found to require up to 29% correction to the ^{238}U fission rate. The fission rate due to ^{235}U impurity is less than 10% for Westinghouse and Combustion Engineering plants and less than 4% for Babcock and Wilcox plants. Further quality assurance overchecks on fissile impurities in ^{238}U and ^{237}Np dosimeters are needed. In addition, further assessment of the true uncertainty in the a priori neutron spectrum at the surveillance capsule is needed. Data for this assessment is available but needs to be incorporated into the analysis.

ACKNOWLEDGEMENTS

This work was supported by contract with the Nuclear Regulatory Commission (NRC). Special acknowledgment is due to C. Z. Serpan and N. Randall of NRC for their efforts to initiate and support this re-evaluation work as part of the LWR Pressure Vessel Surveillance Dosimetry Improvement Program. This work would not be possible without the support, assistance, and helpful discussions with staff members at EPRI, the reactor vendors, and service laboratories, and the utilities of the nuclear plants involved. In particular: T. U. Marston of EPRI; S. L. Anderson and C. Blackburn of Westinghouse; A. Lowe and C. Whitmarsh of B&W; G Cavanaugh of CE; E. B. Norris of SWRI; J. Perrin of BMI; and R. Wullaert of Fracture Control Corporation. The contributions of G. L. Guthrie and F. A. Schmittroth of HEDL are also greatfully acknowledged.

REFERENCES

1. W. N. McElroy, et. al, "LWR Pressure Vessel Surveillance Dosimetry Improvement Program, 1980 Annual Report", NUREG/CR-1747, HEDL-TME 80-73 (April, 1981).

2. W. N. McElroy, et.al, "Surveillance Dosimetry of Operating Power Plants," Proceedings of the 4th ASTM-Euratom International Symposium on Reactor Dosimetry, March 22-26, 1982, Natural Bureau of Standards, Gaithersburg, Maryland; HEDL-SA 2546, (Feb. 1982).

3. ASTM E706-81, "Standard Master Matrix for LWR PV Surveillance Standards," ASTM Annual Book of Standards, Part 45 (1981).

4. MPC Subcommittee 6 on Nuclear Materials, "Prediction of the Shift in the Brittle-Ductile Transition Temperature of LWR Pressure Vessel Materials, "Final Report to ASTM Subcommitte E10.02 (June, 1979).

5. W. N. McElroy, et.al, "LWR PV Surveillance Dosimetry Improvement Program: PCA Experiments and Blind Test", NUREG/CR-1861, HEDL-TME 80-87 (July 1981).

6. J. Grundl, et. al, "NRC-EPRI Studies of Pressure-Vessel-Cavity Neutron Fields", Proceedings of the NRC Ninth Water Reactor Safety Information Meeting, NBS, Washington DC, Oct. 26-30, 1981.

7. S. L. Anderson, "Characterization of the Neutron Environment for Commercial LWR Pressure Vessel Surveillance Programs", NUREG/CR-0004, Vol. 3, p. 1093, Proceedings of Second ASTM-Euratom Symposium on Reactor Dosimetry, Palo Alto, California, Oct 3-7, 1977.

8. W. N. McElroy, et. al, "LWR Pressure Vessel Surveillance Dosimetry Improvement Program," 1979 Annual Report, NUREG/CR-1291; HEDL-SA 1949 (Feb, 1980).

9. J. Strosnider and C. Monseprate with Appendix Prepared by L. D. Kenworthy and C. D. Tether, "MATSURV -- Computerized Reactor Pressure Vessel Materials Information System, NUREG 0688 (Oct 1980).

10. T. U. Marston and K. E. Stahlkopf, "Radiation Embrittlement: Significance of its effects on Integrity and Operation of LWR Pressure Vessels", Nuclear Safety 2 (6), p. 724 (November-December, 1978).

11. J. D. Varsik, "Evaluation of Irradiation Response of Reactor Pressure Vessel Materials", TR-MCM-110, Combustion Engineering Inc. Winsor, CT, EPRI RP 1553-1, Semi-Annual Progress Report No. 3, July-December, 1980 (1981).

12. F. A Schmittroth, "FERRET Data Analysis Code," HEDL-TME 79-40, Hanford Engineering Development Laboratory (September 1979).

13. S. Berg and W. N. McElroy, "A Computer Automated Iterative Method for Neutron Flux Spectra Determination by Foil Activation," AFWL-TR-67-41, Vol. 1, Air Force Weapons Laboratory, Kirkland AFB, New Mexico, (July 1967).

14. R. D. Bourquin, "TIMH - A Computer Program for the Determination of Fluence with a Time Varying Flux," BNWL-1492, Battelle Northwest (August 1970). TIMWH is a modified version of the TIMH program.

15. E. P. Lippincott, et al., "EBR-II 75D High Power Dosimetry Test," HEDL-TME 75-86, Hanford Engineering Development Laboratory (1975).

16. The Evaluated Nuclear Data File (ENDF/B) is available from and maintained by the National Nuclear Data Center (NNDC) at Brookhaven National Laboratory, Upton, New York.

17. R. E. Schenter, et. al., "Status of the ENDF/B-V and ENDF/B-VI Fission Yield Files," Ibid Reference 2.

18. R. Gold, et. al., "Photofission Observations in Reactor Environment Using Selected Fission Product Yields, Ibid Reference 2.

19. F. G. Perey, "The Data Covariance Files for ENDF/B-V", ORNL/TM-5839, Oak Ridge National Laboratory (July 1977).

20. ASTM Standard E693-79, ASTM Standard E706 (ID) "Standard Practice for Characterizing Neutron Exposures in Ferritic Steels in Terms of Displacements Per Atom (dpa)," ASTM Annual Book of Standards, Part 45 (1981).

21. E. P. Lippincott and W. N. McElroy, "ASTM, Standard Recommended Guide on Application of ENDF/A Cross Section and Uncertainty File: Establishment of the File," HEDL-SA 1540, paper presented at IAEA Advisory Group Meeting on Nuclear Data for Radiation Damage and Safety, Vienna, Austria, October 12-16, 1981.

22. E. P. Lippincott, et. al., "ASTM ENDF/A Dosimetry Cross Section and Uncertainty Standard," Ibid Reference 2.

23. IAEA, "Advanced Report on IRDF", Ibid Reference 2.

24. D. E. Cullen, N. Kocherov, and P. M. McLaughlin, "The International Reactor Dosimetry File (IRDF-82)", IAEA-NDS-41/R, Rev. 0, International Atomic Energy Agency (January 1982).

25. ASTM Standard E853-81, ASTM Standard E706(IA), "Standard Practice for the Analysis and Interpretation of LWR Surveillance Results," American Society for Testing and Material, Philadelphia, PA, (1982).

Table 1

Re-evaluated Exposure Values and Their Uncertainties for
Light Water Reactor Pressure Vessel Surveillance Capsules

Plant	Unit	Caps	Fluence (ϕt>1 MeV) (n/cm^2) Old	New (% 1σ)	New/Old	dpa (% 1σ)	dpa/ϕt new	dpa/sec	Exposure* Time (Sec)
Westinghouse									
Conn. Yankee		A	2.08 + 18	3.05 + 18 (18)**	1.47	0.00475 (15)	1.55-21	8.83-11	5.377 + 07
Conn. Yankee		F	4.04 + 18	5.03 + 18 (34)	1.25	0.00838 (31)	1.67-21	1.09-10	7.728 + 07
Conn. Yankee		H	1.79 + 19	2.19 + 19 (32)	1.22	0.0362 (30)	1.65-21	1.51-10	2.390 + 08
San Onofre		A	1.20 + 19	2.53 + 19 (29)	2.11	0.0424 (29)	1.68-21	7.90-10	5.846 + 07
San Onofre		D	2.36 + 19	4.09 + 19 (32)	1.73	0.0705 (31)	1.72-21	7.91-10	8.914 + 07
San Onofre		F	5.14 + 19	5.09 + 19 (24)	1.01	0.0944 (26)	1.82-21	3.95-10	2.451 + 08
Turkey Pt	3	S	1.41 + 19	1.75 + 19 (32)	1.24	0.0244 (29)	1.55-21	2.60-10	1.047 + 08
Turkey Pt	3	T	5.68 + 18	7.68 + 18 (11)	1.35	0.0109 (12)	1.41-21	3.13-10	3.473 + 07
Turkey Pt	4	S	1.25 + 19	1.46 + 19 (33)	1.17	0.0241 (30)	1.65-21	2.23-10	1.084 + 08
Turkey Pt	4	T	6.05 + 18	8.33 + 18 (16)	1.38	0.0132 (13)	1.57-21	3.44-10	3.840 + 07
H. B Robinson	2	S	3.02 + 18	5.07 + 18 (30)	1.68	0.00858 (29)	1.69-21	1.96-10	4.385 + 07
H. B Robinson	2	V	4.51 + 18	7.77 + 18 (29)	1.72	0.0123 (27)	1.59-21	1.16-10	1.061 + 08
Surry	1	T	2.50 + 18	2.87 + 18 (12)	1.15	0.00470 (14)	1.64-21	1.39-10	3.378 + 07
Surry	2	X	3.02 + 18	3.02 + 18 (12)	1.00	0.00488 (13)	1.61-21	1.32-10	3.689 + 07
Pr Island	1	V	5.21 + 18	6.16 + 18 (13)	1.18	0.0105 (17)	1.71-21	2.42-10	4.350 + 07
Pr Island	2	V	5.49 + 18	6.86 + 18 (11)	1.25	0.0118 (14)	1.73-21	2.66-10	4.454 + 07
R. E. Ginna	1	R	7.60 + 18	1.18 + 19 (12)	1.55	0.0218 (14)	1.85-21	2.53-10	8.628 + 07
R. E. Ginna	1	V	4.90 + 18	4.89 + 18 (16)	1.00	0.0872 (23)	1.78-21	2.22-10	3.923 + 07
Kewaunee		V	5.59 + 18	6.60 + 18 (11)	1.18	0.0116 (14)	1.77-21	2.80-10	4.167 + 07
Pt. Beach	1	S	--	8.44 + 18 (11)	--	0.0149 (13)	1.76-21	1.28-10	1.163 + 08
Pt. Beach	1	R	2.22 + 19	2.34 + 19 (11)	1.01	0.0416 (14)	1.78-21	2.55-10	1.632 + 08
Pt. Beach		T	9.45 + 18	9.43 + 18 (12)	1.00	0.0160 (13)	1.70-21	1.46-10	1.098 + 08
Pt. Beach		V	4.74 + 18	7.48 + 18 (13)	1.58	0.0122 (13)	1.63-21	2.52-10	4.859 + 07
Pt. Beach		R	2.01 + 19	2.42 + 19 (12)	1.20	0.0431 (14)	1.78-21	2.68-10	1.609 + 08
D. C. Cook	1	T	1.80 + 18	3.40 + 18 (30)	1.89	0.00599 (29)	1.76-21	1.50-10	3.991 + 07
Indian Pt	2	T	2.02 + 18	3.77 + 18 (31)	1.87	0.00638 (31)	1.69-21	1.43-10	4.473 + 07
Indian Pt	3	T	2.92 + 18	3.32 + 18 (29)	1.14	0.00550 (28)	1.66-21	1.31-10	4.211 + 07
Zion	1	T	1.80 + 18	2.83 + 18 (12)	1.57	0.00474 (14)	1.68-21	1.35-10	3.511 + 07
Zion	1	U	8.92 + 18	1.00 + 19 (12)	1.12	0.0169 (13)	1.68-21	1.52-10	1.11 + 08
Zion	2	U	2.00 + 18	2.86 + 18 (12)	1.43	0.00475 (14)	1.66-21	1.19-10	4.008 + 07
Salem	1	T	2.56 + 18	2.97 + 18 (30)	1.16	0.00496 (28)	1.67-21	1.45-10	3.422 + 07
Combustion Engineering									
Palisades		A240	4.40 + 19	5.96 + 19 (30)	1.35	0.0975 (31)	1.64-21	1.37-09	7.13 + 07
Fort Calhoun		W225	7.10 + 18	6.13 + 18 (17)	1.20	0.0942 (19)	1.48-21	1.11-10	8.20 + 07
Maine Yankee		1	1.30 + 19	2.10 + 19 (23)	1.62	0.0356 (25)	1.69-21	1.28-09	2.776 + 07
Maine Yankee		2	8.84 + 19	8.73 + 19 (16)	0.99	0.141 (20)	1.59-21	9.79-09	1.446 + 08
Maine Yankee		W263	6.90 + 18	6.66 + 18 (15)	0.97	0.010 (16)	1.50-21	6.94-11	1.446 + 08
Babcock & Wilcox									
Oconee	1	F	8.70 + 17	6.88 + 17 (27)	0.79	0.00095 (21)	1.38-21	3.60-11	2.625 + 07
Oconee	1	E	1.50 + 18	1.65 + 18 (13)	1.10	0.0022 (12)	1.34-21	4.30-11	5.166 + 07
Oconee	2	C	9.43 + 17	9.92 + 17 (11)	1.05	0.00144 (10)	1.54-21	3.80-11	3.802 + 07
Oconee	3	A	7.39 + 17	8.52 + 17 (11)	1.15	0.00117 (10)	1.37-21	3.91-11	2.981 + 07
Three Mile Is.	1	E	1.07 + 18	1.16 + 18 (10)	1.08	0.00158 (10)	1.36-21	3.91-11	4.036 + 07

*Equivalent constant power level exposure time.
**3.05 + 18 reads 3.05×10^{18} with a 18% (1σ) uncertainty.

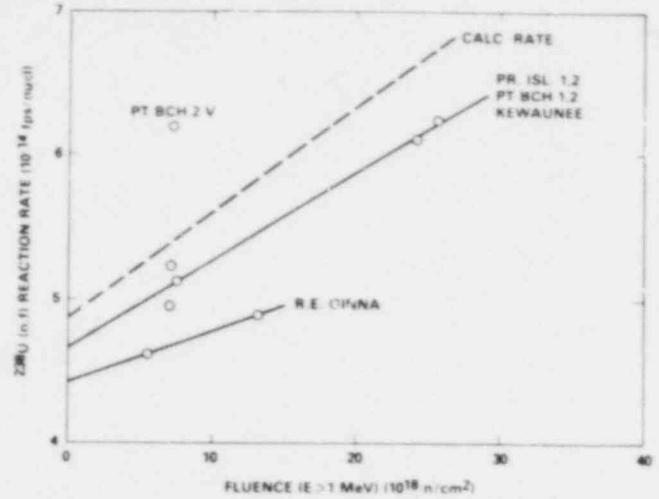

Figure 1. ^{238}U fission rate with burn-in of ^{239}Pu as a function of fluence (E>1MeV) in two loop Westinghouse plants.

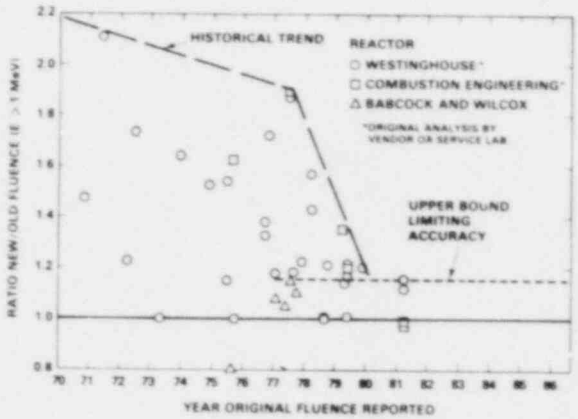

Figure 3. Ratio of new fluence/old fluence as a function of date that old fluence was reported.

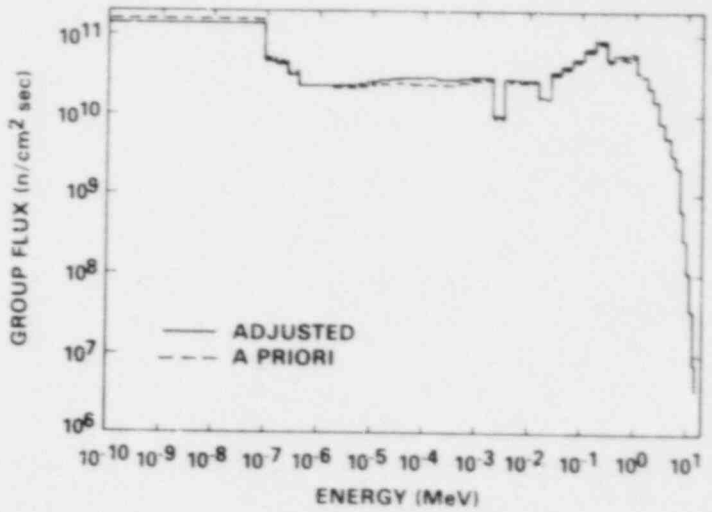

Figure 2a. Adjusted and a priori group fluxes for a Surveillance capsule from a Westinghouse two loop generic plant design.

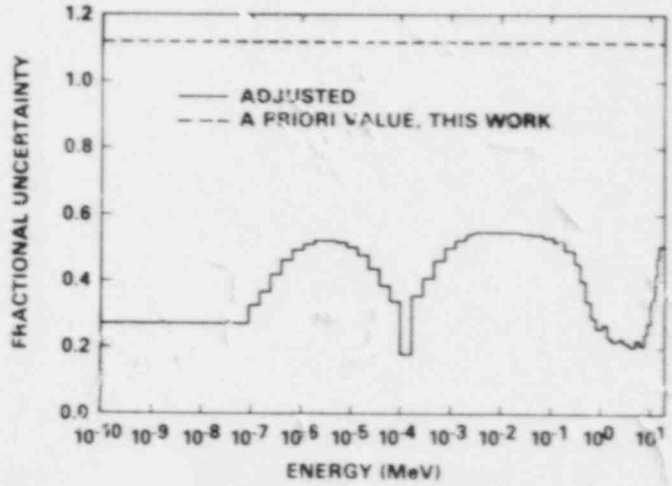

Figure 2b. Fractional uncertainty in group fluxes for a surveillance capsule from a Westinghouse two loop generic plant design.

Table 2

Relative Reaction Rates For Two-Loop Westinghouse Plants at 1520 Megawatts.

Relative Reaction Rates

Plant	Caps	$^{54}Fe(n,p)^{54}Mn$	$^{58}Ni(n,p)^{58}Co$	$^{63}Cu(n,a)^{60}Co$	$^{237}Np(n,f)(cd)$	$^{238}U(n,f)(cd)$	$^{59}Co(n,\gamma)^{60}Co(b)$	$^{59}Co(n,\gamma)^{60}Co(cd)$
R. E. Ginna	R	1.40*	0.98	0.91	1.08	0.94	--	--
R. E. Ginna	V	1.01	1.03	1.05	0.55*	0.94	--	--
Prairie Isl. 1	V	0.95	0.99	0.96	0.85	0.96	0.92	0.96
Prairie Isl. 2	V	0.96	1.02	0.96	0.98	0.99	0.90	--
Pt. Beach 1	R	1.07	0.91	1.11	1.03	0.97	0.93	1.16
Pt. Beach 2	V	1.03	0.92	0 98	0.98	1.22	0.95	0.80
Pt. Beach 2	R	1.01	1.19	1.06	1.04	1.01	1.17	0.92
Kewaunee	V	0.97	0.98	0.97	1.05	0.98	1.13	1.16
Average		7.67×10^{-15}	9.75×10^{-15}	6.43×10^{-17}	4.26×10^{-13}	4.31×10^{-14}	8.45×10^{-12}	3.92×10^{-12}
1 std. dev. (%)		4.1	8.7	6.6	7.4	9.1	12	13
Ratio meas/calc		0.98	0.90	1.02	1.05	0.97	0.81	1.17

b, cd Bare and cadmium covered respectively
* Not used to determine average or standard deviation

Table 3

Relative Reaction Rates For Four-Loop Westinghouse Plants at 3565 Megawatts.

Relative Reaction Rates

Plant	Caps	$^{54}Fe(n,p)^{54}Mn$	$^{58}Ni(n,p)^{58}Co$	$^{63}Cu(n,a)^{60}Co$	$^{237}Np(n,f)(cd)$	$^{238}U(n,f)(cd)$	$^{59}Co(n,\gamma)^{60}Co(b)$	$^{59}Co(n,\gamma)^{60}Co(cd)$
Cook 1	T	1.04	0.91	1.01	4.9*	9.7*	1.17	0.99
Indian Pt. 2	T	0.97	1.10	0.95	--	--	1.34	1.41
Indian Pt. 3	T	1.17*	1.06	1.04	--	--	0.89	0.88
Zion 1	T	1.03	1.05	1.14	0.09	1.00	0.84	0.85
Zion 1	U	1.00	0.86	0.91	1.15	1.1†	1.18	1.36
Zion 2	U	0.96	1.08	0.78*	0.87	0.86	0.78	0.88
Salem 1	T	0.93	0.93	0.90	--	--	0.81	0.64
Average		5.59×10^{-15}	7.52×10^{-15}	5.90×10^{-17}	2.18×10^{-13}	3.09×10^{-14}	4.46×10^{-12}	2.32×10^{-12}
1 std. dev. (%)		4.7	8.4	8.3	12	14	22	28
Ratio Meas/Calc		1.04	1.04	1.24	0.94	1.08	1.25	1.65

b, cd Bare and cadmium covered respectively
* Not used to determine average or standard deviation

Table 4

Relative Reaction Rates For Four-Loop Babcock and Wilcox Plants at 2568 Megawatts.

Relative Reaction Rates

Plant	Caps	$^{54}Fe(n,p)^{54}Mn$	$^{58}Ni(n,p)^{58}Co$	$^{58}Fe(n,\gamma)^{59}Fe$	$^{238}U(n,f)$ (cd)	$^{237}Np(n,f)$ (cd)	$^{59}Co(n,\gamma)^{60}Co(b)$	$^{59}Co(n,\gamma)^{60}Co(cd)$
Oconne 1	F	0.94	1.04	--	1.43*	1.51*	0.91	1.09
Oconne 1	E	1.10	1.07	--	1.06	1.16	1.17	0.97
Oconne 2	C	1.00	0.92	1.06	0.91	0.88	1.03	2.73*
Oconne 3	A	0.98	0.99	0.92	1.98	0.96	0.97	1.03
Three Mile Is. 1	E	0.99	0.98	1.03	1.04	0.99	0.93	0.93
Average		2.67×10^{-15}	3.74×10^{-15}	5.24×10^{-14}	1.21×10^{-14}	6.09×10^{-14}	1.22×10^{-12}	1.97×10^{-13}
1 std. dev. (%)		5.9	5.8	7.3	6.6	11.7	10.9	2.0
Ratio Meas/Calc		0.85	0.92	1.64	1.04	1.02	1.03	0.65

b, cd Bare and cadmium covered respectively
* Not used to determine average or standard deviation

THE IAEA INTERNATIONAL REACTOR DOSIMETRY FILE (IRDF-82)

D.E. Cullen, N.P. Kocherov, P.M. McLaughlin
Nuclear Data Section
International Atomic Energy Agency
A-1400 Vienna, Austria

ABSTRACT

The contents of the International Reactor Dosimetry File which was released by the Nuclear Data Section of the IAEA in February 1982 is described. The calculated averages of dosimetry reaction cross sections for 10 benchmark neutron fields are presented. In case of ^{252}Cf and ^{235}U the calculated averages are compared to available experimental internal data for these fission neutron fields.

I. Introduction

The 1982 version of the International Reactor Dosimetry File (IRDF-82) is now available through the Nuclear Data Section of the International Atomic Energy Agency. The purpose of this file is to provide the international reactor dosimetry community with a comprehensive set of dosimetry reaction cross sections (and their uncertainties) which can be used for the spectra characterization of neutron fields, including, for example, the unfolding of neutron spectra from in-pile multiple foil reaction rate measurements and the estimation of radiation damage in fission and fusion reactors.

The 1982 version of the International Reactor Dosimetry File (IRDF-82) is composed of two different parts. The first part is made up of a collection of Dosimetry cross sections and the second part contains a collection of benchmark spectra. For ease of use in Dosimetry applications both cross sections and spectra are distributed in multigroup (as opposed to continuous energy) form. Each of these two parts is in the ENDF/B-V format [1] as a separate computer file.

II. Dosimetry Cross Sections

The IRDF-82 Dosimetry cross section library contains the following data,

(1.) The entire ENDF/B-V Dosimetry Library (Mod. 1) as created at Brookhaven National Laboratory [2] in the form of 620 group averaged cross sections, using the SAND-II [3] group structure.

(2.) The reactions $^{19}F(n,2n)$, $^{24}Mg(n,p)$, $^{31}P(n,p)$, $^{29}Cu(n,2n)$, $^{64}Zn(n,p)$, $^{90}Zr(n,2n)$, $^{93}Nb(n,n')$ and $^{103}Rh(n,n')$, supplied by Vonach [4]. This data was converted to the ENDF/B-V format, [5] which in turn was converted to 620 group (SAND-II) form [6] at the Nuclear Data Section.

(3.) The reaction $^{23}Na(n,2n)$ provided by Marcinkowski [7]. This data was converted to the ENDF/B-V format [5] and then converted to 620 group (SAND-II) format [6] at the Nuclear Data Section.

(4.) The reaction $^{241}Am(n,f)$ as supplied by Patrick [8]. This data was converted to the ENDF/B-V format at Stuttgart [9] and then converted to 620 group (SAND-II) form [6] at the Nuclear Data Section.

(5.) ASTM and EUR standards damage cross sections for iron as provided by Zijp [10] in the form of 620 group (SAND-II) cross sections. This data was converted to the ENDF/B-V format at the Nuclear Data Section.

With the exception of the $^{241}Am(n,f)$ and the two damage cross sections, all other reactions have accompanying uncertainty information.

All of this data is presented in the standard ENDF/B-V format [1]. However, since ENDF/B-V does not have an MT [2] number corresponding to damage cross sections the convention was arbitrarily introduced to define two new MT numbers (see: ref. 1 for a definition of MT numbers).

MT = 800 - ASTM iron damage
= 801 - EUR iron damage.

See Table I for a complete list of materials with dosimetry cross sections in the IRDF-82 library. Spectra average cross sections are presented in Tables II and III, and comparison to ^{252}Cf and ^{235}U experimentally measured spectra averages are presented in Table IV.

III. Benchmark Spectra

The IRDF-82 Benchmark Spectra library contains ten benchmark spectra including,

(1.) The NBS ^{252}Cf spontaneous fission; the NBS ^{235}U and ENDF/B-V ^{235}U thermal fission, the Intermediate-Energy Standard Neutron Field (ISNF), the Coupled Fast Reactivity Measurement Facility (CFRMF), the 10 % Enriched Uranium Cylindrical Critical Assembly (BIG-TEN) and the Coupled Thermal/Fast Uranium and Boron Carbide Spherical Assembly (SIGMA-SIGMA) spectra, all of which were provided by Eisenhauer [11] in 620 group (SAND-II) form.

(2.) The ORR and YAYOI spectra, which were provided by Greenwood [12] in 100 group form.

(3.) The Central Zone Flux of the NEACRP Benchmark Spectra provided by Goel [13] in 208 group form.

All spectra are presented without uncertainty information.

All of these spectra were converted to the ENDF/B-V format at the Nuclear Data Section. In an attempt to simplify later processing and use of this data each spectrum is presented in the ENDF/B-V [1] format as section MF=3, MT=1 of a separate material (MAT). The spectra are presented in the form of group averages (not group integrals). If for any application group integrals are required, each group average may be converted to a group integral over the same group by simply multiplying by the width of the group.

See Tables II and III for spectra averaged cross sections and Table IV for comparison to experimentally measured spectra averages.

IV. Summary

The initial IRDF as well as future updated versions will be maintained by IAEA/NDS and will be freely available upon request from IAEA/NDS. Updating of the file will be performed by the IAEA/NDS with corrections and additions to be released in a timely manner.

Table 1: Contents of IRDF-82

IZ EL A	MAT NO.	SPECIFICATION	LAB	DATE	AUTHOR	REFERENCE
3-Li- 6g	1424	Neutron + error files	LASL	DEC78	L.STEWART, G.HALE, P.YOUNG	
5-B - 10g	1425	Neutron + error files	LASL	JAN79	L.STEWART, G.HALE, P.YOUNG	
9-F - 19g	920	Neutron + error files	ZAUSTRK	79	S.TAGESEN,H.VONACH,B.STROHMAIER	FIN.REP.ON RC,80
11-Na- 23g	1120	Neutron + error files	ZPOLIB	FEB79	ADAMSKI, HERMAN AND MARCINKOWSKI	R,INR-1809,9,79
11-Na- 23g	1311	Neutron (RP) + error files	ORNL	DEC77	D.C.LARSON	
12-Mg- 24g	1220	Neutron + error files	ZAUSTRK	79	S.TAGESEN,H.VONACH,B.STROHMAIER	B,FH-DAT,13-1,79
13-Al- 27g	1313	Neutron + error files	LASL	DEC73	P.G. YOUNG, D.G. FOSTER, JR.	LA-4726 (1973).
15-P - 31g	1520	Neutron + error files	ZAUSTRK	79	S.TAGESEN,H.VONACH,B.STROHMAIER	FIN.REP.ON RC,80
16-S - 32g	1439	Neutron + error files	BNL	APR79	DIVADEENAM	
21-Sc- 45g	1426	Neutron (RP) + error files	BNL	JUL79	MAGURNO AND MUGHABGHAB	
22-Ti- 46g	1427	Neutron + error files	ANL	JAN77	C.PHILIS,O.BERSILLON,D.SMITH,ETC.	
22-Ti- 47g	1428	Neutron + error files	ANL	JAN77	C.PHILIS,O.BERSILLON,D.SMITH,ETC	
22-Ti- 48g	1429	Neutron + error files	ANL	JAN77	C.PHILIS,O.BERSILLON,D.SMITH ETC.	
25-Mn- 55g	1325	Neutron + error files	BNR	MAR77	S.F. MUGHABGHAB	
26-Fe- 0g	8000	Neutron cross sections only	FETTEN	79	W.L.ZIJP	PRIVATE COM.
26-Fe- 0g	8001	Neutron cross sections only	FETTEN	79	W.L.ZIJP	PRIVATE COM.
26-Fe- 54g	1430	Neutron + error files	HEIL	JUN79	R.SCHENTER F.SCHMITTROTH F.MANN	
26-Fe- 56g	1431	Neutron + error files	ORNL	JUL78	C.Y.FU	
26-Fe- 58g	1432	Neutron (RP) + error files	HEIL	JUN79	R.SCHENTER F.SCHMITTROTH F.MANN	
27-Co- 59g	1327	Neutron (RP) + error files	BNL	JUN77	S.MUGHABGHAB	
28-Ni- 58g	1433	Neutron + error files	BNL	MAR77	M.DIVADEENAM	
28-Ni- 60g	1434	Neutron + error files	BNL	MAR77	M.DIVADEENAM	
29-Cu- 63g	2920	Neutron + error files	ZAUSTRK	79	S.TAGESEN,H.VONACH,B.STROHMAIER	B,FH-DAT,13-1,79
29-Cu- 63g	1435	Neutron (RP) + error files	ORNL	JUL78	C.Y.FU	
29-Cu- 65g	1436	Neutron + error files	ORNL	JUL78	C.Y.FU	
30-Zn- 64g	3020	Neutron + error files	ZAUSTRK	79	S.TAGESEN,H.VONACH,B.STROHMAIER	B,FH-DAT,13-1,79
40-Zr- 90g	4020	Neutron + error files	ZAUSTRK	79	S.TAGESEN,H.VONACH,B.STROHMAIER	B,FH-DAT,13-1,79
41-Nb- 93g	4120	Neutron + error files	ZAUSTRK	79	S.TAGESEN,H.VONACH,B.STROHMAIER	FIN.REP.ON RC,80
45-Rh-103g	4520	Neutron + error files	ZAUSIRK	79	S.TAGESEN,H.VONACH,B.STROHMAIER	FIN.REP.ON RC,80
49-In-115g	1437	Neutron (RP) + error files	HEIL/ANL	JAN78	F.SCHMITTROTH,R.E.SMITH	
53-I -127g	1438	Neutron + error files	STANFORD	AUG72	R.SHER	
79-Au-197g	1379	Neutron (RP) + error files	BNL	FEB77	S.F.MUGHABGHAB	
90-Th-232g	1390	Neutron (RP) + error files	BNL	DEC77	BHAT,SMITH,LEONARD,DESAUSSURE ETAL	
92-U -235g	1395	Neutron (RP) + error files	BNL	APR77	M.R.BHAT	
92-U -238g	1396	Neutron (RP) + error files	ANL+	JUN77	E.FENNINGTON,A.SMITH,W.POENITZ	ANL/NDM-32
93-Np-237g	1337	Neutron (RP) + error files	HEIL,SRL,+	APR78	MANN,BENJAMIN,SMITH,STEIN,REICH,+	HEIL TME 77-54
94-Pu-239g	1397	Neutron (RP) + error files	GE-FRKD	OCT76	E.KUJAWSKI,L.STEWART(LASL)	
95-Am-241g	1009	Neutron cross sections only	AERE	79	J.E.LYNN,B.H.PATRICK,M.G.SOWERBY+	AERE-R 8528

			SPECTRUM	CF-252 FISS (NBS)	U-235 FISS (NBS)	U-235 FISS (ENDF/B-V)	ISNF (NBS)	CFRM (IDAHO)
			NUMBER OF GROUPS	620	620	620	620	459
			SPECTRUM ENERGY RANGE IS FROM	1.0000- 4	1.0000- 4	1.0000- 4	1.0000- 4	4.0000- 1
			TO (EV)	1.8000+ 7	1.8000+ 7	1.8000+ 7	1.8000+ 7	1.8000+ 7
			SPECTRUM AVERAGED ENERGY (EV)	2.1194+ 6	1.9771+ 6	2.0313+ 6	1.0071+ 6	7.4135+ 5
ISOTOPE	MAT	GROUPS	THRESHOLD (EV)	REACTION	SPECTRUM AVERAGES (BARNS)				
3-LI- 6	6424	620	1.000- 4	HELIUM PRODUCTION	4.6460- 1	4.6500- 1	4.5452- 1	7.9777- 1	9.1544- 1
5-B - 10	6425	620	1.000- 4	HELIUM PRODUCTION	4.8886- 1	4.9924- 1	4.9060- 1	1.7054+ 0	1.6752+ 0
9-F - 19	920	70	1.100+ 7	(N,2N)	1.5712- 5	6.6359- 6	6.4621- 6	1.8171- 6	2.0708- 6
11-NA- 23	1120	51	1.290+ 7	(N,2N)	6.4828- 6	2.4569- 6	2.3020- 6	6.6845- 7	9.7895- 7
11-NA- 23	6311	620	1.000- 4	(N,GAMMA)	2.7116- 4	2.6170- 4	2.7498- 4	1.9173- 3	1.5083- 3
12-MG- 24	1220	131	4.900+ 6	(N,P)	2.1575- 3	1.4535- 3	1.5073- 3	4.0756- 4	3.6636- 4
13-AL- 27	6313	162	1.800+ 6	(N,P)	5.1382- 3	4.1215- 3	4.2624- 3	1.2439- 3	9.4207- 4
13-AL- 27	6313	148	3.200+ 6	(N,ALPHA)	1.0588- 3	6.9337- 4	7.1943- 4	1.9392- 4	1.7639- 4
15-P - 31	1520	165	1.500+ 6	(N,P)	3.0637- 2	2.7397- 2	2.8540- 2	1.0137- 2	6.3510- 3
16-S - 32	6439	172	9.200+ 5	(N,P)	7.5999- 2	6.7609- 2	7.0494- 2	2.4256- 2	1.5484- 2
21-SC- 45	6426	620	1.000- 4	(N,GAMMA)	5.2595- 3	5.6398- 3	5.4471- 3	2.7773- 2	2.4414- 2
22-TI- 46	6427	164	1.600+ 6	(N,P)	1.3469- 2	1.0812- 2	1.1173- 2	3.2432- 3	2.4576- 3
22-TI- 47	6428	74	1.060+ 7	(N,N'P)	2.0623- 5	8.4689- 6	8.1654- 6	2.3146- 6	2.8943- 6
22-TI- 47	6428	620	1.000- 4	(N,P)	2.4065- 2	2.1589- 2	2.2458- 2	8.3019- 3	5.1317- 3
22-TI- 48	6429	64	1.160+ 7	(N,N'P)	3.4358- 6	1.3641- 6	1.3001- 6	3.7138- 7	4.9173- 7
22-TI- 48	6429	140	3.200+ 6	(N,P)	4.0912- 4	2.7258- 4	2.8170- 4	7.6616- 5	6.8272- 5
25-MN- 55	6325	76	1.040+ 7	(N,2N)	4.4027- 4	2.0164- 4	2.0114- 4	5.5366- 5	5.6360- 5
26-FE- 0	8000	620	1.000- 4	DAMAGE (ASTM)	8.9510+ 2	8.5415+ 2	8.7405+ 2	4.8778+ 2	3.8698+ 2
26-FE- 0	8001	620	1.000- 4	DAMAGE (EUR)	8.6642+ 2	8.3026+ 2	8.4945+ 2	4.8182+ 2	3.8161+ 2
26-FE- 54	6430	620	1.000- 4	(N,P)	8.8255- 2	7.7821- 2	8.1021- 2	2.7384- 2	1.7802- 2
26-FE- 56	6431	151	2.900+ 6	(N,P)	1.4144- 3	1.0056- 3	1.0364- 3	2.8561- 4	2.4420- 4
26-FE- 58	6432	620	1.000- 4	(N,GAMMA)	1.6605- 3	1.7122- 3	1.6874- 3	7.1908- 3	6.6418- 3
27-CO- 59	6327	74	1.060+ 7	(N,2N)	4.0494- 4	1.8292- 4	1.8179- 4	5.0212- 5	5.1605- 5
27-CO- 59	6327	620	1.000- 4	(N,GAMMA)	6.0278- 3	6.2781- 3	6.1738- 3	4.2951- 2	8.7271- 2
27-CO- 59	6327	125	5.500+ 6	(N,ALPHA)	2.1616- 4	1.4483- 4	1.4975- 4	4.0713- 5	3.6282- 5
28-NI- 58	6433	56	1.240+ 7	(N,2N)	7.2343- 6	2.8593- 6	2.7222- 6	7.8093- 7	1.0516- 6
28-NI- 58	6433	620	1.000- 4	(N,P)	1.1381- 1	1.0088- 1	1.0498- 1	3.6556- 2	2.3411- 2
28-NI- 60	6434	155	2.500+ 6	(N,P)	3.4422- 3	2.5282- 3	2.6077- 3	7.2564- 4	6.0329- 4
29-CU- 63	2920	68	1.120+ 7	(N,2N)	1.9282- 4	8.2463- 5	8.0633- 5	2.2596- 5	2.4688- 5
29-CU- 63	6435	620	1.000- 4	(N,GAMMA)	9.6494- 3	1.0076- 2	9.8682- 3	5.2679- 2	4.6422- 2
29-CU- 63	6435	163	1.700+ 6	(N,ALPHA)	7.5813- 4	5.4024- 4	5.5818- 4	1.5467- 4	1.3103- 4
29-CU- 65	6436	80	1.000+ 7	(N,2N)	6.4913- 4	3.0569- 4	3.0707- 4	8.3981- 5	8.5312- 5
30-ZN- 64	3020	171	9.600+ 5	(N,P)	3.9234- 2	3.4662- 2	3.6125- 2	1.2139- 2	7.9024- 3
40-ZR- 90	4020	59	1.210+ 7	(N,2N)	1.9773- 4	8.0081- 5	7.6911- 5	2.1900- 5	2.7505- 5
41-NB- 93	4120	209	1.350+ 5	(N,N') FIRST LEVEL	1.6160- 1	1.5526- 1	1.6016- 1	7.8908- 2	4.9375- 2
45-RH-103	4520	215	1.000+ 5	(N,N') FIRST LEVEL	7.1216- 1	6.8896- 1	7.0505- 1	3.8757- 1	2.7967- 1
49-IN-115	6437	193	3.200+ 5	(N,N') FIRST LEVEL	1.8192- 1	1.7338- 1	1.7925- 1	8.4013- 2	4.9592- 2
49-IN-115	6437	620	1.000- 4	(N,GAMMA)	1.2124- 1	1.2659- 1	1.2464- 1	2.8909- 1	2.8222- 1
53-I -127	6438	88	9.200+ 6	(N,2N)	2.3108- 3	1.1862- 3	1.2135- 3	3.2605- 4	3.2163- 4
79-AU-197	6379	620	1.000- 4	(N,GAMMA)	7.6324- 2	8.0944- 2	7.8270- 2	4.0347- 1	4.0266- 1
90-TH-232	6390	410	5.000+ 0	FISSION	7.8066- 2	7.2399- 2	7.5038- 2	3.2583- 2	1.8616- 2
90-TH-232	6390	620	1.000- 4	(N,GAMMA)	8.9676- 2	9.4219- 2	9.1950- 2	2.5743- 1	2.6330- 1
92-U -235	6395	620	1.000- 4	FISSION	1.2358+ 0	1.2360+ 0	1.2359+ 0	1.6141+ 0	1.5806+ 0
92-U -238	6398	620	1.000- 4	FISSION	3.1358- 1	2.9464- 1	3.0518- 1	1.3713- 1	7.7223- 2
92-U -238	6398	620	1.000- 4	(N,GAMMA)	6.8334- 2	7.2060- 2	7.0251- 2	2.2703- 1	2.3406- 1
93-NP-237	6337	620	1.000- 4	FISSION	1.3520+ 0	1.3219+ 0	1.3468+ 0	7.9257- 1	5.8541- 1
94-PU-239	6399	620	1.000- 4	FISSION	1.7918+ 0	1.7855+ 0	1.7910+ 0	1.8234+ 0	1.7872+ 0
95-AM-241	1009	620	1.000- 4	FISSION	1.4264+ 0	1.3819+ 0	1.4171+ 0	7.6305- 1	4.9229- 1

Table II: IRDF-82 Spectra Averaged Cross Sections

Table III: IRDF-82 Spectra Averaged Cross Sections

			BIG-TEN (LASL)	SIGMA-SIGMA (MOL)	ORR (ARGONNE)	YAYOI (ARGONNE)	NEACRP (KARLSRUHE)
SPECTRUM							
NUMBER OF GROUPS			395	429	100	100	208
SPECTRUM ENERGY RANGE IS FROM			1.0000+ 1	4.0000- 1	1.0000- 4	1.0000- 4	1.4663- 2
TO (EV)			1.8000+ 7	1.5000+ 7	2.0000+ 7	2.0000+ 7	1.0500+ 7
SPECTRUM AVERAGED ENERGY (EV)			6.0221+ 5	7.6139+ 5	5.9629+ 5	1.3877+ 6	4.3223+ 5
ISOTOPE	MAT	GROUPS	THRESHOLD (EV)	REACTION	SPECTRUM AVERAGES (BARNS)				
3-LI- 6	6424	620	1.000- 4	HELIUM PRODUCTION	8.9788- 1	8.6618- 1	2.1130+ 2	5.9875- 1	1.0775+ 0
5-B - 10	6425	620	1.000- 4	HELIUM PRODUCTION	1.1935+ 0	1.4810+ 0	8.6519+ 2	6.7198- 1	2.6701+ 0
9-F - 19	920	70	1.100+ 7	(N,2N)	1.8106- 6	1.1025- 6	4.0671- 6	9.0789- 6	0.0 + 0
11-NA- 23	1120	51	1.270+ 7	(N,2N)	7.3059- 7	2.2842- 7	2.2708- 6	4.4317- 6	0.0 + 0
11-NA- 23	6311	620	1.000- 4	(N,GAMMA)	6.4668- 4	1.1195- 3	1.2051- 1	3.8684- 4	1.6064- 3
12-MG- 24	1220	131	4.900+ 6	(N,P)	2.6023- 4	3.2212- 4	3.7045- 4	9.7495- 4	1.1686- 4
13-AL- 27	6313	162	1.800+ 6	(N,P)	6.4781- 4	8.7072- 4	1.0422- 3	2.3772- 3	4.0361- 4
13-AL- 27	6313	148	3.200+ 6	(N,ALPHA)	1.2752- 4	1.5376- 4	1.7605- 4	4.8320- 4	5.2859- 5
15-P - 31	1520	165	1.500+ 6	(N,P)	4.3118- 3	6.3249- 3	7.1466- 3	1.5969- 2	3.3082- 3
16-S - 32	6439	172	9.200+ 5	(N,P)	1.0564- 2	1.5235- 2	1.7459- 2	3.9128- 2	7.8640- 3
21-SC- 45	6426	620	1.000- 4	(N,GAMMA)	1.8844- 2	2.2776- 2	6.1330+ 0	9.1550- 3	4.3287- 2
22-TI- 46	6427	164	1.600+ 6	(N,P)	1.6906- 3	2.2447- 3	2.7295- 3	6.2080- 3	1.0551- 3
22-TI- 47	6428	74	1.060+ 7	(N,N'P)	2.3578- 6	1.2010- 6	5.9895- 6	1.2628- 5	0.0 + 0
22-TI- 47	6428	620	1.000- 4	(N,P)	3.4973- 3	5.1651- 3	5.6953- 3	1.2808- 2	2.6638- 3
22-TI- 48	6429	64	1.160+ 7	(N,N'P)	3.9137- 7	1.6729- 7	1.0986- 6	2.2089- 6	0.0 + 0
22-TI- 48	6429	148	3.200+ 6	(N,P)	4.9319- 5	5.9992- 5	7.0926- 5	1.8590- 4	2.1057- 5
25-MN- 55	6325	76	1.040+ 7	(N,2N)	5.1393- 5	3.9570- 5	9.1819- 5	2.2546- 4	2.0483- 8
26-FE- 0	8000	620	1.000- 4	DAMAGE (ASTM)	3.3876+ 2	3.9774+ 2	2.8196+ 2	6.3853+ 2	2.4957+ 2
26-FE- 0	8001	620	1.000- 4	DAMAGE (EUR)	3.3425+ 2	3.9293+ 2	2.7602+ 2	6.2447+ 2	2.5180+ 2
26-FE- 54	6430	620	1.000- 4	(N,P)	1.2146- 2	1.7456- 2	2.0075- 2	4.4850- 2	8.9323- 3
26-FE- 56	6431	151	2.900+ 6	(N,P)	1.7141- 4	2.2005- 4	2.5828- 4	6.3280- 4	8.6578- 5
26-FE- 58	6432	620	1.000- 4	(N,GAMMA)	3.4997- 3	6.2083- 3	2.7358- 1	2.1834- 3	1.1490- 2
27-CO- 59	6327	74	1.060+ 7	(N,2N)	4.7182- 5	3.5325- 5	8.7186- 5	2.1082- 4	0.0 + 0
27-CO- 59	6327	620	1.000- 4	(N,GAMMA)	1.2501- 2	4.2104- 2	9.8651+ 0	7.9656- 3	3.6950- 2
27-CO- 59	6327	125	5.500+ 6	(N,ALPHA)	2.6063- 5	3.2027- 5	3.7269- 5	9.8072- 5	1.1592- 5
28-NI- 58	6433	56	1.240+ 7	(N,2N)	8.2365- 7	3.7525- 7	2.2344- 6	4.6356- 6	0.0 + 0
28-NI- 58	6433	620	1.000- 4	(N,P)	1.5972- 2	2.3139- 2	2.6200- 2	5.8668- 2	1.1864- 2
28-NI- 60	6434	155	2.500+ 6	(N,P)	4.1972- 4	5.4362- 4	6.4051- 4	1.5497- 3	2.2917- 4
29-CU- 63	2920	68	1.120+ 7	(N,2N)	2.2262- 5	1.4248- 5	4.8214- 5	1.0901- 4	0.0 + 0
29-CU- 63	6435	620	1.000- 4	(N,GAMMA)	2.2065- 2	3.6533- 2	1.0733+ 0	1.3414- 2	7.2055- 2
29-CU- 63	6435	163	1.700+ 6	(N,ALPHA)	9.2342- 5	1.1694- 4	1.3656- 4	3.4394- 4	4.6628- 5
29-CU- 65	6436	80	1.000+ 7	(N,2N)	7.6062- 5	6.1474- 5	1.2742- 4	3.2236- 4	4.4088- 7
30-ZN- 64	3020	171	9.600+ 5	(N,P)	5.3973- 3	7.7604- 3	8.9363- 3	1.9986- 2	3.9661- 3
40-ZR- 90	4020	59	1.210+ 7	(N,2N)	2.2625- 5	1.1848- 5	5.7136- 5	1.2230- 4	0.0 + 0
41-NB- 93	4120	209	1.350+ 5	(N,N') FIRST LEVEL	3.6112- 2	5.2271- 2	4.5111- 2	1.0509- 1	2.7608- 2
45-RH-103	4520	215	1.000+ 5	(N,N') FIRST LEVEL	2.2319- 1	2.9227- 1	2.1313- 1	5.0898- 1	1.5964- 1
49-IN-115	6437	193	3.200+ 5	(N,N') FIRST LEVEL	3.4537- 2	5.2569- 2	4.9148- 2	1.1324- 1	2.7619- 2
49-IN-115	6437	620	1.000- 4	(N,GAMMA)	2.1865- 1	2.6289- 1	1.1973+ 2	1.5482- 1	4.0871- 1
53-I -127	6438	88	9.200+ 6	(N,2N)	2.7342- 4	2.5299- 4	3.8598- 4	1.0987- 3	2.4795- 5
79-AU-197	6379	620	1.000- 4	(N,GAMMA)	2.1268- 1	3.3537- 1	6.3461+ 1	1.2029- 1	6.2426- 1
90-TH-232	6390	410	5.000+ 0	FISSION	1.2645- 2	1.9606- 2	2.0097- 2	4.5529- 2	1.0256- 2
90-TH-232	6390	620	1.000- 4	(N,GAMMA)	1.2189- 1	2.3548- 1	4.1004+ 0	1.2342- 1	3.6763- 1
92-U -235	6395	620	1.000- 4	FISSION	1.3657+ 0	1.5049+ 0	1.3039+ 2	1.2603+ 0	1.8911+ 0
92-U -238	6398	620	1.000- 4	FISSION	5.2575- 2	8.2130- 2	8.2518- 2	1.8711- 1	4.3207- 2
92-U -238	6398	620	1.000- 4	(N,GAMMA)	1.5058- 1	2.0937- 1	1.0372+ 1	9.6809- 2	3.3498- 1
93-NP-237	6337	620	1.000- 4	FISSION	4.6708- 1	6.1326- 1	4.2887- 1	1.0208+ 0	3.3176- 1
94-PU-239	6399	620	1.000- 4	FISSION	1.6199+ 0	1.7522+ 0	2.0778+ 2	1.7224+ 0	1.7998+ 0
95-AM-241	1009	620	1.000- 4	FISSION	3.5943- 1	5.1993- 1	1.5281+ 0	9.8590- 1	2.8374- 1

V. References

[1] GARBER, D., et al., Data Formats and Procedures for the Evaluated Nuclear Data File, ENDF, BNL-NCS-50496 (ENDF-102), Brookhaven (1975).

[2] MAGURNO, B.: Private Communication, Brookhaven (1981).

[3] SIMONS, R.L. and MCELROY, W.M.: Evaluated Reference Cross Section Libraries", BNWL-1312, Richland (1970).

[4] TAGESEN, S., VONACH, H., and STROHMAIER, B., Physics Data - Nr. 13-1 (1979) and No. 13-2 (1980), Vienna.

[5] PRONYAEV, V., and SCHWERER, O., Private Communication, IAEA, Vienna (1981).

[6] CULLEN, D.E., Program GROUPIE (Version 79-1): Calculation of Bondarenko self-shielded cross sections and multiband parameters from data in the ENDF/B format", UCRL-50400, Vol. 17, part D, Livermore (1980).

[7] MARCINKOWSKI, Private Communication, Warsaw, (1980).

[8] PATRICK, B., AERE-R-8528, Harwell (1979).

[9] MATTES, M., Private Communication, Stuttgart (1981).

[10] ZIJP, W.L., Private Communication, Petten (1981).

[11] EISENHAUER, C., Private Communication, National Bureau of Standards, Washington (1980).

[12] GREENWOOD, L., Private Communication, Argonne, (1981).

[13] GOEL, B., Private Communication, Karlsruhe (1981).

VI. Comparison to Experimental Measurements

The calculated average cross sections for ^{252}Cf and ^{235}U fission spectra were compared with results of integral measurements. The experimental spectral averaged cross section data were compiled from recent publications. Most of the data for ^{252}Cf spectrum were supplied to us by W. Mannhart [2] who made evaluations of available experimental data. The results of comparison are shown in Table IV. The numbers in parentheses after the experimental values refer to the references listed at the end of this paper. As can be seen from the table the agreement between calculated and measured values varies significantly from one reaction to another and for 9 reactions it is worse than 10 %. The cross-section data for these reactions will be under constant review by the Nuclear Data Section and will be updated when new reliable data appear. This table also shows the accuracy range which might be expected in case of different detectors and might be useful for selection of composition of activation detector sets.

Comparing the two ^{235}U spectrum evaluations one might see that they contribute up to 6% difference in deviations from experiment. This shows that more precise knowledge of this spectrum and further evaluations are needed.

COMPARISON OF EXPERIMENTIALLY MEASURED AND CALCULATED CF-252 AND U-235 FISSION SPECTRA AVERAGES

ISOTOPE	MAT	GROUPS	THRESHOLD (EV)	REACTION	EXPERIMENTAL VALUES CF-252 FISS (MILLIBARNS)		EXPERIMENTAL VALUES U-235 FISS (MILLIBARNS)		EXPERIMENTAL ERROR (PER-CENT)	COMPARISON TO CALCULATIONS (EVAL-EXP)/EVAL CF-252 FISS (NBS) (PER-CENT)	U-235 FISS (NBS) (PER-CENT)	U-235 FISS (ENDF/B-V) (PER-CENT)
3-LI- 6	6424	620	1.000- 4	HELIUM PRODUCTION								
5-B - 10	6425	620	1.000- 4	HELIUM PRODUCTION								
9-F - 19	920	70	1.100+ 7	(N,2N)	0.0108	(1)			15	+30		
11-NA- 23	1120	51	1.290+ 7	(N,2N)								
11-NA- 23	4311	620	1.000- 4	(N,GAMMA)	0.335	(1)			4	-24		
12-MG- 24	1220	131	4.900+ 6	(N,P)	1.918	(2)			4.9	+11		
13-AL- 27	6313	162	1.800+ 6	(N,P)	4.862	(2)			3.55	+5		
13-AL- 27	6313	148	3.200+ 6	(N,ALPHA)	1.014	(2)			2	+4		
15-P - 31	1520	165	1.500+ 6	(N,P)			33.5	(3)	6		-22	-17
16-S - 32	6439	172	9.200+ 5	(N,P)	71.78	(2)			4.5	+6		
21-SC- 45	6426	620	1.000- 4	(N,GAMMA)								
22-TI- 46	6427	164	1.600+ 6	(N,P)	14.11	(2)			2.2	-5		
22-TI- 47	6428	74	1.060+ 7	(N,N'P)								
22-TI- 47	6428	620	1.000- 4	(N,P)	19.26	(2)			2.12	+20		
22-TI- 48	6429	64	1.160+ 7	(N,N'P)					5	+7		
22-TI- 48	6429	148	3.200+ 6	(N,P)	0.38	(1)						
25-MN- 55	6325	76	1.040+ 7	(N,2N)			0.202	(4)	5		-0.2	-0.4
26-FE- 0	8000	620	1.000- 4	DAMAGE (ASTM)								
26-FE- 0	8001	620	1.000- 4	DAMAGE (EUR)								
26-FE- 54	6430	620	1.000- 4	(N,P)	86.55	(2)			2.12	+2		
26-FE- 56	6431	151	2.900+ 6	(N,P)	1.459	(2)			2.36	-3		
26-FE- 58	6432	620	1.000- 4	(N,GAMMA)			0.227	(4)			-24	-25
27-CO- 59	6327	74	1.060+ 7	(N,2N)	6.97	(1)			5	-16		
27-CO- 59	6327	620	1.000- 4	(N,GAMMA)	0.2186	(1)			7.41	+1		
27-CO- 59	6327	125	5.500+ 6	(N,ALPHA)			0.0036	(4)	7		-26	-32
28-NI- 58	6433	56	1.240+ 7	(N,2N)	115.4	(2)			1.67	-1.4		
28-NI- 58	6433	620	1.000- 4	(N,P)	0.3	(1)			9	-56		
28-NI- 60	6434	155	2.500+ 6	(N,P)	0.709	(5)			2	+6		
29-CU- 63	2920	68	1.120+ 7	(N,2N)	40.14	(2)			2.46	-2		
29-CU- 63	6435	620	1.000- 4	(N,GAMMA)	0.267	(1)			9	-35		
29-CU- 63	6435	163	1.700+ 6	(N,ALPHA)								
29-CU- 65	6436	80	1.000+ 7	(N,2N)								
30-ZN- 64	3020	171	9.600+ 5	(N,P)								
40-ZR- 90	4020	59	1.210+ 7	(N,2N)								
41-NB- 93	4120	209	1.350+ 5	(N,N') FIRST LEVEL								
45-RH-103	4520	215	1.000+ 5	(N,N') FIRST LEVEL	197.9	(2)			2.19	-9		
49-IN-115	6437	193	3.200+ 5	(N,N') FIRST LEVEL	125.7	(2)			2.96	-4		
49-IN-115	6437	620	1.000- 4	(N,GAMMA)			1.04	(4)			+12	+14
53-I -127	6438	88	9.200+ 6	(N,2N)	76.83	(2)			2.27	-1		
79-AU-197	6379	620	1.000- 4	(N,GAMMA)	84.7	(6)			17	-8		
90-TH-232	6390	410	5.000+ 0	FISSION								
90-TH-232	6390	620	1.000- 4	(N,GAMMA)								
92-U -235	6395	620	1.000- 4	FISSION	1204	(2)			1.61	+3		
92-U -238	6398	620	1.000- 4	FISSION	319.1	(2)			2.08	-2		
92-U -238	6398	620	1.000- 4	(N,GAMMA)								
93-NP-237	6337	620	1.000- 4	FISSION	1339	(2)			2.14	+1		
94-PU-239	6399	620	1.000- 4	FISSION	1798	(2)			1.83	+0.3		
95-AM-241	1009	620	1.000- 4	FISSION								

Table IV: Comparison to 235-U and 252-Cf Experimentally Measured Spectra Averages

REFERENCES FOR TABLE IV.

[1] DEZSOE, Z., and CSIKAI, J., Proc. Kiev Conf. on Neutron Phys., (1977) 32.

[2] MANNHART, W., Private Communication, P.T.B., Braunschweig, (1980).

[3] KOBAYASHI, K., and KIMURA, I., NEANDC(J)61, (1979) 81.

[4] KOBAYASHI, K., and KIMURA, I., INEANDC(J)67, (1980) 42-43.

[5] WINKLER, G., et al., Nuc. Sci. and Eng. 78, (1981) 415.

[6] DEZSOE, Z., and CSIKAI, J., Proc. VIIth Symposium on Interactions of Fast Neutrons, Gaussig, (1977).

PSF INTERLABORATORY COMPARISON

L. S. Kellogg and E. P. Lippincott
Westinghouse Hanford Company
Hanford Engineering Development Laboratory
Richland, Washington, U.S.A.

ABSTRACT

Two experiments for interlaboratory verification of radiometric analysis methods have been conducted with dosimeters irradiated in the Oak Ridge Research Reactor (ORR) Poolside Facility (PSF) Simulated Dosimeter Measurement Facility (SDMF). In preliminary analysis of data supplied by the six participants, biases as large as 60% were observed which could lead to errors of this general magnitude in reported surveillance capsule fluence values. As a result of these comparisons, problems were identified and the spread in final values was greatly reduced.

Relative agreement among the final results reported by four of the laboratories now appear to be satisfactory (the non-fission dosimeter results generally falling within ±5% and the fission dosimeter results within ±10%), though improvement is required in order to routinely meet Reactor Vessel Material Surveillance Program goals. Results from two of the laboratories, while not extremely out of these ranges, appear to be relatively consistantly biased. These results demonstrate the on-going need for periodic counting laboratory intercalibrations.

INTRODUCTION

It is currently accepted that the accuracy goal for reported neutron exposure parameters [flux and fluence (E<0.1 and 1.0 MeV) and dpa] is in the 5 to 15% (1σ) range in order to meet the Reactor Vessel Material Surveillance Program Requirements.[1,5] To achieve and maintain this level of accuracy, the reactor physics calculational and dosimetry measurement results must routinely be in the same range or better. It has been shown that this level of accuracy can be obtained but only through careful standardization, which include interlaboratory program work using benchmark (verification) facilities.[6-9] In support of this effort two experiments were designed and irradiated in the Oak Ridge Research Reactor Simulated Dosimeter Measurement Facility (ORR-SDMF) benchmark facility. The participation of those laboratories routinely involved in the analysis of Light Water Reactor (LWR) Surveillance capsules was enlisted to provide results to be compared with those obtained at HEDL [whose radiometric laboratory had previously been intercalibrated through the Interlaboratory Reaction Rate

(ILRR) program].[8,9] Four vendors (Babcock and Wilcox, Combustion Engineering, General Electric, and Westinghouse) and two service laboratories (Battelle Memorial Institute and Southwest Research Institute) volunteered their participation. These laboratories have been kept anonymous in the report of these intercomparisons.

EXPERIMENTAL DESCRIPTION

The Dosimeter sets fabricated at HEDL included six replicate samples of each dosimeter and were designed to minimize spatial effects. The design of typical capsules is illustrated in Figures 1 and 2. Capsules of similar design but without the gadolinium shield were also used in the first irradiation. This first experiment was included as an integral part of the PSF Surveillance Capsule Perturbation Experiment[6] and dosimeters were placed in both the Thermal Shield Back (TSB) and Pressure Vessel Face (PVF) simulated surveillance capsules. The location of the two capsules are shown in Figure 3. Figure 4 shows the dosimetry arrangement in each capsule. Those dosimetry capsules labeled HF and HNF contain the interlaboratory comparison samples. The HF capsules contain bare or Gd covered fissionable and Co/Al monitors arranged as in Figure 2. The HNF capsules have bare or Gd covered non-fission wires arranged as in Figure 1.

The second set of intercomparison samples was included in the first metallurgical simulated surveillance capsule (SSC-1) experiment.[10] Figure 5 shows the SSC-1 ORR-SDMF configuration and the dosimetry placement within the experiment is indicted in Figure 6. The HF comparison samples were placed in hole B-block 38 and the HNF samples in hole D-block 37.

After irradiation, the assemblies were dismantled at ORNL and the individual dosimeter capsules shipped to HEDL. The capsules were opened and the individual samples were identified by unloading sequence and sample weight or ID designation. All samples were counted at HEDL to provide both comparative HEDL absolute activities and also to provide a normalization base to compensate for any gradient or self shielding effects and eliminate any errors in the sample weights. Relative normalizations we e obtained at HEDL to an accuracy of better than 1.5%.

Along with the dosimeter sets, each participant was provided all basic information concerning the dosimetry materials, as well as the irradiation information provided by ORNL to allow calculation of both absolute specific activities and reation rates. These data included the individual dosimetry "As-Built" sheets (describing materials, form and encapsulation)[10], dosimeter (QA) information (Table 1) and the individual location and time history information (Table 2).

ANALYTICAL METHODS

All participating laboratories utilized high resolution Ge or GeLi detectors in conjunction with 2048 to 8196 multichannel analyzer systems for analysis of the dosimeter gamma spectra. Analysis of low activity reactions [e.g. $^{63}Cu(n,\alpha)^{60}Co$] was also made by a few of the participants

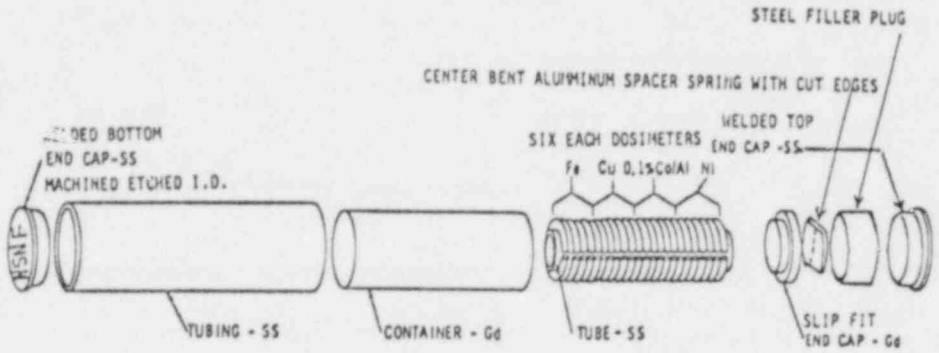

FIGURE 1. HEDL Surveillance Capsule - Non - Fissionable Materials
(1 Set HEDL/ Vendor/Service Laboratory Counting)

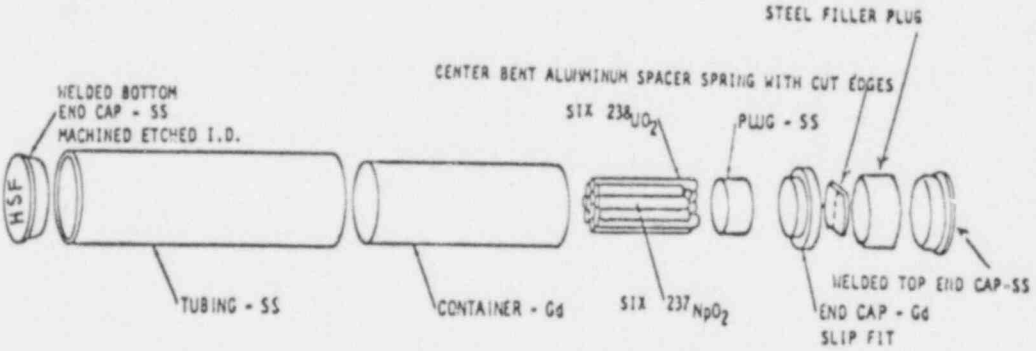

FIGURE 2. HEDL Surveillance Capsule - Fissionable Materials
(1 Set HEDL/Vendor/Service Laboratory Counting)

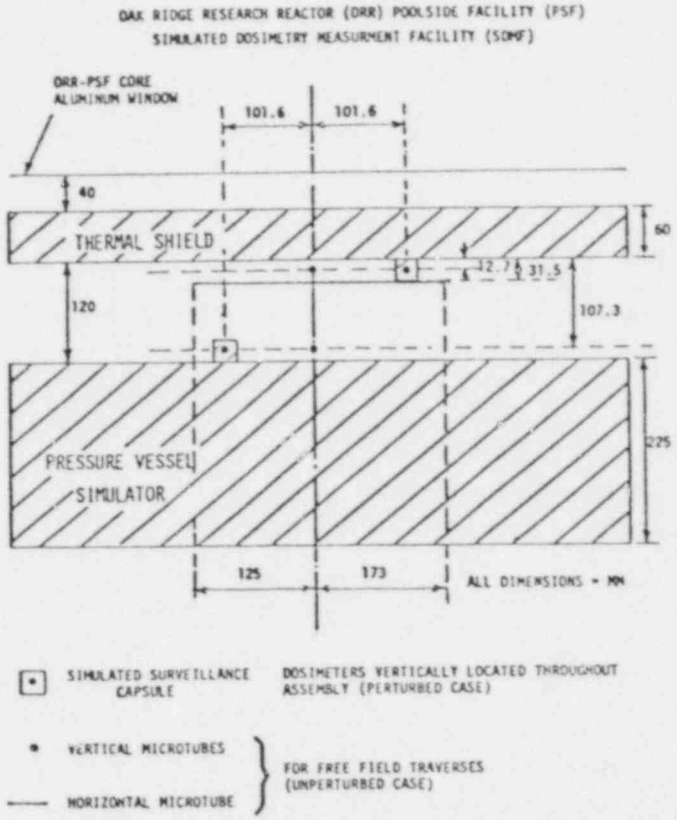

FIGURE 3. PSF-SDMF Perturbation Test Experimental Configuration (Horizontal Cut at Maximum Axial Flux)

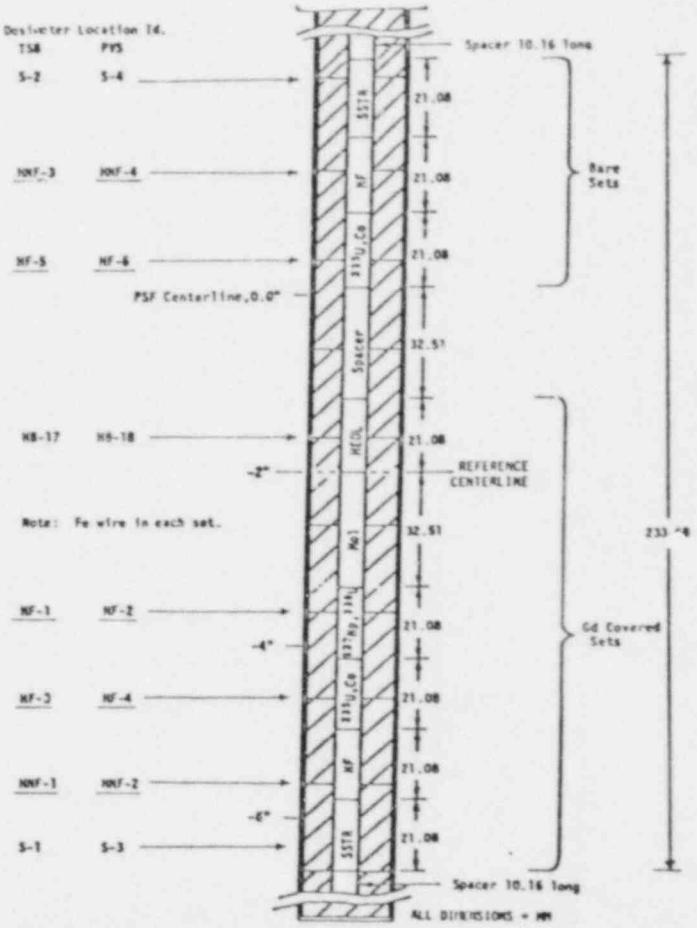

FIGURE 4. Axial Distribution of Dosimetry Sets in Similated Surveillance Capsule

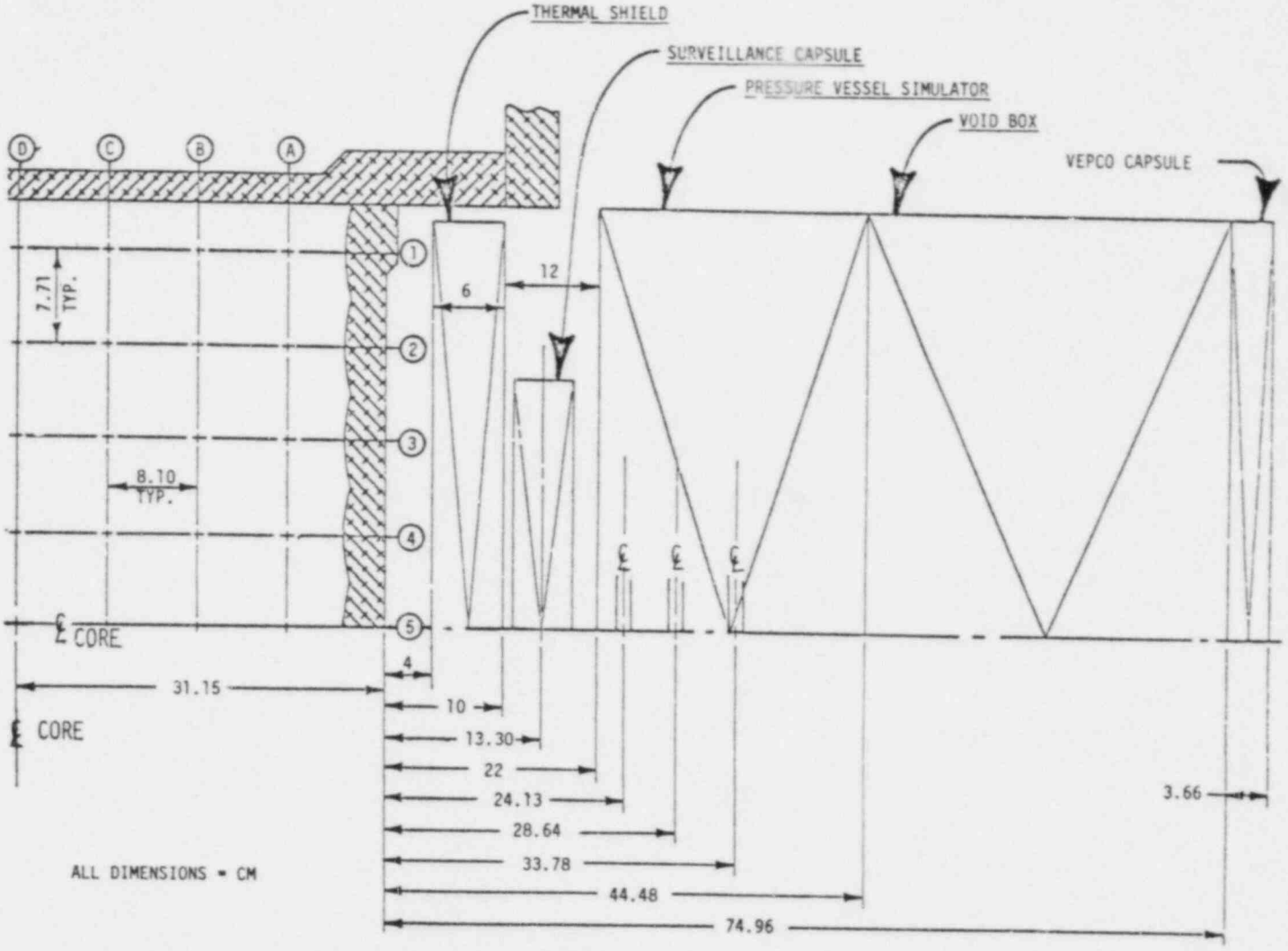

FIGURE 5 ORR-SDMF 4/12 Configuration (SSC-1)

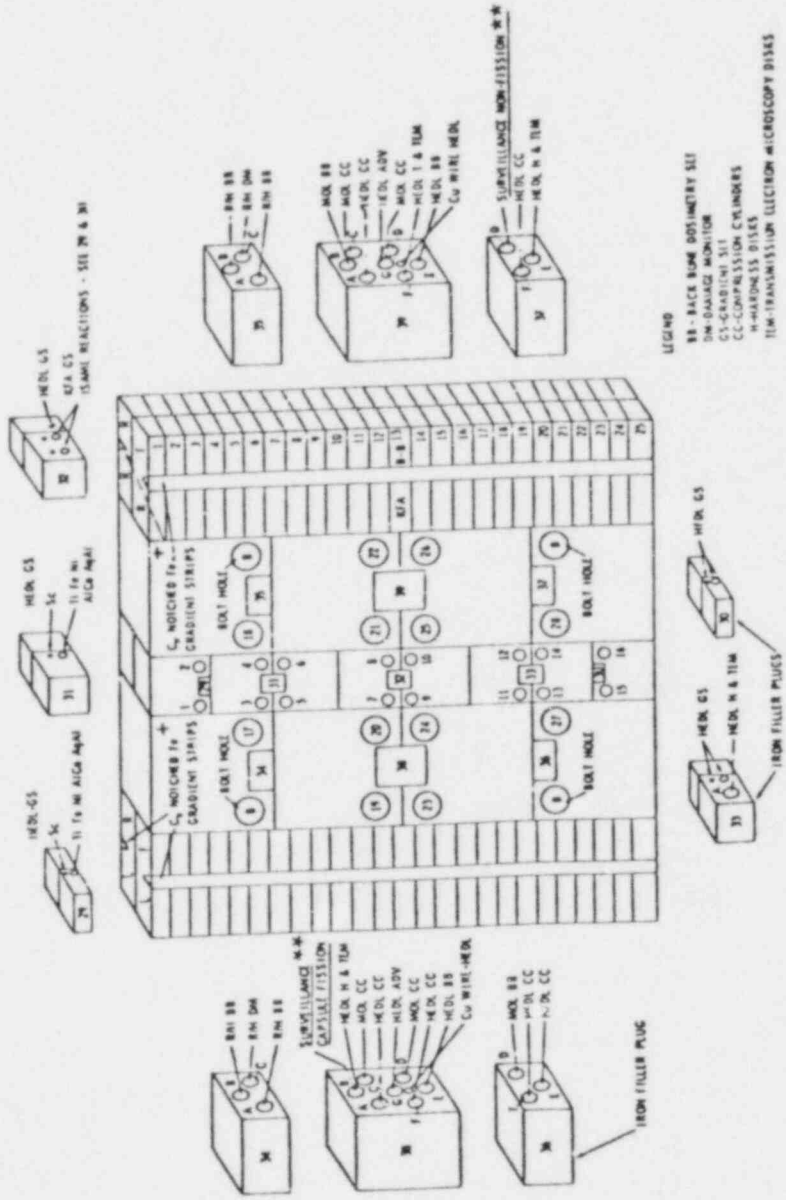

+Fe wire ~ 0.010" OD placed in ~ 0.020 OD ss tubing.
**Interlaboratory comparison dosimeters

Figure 6. SSC-1 Specimen Configuration

TABLE 1

DOSIMETRY FOIL QA DATA

Dosimeter	Form	ρ	Batch	Target Element[a,b] (wt.%)	Isotopic Wt. % [a,b] 233	234	235	236	237	238	239
^{235}U	18.6 mil UO_2 Wire	8.68	264C	87.97	<0.005	0.034(1)	99.89(1)	0.025(1)		0.053(2)	
^{238}U	17.5 mil UO_2 Wire	9.62	ES-Z	87.75	<0.001	<0.001	0.0012(1)	<0.001		99.999(1)	
^{237}Np	19.7 mil NpO_2 Wire	4.92	HP-24	87.4			<0.0005	<0.0005	99.99(1)	≤0.003	≤0.003

The above foils are encapsulated in 0.035" OD vanadium capsules (~40 ppm Ta impurity) wall thickness ~0.006".

Capsule lengths are: ^{235}U - 0.190", ^{238}U - 0.310", ^{237}Np - 0.340".

Dosimeter	Form	Batch	Isotopic	Target Element and Impurity Content (Wt.%) Ni	Fe	Cu	Ti	Co	Al	Ag	Cr	Mg	Si	Mn
Ni[a]	20 mil Wire (0.51 mm)	S.E.	Natural	Balance	<0.0003			<0.0001		<0.0001		<0.0002	<0.0003	
Fe[c]	20 mil Wire	2	"	0.0041	Balance			<0.0058			0.0018			
Cu[a,d]	20 mil Wire	CPO 3054	"			99.999		<0.0003		0.0002		0.0001	0.0001	
Ti[a]	20 mil Wire	139 W	"		0.008	0.001	99.917		0.0001		0.003	0.001	0.005	0.02
Co/Al[a]	20 mil Wire	SRM 953	"					0.116	Balance					

(a) Elemental, isotopic and/or impurity analysis provided by vendor. Assigned errors, i.e. (1), represents value error in the last significant figures.
(b) QA also performed at HEDL. Values supplied by ORNL were confirmed within the error assignments.
(c) Impurity analysis performed at HEDL utilizing activation analysis. Analysis was not made for impurity products with t 1/2 <~2 hr.
(d) Co analysis was made at HEDL by spark source mass spectrometry.

TABLE 2

IRRADIATION HISTORY AND LOCATION

FIRST ORR-SDMF IRRADIATION
(Perturbation Experiment)

Start of Irradiation	1530 EST	1/31/80
End of Irradiation	1530 EST	2/9/80
Total Duration		9.00 days
Nominal Reactor Power		30 MW

Irradiation can be treated as a square wave function.

Sample locations

X coordinate: TSB - 101.6 mm South of Core C_L

PVS - 101.6 mm North of Core C_L

Y coordinate: Referenced to ORR Core Al window:

TSB - 112.7 mm

PVS - 207.3 mm

Z coordinate: Approximate location referenced between Reference Core C_L(maximum flux) rather than actual Core C_L and approximate location of mid-point of each replicate sample group. Actual sample position depends on sample location within set and adjustments will be made later if required.

Gadolinium Covered Capsules: HF-1, HF-2, HF-3, HF-4, HNF-1, HNF-2

Bare Capsules: HF-5, HF-6, HNF-3, HNF-4

SECOND ORR-SDMF IRRADIATION
(SSC-1 Experiment)

Inserted	Retracted or ORR Down
April 30, 1980 13:34	
May 8, 1980 16:43	May 8, 1980 7:00
May 16, 1980 9:67	May 14, 1980 13:30
May 22, 1980 10:49	May 21, 1980 2:17
June 12, 1980 9:20	June 6, 1980 24:00
	June 23, 1980 12:53

(All times Eastern Daylight Time)

Nominal Reactor Power 30MW

Sample Locations

X coordinate: HSF 38B 49.9 mm South of Core C_L

HSNF 37D 47.2 mm North of Core C_L

(individual dosimeter locations vary from this mid point location)

Y coordinate: Referenced to ORR Al window

HSF 38B 133.0 mm

(individual dosimeters may vary by ± 1.1 mm)

HSNF 37D 139.9 mm

Z coordinate: Referenced to Reference Core C_L (maximum flux) rather than actual Core C_L and mid point of each capsule. Actual position of individual HSF samples may vary by ± 1.1 mm

HSF 38B 7.9 mm

HSNF 37D -67.5 mm

using NaI(Tl) detectors. All non-fissile dosimeters were analyzed non-destructively but some of the participating laboratories destructively analyzed the fissionable dosimeters in accordance with their routine surveillance capsule dosimeter techniques. Difficulties were encountered by some of the participants due to the much higher activities of some of the dosimeters compared to the routine surveillance sample activities normally encountered.

REVIEW OF INITIAL DATA

An initial review of the individual preliminary results was conducted. Outlying values were anticipated but consistant discrepancies as large as 60% were observed. Individual discussions were held with each participant concerning their data and the possible discrepancies that existed. Analytical and calibration techniques, nuclear parameters being used and corrections identified and applied to the observed counting data were reviewed. In almost all cases at least one or more problems were identified, though some were relatively insignificant. Some of the more important problems identified, and their affect on the reported data, are shown in Table 3.

COUNTING RESULTS

All final reported specific activities, calculated to end of irradiation (EOI), are listed in Tables 4 and 5 (not all participants reported reaction rates). To determine the range of values that might be expected from the laboratories performing the analysis, the participants' data was first normalized using the HEDL observed sample to mean ratio and the ratio of the highest to lowest reported result determined. These maximum range values, including those calculated after the first corrections had been received, are listed in Table 6. The absolute HEDL values were not included in this comparison and correlation of the individual measured activities to the HEDL measured activities are presented separately in Table 7.

TABLE 3

IDENTIFIED PROBLEMS AND ESTIMATED EFFECT

Problem	Effect on Data
1. Faulty calibration standards	10 to 100% depending on energy region
2. Faulty nuclear parameter data	0 to 2% on specific results
3. No correction for external or self shielding	0 to 4% depending upon reaction and analysis technique
4. Error in conversion of specific activity to reaction rate	0% on specific activity up to 4% on specific reaction rates
5. No coincidence loss corrections for high count rate samples	Estimated at up to 6%

TABLE 4

INTERLABORATORY COMPARISON OF RADIOMETRIC(RM) DATA FIRST ORR-SDMF TEST

Non Fission Foil Sets DPS/mg @ EOI (a)

Dosimeter Set Reaction	Laboratory	HNF-1 (E+5)		HNF-3 (E+5)		HFN-2 (E+4)		HNF-4 (E+4)	
$^{58}Ni(n,p)$	A	4.60	4.493	4.26	4.170	8.17	7.984	7.73	7.480
	B	4.18	4.497	3.90	4.164	7.30	7.986	6.78	7.470
	C	4.33	4.510	4.04	4.192	7.98	7.968	7.43	7.493
	D	4.58	4.486	4.22	4.163	7.97	8.045	7.50	7.465
	E[b]	4.44	4.512	4.05	4.158	7.79	8.016	7.32	7.472
	F	4.430	4.510	4.187	4.177	8.203	8.027	7.728	7.438
		(E+3)		(E+3)		(E+3)		(E+3)	
$^{46}Ti(n,p)$	A	5.72	5.59[c]	5.43	5.371	1.22	1.154	1.17	1.119
	B	5.00	5.59	4.65	5.40	1.07	1.157	1.11	1.125
	C	5.75	5.55	5.55	5.30	1.24	1.159	1.21	1.122
	D	5.68	5.60	5.49	5.37	1.23	1.163	1.17	1.119
	E[b]	5.56	5.60	5.23	5.343	1.16	1.170	1.11	1.107
	F	5.677	5.557	5.427	5.33	1.206	1.141	1.175	1.130
		(E+1)		(E+1)		(E+1)		(E+1)	
$^{63}Cu(n,\alpha)$	A	8.19	8.048	7.89	7.688	1.90	1.880	1.91	1.825
	B	7.98	8.166	7.63	7.509	1.88	1.854	1.82	1.787
	C	8.56	8.031	8.11	7.870	2.02	1.864	1.90	1.784
	D	8.06	8.069	7.87	7.730	1.92	1.864	1.82	1.814
	E[b]	7.82	8.002	7.56	7.714	1.84	1.851	1.78	1.819
	F	8.444	7.815	7.946	7.789	1.994	1.886	1.935	1.811
		(E+3)		(E+3)		(E+3)		(E+3)	
$^{54}Fe(n,p)$	A	6.86	6.659	6.67	6.633	1.26	1.233	1.23	1.155
	B	6.27	6.692	5.93	6.608	1.15	1.245	1.08	1.168
	C	6.89	6.758	6.58	6.573	1.27	1.248	1.25	1.194
	D	6.79	6.646	6.45	6.600	1.25	1.234	1.20	1.182
	E[b]	6.70	6.674	6.40	6.622	1.21	1.260	1.18	1.172
	F	6.650	6.628	6.289	6.560	1.242	1.239	1.160	1.183
		(E+3)		(E+4)		(E+3)		(E+4)	
$^{58}FE(n,\gamma)$	A	6.45	6.352	6.71	6.688	8.32	8.746	2.29	2.246
	B		6.530		6.630		9.067		2.241
	C		6.569		6.627		9.104		2.240
	D		6.517		6.654		8.950		2.244
	E[b]	6.62	6.542	6.62	6.674	8.78	9.049	2.32	2.247
	F		6.610		6.540		8.948		2.249

(a) The first column under each heading are those data reported by the participants, with any subsequent corrections made by HEDL. The second column of data is the corresponding HEDL analysis. Results are to exponent in parenthesis [e.g., 4.60 (E+5) reads 4.60×10^5].

(b) The participant reported the specific activity as per mg target isotope. For comparison with the other reported values, the reported numbers were multiplied by the atom fraction used by the participant.

(c) Only two absolute counts were made on these sets. All of the samples in these sets were counted on a non-calibrated system for determination of the relative ratios. Correlations were made between those samples counted on both systems and absolute values were than calculated for the remaining samples in the sets.

TABLE 5

INTERLABORATORY COMPARISON OF RADIOMETRIC(RM) DATA
FIRST ORR-SDMF TEST

Fission Foil Se - DPS/mg @ EOI

Dosimeter Set	Laboratory	$^{235}U(n,f)$ (a) ^{140}Ba (E+5)		^{105}Ru (E+5)		^{95}Zr		^{137}Cs (E+3)	$^{59}Co(n,\gamma)$ (E+5)	
MF-3	A	25.2	25.20	51.3	48.73	69.			34.0	33.06
	B (b)		25.82		49.73	F			32.3	32.81
	C (b)		24.58	40.9	47.06			31.6	35.5	33.04
	D (c)	24.4	25.51	46.9	48.44			35.5	31.6	31.26
	E	23.2	24.85	48.1	47.68	60.6		35.4	33.0	33.29
	F		24.94		47.95		62.92		30.6	30.93
MF-5	A	361	329.8	651	601.3	858	812.0		172	171.9
	B (b)		326.5		588.7	668	780.4		161	173.9
	C (b)		330.9	640	602.6	875	800.6	470	184	173.0
	D (c)	294	324.5	528	580.2	788	770.6	535	168	169.7
	E	321	335.3	605	595.8	787	810.8	462	165	167.7
	F		327.2		586.1		781.9		172	172.9
MF-4	A	3.38	3.409	6.72	6.505	8.49	8.699		4.08	3.989
	B (b)		3.555		6.543	8.50	9.101		3.90	3.973
	C (b)		3.497	6.15	6.521	8.02	9.059	4.57	4.33	4.019
	D (c)	3.32	3.586	6.47	6.641	9.25	9.259	4.69	4.04	3.978
	E	3.37	3.561	6.77	6.562	8.39	9.155	4.87	3.98	3.873
	F		3.670		6.666		9.322		4.110	4.058
MF-6	A	123.	126.7	228	214.3	304	294.7		52.9	51.89
	B (b)		121.9		202.9	267	274.9		48.8	53.75
	C (b)		121.9		204.0	250	277.4	156	58.0	54.33
	D (c)	106	124.4	193	210.2	290	285.6	152	57.2	55.15
	E	111	127.7	215	212.9	278	293.3	167	52.8	53.06
	F		130.3		214.7		296.8		58.8	57.45

Dosimeter Set	Laboratory	$^{237}Np(n,f)$ (E+5)		(E+4)		(E+4)		(E+2)
MF-1	A	11.2	11.08	44.5	45.18	27.1	27.27	
	B (b)		11.80		44.12	30.7	27.76	
	C (b)		11.67	39.6	43.10	29.8	27.26	16.9
	D	11.0	11.75	41.8	43.71	28.8	27.66	18.6
	E	10.3	11.61	43.2	43.60	26.1	27.30	17.6
	F	10.5	11.12	39.7	41.38	25.6	25.98	18.5
MF-2	A	1.35	1.307	5.24	5.033	3.23	3.167	
	B (b)		1.375		5.032	3.41	3.236	
	C (b)		1.406	4.79	5.147	3.16	3.318	2.16
	D	1.31	1.322	5.12	4.975	3.52	3.185	2.09
	E	1.20	1.582	4.99	5.159	3.12	3.210	2.13
	F	1.27	1.310	4.92	5.040	3.18	3.220	2.27

Dosimeter Set	Laboratory	$^{238}U(n,f)$ (E+8)		(E+8)		(E+8)		(E+1)
MF-1	A	17.4	16.90	7.06	6.693	35.5	34.98	
	B (b)		16.98		6.823	35.9	34.99	
	C (b)		17.67	6.71	7.011	34.4	36.52	24.8
	D	16.8	16.46	6.46	6.587	36.3	33.44	23.6
	E	16.0	16.95	6.79	6.759	34.2	35.10	25.8
	F	17.1	17.16	6.51	6.865	34.1	35.64	25.4
MF-2	A	2.79	2.722	1.11	1.070	0.572	0.5812	
	B (b)		2.740		1.056	0.596	0.5708	
	C (b)		2.695	0.922	1.033	0.558	0.5802	3.74
	D	2.65	2.792	1.08	1.057	0.616	0.5847	4.15
	E	2.49	2.679	1.01	1.036	0.530	0.5676	3.81
	F	2.74	2.777	1.04	1.059	0.555	0.5750	4.02

(a) The first column under each heading are those data reported by the participant with any necessary corrections. The second column is the corresponding HEDL data. The value in parens (E+5) is the exponent for the data following it ((E+5) 25.2 should read 25.2×10^5).

(b) Corrections were made for elemental and isotopic composition.

(c) Correction made for Co alloy content

TABLE 6

INTERLABORATORY COMPARISON OF RADIOMETRIC (RM) ANALYSIS PROCEDURES AND DATA[a]
[Range Evaluation (Maxima/Minima) of RM Results Based on First PSF-SDMF TEST]

Sensor[b] Set No.	$^{58}Ni(n,p)$ Ratio 1	Ratio 2	Ratio 3	Labs	$^{46}Ti(n,p)$ Ratio 1	Ratio 2	Ratio 3	Labs	$^{63}Cu(n,\alpha)$ Ratio 1	Ratio 2	Ratio 3	Labs	$^{54}Fe(n,p)$ Ratio 1	Ratio 2	Ratio 3	Labs
HNF - 1	1.14 C/B	1.10 A/B	1.07 A/C	6	1.39 C/B	1.16 C/B	1.04 C/E	6	1.11 F/B	---	1.09 F/E	6	1.38 C/B	1.10 A/B	1.03 A/F	6
HNF - 3	1.28 C/B	1.09 A/B	1.05 A/C	6	1.48 C/B	1.21 C/B	1.07 C/E	6	1.05 C/E	1.06 C/F	---	6	1.27 C/B	1.12 A/B	1.06 A/F	6
HNF - 2	1.25 C/B	1.13 F/B	1.06 F/E	6	1.42 C/B	1.14 A/B	1.07 A/E	6	1.06 C/E	1.09 C/E	---	6	1.46 C/B	1.11 A/B	1.07 A/E	6
HNF - 4	1.28 C/B	1.14 F/B	1.06 F/E	6	1.41 C/B	1.09 C/B	1.08 C/E	6	1.08 C/E	1.09 F/E	---	6	1.43 C/B	1.15 A/B	1.09 A/E	6

	$^{58}Fe(n,\gamma)$ Ratio 1	Ratio 2	Ratio 3	Labs
HNF - 1	1.15 C/A	1.03 E/A	1.03 E/A	3[c]
HNF - 3	1.02 C/E	1.02 A/E	1.02 A/E	3
HNF - 2	1.23 C/A	1.04 E/A	1.04 E/A	3
HNF - 4	1.12 C/E	1.01 A/E	1.01 A/E	3

Sensor Set No.	$^{59}Co/Al(n,\gamma)$ Ratio 1	Ratio 2	Ratio 3	Labs
HF - 3	1.15 C/B	1.04 C/B	1.04 A/F	6
HF - 5	1.15 C/B	1.15 C/B	1.08 C/E	3
HF - 4	1.06 F/B	1.10 C/B	1.06 C/F	6
HF - 6	1.23 C/B	1.17 C/B	1.07 C/E	6

	$^{235}U(n,f)^{140}Ba$ Ratio 1	Ratio 2	Ratio 3	Labs	$^{235}U(n,f)^{103}Ru$ Ratio 1	Ratio 2	Ratio 3	Labs	$^{235}U(n,f)^{95}Zr$ Ratio 1	Ratio 2	Ratio 3	Labs	$^{235}U(n,f)^{137}Cs$ Ratio 1	Ratio 2	Ratio 3	Labs
HF - 3	1.07 A/E	---	---	3	1.19 C/D	1.21 A/C	1.09 A/D	4	1.09 D/C	1.17 A/C	1.04 A/F	5	---	1.11 E/C	---	3
HF - 5	1.20 A/D	---	---	3	1.73 C/D	1.19 A/D	1.05 A/E	4	1.51 C/B	1.28 C/B	1.09 D/E	5	---	1.14 C/D	---	3
HF - 4	1.07 A/D	---	---	3	1.30 C/D	1.09 E/C	---	4	1.13 D/C	1.14 D/C	1.09 D/E	5	---	1.05 E/C	---	3
HF - 6	1.13 A/D	---	---	3	1.43 C/D	1.14 A/D	---	4	1.15 C/E	1.14 A/C	1.09 A/E	5	---	1.07 E/D	---	3

	$^{237}Np(n,f)^{140}Ba$ Ratio 1	Ratio 2	Ratio 3	Labs	$^{237}Np(n,f)^{103}Ru$ Ratio 1	Ratio 2	Ratio 3	Labs	$^{237}Np(n,f)^{95}Zr$ Ratio 1	Ratio 2	Ratio 3	Labs	$^{237}U(n,f)^{137}Cs$ Ratio 1	Ratio 2	Ratio 3	Labs
HF - 1	1.14 A/F	---	1.08 A/D	4	1.37 C/F	1.11 A/C	1.08 A/D	5	1.16 A/E	1.21 B/C	1.04 A/E	6	---	1.15 F/C	1.09 D/C	4
HF - 2	1.19 A/E	---	1.06 A/F	4	1.27 C/F	1.12 A/C	1.08 A/E	5	1.16 D/C	---	---	6	---	1.12 F/D	1.03 E/D	4

	$^{238}U(n,f)^{140}Ba$ Ratio 1	Ratio 2	Ratio 3	Labs	$^{238}U(n,f)^{103}Ru$ Ratio 1	Ratio 2	Ratio 3	Labs	$^{238}U(n,f)^{95}Zr$ Ratio 1	Ratio 2	Ratio 3	Labs	$^{238}U(n,f)^{137}Cs$ Ratio 1	Ratio 2	Ratio 3	Labs
HF - 1	1.09 A/E	---	1.04 A/F	4	1.44 C/F	1.11 A/F	1.06 E/F	5	1.16 C/F	1.15 D/C	1.04 A/E	6	---	1.08 E/C	---	4
HF - 2	1.09 A/E	---	---	4	1.27 C/F	1.16 A/C	1.06 A/E	5	1.13 D/E	1.08 B/C	---	6	---	1.09 D/C	---	4

(a)Four vendors and two service laboratories participated in this test. All laboratories remain anonymous for these intercomparisons and are identified only as Laboratories A, B, C, D, E and F. The table evaluation shows the present laboratory-to-laboratory comparative status but also shows the improvement in the data comparisons (Ratios 2 and 3) as a result of interim evaluations and discussions with participants. Ratio 2 was obtained after discussions with participants and subsequent reworking of data by participants. For Ratio 3, and for the case of nonfissile sensors, the results from Laboratory B appeared to be consistently biased low and were, therefore, not used. In the case of the fissile sensors, if a participant appeared to be definitely biased, those results were not used in Ratio 3.

(b)HNF-X and HF-X are sensor set identification numbers for specific perturbed locations in 1-in. x 1-in. stainless steel simulated surveillance capsules for this first PSF-SDMF test.

(c)Results for the $^{58}Fe(n,\gamma)$ reaction were not reported by one laboratory after preliminary recalibration of their counting system.

TABLE 7

RELATIVE RATIO FIRST ORR-SDMF TEST (X/HEDL)-1 %

Set ID	Reaction	LABORATORY A	B	C	D	E	F
HNF-1	$^{58}Ni(n,p)$	2.38	- 7.05	-3.99	2.10	-1.60	-1.77
-3		2.16	- 6.34	-3.63	1.37	-2.60	0.24
-2		2.33	- 8.59	0.15	-0.93	-2.82	2.69
-4		3.34	- 9.24	-0.84	0.47	-2.03	3.90
HNF-1	$^{46}Ti(n,p)$	2.33	-10.6	3.60	1.43	-0.71	2.16
-3		1.10	-13.9	4.72	2.23	-2.11	1.82
-2		5.72	-7.52	6.98	5.76	-0.85	5.26
-4		4.56	-1.33	7.84	4.56	0.27	3.98
HNF-1	$^{63}Cu(n,\alpha)$	1.76	-3.38	8.59	-1.12	-2.27	8.05
-3		2.63	1.61	3.05	1.81	-2.00	2.01
-2		1.36	1.40	8.37	3.00	0.59	5.73
-4		4.66	1.85	6.50	2.00	2.14	6.85
HNF-1	$^{54}Fe(n,p)$	3.02	-6.31	1.95	-3.73	0.39	-5.37
-3		0.56	-10.26	0.11	-2.27	-3.35	-4.13
-2		2.19	-7.63	1.76	1.30	-3.96	0.24
-4		6.49	-7.53	4.69	1.52	0.68	-1.94
HNF-1	$^{58}Fe(n,\gamma)$	1.54				1.19	
-3		3.29				0.81	
-2		-4.87				-2.97	
-4		1.96				3.25	
HNF-3	$^{59}Co(n,\gamma)$	2.84	-1.55	7.45	1.09	1.83	-1.07
-5		0.06	-7.42	6.36	-1.00	-1.61	-0.52
-4		2.28	-1.84	7.74	1.56	2.82	1.28
-6		1.95	-9.21	6.76	3.72	-0.49	2.35

Set ID	Reaction	LABORATORY A	B	C	D	E	F
HF-3	$^{235}U(n,f)^{140}Ba$	0.00			- 4.35	- 6.68	
HF-5		9.46			- 9.40	- 4.26	
HF-4		9.39			- 7.42	- 5.36	
HF-6		-2.92			-14.79	-13.08	
HF-3	$^{235}U(n,f)^{103}Ru$	5.27		-13.09	- 3.18	0.88	
HF-5		8.27		6.21	- 9.60	1.54	
HF-4		3.31		- 5.59	- 2.57	3.17	
HF-6		6.39		- 6.37	- 8.18	0.99	
HF-3	$^{235}U(n,f)^{95}Zr$	0.76	0.00	-13.49	4.99	- 2.84	
HF-5		5.67	-14.40	9.29	2.26	- 3.31	
HF-4		-2.40	- 6.49	-11.47	- 0.10	- 8.36	
HF-6		3.16	- 1.78	- 6.99	1.54	- 5.22	
HF-1	$^{237}Np(n,f)^{140}Ba$	1.27			- 6.38	-11.28	-5.58
HF-2		3.29			- 0.91	-13.29	-3.05
HF-1	$^{237}Np(n,f)^{103}Ru$	3.06		-31.26	- 4.37	- 0.92	-4.06
HF-2		4.11		- 6.94	2.91	- 3.28	-2.38
HF-1	$^{237}Np(n,f)^{95}Zr$	-0.22	10.59	- 9.06	4.12	- 4.40	-1.46
HF-2		1.99	5.38	- 4.76	10.83	- 2.80	-1.24
HF-1	$^{238}U(n,f)^{140}Ba$	2.96			- 2.19	- 5.60	-0.35
HF-2		0.65			- 0.40	- 7.05	-1.33
HF-1	$^{238}U(n,f)^{103}Ru$	5.48		- 4.29	- 1.93	0.46	-5.17
HF-2		3.74		1.65	2.08	- 2.51	-1.79
HF-1	$^{238}U(n,f)^{95}Zr$	1.72	2.60	- 5.81	8.55	- 2.56	1.37
HF-2		-1.58	4.41	- 2.83	5.35	- 6.62	-3.48

TABLE 8

INTERLABORATORY COMPARISON OF RADIOMETRIC (RM) DATA
SECOND PSF-SDMF TEST

Non-Fission Foil Sets (DPS/mg @ EOI)[a]

Dosimeter Set	Laboratory	Reaction					
		$^{58}Ni(n,p)$ (E+6)		$^{63}Cu(n,\alpha)$ (E+2)		$^{54}Fe(n,p)$ (E+4)	
HSNF	A	1.16	1.144	2.41	2.389	2.06	2.020
	B		1.137		2.377		2.016
	C-1[b]	1.03	1.138	2.31	2.399	1.87	2.019
	C-2	1.06		2.35		1.95	
	D	1.13	1.141	2.43	2.386	2.01	1.995
	E		1.141		2.400		2.011
	F		1.132		2.384		2.003
		$^{58}Fe(n,\gamma)$ (E+4)		$^{59}Co(n,\gamma)$ (E+4)			
HSNF	A	1.82	1.818	1.40	1.382		
	B		1.825		1.391		
	C-1[b]	1.79	1.836	1.33	1.390		
	C-2	1.84		1.37			
	D	1.84	1.801	1.42	1.397		
	E		1.628		1.383		
	F		1.836		1.834		

(a) The first column listed under each heading are those data reported by the participants, the second column is the HEDL data. The number in parens is the exponent for those numbers following [eg. 1.16 (E+6) should read 1.16×10^6].

(b) Two individuals ran separate analyses for this laboratory and both values are reported.

A comparison of the relative ratios listed in the vertical columns of Table 7 demonstrates whether a particular laboratory appears to be consistently biased. It would appear that laboratory B is generally biased low by ~6 to 10%, and laboratory C appears generally biased high by ~4 to 7%. By reading across this table, one can observe whether an apparent bias exists in the analysis of a particular dosimeter reaction. It appears that the HEDL analysis of both the $^{63}Cu(n,\alpha)$ and $^{46}Ti(n,p)$ reactions appear biased low by ~2% relative to the other labs.

The individual results for the second ORR-SDMF test are listed in Tables 8 and 9. Unfortunately, only three of the six laboratories have reported results at this time. Two separate sets of results are reported by laboratory C. Counting was done by two different individuals and since a difference was observed, both sets of results were reported and are treated separately in the comparisons. It was anticipated this second test would show improved correlations and indeed the ratios relative to HEDL, Table 10, indicate a consistently better agreement. All comparisons with two of the three reporting participants fall within ~±4%. Laboratory C still appears to be biased, though this time a low bias is indicated while the first test indicated a high bias.

TABLE 9

INTERLABORATORY COMPARISON OF RADIOMETRIC (RM) DATA -- SECOND PSF-SDMF TEST

Fission Foil Sets -- DPS/mg @ EOI[a]

Dosimeter Set	Laboratory	$^{238}U(n,f)$ $^{140}Ba(n,f)$ (E+5)	$^{103}Ru(n,f)$ (E+5)		$^{95}Zr(n,f)$ (E+5)		$^{137}Cs(n,f)$ (E+2)	
HNF-388	A	3.064	2.05	2.003	1.15	1.159		10.95
	B	3.153		2.053		1.207		10.92
	C-1[b]	2.863	1.74	1.975	1.01	1.142	9.40	11.30
	C-2		1.80		1.05	(1.16)	9.68	(10.4)
	D	3.093		1.998		1.163	10.3	10.16
	E	3.089		2.034		1.183		10.96
	F	2.989		2.022		1.174		10.50

Dosimeter Set	Laboratory	$^{237}Np(n,f)$ $^{140}Ba(n,f)$ (E+6)	$^{103}Ru(n,f)$ (E+5)		$^{95}Zr(n,f)$ (E+5)		$^{137}Cs(n,f)$ (E+3)	
HNF-388	A	2.017	1.36	1.315	9.42	9.571		8.368
	B	1.956		1.287		9.375		8.156
	C-1[b]	2.097	1.22	1.351	8.72	9.793	7.82	8.484
	C-2		1.21		8.65	(9.24)	7.73	(8.37)
	D	2.005		1.302		9.431	8.31	8.169
	E	2.081		1.310		9.456		8.591
	F	2.088		1.332		9.602		9.308

[a] The first column listed under each heading are those data reported by the participants, the second column is the HEDL data. Result exponents are given in parens [eg. 3.064 (E+5) should read 3.064×10^5].

[b] Two individuals ran separate analyses for this laboratory and both values are reported. The values in parens are from recent counts and were used in the C-2 comparison for Table 10.

TABLE 10

RELATIVE RATIO SECOND ORR-SDMF TEST [X/HEDL -1] %

Reaction		Laboratory A	B	C-1	C-2	D	E	F
$^{58}Ni(n,p)$		1.40		- 9.57	- 6.85	-0.96		
$^{63}Cu(n,\alpha)$		0.88		- 3.71	- 2.04	1.84		
$^{54}Fe(n,p)$		1.98		- 7.38	- 3.42	0.75		
$^{58}Fe(n,\gamma)$		0.11		- 2.51	0.22	2.17		
$^{59}Co(n,\gamma)$		1.30		- 4.32	- 1.44	1.65		
$^{237}Np(n,f)$	^{103}Ru	3.42		- 9.70	-10.4			
	^{95}Zr	- 1.58		-10.9	- 5.6			
	^{137}Cs			- 7.83	- 1.34	1.73		
$^{238}U(n,f)$	^{103}Ru	2.09		-11.9	- 8.86			
	^{95}Zr	- 0.78		-11.6	1.58			
	^{137}Cs			-16.8	-7.96	1.38		

CONCLUSIONS

Intercomparisons of dosimetry results from six service laboratories have provided exprimental estimates of accuracies of measured reaction rates. Preliminary results were distributed over a range of relative values as large as 60%. Had results from a single laboratory been used to derive surveillance capsule fluence values, which are often based on only one or two reactions, a bias of 40% or more could easily have been introduced. Following discussions of the preliminary analysis results and identification of existing problems, these biases were generally reduced to below 15%.

While the agreement among the majority of the laboratories participating in the interlaboratory comparisons is generally satisfactory (non-fissile dosimeter results generally falling within ±5% and the fissionable dosimeter results falling within ±10%.), improvement is still required in order to routinely meet the Reactor Vessel Materials Surveillance Program Requirement goals. The results obtained from these tests along with the subsequent corrections indicate that a critical review of both analytical and calculational techniques must be conducted on a periodic basis by all of the laboratories. In addition, it is recommended that each laboratory review and utilize, where possible, the appropriate ASTM Standard Methods and Guides, maintain system calibration and/or control documentation, and continue in this or similar programs utilizing existing benchmark facilities for verification purposes and direct correlations.

REFERENCES

1. ASTM Standard E706-81, "Master Matrix for LWR Pressure Vessel Surveillance Standards," 1981 Annual Book of ASTM Standards, American Society for Testing and Materials, Philadelphia, PA, 1981.

2. W. N. McElroy, "Surveillance Dosimetry of Nuclear Power Plants," Fourth ASTM-EURATOM Symposium on Reactor Dosimetry, Washington, DC, March 1982.

3. W. N. McElroy et al., LWR Pressure Vessel Surveillance Dosimetry Improvement Program: PCA Blind Test, NUREG/CR-1861, HEDL-TME 80-81 Hanford Engineering Development Laboratory, Richland, WA, July 1981.

4. F. J. Rahn et al., "Trends in Light Water Reactor Dosimetry Programs," Proceedings of the Second ASTM-EURATOM Symposium on Reactor Dosimetry, NUREG/CR-0004 Vol. III, p. 1064, US Nuclear Regulatory Commission, Washington, DC, October 1977.

5. F. B. K. Kam, compiler, Proceedings of the Second ASTM-EURATOM Symposium on Reactor Dosimetry, Washington, DC, March 1982. (in preparation)

6. H. Tourwe, G. Minsart, "Surveillance Capsule Perturbation Studies in the PSF 4/12 Configuration," Fourth ASTM-EURATOM Symposium on Reactor Dosimetry, Washington, DC, March 1982.

7. W. N. McElroy et al., LWR Pressure Vessel Surveillance Dosimetry Improvement Program: 1980 Annual Report, NUREG/CR-1747, HEDL-TME 80-73, Hanford Engineering Development Laboratory, Richland, WA, April 1981.

8. R. C. Greenwood et al., "Radiometric Reaction Rate Measurements in CFRMF and BIG-10," Proceedings of the Second ASTM-EURATOM Symposium on Reactor Dosimetry, NUREG/CP-0004 Vol. III, p. 1207, US Nuclear Regulatory Commission, Washington, DC, October 1977.

9. D. M. Gilliam et al., "Reference and Standard Benchmark Field Concensus Fission Yields for US Reactor Dosimetry Programs," NUREG/CP-0004 Vol. III, p. 1289, US Nuclear Regulatory Commission, Washington, DC, October 1977.

10. E. P. Lippincott et al., Fabrication Data Package for HEDL Dosimetry in the ORNL Poolside Facility LWR Pressure Vessel Mockup Irradiation, HEDL-TC-2065, Hanford Engineering Development Laboratory, Richland, WA, September 1981.

Session C.3
Fusion-II

TOKAMAK FUSION TEST REACTOR FUSION-REACTION-PRODUCTS DIAGNOSTICS*

H. W. Hendel,+ K. Matsuoka,++ and L. E. Samuelson
Princeton University Plasma Physics Laboratory
Princeton, NJ, USA

ABSTRACT

The Tokamak Fusion Test Reactor (TFTR) at Princeton University Plasma Physics Laboratory has been designed to achieve reactor-like plasmas with a power multiplication factor $Q \simeq 1$ (= fusion power generated/heating power required to maintain steady state), i.e., power break-even, at ~20 MW and ~6 10^{18} n/s, during a part of the ~ 1 s plasma pulse. After the initial hydrogen and deuterium operation with lower neutron yield and device activation, high-power pulses in tritium plasmas with deuterium neutral-beam injection will demonstrate $Q \simeq 1$, in the mid-1980's. To measure, with the desired precision and over the required flux ranges for D-H, D-D and D-T plasmas the important parameters such as Q, beam-ion energy distribution and loss rate, ion temperature, tritium confinement in D-D plasmas, and the radial and temporal dependences, we use four different diagnostic systems: 1) a pneumatic neutron activation system with eight irradiation stations, 2) two ^{235}U and four ^{238}U fission detectors, 3) a collimator-spectrometer (~150t) with NE213 and ^{3}He detectors and a proton recoil telescope, and 4) a multi-channel collimator using NE213 detectors.

INTRODUCTION

The Tokamak Fusion Test Reactor (TFTR) at Princeton University Plasma Physics Laboratory has been designed to achieve reactor-like plasmas with a power multiplication factor[1] $Q \simeq 1$ (= fusion power generated/heating power required to maintain steady state), i.e., power break-even, at the level of ~20MW and ~6 10^{18} n/s during a part of the ~ 1 s plasma pulse. TFTR will operate initially with hydrogen and deuterium plasmas which yield relatively low neutron fluxes and thus low device activation. Later, in the mid-1980's, TFTR will generate high fusion-power pulses with tritium plasmas and deuterium neutral-beam injection for demonstration of $Q \simeq 1$. This important Q-measurement

* Work performed under DoE Contract No. DE-AC02-76-CHO-3073
+ On leave from RCA David Sarnoff Research Center, Princeton, NJ.
++ Institute of Plasma Physics, Nagoya University, Nagoya, Japan.

thus largely determines the neutron diagnostics to be used on TFTR, but other fusion and plasma parameters will also be evaluated.

Present tokamaks produce up to 10^{14} n/s.[2] The higher production rates expected on TFTR (up to 10^{19} n/s) will allow use of higher energy-resolution detectors and will result in better spatial and temporal resolutions. In addition, TFTR will generate the first fusion-reactor-like plasmas, with good confinement of D-T produced alpha particles, a requirement for ignition. Below, we will give some background on the properties of the TFTR neutron source and describe the diagnostic systems to be used for their measurements.[3] Alpha-particle loss measurements, although planned, will not be discussed.

THE TFTR PLASMA AS A NEUTRON SOURCE

The TFTR is a geometrically extended, large-size toroidal ($r \simeq 50$cm, $R \simeq 250$cm) plasma neutron source, with temporal variations (due to heating, losses and relaxation), spatial variations (especially during radial compression heating) and neutron energy spectrum variations (determined largely by the dominance of either maxwellian-plasma or beam-plasma reactions) occuring during the approximately one-second-duration discharge. Typically, during this pulse, the plasma may be ohmically heated for 0.1s, neutral-beam-injection heated for a few 0.1s, possibly compression heated during 0.03s and confined and relaxed during another few 0.1s. Thus, the plasma neutron source is determined mainly by the ion type, ion density, and ion temperature (or energy) and the temporal and spatial evolutions of the latter two parameters as prescribed by the heating methods and by the losses. Successful heating and confinement will result in high fusion reaction rates, and thus both the reaction rates and the underlying factors that produced them are considered the measurement goals of the TFTR neutron diagnostics.

Generally, the TFTR ion density is expected to be $\sim 5\ 10^{13}$cm^{-3} and the temperature 5-20 keV. After initial ohmic heating, neutral D-beam-injection will produce about 10^{15} n/s in D-H, 10^{16} n/s in D-D and 10^{18} n/s in D-T plasmas. At the lower limit, thermal D-D plasmas (without neutral-beam injection) at 0.5 keV temperature will produce $\sim 10^{10}$ n/s, while at the upper limit, expected reaction rates in D-T plasmas for intense neutral-beam injection (with strong radial plasma compression) may reach 10^{19} n/s. With minor and major radii of 1.1 and 2.6m for the TFTR vacuum vessel, the flux at the location of the vacuum vessel wall, uncollimated, will be up to 10^{13} n/cm^{2}s and in collimated geometry, for a field of view of 10cm diameter, at representative detector locations (4-5m), $\lesssim 5\ 10^{9}$ n/cm^{2}s.

The neutron energy spectrum for an isotropic, maxwellian plasma has a single line (neglecting scattered neutrons) with full-width half maximum

$$\text{FWHM} \simeq 80\sqrt{T_i}\ (\text{keV}) \text{ for D-D},$$

$$\simeq 180\sqrt{T_i}\ (\text{keV}) \text{ for D-T}.$$

In D-D plasmas, a small ($\sim$ 5%) D-T component will occur, due to tritium production from the D-D reaction. The study of tritium confinement in D-D plasmas allows conclusions to be drawn on the confinement of alpha particles in D-T plasmas. In D-T plasmas, the T-T reaction will be present, but due to the broad energy spectrum of the T-T neutrons and their low flux, it may not be possible to distinguish T-T neutrons from downscattered D-T neutrons. With neutral-beam injection, the neutron peak energy seen depends on the direction of observation. Two directions, perpendicular (radial) and tangential, are of interest for high energy-resolution measurements. For co- and counter-injection, at 120 keV beam energy, two neutron energy peaks will be seen for tangential, collimated observation with a peak separation of 8% of the peak energy (14 Mev) and a FWHM of $\lesssim$ 3% for D-T and 25% and $\lesssim$ 8% for D-D plasmas (2.5 MeV). Here, the peak separation is determined by the beam-ion energy and the FWHM by the plasma-ion temperature. Without collimation, the FWHM of the beam-driven plasma will be slightly wider due to integration over a larger angle of observation.

Different plasma scenarios will be used on TFTR. Two important cases are the high-current, full-bore plasma and the strong-compression plasma. The latter is predicted to result in the highest Q-values at 1MA plasma current and imposes interesting measurement problems. Adiabatic compression must be performed during times $t_c << t_E \sim 100$ ms, the energy confinement time. Compression times of 30 ms are assumed, so that a time resolution of 1 - 10 ms is required to resolve compression effects. Compression moves the plasma (by $\sim$ 75cm) from a radial position near the outer part of the vacuum vessel into the region near the center of the torus, where the magnetic field strength is higher. According to TFTR computer calculations using the BALDUR one-dimensional plasma transport code[1] (and previous density and temperature measurements from an earlier PPL tokamak) compression raises ion density and energy, which in turn increases the peak fusion-reaction rate by more than a factor of 5 and the total (pulse-averaged) reaction rate by a factor of 3.5. To resolve the radial reaction-rate profiles in both the pre- and the post-compression locations and during the compression itself, it is desirable to view almost the full vacuum vessel diameter with a radial array of channels and to have count rates of 10^5 - 10^6 c/s, for a statistical error of 10 - 3% (in a 1 ms counting interval). Thus, the dynamic range of the counting equipment is severely limited.

Besides the direct source neutrons, scattered neutrons will be present and their contribution may be difficult to estimate. In tokamak geometry, vacuum vessel, magnetic field coils, support structures and diagnostic equipment are located near neutron source and detectors and produce a large flux of scattered neutrons.[4] Since the geometry cannot be changed, the scattered flux must be accounted for when uncollimated detectors are used or suppressed by collimation. In typical detector locations, the collided flux is ~50% of the total flux for D-T plasmas, and even higher for D-D plasmas. If collimated geometry is used, scatterers will be included in the field of view where the line-of-sight intersects the vacuum vessel. To make full use of the collimated geometry, the effects of these scatterers must be made negligible.

Neutrons will also be produced in γ-n and e-n reactions, but these reactions will be important only during run-away electron production and can thus be rejected easily. Their source will generally be near the plasma limiter, where the electrons impact, i.e., will be localized.

Gamma-radiation fluxes will be comparable numerically to the neutron fluxes and thus effective γ-n discrimination is important. The magnetic field intensity is <0.1T in typical detector locations, but 5T near the vacuum vessel wall.

The precision of the (uncollided) flux measurement expected is ~15%, which, together with a similar error for the measurement of the power deposited into the plasma by the neutral beams, leads to an error of ~20% for Q. The best Q values will exist over times comparable to the compression time, so that time resolved Q-measurements will be of interest. From the details of the neutron-energy spectrum discussed above, it can be seen that an energy resolution $\Delta E/E$ = 3-10% is desirable to resolve the features of the neutron energy spectrum. The radial source location should be determined with ~5cm error, to allow the relation of fusion reaction rates to the local flux (e.g., for T-breeding experiments).

To measure the important parameters such as Q, beam-ion (from neutral-beam injection) energy distributions and loss rates, ion temperatures, and the radial and temporal dependences of these parameters with this precision, and over the expected flux range of more than four orders of magnitude for D-H, D-D and D-T plasmas, we use four different diagnostic systems (two uncollimated and two collimated): 1) Neutron Activation System, 2) Fission Detector System, 3) Collimator-Spectrometer, and 4) Multi-Channel Collimator. The arrangement of three of these systems on TFTR is shown in Fig. 1. The Fission Detectors are not indicated; they are distributed around the torus. These four diagnostic systems will now be discussed in greater detail.

NEUTRON ACTIVATION SYSTEM

The Neutron Activation System measures the uncollimated, absolute, global neutron source strength, without interference from γ-radiation and em noise. From comparison of the irradiation stations located around the toroidal and poloidal circumferences of the torus, toroidal uniformity of the source can be established and the radial location of the fusing part of the plasma column can be derived. A selection of activation foils with different cross sections is available and due to the small size of these detectors and their insensitivity to magnetic fields, they can be used in the inner region of the torus. The pneumatic transport system which transfers the foils to the irradiation stations can also transport dosimeters into these locations, either to measure the γ-flux during or the activation after a discharge.

Employing a set of activation foils, neutron energy resolution of ~15% for D-T and ~20% for D-D neutrons can be obtained with computer unfolding. However, even with this energy resolution it can be shown[4] that the scattered source-energy flux at the foil location will be (for uncollimated geometry) 20-30% of the total flux for D-T, and ~50% for D-D. Thus, corrections of the measured flux, invoking calculations and

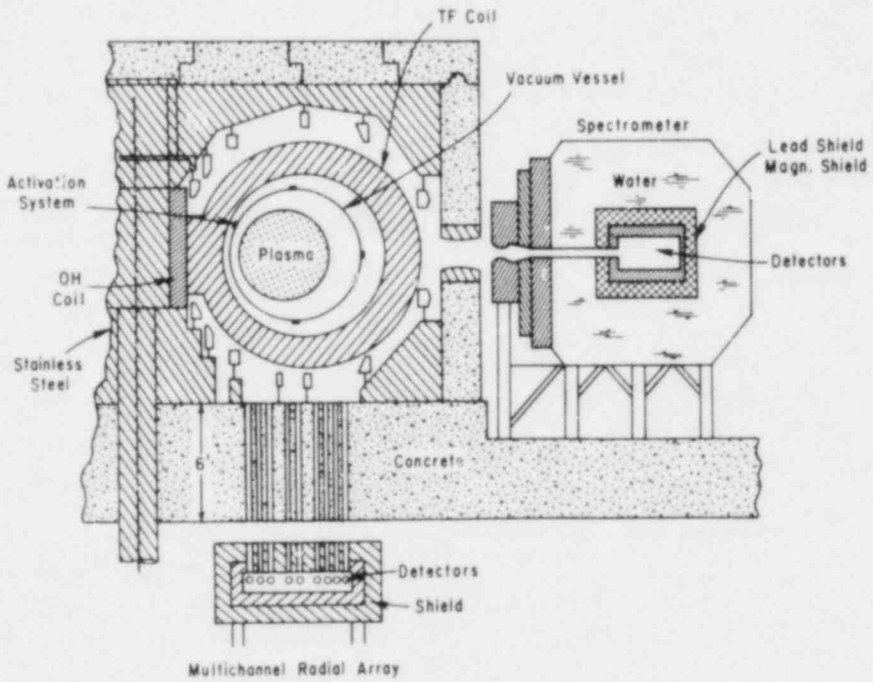

Fig. 1. Arrangement of Neutron Diagnostics on TFTR. Fission Detectors are not shown.

additional measurements using well- known neutron calibration sources inside the TFTR vacuum vessel, will be required to reduce the flux error. We also note that the activation system does not have any time resolution, a disadvantage especially in the time-varying compression scenario, and that the foil selection is limited, particularly for D-D, due to the low fluence of present tokamaks.

Eight Cd-clad irradiation stations are arranged around the toroidal (4) and poloidal (4) circumferences of TFTR. Polyethelene capsules (1 inch o.d.) carrying the activation foils are moved consecutively pneumatically from the loader-hopper to the tokamak (~ 150 m). After irradiation, the capsules are transferred to a γ-counting station, and drop computer-controlled through a number of counting distances until the count rate is optimized, when they are counted. Both Ge(Li) and NaI detectors are used. Finally, the spectrum is analyzed and the uncollided neutron flux determined. It is expected that after an initial period, when uniformity of the neutron emission and the energy spectrum are established, the Activation System can be operated with a reduced compliment of foils and capsules, and flux measurements can be completed between shots (5 minutes). A schematic of the pneumatic transfer system and the arrangement of the irradiation stations is given in Fig. 2. Since the air slug returning with the capsules from the TFTR Test Cell is radioactive, it is moved back into the Test Cell for cooling-off, without allowing it to enter the counting area. A proto-type pneumatic system containing all major elements together with the control logic has been operated reliably for more than 12000 cycles. Activation foil sets will be calibrated with a neutron generator prior to TFTR use.

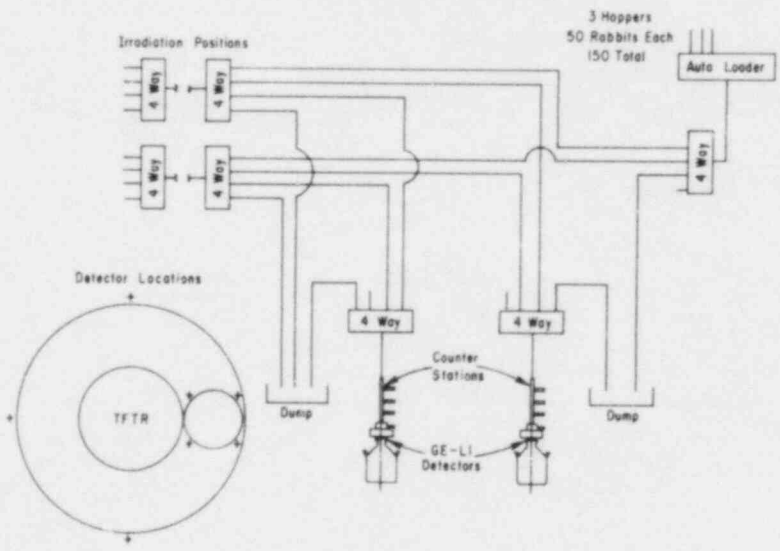

Fig. 2. Neutron Activation System. Transport system routing.

THE FISSION DETECTOR REACTOR-RANGE SYSTEM

The Fission Detector System provides the time-resolution for folding into the Neutron Activation System results. By pairing a ^{235}U and a ^{238}U detector a dynamic range of over nine orders of magnitude in flux can be covered (10^4 - 10^{13} n/cm^{2}s), thus guaranteeing reactor-range time-resolved monitoring for all possible source strengths.

Fission detectors offer the advantages of excellent γ-ray discrimination, of insensitivity to high magnetic fields due to their collision-dominated plasma (we observed no effect on detector characteristics up to 0.3T, the highest field used in our test), and of the presence of internal alpha background useful for threshold calibration and for deriving an operating-status signal between plasma discharges. Fission counter-ionization chambers (Reuter-Stokes RS-C3-2510-114) can be operated in the counting, direct current, and mean-square-voltage (msv) modes. In the counting and the msv modes of operation 10^6 R/hr of γ background will be discriminated against, and the dynamic range of one detector covers approximately six orders of magnitude, for our purposes, up to 10^9 c/s equivalent. Thus, in the msv and in the current modes good statistics can be obtained during short times of observation. The fission-detector circuitry by Gamma-Metrics gives ~20μs time response, both in the msv and the current modes. Due to the inherent γ-ray rejection of the msv (Campbell) mode by about a factor of 10^3, comparison of both the msv and current mode signals can be used to indicate freedom from γ-radiation contributions for the msv-mode signal. ^{235}U detectors have no energy resolution but high detection efficiency, ~10^{-1} c/nv, with moderator. ^{238}U detectors have a threshold at about 1 MeV but lower detection efficiency, ~ 10^{-4} c/nv. We use two ^{235}U and four ^{238}U detectors. Both types of fission detector are surrounded by 10 cm Pb to attenuate background γ-radiation and by an electrostatic shield. The ^{235}U detectors in addition are enclosed with 5 cm polyethelene for neutron moderation and, on the outside, a boron layer to remove background thermal neutrons.

NEUTRON COLLIMATOR SPECTROMETER

The Neutron Collimator-Spectrometer measures the neutron spectrum with high energy resolution, spatially and temporally resolved, for determination of Q, details of the neutrons origin, specific reactions, beam-energy distribution, beam-ion loss rates, $Z_{effective}$, triton confinement in D-D plasmas, and ion temperature. We require resolution of all energy lines, coverage of D-H to D-T flux ranges, spatial resolution with a diameter of the field of view ≃10cm, and suppression of background gammas and scattered neutrons to ≤ 1%. The temporal resolution is specified as one spectrum every 30 ms at standard D-D expected operating conditions (~ 25 KW fusion power generated).

Observations are to be made both in the tangential direction (to observe beam-plasma effects), with the possibility of covering as much of the vacuum vessel diameter as possible to accomodate different plasma scenarios, and in the radial direction (to observe the maxwellian plasma effects). Thus, the viewing direction must be located in the horizontal plane.

Since little prior work had been reported on well-collimated, high-energy-resolution measurements of the neutrons from an extended 14 MeV source, extensive design calculations for a 14 MeV neutron collimator (a slab of iron between source and detector with one cylindrical collimating channel) in TFTR geometry were performed by Lillie et al.,[5] using the discrete coordinates code DOT III. It was shown that the background γ-flux and the neutrons scattered in the collimator and those originating from the source outside the field of view can be suppressed to $\leq 1\%$ of the direct, uncollided collimated source neutron flux. No scatterers besides the collimator itself (i.e., no TFTR structures) were invoked in the model, but the effects of neutron scattering on tokamak neutron diagnostics were discussed later.[6] The design of the collimator for the high-energy resolution Neutron Spectrometer and for the Multi- Channel Collimator described below is based on these calculations and that of the remainder of the collimator shield on ANISN calculations. Cost, ease of handling, and operating schedule considerations made water the preferred bulk shielding material and the collimator was designed for D-D operation and later up-grading to D-T.

The collimator-shield size is determined by the extended neutron source. Generally, the collimated source-neutron flux at the detector is $\sim 10^{-3}$ times the total, uncollimated source-energy flux incident on the collimator-front face and for the source-energy flux incident on the collimator sides we have assumed 1/10 of the front-face flux. The γ-background flux incident is similar numerically to the neutron flux for D-T plasmas (in the 2-4 MeV gamma-energy region, which we have used in the calculations due to the minimum in the linear absorption coefficient at this energy for Pb), and is over an order of magnitude lower for D-D plasmas. A Pb layer of 15 cm thickness reduces the Test Cell γ-background sufficiently. Although designed for D-D plasmas, the water collimator size is determined by the ~5% 14 MeV D-T neutron component, i.e., the shield is overdesigned for the 2.5 MeV D-D flux. Boron addition to the water is thus not required, since for the 14 MeV neutron flux incident the largest flux behind the Pb shield occurs in the <1 MeV neutron groups (and not in the γ-groups).

To cover the range of fluxes and the two different neutron energies, three types of detectors are required. The detectors and their ranges are shown in Table 1. All detectors must discriminate against γ-flux incident through the collimator channel, approximately equal to the neutron flux.

Table 1. Neutron Spectrometers

DETECTOR	NEUTRONS	(R) BEST RESOLUTION (%)	(η) EFFICIENCY PER cm^2	(A) TYPICAL AREA (cm^2)	FLUENCE/cm^2 FOR GOOD SPECTRUM	MAXIMUM USABLE FLUX $\frac{}{cm^2\text{-sec}}$	DRAWBACKS
He^3 SANDWICH (SILICON BARRIER DET.)	D-D	2	10^{-6}-10^{-4}	3	3×10^6 - 3×10^8	10^{10}	D-D ONLY
NE213 PROTON-RECOIL SCINTILLATOR	D-D	6	.1	3	3×10^5	3×10^6	UNFOLDING NECESSARY
	D-T	4	.03	3	10^6	10^7	
PROTON-RECOIL TELESCOPE	D-T	2	10^{-6} 2×10^{-5}	7	7×10^6- 10^8	10^{11}	D-T ONLY LARGE EXPENSIVE

MULTI-CHANNEL COLLIMATOR

The Multi-Channel Collimator measures the time-resolved, radial profiles of the fusion reaction rates and thus the local, temporal Q. It views in the vertical direction and uses the 6' thick concrete TFTR Test Cell floor as the front shield containing nine collimator channels. The source neutron flux incident on the detectors can be adjusted manually by collimator-channel inserts. Extended source and scatterer effects are minimized by making vacuum vessel windows thin and using low-Z materials, incorporating throats in the collimator channels, using detectors having $\Delta E/E \leq 10\%$ and providing additional shielding surrounding the detectors. The fields of view of the nine collimator channels cover the locations of the precompressed, high-current and compressed plasmas, with ~35% of the former and ~ 15% of the latter fusion-reaction-rate profiles being missed, near the vacuum vessel wall, since no port holes exist in these regions.

NE213 detectors will be used to obtain sufficient detection efficiency for low reaction rate D-D plasmas and energy resolution to detect 14 MeV neutrons from D-D plasmas. Pulse shape discrimination is required to reject γ-radiation, since for D-T plasmas the chord-line-integrated neutron emissivity is similar to the emissivity of γ's from the vacuum vessel in the field of view for the central collimator channel and even for D-D plasmas the ratio of neutron to γ fluxes may be less than one in the shoulders of the radial fusion reaction rate profile. Since a minimum of 10^4 counts is required for an acceptable energy spectrum and flux measurement, high count rates of the NE213 detectors are desirable to obtain results during compression or other fast events. Count rates of up to 5 10^6 c/s have been obtained under similar conditions.[7] Cross talk between detectors and channels has been calculated and found to be negligible for the geometry used. The radiation field in the Basement is less severe than that in the Test Cell above, so that the shield size can be made smaller than that of the

high-energy-resolution collimator above. Magnetic shielding for the photomultipliers is required.

CONCLUSION

The achievement of fusion-reactor-like plasmas and power break-even expected in TFTR during a part of the ~1 s plasma duration calls for interesting and novel neutron diagnostics capable of measuring Q and certain plasma parameters with good temporal, spatial and energy resolutions in the presence of the extended, fast-changing fusion neutron source surrounded by large scatterers. The TFTR Neutron Diagnostic is based on well-tested methods and equipment where possible. It should be able to generate the important neutron-related measurements and results on TFTR and indicate directions for the evolution of future fusion reactor neutron diagnostics systems.

Acknowledgement

We gratefully acknowledge contributions from Drs. S. W. Seiler and K.M. Young during the course of this work.

REFERENCES

1. C. E. Singer, D. R. Mikkelsen, F. P. G. Seidl, D. L. Hwang, J. Hovey, D. E. Post, A. E. Silverman, D. M. Meade, and J. A. Schmidt, PPPL TFTR Physics Group Report #41, February 1982.

2. J. D. Strachan, P. L. Colestock, S. L. Davis, D. Eames, P. C. Efthimion, H. P. Eubank, R. J. Goldston, L. R. Grisham, R. J. Hawryluk, J. C. Hosea, J. Hovey, D. L. Jassby, D. W. Johnson, A. H. Mirin, G. Schilling, R. Stooksberry, L. D. Stewart, and H. H. Towner, Nuclear Fusion 21, 67 (1981).

3. H. W. Hendel and S. W. Seiler, Bull. APS 23, 701 (1978).

4. Long-Poe Ku, PPPL-1711, September 1980.

5. R. A. Lillie, R. G. Alsmiller, Jr., and J. T. Mihalczo, Nucl. Technology, 43, 373 (1979).

6. H.W. Hendel, K. Matsuoka and L. E. Samuelson, Bull. APS 26, 965 (1981). G. Zankl, J. D. Strachan, R. Lewis, W. Pettus, and J. Schmotzer, Nucl. Instr. and Meth. 185, 321 (1981).

7. H. P. Spracklen, UCRL-86021, presented at IEEE Nucl. Science Symposium, San Francisco, CA October 1981.

NEUTRON DOSIMETRY FOR THE TFTR LITHIUM BLANKET MODULE PROGRAM*

Y. D. Harker, F. Y. Tsang, A. J. Caffrey
EG&G Idaho, Inc., Idaho Falls, ID 83415

and

W. G. Homeyer, B. A. Engholm
General Atomic Co., San Diego, CA 92138

ABSTRACT

The Tokamak Fusion Test Reactor (TFTR) Lithium Blanket Module (LBM) program is a first-of-a-kind neutronics experiment involving a prototypical fusion reactor blanket module with a distributed neutron source from the plasma of the TFTR at Princeton Plasma Physics Laboratory. The objectives of the LBM program are: (1) to test the capabilities of neutron transport codes when applied to fusion test reactor blanket conditions, and (2) to obtain tritium breeding performance data on a typical design concept of a fusion-reactor blanket.

This paper addresses the issues relative to the measurement of neutron fields in the LBM, presents the results of preliminary design studies concerning neutron measurements and also presents the results of blanket mockup experiments performed at the Idaho National Engineering Laboratory (INEL).

INTRODUCTION+

The TFTR is unique in the U.S. Fusion Program as a near-term magnetic confinement fusion device offering a reactor-prototypical, extended fusion neutron source which can be used for blanket module integral neutronics experiments. As such, it presents an unparalleled opportunity to enhance the development of fusion reactor blankets through a program of design, experiments, and analysis.

* Work sponsored by the Electric Power Research Institute under contract No. RP-1748 through the Princeton University. The Tokamak Fusion Test Reactor is operated by Princeton University for the U.S. Department of Energy. Test space on the TFTR for the LBM and associated equipment is provided through an arrangement between EPRI and U.S. DOE.

+ The introduction to this paper is an abridgement of information contained in TFTR LBM program documents (Ref. 1-5).

The principal objective of the LBM program is to perform a series of neutron transport and tritium-breeding experiments using the toroidal fusion neutron source of the TFTR and to compare the data obtained in these experiments with the predictions of blanket design codes. The program will thus indicate, from comparisons between calculated performance and measured parameters, the extent to which the design codes are presently sufficient for fusion reactor design, and will identify improvements that can be made. This effort thereby can lead to increased confidence in the usefulness and credibility of fusion reactor blanket design codes that will be applied to the design of reactor blanket systems after the TFTR.

A parallel objective of the program is to obtain operational experience in the following areas of fusion blanket technology:

- o fabrication of breeding elements,
- o blanket dosimetry measurements in a tokamak reactor environment,
- o remote handling of blanket modules and dosimetry,
- o electromagnetic isolation of blanket modules from the tokamak plasma,
- o operational and safety aspects of integrating a blanket module into a D-T tokamak reactor assembly.

Passive neutron dosimetry using activation foils and wires is the primary measurement technique to be used to characterize the neutron environment inside and at the surfaces of the LBM. Active neutron detectors, will be used to supplement the activation measurements; however the extent of their use will depend on studies still in progress. The fundamental data to be obtained from these measurements will be "integral reaction" data (i.e., number of neutron reactions of a specific type occurring per dosimeter nuclide atom in a TFTR run). The measured reaction data will form the basis of comparison with neutron transport calculational and modeling techniques. The integral reaction data will also be used to obtain neutron spectral data via the least-squares adjustment code, FERRET[6]. The spectral data will be used in the LBM program to define the neutron fluence fields in and around the LBM and in turn aid in the interpretation of comparisons of measured dosimeter reaction and tritium production data with corresponding results from neutronic design codes.

EXPERIMENTAL PROGRAM

Description of LBM on TFTR

The TFTR facility plan with the LBM in place is shown in Figure 1. As indicated in the figure, the LBM will be located on a pallet and

support structure, opposite a vacuum vessel access port in a space between two adjacent toroidal field coils. The LBM will be positioned so that it is centered at the midplane of the fusion plasma.

Figure 2 is a pictorial view of the LBM by itself. It is an 80 cm x 80 cm x 100 cm box of a hexagonal array of ~ 900 rods containing cylindrical pellets of naturally enriched Li_2O clad in stainless steel tubing. The rod placement and construction are designed to represent a prototypical blanket design involving solid breeder material, stainless steel cladding and gas cooling.

The LBM has been divided into two regions or zones; i.e., the central zone and the outer or buffer zone. As far as dosimeter measurements are concerned, the central zone is of principal interest. The size of the buffer zone has been chosen such that the neutron fields in the central zone are representative of those fields one might expect in full coverage fusion blankets. The LBM will be built so that practically all breeder rods in the central zone are available for installation of dosimeter foil packages and all tri-cusp channels between adjacent breeder rods in that zone are available for installation of dosimeter wires. In the buffer zone only selected breeder rods and tri-cusp channels are available for dosimeter placement.

Dosimeter Material Selection

In selecting the dosimeter materials for this program, the following items were considered:

- o physical and time constraints on the measurements,
- o quality of support data; e.g., neutron cross sections and decay data.,
- o detector energy response range,
- o post-irradiation analyses of dosimeter samples.

Accuracy Requirements. While tritium production is not the only parameter of interest, it serves as the basis for determining the accuracy to which the dosimetry measurements must be performed. In this context, the following requirements were established:

- o tritium prod./front face fluence (@ source energy) $\pm$ 15% (1σ),
- o front face fluence (@ source energy) $\pm$ 13% (1σ),
- o tritium production $\pm$ 8% (1σ)
- o dosimeter reaction data $\pm$ 6-10% (1σ)*

Spectral Requirements. As mentioned above, neutron spectra will be needed to aid in interpreting tritium production and other integral parameters. Once again the basis for determining energy range, uncer-

* A dosimeter reaction datum is defined as the number of activated atoms produced per target atom from a particular dosimeter reaction.

tainty and resolution requirements is tritium breeding. This includes tritium produced from ^{6}Li and ^{7}Li interactions; therefore complete neutron spectrum knowledge from thermal to 16 MeV is needed. As far as the accuracy requirements on the spectral data are concerned, it was determined that $\pm$ 20-30% (1σ) uncertainties on the neutron flux/fluence values over the non-source energy portions of each spectrum and $\pm$ 10-13% uncertainty on the source energy flux/fluence of each front face spectrum are consistent with the accuracy requirements on the integral parameters identified above.

Experimental Limitations. The TFTR will be operating with various plasma compositions, however the LBM measurements will utilize neutrons from deuterium-deuterium (D-D) and deuterium-tritium (D-T) plasmas. Estimates of neutron intensity and fluence at the front face of the LBM are given in Table 1. A run referred to in this table is a sequence of pulses covering a time period of nominally eight hours. The measurements are planned around exposing dosimeter samples for one run and then removing them for gamma spectrum analysis. Removal of these samples will depend on radiation fields inside the TFTR test chamber. Current estimates indicate that manual removal of samples can commence 12 hours following a D-D run and 24 hours following a D-T run. Remote removal of samples in the central region is provided so that these samples can be processed almost immediately following a run. The time allowed for counting all samples from a run is 72 hours following shutdown. In some cases, however, this time window may be shortened in order to prepare for the next TFTR run.

Table 1. Reference Neutron Production Parameters[a] For the LBM Program Of Experiments And Analysis

	Deuterium-Fueled Plasmas	Deuterium-Tritium Fueled Plasmas
Date of first run	First half of 1984	Second half of 1985
Typical integrated fusion-neutron current per run[b]	2.5×10^{11} n/cm^2 @ 2.45 MeV	5×10^{12} n/cm^2 @ 14.1 MeV
Total fusion-neutron production per run (vessel area = 116m^2)	$\simeq 2.5 \times 10^{17}$	$\simeq 5 \times 10^{18}$
Nominal frequency of runs	2 per month	5 per year
Typical breakdown of a run into a series of pulses		
Interval between pulses	600 s	600 to 1200 s
Number of pulses per run	25	10

[a] From reference 5, page 8-10.

[b] At interior surface of the vacuum vessel.

Dosimeter Reactions. Based on the above criteria and limitations, the set of reactions given in Table 2 have been selected for possible use in the LBM measurements. There is in progress at INEL a dosimetry demonstration experiment. The neutron generator facility used in these measurements is described in the paper by Tsang[7] at this symposium. The blanket mockup assembly for the LBM demonstration measurements is an array of 61 hexagonal cannisters made of 0.9 mm thick aluminum (outside dimensions on each cannister: 54 cm long x 4.3 cm flat to flat). Each cannister is filled with Li_2CO_3 packed to 43% theoretical density. In addition to the Li_2CO_3/neutron generator measurements, there were also irradiations performed in the Coupled Fast Reactivity Measurements Facility (CFRMF)[8]. The CFRMF irradiations duplicated LBM fluence and spectrum under D-D operation of the TFTR and the Li_2CO_3/neutron generator irradiations duplicated the conditions under D-T operation of the TFTR. The objective of this experiment is to demonstrate the feasibility of using this set of dosimeters in the LBM program. The last column of Table 2 is the status of testing of dosimeter reactions, and so far that testing has evaluated reactions on the basis of sufficient counting intensity. Examples of count data are given in Table 3. Future tests will involve spectrum adjustment analysis as well.

Energy response is a primary consideration in selecting the set of dosimeter reactions. It should be emphasized that in the TFTR LBM program the primary points of comparison between measured and calculated results will be tritium production and integrated dosimeter responses as functions of position in the LBM. Comparing calculated and measured neutron spectra (the latter obtained by spectrum adjustment using dosimeter response data) will aid in the interpretation of the integral results. Nevertheless, the examination of candidate dosimeter reactions on the basis of energy response is best accomplished if one considers each reaction according to its importance in spectrum unfolding (adjustment). From our examination of this subject and other factors relative to this application, the following noteworthy items have been identified.

1. No specific reaction is uniquely sensitive to the spectrum in the energy ranges, 10^{-5} to 3×10^{-4} MeV, 10^{-2} to 0.4 MeV and 4 MeV to 13 MeV. So in a neutron spectrum adjustment analysis, one would expect little change in the shape of the input spectrum in these energy regions. However, the normalization in these regions should be improved.

2. Dosimeters with thresholds above 1 MeV have a response contribution in the 14-MeV group which dominates the total integral response. So, for reactions like $^{64}Zn(n,p)$ which one would use to characterize the neutron spectrum between 4 MeV and 13 MeV, the sensitivity in that energy range is masked by its greater sensitivity to the large 14-MeV group. However, in the spectrum analysis with FERRET, one can solve a multistep problem in which the 14 MeV flux is first adjusted by the $^{90}Zr(n,2n)$ or $^{197}Au(n,2n)$ reactions only. A second analysis could then be made with the 14 MeV flux fixed and the input spectrum could be adjusted based on the remaining measured integral rates.

Table 2. Reference Set of Activation Foils for Lithium Blanket Module

Material and Reaction	Energy Threshold	Reaction-Product Half Life	Comments	Qualification[a] Status for LBM
$^{63}Cu(n,\gamma)^{64}Cu$	Thermal	12.7 h	Resonances at 0.7, 2, 4 keV, self-shielding corrections; Requires isotopic enrichment; ENDF/B-V-D	CFRMF, OK
$^{197}Au(n,\gamma)^{198}Au$	Thermal	2.96 d	Resonance at 5 eV, self-shielding correction; ENDF/B-V-D	CFRMF, OK
$^{235}U(n,f)$	Thermal	h to d	Complicated γ spectra Requires clad foils, ENDF/B-V-D	NYT
$^{237}Np(n,f)$	~0.5 MeV	h to d	Complicated γ spectra Requires clad foils, ENDF/B-V-D	NYT
$^{238}U(n,f)$	~1 MeV	h to d	Complicated γ spectra Requires clad foils, ENDF/B-V-D	NYT
$^{115}In(n,n')^{115m}In$	~0.8 MeV	4.5 h	Short half-life, requires some cross section improvement, ENDF/B-V-D	CFRMF, OK N-GEN/BL, OK
$^{64}Zn(n,p)^{64}Cu$	~2 MeV	12.7 h	New cross-section evaluation available	CFRMF, OK N-GEN/BL, OK
$^{47}Ti(n,p)^{47}Sc$	~3 MeV	3.4 d	Requires some cross section improvement, ENDF/B-V-D, possible low activity	NYT
$^{24}Mg(n,p)^{24}Na$	~6 MeV	15.0 h	Dosimeter materials must be free of Na contamination, new cross-evaluation available	NYT
$^{48}Ti(n,p)^{48}Sc$	~6.8 MeV	43.7 h	Requires cross-section improvement, ENDF/B-V-D	NYT
$^{27}Al(n,\alpha)^{24}Na$	~8 MeV	15.0 h	Dosimeter materials must be free of Na contamination ENDF/B-V-D	N-GEN/BL, OK
$^{197}Au(n,2n)^{196}Au$	~10 MeV	6.17 d	Requires some cross-section improvement, ENDF/B-V	N-GEN/BL, OK
$^{65}Cu(n,2n)^{64}Cu$	~11 MeV	12.7 h	Requires isotopic enrichment ENDF/B-V-D	N-GEN/BL, OK
$^{90}Zr(n,2n)^{89}Zr$	~13 MeV	78.5 h	New cross-section evaluation available	NYT
$^{58}Ni(n,2n)^{57}Ni$	~13 MeV	36.1 h	Activation too low in N-GEN Test	N-GEN/BL, not satisfactory

[a]Qualification in CFRMF or 14-MeV neutron generator blanket assembly is established or Not-Yet-Tested (NYT). An OK indicates that sufficient activity was produced so that the reaction is suitable for dosimetry use in the LBM program.

The reaction ^{115}In (n,n') is important to this energy range because its relative sensitivity to the 14-MeV group is less than those of other threshold reactions and indeed is one reaction whose response focuses on the 1-10 MeV range. However, the accuracy of the current cross section data (± 15%) for this reaction needs to be reduced to ~ ± 5%.

3. $^{235}U(n,f)$ has a response which is nearly uniformly distributed over the entire energy range.

4. Foils or wires of Au and Cu probably will be thick enough to require sizable resonance self-shielding corrections.

5. It is our plan to use both $^{197}Au(n,2n)$ and $^{90}Zr(n,2n)$ to monitor the 14 MeV fluence. The gold reaction cross section has an uncertainty of ± 11% in that energy range which is marginally satisfactory and should be reduced to ~ ± 5%. The uncertainty for the zirconium reaction is ± 4% which is satisfactory.

Table 3. D-T Simulation in Li_2CO_3 Blanket -- Neutron Generator

Foil	Reaction	E_γ (keV)	T_{wait} (min)(a)	Counts(b)	T_{1000} (min)(c)
In	$^{115}In(n,n')$	336	34	3904	158
Cu	$^{65}Cu(n,2n)$	511	126	6618	80
Au	$^{197}Au(n,2n)$	356	218	3594	50
Zn	$^{64}Zn(n,p)$	511	1389	410	43
Al	$^{27}Al(n,\alpha)$	1368	1310	917	20

(a) T_{wait} is the time from the end of the irradiation to the start of count.

(b) All foils counted for 1000 s.

(c) T_{1000} is the time in minutes required to achieve a peak area of 1000 counts at a T_{wait} of 24 h. This would be reduced by a factor of 30 for a single nominal D-T pulse. The times given are representative and will depend on the efficiency of the detector system used.

Dosimeter Analysis. Following an irradiation the dosimeter samples will be analyzed via gamma spectrometry. Because the gamma spectra are relatively simple with well resolved peaks, sodium iodide spectrometer systems will be used to analyze most non-fissioning samples. Fission foils will be analyzed on Ge(Li) systems. There will be four (4) NaI systems and 2 Ge(Li) systems. Two of the NaI systems will be used to analyze wire samples and the other two will be for foil samples. The Ge(Li) systems will be for foil samples only. Based on our tests so far, the nominal count time to achieve

3% count statistics for a non-fission sample will be ten minutes and for a fission sample will be one hour. Based on these estimates, the throughput of this counting laboratory will be 24 non-fission samples and two fission samples per hour.

All gamma spectral data will be stored for subsequent analyses. The Ge(Li) spectra will be analyzed for gamma-peak areas using the computer program GAUSS[9] and the NaI spectra will be analyzed using basic routines of GAUSS but will be modified to handle the lower resolution gamma spectral data. The gamma peak areas will be converted to reaction data, the units of which are: number of reactions per target atom/14-MeV neutron fluence at the LBM front face.

The reaction data obtained from dosimeters placed in the interior of the LBM will be used to compare directly with calculated reaction data. In order to aid in the interpretation of these comparisons, the measured reaction data will also be used in a least-squares adjustment routine FERRET[6], to derive neutron spectra. FERRET utilizes the covariance data available on dosimeter reaction cross-section data and neutron spectra and can analyze multiple reaction sets simultaneously, thereby generating a set of several adjusted spectra which are consistent from group to group in each spectrum and consistent from spectrum to spectrum. The self-consistent feature will help in interpreting spatial dependence of neutron spectra in the LBM. Reaction data from dosimeters placed to characterize the neutron fields incident on the LBM surfaces will be used to obtain surface neutron fluence spectra. These fluence data will be used in turn to derive surface neutron currents. The latter are input data to neutronic codes utilizing the cell model approach to calculating neutron fields inside the LBM (see the next section of this paper).

Dosimeter Placement. Both foils and wires will be used to characterize the neutron fields in the LBM. The foils will be placed primarily inside the Li_2O breeder rods in pocket cavities between Li_2O pellets. The wires will be assembled in bundles of up to four individual wires and contained in aluminum sheaths. The wire assemblies will be placed in the tri-cusp channels alongside the breeder rods inside the LBM and attached on the outside of the LBM box for surface measurements. The placement of dosimeter samples in a transverse plane of the LBM is shown in Figures 3 and 4. In order to provide a comprehensive mapping of the neutron fields inside the LBM, it is estimated that it will require 25 foil package locations and 12 wire package locations in the central region and 24 foil package locations and 16 wire package locations in the buffer zone.

The philosophy behind the wire/foil approach is that the wires provide good spatial resolution but are limited in spectral definition and the foils provide more accurate absolute data as well as better spectral definition. In addition to mapping the internal neutron field, there will be a comparable effort to map the neutron fields at the surfaces of the LBM. The surface dosimeter data will be used to define surface neutron current sources.

Five of the front face foil positions will be used as normalization points and consequently will be occupied in all runs. There will also be a pneumatic sample transfer system with its irradiation tip outside of the LBM and near its front face. Foils in the pneumatic transfer system will be irradiated on a pulse-to-pulse basis and the data used to define the irradiation history of each run.

This characterization effort will be carried out for both D-D and D-T plasma neutron sources and is expected to take 18 D-D runs and 5 D-T runs to complete.

COMPARISON OF MEASUREMENTS AND CALCULATIONS

The emphasis in the TFTR LBM program is to compare calculated and measured tritium production and integrated dosimeter response data. As a result of the dosimetry qualification experiment, the list of reactions identified in Table 2 will be narrowed down to a primary set for foil dosimeters and a set for wire dosimeters. Based on the data available at this time, the primary set for foil dosimeters will be: $^{90}Zr(n,2n)$ for $E_n \geq 13$ MeV, $^{197}Au(n,2n)$ for $E_n \geq 11$ MeV, $^{27}Al(n,\alpha)$ for $E_n \geq 9$ MeV, $^{64}Zn(n,p)$ for $E_n \geq 4$ MeV, $^{115}In(n,n')$ for $E_n \geq 0.8$ MeV, $^{197}Au(n,\gamma)$ and $^{63}Cu(n,\gamma)$ for thermal $\leq E_n \leq 1$ MeV. The fission reactions $^{235}U(n,f)$ and $^{237}Np(n,f)$ have not, at this time, been adequately tested and if they proved to be suitable for use in the LBM, they will be added to this primary set. The set for wire dosimeters will be: $^{90}Zr(n,2n)$, $^{27}Al(n,\alpha)$, $^{115}In(n,n')$, $^{64}Zn(n,p)$, $^{63}Cu(n,\gamma)$. The gold reactions, $^{197}Au(n,2n)$ and $^{197}Au(n,\gamma)$ are also possible wire dosimeter reactions; however their use will depend on how accurately one can separate the activities from ^{196}Au and ^{198}Au in the same wire using a NaI detector on the wire scanner. Neutron spectra derived from dosimeter data will be used to interpret comparisons of integral data. The surface neutron fluence spectral data will be used to derive neutron surface currents incident on the LBM. The surface currents are needed as input source data for neutronic calculations utilizing an LBM cell model approach (as explained below).

Two approaches to calculating neutron fields in and around the LBM will be pursued. The first approach will treat the LBM as a cell with current sources specified at the surfaces of the cell. The surface neutron fields as measured by dosimetry will be used to specify the surface current sources. The second approach will treat the LBM and TFTR as completely as possible. All dosimetry data, interior as well as surface, will be used to compare with calculated results obtained under this approach.

Comparisons using the second calculational approach will be normalized to the neutron intensity of the TFTR. This type of data will be obtained from measurements performed by the TFTR neutron diagnostics group (a paper describing the TFTR measurements has been presented at this conference by Hendel[10]).

The expected uncertainty on a measured response from a dosimeter is ± 4-10% (1σ) (see Ref. 5, page 8-51). The larger uncertainty would be associated with activation measurements where extremely low-level activities are counted. The uncertainty estimate on a corresponding calculated response is approximately ± 10% (1σ) (see Ref. 5, page 8-57). Therefore, a difference between the measured and calculated response in the range of -15% to +15% would be indicative of agreement and likewise a difference outside that range would be indicative of a possible discrepancy. These estimates are derived for comparisons performed on an absolute basis and therefore include systematic uncertainty estimates. There will be, however, comparisons of response profiles which rely primarily on the precision of the measurements and on smaller uncertainty estimates on the calculated response ratios. At this time, no estimates on the expected range of agreement for the relative profile data have been made.

SUMMARY AND CONCLUSIONS

Program Features

The LBM program is first-of-a-kind neutronics experiment involving a prototypical fusion blanket module with an extended fusion neutron source. The objective of the program is to test neutron transport design codes and modeling techniques as well as obtain important data on tritium breeding. This program relies almost entirely on passive dosimetry for measuring neutron fields and performance parameters.

Challenges to Dosimetry Methods

This program involves low-fluence irradiations and is challenging in that considerable dosimeter data must be acquired in a relatively short period of time following irradiation. This will necessitate automation of the analysis process.

This program will be one of the first if not the first application of full treatment of covariance data and least squares adjustment on a comprehensive set of dosimetry data.

There is a need to improve and expand the dosimeter cross section data files. Improvement in such reaction cross sections as $^{115}In(n,n')$ and $^{197}Au(n,2n)$ would be of benefit to this program. The

desired uncertainties on these reactions are: ± 5% (1σ) for $^{115}In(n,n')$ over the energy range from 1 MeV to 10 MeV and ± 5% (1σ) for $^{197}Au(n,2n)$ over the energy range from 11 MeV to 16 MeV. In terms of energy coverage, there is a need to develop new or improve old dosimetry techniques to measure resonance and intermediate energy neutron flux/fluence. One possibility is further development of the "triple (or sandwich) foil method".[11] This method is applicable to determining neutron fluence at specific energy points in the resonance neutron energy range. We recommend, therefore, that there be continued development of dosimetry data and techniques. Hopefully, the experiences gained in the LBM program will, as a secondary objective, contribute to this development process.

ACKNOWLEDGEMENTS

The authors would like to acknowledge the contributions of the following individuals: R. L. Creeden (GA) who is responsible for the design of the LBM; L. Yang (GA) who is responsible for Li_2O pellet development and tritium analysis; D. L. Jassby (PPPL, Manager of the LBM program), H. Hendel (PPPL) and C. Clifford (PPPL) for their assistance in formulating the experiment and analysis program.

REFERENCES

1. D. L. Jassby, J. File, R. Little and L. M. Lontai, "Lithium Blanket Module Tests on the TFTR," in The Technology of Controlled Nuclear Fusion (Proc. 4th Topical Mtg., King of Prussia, PA, October 1980) Volume III, pp. 782-787.

2. Princeton Plasma Physics Laboratory, Request-for-Proposal for the TFTR Lithium Blanket Module Program, RFP No. 1236 (March, 1980), and updates of the Technical Specification for the TFTR Lithium Blanket Module Program issued by PPPL.

3. W. G. Homeyer, R. L. Creedon, L. Yang, and Y. Harker, "Design of a Lithium Blanket Module for Testing in the TFTR," in Engineering Problems of Fusion Research (Proc. 9th Symposium, Chicago, Il, October, 1981), Volume II, pp. 1988-1991.

4. E. T. Cheng, B. A. Engholm, and S. D. Su, "Neutronic Design for the TFTR Lithium Blanket Module," ibid., pp. 1818-1821.

5. Project Staff General Atomic Co. and EG&G Idaho Inc., "TFTR Lithium Blanket Module (LBM) Program Preliminary Design Report," GA-A16616 (December 1981).

6. F. Schmittroth, "FERRET Data Analysis Code," U.S. DOE Report HEDL-TME 79-10, Hanford Engineering Development Laboratory, Richland, WA (September 1979).

7. F. Y. Tsang, Y. D. Harker, et al., "Fusion-Blanket Dosimetry Program at the Idaho National Engineering Laboratory," Fourth ASTM-EURATOM Symposium on Reactor Dosimetry, National Bureau of Standards, Gaithersburg, Maryland, March 22-26, 1982 (Proceedings to be published).

8. Y. D. Harker, J W Rogers, D. A. Millsap, "Fission Product and Reactor Dosimetry Studies at the Coupled Fast Reactivity Measurements Facility," U.S. DOE Report TREE 1259, March 1978.

9. R. G. Helmer and M. H. Putnam, U.S. AEC Report No. ANCR-1043, 1972; R. G. Helmer, R. L. Heath, M. H. Putnam, and D. H. Gipson, Nucl. Instrum. Methods 57, 46 (1967).

10. H. Hendel, K. Matsuoka, L. E. Samuelson, "TFTR Neutron Diagnostics," Fourth ASTM-EURATOM Symposium on Reactor Dosimetry, National Bureau of Standards, Gaithersburg, Maryland, March 22-26, 1982 (Proceedings to be published).

11. J. Moteff, editor, "Neutron Fluence Measurements," IAEA Tech. Report Series No. 107, International Atomic Energy Agency, Vienna, 1970.

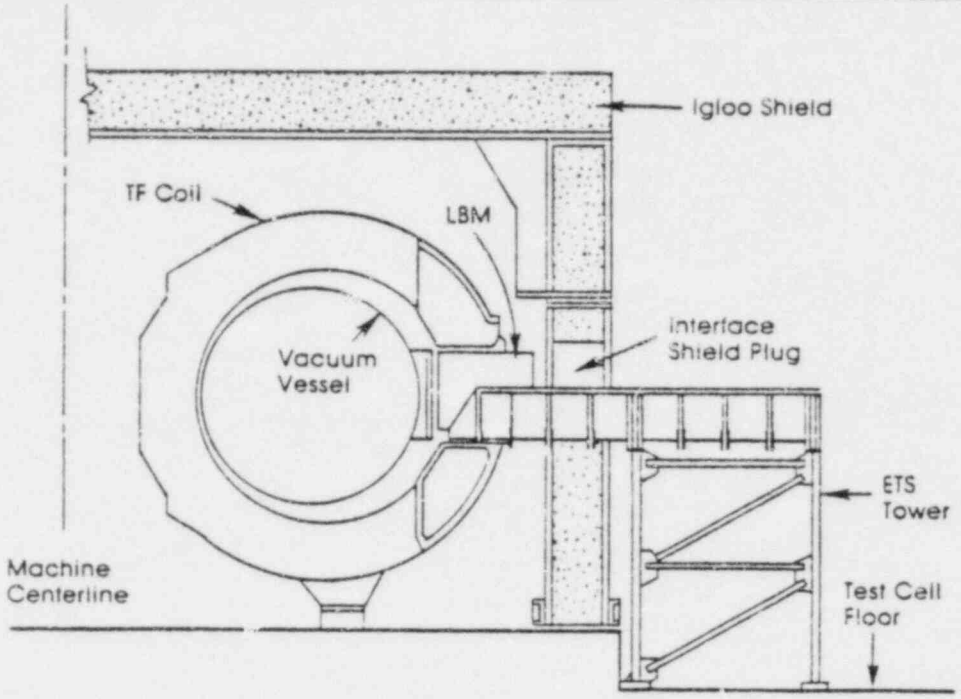

Figure 1. LBM in position in the TFTR (from Ref. 5).

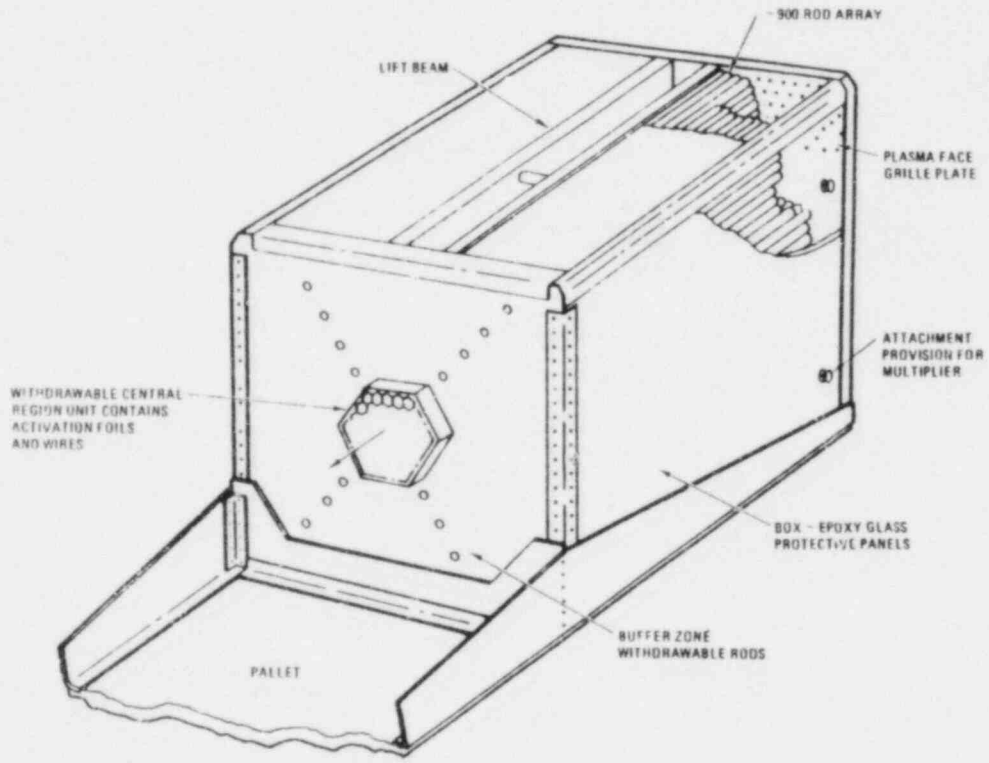

Figure 2. Lithium Blanket Module (from Ref. 5).

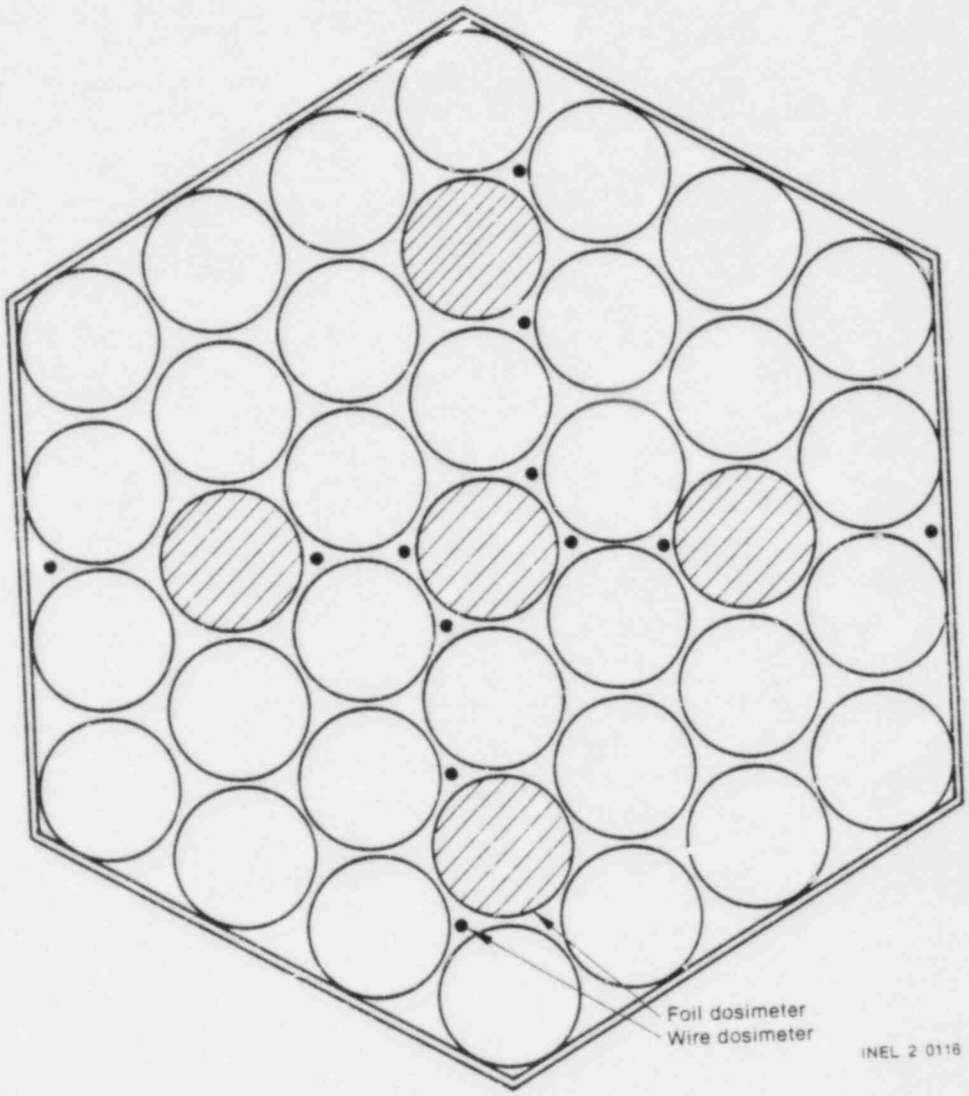

Figure 3. Foil and wire dosimeter placement in central region.

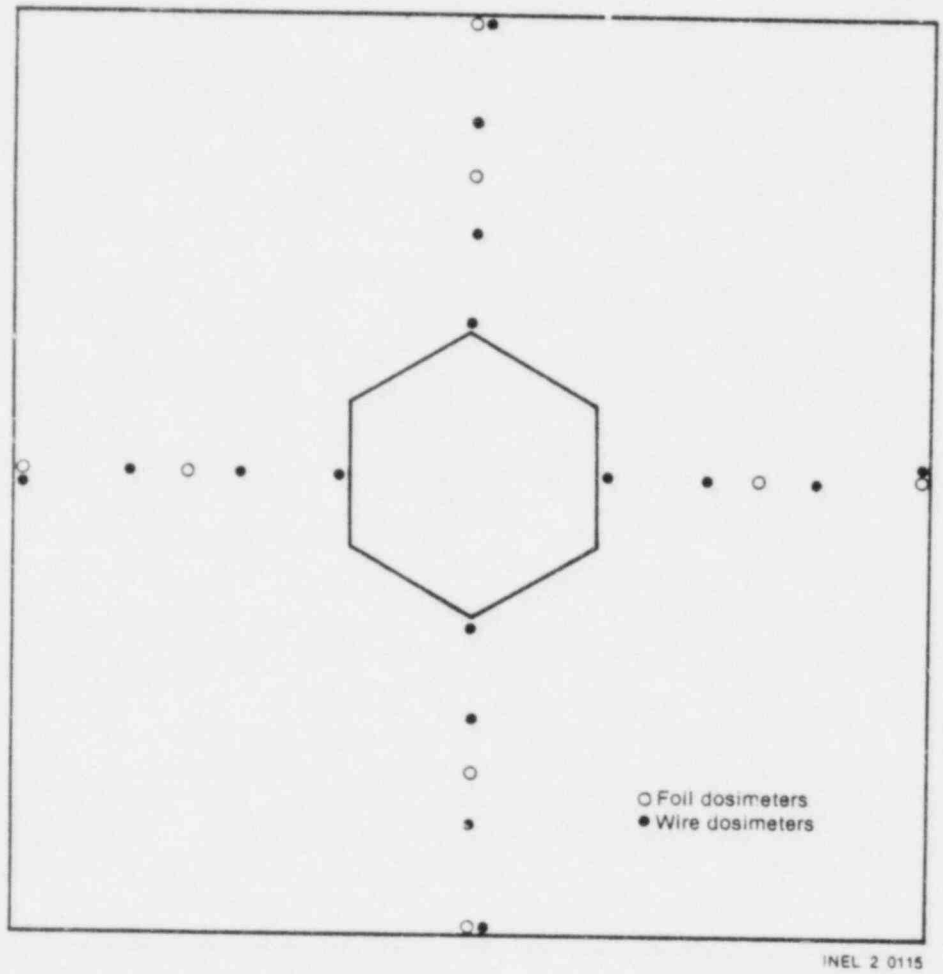

Figure 4. Foil and wire dosimeter placement in buffer zone.

FUSION-BLANKET DOSIMETRY PROGRAM AT THE IDAHO NATIONAL ENGINEERING LABORATORY*

F. Y. Tsang, Y. D. Harker, R. A. Anderl and D. W. Nigg
EG&G Idaho, Inc.
Idaho Falls, Idaho 83415 USA

ABSTRACT

The Fusion-Blanket Dosimetry Program at the Idaho National Engineering Laboratory (INEL) is directed toward the development and application of passive dosimetry to characterize neutron environment in fusion-blanket assemblies. To date, a series of experiments has been performed with a selected set of dosimeters to obtain neutron spectra and integrated neutron fluence data in a lead assembly using a 14-MeV neutron generator. Integral reaction data for each irradiation experiment were derived from gamma spectrometry measurements on the activation products for each dosimeter. These integral data were used in a least-squares adjustment analysis code to characterize the neutron environment in the lead assembly. The 14-MeV neutron fluence estimates obtained from the different threshold detectors are in agreement within $\pm$ 11% (1σ) at the 10^9 n/cm^2 fluence level. All three sets of measured integral reaction data (each set contains broad response and threshold detectors) are consistent with the estimated uncertainties, and the uncertainty of the total neutron fluence was determined to be $\pm$ 9.4% (1σ) at the 10^{10} n/cm^2 fluence level. These series of measurements demonstrate the feasibility to obtain reasonably accurate neutron spectrum and fluence data by using passive dosimetry in a low-neutron-fluence simulated fusion blanket environment in conjunction with a least-squares analysis to refine the neutron spectrum shape derived from a relatively simple neutronic calculation.

1.0 INTRODUCTION

The role of integral neutronic experiments is recognized as an important part of the fusion reactor blanket development program. The first generation of these experiments will utilize point neutron sources, and, in the future, distributed sources from fusion devices: e.g., TFTR and FED. These experiments will require neutron field

* Work supported by the U. S. Department of Energy under DOE Contract No. DE-AC07-76ID01570.

characterization over the entire neutron energy range from thermal to 16 MeV. This type of information will probably be obtained under low-neutron-fluence conditions. Passive neutron dosimetry is expected to have a major role in these types of measurements and therefore, it is important to assess this technology relative to its applicability in an expected fusion blanket environment.

A series of fusion-reactor blanket mockup integral experiments is being performed at the Idaho National Engineering Laboratory (INEL). These experiments are aimed towards the development of dosimetry techniques and materials that are applicable to low-neutron-fluence fusion reactor blanket environments. The INEL experiments emphasize; (a) establishing reproducibility in neutron fluence measurements in simulated fusion blanket mockups, (b) identifying deficiencies in both cross-section data base and the experimental techniques, (c) comparing experimental results with those from neutronic calculations of varying degrees of sophistication, and (d) applying least-squares adjustment techniques to refine the spectrum characterization. To date, measurements of integral reaction data in passive dosimeters, particularly threshold detectors, have been performed. The integral data were used in a least-squares adjustment analysis code - FERRET[1] - to adjust a neutron spectrum obtained from a neutron transport calculation for the lead-blanket assembly. The results and some observations are reported in this paper. Section 2 contains the description of the experimental facility, mockup blanket assembly, and dosimeter materials. The calculational models and the experimental results are described in Section 3 and Section 4, respectively. Section 5 contains the discussion and Section 6 is the conclusion.

2.0 EXPERIMENTAL SETUP

The experimental facility for the INEL fusion-blanket dosimetry experiment is shown in Figure 1. Deuterons, in the 14-MeV neutron generator, are accelerated to a kinetic energy of 200 keV and are incident onto a 0.025 cm-thick titanium-tritide copper backed target with a tritium loading of 0.62 Ci/cm^2. The 14-MeV neutrons are produced via the ^{3}H(d,n)^{4}He reaction.

For the series of dosimetry experiments reported here, the blanket is represented by a 66-cm lead (Pb) cube. Lead was chosen because of its high inelastic scattering cross section, availability and easy geometry setup. The target is positioned at the center of the cube at the end of a re-entrant channel. The outer surfaces of the blanket are covered first with 0.05-cm thick Cd metal and then with 5.1-cm thick polyethylene. The purpose of the Cd/poly shield is to decouple the Pb blanket from neutrons that escape and return after scattering with the surrounding structural materials (room return). This is necessary to simplify the neutronic calculations.

A set of dosimeter materials with their energy response ranges important to fusion reactor blanket neutron spectra is listed in Table 1. This set of dosimeters represents a preliminary selection of suitable dosimeters and an expanded set will be selected and incorporated in future experiments. Cross sections for each of these reactions are in ENDF/B-V, and all but the $^{197}Au(n,2n)$ and $^{90}Zr(n,2n)$ are in the dosimetry file. Each irradiation experiment consisted of positioning a set of circular dosimeter foils in a slot in the lead assembly 4.5 cm from the source on the central axis of the assembly. A ^{235}U fission chamber surrounded by 7.5 cm thick paraffin was positioned outside the lead/Cd/polyethylene assembly and was used to monitor relative neutron intensity as a function of irradiation time.

Table 1. Selected Dosimeter Materials for Use in the Pb Blanket Experiments

Reaction and Products	Half-Life
$^{197}Au(n,\gamma)^{198}Au$	2.96 day
$^{197}Au(n,2n)^{196}Au$	6.17 day
$^{90}Zr(n,2n)^{89}Zr$	78.5 hr
$^{115}In(n,n')^{115m}In$	4.5 hr
$^{115}In(n,\gamma)^{116}In$	54.2 min
$^{59}Co(n,\alpha)^{56}Mn$	2.58 hr

3.0 CALCULATIONS

3.1 Dosimeter Weighting Spectrum

Preliminary analysis[2] and subsequent studies have clearly indicated the importance of the weighting spectrum in collapsing cross sections for dosimetry purposes. It was determined in the original analysis that there was an apparent discrepancy in the measured 14-MeV neutron fluence determined from the different threshold detectors. Subsequent analysis demonstrated that the discrepancy was partially due to spectral shape distribution of the source neutron weighting spectrum. An isotropic neutron source distribution with a mean energy of 14.25 MeV was used in the original collapsing process. A more extensive investigation into the angular and energy distribution of the source neutrons produced by a deuteron accelerator with a tritium target for the dosimetry blanket experiments was performed.[3,4] From this investigation the mean energy of the neutron source was determined to be 14.92 MeV. The calculated energy and angular distributed source-spectrum was used in the neutron transport calculations to determine a weighting spectrum for collapsing group cross section data in the new analysis.

3.2 Assembly Neutron Analysis

The calculated spectrum reported here were obtained from a 45-group S_8P_3 ANISN[5] calculation in spherical geometry using the BUGLE[6] cross section library. The calculational model included a centrally-located fusion neutron source with the appropriate energy dependence (averaged over all source neutron emission angles). This will produce a computed spectrum in the source energy range of 13 to 15.15 MeV which is biased toward the lower energies of the source energy range as compared to the source spectrum actually seen by the dosimeter foils located along the beam axis directly in front of the generator target. For neutron energies below the source range, the spherical approximation should be adequate. Future work will be based on exact geometry, fine-group Monte Carlo calculations with the energy and angular dependence of the fusion source explicitly represented. The calculated spectrum in the Pb blanket at 4.5 cm from the source was used as input to the FERRET code for neutron spectra analysis.

4.0 EXPERIMENTAL RESULTS AND LEAST-SQUARES ANALYSIS

The set of dosimeter materials that is listed in Table 1 was irradiated in the lead assembly at a distance of 4.5 cm from the tritium target. Three sets of experiments were performed. The number of dosimeter foils that could be irradiated per run for each experiment depended on the reaction product half-lives and the gamma-ray counting systems available. The irradiation history for each run was obtained from a strip chart recorder which monitored the count rate from a fission chamber fixed next to the lead blanket. The run-to-run neutron history due to the tritium target depletion was used to obtain the normalized total number of reactions for each individual dosimeter.

The gamma spectrometer used in these three sets of experiments is described in reference 2. The units of the experimental values listed in Table 2 are expressed in total number of reactions per nucleus. Also listed in the table are calculated 95% reaction response ranges of the dosimeter foils.

In these experiments the neutron spectrum from the ANISN calculations was used as the *a priori* spectrum in the FERRET analysis code. The three sets of the measured integral activities listed in Table 2 and the uncertainties listed in Table 3 were used as part of the input parameters. The values in Table 3 represent the conservative estimates on the source of errors that included counting, positioning, cross sections, and detector efficiency.

The cross section values used in the spectrum analysis were processed from ENDF/B-V into the SAND-II 620-group structure, and collapsed to 45 groups using the representative weighting spectrum as described in Section 3.0. The broad response detector cross sections

Table 2. Measured and Calculated Integral Reaction Quantities For The Lead Blanket Experiment

Reaction	Integral Reaction Values		Ratio of Measured to Calculated Integral Reaction Values	
	Measured	Calculated	Unadjusted†	Adjusted†
Nov 80:				
$^{59}Co(n,\alpha)$	2.34(± 14%) -16*	1.90(± 10%) -16	1.31	1.23
$^{197}Au(n,\gamma)$	3.59(± 12%) -14	3.29(± 9%) -14	0.96	1.09
$^{115}In(n,n')$	3.43(± 12%) -15	3.46(± 14%) -15	0.92	0.99
$^{115}In(n,\gamma)$	3.05(± 12%) -14	3.54(± 10%) -14	0.64	0.86
$^{197}Au(n,2n)$	1.21(± 14%) -14	1.30(± 11%) -14	0.92	0.93
$^{90}Zr(n,2n)$	3.07(± 14%) -15	3.63(± 12%) -15	0.65	0.85
April 81:				
$^{59}Co(n,\alpha)$	2.60(± 10%) -16	2.10(± 9%) -16	1.46	1.24
$^{197}Au(n,\gamma)$	3.65(± 8%) -14	3.37(± 7%) -14	0.98	1.08
$^{115}In(n,n')$	3.63(± 8%) -15	3.62(± 13%) -15	0.98	1.00
$^{115}In(n,\gamma)$	3.16(± 8%) -14	3.52(± 8%) -14	0.66	0.90
$^{197}Au(n,2n)$	1.28(± 10%) -14	1.43(± 10%) -14	0.98	0.90
$^{90}Zr(n,2n)$	3.61(± 10%) -15	4.03(± 10%) -15	0.76	0.90
June 81:				
$^{59}Co(n,\alpha)$	1.59(± 10%) -16	1.92(± 9%) -16	0.89	0.83
$^{197}Au(n,\gamma)$	4.27(± 8%) -14	3.68(± 7%) -14	1.15	1.16
$^{115}In(n,n')$	3.16(± 8%) -15	3.21(± 13%) -15	0.85	0.98
$^{115}In(n,\gamma)$	3.08(± 8%) -14	3.67(± 8%) -14	0.65	0.84
$^{197}Au(n,2n)$	1.47(± 10%) -14	1.31(± 10%) -14	1.12	1.12
$^{90}Zr(n,2n)$	3.89(± 10%) -15	3.69(± 11%) -15	0.82	1.05

	95% Reaction Response Range (MeV)
$^{59}Co(n,\alpha)$	13.0 - 14.4
$^{197}Au(n,\gamma)$	2.7-7 - 3.6-1
$^{115}In(n,n')$	1.10 - 14.2
$^{115}In(n,\gamma)$	2.4-7 - 5.0-1
$^{197}Au(n,2n)$	13.3 - 14.5
$^{90}Zr(n,2n)$	13.6 - 14.5

* 2.34×10^{-16} is written as 2.34-16 for brevity. Each value represents the total number of reactions per atom for the irradiation time period of the experiment.

† Unadjusted values are calculated from the a priori spectra, while the adjusted values are determined from the final spectra after 6 iterations.

Table 3. Uncertainty and Correlation Input to FERRET Analysis Code

a.	Input spectrum normalization uncertainty	± 20%
b.	Individual spectral group uncertainties	± 20%
c.	Group to group correlation parameter	1.5 group
d.	Nov 80 measurement reaction data uncertainties	
	Threshold detectors*	± 14%
	Broad response detectors*	± 12%
e.	April 81 and June 81 measurement reaction data uncertainties	
	Threshold detectors	± 10%
	Broad response detectors	± 8%

* Threshold detectors - $^{197}Au(n,2n)$, $^{90}Zr(n,2n)$, and $^{59}Co(n,\alpha)$.

Broad response detectors - $^{197}Au(n,\gamma)$, $^{115}In(n,\gamma)$, and $^{115}In(n,n')$.

for $^{197}Au(n,\gamma)$ and $^{115}In(n,\gamma)$ were corrected for the self-shielding effects. Cross section covariance matrices for the FERRET analysis were processed from ENDF/B-V with the PUFF2[7] code.

A simultaneous least-squares adjustment analysis was done for the integral data. This approach demands that the cross-section adjustments made must be common and consistent with respect to each integral experiment. An adjusted spectrum from one of the experiments is compared to the input spectrum in Figure 2. Corresponding estimated input and adjusted uncertainties for this spectrum are given in Figure 3. These figures demonstrate the typical adjustments made in the input spectrum characterization for these irradiation experiments.

5.0 DISCUSSION

The integral neutron fluence and the 14-MeV neutron fluence for the three experiments are summarized in Table 4.

From Tables 2 and 4, and Figures 2 and 3, the following can be summarized:

1. The experiment demonstrates the capability to use selected passive broad-response and threshold detectors in a low-neutron-fluence fusion environment to obtain reasonably accurate neutron spectrum and fluence data with a moderate-intense facility.

Table 4. Measured Neutron Fluences from the Pb Blanket Experiments

Case	Integral Fluence (n/cm^2)	14-MeV Neutron Fluence (n/cm^2)
1. Unadjusted value from input spectrum	6.21(± 16%) +10	3.90(± 28%) +9
2. Adjusted values		
(Nov 80)	5.69(± 9.2%) +10	3.94(± 12%) +9
(April 81)	5.93(± 8.3%) +10	4.40(± 10%) +9
(June 81)	6.03(± 8.6%) +10	4.00(± 10%) +9

2. Better agreement was obtained in 14-MeV neutron fluence from the different threshold reactions by incorporating a more representative neutron source distribution in the neutron weighting spectrum. The uncertainty of the 14-MeV neutron fluence estimates was determined to be ± 11% (1σ) at the 10^9 n/cm^2 fluence level.

3. The integral neutron fluences from the final adjusted spectra for this series of experiments are consistent and the uncertainty was determined to be ± 9.4% (1σ) at the 10^{10} n/cm^2 fluence level.

4. The response functions obtained from the FERRET analysis for the set of dosimeters indicate the lack of threshold detectors in this analysis that are responsive between 0.1 MeV to 10 MeV.

5. The present analysis demonstrates the importance of the $^{115}In(n,n')$ reaction to bridge the resonance and fusion source regions in the neutron spectrum. Other possible broad response reactions that are able to complement the $^{115}In(n,n')$ reaction include $^{237}Np(n,f)$, $^{235}U(n,f)$, and $^{64}Zn(n,p)$.

6. As seen from Table 2, consistency was obtained between measured integral reaction quantities for a given experiment and between the three sets of measurements.

7. A relatively simple neutronic calculation can be used to obtain a reasonable input spectrum which can be refined using passive neutron dosimetry and least-squares adjustment analysis.

6.0 CONCLUSION

At this point in the INEL program, the experimental results demonstrate the feasibility of using passive neutron dosimetry to determine neutron spectra and integral fluence data in a low-neutron fluence fusion reactor blanket environment with a moderate-intense facility. Estimates of the 14-MeV neutron fluence, obtained from the different threshold detectors, are in agreement within $\pm$ 11% (1σ) at the 10^9 n/cm^2 fluence level. All three sets of measured integral reaction data are consistent with the estimated uncertainties, and the uncertainty of the total neutron fluence was determined to be $\pm$ 9.4% (1σ) at the 10^{10} n/cm^2 fluence level. The analysis indicates the lack of broad responsive detectors between 0.1 MeV to 10 MeV and the broad energy group structure used in the neutronic calculations. The measured integral reaction data are consistent for a given experiment and also for the three sets of measurements. Refinement in the calculated integral reaction quantities can be obtained by using the unadjusted values.

Future dosimetry experiments include more testing using different dosimeters such as ^{235}U(n,f), ^{237}Np(n,f), and ^{64}Zn(n,p) reactions. Other blanket assembly materials, such as Li_2CO_3/stainless steel and Li_2CO_3/Be, are beneficial to determine the applicability of dosimeters in tritium breeding environments. Future neutronic calculations will be based on Monte Carlo methods and will include the use of a finer energy group structure. Data analysis will use a more sophisticated approach to resolve the 14-MeV neutron peak response and broad energy response by incorporating both source neutron threshold detectors and broad response detectors.

REFERENCES

1. F. Schmittroth, "FERRET Data Analysis Code," HEDL-TME 79-40 (Sept. 79).

2. F. Y. Tsang et al., "Low-Neutron Fluence Fusion-Blanket Dosimetry Experiment," CONF-801011, Vol. III, page 731 (July 1981).

3. Private Communication from D. W. Nigg (January 1981).

4. Private Communication from D. W. Nigg (March 1981).

5. ANISN-W, "Multigroup One Dimensional Discrete Ordinate Transport Code with Anisotropic Scattering," Radiation Shielding Information Center (RSIC), CCC-255 (Aug 1975).

6. Radiation Shielding Information Center (RSIC), BUGLE, Coupled 45 neutron, 16 gamma ray P_3 cross section for studies by the ANS 6.1.2 shielding standards working group on multigroup cross sections, DLC-47/BUGLE, (Oct. 1977).

7. "PUFF2 - Determination of Multigroup Covariance Matrices from ENDF/B-V Uncertainty Files," RSIC Computer Code Collection, PSR-157 (1980).

Fusion Dosimetry Experiment at the INEL

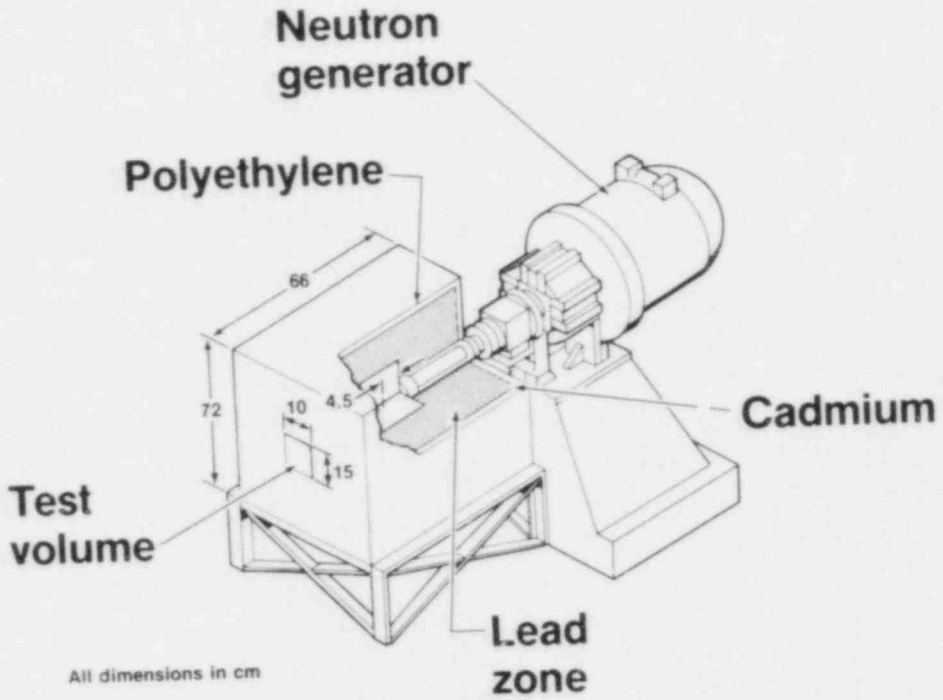

Fig. 1. Experimental setup used for the fusion-blanket dosimetry experiment.

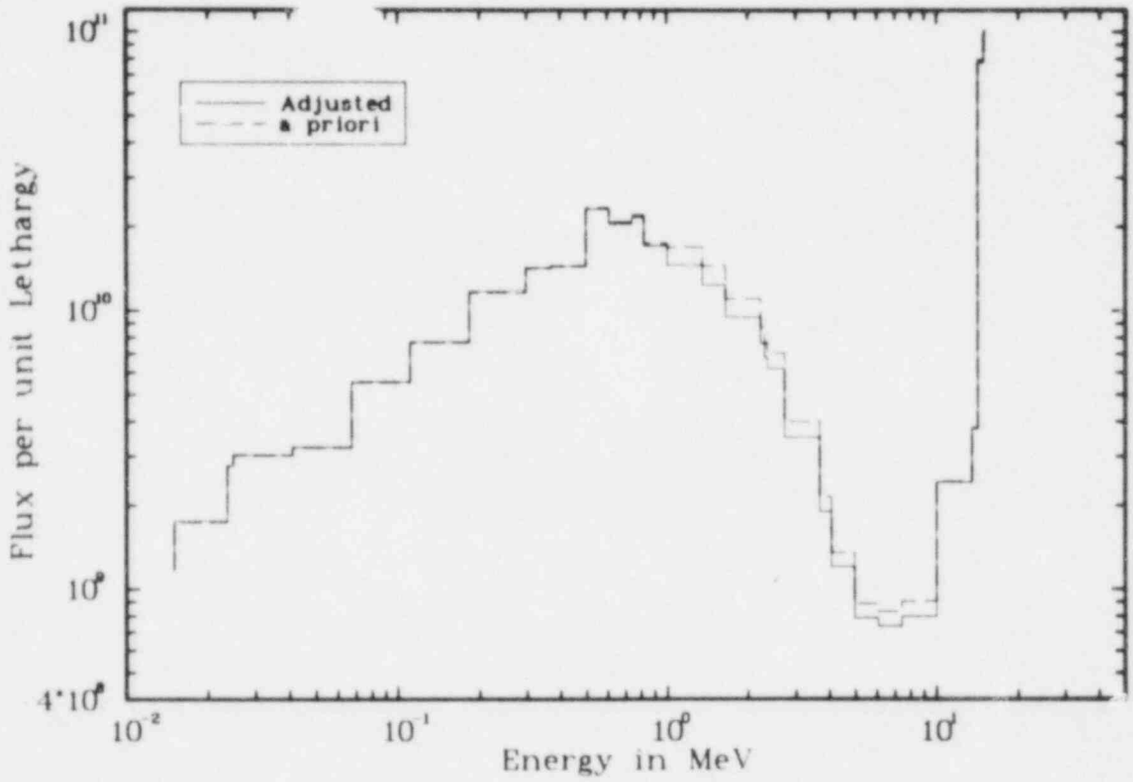

Fig. 2. Comparison of the adjusted and a priori spectra in the lead assembly. The a priori spectrum from the ANISN calculation was the trial spectrum for the FERRET analysis.

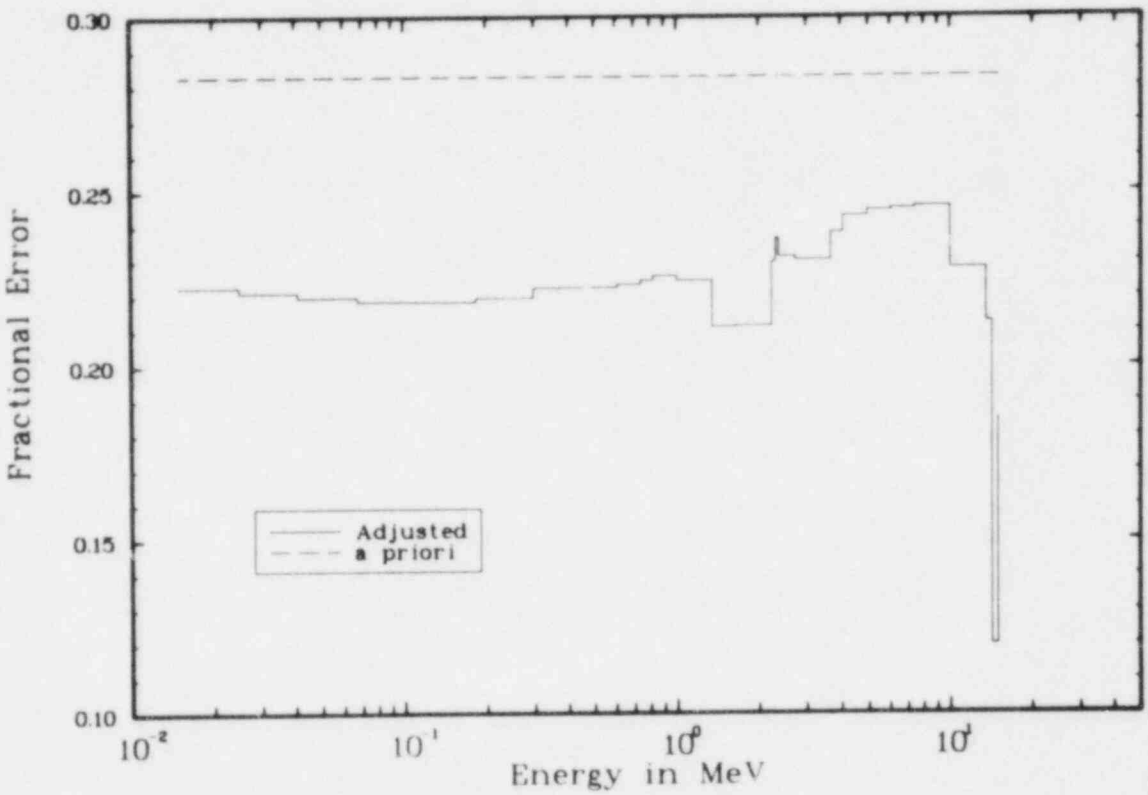

Fig. 3. Uncertainty in the lead assembly spectrum. The a priori uncertainty curve was the uncertainty in the trial spectrum for the FERRET analysis. The final uncertainty curve was derived from the FERRET analysis.

Fast Neutron Dosimetry of Spallation Neutron Sources

F. Hegedüs
Swiss Federal Institute for Reactor Research
CH - 5303 Würenlingen (Switzerland)

1. Introduction

The Swiss Nuclear Institute (SIN) is building a spallation neutron source. The principle is the following: in a cylindrical liquid heavy metal (Pb-Bi) target bombarded by a 590 MeV proton beam ($\sim$ 1 mA), fast neutrons with energies of a few MeV are produced. In the D_2O moderator, which surrounds the target, the fast neutrons are slowed down to thermal energies.

For the purpose of a fusion first wall material damage simulation, the intense fast neutron field could be of interest. The suitability of a spallation source for this purpose depends mainly on the magnitude of the integrated fast neutron flux (E>0.1 MeV) and on the shape of the neutron spectrum. For this reason, fast neutron flux and spectrum measurements were performed at several possible locations around a mock-up target at SIN.

2. Description of the Experimental Set-up

The spallation source mock-up consisted of a cylindrical lead target (d = 15 cm, l = 60 cm) which was bombarded with a low current (1.0 nA) proton beam of 590 MeV. The incident beam was along the axis of the cylindrical target which was surrounded by D_2O moderator. The fast neutron flux measurements were done in two empty channels (d = 10 cm) leading to the target (Fig. 1). The channels have traversed the D_2O tank just below the target channel. The angle between the beam direction and the channel axis was 90° and 150°. It was assumed that the maximum fast neutron intensity point (point source) is at a depth of 10 cm from the front side of the target (see Fig. 1). Both channel axes were 13 cm below this point.

3. Measurement Technique and Fast Neutron Spectrum Evaluation

In order to measure in situ the fast neutron spectrum, the multi-foil threshold activation method was used. A detector sandwich contained 7 foils (d = 2,5 cm); their characteristics are given in Table 1. The location of the 9 measuring positions is shown in Fig. 1. During the activation the proton beam current was monitored. In order to reduce parasitic activation due to thermal neutrons, the foil sandwich was enclosed in cadmium (thickness: 0.1 cm). The induced activities were measured by means of a Ge(Li) gamma spectrometer with the exception of rhodium whose X-ray activity was counted by means of a pure Ge detector.

The reaction rates were calculated from the measured activities by using the nuclear constants given in Ref. 1. The unfolding code SAND, with the cross section library of Greenwood (Ref. 2) was used to evaluate the neutron spectrum. Time-of-flight spectra measured

by KfK at SIN (Ref. 3) and by LASL at LAMPF (Ref. 4) were used as input spectra for SAND. It was found that the resulting spectrum for neutron energies below 30 MeV is practically independent of the input spectrum.

It was found that the reaction rate of ^{56}Fe (n,p) is too high. This effect is probably due to higher energy reactions. Therefore the spectrum unfolding was done without iron.

4. Results

By comparison of the shapes of the evaluated spectra, it was found that the spectra far away from the point source are softer than the ones in the nearer positions. Fig. 2 shows the spectra in Pos. 3 and 5. The distance between the two positions was 27 cm. The third spectrum shown in Fig. 2 was measured by TOF (Ref. 3). The shape of the TOF spectrum for 8 <E<30 MeV is similar to our spectrum. Below 8 MeV, our spectrum is softer. This effect probably could be due to the higher inelastic contribution for our 15 cm target than for the target of 10 cm used in the TOF measurement.

The integrated neutron flux (E>0.1 MeV) as a function of the distance between the assumed point source position (see Fig. 1) and the measuring position is shown in Fig. 3.

It was estimated that the agreement between our results and the TOF integrated flux, for energies above 3 MeV, was better than 30 %.

5. Conclusion

The SIN spallation source could be useful for fusion fist wall material studies provided that:

- the location of the material samples would be situated at least 10 cm from the assumed point source;
- the proton current would be at least 1,5 mA.

If these conditions are satisfied, the neutron flux (E>0.1 MeV) will be $\sim 6 \cdot 10^{13}$ cm^{2} sec^{-1} in the position of the material samples. During 3 - 4 months irradiations, significant productiong of helium gas and atomic displacements could be achieved.

References:

1. W.L. Zijp and J.H. Baard: ECN-70 (1979)
2. L.R. Greenwood: ANL/FPP/TM-115 (1978)
3. S. Cierjacks, M.T. Rainbow, M.T. Swinhoe and L. Buth: KfK 3079 B (1980)
4. R. Dierckx: Private communication (1980)

Table 1: Characteristics of the Threshold Activation Detectors (d = 2,5 cm)

Detector	Thickness g/cm^2	Reaction	Half life
Rh met.	0.07	^{103}Rh (n,n') ^{103m}Rh	57,0 m
In met.	0.6	^{115}In (n,n') $^{115m}/n$	4,49 h
Ni met.	0.12	^{58}Ni (n,p) ^{58}Co	1699 h
Fe met.	0.05	^{56}Fe (n,p) ^{56}Mn	2.58 h
Al met.	0.4	^{27}Al (n,α) ^{24}Na	15,0 h
Nb_2O_5 powder	0.3	^{93}Nb (n,2n) ^{92m}Nb	244 h
Zr met.	0.03	Zr (n,x) ^{89}Zr	78,4 h

FIG. 1. TOP VIEW OF THE EXPERIMENTAL SET-UP

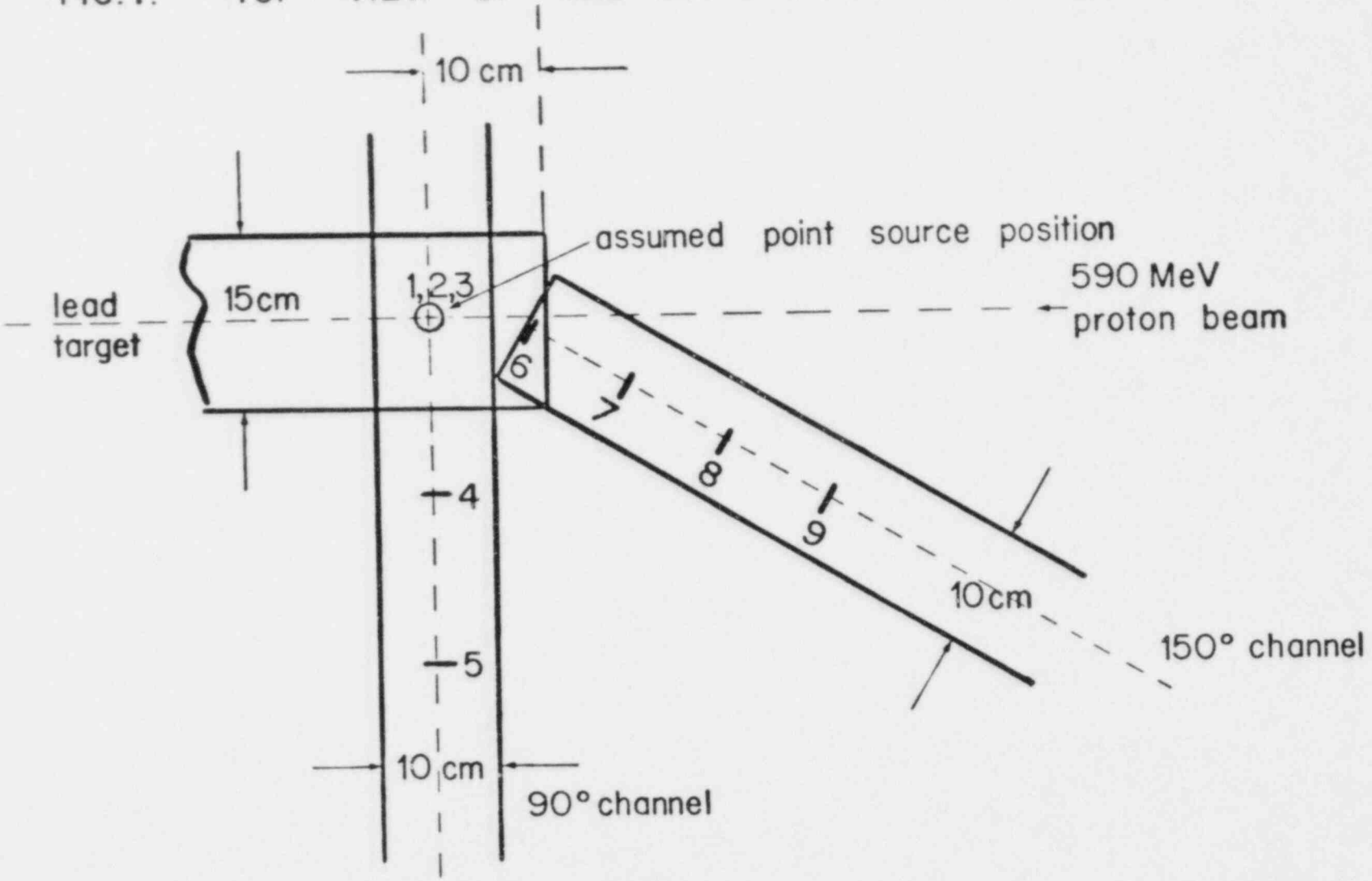

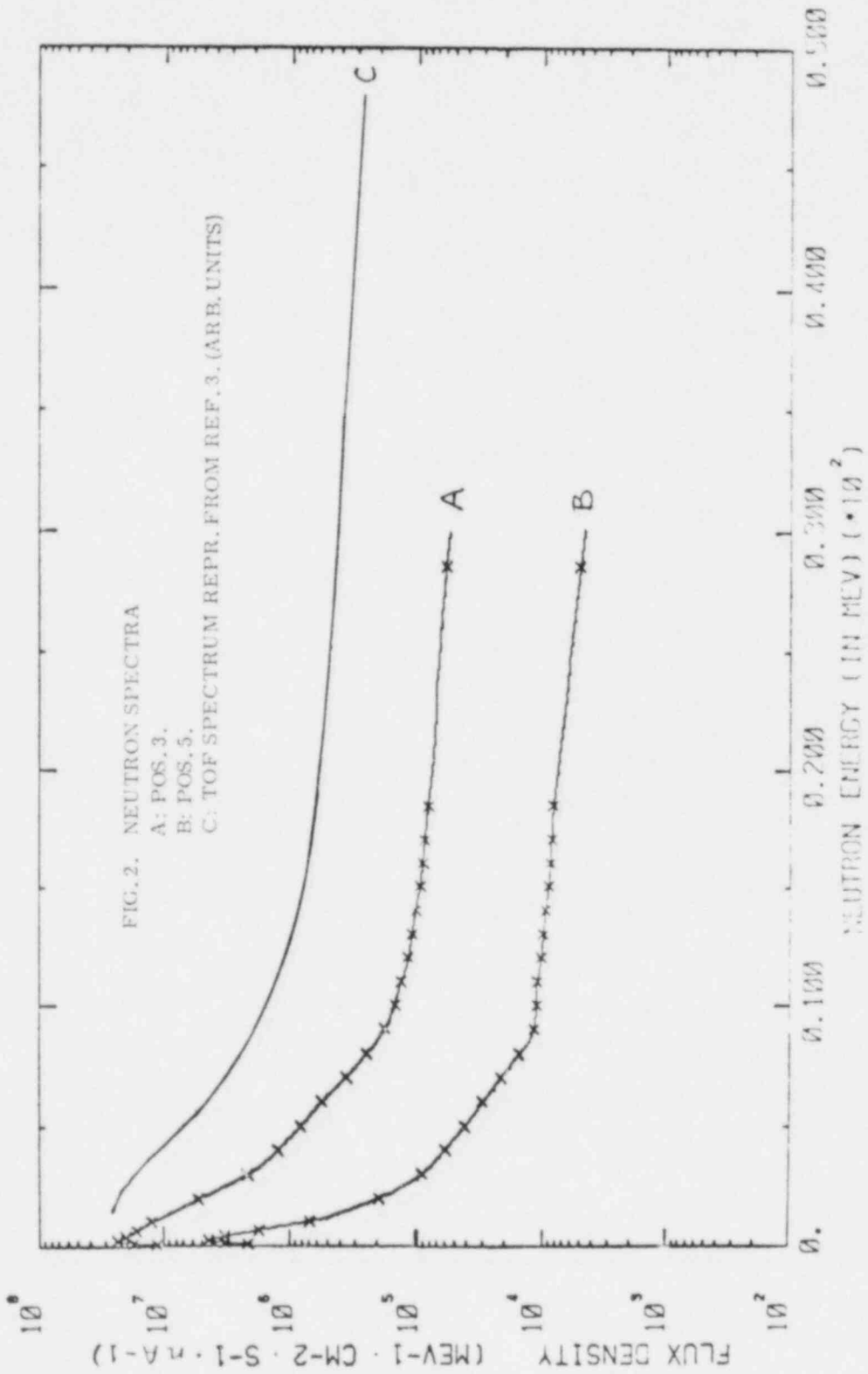

FIG. 2. NEUTRON SPECTRA
A: POS. 3.
B: POS. 5.
C: TOF SPECTRUM REPR. FROM REF. 3. (ARB. UNITS)

FIG. 3. FAST NEUTRON FLUX DENSITY (E>0.1 MeV)
VS. DISTANCE FROM THE ASSUMED POINT SOURCE

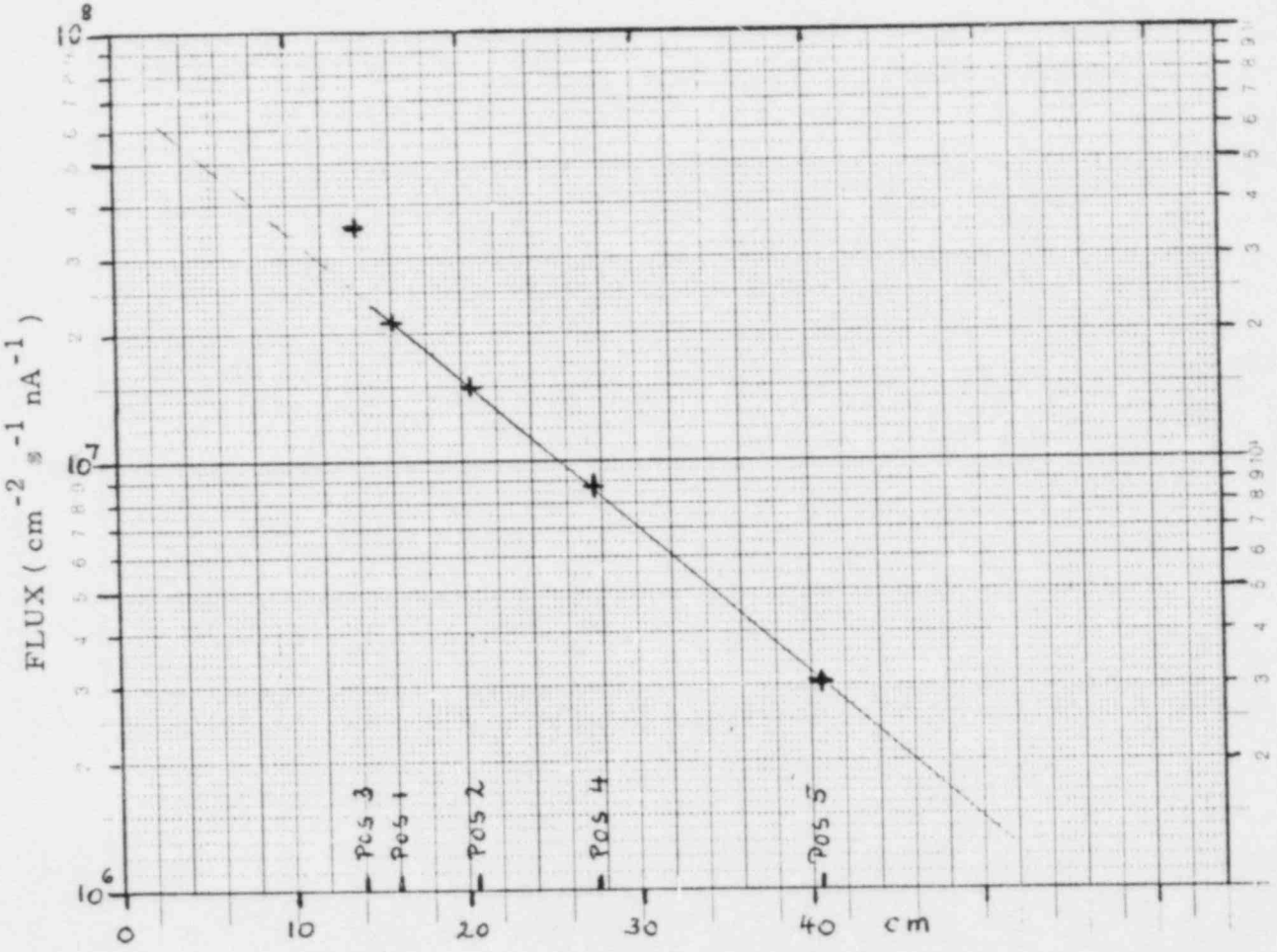

A REVIEW OF HELIUM ACCUMULATION NEUTRON DOSIMETRY FOR FUSION NEUTRON TEST ENVIRONMENTS

D. W. Kneff and Harry Farrar IV
Rockwell International Corporation
Canoga Park, California 91304, USA

and

L. R. Greenwood
Argonne National Laboratory
Argonne, Illinois 60439, USA

ABSTRACT

The current status of helium accumulation neutron dosimetry for fusion neutron test environments is reviewed. The technique has been used in conjunction with radiometric dosimetry to characterize a variety of neutron fields, including those produced by mixed-spectrum fission reactors and by T(d,n) and Be(d,n) source reactions. Neutron energy spectrum unfolding has been demonstrated for both mixed-spectrum reactor and Be(d,n) neutron environments using combined radiometric and helium accumulation measurements.

INTRODUCTION

The full interpretation of a given neutron irradiation test requires that the neutron field be characterized in detail for that particular test. This detailed characterization is particularly important for the fast neutron sources used for the irradiation testing of candidate fusion reactor materials. These neutron sources typically have steep neutron fluence gradients over the small volumes available for irradiation experiments and in many cases they also exhibit large energy spectrum gradients. Passive dosimetry provides the most accurate available neutron field characterization for fast, as well as fission reactor, fusion neutron test environments.

Radiometric (activation) dosimetry is the most-developed passive dosimetry technique.[1] Other passive techniques are also being developed, including helium accumulation neutron dosimetry[2] and solid-state track recorders.[3] Helium accumulation techniques have been demonstrated in a number of recent fusion-related irradiation experiments, where they have been used to complement radiometric dosimetry in the characterization of these neutron environments. The complementary nature of the techniques

has been demonstrated in two ways: helium accumulation measurements have provided additional details in neutron fluence gradients to refine radiometric fluence profile mapping, and they have recently been combined with activation reaction rates in neutron energy spectrum unfolding. The latter application is of particular value for long-term (≥ weeks) irradiations, where the number of available radiometric fluence dosimeters with adequately long half-lives is limited.

This paper reviews the current status of helium accumulation neutron dosimetry for fusion neutron test environments. Applications to date have included both fast and fission reactor neutron fields.

HELIUM ACCUMULATION TECHNIQUE

The helium accumulation neutron dosimetry technique is based on the neutron irradiation of one or more selected materials and the subsequent measurement by high-sensitivity gas mass spectrometry of the amount of helium generated.[4] Materials that have been irradiated specifically for helium accumulation dosimetry include bare and encapsulated pure element and alloy wires, and encapsulated compounds (crystals and powders). In some cases, dosimetry can also be provided by the helium analysis of the actual samples being tested or by analysis of segments of their experimental support assemblies. The compositions of the dosimetry materials must be known, including the presence of any helium-producing contaminants (such as boron, where parts-per-million concentrations can produce significant helium in fission reactor neutron environments with large thermal neutron components). The unirradiated materials must also be characterized for any possible helium introduced during their manufacture. Contaminants are generally not of concern in test specimens irradiated for damage measurements, because the total helium generation in these samples is one of the quantities of interest.

Helium accumulation is attractive for passive neutron dosimetry because of the small size of the monitors (a few milligrams for unencapsulated wires), the fact that the reaction product (helium) is stable, the large range of helium concentrations that can be measured (>8 orders of magnitude), and the wide range of helium-producing materials that can be used. The large materials selection permits the use of materials whose helium generation is sensitive to different ranges of neutron energies. A number of current dosimetry experiments are using materials that will be analyzed for both activation yields and helium generation. Since these reactions have different energy sensitivities (including multiple activation reactions in a given material), this multiple dosimetry with a single material will be particularly advantageous for characterizing test environments with very restricted irradiation volumes.

MIXED-SPECTRUM REACTORS

Many fusion materials radiation damage experiments are presently performed in mixed-spectrum (comparable thermal and fission-spectrum neutron component) reactors, because of flux limitations in existing high-energy neutron sources.[5] Reactors used in the United States for these experiments include the Oak Ridge Research Reactor (ORR) and High Flux Isotopes Reactor (HFIR) at the Oak Ridge National Laboratory, and the Omega West Reactor (OWR) at the Los Alamos National Laboratory. Combinations of helium accumulation and radiometric dosimetry have been included in eleven experiments in these three reactors, and limited results are now available for ORR and OWR. The objectives of the initial reactor dosimetry experiments are threefold: (1) to provide helium concentration measurements that can be used directly by materials scientists to design and evaluate their experiments; (2) to make integral cross section tests by comparing helium generation measurements with predictions based on radiometric fluence determinations and helium production cross section files; and (3) to demonstrate neutron spectrum unfolding using combined helium accumulation plus activation neutron dosimetry.

Direct comparisons between helium generation measurements and predictions based on cross section evaluations have been made for Al, Fe, Cu, Ni, and Ti samples irradiated in the ORR fusion materials experiment MFE1, and for Ni from the ORR experiment MFE4A. The comparisons made using MFE1 data are summarized in Table 1. The predictions for Al, Fe, Cu, and Ti were made by combining ENDF/B-IV (n,α) cross section evaluations[6] (the Al and Fe evaluations are the same in ENDF/B-V) with the radiometric fluence and energy spectrum determinations from the MFE1 experiment. The ratios in Table 1 for three of these four materials show large (19%-46%) differences. Since the fluence spectrum is known to within 10% uncertainties, the results suggest discrepancies in the evaluated (n,α) cross sections. Predictions for both MFE1 and MFE4A nickel were first made using nickel reaction rates derived directly from the empirical ^{58}Ni gas production equation established from helium measurements in HFIR.[7] The predictions differed from the ORR data by 15-20%, suggesting differences between the ORR and HFIR neutron spectra. These nickel reaction rates were then

Table 1. Summary Comparison of Helium Measurements and Calculations for ORR-MFE1

Material	^4He Ratio: $\frac{\text{Calculated}}{\text{Measured}}$	Material	^4He Ratio: $\frac{\text{Calculated}}{\text{Measured}}$
Al	1.05 ± 0.02	Cu	0.81 ± 0.04
Ti	0.54 ± 0.04	Ni	1.00 ± 0.03
Fe	0.79 ± 0.06		

adjusted for ORR by comparison with other (n,γ) reaction rates measured in ORR. The adjusted helium generation predictions agree with the ORR measurements, as shown in Table 1 for MFE1. The results for the five ORR materials indicate that for the accurate determination of helium production in a given material, that material should be included in the mixed-spectrum reactor irradiation of interest.

Spectral unfolding in a mixed-spectrum reactor using combined helium accumulation and radiometric dosimetry has been demonstrated for the Omega West Reactor. A number of helium accumulation dosimeters were incorporated in an OWR spectral characterization irradiation, including Al-Li and Al-B alloy wires. Spectral unfolding calculations were performed, both with and without the helium accumulation data, using the computer code STAY'SL.[8] The spectral unfolding results obtained with the inclusion of ^{6}Li, ^{10}B, and Cu helium production reaction rates are shown in Fig. 1, and the reactions used in the unfolding are summarized in Table 2. ENDF/B-V (n,α) cross sections[6] were used for the helium generation reactions; the unfolding results indicate that these cross sections are consistent with the ENDF/B-V radiometric cross sections.[6] Spectral unfolding without the helium data generated a nearly identical spectrum. Since this OWR experiment utilized a large number of radiometric reactions, helium accumulation measurements were included primarily to demonstrate combined unfolding. Long-term reactor experiments now in progress in HFIR and ORR, on the other hand, have limited radiometric dosimetry, due to long irradiation times and burn-up by the high fluxes. Helium accumulation is expected to contribute significantly to the spectral unfolding for these irradiations.

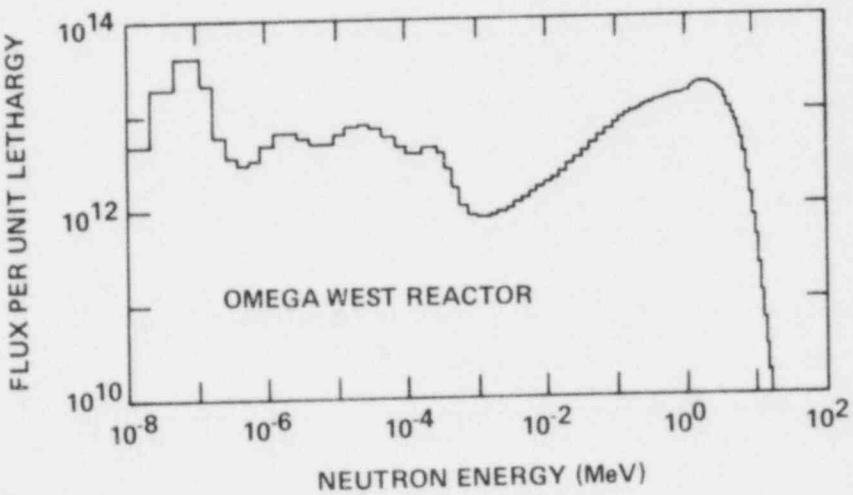

Fig. 1. Unfolded Flux Spectrum for the Omega West Reactor at 8 MW, Core Center.

Table 2. Dosimetry Reactions Used for OWR Spectral Unfolding

Reaction		Energy Range* (MeV)	Average Deviation†
$^{6}Li(n,X)helium$		$1 \times 10^{-9} - 4 \times 10^{-7}$	-0.1%
$^{10}B(n,X)helium$		$1 \times 10^{-9} - 4 \times 10^{-7}$	+0.0%
$^{45}Sc(n,\gamma)^{46}Sc$		$1 \times 10^{-9} - 4 \times 10^{-7}$	-5.7%
$^{59}Co(n,\gamma)^{60}Co$		$1 \times 10^{-9} - 1 \times 10^{-4}$	+1.8%
$^{58}Fe(n,\gamma)^{59}Fe$		$1 \times 10^{-9} - 2 \times 10^{-4}$	+4.1%
$^{176}Lu(n,\gamma)^{177}Lu$		$1 \times 10^{-8} - 1 \times 10^{-7}$	+4.3%
$^{197}Au(n,\gamma)^{198}Au$		$1 \times 10^{-8} - 4 \times 10^{-6}$	-1.1%
$^{235}U(n,f)$		$1 \times 10^{-8} - 2 \times 10^{-6}$	+0.5%
$^{238}U(n,\gamma)^{239}U$		$2 \times 10^{-8} - 2 \times 10^{-4}$	-4.0%
$^{176}Lu(n,\gamma)^{177}Lu$	**	$8 \times 10^{-8} - 9 \times 10^{-6}$	+7.2%
$^{45}Sc(n,\gamma)^{46}Sc$	**	$8 \times 10^{-8} - 2 \times 10^{-5}$	-2.4%
$^{10}B(n,X)helium$	**	$8 \times 10^{-8} - 2 \times 10^{-5}$	+0.5%
$^{6}Li(n,X)helium$	**	$8 \times 10^{-8} - 3 \times 10^{-5}$	-2.4%
$^{59}Co(n,\gamma)^{60}Co$	**	$8 \times 10^{-8} - 1 \times 10^{-4}$	-0.6%
$^{58}Fe(n,\gamma)^{59}Fe$	**	$8 \times 10^{-8} - 3 \times 10^{-4}$	+3.8%
$^{235}U(n,f)$	**	$8 \times 10^{-8} - 3 \times 10^{-4}$	+1.3%
$^{63}Cu(n,\gamma)^{64}Cu$	**	$8 \times 10^{-8} - 7 \times 10^{-3}$	-8.3%
$^{237}Np(n,\gamma)^{238}Np$	**	$1 \times 10^{-7} - 1 \times 10^{-4}$	+15.2%
$^{197}Au(n,\gamma)^{198}Au$	**	$8 \times 10^{-7} - 6 \times 10^{-6}$	+1.1%
$^{238}U(n,\gamma)^{239}U$	**	$4 \times 10^{-6} - 2 \times 10^{-4}$	-0.2%
$^{237}Np(n,f)$		0.36 - 5.0	+1.6%
$^{238}U(n,f)$		1.4 - 6.0	-0.1%
$^{54}Fe(n,p)^{54}Mn$		2.0 - 6.7	+1.3%
$^{58}Ni(n,p)^{58}Co$		2.0 - 6.7	-4.2%
$^{46}Ti(n,p)^{46}Sc$		3.7 - 9.0	-1.6%
$^{60}Ni(n,p)^{60}Co$		4.5 - 10	-9.1%
$^{63}Cu(n,\alpha)^{60}Co$		4.5 - 10	+2.6%
$Cu(n,X)helium$		5.0 - 11	+4.0%
$^{54}Fe(n,\alpha)^{51}Cr$		5.0 - 11	+6.4%
$^{48}Ti(n,p)^{48}Sc$		5.5 - 12	+6.1%
$^{27}Al(n,\alpha)^{24}Na$		6.0 - 12	-1.3%
$^{93}Nb(n,2n)^{92m}Nb$		9.0 - 14	+3.3%
$^{55}Mn(n,2n)^{54}Mn$		11 - 17	+1.8%
$^{90}Zr(n,2n)^{89}Zr$		12 - 18	-4.1%

*90% response range
†Percentage deviations between measured and calculated reaction integrals
**Gadolinium cover foil

FAST MONOENERGETIC NEUTRON SOURCES

Fast, approximately monoenergetic neutron sources with high neutron yields for fusion materials tests have been limited to T(d,n) reactions. The most intense ~14.8-MeV T(d,n) neutron fluxes in the United States are generated by the Rotating Target Neutron Sources-I and -II (RTNS-I, II) at the Lawrence Livermore National Laboratory (LLNL). Three source characterization experiments have been performed at those facilities using combined helium accumulation and radiometric dosimetry. They demonstrate the use of helium accumulation measurements to refine the fluence profiles deduced using radiometric data.

The irradiation geometry for the RTNS-II characterization experiment is shown in Fig. 2. The miniature sample capsule for each of the RTNS experiments was irradiated in close proximity to the neutron source, as demonstrated by Fig. 2, and thus in the region of highest available source intensity. This region also has large fluence gradients. The capsule for each of the three irradiations was generally similar in geometry to that shown in Fig. 3. Each capsule was irradiated to measure the helium generation cross sections of several different pure elements and separated isotopes. The accuracy of these final cross section results is limited to the accuracy to which the neutron fluence at each sample location could be determined. Dosimetry for each capsule consisted basically of a set of concentric pure element wire rings sandwiched between stacks of radiometric foils. After irradiation, the wires and foils were segmented and analyzed, respectively, for generated helium and activity levels.

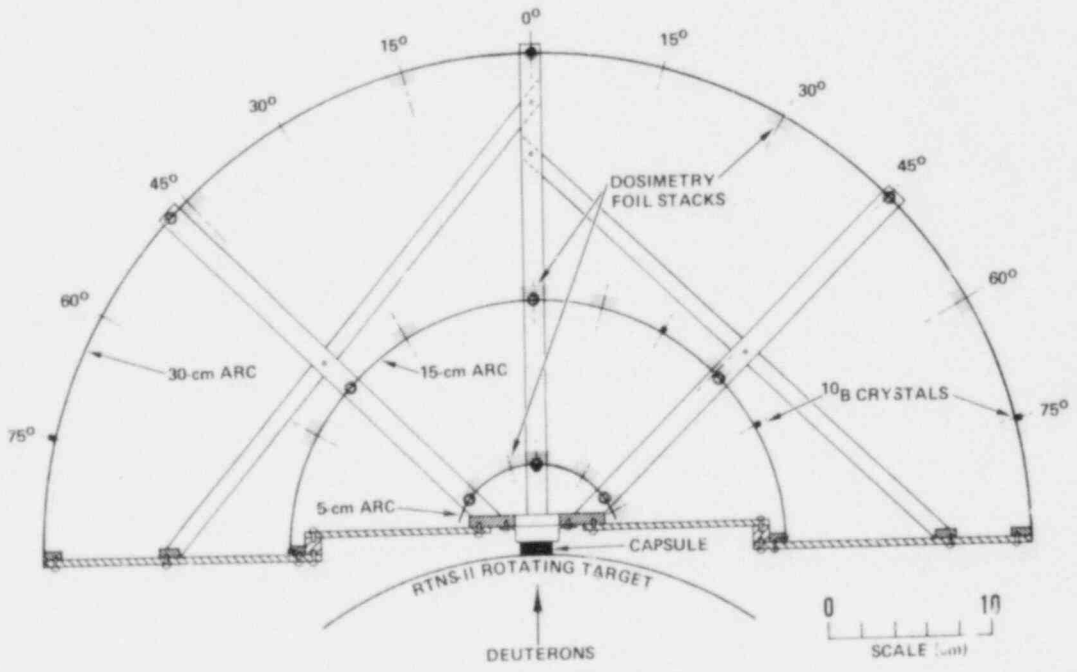

Fig. 2. Irradiation Geometry for the RTNS-II Characterization Experiment.

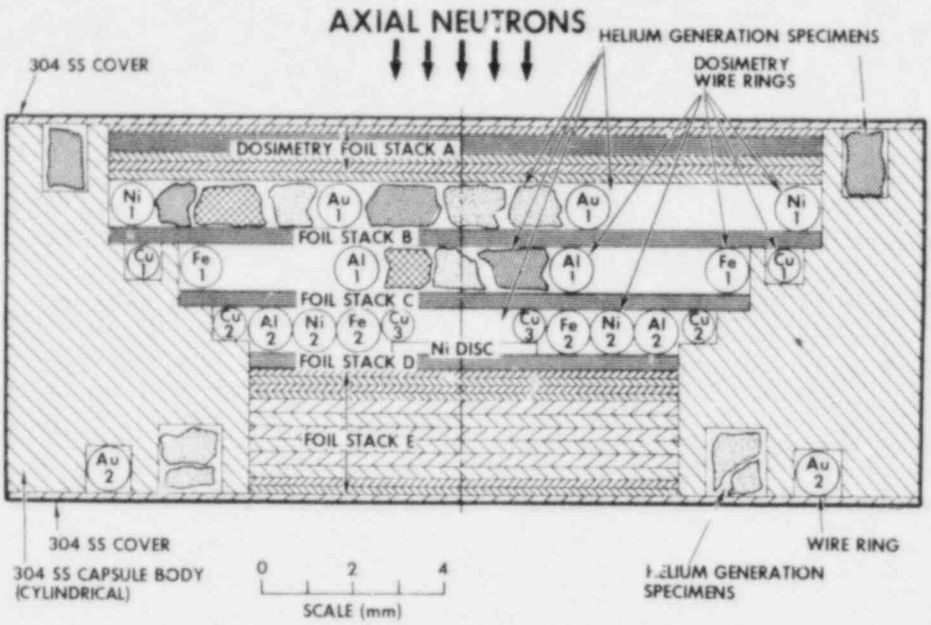

Fig. 3. Be(d,n) High-Flux Irradiation Capsule.

Fluence mapping for the volume of each irradiation capsule was performed by first constructing an average map from the radiometric dosimetry data, assuming a circular deuteron beam shape. Any offset (typically ~1-2 mm) of the capsule from the neutron source axis was determined using a series of least-squares fits across the segmented foil data. This offset was incorporated in a multiple regression analysis to calculate the constants in an initial empirical model of the fluence profiles. The results of the empirical map derived for the second RTNS-I experiment are depicted in Fig. 4a, where contours of constant neutron fluence are plotted for one sample layer of the capsule.[9]

The average map was then refined using the helium accumulation dosimetry data. The use of helium accumulation in this application relies on the slowly varying total helium generation cross sections as a function of energy for the dosimetry materials in the 15-MeV energy region, and the nearly constant neutron energy throughout the irradiation volume. The helium concentrations generated as a function of position within each dosimetry material then provide a measure of the fluence gradients. For example, Fig. 5 shows the measured helium concentrations in segments from three of the ten dosimetry wires from the second RTNS-I irradiation, along with the average fluence profile calculated from the radiometric data (dashed curves). These comparisons were used to adjust the fluence map for the observed differences. The adjusted map is also shown in Fig. 5, where it is represented by the solid curves. The resulting contours that correspond to the geometry in Fig. 4a are shown in Fig. 4b. For this irradiation, the adjusted map[9] disclosed a 10% higher fluence maximum than the average map, and revealed fluence profile details (including a non-symmetric shape) not apparent from the radiometric data. The overall

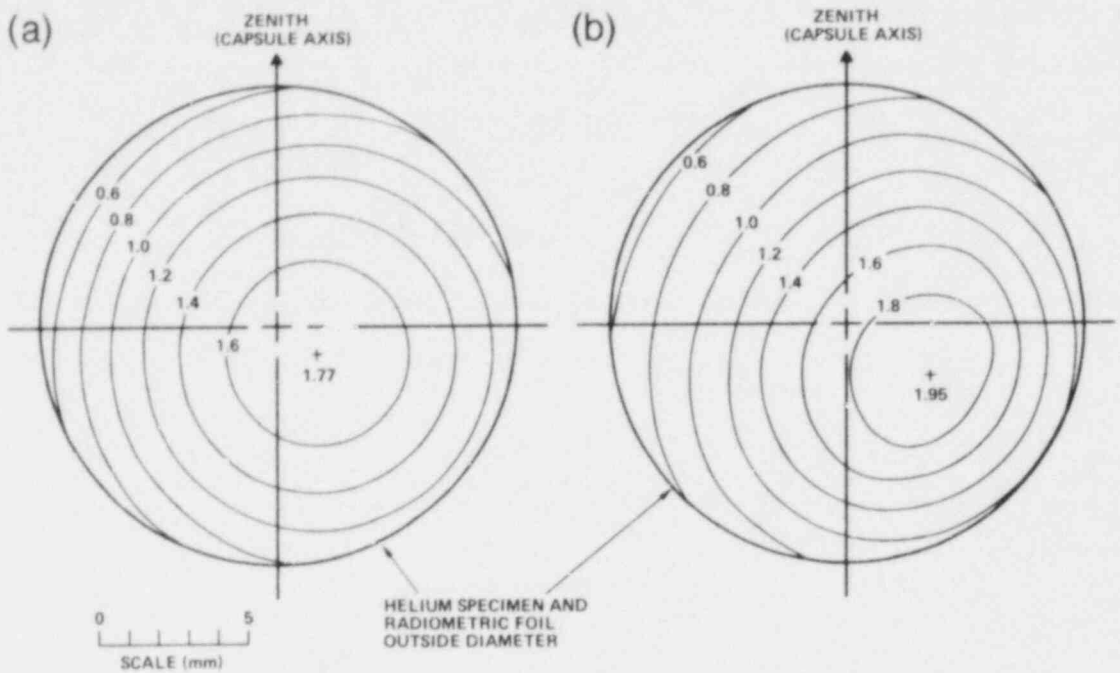

Fig. 4. Contours of Constant Neutron Fluence for One Plane of the Irradiation Capsule from the Second RTNS-I Experiment (Units of 10^{17} n/cm^2): (a) Based on Radiometric Dosimetry and Assuming a Symmetric Profile; (b) With Refinements Made Based on Helium Accumulation Dosimetry.

normalization for this map was based on the $^{93}Nb(n,2n)^{92m}Nb$ activation cross section, and the relative map uncertainty was estimated to be ~5%.

A similar analysis for the first RTNS-I source characterization experiment showed that the time-averaged neutron profile was elliptical in shape for that irradiation.[2] It is clear that such variations from irradiation to irradiation make helium accumulation a valuable dosimetry tool in those applications where an accurate knowledge of the neutron fluence is required. The RTNS-II helium measurements showed that the fluence profile for that irradiation was symmetric, as expected because of the larger neutron source spot (larger deuteron beam diameter) in close proximity to the capsule. No adjustments were made to the average radiometric fluence map for the RTNS-II irradiation.

FAST NEUTRON SOURCES WITH BROAD ENERGY DISTRIBUTIONS

Two experiments have been performed using helium accumulation dosimetry to characterize high-energy neutron fields with broad energy distributions: one Be(d,n) irradiation using 30-MeV deuterons, and one

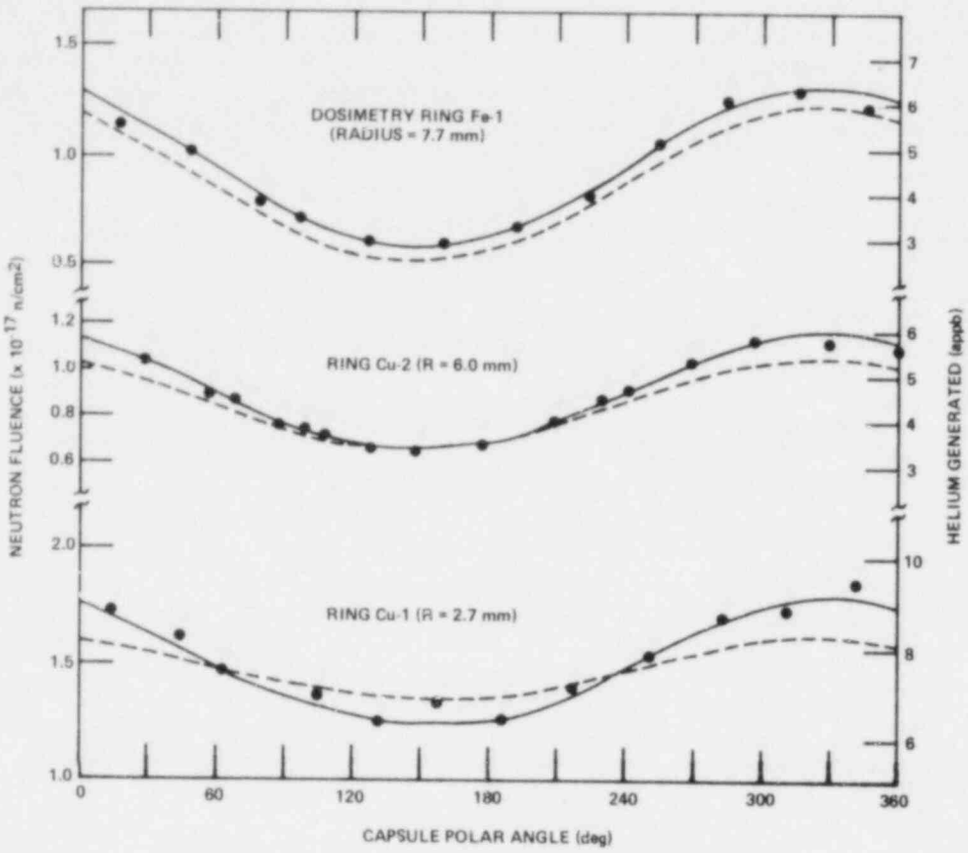

Fig. 5. Measured Helium Generation Concentrations in Three of the Ten Segmented Dosimetry Wires from the Second RTNS-I Irradiation, Plus Neutron Fluence Calculations Based on Radiometric Dosimetry (Dashed Curves) and Radiometric Plus Helium Accumulation Dosimetry (Solid Curves).

scoping experiment in the Los Alamos Meson Physics Facility (LAMPF) at the Radiation Effects Facility (R.E.F.). The LAMPF neutron environment was produced by 800-MeV proton bombardment of a copper beam stop. The neutron yield peaked in the ~100-500 keV energy region, and extended up to about 100 MeV. Helium accumulation dosimeters included ^{6}Li, ^{10}B, Al, Fe, Ni, Cu, and Au, and were irradiated in two R.E.F. configurations. Helium accumulation results were generally consistent with other dosimetry results. They demonstrated that helium accumulation neutron dosimetry is an effective technique for this type of neutron spectrum, and is particularly suited for monitoring irradiation-to-irradiation fluence variations once the neutron spectrum has been characterized.

The Be(d,n) reaction, and similarly the Li(d,n) reaction (the source reaction for the Fusion Materials Irradiation Test Facility, FMIT), produces a neutron field with steep fluence gradients and, in addition, large differences in the neutron energy spectrum at different source angles. The Be(d,n) neutron environment was characterized in a joint helium

accumulation-plus-radiometric dosimetry experiment performed at the University of California at Davis.[10] The experiment used a geometry similar to that shown in Fig. 2. In this case, the irradiation capsule, shown in Fig. 3, was positioned ~1 cm from the beryllium target. A large number of radiometric dosimeters were incorporated in this experiment. Most of the source characterization was performed by unfolding the neutron spectrum distributions at well-defined angles using stacks of radiometric foils mounted on the three large arcs behind the irradiation capsule,[10] as shown in Fig. 2.

The helium accumulation dosimetry rings incorporated within the capsule (Fig. 3) were used in the characterization of the capsule irradiation volume. At this close source distance, the fluence varies rapidly with position and the finite source size affects the shape of the energy spectrum. Any capsule offset from the neutron source axis is also important; this was determined to be ~1.3 mm, based on comparisons of the measured helium concentration variations around the dosimetry rings with a fluence model of the neutron source distribution. This small offset produced nearly factor-of-two differences in fluence at symmetric locations around the capsule, demonstrating the steep gradients present and the need for in-situ passive dosimetry in the high-flux regions of Be(d,n) and, by implication, Li(d,n) test environments. Neutron fluences were calculated for the capsule region by integrating the angular yields determined from the radiometric dosimeters on the arcs over the neutron source and capsule radiometric foil geometries, accounting for the capsule offset.[10] These results were used to derive total helium generation cross sections for several materials incorporated in the capsule.[11]

Helium accumulation results have now also been used to demonstrate combined helium accumulation/radiometric spectrum unfolding in the capsule region. The helium analysis results from the segmented Al, Fe, and Cu dosimetry rings were geometrically extrapolated to the plane of radiometric foil stack C (Fig. 3). Spectral unfolding was performed at 0° in this plane, using the code STAY'SL and the reactions listed in Table 3. Radiometric cross sections for neutron energies ≤20 MeV were based on ENDF/B-V, and cross sections >20 MeV were taken from Ref. 12. ENDF/B-V (n,α) cross sections were used for Cu and Al helium production below the (n,nα) thresholds (~12 MeV), and the (n,total helium) statistical model calculations of F. M. Mann were used at higher energies.[13] The Fe(n,total helium) cross section was taken from Arthur and Young.[14] The resulting unfolded neutron energy spectrum is shown in Fig. 6.

The results demonstrate the feasibility of using combined helium accumulation/radiometric spectrum unfolding for broad neutron energy distributions. In the present case, the helium accumulation materials used in the unfolding were based in part on the availability of energy-dependent total helium production cross section information. The unfolding demonstrates their similar energy sensitivities (Table 3). Future work will investigate materials with different expected energy responses, such as gold for higher energies.

Table 3. Dosimetry Reactions Used for Be(d,n) Neutron Spectrum Unfolding

Reaction	Energy Range* (MeV)	Average Deviation†
$^{59}Co(n,\gamma)^{60}Co$	10^{-4} - 13.5	-1.9%
$^{197}Au(n,\gamma)^{198}Au$	10^{-3} - 4.0	-0.1%
$^{58}Ni(n,p)^{58}Co$	3.0 - 17.5	+6.6%
$^{54,56}Fe(n,X)^{54}Mn$	3.5 - 25	-6.8%
$^{59}Co(n,p)^{59}Fe$	6.5 - 19	-2.6%
$^{60}Ni(n,p)^{60}Co$	7.0 - 19.5	+9.1%
$^{27}Al(n,\alpha)^{24}Na$	8.5 - 18.5	-0.9%
$^{54}Fe(n,\alpha)^{51}Cr$	8.5 - 22	-2.7%
Fe(n,X)helium	8.5 - 25	+16.0%
Al(n,X)helium	9.0 - 25	+0.6%
Cu(n,X)helium	9.0 - 26	-1.9%
$^{197}Au(n,2n)^{196}Au$	10 - 20	+0.5%
$^{93}Nb(n,2n)^{92m}Nb$	10.5 - 20	-12.0%
$^{59}Co(n,2n)^{58}Co$	12 - 23	-3.8%
$^{90}Zr(n,2n)^{89}Zr$	13 - 25	-1.1%
$^{58}Ni(n,2n)^{57}Ni$	13.5 - 24	+15.4%
$^{197}Au(n,3n)^{195}Au$	17 - 27	-10.2%
$^{59}Co(n,3n)^{57}Co$	21 - 30	+3.8%
$^{197}Au(n,4n)^{194}Au$	25 - 32	+1.5%

*90% response range
†Percentage deviations between measured and calculated reaction integrals

Since this Be(d,n) experiment included a large number of radiometric dosimetry reactions for extensive source characterization, the emphasis on further experiment analyses will be on integrally testing (n,total helium) cross section evaluations by comparison with the helium measurements. Such integral testing has been demonstrated for this experiment.[10] Comparisons made at multiple neutron source angles should also provide some energy-dependent information, since the neutron energy spectrum changes rapidly with source angle.

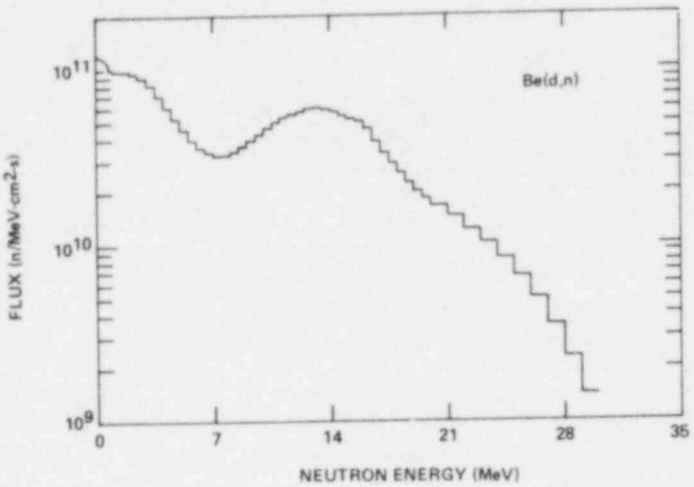

Fig. 6. Unfolded Flux Spectrum for the Be(d,n) Reaction at 0^{o} for 30-MeV Deuterons, 17 mm from the Beryllium Target.

CONCLUSIONS

The dosimetry work performed to date demonstrates the use of helium accumulation neutron dosimetry in fusion neutron test environment characterization. The goal of future dosimetry work will be to develop and use optimum sets of energy-dependent helium accumulation dosimeters, in combination with radiometric dosimeters, on a routine basis in both fission reactor and fast neutron environments used for fusion materials testing.

ACKNOWLEDGEMENTS

The T(d,n) and Be(d,n) irradiations were joint experiments with M. W. Guinan (LLNL). The technical support of B. M. Oliver, M. M. Nakata, and J. G. Bradley (Rockwell International) is gratefully acknowledged, as are the encouragement and support of this work by M. M. Cohen and T. C. Reuther, Jr. of the U.S. Department of Energy's Office of Fusion Energy. This work was supported by the U.S. DOE's Materials Irradiation Effects Branch of the Office of Fusion Energy.

REFERENCES

1. L. R. Greenwood, "Review of Source Characterization for Fusion Materials Irradiations," in Proc. Symp. on Neutron Cross-Sections

from 10 to 50 MeV, M. R. Bhat and S. Pearlstein, eds., Brookhaven National Laboratory, BNL-NCS-51245 (1980) pp. 75-98

2. D. W. Kneff and H. Farrar IV, "Helium Accumulation Fluence Dosimetry for Fusion Reactor Materials Irradiations," J. Nucl. Mater. 85 & 86, 479 (1979)

3. F. H. Ruddy, C. C. Preston, R. Gold, E. V. Benton, and J. H. Roberts, "CR-39 Polymer, A Promising New Solid State Track Recorder for High Energy Neutron Applications," in Proc. Symp. on Neutron Cross-Sections from 10 to 50 MeV, M. R. Bhat and S. Pearlstein, eds., Brookhaven National Laboratory, BNL-NCS-51245 (1980) pp. 599-616

4. H. Farrar IV, W. N. McElroy, and E. P. Lippincott, "Helium Production Cross Section of Boron for Fast-Reactor Neutron Spectra," Nucl. Technol. 25, 305 (1975)

5. R. E. Gold, E. E. Bloom, F. W. Clinard, D. L. Smith, R. D. Stevenson, and W. G. Wolfer, "Materials Technology for Fusion: Current Status and Future Requirements," Nucl. Technol./Fusion 1, 169 (1981)

6. National Nuclear Data Center, Brookhaven National Laboratory

7. T. A. Gabriel, B. L. Bishop, and F. W. Wiffen, "Calculated Irradiation Response of Materials Using Fission Reactor (HFIR, ORR, and EBR-II) Neutron Spectra," Oak Ridge National Laboratory, ORNL/TM-6361 (1979); F. W. Wiffen, E. J. Allen, H. Farrar IV, E. E. Bloom, T. A. Gabriel, H. T. Kerr, and F. G. Perey, "The Production Rate of Helium During Irradiation of Nickel in Thermal Spectrum Fission Reactors," J. Nucl. Mater. (1982, to be published)

8. F. G. Perey, "Least Squares Dosimetry Unfolding: The Program STAY'SL," Oak Ridge National Laboratory, ORNL/TM-6062 (1977); as modified by L. R. Greenwood, Argonne National Laboratory (1979)

9. D. W. Kneff, B. M. Oliver, M. M. Nakata, and H. Farrar IV, "Helium Generation Cross Sections for Fast Neutrons," in Proc. Symp. on Neutron Cross-Sections from 10 to 50 MeV, M. R. Bhat and S. Pearlstein, eds., Brookhaven National Laboratory, BNL-NCS-51245 (1980) pp. 289-300

10. D. W. Kneff, H. Farrar IV, and L. R. Greenwood, "Characterization of the Be(d,n) Neutron Field by Passive Dosimetry Techniques," ibid, pp. 113-132

11. D. W. Kneff, B. M. Oliver, M. M. Nakata, and H. Farrar IV, "Experimental Helium Generation Cross Sections for Fast Neutrons," J. Nucl. Mater. (to be published)

12. L. R. Greenwood, "Extrapolated Neutron Activation Cross Sections for Dosimetry to 44 MeV," Argonne National Laboratory, ANL/FPP/TM-115 (1978)

13. D. W. Kneff, H. Farrar IV, F. M. Mann, and R. E. Schenter, "Experimental and Theoretical Determination of Helium Production in Copper and Aluminum by 14.8-MeV Neutrons," Nucl. Technol. 49, 498 (1980)

14. E. D. Arthur and P. G. Young, "Evaluated Neutron-Induced Cross Sections for $^{54,56}Fe$ to 40 MeV," Los Alamos National Laboratory, LA-8626-MS (1980)

Session D.1
Light Water Reactors-III

STATUS OF REGULATORY DEMANDS IN THE U.S. ON THE APPLICATION OF PRESSURE VESSEL DOSIMETRY

P. N. Randall
U.S. Nuclear Regulatory Commission
Washington, DC 20545

ABSTRACT

Regulatory demands for information about neutron radiation embrittlement of reactor vessel beltline materials have increased sharply in scope and in need for reliability. Setting pressure temperature limits for normal operation continues to require accurate predictions of fluence at the location of the most sensitive material. Surveillance results occasionally provide a technical surprise, indicating that there is room for improvement in reactor physics calculations. But, the recent increase in scope of regulatory demands for improved dosimetry has been caused by the growing realization that overcooling transients can threaten vessel integrity under certain conditions. While the systems scenarios may vary, the common features of the overcooling transients that are of concern are: 1) a drop in reactor coolant temperature, which could give the beltline a thermal shock sufficient to cause small cracks to pop in to considerable depth, and 2) repressurization while the vessel remains relatively cool, which could drive the crack through the remaining ligament. Only after some years of neutron radiation will the embrittlement of the material be sufficient for such an event to occur, and only then in radiation sensitive material such as high-copper welds. Thus, there is great demand for fluence calculations aimed at specific locations in the beltline, which requires detailed knowledge of azimuthal, axial and radial distribution of fluence through the vessel wall. In addition, there are proposed changes in core configuration to reduce flux peaks, which must be evaluated.

INTRODUCTION

The purpose of this paper is to tell practitioners of the dosimetry arts how their findings are applied by regulatory people. The paper is written from the perspective of a fracture mechanics practitioner, and its theme is that the ultimate goal of neutron dosimetry is fracture control of reactor vessel beltlines under normal and accident loads. As diagrammed in Figure 1, fracture analyses require material properties information, especially about neutron embrittlement, which in turn requires a reliable measure of neutron fluence, one that correlates with damage to the material as a function of its chemical composition, irradiation temperature and time of exposure.

Current studies of pressurized thermal shock, which is a potential threat to the integrity of reactor vessel beltlines, have caused a quantum jump in the demand for good information about neutron embrittlement of the materials in those vessels. The calculation of pressure-temperature limits for normal operation has always demanded such information, but it was possible to cover our ignorance with large margins more readily for the stresses caused by normal operation than it is for the stresses superimposed by a thermal shock transient.

FRACTURE ANALYSIS

Because the application of neutron dosimetry is materials property information for use in fracture analysis, it seems worthwhile to devote pages to a discussion of current fracture analysis procedures. Size effect is the principal impediment to the measurement of fracture toughness for use in an analysis of a reactor vessel. Beltline wall thicknesses range from about 6 to 9 inches, hence full-thickness compact toughness specimens of irradiation material would be the size of a suitcase and are almost unheard-of. Questions of scale-up underlie much of the art of fracture analysis for reactor vessels.

Fracture analyses done for regulatory purposes solve the size-effect problem by the use of a reference toughness curve that is given in the ASME code.[1] The reference toughness K_{IR} values, given as a function of temperature, are analogous to allowable stress values. The K_{IR} curve was derived from a curve drawn as a lower bound to a set of large-scale tests performed for the HSST program. All of the specimens were cut from one 12-inch thick plate of A533-B steel, Plate 02.

To make the curve application to another material, the reference (transition) temperature of the material in question is compared to that of Plate 02 and the temperature scale is indexed accordingly. The ASME Code defines the indexing procedure in terms of the reference temperature, RT_{NDT}, which is the highest of three temperatures: 1) the drop weight nil-ductility transition temperature, 2) the Charpy 50 ft lb transition temperature minus 60°F, and 3) the Charpy 35 mil lateral expansion temperature minus 60°F. The ASME Code does not define RT_{NDT} for an irradiated material. That definition is given in Appendix G, 10 CFR Part 50 of the federal regulations as "... the reference temperature as adjusted for irradiation effects ... by adding to RT_{NDT} the temperature shift in the average Charpy curve for the irradiated material relative to that for the unirradiated material, measured at the 30 ft lb level. (Until recently the regulation referred to the 50 ft lb and 35 mil lateral expansion levels.) Figure 2 illustrates the case when drop weight NDTT governs. The terminology has been treated somewhat loosely. It is now common to refer to the ASME Code procedure as the measurement of "initial RT_{NDT}" and the term RT_{NDT}, when applied to irradiated material after exposure, is the sum of the initial RT_{NDT} and the ΔRT_{NDT} caused by irradiation.

One might well ask where is the proof that the K_{IR} curve, adjusted on the basis of the Charpy shift, properly represents the effect of temperature on fracture toughness of an irradiated material. The evidence we have is reassuring, but it is fragmentary. There is now an NRC sponsored program underway at Oak Ridge with the objective of gathering such evidence.

The foregoing definition of RT_{NDT} is nothing new to many readers. It was put in to clear up a common misunderstanding that the RT_{NDT} of irradiated material was measured by applying the ASME Code procedure. It is not. Another reason to repeat the definition of RT_{NDT} is to emphasize that the Charpy 30 ft lb shift is the salient feature of the linkage of dosimetry to fracture mechanics.

Figure 3 is intended to emphasize the tenuous nature of the link provided by the Charpy shift between two sophisticated technologies, dosimetry and fracture mechanics. It has the benefit of tradition, perhaps, and nothing better has appeared to take its place. Yet everyone knows that scatter in Charpy values in the transition region, coupled with the fact that the shift is the difference between two transition temperatures, contributes to the problem of drawing trend curves that relate shift to fluence. For this reason, small shifts are hardest to measure accurately. For example, the MPC task group that drew the trend curves[2] now being included in the ASTM standard had difficulty finding a lower cutoff value of fluence at which the shift was essentially zero. In the data base, negative values had been recorded as zero, and even at fluences of 10^{16} n/cm^2 some of the positive values seemed significant. This was probably because of scatter, but the question could not be answered without a detailed re-examination of the zero-shift data points.

One final aspect of fracture analysis to be discussed is the geometry of the postulated flaws. Figure 4a is a longitudinal section of the beltline wall showing the "1/4 T" (or 3/4 T) flaw that is specified by the ASME Code and NRC regulations for the calculation of pressure-temperature limits. Fluence estimates are made for the bottom of the semielliptical flaw. For the stress gradients encountered in normal operation, the stress intensity factor is highest there. The flaws shown in Figure 4b are typical of the range of sizes considered in thermal shock analyses, where the thermal stress gradient is quite steep. The flaws are considered to have a straight crack front and sufficient length to be considered a continuous "infinitely long" flaw. For shallow cracks (less tha 1/10 T) the usual rule of thumb of fracture mechanics applies, i.e., for a crack length greater tha 10 times the depth, K_I changes very little with greater length. For deep cracks (greater than 1/2 T) however, thermal stresses form a cusp in the cylinder, the uncracked ligament acts as a hinge, and the crack tip sustains an increase in K_I as a result.

For this case, crack length is assumed to be sufficient to prevent restraint of the cusp formation by uncracked parts of the cylinder. This problem in shell theory has not been worked out to my knowledge. It is simply assumed that the crack is long enough to permit full development of the cusp.

FLUENCE PREDICTION

As indicated in Figure 1, the salient quantity in fluence prediction is an estimate of the peak fluence per EFPY, i.e., the highest fluence on the inside wall of the vessel per effective full power year. For an operating reactor, the current value of EFPY is obtained simply by dividing the total megawatt hours thermal produced to date by the rated thermal power for the plant, and converting hours to years. For the future, EFPY is normally considered to be 0.8 times calendar years. The technology involved in making the calculation of fluence per EFPY has improved in recent years. The history of changes in reported fluence values reveals some very wide swings, typically involving a sharp increase in the estimate after examination of the first surveillance capsule. Part of the improvement has come through the development of two-dimensional transport codes and part through refinements in dosimetry.

Clearly, one of the regulatory demands that has been sharpened by the thermal shock studies is the requirement to estimate fluence as a function of azimuthal position. This information is required to compare surveillance results with transport calculations. Surveillance capsules are not always at the peak azimuthal location. Knowledge of the azimuthal variation of fluence is also required to find the fluence at the critical material. In many vessels, the critical material is a longitudinal beltline weld, because the welds have the highest copper content. Knowing this, the designer often attempted to rotate the shell course so the welds were not at the peak azimuthal fluence location. For vessels made with two plates per shell course, this technique reduced the fluence on the longitudinal welds to less than one third of the peak, in some cases, -- reactor cores normally being arranged in a square grid with some corner elements removed. Unfortunately, many vessels have three plates per shell course.

It is obviously important that the transport calculation be capable of accounting for the attenuation of fluence in the radial direction to relate capsule fluence to that at the vessel I.D. wall and at locations in the wall at the critical location on the crack front of the postulated flaw. Finally, the axial variation of fluence must be understood as well.

The acceptable level of uncertainty in fluence estimates is a matter of much recent debate. Also, there is much discussion about the accuracy of the trend curves, and errors in fluence affect the data base. In this regard, the regulatory demand is for only moderate accuracy but for a high level of confidence that the stated uncertainty is not exceeded. At the moment we would be satisfied if we had 99.9 percent confidence that the value was not off by a factor of 2. The reason for acceptance of a fairly wide uncertainty band is the well-known fact that the shift in RT_{NDT} varies with fluence taken to some fractional power. Thus, the uncertainty in ΔRT_{NDT} produced by an uncertainty of 30 percent in fluence is ±14 percent if the exponent is 0.50, and decreases to 5 percent if the exponent is 0.20. As described below, the trend is toward the latter value.

TREND CURVES

There is a strong interest in knowing the relationship of ΔRT_{NDT} to neutron fluence, however measured. Most of the effort at finding the relationship depends on curve fitting some data base. Theoretical bases have been proposed, but none have proven useful. Using plots on log-log paper, a slop of 0.50 has been used in R.G. 1.99, but to avoid over-prediction at high fluences and high copper content, a cut-off line with a slope of 0.195 had to be used. Westinghouse trend curves have a slope of 0.25. The MPC curve fitting activity yielded a mean curve slope of 0.31. The author fitted a PWR surveillance data base with two sets of curves, one for high nickel material with a slope of 0.35 and one for low nickel material with a slope of 0.25 at low fluences and 0.15 at high fluences.[3] These were bounding curves drawn to fall above about 95 percent of the data. George Guthrie then fitted the PWR surveillance data base with mean curves using a nonlinear regression technique.[4] He found the best fit using a slope of 0.22 for both low and high nickel materials. He has not yet tried "broken back" curves or any function other than a power law.

Should the trend curves be changed to substitute dpa for n/cm^2 (E>1 MeV)? There are a few reports of efforts to discover if damage correlation goes better with dpa. At the moment, the regulatory efforts to modernize Reg. Guide 1.99 do not include this change, because only part of the data base is available in terms of dpa, and because the advantages have not been shown clearly.

In relating ΔRT_{NDT} to fluence, the conventional measure of fluence, n/cm^2 (E>1 MeV) has seemed adequate. The reason given has been that the neutron energy spectrum did not differ too much from the surveillance capsule to the vessel wall, provided one was interested only in 1/4 T cracks.

Differences between power reactor spectra and test reactor spectra were certainly recognized, but other differences such as exposure time were also recognized and it was not possible to separate out the spectral effects. Sophisticated efforts to develop damage function analyses of neutron embrittlement were made some 10 years ago.[5] Now there is an ASTM standard on the calculation of displacements per atom (dpa).[6] Quoting from paragraph 3.2 of this Standard, "A primary source of neutron radiation damage in metals is the displacement of atoms from their normal lattice sites. Hence an appropriate damage exposure index is the number of times, on the average, that an atom has been displaced during an irradiation."

The thermal shock analyses have brought this factor greater attention, as has the estimation of damage to reactor vessel supports, because in both cases ignoring spectral effects is unconservative. In thermal shock analyses we are tentatively planning to change the attenuation expression used for calculating fluence at the crack tip, knowing fluence at the vessel inside surface to correspond to the change in dpa through the wall.

To complete the discussion of trend curves, copper remains the most potent element in everyone's trend curve formulation. Phosphorus has been discarded in our current treatment of the data, largely as a result of the MPC work which failed to find a phosphorus effect, and the fact that phosphorus does not vary widely in the data base.

Nickel is the current favorite for study. A number of reports have shown that low nickel is beneficial. The analysis of the PWR surveillance data mentioned above showed that the data most overpredicted by R.G.1.99 are the low-nickel data for A302-B steel and welds having nickel content less than 0.2 percent. Guthrie found that a copper-nickel product term in the multiplier of the expression for the trend curves gave a better fit of the data.

$$\Delta RT_{NDT} = [-5 + 480\ Cu + 270\ Cu\ Ni]\ [\frac{f}{10^{19}}]^{0.22}$$

He tried both a nickel term and a copper-nickel term with equally good results. Currently, the Cu Ni term is being used because Hawthorne has reported that nickel by itself does not seem to make the steel sensitive to neutron radiation. Work being sponsored by EPRI at Combustion Engineering has led to some rechecking of their "chemical factor", which included nickel, cooper and several other elements, but the results have not been published. It now appears that the next revision of Reg. Guide 1.99, (Revision 2) will either incorporate a nickel term in the expression for ΔRT_{NDT} or will provide separate sets of curves for "low" and "high" nickel content.

Some future revision of Reg. Guide 1.99 should include a factor for the time and temperature of irradiation. In the MPC trend curve activity[2] an effort was made to find a difference between test reactor data and surveillance data, but no clear-cut trend could be detected. We do see a growing need to quantify differences in ΔRT_{NDT} caused by exposure to different irradiation temperatures. This must involve the dosimetry practitioners because gamma heating is obviously involved. There is considerable disagreement about the importance of 30 or 50 degrees difference in test temperature at a nominal temperature of 550 deg. F. Much of the data is more than 20 years old. Much of the disagreement may result from the interaction of residual elements such as copper with the time-temperature effect. In approximate terms, chemical composition of reactor vessel steels is believed to be unimportant at temperatures up to about 350 deg. F and again at temperatures above about 750 deg. F, but composition may have a significant effect on the temperature at which the transition from high to low levels of damage occurs.

The physical picture of time-temperature-compositional effects needs to be quantified for elements that are now known to make steels sensitive to radiation -- copper and nickel and perhaps others as well. The results would be useful in correlation of test reactor and surveillance data, in evaluation of deliberate changes in reactor operating temperature, and as a supplement to annealing studies.

CONCLUSION

This has been a paper about fracture analysis of reactor vessel beltlines, a unique problem in which the fracture toughness of the material undergoes a progressive change for the worse in the service environment. Neutron dosimetry is the tool used to measure the hostility of that environment. If there was a period of complacency some time back when some felt they knew all they needed to know about neutron dosimetry, that feeling was dissipated by the discovery that pressurized thermal shock could cause fracture of a highly irradiated vessel. So now you have an eager customer. His loudest regulatory demand for good dosimetry is for assurance that errors in fluence of a factor of two are a thing of the past, that there are no more technical surprises. Next, he wants a more sophisticated measure of fluence, one that accounts for differences in neutron energy spectra. To account for time-temperature effects, he wants to understand gamma heating. And, of most importance, he wants all of this correlated with the embrittlement of the reactor vessel materials.

REFERENCES

1. ASME Boiler and Pressure Vessel Code Section III Appendix G, "Protection Against Non-Ductile Failure."

2. Metal Properties Council Subcommittee 6 on Nuclear Materials, "Prediction of the Shift in the Brittle-Ductile Transition Temperature of LWR Pressure Vessel Materials" Report to ASTM Committee E 10.02 on Behavior and Use of Metallic Materials in Nuclear Systems. To be published by MPC.

3. P. N.Randall, "The Status of Trend Curves and Surveillance Results in U.S. Regulatory Activities." Paper given at IAEA Specialists meeting in Vienna, October 20, 1981.

4. Private Communication. To be published in Quarterly Progress Reports of LWR Dosimetry Improvement Program.

5. C. Z. Serpan, Jr., "Damage Function Analysis of Neutron-Induced Embrittlement in A302B Steel at 550F (288C) ASTM STP 529, 1973."

6. ASTM 693-79. Standard Practice for Characterizing Neutron Exposures in Ferritic Steels in Terms of Displacements Per Atom (dpa).

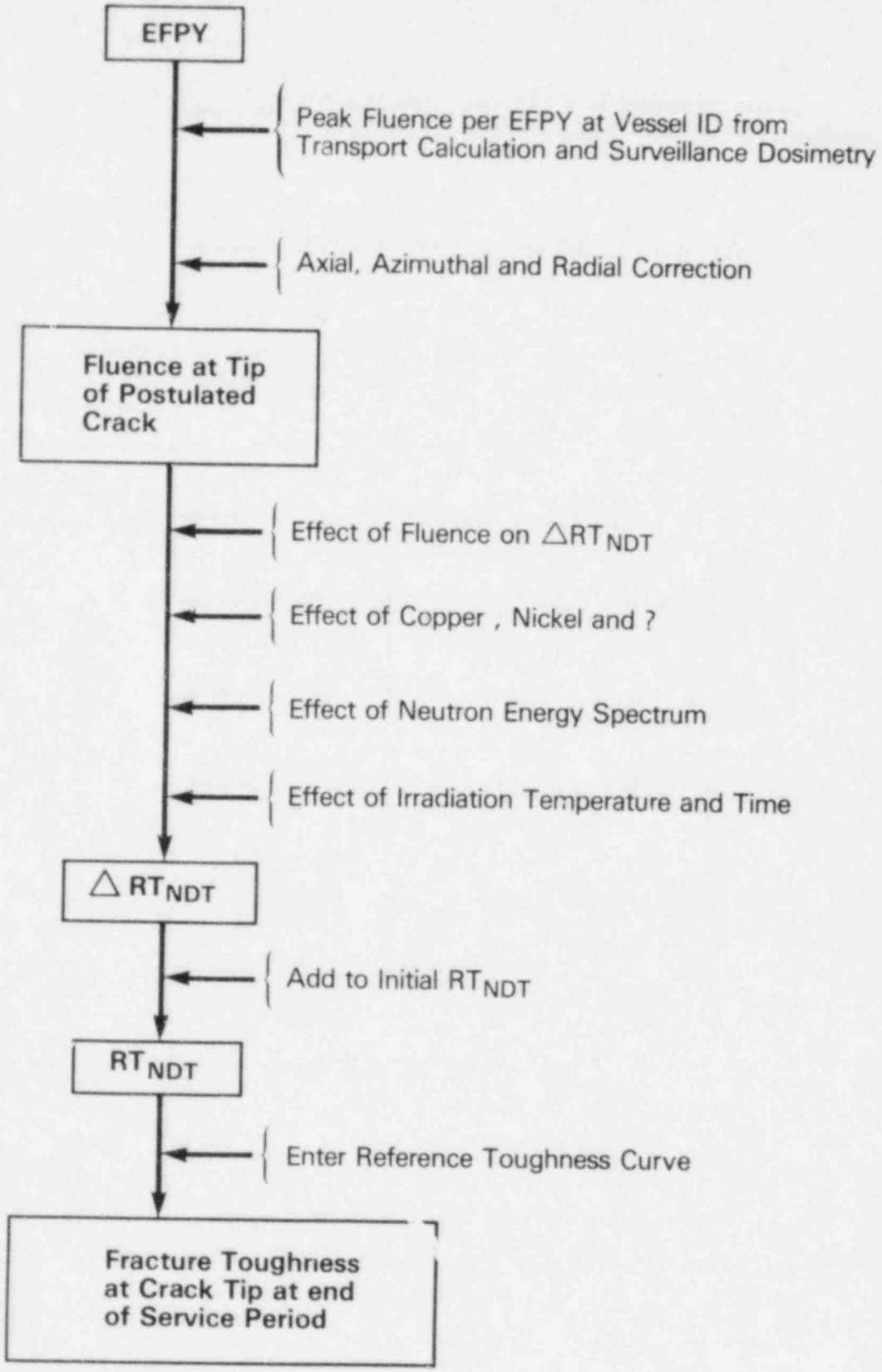

Figure 1. Flow Sheet for the Application of Neutron Dosimetry to Fracture Analysis

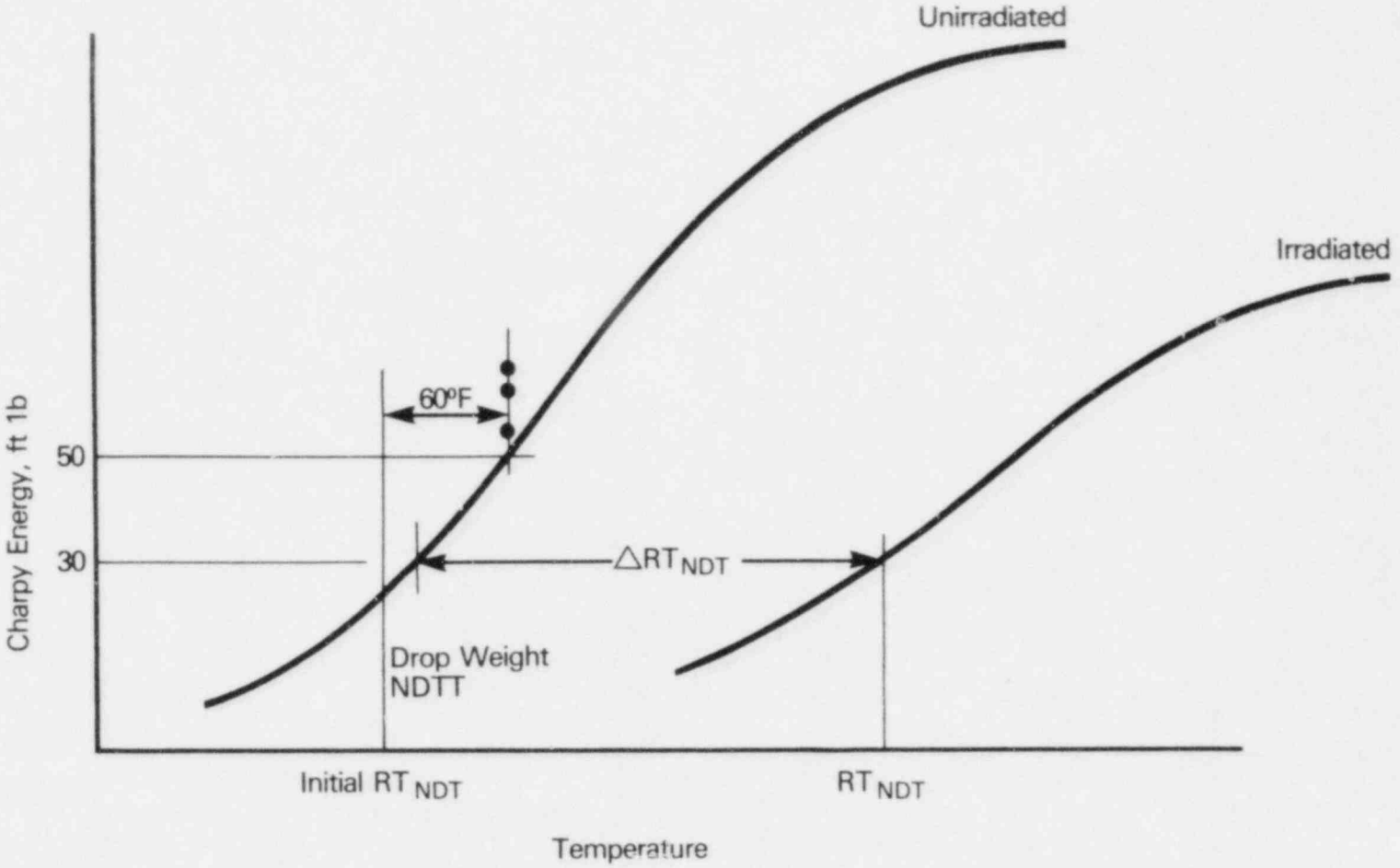

1020

Figure 2. Definition of initial RT_{NDT} when the drop weight test governs

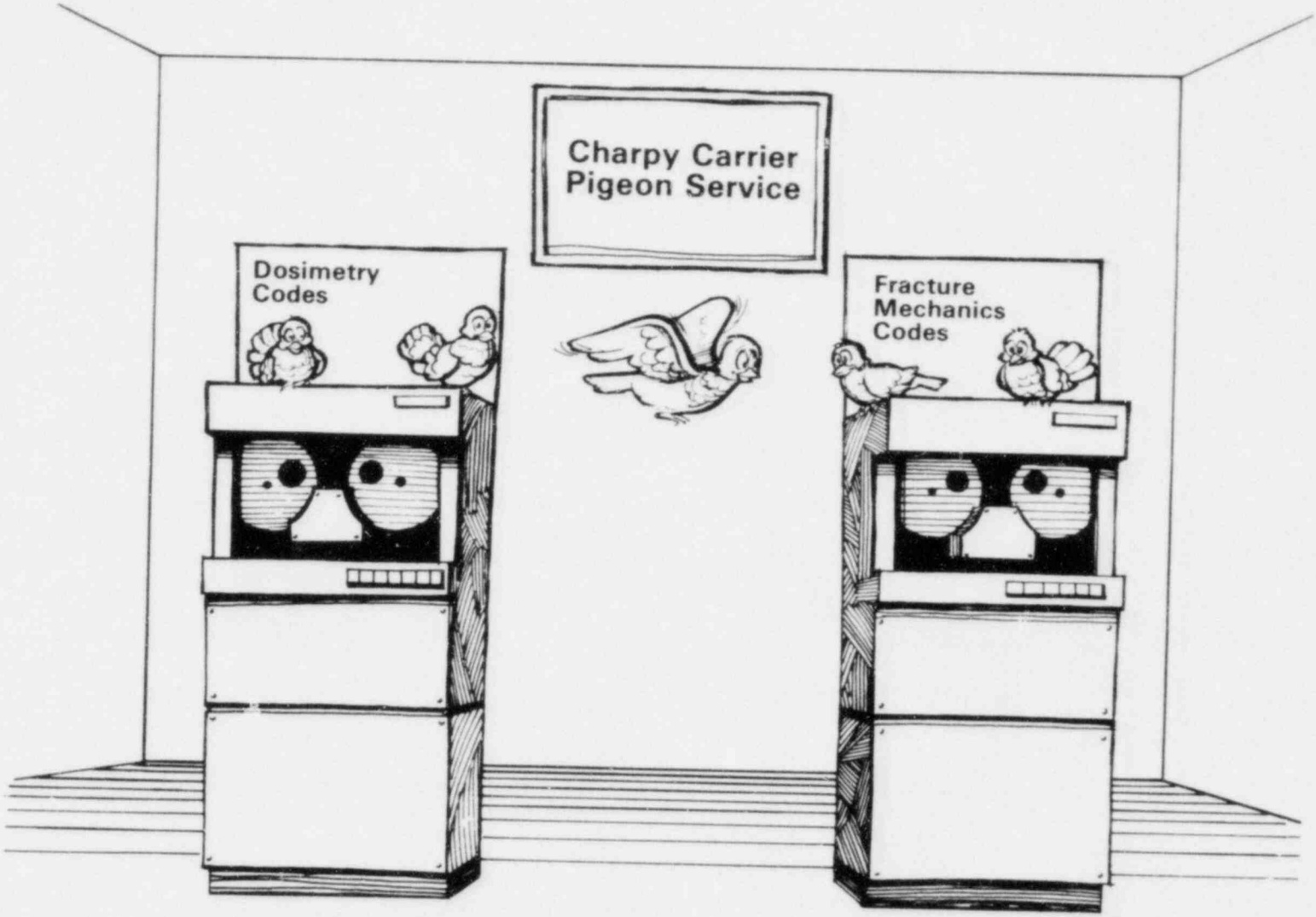

Figure 3. The link between transport codes used for dosimetry and fracture analysis codes is a set of Charpy tests used to measure damage.

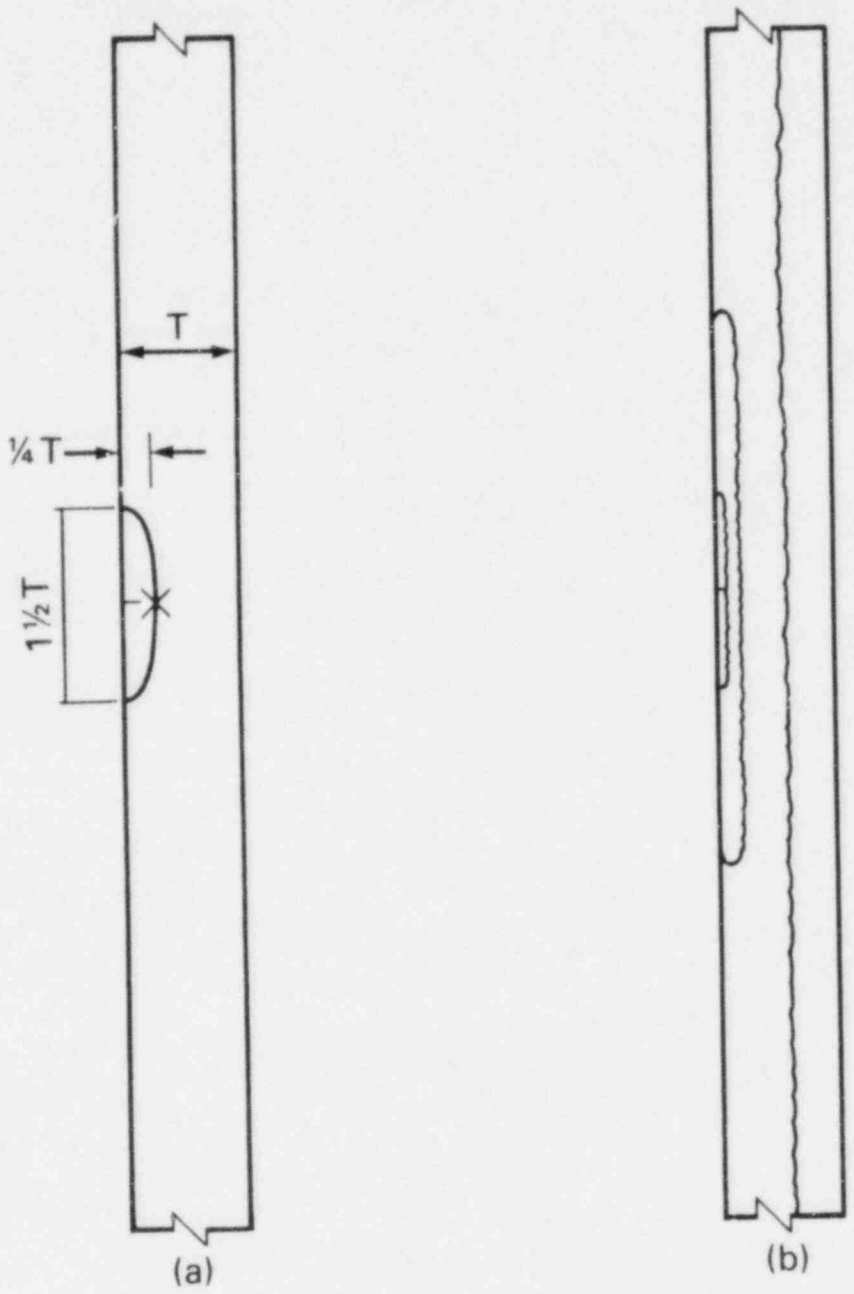

Figure 4. Type of flaw postulated for calculation of pressure-temperature limits (a) and for pressurized thermal shock calculations (b).

NEUTRON EXPOSURE PARAMETERS FOR THE FOURTH HSST SERIES OF METALLURGICAL IRRADIATION CAPSULES*

F. B. K. Kam, F. W. Stallmann, C. A. Baldwin, and A. Fabry†

Oak Ridge National Laboratory
Oak Ridge, Tennessee 37830

†CEN/SCK, Mol, Belgium

ABSTRACT

The neutron exposure parameters for the Heavy Section Steel Technology (HSST) Experiments performed at the Oak Ridge National Laboratory (ORNL) can be determined conservatively to ±10% (1σ) variance.

The neutron exposure parameters used for this study were fluence greater than 1 MeV, fluence greater than 0.1 MeV, and displacements per atom (dpa). Measured reaction rates, calculated neutron transport fluxes, and cross sections values were combined in the logarithmic least square adjustment code LSL.[1]

1. Introduction

The U.S. Nuclear Regulatory Commission (NRC) is conducting an extensive research program[2,3] to study fracture toughness of irradiated pressure vessel materials in the upper transition region and to investigate the applicability of small specimen test results to thick-section materials. This study has been extended to the study of upper-shelf behavior (plastic behavior). The first three irradiation experiments (nine capsules) contained fracture toughness specimens of four-inch (4T-CS) and a number of smaller specimens of low-shelf weldments.

*Research sponsored by the Division of Reactor Safety Research, U.S. Nuclear Regulatory Commission under Interagency Agreement DOE 40-551-75 with the U.S. Department of Energy under contract W-7405-eng-26 with the Union Carbide Corporation.

The fourth HSST irradiation series (four capsules) is primarily designed to obtain statistical data on the fracture toughness of "current practice" weldments. Each of the capsules contains one-inch-thick fracture toughness (1T-CS), Charpy V-notch, and tension test specimens (Figs. 1 and 2).

In support of the material irradiation experiments, a neutron characterization program was initiated to provide accurate exposure parameters for correlation with the property change rate data. The dosimetry results of the second and third HSST series have been reported in Refs. 4 and 5. The experience gained in these two experiments have led to modifications in the composition and distribution of the dosimeters which monitor the flux spectrun in the irradiated steel specimens. In addition, multiple foil sets were irradiated in simulated HSST irradiation capsules to obtain detailed neutron spectrum information. This dosimetry experiment was a joint effort between CEN/SCK, Mol, Belgium and ORNL. The methods and techniques of measurement, calculation, and analysis are the same as applied to the neutron spectral characterization of the PCA experiments and Blind Test.[6]

2. Results

The results reported in this paper are for capsules A and B of the fourth HSST irradiation series (Fig. 3). Tables 1 and 2 show the exposure parameters (fluence > 1 MeV, fluence > 0.1 MeV and dpa) for each specimen in capsule A. For the 1T-CT specimens, the exposure values represent values at the crack tip. For the charpy specimens, the values are given at the apex of the v-notch. Similarly Tables 3 and 4 represent the exposure values for capsule B. A 3-dimensional map for the exposure parameters has been determined. This map has the form

$$\phi(x,y,z) = \phi_o \cos B_x (x-x_o) \cos B_y (y-y_o) e^{-\lambda z} \quad . \qquad (1)$$

Preliminary estimates yield a ±10% (1σ) variance for the exposure parameters obtained from equation (1).

A technical report will be issued at a later date with a detailed uncertainty analysis and the methodology that was used to arrive at the

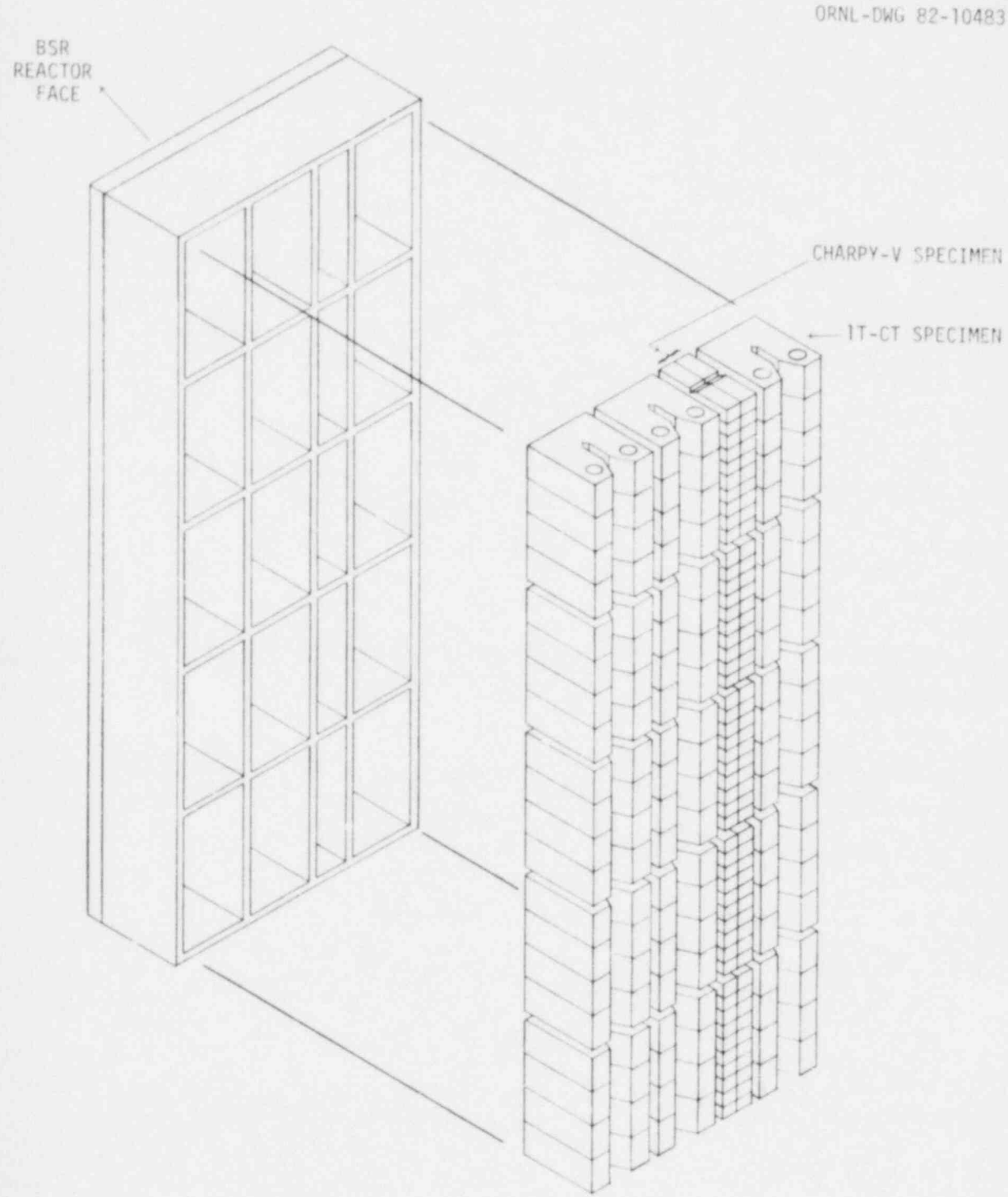

Fig. 1. Fourth HSST Series of Irradiation Capsules

1	21	41	42	141
		43	44	
		45	46	
2	22	47	48	142
		49	50	
3	23	51	52	143
		53	54	
		55	56	
4	24	57	58	144
		59	60	
5	25	61	62	145
		63	64	
		65	66	
6	26	67	68	146
		69	70	
7	27	71	72	147
		73	74	
		75	76	
8	28	77	78	148
		79	80	
9	29	81	82	149
		83	84	
		85	86	
10	30	87	88	150
		89	90	
11	31	91	92	151
		93	94	
		95	96	
12	32	97	98	152
		99	100	
13	33	101	102	153
		103	104	
		105	106	
14	34	107	108	154
		109	110	
15	35	111	112	155
		113	114	
		115	116	
16	36	117	118	156
		119	120	
17	37	121	122	157
		123	124	
		125	126	
18	38	127	128	158
		128	130	
19	39	131	132	159
		133	134	
		135	136	
20	40	137	138	160
		139	140	

Fig. 2. Specimen Position Numbers for Fourth HSST Series Irradiation Capsules.

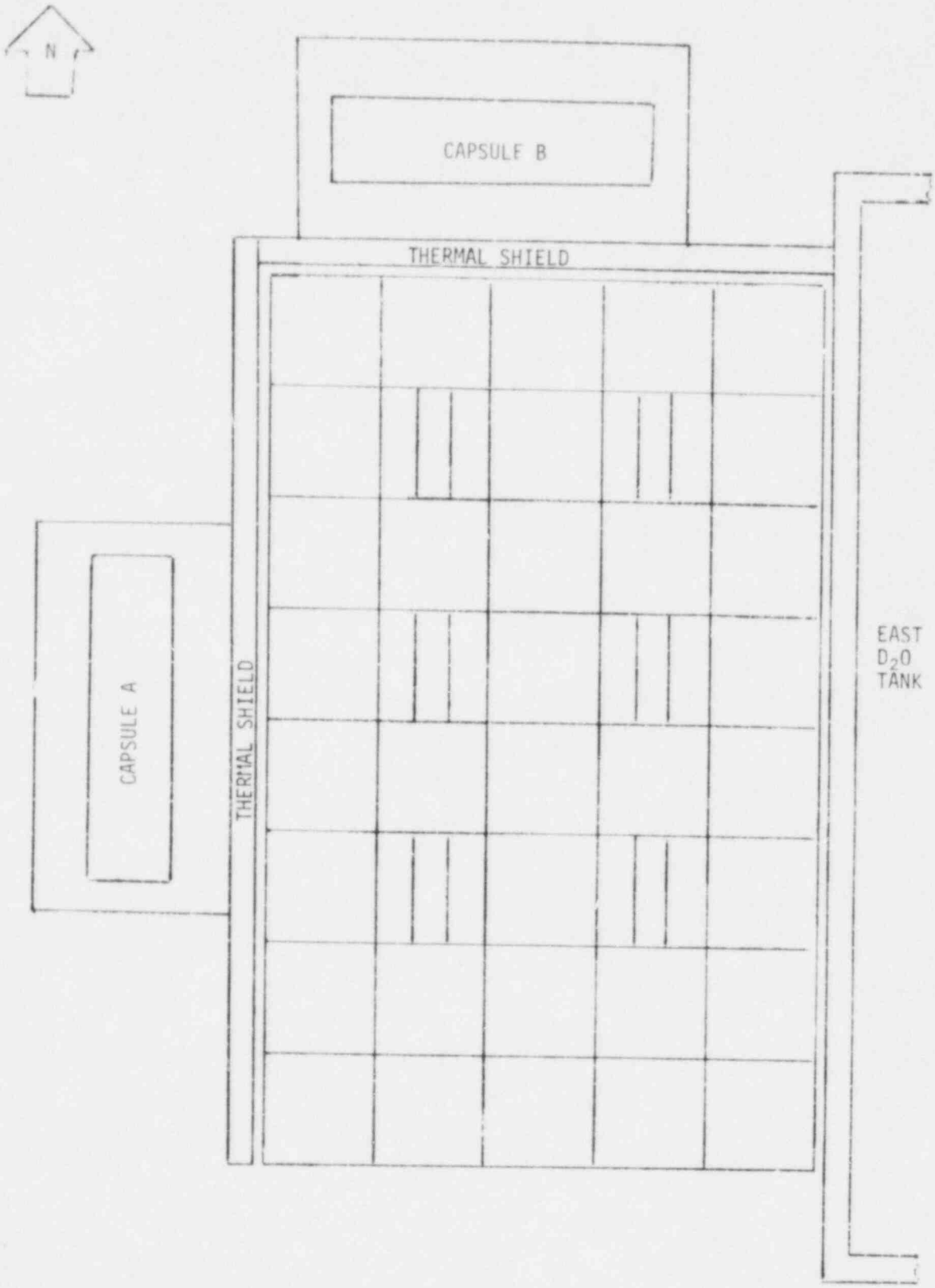

Fig. 3. Fourth HSST Experimental Configuration.

Table 1. Exposure Parameters for Capsule A 1T-CT Specimens

Specimen Position No.	Fluence >1 MeV	Fluence >.1 MeV	DPA	Specimen Position No.	Fluence >1 MeV	Fluence >.1 MeV	DPA	Specimen Position No.	Fluence >1 MeV	Fluence >.1 MeV	DPA
1	7.9485E+18	2.6420E+19	1.2545E-02	21	1.0480E+19	3.6404E+19	1.6890E-02	141	8.8131E+18	3.0132E+19	1.4112E-02
2	1.0668E+19	3.5955E+19	1.6933E-02	22	1.3109E+19	4.6066E+19	2.1232E-02	142	1.0917E+19	3.7778E+19	1.7570E-02
3	1.3254E 19	4.5022E+19	2.1107E-02	23	1.5589E+19	5.5174E+19	2.1232E-02	143	1.2899E+19	4.4977E+19	2.0826E-02
4	1.5676E+19	5.3500E+19	2.5012E-02	24	1.7891E+19	6.3618E+19	2.9125E-02	144	1.4737E+19	5.1645E+19	2.3842E-02
5	1.8467E+19	6.3250E+19	2.9508E-02	25	2.0517E+19	7.3227E+19	3.3452E-02	145	1.6830E+19	5.9224E+19	2.7275E-02
6	2.0406E+19	7.0000E+19	3.2627E-02	26	2.2321E+19	7.9801E+19	3.6419E-02	146	1.8266E+19	6.4404E+19	2.9626E-02
7	2.2092E+19	7.5836E+19	3.5331E-02	27	2.3871E+19	8.5414E+19	3.8960E-02	147	1.9497E+19	6.8822E+19	3.1636E-02
8	2.3502E+19	8.0684E+19	3.7587E-02	28	2.5148E+19	9.0000E+19	4.1045E-02	148	2.0510E+19	7.2428E+19	3.3284E-02
9	2.4875E+19	8.5332E+19	3.9767E-02	29	2.6358E+19	9.4272E+19	4.3006E-02	149	2.1467E+19	7.5780E+19	3.4829E-02
10	2.5600E+19	8.7715E+19	4.0904E-02	30	2.6966E+19	9.6334E+19	4.3972E-02	150	2.1945E+19	7.7392E+19	3.5586E-02
11	2.6007E+19	8.8953E+19	4.1521E-02	31	2.7266E+19	9.7237E+19	4.4424E-02	151	2.2177E+19	7.8090E+19	3.5935E-02
12	2.6090E+19	8.9031E+19	4.1611E-02	32	2.7255E+19	9.6969E+19	4.4357E-02	152	2.2160E+19	7.7864E+19	3.5872E-02
13	2.5728E+19	8.7457E+19	4.0963E-02	33	2.6793E+19	9.4949E+19	4.3524E-02	153	2.1781E+19	7.7864E+19	3.5198E-02
14	2.5079E+19	8.4921E+19	3.9862E-02	34	2.6982E+19	9.2060E+19	4.2289E-02	154	2.1206E+19	7.3960E+19	3.4209E-02
15	2.4118E+19	8.1277E+19	3.8254E-02	35	2.5073E+19	8.8062E+19	4.0560E-02	155	2.0393E+19	7.0792E+19	3.2826E-02
16	2.2857E+19	7.6573E+19	3.6160E-02	36	2.3777E+19	8.3005E+19	3.8356E-02	156	1.9351E+19	6.6788E+19	3.1067E-02
17	2.0848E+19	6.9168E+19	3.2842E-02	37	2.1743E+19	7.5151E+19	3.4914E-02	157	1.7717E+19	6/0572E+19	2.8322E-02
18	1.8969E+19	6.2305E+19	2.9752E-02	38	1.9858E+19	6.7933E+19	3.1737E-02	158	1.6204E+19	5.4859E+19	2.5789E-02
19	1.6854E+19	5.4629E+19	2.6285E-02	39	1.7746E+19	5.9897E+19	2.8189E-02	159	1.4510E+19	4.8498E+19	2.2960E-02
20	1.4530E+19	4.6241E+19	2.2483E-02	40	1.5432E+19	5.1141E+19	2.4311E-02	160	1.2652E+19	4.1563E+19	1.9867E-02

Table 2. Exposure Parameters for Capsule A Charpy Specimens

Specimen Position No.	Fluence >1 MeV	Fluence >.1 MeV	DPA	Specimen Position No.	Fluence >1 MeV	Fluence >.1 MeV	DPA
41	7.6558E+18	2.7335E+19	1.2598E-02	42	7.5128E+18	2.6789E+19	1.2372E-02
43	8.5618E+18	3.0795E+19	1.4133E-02	44	8.4019E+18	3.0179E+19	1.3880E-02
45	9.4528E+18	3.4196E+19	1.5643E-02	46	9.2762E+18	3.3513E+19	1.5362E-02
47	1.0327E+19	3.7534E+19	1.7124E-02	48	1.0134E+19	3.6784E+19	1.6816E-02
49	1.1183E+19	4.0802E+19	1.8574E-02	50	1.0974E+19	3.9987E+19	1.8240E-02
51	1.2015E+19	4.3993E+19	1.9990E-02	52	1.1795E+19	4.3114E+19	1.9631E-02
53	1.2834E+19	4.7102E+19	2.1370E-02	54	1.2594E+19	4.6161E+19	2.0986E-02
55	1.3626E+19	5.0123E+19	2.2711E-02	56	1.3372E+19	4.9122E+19	2.2303E-02
57	1.4394E+19	5.3050E+19	2.4011E-02	58	1.4125E+19	5.1990E+19	2.3580E-02
59	1.5137E+19	5.5878E+19	2.5268E-02	60	1.4854E+19	5.4762E+19	2.4814E-02
61	1.6437E+19	6.0820E+19	2.7465E-02	62	1.6129E+19	5.9605E+19	2.6971E-02
63	1.7100E+19	6.3337E+19	2.8585E-02	64	1.6780E+19	6.2072E+19	2.8071E-02
65	1.7733E+19	6.5736E+19	2.9653E-02	66	1.7401E+19	6.4423E+19	2.9121E-02
67	1.8334E+19	6.8012E+19	3.0667E-02	68	1.7992E+19	6.6654E+19	3.0117E-02
69	1.8903E+19	7.0161E+19	3.1626E-02	70	1.8550E+19	6.8759E+19	3.1058E-02
71	1.9439E+19	7.2178E+19	3.2527E-02	72	1.9076E+19	7.0736E+19	3.1943E-02
73	1.9940E+19	7.4061E+19	3.3370E-02	74	1.9568E+19	7.2581E+19	3.2770E-02
75	2.0406E+19	7.5805E+19	3.4151E-02	76	2.0025E+19	7.4290E+19	3.3538E-02
77	2.0836E+19	7.7407E+19	3.4871E-02	78	2.0447E+19	7.5861E+19	3.4245E-02
79	2.1229E+19	7.8864E+19	3.5527E-02	80	2.0833E+19	7.7289E+19	3.4889E-02
81	2.1860E+19	8.1181E+19	3.6576E-02	82	2.1452E+19	7.9559E+19	3.5919E-02
83	2.2144E+19	8.2210E+19	3.7045E-02	84	2.1730E+19	8.0568E+19	3.6380E-02
85	2.2389E+19	8.3086E+19	3.7447E-02	86	2.1971E+19	8.1426E+19	3.6774E-02
87	2.2594E+19	8.3806E+19	3.7781E-02	88	2.2172E+19	8.2132E+19	3.7102E-02
89	2.2760E+19	8.4569E+19	3.8046E-02	90	2.2334E+19	8.2684E+19	3.7363E-02
91	2.2885E+19	8.4775E+19	3.8242E-02	92	2.2457E+19	8.3081E+19	3.7556E-02
93	2.2969E+19	8.5022E+19	3.8369E-02	94	2.2540E+19	8.3324E+19	3.7680E-02
95	2.3013E+19	8.5110E+19	3.8426E-02	96	2.2583E+19	8.3410E+19	3.7736E-02
97	2.3016E+19	8.5039E+19	3.8414E-02	98	2.2586E+19	8.3340E+19	3.7724E-02
99	2.2979E+19	8.4808E+19	3.8332E-02	100	2.2550E+19	8.3114E+19	3.7643E-02
101	2.2803E+19	8.3967E+19	3.7997E-02	102	2.2377E+19	8.2290E+19	3.7315E-02
103	2.2650E+19	8.3288E+19	3.7718E-02	104	2.2227E+19	8.1624E+19	3.7040E-02
105	2.2458E+19	8.2453E+19	3.7370E-02	106	2.2038E+19	8.0806E+19	3.6699E-02
107	2.2225E+19	8.1463E+19	3.6954E-02	108	2.1810E+19	7.9836E+19	3.6290E-02
109	2.1953E+19	8.0321E+19	3.6471E-02	110	2.1543E+19	7.8717E+19	3.5816E-02
111	2.1643E+19	7.9029E+19	3.5922E-02	112	2.1238E+19	7.7451E+19	3.5277E-02
113	2.1294E+19	7.7589E+19	3.5307E-02	114	2.0896E+19	7.6040E+19	3.4673E-02
115	2.0907E+19	7.6004E+19	3.4629E-02	116	2.0517E+19	7.4486E+19	3.4007E-02
117	2.0484E+19	7.4277E+19	3.3888E-02	118	2.0101E+19	7.2794E+19	3.3279E-02,
119	2.0024E+19	7.2411E+19	3.3085E-02	120	1.9650E+19	7.0965E+19	3.2491E-02
121	1.9083E+19	6.8614E+19	3.1446E-02	122	1.8726E+19	6.7243E+19	3.0882E-02
123	1.8524E+19	6.6372E+19	3.0477E-02	124	1.8178E+19	6.5046E+19	2.9930E-02
125	1.7933E+19	6.4007E+19	2.9452E-02	126	1.7598E+19	6.2728E+19	2.8923E-02
127	1.7311E+19	6.1521E+19	2.8374E-02	128	1.6987E+19	6.0292E+19	2.7864E-02
129	1.6657E+19	5.8921E+19	2.7244E-02	130	1.6346E+19	5.7744E+19	2.6755E-02
131	1.5974E+19	5.6210E+19	2.6064E-02	132	1.5676E+19	5.5088E+19	2.5597E-02
133	1.5974E+19	5.3395E+19	2.4838E-02	134	1.4978E+19	5.2328E+19	2.4392E-02
135	1.4525E+19	5.0479E+19	2.3566E-02	136	1.4254E+19	4.9471E+19	2.3143E-02
137	1.3762E+19	4.7469E+19	2.2252E-02	138	1.3505E+19	4.6521E+19	2.1852E-02
139	1.2973E+19	4.4370E+19	2.0897E-02	140	1.2731E+19	4.3484E+19	2.0522E-02

Table 3. Exposure Parameters for Capsule B 1T-CT Specimens

Specimen Position No.	Fluence 1 MeV	Fluence .1 MeV	DPA	Specimen Position No.	Fluence 1 MeV	Fluence .1 MeV	DPA	Specimen Position No.	Fluence 1 MeV	Fluence .1 MeV	DPA
1	5.5006E+18	1.8511E+19	8.7261E-03	21	6.9316E+18	2.4142E+19	1.1131E-02	141	5.6745E+18	1.9113E+19	9.0076E-03
2	7.1566E+18	2.4418E+19	1.1410E-02	22	8.8069E+18	3.0995E+19	1.4212E-02	142	7.1586E+18	2.4395E+19	1.1409E-02
3	8.7272E+18	3.0017E+19	1.3955E-02	23	1.0579E+19	3.7464E+19	1.7121E-02	143	8.5609E+18	2.9382E+19	1.3677E-02
4	1.0194E+19	3.5238E+19	1.6330E-02	24	1.2226E+19	4.3471E+19	1.9824E-02	144	9.8654E+18	3.4015E+19	1.5795E-02
5	1.1879E+19	4.1222E+19	1.9055E-02	25	1.4109E+19	5.0315E+19	2.2909E-02	145	1.1358E+19	3.9299E+19	1.8193E-02
6	1.3047E+19	4.5350E+19	2.0939E-02	26	1.5405E+19	5.5005E+19	2.5028E-02	146	1.2387E+19	4.2925E+19	1.8193E-02
7	1.4060E+19	4.8907E+19	2.2567E-02	27	1.6521E+19	5.9014E+19	2.6844E-02	147	1.3275E+19	4.6033E+19	2.1273E-02
8	1.4905E+19	5.1849E+19	2.3919E-02	28	1.7442E+19	6.2294E+19	2.8338E-02	148	1.4011E+19	4.8584E+19	2.2448E-02
9	1.5724E+19	5.4649E+19	2.5219E-02	29	1.8318E+19	6.5355E+19	2.9745E-02	149	1.4717E+19	5.0984E+19	2.3565E-02
10	1.6153E+19	5.6064E+19	2.5888E-02	30	1.8760E+19	6.6839E+19	3.0442E-02	150	1.5079E+19	5.2166E+19	2.4127E-02
11	1.6390E+19	5.6773E+19	2.6242E-02	31	1.8982E+19	6.7495E+19	3.0772E-02	151	1.5270E+19	5.2717E+19	2.4407E-02
12	1.6432E+19	5.6768E+19	2.6275E-02	32	1.8982E+19	6.7318E+19	3.0731E-02	152	1.5285E+19	5.2632E+19	2.4401E-02
13	1.6203E+19	5.5731E+19	2.5854E-02	33	1.8659E+19	6.5894E+19	3.0146E-02	153	1.5054E+19	5.1608E+19	2.3983E-02
14	1.5803E+19	5.4117E+19	2.5164E-02	34	1.8156E+19	6.3846E+19	2.9272E-02	154	1.4676E+19	5.0092E+19	2.3334E-02
15	1.5215E+19	5.1822E+19	2.4167E-02	35	1.7440E+19	6.1009E+19	2.8045E-02	155	1.4131E+19	4.7971E+19	2.2413E-02
16	1.4445E+19	4.8874E+19	2.2875E-02	36	1.6518E+19	5.7418E+19	2.6481E-02	156	1.3424E+19	4.5270E+19	2.1229E-02
17	1.3221E+19	4.4249E+19	2.0833E-02	37	1.5070E+19	5.1839E+19	2.4036E-02	157	1.2307E+19	4.1057E+19	1.9369E-02
18	1.2077E+19	3.9969E+19	1.8934E-02	38	1.3727E+19	4.6714E+19	2.1780E-02	158	1.1266E+19	3.7172E+19	1.7646E-02
19	1.0789E+19	3.5187E+19	1.6805E-02	39	1.2223E+19	4.1011E+19	1.9262E-02	159	1.0097E+19	3.2838E+19	1.5716E-02
20	9.3728E+18	2.9962E+19	1.4470E-02	40	1.0575E+19	3.4801E+19	1.6512E-02	160	8.8122E+18	2.8107E+19	1.3603E-02

Table 4. Exposure Parameters for Capsule B Charpy Specimens

SPECIMEN POSITION No.	FLUENCE >1 MeV	FLUENCE >.1 MeV	DPA	SPECIMEN POSITION No.	FLUENCE >1 MeV	FLUENCE >.1 MeV	DPA
41	5.5840E+18	1.9859E+19	9.1671E-03	42	5.4686E+18	1.9481E+19	8.9778E-03
43	6.2505E+18	2.2376E+19	1.0289E-02	44	6.1251E+18	2.1838E+19	1.0076E-02
45	6.9059E+18	2.4851E+19	1.1392E-02	46	6.7631E+18	2.4253E+19	1.1157E-02
47	7.5491E+18	2.7280E+19	1.2474E-02	48	7.397 E+18	2.6623E+19	1.2217E-02
49	8.1790E+18	2.9657E+19	1.3534E-02	50	8.0 0E+18	2.8944E+19	1.3254E-02
51	8.7945E+18	3.1980E+19	1.4569E-02	52	8.6 7E+18	3.1210E+19	1.4268E-02
53	9.3945E+18	3.4242E+19	1.5578E-02	54	9. 02E+18	3.3419E+19	1.5256E-02
55	9.9778E+18	3.6441E+19	1.6559E-02	56	9. 15E+18	3.5564E+19	1.6217E-02
57	1.0544E+19	3.8571E+19	1.7509E-02	58	1 26E+19	3.7644E+19	1.7148E-02
59	1.1091E+19	4.0630E+19	1.8428E-02	60	1.0861E+19	3.9652E+19	1.8048E-02
61	1.2049E+19	4.4228E+19	2.0036E-02	62	1.1799E+19	4.3164E+19	1.9622E-02
63	1.2538E+19	4.6060E+19	2.0855E-02	64	1.2278E+19	4.4952E+19	2.0425E-02
65	1.3004E+19	4.7807E+19	2.1637E-02	66	1.2736E+19	4.6657E+19	2.1191E-02
67	1.3448E+19	4.9464E+19	2.2380E-02	68	1.3170E+19	4.8274E+19	2.1918E-02
69	1.3868E+19	5.1029E+19	2.3082E-02	70	1.3582E+19	4.9802E+19	2.2608E-02
71	1.4264E+19	5.2499E+19	2.3743E-02	72	1.3969E+19	5.1236E+19	2.3252E-02
73	1.4635E+19	5.3870E+19	2.4360E-02	74	1.4332E+19	5.2574E+19	2.3857E-02
75	1.4979E+19	5.5141E+19	2.4933E-02	76	1.4670E+19	5.3815E+19	2.4418E-02
77	1.5297E+19	5.6309E+19	2.5461E-02	78	1.4981E+19	5.4954E+19	2.4935E-02
79	1.5589E+19	5.7371E+19	2.5943E-02	80	1.5266E+19	5.5991E+19	2.5407E-02
81	1.6057E+19	5.9061E+19	2.6714E-02	82	1.5725E+19	5.7641E+19	2.6172E-02
83	1.6268E+19	5.9812E+19	2.7059E-02	84	1.5932E+19	5.8374E+19	2.6503E-02
85	1.6451E+19	6.0452E+19	2.7355E-02	86	1.6110E+19	5.8998E+19	2.6791E-02
87	1.6604E+19	6.0979E+19	2.7602E-02	88	1.6261E+19	5.9512E+19	2.7032E-02
89	1.6728E+19	6.1392E+19	2.7799E-02	90	1.6382E+19	5.9915E+19	2.7225E-02
91	1.6823E+19	6.1690E+19	2.7945E-02	92	1.6475E+19	6.0206E+19	2.7368E-02
93	1.6888E+19	6.1873E+19	2.8041E-02	94	1.6539E+19	6.0384E+19	2.7462E-02
95	1.6923E+19	6.1940E+19	2.8086E-02	96	1.6573E+19	6.0450E+19	2.7506E-02
97	1.6928E+19	6.1891E+19	2.8080E-02	98	1.6578E+19	6.0402E+19	2.7501E-02
99	1.6904E+19	6.1727E+19	2.8024E-02	100	1.6554E+19	6.0242E+19	2.7443E-02
101	1.6780E+19	6.1121E+19	2.7765E-02	102	1.6433E+19	5.9631E+19	2.7212E-02
103	1.6671E+19	6.0630E+19	2.7585E-02	104	1.6326E+19	5.9171E+19	2.7015E-02
105	1.6532E+19	6.0026E+19	2.7334E-02	106	1.6190E+19	5.8582E+19	2.6770E-02
107	1.6364E+19	5.9309E+19	2.7014E-02	108	1.6026E+19	5.7823E+19	2.6476E-02
109	1.6168E+19	5.8482E+19	2.6685E-02	110	1.5833E+19	5.7075E+19	2.6134E-02
111	1.5942E+19	5.7545E+19	2.6287E-02	112	1.5613E+19	5.6161E+19	2.5744E-02
113	1.5689E+19	5.6501E+19	2.5842E-02	114	1.5365E+19	5.5142E+19	2.5308E-02
115	1.5408E+19	5.5352E+19	2.5350E-02	116	1.5089E+19	5.4020E+19	2.4826E-02
117	1.5099E+19	5.4099E+19	2.4812E-02	118	1.4787E+19	5.2797E+19	2.4300E-02
119	1.4764E+19	5.2745E+19	2.4229E-02	120	1.4459E+19	5.1476E+19	2.3729E-02
121	1.4078E+19	4.9988E+19	2.3039E-02	122	1.3787E+19	4.7875E+19	2.2563E-02
123	1.3671E+19	4.8361E+19	2.2334E-02	124	1.3388E+19	4.7197E+19	2.1873E-02
125	1.3239E+19	4.6643E+19	2.1588E-02	126	1.2965E+19	4.5521E+19	2.1143E-02
127	1.2784E+19	4.4838E+19	2.0804E-02	128	1.2520E+19	4.3759E+19	2.0378E-02
129	1.2307E+19	4.2949E+19	1.9982E-02	130	1.2052E+19	4.1916E+19	1.9569E-02
131	1.1807E+19	4.0980E+19	1.9124E-02	132	1.1563E+19	3.9995E+19	1.8729E-02
133	1.1287E+19	3.8935E+19	1.8231E-02	134	1.1054E+19	3.7998E+19	1.7854E-02
135	1.0747E+19	3.6817E+19	1.7305E-02	136	1.0525E+19	3.5931E+19	1.6947E-02
137	1.0188E+19	3.4630E+19	1.6347E-02	138	9.9775E+18	3.3797E+19	1.6010E-02
139	9.6111E+18	3.2378E+19	1.5360E-02	140	9.4124E+18	3.1599E+19	1.5040E-02

values. Preliminary results of the uncertainty analysis can be found in Ref. 7.

3. Conclusions and Recommendations

The results achieved in the analysis of the fourth HSST experiments indicate that for a reasonable amount of time and funds, a considerable improvement in accuracy is attainable. The following steps are suggested for the analysis of exposure parameters from test reactor experiments.

1. ^{237}Np (n,f) and ^{238}U (n,f) sensors with gadolinium or CdO covers be included in the dosimetry multiple foil sets at select locations.
2. Single wire sensors should be placed at as many locations as feasible to obtain a complete and accurate spatial distribution of fast fluxes.
3. Good calculations for the source term in the core and the transport of neutrons from the core to the experiment.
4. A cross section data base for the reaction rate cross section and their variances and covariances.
5. A least square adjustment method to combine the reaction rate data, the calculated fluxes, and cross section values and arrive at an overall uncertainty for the exposure parameter of interest.

REFERENCES

1. F. W. Stallmann, "LSL, A Logarithmic Least Squares Adjustment Method," Proceedings of the Fourth ASTM-EURATOM Symposium on Reactor Dosimetry (to be published).
2. F. J. Witt, "The USAEC Heavy Section Steel Technology Program: Objectives and Status," Nucl. Eng. Des. 20(1), pp. 169-180 (June 1972).
3. G. D. Whitman and R. H. Bryan, Heavy-Section Steel Technology Program Quarterly Progress Report for Jan.-Mar. 1981, NUREG/CR-2141/VI, ORNL/TM-7822 (June 1981).
4. F. W. Stallmann and F. B. K. Kam, Neutron Spectral Characterization of the Second Nuclear Regulatory Commission Heavy Section Steel Technology 4T-CT Irradiation Experiment, ORNL/NUREG/TM-285 (Dec. 1978).
5. F. W. Stallmann and F. B. K. Kam, "Neutron Spectral Characterization of the NRC-HSST Experiments," Proceedings of the Third ASTM-EURATOM Symposium on Reactor Dosimetry, EUR 5667, Vol. 1, pp. 198-207 (1980).

6. W. N. McElroy (Editor), LWR Pressure Vessel Surveillance Dosimetry Improvement Program: PCA Experiments and Blind Test, NUREG/CR-1861 (July 1981).

7. F. W. Stallmann, "Uncertainties in the Estimation of Radiation Damage Parameters," Proceedings of the Fourth ASTM-EURATOM Symposium on Reactor Dosimetry (to be published).

CHARACTERIZATION OF THE NEUTRON ENVIRONMENT INSIDE THE PRIMARY CONTAINMENT OF CAORSO NUCLEAR POWER PLANT.

E.Borioli, G.Garagnani, G.Sandrelli
ENEL, Ente Nazionale per l'Energia Elettrica, DSR/CRTN-Milano and DCO/CTN-Roma, Italy
A.Cesana, A.Foglio Para, V.Sangiust, M.Terrani, S.Terrani
Politecnico di Milano, Istituto Ingegneria Nucleare - CESNEF Milano, Italy

ABSTRACT

Extensive neutron flux measurements were performed inside the drywell of Caorso (Italy) nuclear power plant, a 2600 MW_{th} BWR. The activation technique was used together with the fission track measurement in solid state detectors, with natural or depleted uranium as converter materials. The results were of utility to assess neutron dose rates and related quantities, such as the reliability functions of the exposed materials.

Additional measurements are planned at the pressure vessel outer surface by means of the multiple foil activation technique, for an experimental validation of shielding and streaming calculations relating to the neutron environment between the pressure vessel and the sacrificial shield.

INTRODUCTION

A mapping of the neutron flux has been performed inside the drywell of Caorso nuclear power plant, a 2600 MW_{th} BWR, in order to estimate the neutron dose rates and consequently the reliability functions of the exposed materials in as many positions as possible.

Computed neutron flux energy shapes and intensities were available only in some selected points[1]. In most points of interest, guessed values of the intensity but scarce or no information on the neutron energy distribution were available. Relatively hard neutron spectra were however foreseen[2], with intensities ranging from 10^3 to 10^5 n/cm^2s.

As the measurements were to be performed during the preliminary runs of the plant before normal operation, some limitations conditioned the planning of the experiment. In

particular:
1- The exact irradiation time could not be previously fixed (with a possible range from some weeks to some months), because the irradiations had to coincide with a period of overall correct performance of the plant.
2- Neither the cooling time of the induced activities could be foreseen and might vary from one to several days, in connection with the possibility of removing the detectors after a non planned shut-down. In addition, the shut-down might be preceded by a period of reduced power of the plant.

Moreover, as above said, the neutron flux could exhibit variations by factors of two or three decades from zone to zone, with no 'a priori' possibility, for practical reasons, of placing detectors of different masses in the various points.

Considering the limitations above mentioned and the necessity of getting information in a very large region of the drywell, it was not possible to use a high number of detectors in each measure point.

One hundred measure points were selected where the following detectors were utilized:
a) Bare and cadmium covered gold foils;
b) gold foils enclosed at the center of Bonner spheres[3];
c) nickel foils;
d) solid state track detectors SSTD[4], partially cadmium covered, with natural or depleted uranium as fissionable material.

Additional measurements are planned at the pressure vessel outer surface for an experimental validation of shielding and streaming calculations[1,5] carried out between the pressure vessel and the sacrificial shield. Computed neutron flux energy shapes are available along the vessel surface, with intensities ranging from 10^7 to 10^9 n/cm^{2}s. The measurements will be performed utilizing the multiple foil activation technique with the following detectors: Fe, Ni, Co, Cu, Zr, Au. An irradiation time of one year and a cooling time of ten days are foreseen.

EXPERIMENTAL

Characteristics of the detectors placed inside the drywell

The gold detectors were selected in expectation of a normal plant operation. It was required that the plant power level in the last week should be not too low compared with the maximum power level and that the cooling time after ir-

radiation should be not too long. In order to detect fluxes down to 10^3 n/cm^{2}s with a reasonable statistical accuracy, gold foils 7-mm-diam, 0.1-mm-thick were employed. Bonner detectors were made of Moplen in the form of a 4.5-inch-diam sphere, covered with cadmium.

The nickel foils were used to implement the information on the fast portion of the spectrum given by Bonner spheres. In order to detect low intensity fast neutron fluxes, also these foils were massive, 50-mm-diam and 5-mm-thick.

The SSTD detectors could obviously show a saturated response, in terms of readability at high fluences, but their permanent recording should counterbalance a possible too long cooling time before the activation measurements. Moreover, the uranium converters could be also used for a lirect determination of (n,γ) or (n,fission) reaction rates via gamma counting. In most detectors the converter was natural uranium in metallic form, 12.7-mm-diam, 0.18-mm-thick, but depleted uranium was also used, with a ^{235}U content of 360 ppm. Makrofol was used as detecting material.

In order to avoid interference effects, Bonner spheres and the other detectors were set about 50 cm apart.

Measurement techniques

Gold foils were usually beta counted by a set of G.M. detectors. Gamma counting by a Ge-Li detector was used to determine the reaction rates for ^{58}Ni(n,p) and ^{238}U(n,γ). Makrofol etching and track visual counting for the SSTD detectors were carried out with the usual procedures.

RESULTS AND CONCLUSIONS

The following reactions were used for the neutron flux determination:

^{197}Au(n,γ)	in bare, cadmium covered gold foils and in Bonner spheres;
^{58}Ni(n,p)	in nickel foils;
^{235}U(n,f), ^{238}U(n,f)	in bare and cadmium covered uranium converters.

In many points not all the above mentioned detectors were effectively utilized; for instance the bare zone of the track detectors showed frequently a nearly saturated response, so that the reading resulted problematic and often impossible. To implement the experimental information in some selected

points also the reaction rate of $^{238}U(n,\gamma)$ was measured in the uranium converters.

The reaction rate data were analyzed by means of the SAND-II code in order to derive the neutron flux in each of the 100 measure points.

The input spectrum employed for the adjustment procedure was obtained through a DOT-3.5 calculation performed at the ENEL-Thermal and Nuclear Research Center[1]. A 40 energy group structure[6] between 10^{-10} and 18 MeV was adopted. The cross section library in the same group structure was derived from the ENDF B/IV file, using the input spectrum mentioned above as weight function.

If necessary, as in the case of gold foils, a self-shielding correction, derived through the code SELF[7], was included in the cross section; in the case of nickel foils, the edge effect during irradiation was taken into account appropriately. The fission rates from the SSTD detectors, with natural or depleted uranium, were interpreted using cross sections derived by properly weighting the ^{235}U and ^{238}U fission cross sections.

Finally, the effective cross section for Bonner detectors was obtained through an ANISN[8,9] evaluation of the neutron spectrum at the center of the sphere, considering different neutron energies at the sphere surface. Irradiations with a Pu-Be source confirmed those evaluations.

It is not convenient to report here the results obtained for all the measure points. Moreover, since an adjustment procedure with a low number of reactions is something between a normalization of the input flux and a real flux measurement, the detailed flux shapes are scarcely significant.

For these reasons in Table 1 we report only the minimum and maximum values of the neutron fluxes measured in the different zones of the drywell, the location of which is shown in Fig.1, with the following large group structure:
a) thermal group, from 10^{-4} to 0.69 eV
b) first epithermal group, from 0.69 eV to 17 keV
c) second epithermal group, from 17 keV to 0.55 MeV
d) fast group, from 0.55 to 18 MeV.

The choice of the energy limits is such as to have nearly constant RBE values within each of the four groups.The accuracy of the results in each large neutron group was estimated at ± 20%.

Table 1. Minimum and maximum values of the fluxes in the drywell zones ($n/cm^2.s$ at maximum power).

Group / Zone	a	b	c	d
1	$1.4\ 10^5$ $1.6\ 10^5$	$9.2\ 10^5$ $1.2\ 10^6$	$8.7\ 10^5$ $1.2\ 10^6$	$3.4\ 10^5$ $4.5\ 10^5$
2	$3.3\ 10^4$ $2.4\ 10^5$	$4.5\ 10^5$ $2.5\ 10^6$	$4.2\ 10^5$ $2.9\ 10^6$	$1.6\ 10^5$ $1.1\ 10^6$
3	$1.6\ 10^3$ $1.8\ 10^3$	$3.3\ 10^3$ $7.4\ 10^3$	$3.5\ 10^3$ $6.8\ 10^3$	$1.4\ 10^3$ $2.7\ 10^3$
4/5	$4.6\ 10^2$ $1.2\ 10^4$	$4.3\ 10^3$ $7.2\ 10^4$	$3.7\ 10^3$ $9.1\ 10^4$	$1.4\ 10^3$ $3.6\ 10^4$

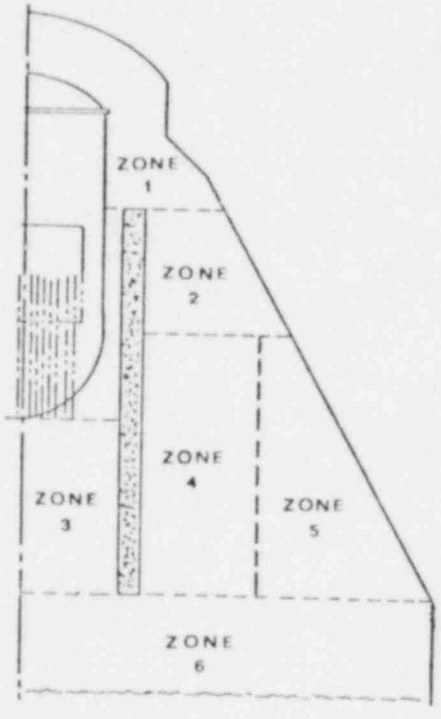

Fig.1. Drywell zones.

The collected data are now being analyzed from the point of view of: 1) estimating the possible radiation damage on exposed materials (e.g., plastics and in general insulating materials of electric components) and 2) estimating the gamma field deriving from the activation of the materials present in the drywell. Points 1) and 2) are of importance for assessing the reliability of the electrical components and for determining a safe time delay before entering into the drywell after a shut-down.

As a conclusion, we may say that the advantages and drawbacks of the different employed techniques have been well established by treating the data from several hundreds of

detectors. The considerable experience gained in managing extensive neutron flux mapping will be of utility for a probable future extension of this kind of measurements in Italian nuclear power plants.

ACKNOWLEDGEMENT

The authors want to thank E. Brega and G. Alloggio of ENEL - Thermal and Nuclear Research Center for the ANISN calculations, P. Saronni of CESNEF for the cooperation in the SSTD technique and S. Lanza of Caorso Power plant for the support in the experiment setting up.

REFERENCES

1. P. Barbucci and F. Di Pasquantonio, Verifica degli Schermi dell'Edificio Reattore della Centrale di Caorso e Analisi dello Streaming nel Canale tra il Vessel e lo Schermo Sacrificiale, Ente Nazionale per l'Energia Elettrica, Direzione Studi e Ricerche, Centro Ricerca Termica e Nucleare, Milano, Italy, Report N6-4 (Dec. 1976).

2. Ente Nazionale per l'Energia Elettrica, Italy, Private Communication.

3. R. L. Bramblett, R. I. Ewing, and T. W. Bonner, "A New Type of Neutron Spectrometer," Nucl. Instr. Methods, 9, 1 (1960).

4. R. L. Fleischer, P. B. Price, and R. M. Walker, Nuclear Tracks in Solids, University of California Press, Berkeley, CA, 1975.

5. P. Barbucci and F. Di Pasquantonio, "Neutron and Gamma Ray Streaming in the Annulus between the Reactor Pressure Vessel and Sacrificial Shield of the Caorso Nuclear Power Station," Proc. 5th International Conference on Reactor Shielding, Knoxville, Tenn., USA, April 18-23, 1977, Science Press, Princeton, p.205, 1977.

6. A. Cesana, G. Sandrelli, V. Sangiust, and M. Terrani, "The Group Structure of Cross Section Libraries in Neutron Activation Spectrometry," Nucl. Sci. Eng., to be published.

7. W. L. Zijp and H. J. Nolthenius, Neutron Selfshielding of Activation Detectors Used in Spectrum Unfolding, Netherland Report RCN-231 (September, 1975).

8. W. W. Engle jr., ANISN, A One Dimensional Discrete Ordina-

tes Transport Code with Anisotropic Scattering, U.S.A. Report ORNL K-1693, (1973).

9. P. Barbucci and F. Di Pasquantonio, "Exponential Supplementary Equations for S_N Methods: the One Dimensional Case," Nucl. Sci. Eng. 63, 179 (1977).

SPECTRAL ANALYSIS OF A BWR VESSEL

E. B. Norris
Southwest Research Institute
San Antonio, Texas

ABSTRACT

The vessel wall neutron dosimeter capsule was removed from Browns Ferry Unit 3 after 1-1/2 effective full power years of operation to provide a check on the neutronic design calculations. The cross sections required for this dosimetry analysis were derived using a two-dimensional discrete ordinates transport calculation for the horizontal plane at midcore height. To fulfil general vendor and utility needs, an independent multiple-dosimeter analysis was conducted during the same exposure period by another laboratory. Integral cross sections determined experimentally at three locations show very good agreement with those calculated in support of the vessel wall dosimeter analysis. As a result, it is concluded that the two-dimensional discrete ordinates code can be used with confidence to provide the spectral information needed for pressure vessel surveillance dosimetry analyses.

INTRODUCTION

The Browns Ferry Unit 3 Nuclear Plant is a 1065 Mwe Boiling Water Reactor (BWR) built by General Electric (GE). Three vessel material mechanical property surveillance capsules and one vessel wall dosimeter capsule had been installed in the pressure vessel by GE prior to startup to fulfil the regulatory requirements for monitoring vessel steel embrittlement.[1] GE augmented the surveillance program by conducting an experiment during core cycle 1 which allowed a more thorough estimation of the spectral response of the dosimeter materials.[2]

The vessel wall dosimeter capsule, also removed at the end of core cycle 1, was shipped to Southwest Research Institute (SwRI) for analysis. SwRI performed a two-dimensional discrete ordinates transport calculation to provide the spectral information needed to compute the reaction cross sections at the capsule location.[3] Although the differences in the R-θ positions of the standard and augmented program dosimetry capsules were such that the results cannot be compared directly, three of the latter were closely modeled at four mesh points used in the transport calculation.

This paper presents a comparison of the fast neutron cross sections determined by two independent studies for the Fe-54(n,p), Ni-58(n,p), Cu-63(n,α), Np-237(n,f) and U-238(n,f) reactions.

EXPERIMENTAL AND COMPUTATIONAL METHODS

In-vessel Neutron Spectral Analysis

The experimental procedures employed by GE have been described in detail elsewhere.[2] Briefly, groups of neutron dosimeters were supported by fixtures attached to the O.D. of the core shroud at the core-midplane and at the core-top-edge elevations. The neutron dosimeters included oxides of U-235, U-238, Np-237 and Th-232; salts of Ag, Sc, and U-235; and Fe, Ni, Cu, Ti and AlCo wires.

Neutron differential flux density spectra were generated for six locations. Integral flux densities (and fluences) above various threshold energies were determined at the dosimeter positions and were extrapolated to the shroud and vessel wall. Fast cross sections for selected dosimeter reactions were calculated by dividing the measured reaction rates by the appropriate integral fast flux densities.

Discrete Ordinates Transport Computation

The neutron flux energy and spatial distribution in the vessel at the core midplane was calculated by SwRI using the DOT 3.5 two-dimensional discrete ordinates transport code, a 22 group neutron cross section library (CASK), a P_1 expansion of the scattering matrix and an S_8 order of angular quadrature. A one-eighth segment, shown in Figure 1, was taken to be representative because of the symmetry involved. The boundaries of the core, core shroud, jet pumps, and vessel wall were described in R-θ coordinates and the materials within each region were homogenized over their respective areas. The coolant outside the core was assumed to have no voids. An average power distribution in the core was derived from operational records.

Four of the mesh points used in the model correspond closely to the locations of three dosimeter sets placed at the core midplane in the GE experiment:

Experimental Location	Computational Location
R = 267cm; θ = 3.75°	R = 270cm; θ = 4.1°
R = 267cm; θ = 45°	R = 270cm; θ = 44°
R = 312cm; θ = 45°	R = 307cm; θ = 44° and R = 318cm; θ = 44°

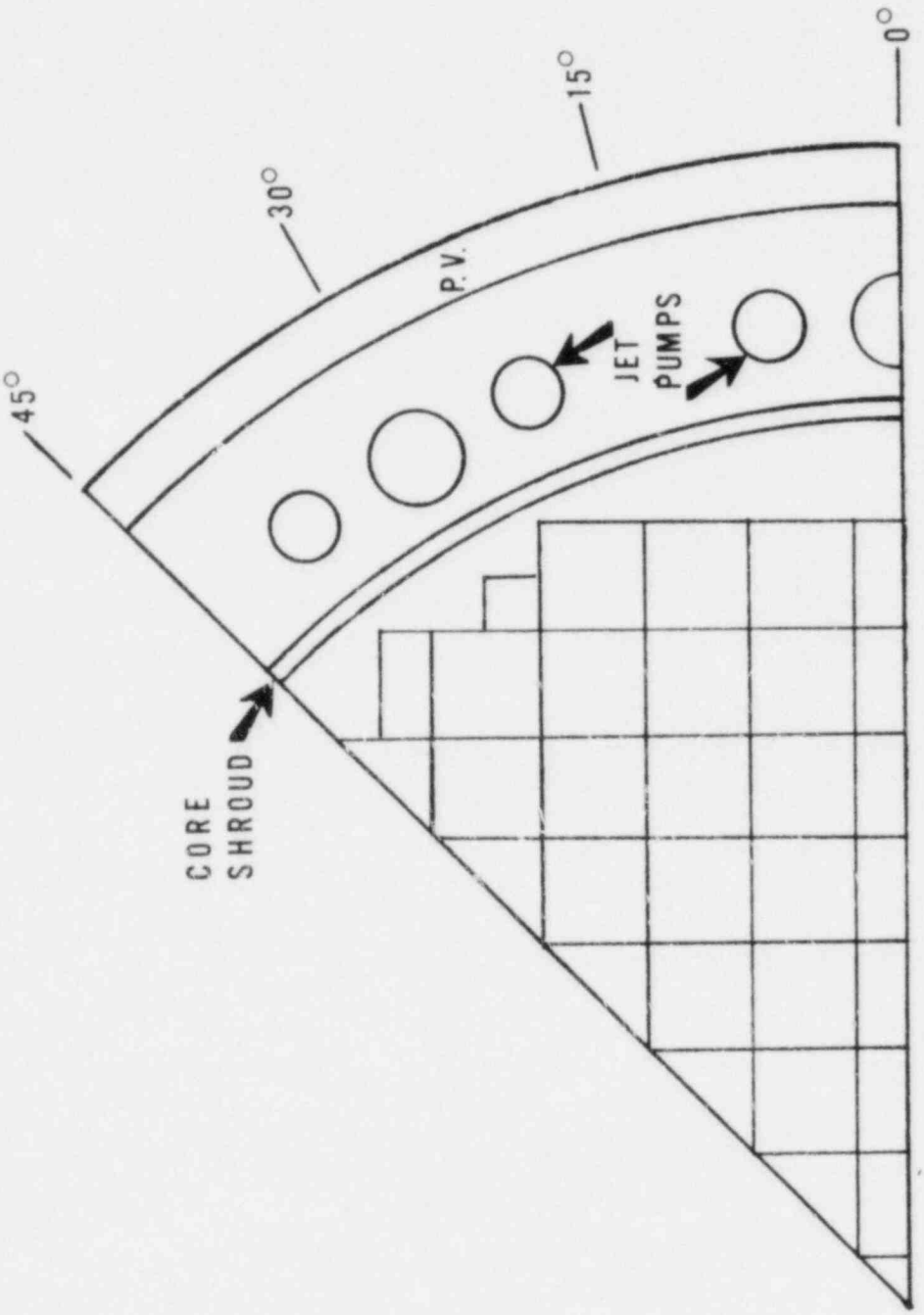

Figure 1. One-eighth Segment Browns Ferry Unit 3 Core Midplane.

The neutron spectra above 0.11 MeV calculated for each of these computational locations are presented in Table 1.

Spectrum-averaged cross sections were calculated for the dosimeter reactions of interest by the relationship:

$$\bar{\sigma}(E > 1\ \text{MeV}) = \frac{\sum_{1}^{m} \sigma\ (E)\ \phi\ (E)\ d\ E}{\sum_{1}^{m} \phi\ (E)\ d\ E} \qquad (1)$$

The group cross sections, σ (E), were obtained by collapsing data from the Evaluated Nuclear Data File/B into the group structure given in Table 1.

RESULTS AND CONCLUSIONS

The fast cross sections, E>1MeV, determined independently by two laboratories at three positions in the water annulus between the core shroud and the pressure vessel, are given in Table 2. Several observations concerning these results are presented below:

1. Fast cross sections obtained from spectra calculated with a two-dimensional discrete ordinates transport code are in good agreement with those obtained using a spectrum unfolding method.

2. The best agreement between the independently determined fast cross sections occurred at the near-vessel positions where corresponding values are within ±5% of the averages

3. The fast cross sections for the non-fission reactions are strongly dependent on their positions relative to the reactor core and internals.

These observations indicate that a transport calculation can provide the spectral information needed to carry out reactor pressure vessel surveillance dosimetry analyses. Also, a two-dimensional calculation is preferred to adequately account for the influence of the nearby core and internal support structure elements.

Table 1. Calculated Neutron Energy Spectra

Energy Group m	Energy Range (MeV)	Relative Flux @θ=4.1° & R=270cm	Relative Flux @θ=44° & R=270cm	Relative Flux @θ=44° & R=307cm	Relative Flux @θ=44° & R=318cm
1	12.2-15.0	5.84×10^{-7}	3.85×10^{-7}	1.37×10^{-6}	1.42×10^{-6}
2	10.0-12.2	3.44×10^{-3}	2.37×10^{-3}	6.92×10^{-3}	6.84×10^{-3}
3	8.18-10.0	1.17×10^{-2}	8.22×10^{-3}	2.23×10^{-2}	2.16×10^{-2}
4	6.36-8.18	3.29×10^{-2}	2.43×10^{-2}	5.84×10^{-2}	5.50×10^{-2}
5	4.96-6.36	5.54×10^{-2}	4.45×10^{-2}	8.84×10^{-2}	8.02×10^{-2}
6	4.06-4.96	4.91×10^{-2}	4.32×10^{-2}	7.41×10^{-2}	6.51×10^{-2}
7	3.01-4.06	6.50×10^{-2}	6.33×10^{-2}	8.76×10^{-2}	7.57×10^{-2}
8	2.35-3.01	8.73×10^{-2}	8.84×10^{-2}	1.07×10^{-1}	9.55×10^{-2}
9	1.83-2.35	8.21×10^{-2}	8.36×10^{-2}	8.55×10^{-2}	8.09×10^{-2}
10	1.11-1.83	1.61×10^{-1}	1.68×10^{-1}	1.39×10^{-1}	1.37×10^{-1}
11	1.00-1.11	3.70×10^{-2}	3.77×10^{-2}	2.43×10^{-2}	1.56×10^{-2}
12	0.55-1.00	1.53×10^{-1}	1.61×10^{-1}	1.15×10^{-1}	1.43×10^{-1}
13	0.11-0.55	2.63×10^{-1}	2.75×10^{-1}	1.91×10^{-1}	2.23×10^{-1}

Table 2. Fast Cross Sections in Browns Ferry Unit 3 Vessel Spectra

R/θ (cm/deg)	Data Source[a]	Cross Section for Neutrons > 1 MeV (barns)				
		$^{54}Fe(n,p)$	$^{58}Ni(n,p)$	$^{63}Cu(n,\alpha)$	$^{237}Np(n,f)$	$^{238}U(n,f)$
Near-Shroud Positions[b]						
267/3.75	GE	0.14	0.19	0.0018	2.1	0.50
270/4.10	SwRI	0.17	0.21	0.0023	2.0	0.48
267/45	GE	0.12	0.16	0.0014	2.25	0.51
270/44	SwRI	0.15	0.18	0.0017	2.1	0.46
Near-Vessel Positions[b]						
307/44	SwRI	0.22	0.27	0.0035	1.9	0.54
312/45	GE	0.21	0.26	0.0038	1.9	0.54
318/44	SwRI	0.22	0.26	0.0036	2.0	0.54

[a] GE data from reference 2; SwRI data unpublished.

[b] Shroud O.R. = 263 cm; Vessel I.R. = 319 cm.

REFERENCES

1. Title 10, Code of Federal Regulations, Part 50, Appendix H, "Reactor Vessel Material Surveillance Program Requirements."

2. G. C. Martin, Browns Ferry Unit 3 In-Vessel Neutron Spectral Analysis, General Electric Report NEDO-24793 (August, 1980).

3. E. B. Norris, Analysis of the Vessel Wall Neutron Dosimeter from Browns Ferry Unit 3 Pressure Vessel, Southwest Research Institute Report 02-4884-003 (September 1979).

MESURE ET INTERPRETATION DES FLUX DE DOMMAGES DANS LE SIMULATEUR DE CUVE P.W.R. D'OAK-RIDGE (ORR-PSF)

A. Alberman, M. Benoist, M. Thierry
Services des Piles de Saclay
C.E.N./Saclay, 91191 Gif Sur Yvette, France

RESUME

Les rapports dommage/activation (D.A.R.) ont été mesurés dans le simulateur de cuve P.W.R. d'Oak-Rigde (P.S.F.) aux positions "surveillance", 1/4 et 3/4 d'épaisseur de la "cuve". Les deux techniques de dosimétrie G.A.M.I.N. et tungstène ont été mises en oeuvre pour qualifier, avec précision, les emplacements d'irradiation des aciers. Les réponses des dosimètres sont très cohérentes entre elles et indiquent des spectres voisins aux positions "surveillance" et "1/4 d'épaisseur". On montre, d'autre part, que l'analyse des dommages par D.A.R. dans la cuve est conservative (comparaison avec l'expérience DOMPAC présentée au 3ème Symposium ASTM/EURATOM) pour caractériser les flux de dommage acier.

SUMMARY

Damage to activation ratio (DAR) have been measured in the pressure vessel mock-up PSF of the Oak-Ridge reactor, at surveillance, 1/4 and 3/4 thickness positions. G.A.M.I.N. and Tungsten techniques were implemented, providing accurate qualification of steel dosimetry. Results prove surveillance capsule and 1/4 T very similar spectra. Moreover DAR results in the vessel show conservative damage analysis (consistency with DOMPAC experiment presented at the 3rd ASTM/EURATOM symposium) for steel damage fluence determination.

INTRODUCTION

L'amélioration de la dosimétrie de surveillance des cuves PWR fait actuellement l'objet de coopération entre divers pays. La définition des programmes mis en oeuvre a fait l'objet de plusieurs présentations au 3ème symposium ASTM/EURATOM sur la dosimétrie des réacteurs [1, 2] et ne sera pas rappelée ici. Ces programmes sont basés, pour l'essentiel, sur les maquettes de cuve PCA (métrologie basse puissance) et PSF (capsule d'irradiation d'aciers, voir Fig. 1) installées à Oak-Ridge.

Les résultats présentés ici ont été obtenus sur la capsule de dosimétrie pour PSF.

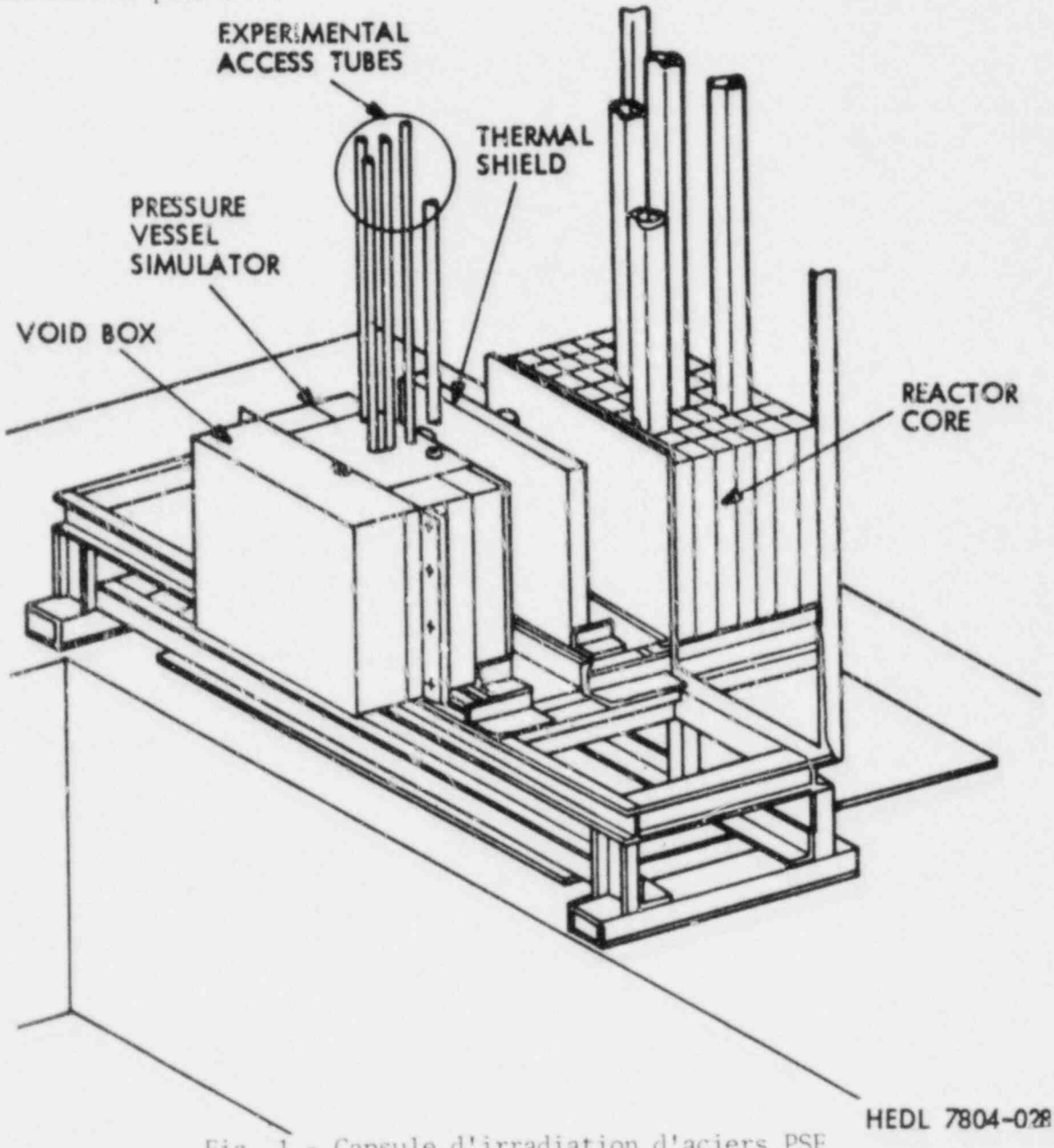

Fig. 1 - Capsule d'irradiation d'aciers PSF

PRINCIPE DE LA DOSIMETRIE

Dispositif

Le dispositif de dosimétrie n'est autre que la masse d'acier équivalente à celle du dispositif d'irradiation PSF. Aux positions d'intérêt, sont percés des trous (Ø 25 mm) centrés sur les milieux d'assemblage.

Trois dosimétries des dommages ont été réalisées aux emplacements :

A : surveillance
B : 1/4 épaisseur (+ 64 mm)
C : 3/4 épaisseur (+ 170 mm).

N. B. : pour l'instant, aucune éprouvette d'acier n'est irradiée en position 3/4. Par contre, dans la mesure où les calculs de déplacements atomiques divergent selon la méthode et ce d'autant plus que l'on pénètre dans l'acier, il a paru intéressant d'y obtenir un point expérimental.

Chargements

Les 3 capsules irradiées comprenaient un chargement identique (voir annexe) de détecteurs de dommages graphite (G.A.M.I.N.) et tungstène (W) positionnés en barillet, de part et d'autre du plan de Ø maximum. Le remplissage était constitué d'acier doux, le tout étant placé dans un tube inox ($Ø_{ext}$ = 25 mm) rendu étanche par un joint élastomère en partie haute. Chaque capsule était munie d'un thermocouple pour mesures au niveau des dosimètres G.A.M.I.N.

Les dosimètres G.A.M.I.N. ont été utilisés jusqu'à présent pour la dosimétrie des aciers de cuve français. Les valeurs de d.p.a. dans le fer, extrapolées de la mesure, ont toujours montré un bon accord avec les résultats observés [3].

Le nouveau dosimètre W [4], dont la réponse est voisine des modèles de dommages acier (d.p.a.), a été également mis en oeuvre afin d'améliorer le niveau des corrélations. La fiabilité de ces dosimètres, dans une géométrie de cuve PWR, a été montrée dans l'expérience DOMPAC [5].

CONDITIONS EXPERIMENTALES

Le tableau I ci-après résume les conditions de dosimétrie dans le P.S.F.

Les irradiations ont été effectuées à faible puissance (30 MW nominal) afin d'éviter des échauffements sur les dosimètres G.A.M.I.N.

Tableau 1

Conteneur	Position	Date début irradiation	Puissance	Température mesurée	Durée
A	Surveillance	26.10.79 à 2h08	7,4 MW	75°C	2h00
B	1/4 épaiss.	26.10.79 à 5h03	16 MW	66°C	12h35
C	3/4 épaiss.	26.10.79 à 5h03	16 MW	52°C	23h00

RESULTATS EXPERIMENTAUX

G.A.M.I.N.

On donne, en annexe, les valeurs $\Delta R/R^C$ de résistivité électrique, linéarisées et ramenées à 40°C (standard d'étalonnage ISIS à Saclay), ainsi que la fluence nickel ϕ^f_{Ni} (moyenne arithmétique des 2 disques Ni) par dosimètre :

$$\phi^f_{Ni} = \int_0^\infty \sigma_{Ni}(E)\,\varphi(E)\,dE \quad / \quad \bar{\sigma}^f_{Ni}$$

où $\bar{\sigma}^f_{Ni}$ est la section efficace ^{58}Ni (n, p) moyennée sur le spectre de fission. On utilise la valeur $\bar{\sigma}^f_{Ni}$ = 101 mbarns.

r est le rapport dommage/activation (sans dimension) expérimental

$$r = 10^{-7}\,\Delta R/R^C \,/\, A_{Ni}$$

avec A_{Ni} : nombre de réactions ^{58}Ni par atome-cible.

Tungstène

On donne également, en annexe, pour chaque détecteur, les valeurs $\Delta R/R^r$ de résistivité, corrigées après déduction de la composante thermique, la fluence de fission ϕ^f_{Ni} et le rapport dommage/activation

$$s = 10^{-5}\,\Delta R/R^r \,/\, A_{Ni}$$

Récapitulatif

On donne, dans le tableau 2, les valeurs moyennes des rapports dommage/activation, mesurées dans les 3 emplacements, avec l'erreur relative sur la moyenne correspondante :

Tableau 2 - Valeurs expérimentales moyennes

Conteneur	Position	G.A.M.I.N.		TUNGSTENE	
		$\bar{r}$	$\Delta\bar{r}/\bar{r}$	$\bar{s}$	$\Delta\bar{s}/\bar{s}$
A	Surveillance	7,00	1,6 %	8,48	1,5 %
B	1/4 épaiss.	9,24	1,9 %	11,78	7 %
C	3/4 épaiss.	24,16	0,9 %	27,60	6,5 %

Ces valeurs sont indiquées sur la figure 2. On remarque la bonne cohérence entre réponses des détecteurs. Les taux de dommages graphite ou tungstène sont voisins entre "surveillance" et "1/4" (écart ∿ 25%). Ils augmentent en éloignement dans le pavé. La figure 3 représente la réponse tungstène en fonction du graphite. On observe le parfait accord des mesures dans les emplacements "cuve" (B et C) avec celles effectuées dans le simulateur DOMPAC [5]. Ces mesures peuvent s'analyser selon une loi puissance du type :

$$s = 1{,}69\ (r)^{0{,}88}$$

FLUENCES DE DOMMAGES - INTERPRETATION

La principale application de cette dosimétrie reste l'étalonnage en dommages des intégrateurs de flux neutroniques pour obtenir les fluences de dommages sur les éprouvettes d'acier.

On déduit les rapports dommages/activation (DAR), exprimés en flux de fission équivalents [6], selon les relations :

graphite $$\frac{\Phi_G}{\Phi_{Ni}} = 0{,}50\ r \qquad [7]$$

tungstène $$\frac{\Phi_W}{\Phi_{Ni}} = 0{,}247\ s \qquad [4]$$

Les coefficients d'étalonnage ont été déduits de corrélations calculs/mesures et correspondent aux modèles de déplacements atomiques (d.p.a).

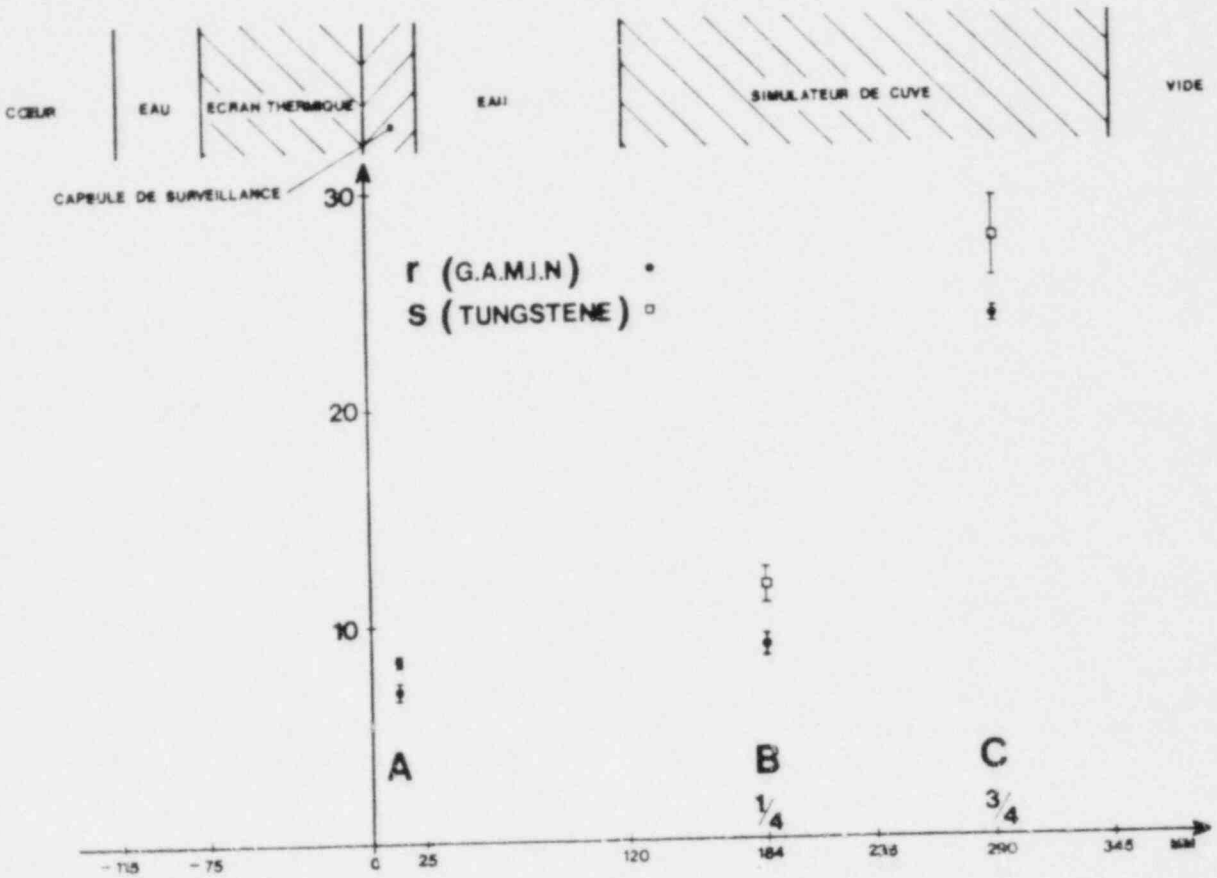

Fig. 2 - Réponses des détecteurs dans le P.S.F.

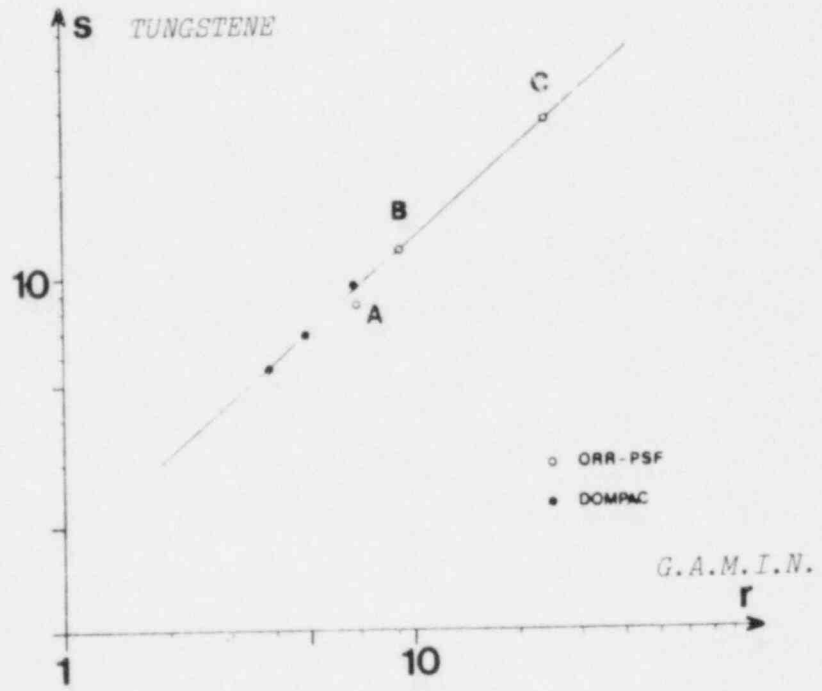

Fig. 3 - Réponses TUNGSTENE/G.A.M.I.N. dans les simulateurs de cuve

Fluences de dommages tungstène :

Un calcul de transport 1D VITAMIN C a été effectué [8] pour la qualification préliminaire de la maquette PSF. Les indices de spectres (DAR) calculés sont un peu forts pour les 2 détecteurs. Dans la mesure où la réponse GAMIN est bien connue (flux de dommage référence), on peut cependant analyser, à l'aide de la courbe s/r (Fig. 3), la sensibilité du tungstène selon les énergies de neutron. Le tableau III donne les pourcentages de réponse tungstène par bandes d'énergie, ainsi que les indices de spectres W/Nickel et W/Ø > 1 MeV rapportés à la capsule de surveillance :

Tableau 3 - Réponse du détecteur W

	Pourcentage de réponse :				W/Ni	W/Ø > 1MeV
	10keV	100keV	1 MeV	10 MeV		
A surveillance	6%	53%	41%		1	1
B 1/4 épaisseur	9%	56%	35%		1,18	1,19
C 3/4 épaisseur	8%	72%	20%		3,25	1,98

De ce qui précède, il apparait que l'analyse des dommages, par rapports dommages/activation, est certainement conservative, le paramètre d'exposition aux neutrons Ø > 1 MeV conduisant ici à des corrélations aberrantes. L'étude d'une fonction de dommages W semi-expérimentale, adaptée au détecteur, est discutée ailleurs à ce symposium [9] .

Conclusions :

a) le rapport des réponses graphite (r) ou tungstène (s) entre les positions 3/4 et 1/4 d'épaisseur est de 2,5 environ.

Ceci montre que la fluence neutronique (Ø > 1 MeV) mesurée par détecteurs d'activation type Ni(n,p), prise comme paramètre d'irradiation, conduit à des résultats aberrants pour l'évaluation des dommages.

b) les positions "surveillance" et "1/4 épaisseur" sont assez voisines du point de vue spectre. Dans le cas d'un éventuel effet de fragilisation observé entre ces 2 positions, il faudrait probablement mettre en cause le niveau de flux relatif ($\simeq 10$).

c) les rapports dommages acier (d.p.a.) / activation dans le pavé peuvent se déduire du rapport dommages graphite / activation pris en référence selon la corrélation :

$$\frac{\phi_{fer}}{\phi_{Ni}} = 0{,}84 \left(\frac{\phi_G}{\phi_{Ni}}\right)^{0{,}70}$$

obtenue par calcul de référence TRIPOLI pour la maquette DOMPAC [5] (835.10^{-24} d.p.a./s par unité de ϕ_{fer}).

d) une corrélation du même type que celle du paragraphe c) ci-dessus peut être obtenue à partir du tungstène, dont la réponse théorique (d.p.a.) est quasi identique à celle du fer (d.p.a.) [4]. Mais les données expérimentales [9] conduisent à une correction de la réponse théorique du tungstène (d.p.a.). Pour fixer les idées, cette dernière peut être approximée par une fonction seuil à environ 0,5 MeV contre environ 0,3 MeV pour la fonction expérimentalement corrigée (N.B. : seuil effectif graphite $\sim$ 75 keV). Dans ces conditions, le dépouillement des éprouvettes d'acier, irradiées dans le PSF, devrait permettre d'améliorer les corrélations avec les modèles de dommages et en particulier avec le tungstène en tant que paramètre d'exposition aux neutrons.

REFERENCES

[1] W.N. McElroy, R. Gold, ...
LWR Pressure Vessel Surveillance Dosimetry Improvement Program
3ème ASTM/EURATOM sur la Dosimétrie, ISPRA, 1979

[2] F.W. Stallmann, A. Fabry, ...
Neutron Spectral Characterization of the PCA-PV Benchmark Facility
3ème ASTM/EURATOM sur la Dosimétrie, ISPRA, 1979

[3] A. Alberman, J.P. Genthon, ...
Damage function for the mechanical properties of steel,
Nucl. Technology 36, 336, 1977

[4] A. Alberman, J.P. Genthon, ...
Le détecteur miniaturisé au tungstène. CEA.CONF.4734
3ème ASTM/EURATOM sur la Dosimétrie, ISPRA, 1979

[5] A. Alberman, M. Faure, ...
Expérience de dosimétrie DOMPAC. Simulation neutronique de l'épaisseur de la cuve d'un réacteur PWR. CEA.CONF.4741
3ème ASTM/EURATOM sur la Dosimétrie, ISPRA, 1979

[6] J.P. Genthon, B.W. Hasenclever, ...
Recommandations sur les mesures des irradiations reçues par les matériaux de structure de piles, EUR.5274, 1975

[7] M. Cance, J.P. Genthon, ...
Le détecteur neutronique au graphite "G.A.M.I.N." CEA.N.1823,1975

[8] C.A. Baldwin, F.B.K. Kam, Communication personnelle

[9] A. Alberman, J.P.Genthon, W.L. Zijp, ...
Nouveau développement de la dosimétrie W,
Communication à ce symposium. (1982)

ANNEXE

CHARGEMENTS ET RESULTATS PAR DETECTEURS

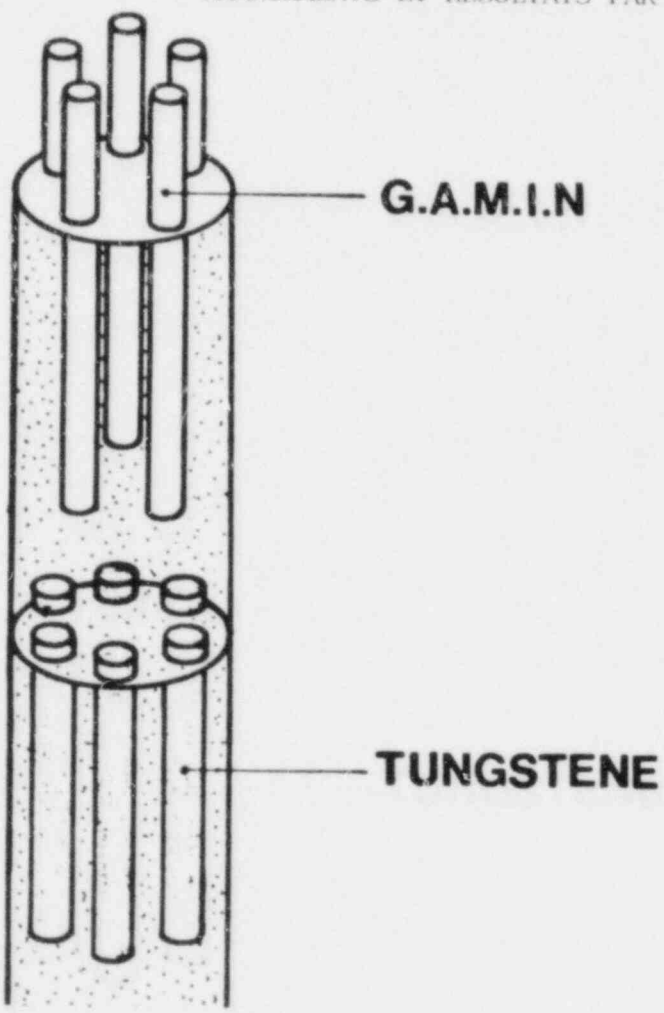

Plan de chargement

A N N E X E (suite)

Conteneur	N° GAMIN	position	$\Delta R/R^c$ (%)	$\phi^f_{Ni}.10^{-15}$ (n.cm^{-2})	r	$\bar{r}$
A Surveillance	40	a	7,019	10,24	6,784	7,00
	41	b	7,234	10,00	7,162	
	42	c	6,618	9,75	6,717	
	43	d	6,077	8,39	7,171	
	44	e	6,479	8,95	7,164	
B 1/4 épaisseur	45	a	9,181	10,20	8,912	9,24
	46	b	9,249	10,34	8,852	
	47	c	8,744	9,21	9,400	
	31	d	8,355	8,59	9,630	
	32	e	8,674	9,11	9,427	
C 3/4 épaisseur	33	a	5,663	2,27	24,70	24,16
	34	b	6,109	2,50	24,19	
	35	c	6,724	2,79	23,86	
	36	d	6,350	2,66	23,59	
	37	e	5,828	2,36	24,45	

Mesures G.A.M.I.N.

Conteneur	N° W	position	$\Delta R/R^r$ (%)	$\phi^f_{Ni}.10^{-15}$ (n.cm^{-2})	s	$\bar{s}$
A Surveillance	141	f	0,102	11,99	8,445	8,48
	142	g	0,097	11,21	8,595	
	143	h	0,084	10,12	8,192	
	155	i	0,089	9,90	8,860	
	156	j	0,091	10,85	8,331	
	157	k	0,186⁂	11,96	-	
B 1/4 épaisseur	158	f	0,119	11,31	10,41	11,78
	159	g	0,113	10,51	10,66	
	160	h	0,212⁂	9,58	-	
	161	i	0,122	9,52	12,66	
	162	j	0,151	10,46	14,30	
	145	k	0,124	11,27	10,88	
C 3/4 épaisseur	146	f	0,095	2,92	32,16	27,60
	148	g	0,073	2,79	25,83	
	149	h	0,065	2,54	25,45	
	150	i	(cassée)	2,48	-	
	151	j	0,193⁂	2,61	-	
	154	k	0,079	2,81	26,97	

Mesures TUNGSTENE

⁂ valeurs aberrantes

A BRIEF ACCOUNT OF THE EFFECT OF OVERCOOLING ACCIDENTS ON THE INTEGRITY OF PWR PRESSURE VESSELS*

R. D. Cheverton
Oak Ridge National Laboratory
Oak Ridge, Tennessee 37830

ABSTRACT

The occurrence in recent years of several pressurized water reactor (PWR) accident initiating events that could lead to severe thermal shock to the reactor pressure vessel, and the growing awareness that copper and nickel in the vessel material significantly enhance radiation damage in the vessel, have resulted in a reevaluation of pressure-vessel integrity during postulated overcooling accidents. Analyses indicate that the accidents of concern are those involving both thermal shock and pressure loadings, and that an accident similar to that at Rancho Seco in 1978 could, under some circumstances and at a time late in the normal life of the vessel, result in propagation of preexistent flaws in the vessel wall to the extent that they might completely penetrate the wall. More severe accidents have been postulated that would result in even shorter permissible lifetimes. However, the state-of-the-art fracture-mechanics analysis may contain excessive conservatism, and this possibility is being investigated. Furthermore, there are several remedial measures, such as fuel shuffling, to reduce the damage rate, and vessel annealing, to restore favorable material properties, that may be practical and used if necessary.

INTRODUCTION

The occurrence in recent years of several pressurized water reactor (PWR) accident initiating events that could lead to severe thermal shock to the reactor pressure vessel,[1,2,3] and the growing awareness that copper and nickel in the vessel material significantly enhance radiation damage in the vessel,[4,5] have resulted in a recent reevaluation of pressure-

*Research sponsored by the Office of Nuclear Regulatory Research, U.S. Nuclear Regulatory Commission under Interagency Agreements 40-551-75 and 40-552-75 with the U.S. Department of Energy under contract W-7405-eng-26 with the Union Carbide Corporation.

vessel integrity during postulated overcooling accidents. Analyses[4] performed following the 1978 Rancho Seco accident[1] indicated that under some circumstances transients of this type might result in failure of the vessel, if the transients occurred late in the normal life of the pressure vessel. Thus, the subject of PWR pressure vessel integrity during overcooling accidents (OCA's) deserved additional attention.

The March of 1981 Commission informed the nuclear utilities of their concerns, and by March 1982 the NRC had officially declared the problem, referred to as pressurized thermal shock (PTS), an unresolved safety issue.

PWR accidents of particular concern are those that allow cool water to come in contact with the inner surface of the pressure vessel at a time when the primary-system pressure is substantial. The rapid cooling of the inner surface results in high thermal stresses and a reduction in the fracture toughness near the inner surface. This introduces the possibility of propagation of preexistent inner-surface flaws (sharp, cracklike defects), and this possiblity increases with reactor operating time because of an additional reduction in fracture toughness that is the result of neutron exposure. Because of this dependence on neutron exposure, the portion of the vessel directly across from the reactor core, where the neutron flux in the vessel wall is a maximum, is of greatest concern.

Thermal shock by itself presumably cannot drive a flaw all the way through the wall; however, if the primary-system pressure were substantial, a potential for vessel failure could exist; that is, a preexistent flaw, under proper circumstances, could penetrate the vessel wall and provide a large enough opening to prevent flooding of the reactor core.

A complete evaluation of the OCA problem in terms of its threat to pressure vessel integrity requires consideration of a number of factors, including postulated accident initiating events, reactor system and operator response to these events, specific design features of the reactor vessel and core that affect fluence-rate and coolant-temperature distributions adjacent to the inner surface of the vessel wall, sensitivity of the vessel material to radiation damage, size, and orientation of preexistent flaws, and remedial measures. This paper examines primarily the fracture-mechanics-related conditions that could lead to a potential for vessel failure.

MECHANISMS AND ACCIDENTS RESULTING IN PRESSURIZED-THERMAL-SHOCK SITUATIONS

There are two basic mechanisms for creating thermal shock to the PWR pressure vessel.[7] One is the injection of cold fluid, and the other is depressurization of the primary or secondary system which reduces the saturation temperature. Cold water can be injected into the primary circuit by means of the emergency core cooling systems and into the secondary

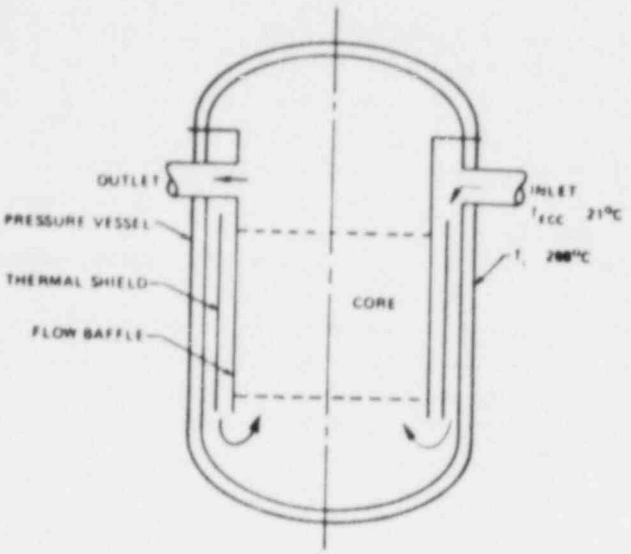

Fig. 1. Schematic cross section of a PWR pressure vessel indicating the flow path of the coolant that can contribute to thermal shock of the vessel.

circuit by means of the feedwater systems, while depressurization can be the result of stuck-open valves, excessive power demands and pipeline failures. In either of these cases cool water eventually enters the vessel through a main coolant line, as indicated in Fig. 1 and passes down through the downcomer region, coming in contact with the inner surface of the vessel wall on the way to cooling the core.

Large decreases in pressure do not necessarily accompany a reduction in coolant temperature, and for those cases where they would, the primary system could be repressurized with the emergency core cooling system. Thus, it is possible for thermal-shock effects and high pressure to co-exist.

Four classes of postulated PWR accidents that can result in pressurized-thermal-shock situations are the large-break loss-of-coolant accident (LBLOCA), the small-break loss-of-coolant accident (SBLOCA), a main steamline break (MSLB) and a runaway feed-water transient (RFT).[7] The 1978 Three Mile Island accident[8] is an example on SBLOCA (stuck-open primary-system relief valve), and the 1978 Rancho Seco accident is an example of an RFT. In the case of an LBLOCA the primary system pressure would drop very quickly to nearly one atmosphere and would remain there; thus, vessel integrity would be retained to the extent of being able to maintain coolant in the vessel.

THE TENDENCY FOR INNER-SURFACE FLAWS TO PROPAGATE DURING THERMAL-SHOCK LOADING ONLY

The tendency for inner-surface flaws to propagate as a result of thermal-shock loading is illustrated in Fig. 2, which shows the temperature, resultant thermal stress, and fracture toughness distributions through the wall of the vessel at a particular time during an LBLOCA. Also included for the same time in the transient are the stress intensity factors (K_I) for long axial flaws of different depths and the radial distribution of the fast neutron fluence. As indicated, the positive gradient in temperature and the steep attenuation of the fluence result in positive gradients in the crack initiation toughness (K_{Ic}) and the crack

arrest toughness (K_{Ia}), and these positive gradients tend to limit crack propagation. However, K also increases with crack depth, except near the back surface, and for the particular case and time analyzed, $K_I \geq K_{Ic}$ for a broad range of crack depths. It is evident that both shallow and deep flaws can initiate, but the positive gradient in toughness provides a mechanism for crack arrest.

If the crack depths corresponding to the initiation and arrest events are plotted as a function of the times in the transient at which the events take place, a set of curves referred to as the critical-crack-depth curves is obtained that indicates the behavior of the flaw during the entire transient. A typical set of critical-crack-depth curves for an LBLOCA is shown in Fig. 3. As indicated by the dashed lines the long axial flaw would propagate in a series of initiation-arrest events and, if warm prestressing were not effective, would penetrate deep into the wall.

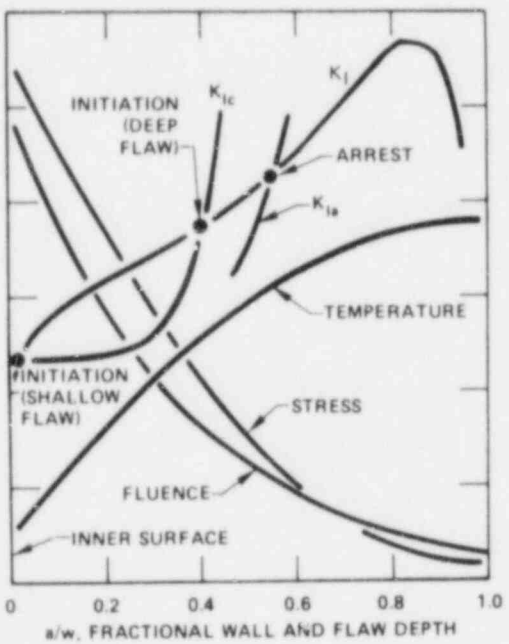

Fig. 2. Mechanisms for crack initiation and arrest at a specific time during a PWR-LBLOCA.

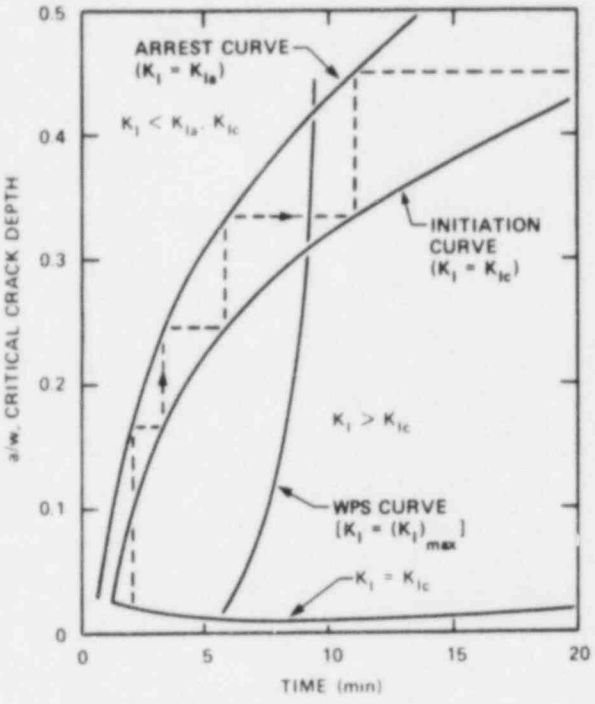

Fig. 3. Critical-crack depth curves for a PWR-LBLOCA, assuming a long axial, high copper and 32 EFPY

Warm prestressing, as referred to above, is a term used to describe a situation where K_I is decreasing with time when K_I becomes equal to K_{Ic} by virtue of a decrease in temperature. It has been postulated and demonstrated experimentally[8,9] that under these conditions a flaw will not propagate; that is, a flaw will not initiate while K_I is decreasing. In Fig. 3 the WPS curve is the locus of points for $K_i = (K_I)_{max}$ $(dK_I/dt = 0)$.

To the left of the WPS curve $dK_I/dt > 0$ and thus crack initiation can take place, but to the right of the WPS curve $dK_I/dt < 0$, and crack initiation will not take place. For the particular case illustrated in Fig. 3, WPS limits crack propagation to ~40% of the wall thickness.

Even if WPS were not effective, the flaw could not completely penetrate the wall under thermal-shock loading conditions only. This is a result of the substantial decrease in K_I as the crack tip approaches the outer surface (see Fig. 2) and has been demonstrated recently in a thermal-shock experiment.[10] However, when pressure is applied in addition to the thermal loading, the possibility of vessel failure (complete penetration of the wall) exists for some assumed conditions.

FRACTURE MECHANICS CALCULATIONAL MODEL

Linear elastic fracture mechanics (LEFM)[11] has been used thus far to analyze the behavior of a flaw during the postulated overcooling accidents. The initial flaw was assumed to be quite long on the vessel surface, to be oriented in an axial direction and to extend radially through the cladding into the base material. Fracture toughness data (K_{Ic} and K_{Ia} vs T - RTNDT, where T is the temperature and RTNDT is the reference nil ductility temperature) were taken from ASME Sect. XI,[12] and the reduction in toughness due to radiation damage was taken from Reg. Guide 1.99, Rev. 1.[13] Since techniques for evaluating the behavior of a flaw when temperatures at the crack tip correspond to and exceed upper shelf (ductile) conditions, it was assumed that crack arrest would not occur if K_I were above an arbitrary upper-shelf toughness value of 220 MPa $m^{1/2}$.

This particular calculational model is believed to be conservative for several reasons: (1) long axial flaws have a greater potential than other flaws for penetrating deep; (2) the cladding may prevent short flaws from extending on the surface to become long flaws; (3) the probability of long flaw existing as an initial flaw and of any flaw extending through the cladding presumably is very small; (4) Reg. Guide 1.99 does not account for variations in the concentration of nickel, and more recent data indicate that vessels with low concentrations of nickel will suffer less damage than presently assumed; and (5) for some of the milder postulated overcooling accidents crack arrest presumably will take place on the upper-shelf portion of the toughness curve, preventing failure of the vessel. Each of these areas is under investigation to determine the degree of conservatism involved.

LOCATION OF SENSITIVE REGIONS OF THE VESSEL WALL

The fracture toughness of the reactor vessel at any point in space and time is a function of the initiation toughness of the material and

the reduction in toughness due to radiation damage. Since radiation damage to the vessel wall is a function of both fast neutron fluence and copper and nickel concentrations it is necessary to locate the areas of the vessel wall where the worst combination of initial toughness, fluence, and copper and nickel concentrations exists. The reduction in fracture toughness due to radiation damage is relatively small if the copper and/or nickel concentrations are low and is large if the concentrations of both are high.

Copper is an impurity in the vessel material, and high concentrations generally are found only in the welds that join the segments of the vessel wall. Nickel is an alloying element in both the base and weld materials, and its concentration covers a broad range among the PWR vessels and is not necessarily the same in the base and weld metals of any particular vessel. Since high concentrations of copper tend to be confined to the welds (there are exceptions), the welds take on special significance.

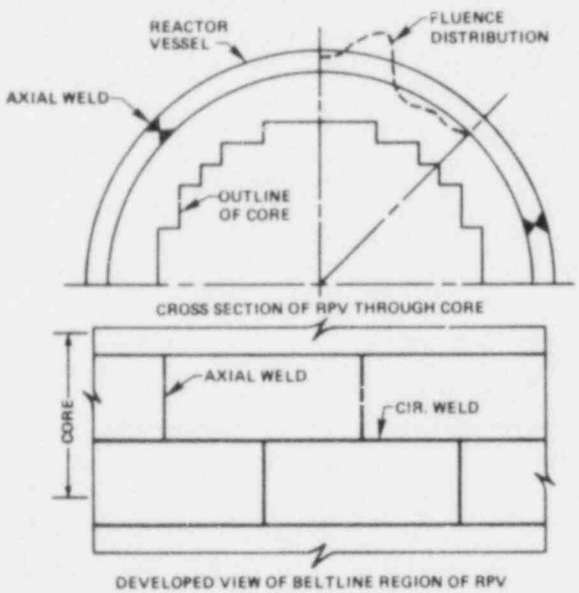

Fig. 4. Peak fluence, maximum concentration of Cu and Ni, and maximum $TRNDT_o$ do not necessarily coincide because of azimuthal variations in fluence and material properties.

As shown in Fig. 4, vessels fabricated from sections of plate have both axial (longitudinal) and circumferential welds, while vessels fabricated from forging rings have only circumferential welds opposite the reactor core. In a plate-type vessel the axial welds tend to be of greater concern than the circumferential welds because, as mentioned above, axially oriented flaws have a greater potential for penetrating deep into the vessel wall during an overcooling accident. However, forged vessels, which have only circumferential welds, are not free from the adverse effects of the same accidents.

The fast neutron fluence in the vessel wall is a maximum at an elevation corresponding to about the horizontal midplane of the reactor core, and, as shown in Fig. 4, there is an azimuthal variation in fluence, resulting from the noncircular geometry of the periphery of the core. Thus, the maximum concentrations of copper and nickel, the maximum fluence and the minimum value of initial toughness do not necessarily coincide. For an accurate specific-plant analysis of the radiation-induced reduction in fracture toughness these space variations must be considered.

ANALYSIS OF THE 1978 RANCHO SECO AND SEVERAL POSTULATED OVERCOOLING ACCIDENTS

Using the fracture-mechanics model described above, pressure-vessel-integrity studies were performed for the 1978 Rancho Seco accident and several postulated accidents,[7] including an LBLOCA, and MSLB, and and RFT that consisted of a turbine trip followed by stuck-open bypass valves. Two different sets of assumptions regarding plant and operator responses to the initiating event were used for the MSLB in an effort to examine and illustrate extremes in the calculated severity of the accidents. For each of the transients considered a typically high copper concentration of 0.31% was assumed to exist in an axially oriented weld, and the initial value of RTNDT was assumed to be −7°C. For the purpose of computing a time in the life of the vessel at which a potential for vessel failure might exist a typical fluence rate of 0.05×10^{19} neutrons/cm²·year was assumed for the inner surface of the vessel at the location of the axial weld.

The LBLOCA constitutes the most severe thermal shock of any of the overcooling accidents, and for this accident the thermal shock is the result of injection of emergency core coolant. The primary-system pressure remains very low, and because of this the calculations indicate that the flaw will not penetrate the wall. Furthermore, WPS would tend to prevent crack propagation beyond midwall thickness. But even without WPS the crack would not penetrate the wall because of the lack of pressure to maintain a high stress intensity factor for very deep flaws.

The Rancho Seco accident[6] involved a loss and then a sudden reapplication of feedwater to a steam generator, resulting in rapid cooling of the primary system while the primary-system pressure was being maintained close to the normal operating level, as shown in Fig. 5. The temperature of the coolant in the cold leg dropped ~180°C in one hour.

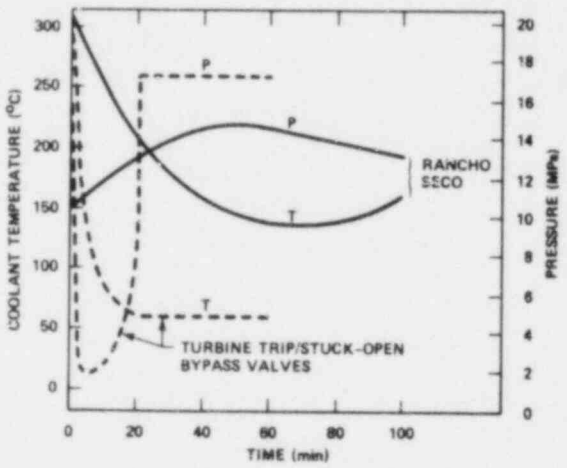

Fig. 5. The 1978 Rancho Seco and a postulated RFT downcomer coolant temperature and pressure transients.

During the specific Rancho Seco transient, the requisite conditions for WPS existed ($dK_I/dt < 0$), and as a result the analysis discussed herein does not predict a reduction in the normal vessel design lifetime [~32 effective full-power years (EFPY)]. However, for an otherwise similar accident the requisite conditions for WPS might not exist as a result of variations in pressure. In this case the calculations indicate a potential for vessel failure at ~17 EFPY.

The postulated turbine-trip accident tends to represent a worst-case situation and may in fact represent an unrealistic set of circumstances insofar as system response is concerned. As indicated in Fig. 5, the transient is much more severe than that for Rancho Seco in that the primary-system temperature drops more rapidly and to a lower value, while repressurizaton by the high-pressure injection system provides a pressure equal to the safety-valve setting. The result of this postulated and possibly exaggerated worst-case accident is a potential for failure of the reactor vessel at about 4 EFPY, with or without WPS.

The two MSLB cases analyzed presumably represent two extremes for the postulated MSLB accident: an exaggerated worst case in the same sense that the turbine-trip case was, and a least-severe situation based on preferred and most-likely system and operator responses. For this latter case a potential for vessel failure is not predicted within the normal lifetime of the power plant. However, for the postulated worst-case situation the calculations indicate a potential for failure at 8 EFPY's, taking advantage of WPS, and 4 EFPY's without WPS.

REMEDIAL MEASURES

Aside from ongoing investigations that may result in the discovery and removal of excessive conservatism in the state-of-the-art fracture-mechanics model, there are several fracture-mechanics-related remedial actions that might be taken to ensure longer permissible vessel lifetimes. They include reducing the uncertainty in the estimation of the fluence in the vessel wall, redesign of the fuel loading to reduce the fluence rate in the wall, and annealing the vessel to restore the original high fracture-toughness values. There is a substantial effort under way to improve the accuracy of fluence determinations,[14] and a few PWR's in the United States, West Germany, and Finland have undergone fuel-loading changes to reduce the fluence in the vessel wall. However, the redesign of a fuel loading is a very complex task, involving a possible reduction in power to accommodate less heat transfer area and/or a less favorable power distribution, changes in control-rod worth and perhaps a shorter fuel-cycle time. Furthermore, if a vessel has already suffered severe radiation damage there is not much to be gained by reducing the fluence rate. For this situation, annealing the vessel may be the answer, but this too is a complex and expensive operation and has not yet been demonstrated on a full-sized PWR vessel.[15]

SUMMARY

A state-of-the-art fracture-mechanics analysis of the 1978 Rancho Seco accident, assuming a typically high concentration of copper to exist

in the vessel material indicates that because of WPS the specific transient would not result in a potential for vessel failure during the normal life of the vessel. However, the requisite conditions for WPS might not exist in an otherwise similar transient. In this case the analysis indicates that a potential for vessel failure would exist at ~17 EFPY. Depending upon the assumptions made regarding reactor system and operator response to the initiating event, potentially more severe transients can result in either no premature failure or failure at times perhaps as short as 4 EFPY.

It appears that the state-of-the-art fracture-mechanics model used for these predictions contains substantial conservatism, and programs are under way to explore this possibility and also to reduce uncertainties in fracture-mechanics-related areas, such as dosimetry, which provide important input to the pressure vessel integrity studies.

REFERENCES

1. (March 20, 1978, Rancho Seco) Nuclear Safety Information Center Accession #0020-138830.

2. (February 26, 1980, Crystal River 3) Nuclear Safety Information Center Accession #0020-160846.

3. (April 23, 1978, Three Mile Island 2) Nuclear Safety Information Center Accession #0020-137918, 137919, 139931.

4. L. E. Steele, *Neutron Irradiation Embrittlement of Reactor Pressure Vessel Steels*, Technical Report Series No. 163, International Atomic Energy Agency, Vienna, 1975.

5. Personal communication with P. N. Randall, U.S. Nuclear Regulatory Commission.

6. R. D. Cheverton, "Parametric Analysis of Rancho Seco Overcooling Accident," March 3, 1981 letter report to Milton Vagins, Division of Reactor Safety Research, U.S. Nuclear Regulatory Commission.

7. R. C. Kryter, R. D. Cheverton, F. B. K. Kam, T. J. Burns, R. A. Hedrick, and C. W. Mayo, *Evaluation of Pressurized Thermal Shock*, NUREG/CR-2083, ORNL/TM-8072. November 1981.

8. F. J. Loss, A. A. Gray, Jr., and J. R. Hawthorne, *Significance of Warm Prestress to Crack Initiation During Thermal Shock*, Naval Research Laboratory, Washington, DC, NRL/NUREG-8165, September 1977.

9. R. D. Cheverton, "Thermal-Shock Investigations," *Heavy-Section Steel Technology Program Quart. Prog. Rep. October-December 1980*, ORNL/-NUREG/TM-437, March 1981, pp. 37-50.

10. R. D. Cheverton, *Heavy-Section Steel Technology Program Quart. Prog. Rep. for October–December 1981*, ORNL/TM-8252, pp. 68–77.

11. S. T. Rolfe and J. M. Barsom, *Fracture and Fatigue Control in Structures, Applications of Fracture Mechanics*, Prentice-Hall, Inc., 1977.

12. T. U. Marston (editor), *Flaw Evaluation Procedures: ASME Section XI*, EPRI NP-719-SR, August 1978.

13. U.S. Nuclear Regulatory Commission, "Effects of Residual Elements on Predicted Radiation Damage to Reactor Pressure Vessel Materials," Reg. Guide 1.99, Rev. 1 (Sept. 16, 1976).

14. J. J. Wagschal, R. E. Maeker, "Surveillance Dosimetry: Achievements and Disappointments," *Proceedings of the Fourth ASTM-Euratom Symposium on Reactor Dosimetry*, March 1982.

15. T. U. Marston et al., "Development of Generic Procedures for Thermal Annealing and Embrittled Reactor Vessel Using a Dry-Anneal Method," EPRI Topical Report, June 1982 (in publication).

LWR PRESSURE VESSEL MONITORING: ABSOLUTE OR RELATIVE DOSIMETRY?

W. Schneider
ZBB, Kernforschungsanlage Jülich, Germany F. R.

ABSTRACT

The neutron fluence monitoring in the LWR pressure vessel surveillance is in principle a task of absolute measurement. However, under particular conditions in practice, it can be carried out by a relative measurement procedure. These conditions will be discussed, and also the possible advantage of applying such a procedure.

1. INTRODUCTION

Absolute measurements and calculations generally require extensive work and a particular degree of experience; if not carried out in a standardized procedure (s. e.g. /I-E706//II, 334/), it is often not easy to judge to which extent the results might be affected by systematic errors.

In this connection it appears of interest to inquire into statements made recently from the metallurgical and the dosimetric side (e. g. /III, M. Brumovsky et al./) saying that the neutron monitoring in the frame of surveillance programmes for the lifetime predetermination of LWR pressure vessels can be carried out also with relative instead of absolute evaluation. Therefore we want to put the following questions up for discussion: firstly, whether such a statement can be taken for justified; and secondly, if so what the advantage of a relative measuring method would be in comparison with the absolute one.

2. LIFETIME PREDICTION AND SURVEILLANCE PROGRAMME MONITORING

When designing a LWR, we have to start with a calculated a b s o l u t e neutron flux density distribution to predict the material properties shift of the pressure vessel which will be expected as induced by fast neutrons. Using correlation curves (s. e. g. /II, 1255//IV, 411/ /IV, 439/), we are able to predict the permissible lifetime of the reactor resulting from those shifts of properties.

If the absolute neutron fluence to be reached which is proportional to this lifetime, will exceed a fixed standard value, it is necessary to perform a surveillance programme for the pressure vessel material in the familiar manner (e. g. /I-E185/).
For such surveillance programmes, the lifetime for the "Service" location of the pressure vessel steel which is the maximum exposed one to embrittlement, may be expressed as follows:

$$t_s = \frac{\Phi(E_L,\vec{r}_A,t_a)}{\overline{\Phi}\,(E_L,\vec{r}_s,t)} \frac{w^A_{St,eff}(E_L)}{w^s_{St,eff}(E_L)} \qquad (1)$$

with:

$\Phi(E_L,\vec{r}_A,t_A)$ the neutron fluence (determined by calculation or measurement) above the lower energy limit E_L, in the Accelerated surveillance position $\vec{r}_A$, for the time t_A

t_A the irradiation time until the vessel steel specimens in the Accelerated position have reached their maximum permissible embrittlement

$\overline{\Phi}(E_L,\vec{r}_s,t)$ the neutron flux density, correspondingly as for the fluence above, but in the Service position $\vec{r}_s$, averaged over the time $0<t<t_s$

$\vec{r}_s$ the Service position taken at the (beltline region of the) inside surface being the maximum exposed region of the vessel wall

$$w^A_{St,eff}(E_L) \equiv \int_0^\infty w_{St}(E)\chi^A_E(E)dE : \int_{E_L}^\infty \chi^A_E(E)dE \qquad (1a)$$

the effective (i.e., above E_L valid) cross-section for displacements in the vessel steel St, determined with the normalized spectral neutron flux density χ^A_E in the A(ccelerated) position.
Eq. (1) takes into account that the neutron exposure of pressure vessel steel has to be given as the number of displacements, as recently recommended /V/; for $w^A_{St,eff} = w^s_{St,eff}$ we would fall back into the old fluence notation.
The idea of a relative evaluation for the pressure vessel surveillance monitoring is then the following: If the damaging exposure ratio between the A(ccelerated) and the S(ervice) positions is known, from the metallurgically found "End of Life" in the A position (i.e., from t_A) the End of

Life for the S position may be extrapolated. Let us assume that we measure $\Phi(\vec{r}_A, t_A)$ and $\phi(\vec{r}_s, t)$ by the same detector type (with measuring reaction i): then eq. (1) would reduce to:

$$t_s = \frac{\bar{I}_i(\vec{r}_A, t)\ t_A\ H(t_A)}{\bar{I}_i(\vec{r}_s, t)\ H(t_s)} \cdot \frac{DAR^A_{Sti}}{DAR^s_{Sti}} \cdot \frac{c_{Ai}}{c_{Si}} \qquad (2)$$

Here is:

$\bar{I}_i(\vec{r}, t)$ the pulse rate measured correspondingly for $\vec{r}=\vec{r}_A, \vec{r}_s$ and averaged over $0<t<t_A$ or t_s, resp.

$H(t_A)$ the irradiation history correction for the Accelerated irradiation

$$DAR^A_{St,i} \equiv \frac{\sigma^f_i}{w^f_{St}} \cdot \frac{w_{St,eff}(E_L)}{\sigma^A_{i,eff}(E_L)} \qquad (2a)$$

the Damage-to-Activation Ratio /1/, with:

$$\sigma^f_i \equiv \int_0^\infty \sigma_i(E)\chi^f_E(E)dE$$

the cross-section of the measuring reaction i averaged over the fission spectrum f

$$w^f_{St} \equiv \int_0^\infty w_{St}(E)\chi^f_E(E)dE$$

the steel displacement cross-section, averaged analogously

$$\sigma^A_{i,eff}(E_L) \equiv \int_0^\infty \sigma_i(E)\chi^A_E(E)dE \ :\ \int_{E_L}^\infty \chi^A_E(E)dE \qquad (2b)$$

the effective measuring reaction cross-section, determined analogously to eq. (1a).

$c_A(c_s)$ correction factors for the measurement in the Accelerated (or: Service) location

In which manner neutron detectors can be applied for such corresponding measurements in the A and S locations will not be discussed here.

3. DISCUSSION OF THE RELATIVE MONITORING EVALUATION

The transition from eq. (1) to (2), i.e., from an absolute to a relative evaluation, should - if worth mentioning further - be made up of more than the change from absolute to relative reaction rates. This latter change solely would bring no bigger uncertainty reduction than about ±5% at most.

Advantages in the application of a relative instead of an absolute evaluation are given if the correction functions - i.e., the quantities beside the $\bar{r}$s - in eq. (2) would more or less cancel against each other or lead to (nearly) constant values; or if the overall uncertainty in the lifetime determination could be decisively reduced in comparison with applying absolute procedures.

Regarding the correction functions in eq. (2), we state at first that the irradiation history corrections H(t) including possible time-dependent **local** flux density-to-reactor power variations /2/ in the two locations A, S are independent **from** each other so that the ratio of the H functions in eq. (2) can generally not be replaced by a constant. This follows from the fact that the irradiation history of the reactor runs faster in the A than in the S location, and that flux-to-power variations may be different in the two locations.

Also for the measuring correction factors c_A, c_S apply generally different values: we expect e. g. for the important photoreaction correction distinctly higher values in the S than in the A location /II, 493/. On the other hand, the $c_A:c_S$ ratio is practically time-independent; so if it has been determined in a benchmark procedure (cf again /II, 493/) tailored to the irradiation environment in question, it may be used as a constant for all reactors belonging to the same design type.

Similarly also the DAR values can be regarded as time-independent. Moreover the ratio $DAR^A:DAR^S$ is to expect to be a constant not very far from unity. This is resulting from the observation that the neutron spectrum between the A and S locations in LWRs does not show large differences particularly if - cf eq. (1) - the inside surface of the vessel wall is taken for the S location; this may be verified using a spectra compilation as, e. g., /3/. The ratio of the DARs may be determined correspondingly to the $c_A: c_S$.

The uncertainties for the measuring correction factors - as well as for the irradiation history incl. the local flux correction - must be assessed for the A and S locations individually. On the other hand, we may expect that the DAR uncertainties in the two locations are relatively strongly correlated, and that the uncertainty to be assigned to the ratio of the DARs is rather small because the value of this ratio as stated should not too much deviate from unity. A general compilation of uncertainty contributions and their values for our problem is given in /I - E706/; cf also /2/.

After this discussion we may rewrite eq. (2) in the following way:

$$t_s = \frac{\bar{I}(\vec{r}_A,t) \cdot t_A \cdot H(t_A)}{\bar{I}(\vec{r}_s,t)\, H(t_s)} \cdot C \qquad (3)$$

where

$$C \equiv \frac{DAR^A}{DAR^s} \cdot \frac{c_A}{c_s}$$

is a dimensionless conversion factor, i.e. a constant specific to a particular LWR line, to be determined with the aid of benchmark or calculational methods.

4. SUMMARY AND CONCLUSION

For neutron monitoring, one may prefer a relative evaluation procedure leading to the wanted absolute value by use of a conversion factor, if:

- the evaluation is easier to be carried out than absolute procedures,
- the conversion factor (as complicated it might be to determine) could be applied as a reference value, not only for a complete surveillance programme but also for all individual reactors of the same LWR line
- the uncertainties an evaluation according to eq. (3) might be affected with could be assessed and checked up in a not too intricate way and would sum up to an overall amount less than with the use of absolute procedures.

Judging the result of our discussion in Section 3 from these criteria, we remark that al least in principle the first two of them can be fulfilled; the uncertainty assessment would be easier if such a unified procedure is applied; the overall uncertainty amount which certainly is hard to preassess might turn out to be somewhat reduced. However, the capability of such a relative evaluation is in our case limited by the facts that an absolute determination cannot be avoided for the first prediction of the lifetime by use of calculation and of correlation curves; and that possible irradiation history (incl. local flux density-to-reactor power) corrections have to be determined to every irradiation individually.

Recognizing this we are concluding that the neutron monitoring for pressure vessel surveillance programmes according to a relative evaluation method as basically outlined above may be advantageous particularly if applied to LWRs produced in

series. Such a procedure should benefit mostly from established reference devices, using benchmark techniques /II, 334//III, W. Schneider//IV, 249/.

REFERENCES
PROCEEDINGS AND COMPILATIONS

/I/ 1981 Annual Book of ASTM Standards, American Society for Testing and Materials, Philadelphia, Pa, USA.

/II/ Proc. 3rd ASTM-Euratom Symposium on Reactor Dosimetry, Ispra, Italy, Oct. 1979, Vols. 1, 2 EUR 6813 (1980).

/III/ IAEA Advisory Group Meeting on Nuclear Data for Radiation Damage Assessment and Related Safety Aspects, Vienna, 12-16 Oct. 1981, (Summary Report edited by N. Kocherov: INDC(NDS)-128/GR).

/IV/ CAPRICE 79 - Correlation Accuracy in Pressure Vessel Steel as Reactor Component Investigation of Change of Material Properties with Exposure Data, Proc. IAEA Technical Committee Meeting, Jülich, Germany F. R., Sept. 1979, Editor W. Schneider, JÜL-Conf-37 (1980).

/V/ IAEA Specialists'Meetings on Radiation Damage Units in Graphite and Ferritic and Austinitic Steels, Seattle, Wa., USA, Oct./Nov. 1972, Nucl. Eng. Design 33, (1975), No. 1.

INDIVIDUAL PAPERS

Papers taken from these Proceedings and Compilations (as /I/ /II/ff, above) are quoted in the text as /I -(Standard no.) E nnn/, /II, page no. in II/ ff, other papers as listed below with single consecutive numbers /1/ff.

/1/ J. P. Genthon, B. Hasenclever,et. al., Recommendations on the Measurement of Irradiation Received by the Structural Materials of Reactors, EUR 5274 d, e, f, n (1975).

/2/ W. Schneider, Comparison and Limitation of Uncertainties in Surveillance and Lifetime Prediction of LWR Pressure Vessels. This Symposium.

/3/ C.Z. Serpan, Jr., B. H. Menke, Nuclear Reactor Neutron Energy Spectra, ASTM Data Series Publications DS 52, ASTM, Philadelphia, Pa., USA (1974).

TESTS ON RADIATION DAMAGE EXPOSURE AND THE ROLE OF ITS LOCATION DEPENDENCY IN BULKY MATERIALS (LIKE PRESSURE VESSEL STEELS)

W. Schneider

ZBB, Kernforschungsanlage Jülich, Germany F. R.

ABSTRACT

In reactor irradiation investigations, generally the neutron spectrum must be known for determining the neutron exposure as irradiation parameter. Moreover, particularly for bulky materials (like steel plates for LWR pressure vessels), the role of the local variation of the neutron spectrum and exposure has to be taken into account.
To investigate this, a special dosimetry test experiment has been started in connection with steel irradiations carried out at Jülich. A report is given on the irradiation device, the detector application, and on the status and the further plan connected with that experiment.

---

1. INTRODUCTION

1.1 General Remarks

For characterizing the neutron effect on reactor materials in material test reactors (MTRs) or on the other hand, during their service in power reactors, the fast neutron fluence

$$\Phi(E_L,\vec{r},t_I) = \int_{E_L}^{\infty} \Phi_E(E,\vec{r},t_I)dE \qquad (1)$$

(above the lower energy limit E_L=0.1 and 1 MeV, in the irradiation position r, during the irradiation time t_I) is used for a long time for the exposure unit (s. e.g. /I-E185/); this procedure has been continued for facilitating the

comparison of newer with older results /II,474/ beside the use of the number of displacements per atom

$$N_M(\vec{r},t_I) = \int_0^\infty w_M(E)\ \Phi_E(E,\vec{r},t_I)dE \qquad (2)$$

(with the damage function $w_M(E)$, for the material M) which has been recommended more recently /I-E693//III//1/.
The selection of the irradiation position r representing the location for an irradiated bulky material (like a thick-wall steel plate) is discussed in Section 1.2. Later on there is reported on the aims and the planning of a dosimetry test experiment (Section 2) for studying the space-dependent effects of the neutron spectrum on the "fluence" or the "displacement number"in a MTR.This study belongs to the extensive irradiation series of large steel specimens at Jülich in the frame of the German project "FKS" (s. Section 2.1). On the neutron detectors and their irradiation, and on the status of that dosimetry experiment is reported in Section 3.

1.2 On the Location Dependency of the Radiation Damage in Bulky Materials

If we want to irradiate a series of large steel specimens in MTR tests, our intention must be to have a neutron fluence distribution over the bulky material as uniformly as possible, and that we at least arrive at a minimum fluence in every point of each specimen.
Such irradiations may simulate the service conditions of reactor materials, like that of the pressure vessel, to a certain degree. However, for the pressure vessel service irradiation itself, it is particularly demanded not to exceed a maximum fluence which (like the maximum number of displaced atoms over the wall) is reached at the inner surface of the vessel wall; besides and for metallurgical reasons too, the fluence is commonly determined in the quarter thickness (T/4) of the vessel wall. At least these two locations have often been recommended and applied for the representative neutron fluence (or displacement number), s. /I-E185//I-E560//II,6/ /II,210//II,249/ and others. Furthermore one expects an influence of the neutron spectrum variation with the penetration depth of the neutrons in the wall on the damaging behaviour according to calculations /2/, resulting in an essential change in material properties.

From another point of view one could expect that property changes in the material occur which are proportional to the spatially integrated neutron absorption (or more refined: to the number of produced displacements) per mass of the

material.

2. A DOSIMETRY TEST EXPERIMENT FOR MATERIAL IRRADIATIONS

2.1 On Steel Irradiations at Jülich (within the German "FKS" Project)

Combined irradiations of large (fracture mechanics) and small specimens of ferritic steels have been started in a threefold arrangement of capsules surrounding the core of the swimming-pool reactor FRJ-1 (as shown in Fig. 1) in 1981, after a preceding prototype irradiation. These irradiations are carried out in the frame of the German research project "Forschungsvorhaben Komponenten-Sicherheit" (FKS, Structural Integrity of Components). On a pilot test and on the planning for this irradiation series and on the preparation of the neutron monitoring for it has been reported at earlier occasions /IV,285//V,459/.

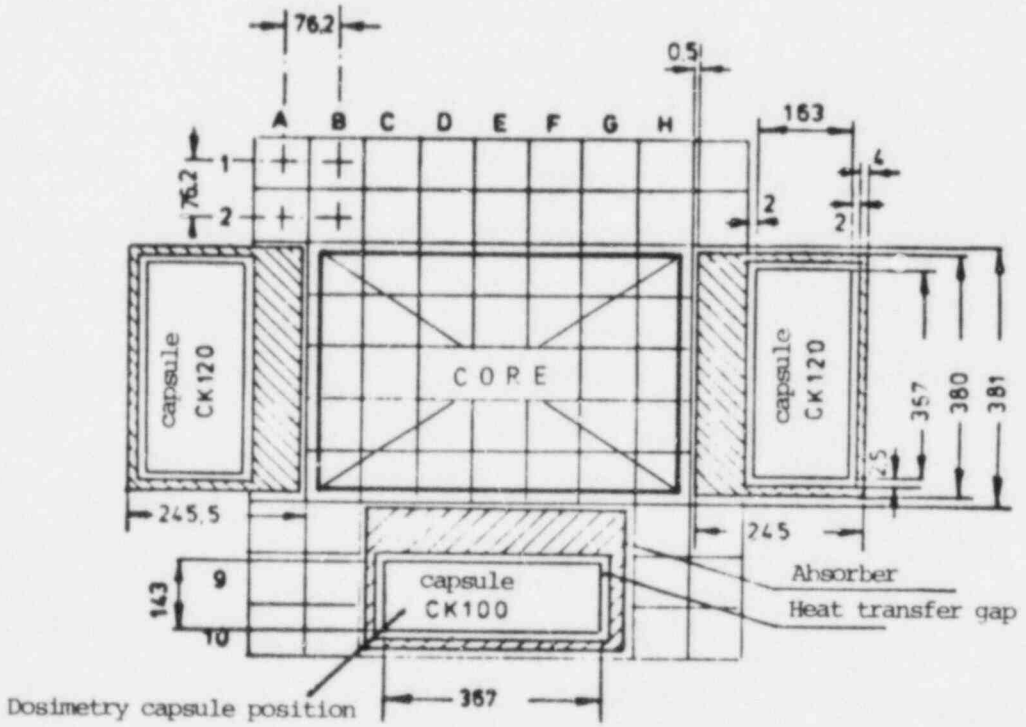

FIG. 1 SPECIMEN ARRANGEMENT FOR THE FKS STEEL IRRADIATION IN THE FRJ-1

Normally all the three irradiation positions are occupied by "standard" capsules (i.e. such ones which contain the steel specimens to be investigated) during the project; in early 1982, transitorily the capsule in the middle position has been replaced by a slightly different "dosimetry capsule" (s. Fig. 1). This peculiar capsule has been built for the Dosimetry Test Experiment the aim of which is outlined in Section 2.2, and the device for it in Section 2.3.

2.2 The Aims of the Dosimetry Test Experiment

It is generally familiar that for evaluating the neutron fluence according to eq. (1) from measurements of atomic reaction rates p_i obtained with the neutron reaction i (=1,..)

$$\Phi(E_L,\vec{r},t_I) = \frac{p_i(\vec{r})t_I}{\sigma^I_{eff,t}(E_L)} H(t_I) \qquad (3)$$

it is necessary to know the spectral neutron flux density for the relevant irradiation environment I, at least in a normalized presentation $\chi^I_E(E)$ so that the effective cross-section for the reaction i in question

$$\sigma^I_{eff,i}(E_L) = \frac{\int_0^\infty \sigma_i(E)\chi^I_E(E)dE}{\int_{E_L}^\infty \chi^I_E(E)dE} \qquad (4)$$

may be determined; in eqs. (3),(4) is: $H(t_I)$ a correction factor for the irradiation history and $\sigma_i(E)$ the energy-dependent cross-section of the reaction i.
The knowledge of the neutron spectrum is wanted all the more for the displacement number determination, according to eq. (2). To attain this knowledge, as a rule calculational information is used which may be of more or less accuracy and suitability. One information which has been made easily available and applied for many years, is based on the assumption of a fission spectrum for the energy distribution of the damaging neutrons. However, after the result of a single neutron spectrum adjustment evaluation in our pilot test to the FKS project /3/, and also from an assessment using other relevant spectral evaluations /2//4/, we have to expect a strong deviation (by nearly the factor two) if we would rely upon the fission neutron spectrum for inside of a thick-wall steel plate instead upon the true spectrum $\chi^I_E(E)$

in the fluence evaluation according to eqs. (3) and (4). Such a serious effect indeed demands to be checked up, not only by elaborate calculations but also from the experimental side: this latter one all the more because we have found a remarkable trend in the shape of the neutron spectrum going from a pure water surrounding over a thin steel bar into a large steel block, all in the same LWR test region /IV,285/ /3/.

For these reasons the Dosimetry Test Experiment has been planned within the FKS irradiation at Jülich. The device (s. Section 2.3) for this experiment should permit the adjustment procedure (as, e.g., applied in /V,208/) for verifying the neutron spectrum experimentally with its variation over a thick-wall steel plate as the contents of the FKS capsules are. For these measurements and for the accompanying flux density gradient measurements radiometric neutron detectors have been provided. Subsequent to these, Damage-to-Activation Ratio (DAR) measurements /1/ have been planned by means of damage detectors (s.Section 3.1) in the same arrangement; this has been done in cooperation between Services des Piles, C. E. N. Saclay, France, and our laboratory, with a twofold aim: firstly for gaining experience with these detectors in different irradiation devices and test environments (cf., e.g., /V,70/); and secondly, for comparing the measured DARs with those obtained from other evaluations,cf eq.(2).

2.3 The Irradiation Device for the Dosimetry Test Experiment

For this a capsule has been prepared with the same dimensions and equipped with the same kind of gamma-ray absorber shield as the "standard" capsules for the FKS irradiations. The dosimetry capsule has been filled with ferritic steel blocks which have been provided with five vertical holes for insertion of neutron detectors (s. Fig. 2). These holes have originally been planned for:

A. studying the variation of the neutron spectrum along the main travelling direction of the neutrons (the x direction, Fig. 2) and also along one perpendicular (viz, the z) direction;
B. mapping the flux density gradient over the steel blocks, particularly for cross-checking the neutron flux density variation in the spectral measurement positions;
C. measuring the DAR by means of damage detectors (cf Sections 2.2, 3.1);
D. the calibration of other special detector types.

The determination of the neutron spectrum variation along the x axis is of special importance because it may (over the variation of the displacement number) influence radiation-induced property changes of the steel remarkably /2/.

Furthermore it has been planned to study the neutron spectrum variation along the z axis too since this variation should be caused nearly purely by the material environment (steel and H_2O mainly), while the neutron intensity should change only slightly in the z direction. Besides, a spectrum variation study in the third Cartesian (y) direction seemed then to be superfluous.

For the spectral sets and the damage detectors, the (wider) stringer holes nos. 1,3,5 have been provided, for the gradient measurements the (narrower ones) nos. 2,4, resp. (Fig.3). Since for practical reasons it was not possible to arrange all the stringer holes along the x axis, the arrangement has been chosen as shown in Fig. 2,viz, the holes nos. 2,3,4 along the y direction, the holes nos. 1,3,5 obliquely between the x and y axes.

The immediate access to the stringers in the Dosimetry capsule has been essential for the capsule design since the stringers should be discharged quickly (i.e., within a few hours after irradiation). During the Dosimetry capsule irradiation (in the middle position), two Standard capsules have remained under irradiation (in the lateral positions, cf Fig. 1) to maintain almost the same neutron population as for the common situation with three Standard capsules simultaneously irradiated.

3. REALIZATION OF THE DOSIMETRY TEST EXPERIMENT

3.1 The Neutron Detector Types

The following types of neutron detectors have been provided (cf Fig. 3):

- (19) sets of radiometric detectors (as under "C_1" in /V,459/, for applying the neutron spectrum adjustment procedure, cf Section 2.2. For a more detailed investigation of the low energy neutrons, the reactions $^{109}Ag(n,\gamma)\,^{110}Ag^m$ and $^{186}W(n,\gamma)\,^{187}W$ have been added. The spectral sets have been planned for insertion into tubular stringers, alternatively with and without Gd cover; 62.5 mm vertical distance between the sets has been chosen, for preventing flux perturbation acting on the non-covered sets by the nearest Gd covers.
- One set of (9) tungsten damage detectors developed at the C.E.N. Saclay /V,1104/and made available from there (cf Section 2.2). These detectors have been designated for adjacent insertion in a stringer into the central hole no.3,

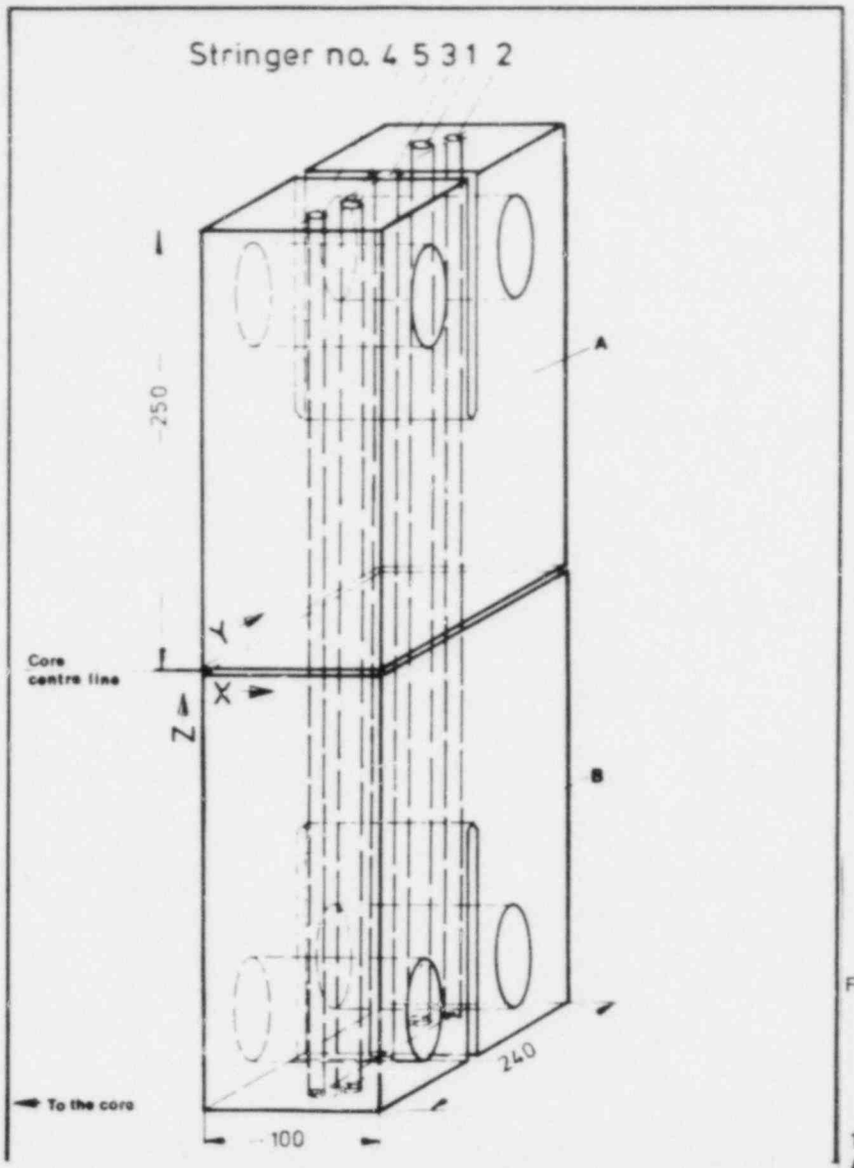

FIG. 2: STRINGER HOLES (1-5) THROUGH THE STEEL SPECIMENS (A,B) FOR THE FKS DOSIMETRY TEST EXPERIMENT

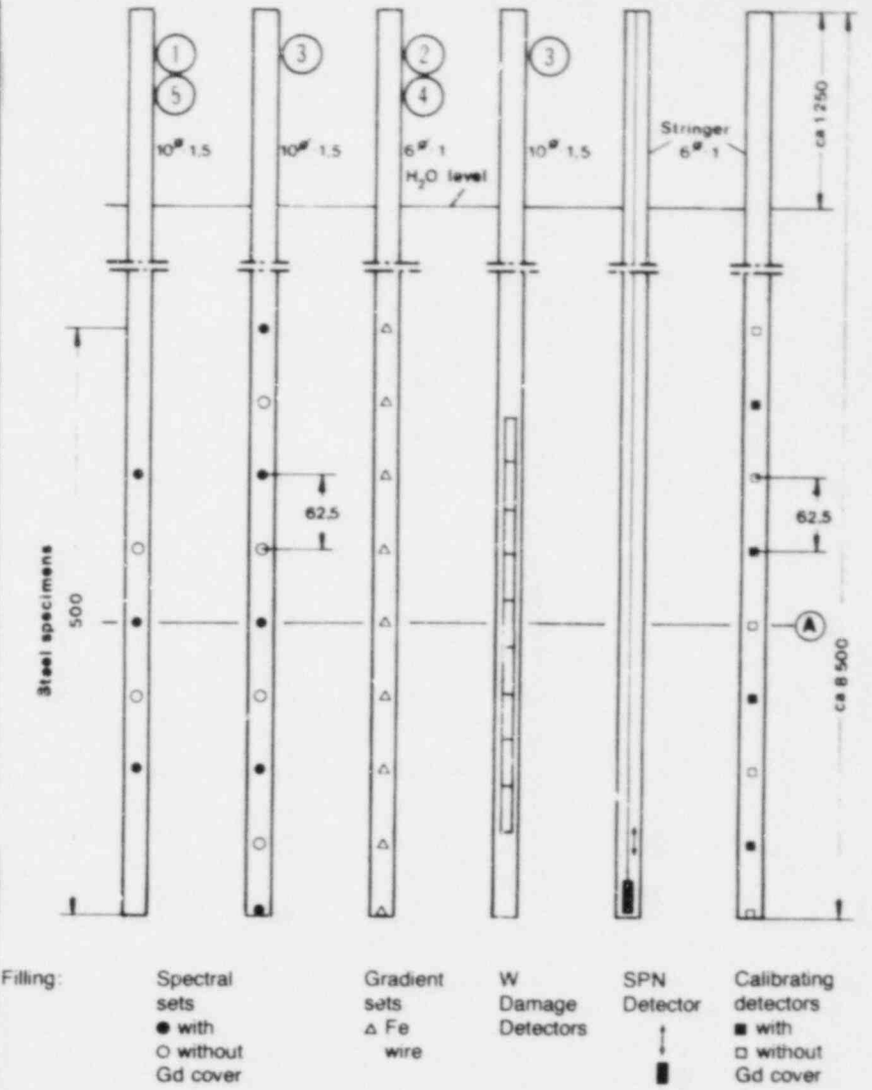

FIG. 3: THE STRINGERS-VERTICAL VIEW AND FILLING WITH DETECTORS

subsequently (or shortly before) the irradiation of the radiometric sets there.
- Two sets of (9) radiometric gradient detectors, using the reaction $^{54}Fe(n,p)^{54}Mn$, for insertion into stringers.
- A third equal set of gradient detectors has been designated for a hole in the absorber shield of the Dosimetry capsule. The averaged flux density ratio of this set to the representative flux density over the capsule allows to preinform about the fluence reached in the Standard capsules at certain times during their irradiation: to each of the Standard capsule irradiations interim fluence values can be obtained by measurements in quickly dischargeable stringers in its absorber shield.
- Other(like SPN) detector types may later on be inserted, to calibrate them in flux density values inside of steel blocks, over the z extension of the capsule (cf Figs. 2,3).

3.2 The Status and the Further Plan for the Experiment

After irradiation, the detectors have been get back out of the stringers in the hot cells of the KFA Jülich. The W damage detectors have been transported to the C. E. N. Saclay for their measurement. The radiometric detectors are at present under measurement in our lab by gamma-ray spectrometry. We expect to have results availabe (incl. the adjustment procedure, the flux mapping, and the discussion) about in one year from now. In this context, the role of the (representative) location for such extensive pieces of material concerning the damaging results of their irradiation - as outlined in Section 1.2 - is intended to be studied more thoroughly.

ACKNOWLEDGMENTS

Concerning the realization of the Dosimetry Test Experiment, I have particularly to name G. Borchardt, H. Küpper, G. Pott, G. Segelhorst, and L. Thöne (all at ZBB, Kernforschungsanlage Jülich) who have decisively contributed to the preparation, the irradiation, and to the subsequent measurements at Jülich. A detailed joint report on the design of the device, on the execution and on the results of this experiment will be published after it will be completed.

A. Alberman, J. P. Genthon, and M. Thierry at Services des Piles, C. E. N. Saclay, France, made it possible for us to arrange the joint project of the W damage detector test within the schedule of our Dosimetry Test Experiment. Also on this W damage detector test a joint publication has been envisaged, after results will have been available.

REFERENCES
PROCEEDINGS AND COMPILATIONS

/I/ 1981 Annual Book of ASTM Standards, American Society for Testing and Materials, Philadelphia, Pa, USA.

/II/ CAPRICE 79 - Correlation Accuracy in Pressure Vessel Steel as Reactor Component Investigation of Change of Material Properties with Exposure Data, Proc. IAEA Technical Committee Meeting, Jülich, Germany F.R., Sept. 1979, Editor W. Schneider, JÜL-Conf-37 (1980).

/III/ IAEA Specialists'Meetings on Radiation Damage Units in Graphite and Ferritic and Austenitic Steel, Seattle, Wa, USA, Oct./Nov. 1972, Nucl.Eng. Design 33 (1975), No. 1.

/IV/ Proc. 2nd ASTM-Euratom Symposium on Reactor Dosimetry, Palo Alto, Ca., USA, Oct. 1977, Vols. 1 to 3, NUREG/CP-0004

/V/ Proc. 3rd ASTM-Euratom Symposium on Reactor Dosimetry, Ispra, Italy, Oct. 1979, Vols. 1, 2. EUR 6813 (1980).

INDIVIDUAL PAPERS

Papers taken from these Proceedings and Compilations (as /I/ /II/ff,above) are quoted in the text as /I -(Standard no.) E nnn/, /II, page no. in II/ ff, other papers as listed below with single consecutive numbers /1/ff.

/1/ J.P. Genthon, B. Hasenclever, et al., Recommendations on the Measurement of Irradiation Received by the Structural Materials of Reactors, EUR 5274 d,e,f,n (1975).

/2/ D.A. Canonico, Transition Temperature Considerations for Thick-Wall Steel Nuclear Pressure Vessels, Nucl. Eng. Design 17, 149-160 (1971).

/3/ G. Borchardt, H. Lang, L. Weise, Irradiation of Pressure Vessel Steel, Neutron Flux Densities, Neutron Spectra and Temperature Fields in Large Specimens, Kerntechnik 19 (1977), Nr. 5, 219-224.

/4/ C. Z. Serpan, Jr., B. H. Menke, Nuclear Reactor Neutron Energy Spectra, ASTM Data Series Publications DS 52, ASTM, Philadelphia, Pa., USA (1974).

Session D.2
Adjustment Codes and Uncertainties

STATUS REPORT ON THE REAL-80 EXERCISE

W.L. Zijp*, H.J. Nolthenius*, E.M. Zsolnay**, E.J. Szondi**,
G.C.H.M. Verhaag*, D.E. Cullen***, C. Ertek***

* Netherlands Energy Research Foundation ECN, Petten, The Netherlands.
** Nuclear Reactor of the Technical University, Budapest, Hungary.
*** International Atomic Energy Agency, Vienna, Austria.

ABSTRACT

This report presents some results of the first phase of the interlaboratory exercise REAL-80 to study uncertainties in integral parameters (such as displacement rate per atom steel, activation rate per atom nickel), derived from spectrum information obtained by means of activation spectrometry in well defined test cases.

INTRODUCTION

In the concluding session of the third ASTM-Euratom Symposium on Reactor Dosimetry (Ispra 1979) there was warm support for the suggestion to organize a follow-up of the previous international activities on the intercomparison of unfolding codes. It was felt that such a study should pay particular attention to the uncertainty of integral parameters (displacement rates and activation rates), derived from neutron flux density spectrum information (based on experimental activation rates) by an unfolding procedure. The REAL-80 exercise was organized by the IAEA in Vienna. The exercise has received the code name REAL-80 (Reaction Rate Estimates, Evaluated by Adjustment Analysis in Leading Laboratories). The analysis of the numerical results of this exercise is being performed (upon request by the IAEA) by a joint team from the Budapest Technical University and the Petten research centre. After preparatory work in various laboratories the exercise started for the participants in February 1981, when the IAEA distributed magnetic tapes with input data required in the exercise together with an information sheet. This information was sent to some prospective 30 participants all over the world.
The first results of the intercomparison were reported at the IAEA Advisory Group Meeting on Nuclear Data for Radiation Damage Assessment and Related Safety Aspects (held in Vienna, 12-16 October 1981.

The participating laboratories were asked to perform the following actions:

- adjust (unfold) the two reactor neutron spectra for the ORR and the YAYOI reactor and make statements, if possible, on the uncertainties and the correlations for the group fluence rates;
- calculate the activation rate of nickel, using the cross-section data for $^{58}Ni(n,p)^{58}Co$, and also the standard deviation in this value;
- calculate the damage rate in iron, using the damage cross-section data supplied, and also the standard deviation in this value;
- submit to the IAEA the requested data on magnetic tape in a prescribed format, preferably within two months after receipt of the IAEA tape with the input data.

It is emphasized that the outcome of the exercise reflects the state-of-the-art in 1981 of the capabilities of laboratories, in deriving values and uncertainties for the predicted number of displacements. All participating laboratories were asked to use their own existing practices.

INPUT DATA

The input neutron spectrum, the group cross-sections and the input reaction rates with their uncertainties in the form of variance-covariance matrices were completely described for the exercise. One input set was derived for the Oak Ridge Research Reactor (ORR). The spectrum is a typical thermal spectrum with a predominant 1/E part. The other set was derived for the central region (inside a vertical penetrating 2 cm diameter gloryhole) of the YAYOI reactor. For the latter spectrum 12 reaction rates could be applied in the input set, and for the ORR set 19 reaction rates were available. The input neutron spectrum for the ORR was calculated with a transport theory code. The input spectrum for the YAYOI reactor was calculated with the one-dimensional ANISN code. The reactor physics codes did not yield directly the variance-covariance matrices for the spectrum, which some adjustment codes require as part of the input. Dr. L.R. Greenwood developed variance-covariance matrices which were suitable for the REAL-80 exercise.
The correlation matrix of the input spectrum was generated with a Gaussian function with a full width at half maximum of 3 groups (within a 100 groups structure) superimposed on a small flat contribution. The correlation matrices for the ORR and for the YAYOI input neutron spectrum were about equal. In the input data set supplied for this exercise the input neutron spectrum and also a set of group cross-section data were available in a 100 groups structure. The primary source of the input cross-section data was the first version of the ENDF/B-V dosimetry file. The input data set contained also the neutron selfshielding factors for the dosimetry detectors of interest. The set contained moreover a cross-section set with a 620 groups structure. This set was derived also from the ENDF/B-V dosimetry file.
In the IAEA input data set the neutron selfshielding and cadmium cover corrections were not supplied for this 620 groups structure. The variances for the 100 groups cross-section data originate also from the ENDF/B-V dosimetry file. For the characterization of the output neutron spectrum

two extra energy dependent cross-section data were supplied: the damage cross-section of steel and the activation cross-section of the reaction $^{58}Ni(n,p)$. The uncertainty for these group cross-section data was 15% for all groups in the 100 groups structure. The correlation function was defined again as a Gaussian with a FWHM of 10 groups.

It will be clear that correct physical information was supplemented with extra data for which the correctness cannot be proved so easily. The influence of these extra informations (especially the correlation matrices of input spectrum, cross-section data and ORR reaction rates, but also the variances of the ORR input neutron spectrum) cannot be estimated easily. For several adjustment codes this variance-covariance information determines magnitude and the energy dependence of the neutron spectrum modifications.
Also the chi-square value which can be calculated for the data set is dependent on the definition of the input data. For the ORR input data set a very small chi-square value can be observed, when a least squares adjustment procedure is applied. This indicates a too good consistency of the input data. This "inconsistency" is probably caused by the extra data but of course also other inconsistencies may be present in the other data part.
The participants had the freedom to use either the 620 groups or the 100 groups cross-section data. In the REAL-80 input data set two different files of displacement cross-sections were given. The ASTM standard procedure E693-79 refers to the calculation of displacement in ferritic steel (iron). In the European Working Group on Reactor Dosimetry (EWGRD) values have been derived for the displacement cross-sections in stainless steel. These data are available in a 620 groups structure. A quantitative comparison of the cross-section curves of the two separate files showed appreciable local differences between the ASTM standard and the Euratom practice, due to different origins for the cross-section data set and different group structures (in combination with conversion procedures for group values). The fission spectrum averaged cross-sections differ however less than 2,5 per cent.

DATA TREATMENT

The IAEA passed all REAL-80 solutions from the participants on magnetic tape to the analyzing laboratories in Budapest and Petten. The magnetic tapes were read and the data could be treated with a few programs. Software was developed to read the data and sort them. Also special calculation and plotting programs had to be written. In the evaluation of the participant data four parts can be distinguished: a) classification of information of the REAL-80 of the participants; b) comparison of integral data supplied by the participants; c) comparison and characterization of the energy dependent neutron spectrum data; d) study of the output correlation matrices with aid of factor analysis.

In most cases the contributions of the participants had to be adapted for application of utility programs. Small deviations of the input format had to be corrected upon request from the participant or because changes were obviously necessary. The integral spectrum data were listed and the neutron spectra were converted to a uniform representation. The neutron spectrum data (i.e. the spectrum and the variances) were converted to a 640 groups structure of the SAND-II type. Due to this approach no spectrum information was lost. For the calculations with the neutron spectra a cross-section library was used in the same structure. The cross-section data were converted also without loss of information. All response calculations were done with the 640 groups structure. The data in the plots of the ratio of output and input spectrum are given in 100 groups structure and were derived from the 640 groups data by an averaging procedure. Furthermore a number of characteristic values and group fluence rates with group width equal to energy decades were calculated. Three categories of output spectrum data were selected: 100 groups, 620 groups and other structures. The correlation matrices were analysed using the method of factor analysis. The original (large) correlation matrices were split up into product of vectors without information loss. These characteristic vectors (factors) were then compared and analysed for the different solutions.

RESPONSES AND ADJUSTMENT CONDITIONS

Altogether 62 solutions from 12 laboratories using 10 different adjustment codes were considered (see table 1). The definition of the exercise allowed the participants to prepare more than one solution for the same problem. As a result, in some cases several solutions were given, either with more than one adjustment code, or with the same code under different conditions. The number of energy groups used in the adjustment procedures was 100 in more than half of the cases, while only 16 per cent of the results was presented in 620 groups structure. Sometimes solutions were based on a group structure different from the 620 groups or the 100 groups of the input specification. In these cases the conversion procedure (with interpolation and extrapolation schemes) was not specified by the participants. This means that the input data for these special group structures may not have unambiguous values. The convergence criteria are not the same for the different adjustment codes. For that reason a comparison of the adjustment results on the point of convergence is not so easy. As common convergence parameter in the analysis of the participants data the so-called Average Relative Deviation (ARD) seems best suited. This parameter is defined as:

$$ARD = \left\{ \sum_{i=1}^{n} \left[(\alpha_i^m - \alpha_i^c) / s_i^m \right]^2 / n \right\}^{\frac{1}{2}} \qquad (1)$$

where:

n = number of input reaction rates;

α_i^m = measured (input) reaction rates;

α_i^c = calculated reaction rate, using the solution spectrum;
s_i^m = estimated uncertainty of the difference between α_i^m and α_i^c.

Another parameter which can be considered to describe the convergence is the standard deviation of the reaction rates, called DEV. This parameter does not apply statistical weights.

$$DEV = \left\{ \sum_{i=1}^{n} \left((\alpha_i^m - \alpha_i^c / \alpha_i^m \right)^2 / (n-1) \right\}^{\frac{1}{2}} \qquad (2)$$

In the calculations of these parameters it was often found that the output spectra were not normalized in the same way. This may be due to the application of different sets of reaction rates in the input of the adjustment, but also properties of the adjustment code itself may be important in this respect. The results obtained are presented in table 2. The data for the "other" groups structures should be interpreted carefully because the convergence parameter for the output spectra with less than 100 groups might be incorrect.

Only five of the adjustment codes (i.e. STAY'SL, NEUPAC, LSL, SENSAK, and SANDBP) provided information on the correlation between the output group fluence rates of the neutron spectrum. Not always information was supplied on the calculation procedure for the covariance data (or the related correlation matrices). The information originated sometimes from the properties of the least squares principle (deterministic model) and sometimes from Monte Carlo variations applied in accordance with the input standard deviations (stochastic process).

NUMERICAL COMPARISON OF OUTPUT DATA

Figs. 1 and 4 show some typical distributions for the ORR and YAYOI spectra, while figs. 2 and 5 show the ratios of output and input spectra. The plots show the various codes give differences in the ratios, thus also differences in the output spectra. In order to compare the overall output spectrum shapes, the energy dependent neutron spectrum data were converted to a decade group structure. The results of the various groupings were then compared. In the comparison the standard deviation of all spectra for each group was calculated together with the average value. In a number of cases a large standard deviation is found. This may be partly due to a few discrepant solutions, which inflates the coefficients of variation for some groupings in an appreciable way. This is demonstrated by calculating the extremes in each grouping for the set of all output spectra (see figs. 3 and 6). These large differences are partly due to different representations of the input spectrum used by the participants, but also the number of groups applied will have influenced the results.

For both the ORR and YAYOI neutron spectra one may conclude that in general the standard deviation of the various output spectra is larger than 10 per cent. Only in some energy regions (between 0,1 and 1 MeV and

between 1 and 10 MeV) the value of the standard deviation is smaller than 10 per cent. This is the region where the threshold detectors have their main response. One should realize that the average value below 0,1 MeV is not representative in case of the YAYOI spectrum, owing to the spread of more orders of magnitude of the group fluence rates (see fig. 6). Characteristic spectrum data derived by the participants for their solutions are listed in table 3. In most cases the coefficients of variation are rather small if the information for the "other" group structures is not considered. In the 620 groups spectra for the YAYOI large deviations for the nickel activation rate are found. The covariance information was made available in the form of correlation matrices in most cases with 100x100 elements (Exceptions: SENSAK with 40x40 and LSL with 20x20 matrix elements). The comparison of such a large amount of data is time consuming and not yet finished. It turned out that the patterns of the correlation matrices based on the STAY'SL least squares approach and based on Monte Carlo variations using the SAND-II approach were significantly different (see figures 7 and 8). This finding is now subject of further study.

From a preliminary analysis of the data the following results can be obtained:

a) In case of STAY'SL type adjustment codes most of the eigen vectors of the input spectrum correlation matrix can be identified also in the solution matrix. The output correlation matrix will be determined by these eigen vectors in the energy regions where the response of the detector set used in the adjustment procedure is poor. These energy regions are: for ORR spectrum: 360 keV < E < 1 MeV, and E > 14 MeV; for YAYOI spectrum: E < 15 keV, 360 keV < E < 1,8 MeV, E > 14 MeV.
The input spectrum correlation matrices of the REAL-80 exercise were artificially generated. Consequently, they cannot describe the real physical correlations present in a reactor neutron spectrum. As the correlation matrices of the adjusted neutron spectra are used in the calculation procedure of uncertainty values for different spectrum characteristics, the replication of the main characteristics of the input correlation matrix will lead in these cases to unrealistic results. This effect clearly shows the urgent need of more realistic (physics based) correlation matrices.

b) The correlation matrices of SAND-type solutions differ strongly from the above written pattern. Correlations in the neutron spectrum originating from reactor physics processes can be observed in these matrices. The pattern of the cross-section curves of the detector set can also be identified in energy dependent importance values of the eigen vectors. This effect has here a more pronounced character than in case of the STAY'SL-type solutions.

c) The numerical evaluation of the correlation matrices having other group structures than the above discussed 100 groups solutions requires a transformation procedure. Nevertheless the statements referring to the role of input correlation matrices in case of the STAY'SL-type solutions are valid also for the results of codes like SENSAK and LSL, which were applied with far less than 100 groups.

GENERAL CONCLUSIONS

1. For the preparation of a complete set of input data, the organizers used numerical data of various nature (experimental reaction rate data; evaluated cross section data; reactor physics based spectrum data; experimental, evaluated and estimated uncertainty data; experimental and artificial correlation data). One should realize that the quality of the results obtained with an adjustment procedure, is heavily based on the amount and quality of the input information actually used.

2. In most cases the participants used in their adjustment procedure not exactly the same input information:
   - not always the complete set of input data was used;
   - sometimes numerical data differing from those in the supplied data set were used (e.g. another cross-section file, another input spectrum etc.).

   It turned out that the solutions could not well be classified according to their adjustment principle, due to these many different conditions for the input.
   In the present situation one of the best criteria to make a classification for the solutions is based on the number of energy groups applied in the adjustment (620 groups, 100 groups, other than 100 groups). It should be realized that even with this classification the solutions within one category are not always directly comparable (presence of "apples" and "oranges").

3. The exercise involved the handling of a large amount of numerical data. During the course of time some contacts between organizers and participants were helpful. In a few cases these contacts have led to modifications in solutions already submitted.

4. There were no two solutions (not even from the STAY'SL type least squares codes) which give identical output data.

5. With respect to the interpretation of the results for the ORR spectrum, one should bear in mind that the whole set of input data was not optimal with respect to the consistency of the data.

6. The spectral shapes of the output spectra show considerable spread, both for the thermal ORR spectrum and for the fast YAYOI spectrum. The integral spectrum parameters, such as $\phi_{>1MeV}$ and $\phi_{>0,1MeV}$, show much less variation.

7. The differences between the solution spectra obtained with the 100 groups and the 620 groups cross-section libraries respectively, can be due to the different physics information present in these two libraries. Furthermore the absence of prescribed self-shielding information may also have had some influence. In cases where the participants used the 620 groups cross-section data, they had to calculate the neutron self-shielding factors themselves; one participant did not take this effect into consideration.

8. Sometimes solutions were based on a group structure different from the 620 groups or the 100 groups of the input specification. In these cases the conversion procedure (with interpolation and extrapolation schemes) were not specified by the participants. This means that the input data for these special group structures may not have unambiguous values. This implies that systematic effects and deviations might have been introduced by the participants choice of an own group structure.

9. During the calculations for the evaluation of the solutions, some difficulties were met in the interpretation of neutron spectra presented in a group structure with less than 100 groups. To obtain correct results for the relevant reaction rates in these cases extra calculations should have been made by the evaluators making use of appropriately weighted few group cross-section data. This approach was not followed, since the 100 groups structure was taken as reference, and reduction to fewer groups gives rise to loss of information with respect to the reference structure. Consequently the evaluation procedure resulted in some differences between evaluators' data and participants' data in the relevant group structures.

10. For the YAYOI spectrum the predicted displacement rates in steel show more agreement than the predicted activation rates in nickel. This may suggest that one has to be very careful in deriving calculated displacement rates from the experimental response from only one (nickel) threshold activation detector and supplementary spectrum information.

11. With respect to the predicted activation rate in nickel we arrived, when taking into account all responses as supplied by the participants, at a coefficient of variation of 2,1 per cent for the ORR spectrum and of 8,8 per cent for the YAYOI spectrum. If only the category of 100 groups solution spectra is considered, then these values become 1,5 per cent for the ORR spectrum, and 6,4 per cent for the YAYOI spectrum.

12. The participants had much freedom in selecting the cross-section data for the prediction of the activation rate in nickel (R_{Ni}) and the displacement rate in steel (R_{dpa}). The supplied input data set comprised 100 groups and 620 groups versions of the relevant cross-sections. Furthermore the 620 groups cross-section library comprised for steel two different displacement cross-section evaluations originating from ASTM and from EURATOM. A rough quantitative comparison of the two cross-section curves showed appreciable local differences. The fission spectrum-averaged cross-sections differ however less than 2,5 per cent. The fact that different cross-section sets were used, will have influenced the results for R_{Ni} and R_{dpa}.

13. For the predicted displacement rate in steel we observed a coefficient of variation of 6 per cent for the ORR spectrum and 2,9 per cent for the YAYOI spectrum, if all of the participant responses are considered.

14. The coefficient of variation for the activation rates in nickel and the displacement rate in steel derived from the sets of responses were less than the largest uncertainties quoted by some participants.

15. When we consider the series of predicted activation rates per atom nickel and predicted displacement rates per atom iron for all solutions, one cannot observe significant differences due to the adjustment algorithm used. The largest deviations from the average value seem to be due to effects originating from group structure and/or changes in the input data.

16. It was observed that the various output spectra were not normalized in the same way. The average value for the ratio of the measured and calculated reaction rates was not in all cases equal to unity. These differences in normalization will directly influence all the integral and spectrum-averaged parameters.

17. The Average Relative Deviation (ARD) parameter was considered as an appropriate measure for the convergence of the solution. It was found that the values for this parameter were not the same for all solutions; this fact in itself will already result in some differences in the integral and spectrum-averaged data.

18. The pattern of the correlation matrix for the output spectrum derived in a deterministic way with the STAY'SL code is clearly different from the patterns of the correlation matrix derived in a stochastic way with Monte Carlo variations using the SAND-II algorithm, without making strict assumptions for the covariance matrix of the input spectrum.

Table 1. Groupings of REAL-80 solutions.*

viewpoint	number of solutions		number of laboratories	
	ORR	YAYOI	ORR	YAYOI
total number considered	30	32	11	12
. in 100 groups	15	18	6	7
. in 620 groups	6	4	3	3
. in other structure	9	10	4	4
. without uncertainties	15	15	2	3
. with uncertainties only for spectrum	4	2	1	1
. with uncertainties for spectrum and characteristics	11	15	8	8
. without correlations	18	17	4	5
. with correlation matrix for spectrum	10	11	7	7
. with correlations for spectrum and reaction rates	1	1	1	1
. with correlations only for reaction rates	1	1	1	1
. SAND-II, SANDBP, SANDPET, SANDMX2	11	12	4	5
. STAY'SL	6	5	3	3
. CRYSTAL BALL	1	1	1	1
. WINDOWS	2	2	1	1
. LOUHI-78	2	2	1	1
. NEUPAC	1	2	1	1
. LSL	3	4	1	1
. RFSP-JÜL	2	2	2	2
. SENSAK	1	1	1	1
. GERDMO2	1	1	1	1

*Some incomplete STAY'SL, ITER and FERRET solutions arrived too late for inclusion in this table.

Table 2. Convergence parameters.

$$ARD = \left\{ \sum_{i=1}^{n} \left| (\alpha_i^m - \alpha_i^c) / s_i^m \right|^2 / n \right\}^{\frac{1}{2}}$$

$$DEV = \left\{ \sum_{i=1}^{n} \left| (\alpha_i^m - \alpha_i^c) / \alpha_i^m \right|^2 / (n-1) \right\}^{\frac{1}{2}} \times 100$$

ORR spectrum:

	IAEA code	$\overline{A_m}/\overline{A_c}$	DEV	ARD
100 groups	000XX (input spectrum)	1,01	10,31	1,11
	006AB	0,999	3,44	0,29
	008FB	0,990	4,03	0,44
	019BD	1,19	6,12	0,60
	023CA	1,01	9,72	1,00
	036AC	1,00	4,87	0,51
	038AC	1,00	3,52	0,35
	045BC	1,01	8,17	0,83
	049DA	1,01	8,34	0,84
	050AA	0,999	3,65	0,31
	051BA	0,996	6,73	0,74
	055BC	0,993	8,59	0,83
	062DA	0,991	7,29	0,82
	067DA	1,01	9,05	0,97
	069AC	0,999	3,71	0,32
	071AC	0,999	3,70	0,32
620 groups	001BB	0,973	15,26	1,59
	018BD	1,13	14,16	1,55
	020BD	1,11	13,16	1,54
	021BD	1,11	13,11	1,53
	064DA	1,01	10,38	1,05
	065DA	1,03	8,99	0,88
other group structure	003EB	0,959	8,30	0,85
	005EB	0,959	8,39	0,92
	031HA	0,906	26,72	2,76
	032HA	0,682	82,93	7,27
	033HA	0,966	6,53	0,73
	034GA	0,898	50,53	4,89
	035GA	0,96	54,18	5,13
	040IA	1,10	9,73	0,93
	043JA	1,14	21,31	2,50

Table 2 (continued).

YAYOI spectrum:

	IAEA code	$\overline{A_m/A_c}$	DEV	ARD
100 groups	Y00XX (input spectrum)	1,03	19,60	2,25
	Y07AB	0,998	7,92	0,72
	Y09FB	0,992	11,10	0,93
	Y10FB	0,981	10,17	0,88
	Y22BD	1,16	15,24	1,81
	Y24CA	0,982	11,29	1,00
	Y37AC	0,975	10,77	0,96
	Y39AC	0,984	10,44	0,91
	Y46BC	0,968	11,39	0,96
	Y47BC	0,967	11,65	1,02
	Y52DA	1,00	11,05	0,95
	Y53AA	0,996	8,50	0,78
	Y54BA	0,992	9,93	0,92
	Y56BC	0,990	11,21	0,97
	Y63BA	0,988	10,04	0,94
	Y68DA	0,986	12,63	1,11
	Y70AC	0,984	10,44	0,91
	Y72BD	0,967	11,29	0,93
	Y73BD	0,970	10,68	0,88
620 groups	Y02BB	1,10	13,18	1,62
	Y48BC	0,964	13,89	1,25
	Y57BC	0,989	13,13	1,22
	Y66BA	0,996	7,86	0,78
other group structure	Y04EB	0,951	11,68	1,37
	Y25HA	0,801	21,00	2,80
	Y26HA	0,794	20,69	2,69
	Y27HA	0,41	62,97	8,26
	Y28HA	0,973	8,70	0,82
	Y29GA	0,754	28,98	3,78
	Y30GA	0,705	30,25	3,78
	Y41IA	0,972	11,53	1,09
	Y44JA	1,09	8,10	0,73
	Y61EB	1,03	19,60	2,25

Table 3. Integral parameters as supplied by participants.

Reference values for input spectrum:

	ϕtot	ϕ > 1 MeV	ϕ > 0,1 MeV	R_{Ni}	Rdpa
ORR	$1,932\times10^{17}$	$3,808\times10^{16}$	$8,127\times10^{16}$	$5,142\times10^{-13}$	$5,450\times10^{-9}$
YAYOI	$1,614\times10^{15}$	$7,473\times10^{14}$	$1,548\times10^{15}$	$9,632\times10^{-15}$	$1,031\times10^{-10}$

		IAFA code	relative values for ϕtot	ϕ > 1 MeV	ϕ > 0,1 MeV	R_{Ni}	Rdpa
ORR spectrum	100 groups	006AB	1,03	1,06	1,01	1,03	1,04
		008FB	1,03	1,06	1,01	1,03	1,04
		019BD	-	-	-	-	-
		023CA	1,02	1,02	1,02	1,01	1,02
		036AC	1,02	1,06	1,01	1,02	1,04
		038AC	1,03	1,06	1,01	1,03	1,05
		045BC	1,00	1,07	1,01	1,03	1,04
		049DA	1,01	1,02	1,01	1,01	1,02
		050AA	1,04	1,06	1,04	1,03	1,05
		051BA	1,04	1,04	1,04	1,00	1,03
		055BC	1,01	1,05	1,02	1,04	1,04
		062BA	1,05	1,03	1,05	1,00	1,03
		067DA	1,00	1,01	1,00	0,99	1,00
		069AC	1,03	1,06	1,03	1,02	1,04
		071AC	-	-	-	-	-
	Aver.		1,024	1,046	1,020	1,018	1,034
	St.d.%		1,52	1,89	1,50	1,49	1,34
	620 groups	001BB	1,06	1,04	1,03	1,04	1,06
		018BD	1,01	1,06	1,04	1,07	1,13
		020BD	-	-	-	-	-
		021BD	-	-	-	-	-
		064BA	1,03	1,08	1,04	1,04	1,06
		065BA	1,00	1,07	1,04	1,02	1,05
	Aver.		1,025	1,063	1,038	1,043	1,075
	St.d.%		2,58	1,61	0,48	1,98	3,44
	other group structure	003EB	1,10	0,981	1,02	1,01	1,06
		005EB	1,01	0,992	0,896	1,03	1,01
		031HA	1,02	1,06	1,02	1,02	1,04
		032HA	1,04	1,08	1,03	1,00	1,04
		033HA	1,03	1,06	1,03	1,02	1,04
		034GA	1,67	1,07	1,51	1,06	1,30
		035GA	1,07	1,06	1,16	1,05	1,12
		040IA	0,932	1,03	0,856	0,980	0,936
		043JA	1,01	1,02	1,00	0,990	1,02
	Aver.		1,098	1,039	1,058	1,018	1,063
	St.d.%		19,98	3,40	17,98	2,59	9,51
Total aver.			1,05	1,046	1,036	1,022	1,050
Total st.d.%			12,38	2,49	10,52	2,11	5,89

Table 3 (continued)

		IAEA code	relative values for				
			ϕtot	ϕ > 1 MeV	ϕ > 0,1 MeV	R_{Ni}	R_{dpa}
YAYOI spectrum	100 groups	Y07AB	1,27	1,18	1,26	0,933	1,16
		Y09FB	1,26	1,18	1,26	1,05	1,18
		Y10FB	1,26	1,19	1,26	1,04	1,18
		Y22BD	1,27	1,12	1,24	0,841	-
		Y24CA	1,26	1,19	1,27	1,06	1,19
		Y37AC	1,24	1,15	1,23	1,03	1,15
		Y39AC	1,24	1,15	1,23	1,04	1,15
		Y46BC	1,29	1,21	1,28	1,09	1,21
		Y47BC	1,28	1,21	1,28	1,09	1,21
		Y52DA	1,23	1,22	1,23	1,03	1,17
		Y53AA	1,25	1,15	1,25	0,948	1,15
		Y54BA	1,24	1,13	1,23	1,00	1,15
		Y56BC	1,25	1,17	1,25	1,05	1,18
		Y63BA	1,25	1,13	1,24	0,994	1,14
		Y68DA	1,20	1,18	1,20	1,08	1,16
		Y70AC	1,24	1,15	1,23	1,04	1,15
		Y72BD	1,28	1,20	1,25	1,10	-
		Y73BD	1,28	1,20	1,26	1,08	-
	Aver.		1,255	1,173	1,247	1,028	1,169
	St.d.%		1,755	2,60	1,65	6,38	1,91
	620 groups	Y02BB	1,34	1,22	1,32	0,870	1,18
		Y48BC	1,23	1,21	1,23	1,10	1,20
		Y57BC	1,20	1,17	1,20	1,05	1,16
		Y66BA	1,31	1,18	1,32	0,92	1,18
	Aver.		1,27	1,195	1,268	0,985	1,18
	St.d.%		5,18	1,99	4,88	10,95	1,38
	other group structure	Y04EB	1,28	1,10	1,27	0,903	1,16
		Y25HA	1,28	1,20	1,28	0,998	1,18
		Y26HA	1,28	1,21	1,28	1,08	1,21
		Y27HA	1,24	1,10	1,23	1,03	1,15
		Y28HA	1,28	1,16	1,29	0,955	1,17
		Y29GA	1,32	1,43	1,38	0,869	1,23
		Y30GA	1,24	1,08	1,29	1,23	1,21
		Y41IA	1,22	0,978	1,22	1,06	1,24
		Y44JA	1,16	1,05	1,15	0,852	1,06
		Y61EB	1,34	1,10	1,33	0,900	1,18
	Aver.		1,263	1,141	1,272	0,9877	1,179
	St.d.%		3,99	10,77	4,91	11,83	4,352
Total aver.			1,260	1,166	1,258	1,010	1,174
Total st.d.%			3,06	6,23	3,45	8,78	2,89

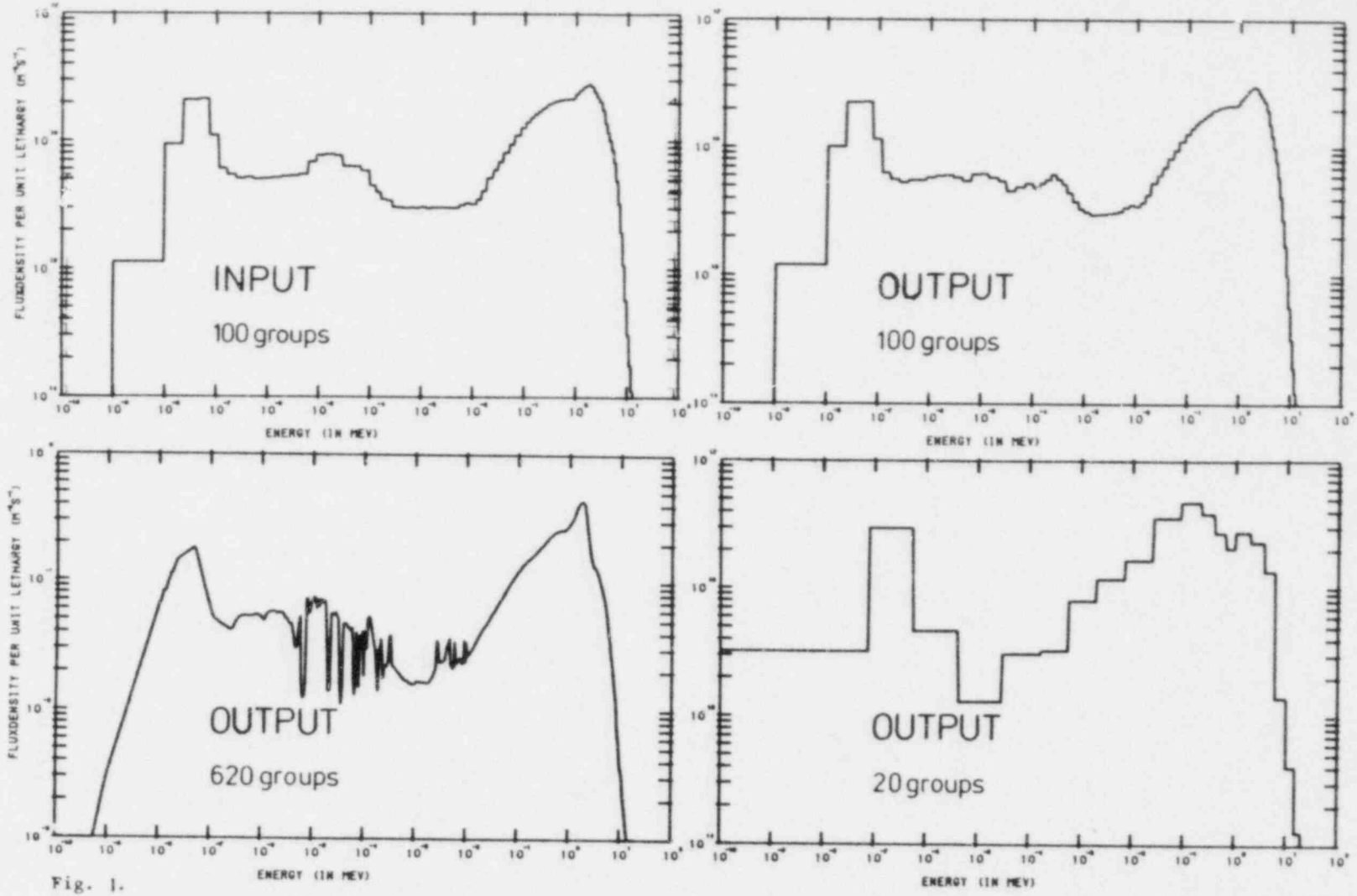

Fig. 1.
Examples of ORR spectra.

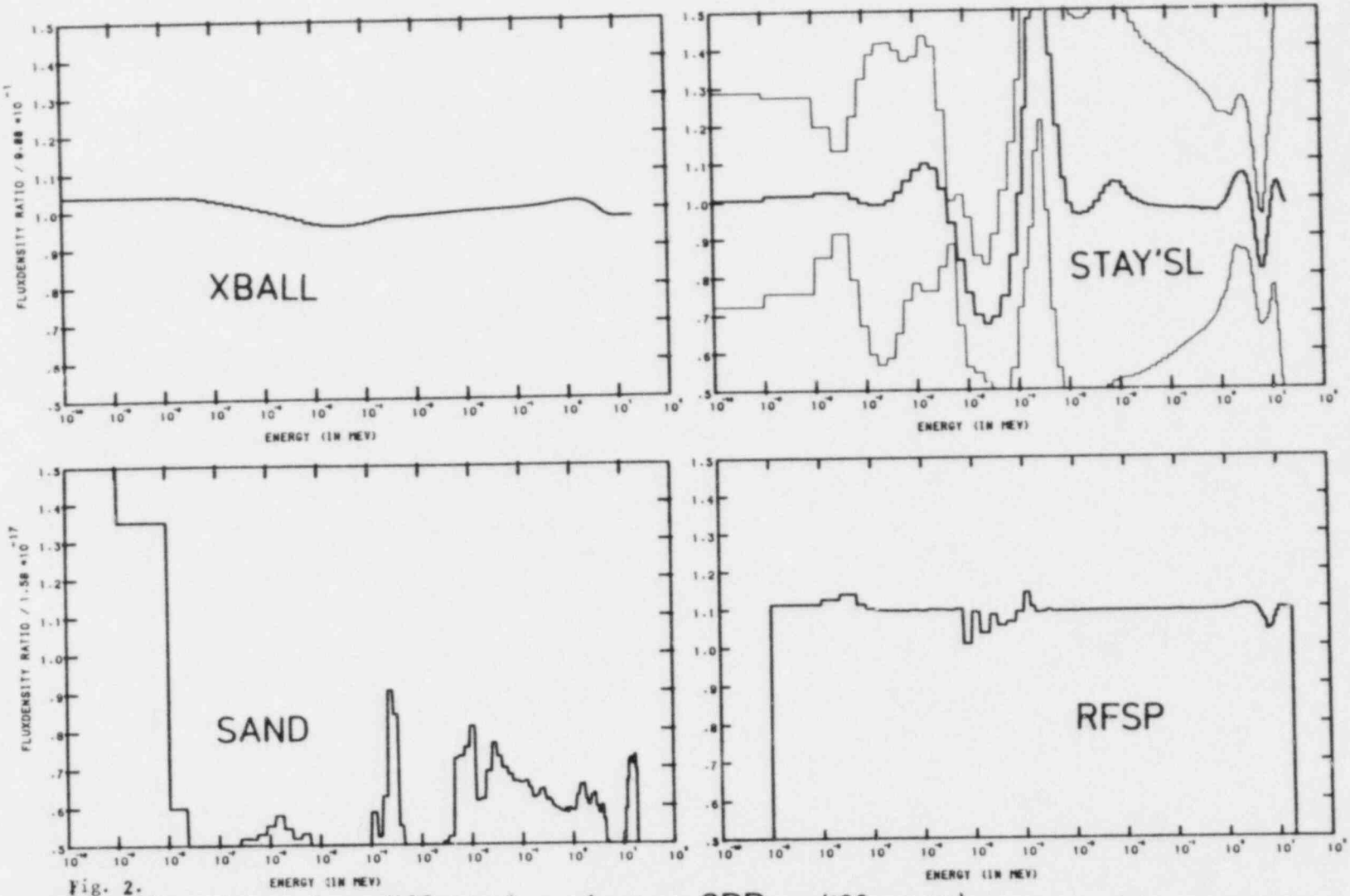

Fig. 2.
Modifications for different codes ORR (100 groups)

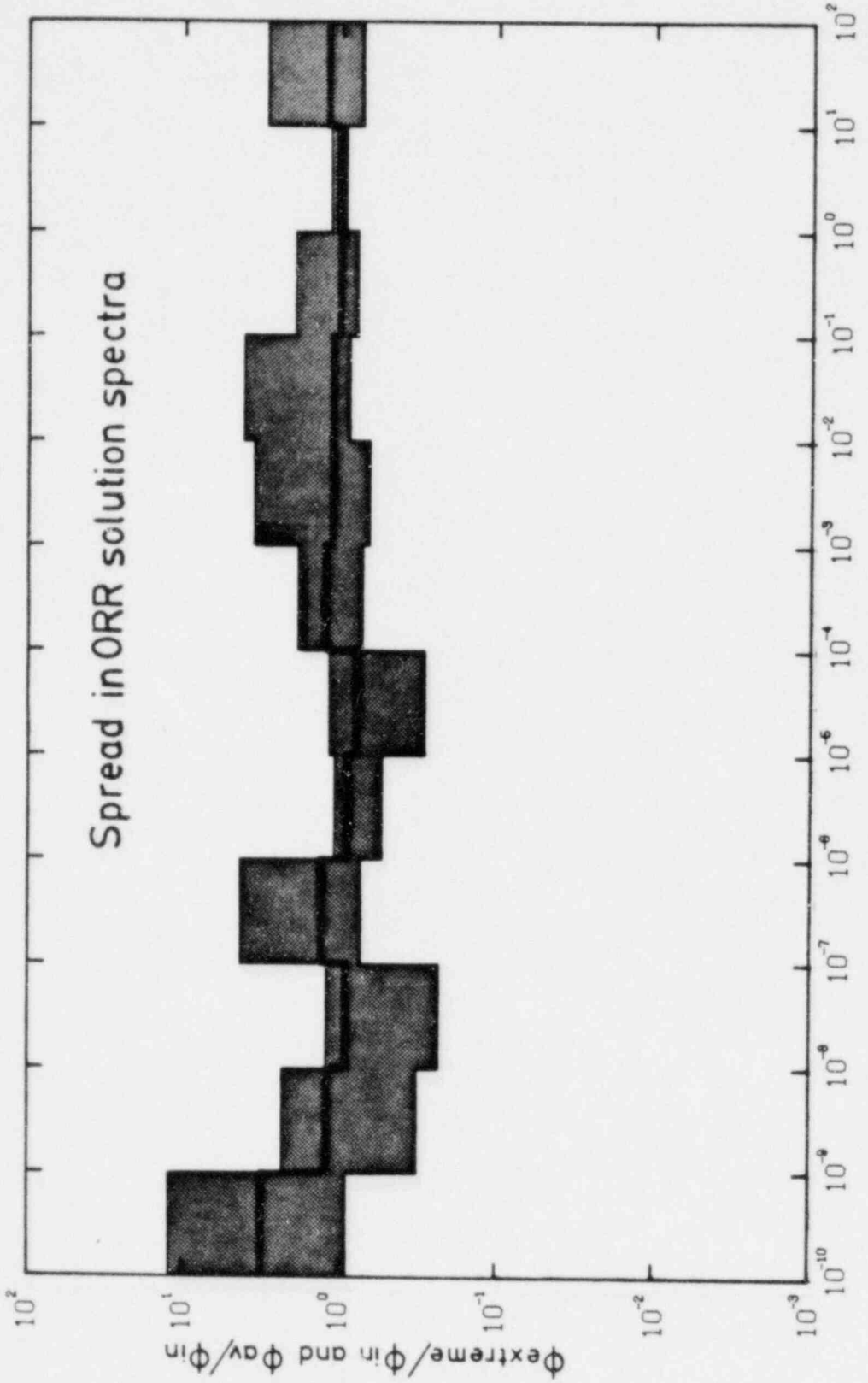
Spread in ORR solution spectra
$\phi_{extreme}/\phi_{in}$ and ϕ_{av}/ϕ_{in}
ENERGY (IN MEV)
10^{2}
10^{1}
10^{0}
10^{-1}
10^{-2}
10^{-3}
10^{-10}
10^{-9}
10^{-8}
10^{-7}
10^{-6}
10^{-5}
10^{-4}
10^{-3}
10^{-2}
10^{-1}
10^{0}
10^{1}
10^{2}

Fig. 3.

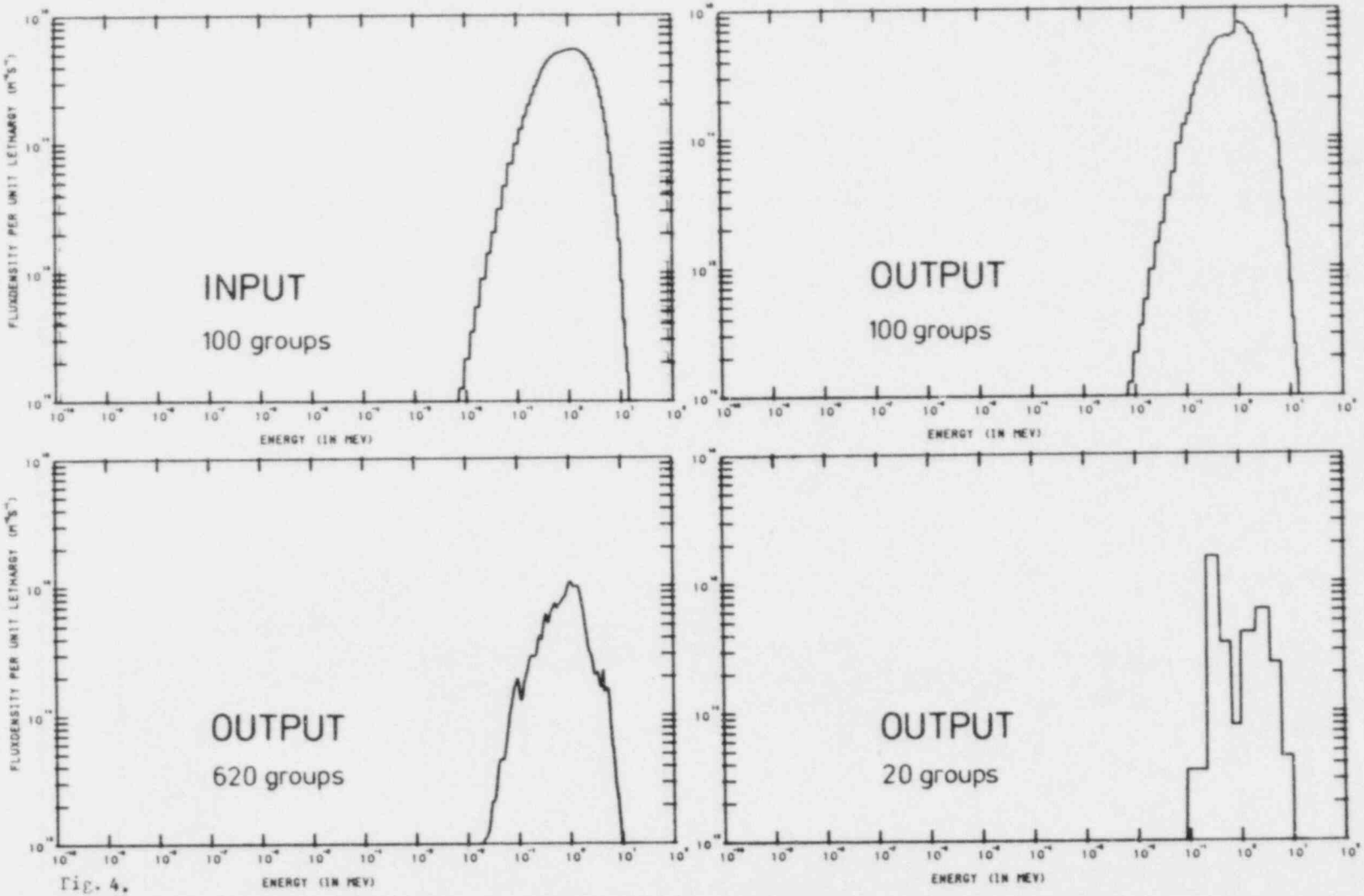

Fig. 4.

Examples of YAYOI Spectra

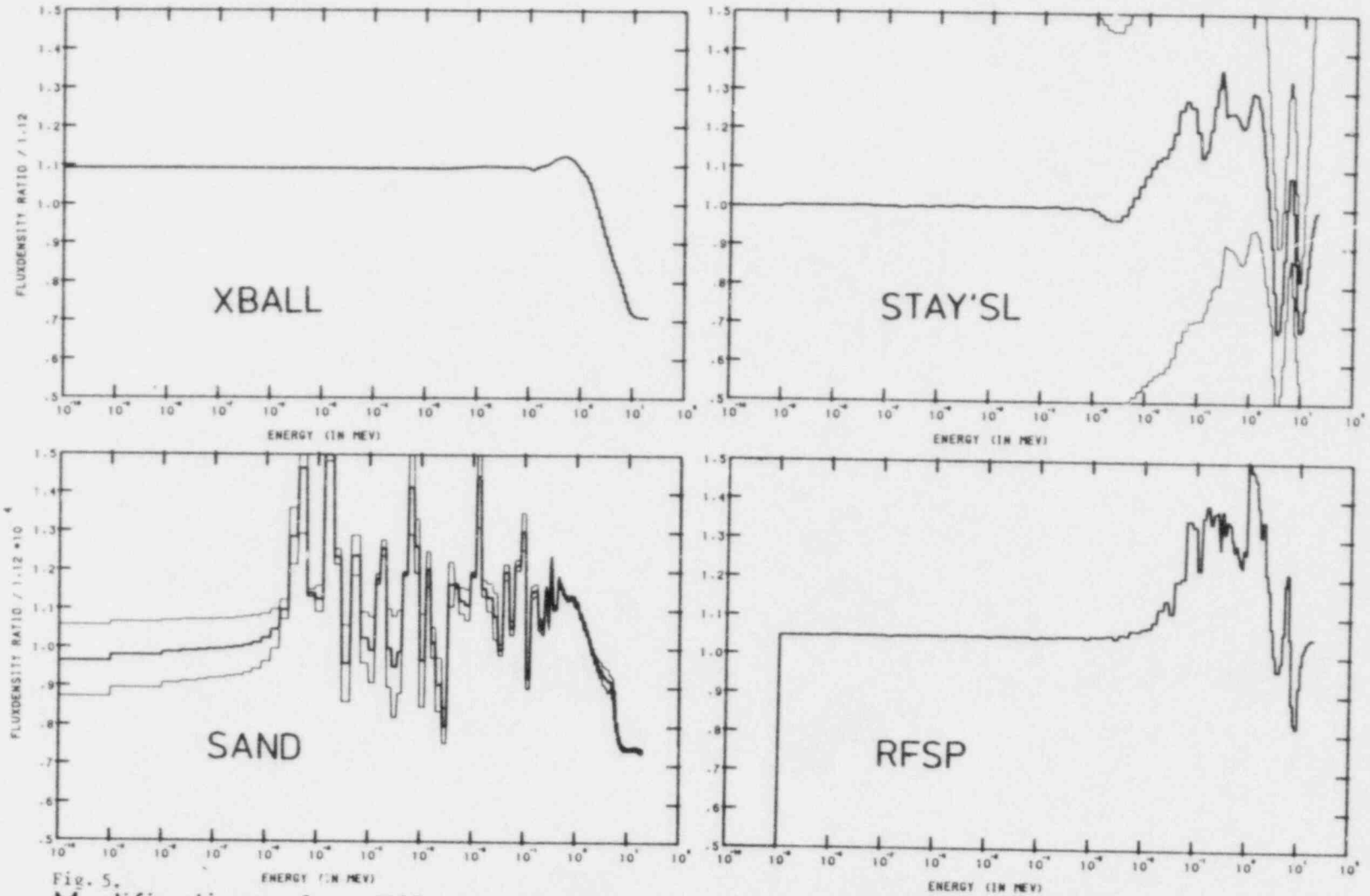

Fig. 5.
Modifications for different codes. YAYOI (100 GROUPS)

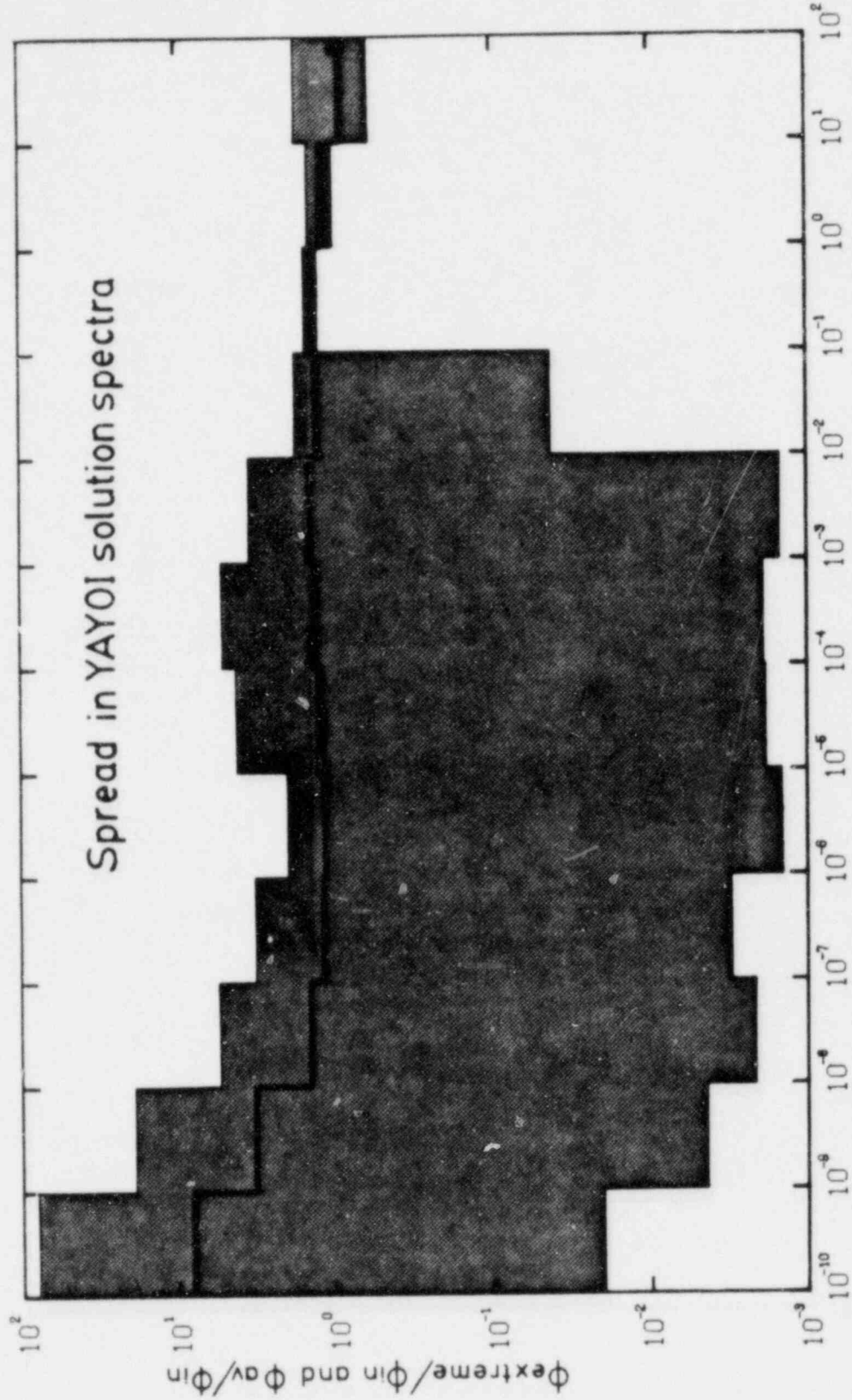
Spread in YAYOI solution spectra
Φextreme/Φin and Φav/Φin
ENERGY (IN MEV)
10^2
10^1
10^0
10^-1
10^-2
10^-3
10^-10
10^-9
10^-8
10^-7
10^-6
10^-5
10^-4
10^-3
10^-2
10^-1
10^0
10^1
10^2

Fig. 6.

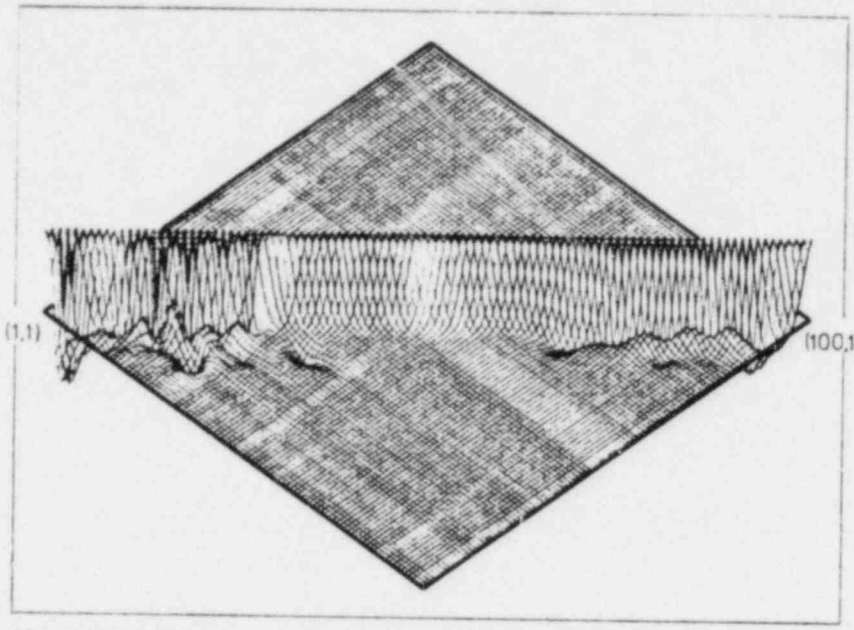

REAL-80 A06AB
Correlation function of group flux densities for ORR (STAY'SL).

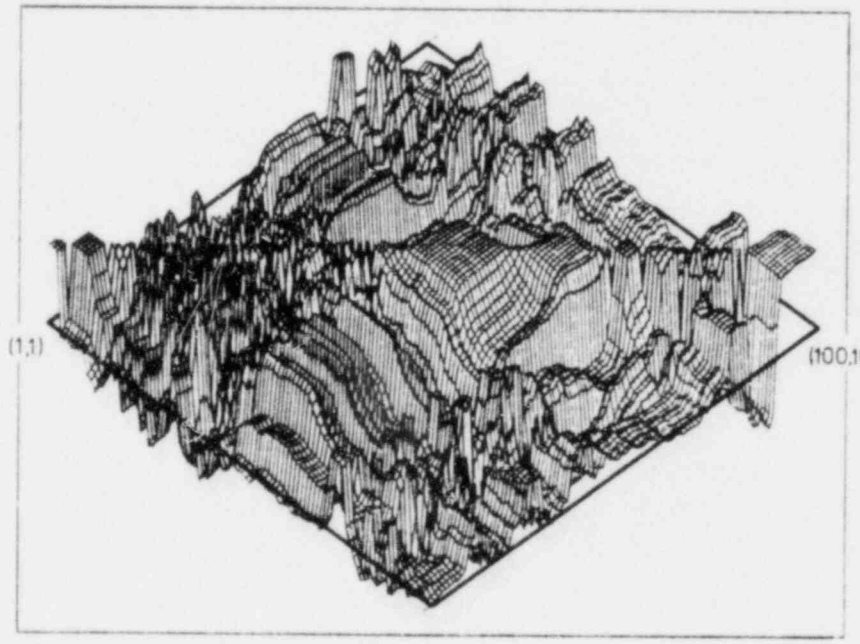

REAL-80 B15BC
Correlation function of group flux densities for ORR (SAND-II).

Fig. 7.

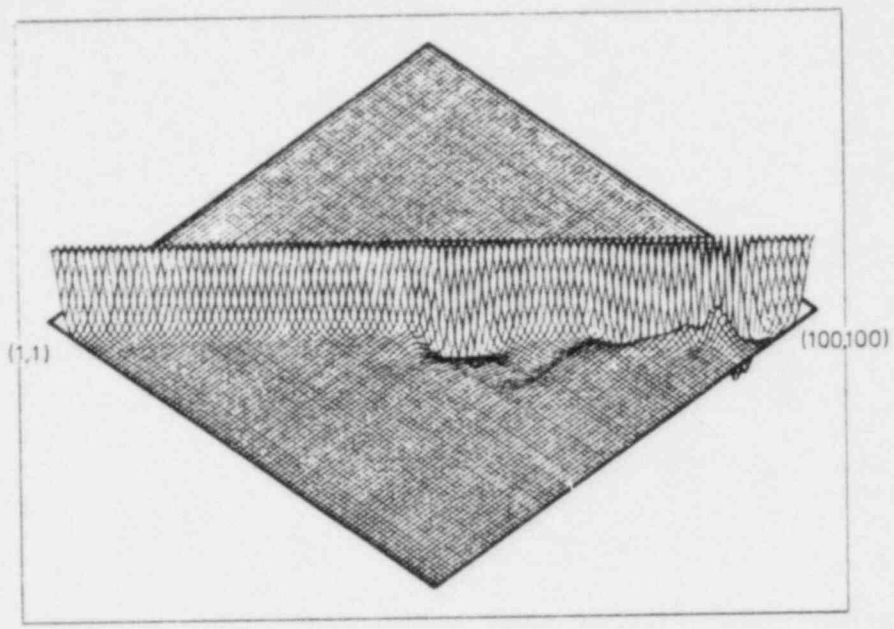

REAL-80 Y07AB

Correlation function of group flux densities for YAYOI (STAY'SL).

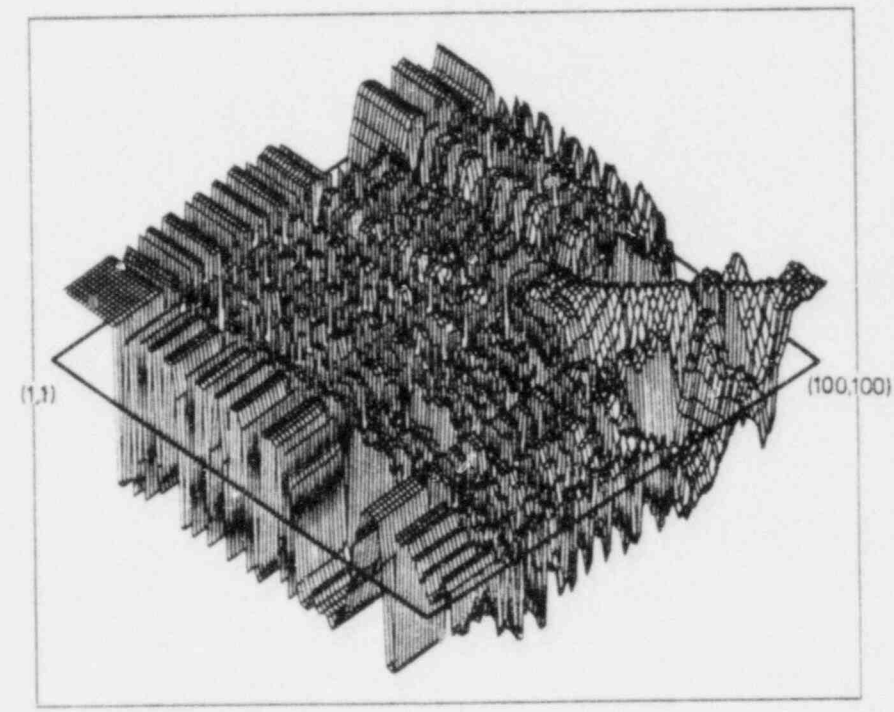

REAL-80 Y16BC

Correlation function of group flux densities for YAYOI (SAND-II).

Fig. 8.

DOSIMETRY EXPERIMENTS IN JOYO

A.Sekiguchi, M.Nakazawa, T.Taniguchi
M.Sasaki*, S.Suzuki* and T.Ohtake*
Univ. of Tokyo, Hongo 7-3-1, Bunkyo-ku, Tokyo, JAPAN
(*)Power Reactor and Nuclear Fuel Development Corporation,
O-arai-cho, Higashi-Ibaraki-gun, Ibaraki-ken, JAPAN

ABSTRACT

JOYO dosimetry test program was started since 1979 to improve and validate the dosimetry technique for the liquid metal cooled fast reactor JOYO. The main research activities have been concentrated to the uncertainty analysis of the dosimetry procedures. The new unfolding code NEUPAC has been developed based on the J1 algorithm that can accept all covariance matrices of inputs. The complementary intercomparison studies have been also performed through the YAYOI blind intercomparison and the PNC/DOE-HEDL dosimetry exchange program.

INTRODUCTION

The experimental fast reactor "JOYO" is the first and only one liquid metal cooled fast reactor in JAPAN, and reached its initial criticality on April 24, 1977. Then, the low power physics tests[1], rated power engineering tests at 50MW operations and 75MW power ascension program have been well completed till the beginning of 1980. At present, the "JOYO Mark-II" program is in progress to be modified as a powerful fast flux irradiation reactor through core-configurations of the various irradiation test devices. The completion of this program is expected on the beginning of 1983.

The purpose of JOYO dosimetry test program since 1979 is the dosimetry improvements and validations for its reactor vessel surveillance test and for the next fuel and material irradiation tests in the "Mark-II" program. Many dosimetry improvements have been made on the suitable dosimeter-set selection, capsule-design and the reaction-rate measurement technique. The new unfolding code NEUPAC (Neutron Unfolding Code Package) has been developed based on the J1 unfolding

algorithm that can accept the covariance matrices of all of the input data such as the reaction-rate, the cross-section and the initial guess spectrum.

Validations of the JOYO dosimetry system have been made through participations to the YAYOI Blind Intercomparison study [2] and PNC/DOE-HEDL dosimetry exchange program [3], both of which have been also presented in this symposium. The main research activities for these improvements and validation works of JOYO dosimetry system have been concentrated to the uncertainty analysis of dosimetry procedures,and their important results are presented here.

UNCERTAINTY ANALYSIS OF REACTION-RATE MEASUREMENTS

Through quantitative survey of every origins of uncertainties in the JOYO reaction-rate measurement system, it can be concluded that the main origin is due to the uncertainty of the γ-ray counting efficiency values. That is depending on the both terms, the uncertainty of the standard γ-ray source intensity for detector calibrations and the interpolation or extrapolation error to draw the efficiency curve using the calibration data.

For the uncertainty values of each standard γ-ray source intensity, we can use assigned values from the source supplier. Their correlative uncertainties between γ-ray sources, however, are expected to be assigned if it exists, for the accurate covariance matrix estimation of the uncertainty.

Careful considerations on the interpolation and extrapolation errors have been made to estimate the covariance matrix of the reaction-rate measurements, which needs the second order derivatives of the efficiency curve when a linear interpolation is applied for the data fitting. Fig.1 shows some typical discrepancies from the linear interpolation curve in the graph of log-log scale for the γ-ray full energy peak efficiency curves for the 55-57 cc Ge detectors. This tendency of the discrepancies, named twisting properties around the $\log \varepsilon(E)$ vs $\log E$ straight line of the Germanium detector peak efficiency curves are found generally for the other size detectors. It can be explained by considering the γ-ray counting process in the full energy peak region through the cascade absorption of photo- and compton-absorption processes in the Germanium detector.

Then $\Delta(\ln \varepsilon(E))$, the interpolation error of $\ln \varepsilon(E)$, can be written like

$$\Delta(\ln \varepsilon(E)) = \frac{1}{2} \ln\frac{E}{E_1} \ln\frac{E_2}{E} (\ln \varepsilon(\tilde{E}))''$$

where $(\ln \varepsilon(\tilde{E}))''$ is the second derivative value typically shown in Fig.2 and $\tilde{E}$ means a proper energy between the efficiency measured points of energy E_1 and E_2.

The covarince matrix due to this interpolation or extrapolation errors can be given like

$$\overline{\Delta(\ln\varepsilon(E))\Delta(\ln\varepsilon(E'))} = \frac{1}{4}\ln\frac{E}{E_1}\ln\frac{E_2}{E}\ln\frac{E'}{E_1}\ln\frac{E_2}{E'} \times \{(\ln\varepsilon(\tilde{E}))''\}^2$$

if the efficiency values at the energy of E and E' are interpolated or extrapolated linearly on the graph of the log-log scale using the measured values of $\varepsilon(E_1)$ and $\varepsilon(E_2)$.

Summary results of the uncertainty analysis in the JOYO reaction-rate measurement system are shown in Table 1, and the present accuracy can be evaluated as ±2 - 5%(1σ) excluding the reactor power uncertainty of 3.47%. This accuracy can be validated independently through the two intercomparison studies of the YAYOI Blind Intercomparison[2] and the PNC/DOE-HEDL dosimetry exchange program[3].

DEVELOPMENTS OF THE UNFOLDING CODE NEUPAC

A new unfolding code NEUPAC has been developed to obtain the neutron flux, spectra and relating integral dose values such as dpa from the multiple reaction-rate data set, that was basing on the J1-unfolding algorithm developed by the authors of University of Tokyo[6]. Some features of this NEUPAC code are

1) uncertainty values of the output values of flux, spectrum and dpa etc.can be obtained accurately depending on the input uncertainty data, that can be given as the exact covariance matrices of the reaction-rate, dosimeter cross-section and initial guess spectrum,
2) the χ-square testing is used to examine the statistical consistency between the whole input data including their assigned uncertainties and also between the output data. This testing is very useful especially to avoid the under-estimates of the uncertainty of initial guess spectra, which is the main reason of under-estimates of the final results, and
3) further sensitivity analysis routine are ready to show how many contributions to the each output uncertainty are made by the respective input uncertainties of reaction-rate data, cross-section values and initial guess spectra.

Additional feature of the NEUPAC code is a new representaion form of the uncertainty inputs of the function values like dosimeter cross-section $\sigma(E)$ and initial guess spectrum $\phi^0(E)$, where the uncertainties of energetically correlated components can be distinguished from uncorrelated components. For example, for $\sigma(E)$, the covariance matrix should be expressed basically by the form of

$$\overline{\Delta\sigma(u_1)\Delta\sigma(u_2)} = S(u_1,u_2) + \gamma^2(u_1)\ \delta(u_1-u_2)$$

and the first and the second terms of the right side mean a correlated and an uncorrelated component respectively, where $\delta(u)$ is the Kronecker's delta function. If this formula is changed into the following actual group averaged expression of calculation basing on the multi-group approximation

$$\overline{\Delta\sigma_g\Delta\sigma_k} = S(u_g,u_k) + \frac{\gamma^2(u_g)}{\Delta u_g}\delta_{gk},$$

it is found that the uncorrelated component of the second term of the right side is depending on the value of group width Δu_g in use. For this reason, in this code, the value of $\gamma^2(u_g)/\Delta u_g$ (g=1,G) can be entered for the inputs of uncorrelated uncertainty independently to $S(u_g,u_k)$. The internal changes of the group width through calculation are made considering the dependency on the group width of $(\gamma^2(u_g)/\Delta u_g)\ \delta_{gk}$. Therfore, a random error component (uncorrelated uncertainty) entered at 5%, for example, in a certain group structure has an internal value of 10% when the group width is lessened to 1/4 time internally. The same inputs of uncertainty are prepared also for the initial spectrum, however, it is a problem how to make these uncertainty of input spectrum.

In order to validate this NEUPAC code, the unfolding of the benchmark reaction-rate data in the Mol-ΣΣ facility has been carried out, and compared with the results of the SAND-II MC [8] code using the same input values except their uncertainty values. Good agreements have obtained between the two results of the NEUPAC and the SAND-II MC code, where the total flux values were estimated respectively as 7.36 ± 0.12 (1σ) and 7.63 ± 0.24(1σ) n/cm^2·sec at the 1MW reactor operation. In this calculation, NEUPAC has used the same SAND-II MC uncertainty table of the dosimeter cross-section but it is assumed as the random-error. Therefore, NEUPAC has given a little smaller value of the standard deviation of the output total flux than the SAND-II MC results, though the uncertainty of the input spectrum was included for the NEUPAC code by about 20% but not for the SAND-II MC code. The unfolded spectrum is shown in Fig.3.

As another test-run of the NEUPAC code, the multiple foil data unfolding of the YAYOI core-center neutron field has been carried out with a special attention to the influences of the covariance terms of initial guess spectra. Typical results are summarized in Table 2, where the covariance terms of initial spectra have been found giving favourable and reasonable effects to the statistical χ-square consistency of the input data and also to the uncertainty reduction of some integral dose values like total flux and dpa quantity.

CONCLUSIONS AND DISCUSSIONS

Succesful developments and validations of the JOYO dosimetry system have been carried out through these two years program. The present accuracy of our reaction-rate measurements can be evaluated within ±2 - 5%(1σ), and this uncertainty is thought mainly due to the calibration procedure of the γ-ray full energy peak efficiency curves of the Germanium detector.

On the uncertainty of the total flux values obtained by the NEUPAC code, it is preliminary estimated as about 10%(1σ), but this values are found depending on the uncertainty data inputs of the reaction cross-section and initial spectra including their covariance components that have never been well validated.

Future programs of this JOYO dosimetry experiments are planned on the following subjects,

1) dosimeter developments such as the long-life Nb dosimeter, SSTR and damage monitors,
2) improvements of the NEUPAC code's cross-section library and initial spectra, especially their covariance input data and
3) dosimetry experiments in the modified MK-II core as a irradiation facility.

REFERENCES

1) S.Nomoto, H.Yamamoto and Y.Sekiguchi, "Physics Experiments at the Start-up of JOYO", IAEA-SM-244/8, Sept. 24-28 (1979)

2) M.Nakazawa et.al., "The YAYOI Blind Intercomparison on Multiple-Foil Reaction-Rate Measurements", UTNL-0099 (1981), to be presented to this symposium.

3) S.Suzuki et.al., "PNC/DOE Collaborative Dosimetry Test in JOYO", to be presented to this symposium.

4) R. J. Gehrke, R. G. Helmer and R. C. Greenwood, Nucl. Instr. and Meth. 147 (1977) 405.

5) Y.Yoshizawa et.al., JAERI-M 8196 (1979)

6) M.Nakazawa and A.Sekiguchi, "Several Applications of J1-Unfolding method of Multiple-Foil Data to Reactor Neutron Dosimetry", EUR-6813, p751 (1979)

7) W. N. McElroy and L. S. Kellog, "Fuels and Materials Fast Reactor Data Developments and Testing", Nucl. Technology 25, 180 (1975)

8) C. A. Oster et.al., "A Monte Carlo Program for SAND-II Error Analysis", HEDL-TME 73-20 (1973)

Table 1 . Evaluated Uncertainties (1σ) of Reaction-rates
in JOYO Surveillance position 9A1

PNC Dosimeter Set

Reaction	Gamma-ray Counting			Nuclear Data			Foil Weight	(I) Reaction-rate ΔR/R**	(II) ΔR/R***
	Statistical	Positioning	Efficiency	Due to $T_{1/2}$	Emission Probability	Isotope Abundance			
$^{63}Cu(n,\alpha)^{60}Co$	0.72%	0.18%	2.70%	0.02%	~0.0%	0.03%	0.06%	4.49%	2.85%
$^{59}Co(n,\gamma)^{60}Co$	0.65	0.20	2.50	0.02	~0.0	~0.0	0.12	4.37	2.66
$^{54}Fe(n,p)^{54}Mn$	1.12	0.18	1.90	0.07	~0.0	1.72	0.19	4.51	2.88
$^{58}Fe(n,\gamma)^{59}Fe$	0.91	0.18	2.91	0.08	1.38	3.3	0.19	5.89	4.76
$^{46}Ti(n,p)^{46}Sc$	0.72	0.18	1.74	0.09	~0.0	1.23	0.11	4.19	2.35
*$^{45}Sc(n,\gamma)^{46}Sc$	0.36	0.13	2.31	0.09	~0.0	~0.0	—	4.19	2.35
$^{58}Ni(n,p)^{58}Co$	0.53	0.20	2.04	0.07	0.17	~0.0	0.20	4.13	2.24
$^{93}Nb(n,n')^{93m}Nb$	0.40	0.18	2.60	2.46	3.45	~0.0	0.31	6.13	5.05
*$^{181}Ta(n,\gamma)^{182}Ta$	0.37	0.20	2.84	0.02	0.92	~0.0	1.10	4.87	3.42

(*) DOE Dosimeter Set

(**) These values are estimated as a root of square sum of independent components of uncertainties, and contain the uncertainty due to the reactor power, which is 3.47 % at 75 MWt power level.

(***) These values are not included the uncertainty due to the reactor power.

Table 2 Influences of the Covariance Matrices in Dosimetry Analysis
(The effects of the covariance matrix of the guess spectra.)

Reaction	Measured value	Unfolding Results				Sensitivity			
		Variance only[1]		Convariance[2]					
		R_C^0/R_m	R_C/R_m	$\Delta(R_C^0/R_m)^*$	(R_C/R_m)	$\frac{\Delta \ln I_1}{\Delta \ln R_C}$	$\frac{\Delta \ln I_1}{\Delta \ln R_C^*}$	$\frac{\Delta \ln I_2}{\Delta \ln R_C}$	$\frac{\Delta \ln I_2}{\Delta \ln R_C^*}$
$^{55}Mn(n,\gamma)$	1.10+09(±5.8%)	0.802±13.0%	0.934± 8.5%	±23.6%	0.955± 8.2%	-0.043	0.015	0.466	0.315
$^{56}Fe(n,p)$	1.27+08(±6.1)	0.773±22.5	0.897± 9.9	±27.1	0.905± 9.9	-0.014	-0.0048	-0.0030	0.056
$^{27}Al(n,p)$	3.87+08(±8.4)	0.953±21.1	0.997±12.5	±27.0	1.032±12.3	-0.0023	0.014	0.0049	0.061
$^{24}Mg(n,p)$	1.51+08(±3.1)	0.786±27.2	0.959±12.4	±29.4	0.957±12.1	-0.0051	-0.0021	-0.0028	0.034
$^{23}Na(n,\gamma)$	7.85+07(±2.7)	0.928±12.4	1.063± 6.6	±23.1	1.092± 6.4	0.069	0.218	0.175	0.239
$^{115}In(n,n')$	1.99+10(±3.2)	0.914±17.2	0.949± 9.3	±24.9	0.973± 9.1	0.249	0.248	-0.032	0.096
$^{197}Au(n,\gamma)$	2.91+10(±3.2)	0.718±12.7	0.896± 7.3	±23.2	0.888± 6.4	0.643	0.487	-0.069	0.107
(X^2 prob.)		(1.6%)	(47%)	(41%)	(31%)				
Total Flux: I_1			2.06+11(±4.5%)		2.01+11(±4.2%)				
DPA : I_2			7.40+09(±15.4%)		8.12+09(±11.5%)				

1) Error covariance matrix of the guess spectra : Diagonal components only 30%

2) Error covariance matrix of the guess spectra : Diagnonal 30%, Off-diagonal 21%

R_C^0 is the reaction-rate value calculated by using the guess spectra.

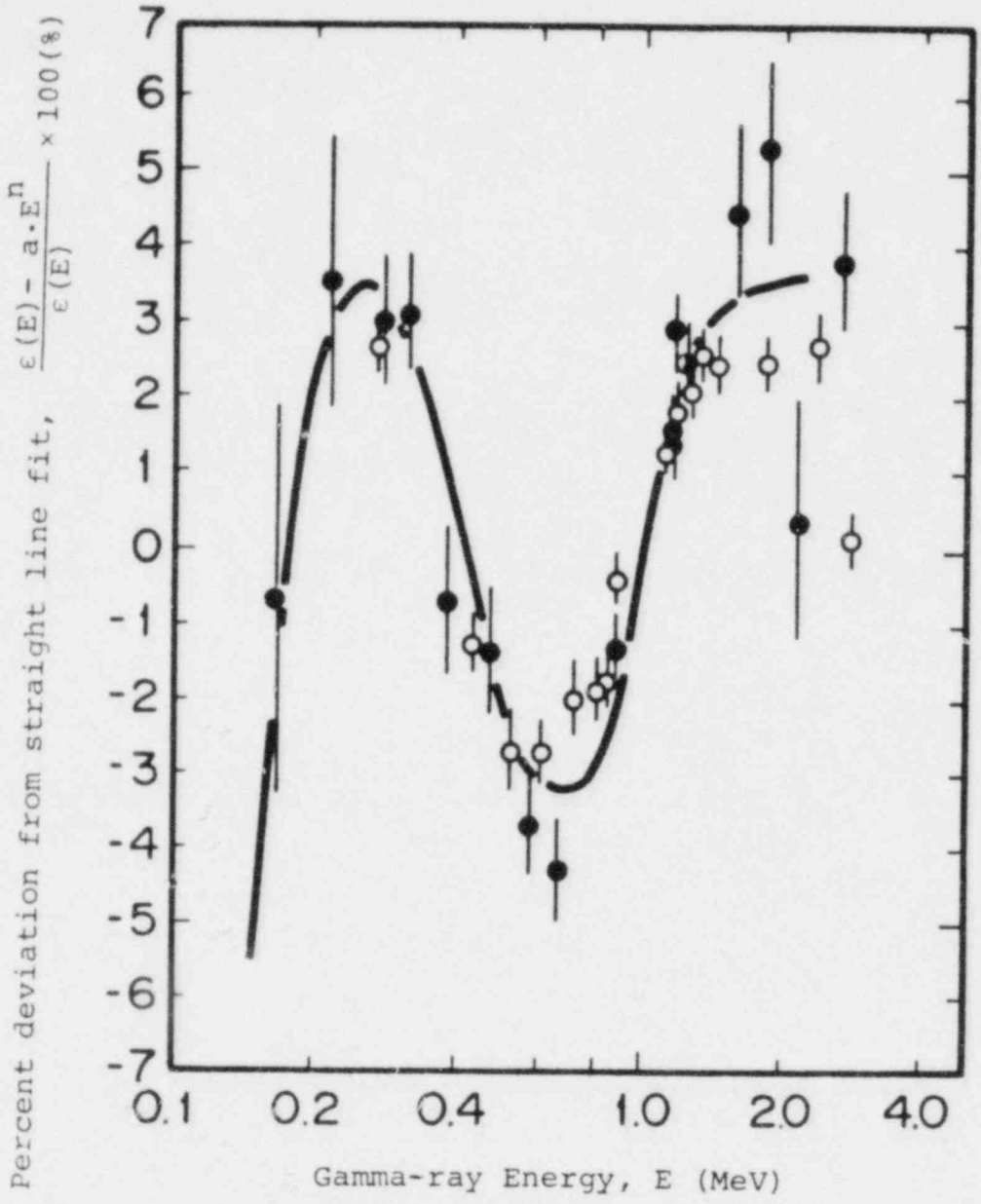

Fig. 1 Relative deviations of the γ-ray full peak efficiency of the 55 cc[4] and 57 cc[5] Ge(Li) detectors between measurements and simple fitting curves.

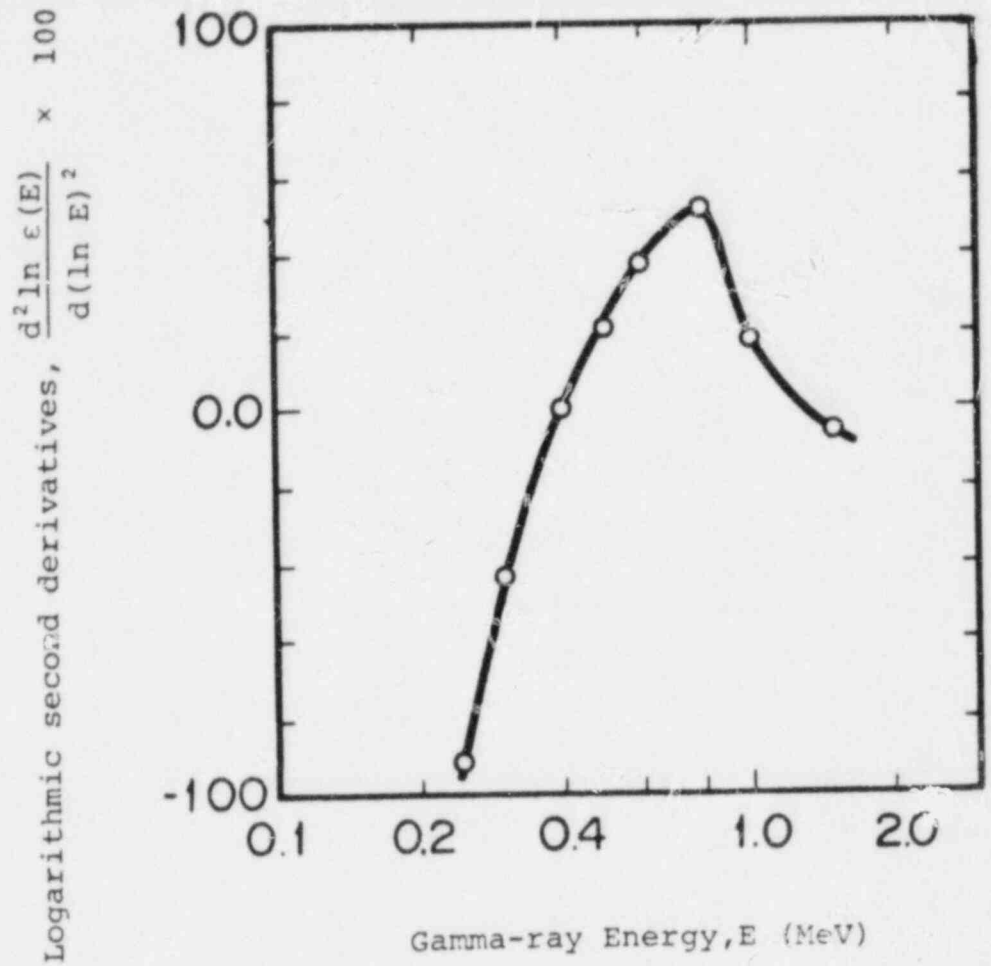

Fig. 2 Logarithmic second derivatives of the full energy peak efficiency $\varepsilon(E)$ of the 55 and 57 cc coaxial Ge(Li) detectors for uncertainty estimations of logarithmic linear interpolation techniques

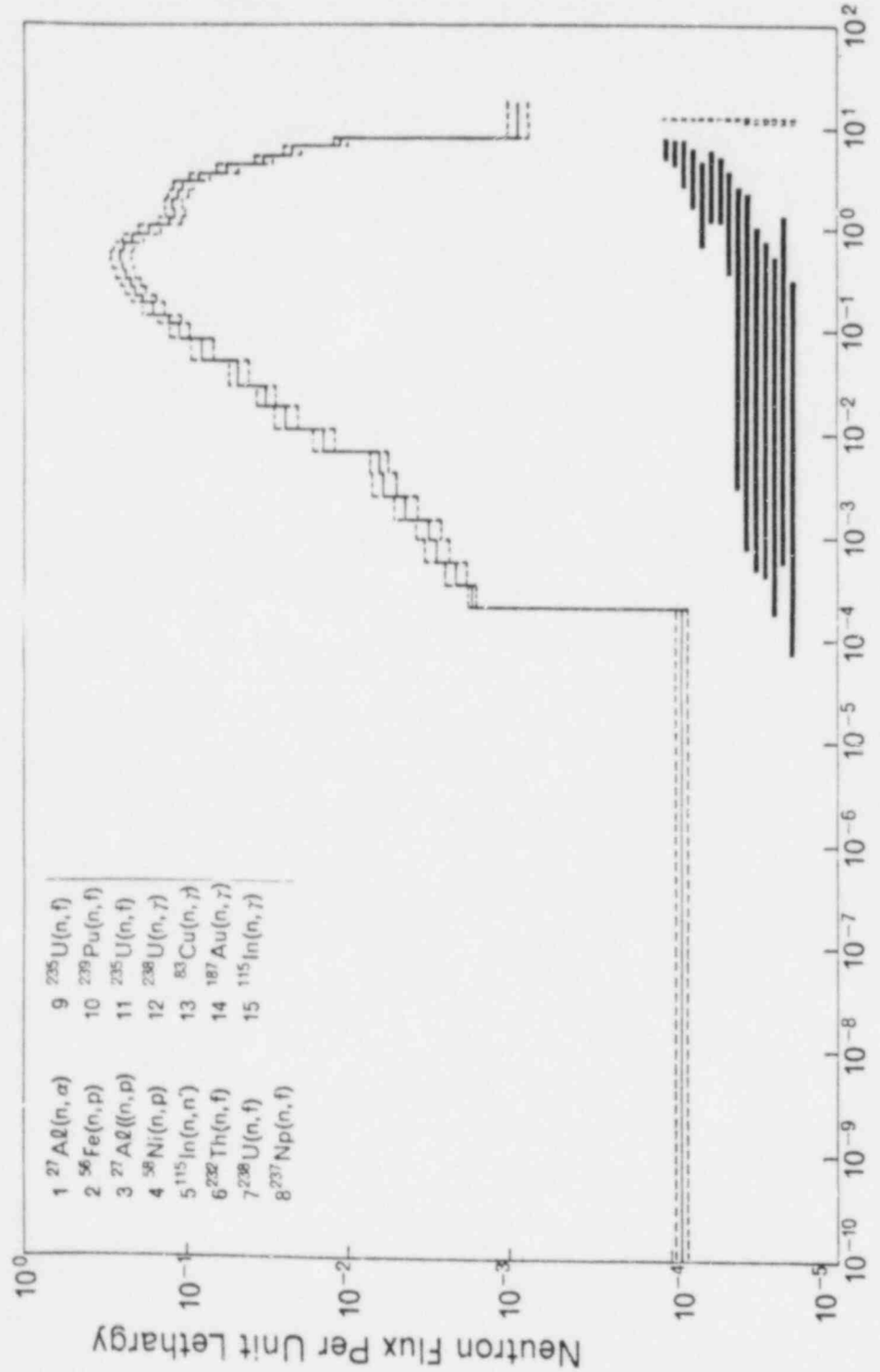

Fig. 3 Benchmark neutron spectrum of the ΣΣ-facility unfolded by the NEUPAC code

LSL - A LOGARITHMIC LEAST SQUARES ADJUSTMENT METHOD*

F. W. Stallmann

Mathematics Department
The University of Tennessee
Knoxville, Tennessee 37916

and

Oak Ridge National Laboratory
Oak Ridge, Tennessee 37830

ABSTRACT

To meet regulatory requirements, spectral unfolding codes must not only provide reliable estimates for spectral parameters, but must also be able to determine the uncertainties associated with these parameters. The newer codes, which are more appropriately called "adjustment codes," use the least squares principle to determine estimates and uncertainties. The principle is simple and straightforward, but there are several different mathematical models to describe the unfolding problem. In addition to a sound mathematical model, ease of use and range of options are important considerations in the construction of adjustment codes.

Based on these considerations, a least squares adjustment code for neutron spectrum unfolding has been constructed some time ago and tentatively named LSL. Its main features are:

- All adjustments and residuals are based on the logarithm of the physical quantities. Thus, variances and covariances are based on log-normal distributions and are given as relative uncertainties, as it is customary for these quantities. All adjusted quantities remain positive after adjustment.

- The input spectrum can be scaled freely to fit the dosimetry measurements. That is, only the shape, but not the magnitude of the input spectrum need to be calculated. This option can be defeated if normalization constants are known apriori.

- Either absolute reaction rates or equivalent fission fluxes can be used as input. The latter has smaller uncertainties and reduces the influence of cross section errors. Additional options are under consideration. The present version has been tested successfully in a variety of applications.

*Research sponsored by the Division of Reactor Safety Research, U.S. Nuclear Regulatory Commission under Interagency Agreement DOE-40-551-75 with the U.S. Department of Energy under contract W-7405-eng-26 with the Union Carbide Corporation.

INTRODUCTION

The philosophy of neutron spectrum unfolding methods has undergone a critical change during the last several years. In older methods the main objective was to find a spectrum which is consistent with neutron dosimetry measurements and is in some unspecified manner similar to a "trial spectrum." More recent procedures like STAY'SL[1] consider instead unfolding as a statistical least squares adjustment method. Such adjustment methods have been used successfully in many other scientific investigations and they are indispensible whenever uncertainties in form of variances and covariances for the processed data are needed. Such uncertainty estimates will be part of the regulatory requirements in the assessment of neutron irradiation damage in reactor pressure vessel and other reactor components. The older unfolding codes do not satisfy these requirements and must be replaced by the more recent adjustment procedures.

The mathematical theory of least squares adjustment is very well established[2] and it remains only to implement this theory in a manner which fits best the given task. Important considerations are the convenience in the preparation of input data and the options available for input and output parameters. The LSL code, which is the subject of this paper, has been constructed with these considerations in mind. Written about two years ago it has been proven to be a very convenient and reliable tool for the determination of damage exposure parameter values and their uncertainties.

COMPUTATIONAL PROCEDURES

At the center of any neutron spectrum adjustment method lies the formula

$$R_{\Phi i} = \int_0^\infty \Phi(E)\, \sigma_i(E) dE \quad , \quad i = 1, 2, \text{lll } k \quad . \qquad (1)$$

This formula describes the relation between the reaction rate (or reaction probability), $R_{\Phi i}$, for the i-th dosimetry reaction in the neutron field Φ, the reaction cross section $\sigma_i(E)$, and the fluence rate (or fluence) spectrum $\Phi(E)$ as a function of the neutron energy E. The terms in formula (1) represent the actual, but unknown, values. In any "real world" experiment only the measured values of the reaction rates and cross sections, $R_{\Phi i}^{meas}$ and σ_i^{meas}, and the calculated spectrum Φ^{calc} are known. The measured and calculated values are considered random variables with a joint normal probability distribution whose variance-covariance matrix is supposed to be known. It is further assumed that formula (1) describes the relation between the expected values of the corresponding random variables. These expected values are estimated by a maximum likelihood procedure, i.e. for

normal distributions a least squares procedure. The estimated values will be designated by $R_{\phi i}^{adj}$, and σ_i^{adj}, and ϕ^{adj} respectively. A detailed description of non-linear, least squares adjustment procedures can be found in Ref. 2. Only those features are discussed which are unique for spectrum adjustment and in particular for the LSL procedure.

The LSL procedure is a logarithmic adjustment procedure, which means that not the original values of formula (1) are adjusted but their logarithm. Another way of saying this is that the adjustment is multiplicative and not additive. Let v be any variable; its adjusted value is then represented by

$$v^{adj} = v\, e^{\delta} \tag{2}$$

where the logarithmic adjustment δ is calculated according to the formulas in Ref. 2. This assures that all adjusted values are strictly positive, which must be required for all variables in spectrum adjustment. The probability distribution is assumed to be log-normal and all variances and covariances must be given in relative terms (percentages). These assumptions are quite natural for the data used in spectrum adjustments. A disadvantage is that the least squares adjustment is strongly non-linear and iterations are needed to obtain consistent results.

The model equations for the least squares adjustment are set up in the following manner: let $R_{\phi i}^{calc}$ be the reaction rate obtained from formula (1) with the calculated spectrum. Since ϕ^{calc} is normally given for a finite number of energy groups we have

$$R_{\phi i}^{calc} = \sum_{j=1}^{n} \sigma_{ij} \phi_j^{calc}, \quad i = 1, 2, \ldots k \tag{3}$$

where σ_{ij} are the group averaged cross sections obtained from a suitable cross section file and ϕ_j^{calc} is the group fluence rate for the j-th energy group. The model equations are then representations of the difference between measured and calculated reaction rates. These are in the simplest case

$$\ln (R_{\phi i}^{meas} / R_{\phi i}^{calc}) = r_i, \quad i = 1, 2, \ldots k \tag{4}$$

That is, the residual r_i is the logarithm of the ratio between measured and calculated reaction rates.

The calculated spectrum may not be normalized to the same power level as present in the experiment, so that the ratio in formula (4) has not the expected value of one but some unknown constant. The formula (4) is replaced in this case by

$$\ln\left(R^{meas}_{\Phi i}/R^{calc}_{\Phi i}\right) - \ln\left(R^{meas}_{\Phi k}/R^{calc}_{\Phi k}\right) = r_i, \quad i = 1, 2, \ldots k-1 \qquad (5)$$

which eliminates the unknown scale factor. This factor can then be obtained as an additional parameter from the adjustment procedure.

The LSL procedure provides also for the case that the reaction rates are not measured directly but are referenced to a standard fission field. The standard field may be described in group fluence rates χ^{calc}_j. The measured reaction rate in this field may be denoted as $R^{meas}_{\chi i}$. The equivalent fission fluence rate is then defined as

$$F^{meas}_{\Phi i} = R^{meas}_{\Phi i}/R^{meas}_{\chi i} \qquad . \qquad (6)$$

The calculated equivalent fluence rate $F^{calc}_{\Phi i}$ is defined in the same manner with

$$R^{calc}_{\chi i} = \sum_{j=1}^{n} \sigma_{ij}\chi^{calc}_j \qquad . \qquad (7)$$

The model equations based on the equivalent fission fluence rate are then

$$\ln\left(F^{meas}_{\Phi i}/F^{calc}_{\Phi i}\right) = r_i, \quad i = 1, 2, \ldots k \qquad (8)$$

or the corresponding system as given in formula (5) if an unknown scale factor is involved.

As in all least squares adjustment methods variances and correlations are required for all input data. For auto-correlations, that is correlations between different energy groups for the same spectrum or cross section values a simplified scheme is used. To each energy group j a numerical value g_j is assigned so that the difference

$$D_{st} = |g_s - g_t| \qquad (9)$$

represents a measure for the distance between the two groups s and t. The auto-correlation for any parameter, say the fluence Φ, is then calculated as the exponential function of D_{st}

$$corr(\Phi_s, \Phi_t) = \exp(-cD_{st}) \qquad (10)$$

where c is an additional parameter which determines the strength of the auto-correlation. This assignment of auto-correlations reduces both storage requirements and computer time. It provides also a fairly good approximation to the cross section covariance data which are given in the ENDF/B-V cross section file. The results of the adjustment procedure don't seem to be very sensitive to changes in the auto-correlation values.

Since the adjustment is nonlinear, iterations are needed to obtain consistent results. The iteration method as described in Ref. 2 works briefly as follows: the adjustment δx for any variable x is calculated through the formula

$$\delta x = -V_{xr} V_r^{-1} \bar{r} \qquad (11)$$

where V_r is the variance-covariance matrix of the residuals r_i as defined in formulas (4), (5), or (8), $\bar{r}$ is the column vector of the residuals r_i and V_{xr} the row vector of convariances between the random variable x and the residuals r_i. The covariance matrices depend on the fluence and cross section values, which should be the adjusted values if formula (11) represents the minimum X^2 solution. Formula (11) is also a linearization which means that the adjustments in this formula do not necessarily reduce the residuals to zero even with the correct covariance matrices. Several steps are usually needed to obtain consistent output data. In each step adjustments are calculated with residuals obtained from adjusted values of the previous step but with fixed covariance matrices until the residuals are reduced to a predetermined small tolerance. The adjusted values are then used to calculate new covariance matrices and the iteration is repeated starting with the original (not adjusted) data. This leads to a new and possibly different set of adjusted data which are again inserted in the covariance matrices until convergence occurs. This process may not converge if the adjustments are too large. Examples of non-convergence have been observed but are rare.

The program has been written for use at the interactive DEC-10 system. Convergence criteria can be specified by given tolerances or can be set interactively by the user at execution time. At present up to 20 reactions and up to 50 energy groups can be handled. Any set of up to 20 integral parameters can be obtained from the adjusted data including variances and correlations.

CONCLUSIONS AND FUTURE PLANS

The LSL program has been tested in several application among them the PCA,[3] REAL-80[4] and the BSR-HSST metallurgical experiments.[5] It is simple, flexible and easy to use and is especially suited for numerical experiments.[6] Work is in progress to make this program available for public use. Additional programs for easy input data preparation will be included. Also planned are provisions for simultaneous adjustment of several correlated neutron spectra and for the extrapolation to spectra which are not acessible to dosimetry as done in Ref. 7.

REFERENCES

1. F. G. Perey, Least Squares Dosimetry Unfolding: The Program STAY'SL, ORNL/TM-6062 (1977).

2. F. W. Stallmann, Theory and Practice of General Adjustment and Model Fitting Procedures, ORNL/TM-7896 (1981).

3. M. N. McElroy, Ed., LWR Pressure Vessel Surveillance Dosimetry Improvement Program: PCA Blind Test, NUREG/CR-1861 (1981).

4. C. Ertek, et al, "Status Report on the REAL 80 Exercise." Proceedings of the Fourth ASTM-EURATOM Symposium on Reactor Dosimetry (1982).

5. F. B. K. Kam, "Characterization of the Fourth HSST Series of Neutron Spectral Metallurgical Irradiation Capsules," Proceedings of the Fourth ASTM-EURATOM Symposium on Reactor Dosimetry (1982).

6. F. W. Stallmann, "Uncertainties in the Estimation of Radiation Damage Parameters," Proceedings of the Fourth ASTM-EURATOM Symposium on Reactor Dosimetry (1982).

7. R. E. Maerker, et al, Development and Demonstration of an Advanced Methodology for LWR Dosimetry Applications, EPRI INP-2188 (1981).

FERRET ADJUSTMENT CODE - STATUS/USE

F. Schmittroth
Westinghouse Hanford Company
Richland, Washington, USA

ABSTRACT

The least-squares data analysis code FERRET is reviewed. Recent enhancements are discussed along with illustrative applications. Particular features noted include the use of differential as well as integral data and additional user options for assigning and storing covariance matrices.

INTRODUCTION

As the demand for accuracy in reactor data has increased, more emphasis has been placed on obtaining reliable and quantitative uncertainties for these data. Economics, safety, and the expense and difficulty of measuring many of the desired parameters encourage one to obtain the maximum benefit from each experiment. FERRET[1,2] is one of a number of least-squares computer codes recently developed that emphasize the rigorous evaluation of both the values and uncertainties of reactor data as well as other parameters (e.g., damage) derived from these data.

The following sections review the formalism upon which FERRET is based, highlight particular features of the code, and illustrate use of the code for a variety of problems.

FORMALISM

The FERRET code is a lognormal[1] least-squares code that minimizes the generalized sum of squared residuals:

$$S^2 = (\bar{f}-A\hat{x})^t M_f^{-1} (\bar{f}-A\hat{x}) + (\hat{z}-\bar{z}_o)^t M_z^{-1} (\hat{z}-\bar{z}_o) \ , \qquad (1)$$

where $\bar{f}$ is a vector of measurements (e.g., reaction rates) that are linearly related to a data vector $\bar{x}$ (e.g., multigroup fluxes):

$$\bar{f} = A\bar{x} \ . \qquad (2)$$

The first term in Equation (1) requires that the "best" estimate, $\bar{x}$, is chosen so that the measured values of $\bar{f}$ and the calculated values of $\bar{f}$ are close with respect to the data covariance matrix M_f for $\bar{f}$. The second term requires that the vector $\bar{x}$ be close to an a priori vector $\bar{x}_o$ in a lognormal sense:

$$\bar{z} = \ln(\bar{x}) \tag{3a}$$

and

$$\bar{z}_o = \ln(\bar{x}_o) \tag{3b}$$

The covariance matrix M_z is a fractional covariance matrix for $\bar{x}$ reflecting the use of a logarithmic development:

$$(M_z)_{ij} = (x_i x_j)^{-1}(M_x)_{ij} . \tag{4}$$

(See Reference (2) for additional details.)

The use of the lognormal distribution for $\bar{x}$ ensures that all components of $\bar{x}$ remain positive. Moreover, it circumvents the difficulty in assigning large a priori uncertainties (e.g., 50%) to physical values that are positive by nature where otherwise the use of symmetric normal uncertainties would imply that negative values are possible. The lognormal formalism introduces fractional or relative uncertainties in a natural and consistent way. FERRET retains the use of absolute uncertainties for the data vector $\bar{f}$ whose smaller uncertainties typically do not warrant the use of logarithmic distributions. (For convenience, however, they are entered as fractional uncertainties in the code).

The minimization of S^2 in Equation (1) is accomplished by linearization of Equation (1) with respect to $\bar{z} = \ln(\bar{x})$ and a iterative application of the usual[3,4] least-squares equations. The process yields a new fractional covariance matrix M_z as well as a "best" estimate $\bar{x}$.

Finally, the a priori logarithmic distributions provide a natural linearization of the non-linear bilinear form

$$R = \phi\sigma \tag{5}$$

where the reaction rate R is given as a product of a cross section and flux. (A sum over energy groups is implied for multigroup problems). Let z_ϕ and z_σ be the respective logarithms of ϕ and σ to find

$$R = e^{z_\phi} e^{z_\sigma} \tag{6}$$

$$R/R^* = e^{(z_\phi - z_\phi^*) + (z_\sigma - z_\sigma^*)} \tag{7}$$

or

$$\frac{R-R^*}{R^*} = (z_\phi - z_\phi^*) + (z_\sigma - z_\sigma^*) \ . \tag{8}$$

where * denotes a convenient expansion point. This form is useful in the simultaneous adjustment of fluxes and cross sections.

FEATURES

Covariance Input

A common criticism[5] of recent least-squares codes is that required input covariance matrices are difficult to obtain. FERRET relieves some of this burden by simple parametric forms related to intuitive concepts and by allowing a stepwise covariance construction that relates to individual sources of uncertainty.

Each covariance matrix is entered as a sum of components

$$M = \sum_k M^{(k)} \ , \tag{9}$$

where each component represents a source of uncertainty that is physically distinct (uncorrelated) from other sources. Each component $M^{(k)}$ can then be specified element by element $\{M_{ij}^{(k)}\}$ or in terms of fractional uncertainties $\{r_i\}$ and a correlation matrix $\{\rho_{ij}\}$:

$$M_{ij}^{(k)} = r_i \ r_j \ \rho_{ij} \ . \tag{10}$$

(Throughout this section all covariance matrices are assumed to be in fractional or relative form, not absolute).

In the absence of a detailed covariance matrix, Equation (10) may be replaced by

$$M_{ij}^{(k)} = c^2 + r_i \ r_j \ \rho_{ij}^{(s)} \tag{11}$$

where c (independent of i and j) is a fractional normalization uncertainty and the correlation matrix

$$\rho_{ij}^{(s)} = (1 - \theta) \ \delta_{ij} + \theta \ e^{-\frac{(\varepsilon_i - \varepsilon_j)^2}{2\gamma^2}} \tag{12}$$

consists of a purely random component δ_{ij} and a short-ranged correlated component with strength θ and range γ. The values $\{\varepsilon_i\}$ represent a simple monotonic function of i. Two simple examples are $\varepsilon_i = i$ and $\varepsilon_i =$ (multigroup energy E_i). The first relates the range of correlation to the index and the second to the energy.

Other recent code enhancements provide additional user options in entering covariance matrices in terms of explicit correlation matrices and uncertainties. Similar options are available for output.

Partitioning and Sequential Data

Two features of the code enable the user to exploit natural divisions in the data in order to enhance computational efficiency and to organize both input and output. The first is partitioning of the parameter vector $\overline{x}$ into a set of subvectors $\{\overline{x}_\sigma\}$, $[\overline{x} = (\overline{x}_1, \overline{x}_2, \overline{x}_3, \ldots)]$.

Equation (2) is replaced by

$$\overline{f} = \sum_\sigma A_\sigma \overline{x}_\sigma \ . \tag{13}$$

A very simple example is given by Equation (8) where the logarithmic flux vector z_ϕ represents one partition of the complete parameter vector and the logarithmic cross section vector z_σ represents a second partition. This partitioning is especially valuable in the simultaneous adjustment of multiple neutron spectra and cross sections. And it can lead to large savings in computer time when some or all a priori correlations between partitions can be neglected (between a flux and a cross section, for example).

In the event the data vector $\overline{f}$ consists of statistically independent subsets $\{\overline{f}_s\}$, $[\overline{f}_1, \overline{f}_2, \ldots)]$, FERRET allows them to be entered sequentially. This procedure can drastically reduce the size of matrices that must be inverted when the dimension of $\overline{f}$ is large. This feature is more an advantage when $\overline{f}$ consists of multiple sets of differential data[6] than for a spectrum unfolding problem where $\overline{f}$ represents a limited number of reaction rates. However, it is also useful when multigroup proton recoil measurements are included with integral reaction rate measurements in spectral adjustments.

Adjusted Libraries

A recent enhancement provides the capability to write an adjusted parameter vector (cross sections, e.g.) to mass storage. In this way cross sections benchmarked in well characterized neutron fields can be used in ensuing analyses. The library format can retain complete covariance information including cross correlations among different cross sections and spectra.

It is worthwhile to note here that it is valid to benchmark cross sections (i.e., adjust them) by measurements in poorly characterized fields. The only caveat is that the uncertainties for these poorly known fields must be large enough to fairly reflect the uncertainties. (Correlations must also be considered).

APPLICATIONS

In this section a few applications of FERRET are reviewed to illustrate its range of application and to expand some of the points discussed above.

Multigroup Spectra and Cross Section Adjustment

The analysis of data from the Pool Critical Assembly (PCA) mockup of an LWR pressure vessel (PV)[8] illustrates three particular features of FERRET beyond simple spectral unfolding. First, well characterized benchmark fields can be included in the analysis (see Table 1, ^{235}U fission spectrum measurements) to constrain the dosimetry cross sections and thereby yield a more accurate PCA spectrum, particularly for poorly known dosimeters. Or alternatively, as noted before, FERRET can create a benchmarked dosimetry cross section library that can be used in subsequent analyses. Whether or not this "benchmarking" yields significant increases in accuracy depends largely on the a priori accuracy of the cross section. Moreover, as is well known[4], improvements in the adjusted cross sections obtained from integral measurements often appear mainly in the covariance matrix. Consequently, these improvements may be apparent only when one calculates uncertainties of derived integral quantities such as dpa.

A second feature noted in Table 1 is the simultaneous adjustment of multiple spectra and cross sections.

Finally, Table 1 indicates the use of both differential and integral data. One does not need to revert to simple C/E comparisons for the differential data after making an adjustment based solely on integral measurements. In this example, a large normalization uncertainty (c in Equation (11)) was assumed for the differential measurements. This device assured that only the shape of the differential measurements (which were arbitrarily normalized in this analysis) was accounted for.

A typical adjusted spectrum and its uncertainty is shown in Figure 1 (other spectra and cross section adjustments are not shown here). Neither, of course, are covariance matrices that are written to a file for subsequent use in the calculation of integral uncertainties.

A preliminary analysis of integral reactions, and $^{10}B(n,He)$ in particular, in the Coupled Fast Reactivity Measurement Facility (CFRMF)[9] further illustrates use of FERRET. In this example, 21 measured reaction rates (including ^{10}B), were used to adjust the corresponding cross sections and the CFRMF spectrum (the measurements, the calculated spectrum, and its covariance matrix were received from R. A. Anderl, see acknowledgement). The a priori flux covariance matrix, which was in 26 energy groups, was expanded to 53 groups with a recently developed code. The corresponding correlation matrix is depicted in Figure 2.

Prior to adjustment, the calculated ^{10}B reaction rate was low by ~14% in this illustrative example. After adjustment the discrepancy was still 10% and well outside estimated uncertainties. To test the possibility that the explicit FORSS[10]-calculated covariance matrix for the CFRMF spectrum was too restrictive, another component of uncertainty was included using the parametric formats. It was assumed to contribute an additional 2% random and 5% normalization uncertainty and could be attributed to modeling errors. Even with this additional freedom in the neutron spectrum, the ^{10}B reaction rate discrepancy was still 9%. It appears unlikely that the difficulty arises from an improper flux. A more likely possibility is a low ^{10}B cross section above 100 keV. However, to obtain a consistent evaluation, present ENDF/B-V uncertainties for $^{10}B(n,He)$ must be markedly increased.

Pointwise Adjustments

FERRET has also been used to make pointwise adjustments of continuous curves. The method[6] is based on a finite element representation using triangle or "roof" functions as depicted in Figure 3. The method has been discussed in detail elsewhere[6], and a single example is briefly reviewed here to illustrate the advantages of least-squares algorithms.

Let the beta and gamma decay heat at time t following an instantaneous fission pulse be given by $f_\beta(t)$ and $f_\gamma(t)$ respectively. One can easily show that the decay heat for a finite irradiation of time T is then given by

$$F_\alpha(t, T) = \int_t^{t+T} f_\alpha(t')dt' \quad (\alpha = \beta,\gamma) \ . \tag{14}$$

Then, with the representation (see Figure 3)

$$f_\alpha(t) = \sum_{i=1}^{N} x_{i\alpha} \Delta_i(t) \qquad (\alpha = \beta,\gamma) \ , \tag{15}$$

Equation (14) becomes

$$F_\alpha(t, T) = \sum_{i=1}^{N} A_i \, x_{i\alpha} \ , \tag{16}$$

where

$$A_i = \int_t^{t+T} \Delta_i(t') \, dt' \tag{17}$$

is an integral over the roof function $\Delta_i(t)$.

A major advantage of this approach is that experimental values for $F_\alpha(t,T)$ for different irradiation periods T can be combined in a single consistent decay heat evaluation.

Furthermore, measurements of the total decay heat, $F(t,T) = F_\beta(t,T) + F_\gamma(t,T)$ can be easily included in an evaluation of the β and γ components since $F(t,T)$ is a linear function of the parameters $\{x_{\beta i}\}$ and $\{x_{\gamma i}\}$ that represent the beta and gamma decay heat functions for a fission pulse.

The same technique provides an effective method to use total cross section measurements in the evaluation of the corresponding partial cross sections.

Other Applications

A different problem, although formally very similar, is illustrated by a recent evaluation of fission product yields and gamma branching ratios measured in the Fast Flux Test Facility (FFTF).

Gamma counting rates of irradiated fissionable isotopes are given by

$$C_{fiks} = \eta\, Y_{fi}\, B_{ik}\, S_s \qquad (18)$$

where Y_{fi} denotes the yield of the i-th fission product for the fissionable nuclide f, and B_{ik} is the k-th gamma branching ratio. The factor S_s allows for self-shielding in sample s while η represents all other factors such as counting efficiency.

In this analysis, the measured counting rates C_{fiks} were used to simultaneously evaluate (adjust) not only the yields and gamma branching ratios but the sample self-shielding factors as well. The success of this approach depends upon the inclusion of multiple fissionable nuclides, fission product nuclides, and gamma branching intensities. Here, isotopes of Pu, U, and Np were all included. The need for a priori values allows the inclusion of prior measurements in the analysis. A comprehensive treatment as described here can take full advantage of highly redundant data to obtain optimum values and to spot outliers. E.g., a well known ^{235}U yield may imply a revised branching ratio which in turn impacts a particular Np yield.

Formally the adjustment of a product of three variables as in Equation (18) is no different than for the bilinear form in Equation (5). Equation (18) is linearized just as in Equation (8) for two variables.

Clearly, the least-squares data adjustment method is applicable to diverse problems. FERRET is designed to address this diversity with a single code so that enhancements for one application can be generally useful. One example is that the FERRET library routines designed for adjusted cross sections can store adjusted gamma branching ratios for future yield measurements.

ACKNOWLEDGEMENT

The assistance of R. A. Anderl in providing CFRMF reaction rates, calculated spectra and a flux covariance matrix is gratefully acknowledged.

REFERENCES

1. F. Schmittroth, "FERRET Data Analysis Code," HEDL-TME 79-40, Hanford Engineering Development Laboratory, Richland, WA (September 1979).

2. F. Schmittroth, Nucl. Sci. Eng., 72, 19-34 (1979).

3. J. B. Dragt, et al., Nucl. Sci. Eng., 62, 119 (1977).

4. F. G. Perey, "Contributions to Few-Channel Spectrum Unfolding," ONRL/TM-6267, Oak Ridge National Laboratory, Oak Ridge, TN (1978).

5. D. L. Smith, "Neutron Dosimetry for Radiation Damage in Fission and Fusion Reactors," Proc. International Conference on Nuclear Cross Sections for Technology, Ed. by J. L. Fowler et al., Knoxville, TN (October 22-26, 1979).

6. F. Schmittroth and R. E. Schenter, Nucl. Sci. Eng., 74, 168-177 (1980).

7. G. K. Schenter and F. Schmittroth, "Beta and Gamma Decay Heat Evaluation for the Thermal Fission of ^{235}U," Proc. International Conference on Nuclear Cross Sections for Technology, Ed. by J. L. Fowler et al., Knoxville, TN (October 22-26, 1979).

8. E. P. Lippincott, et al., "Consistency of Experimental Data and Derived Exposure Parameters Based on Least-Squares Analysis," in LWR Pressure Vessel Surveillance Dosimetry Improvement Program: PCA Experiments and Blind Test, Ed. by W. N. McElroy, NUREG/CR-1861 (July 1981).

9. J. W. Rogers, D. A. Millsap and Y. D. Harkn, "The Coupled Fast Reactivity Measurement Facility," IAEA Consultants Meeting on Integral Cross Section Measurements in Standard Neutron Fields for Reactor Dsoimetry, Vienna, Austria (November 15-19, 1976).

10. C. R. Weisbin, et al., "Application of FORSS Sensitivity and Unicertainty Methodology to Fast Reactor Benchmark Analysis," ORNL/TM-5563, Oak Ridge National Laboratory, Oak Ridge, TN (December 1976).

TABLE 1

Summary of Data Used in a FERRET Analysis of the PCA-PV (LWR Pressure Vessel Mockup)

A priori Values (Multigroup, 53 groups)
1. Transport calculated spectra (3 locations)
2. ENDF/B-V dosimeter cross sections
Integral Data
1. Dosimeter reaction rates
2. ^{235}U fission spectrum measurements
3. Emulsion measurements
Differential Data (Multigroup)
1. Proton-recoil measurements
2. ^{6}Li measurements
3. Emulsion measurements

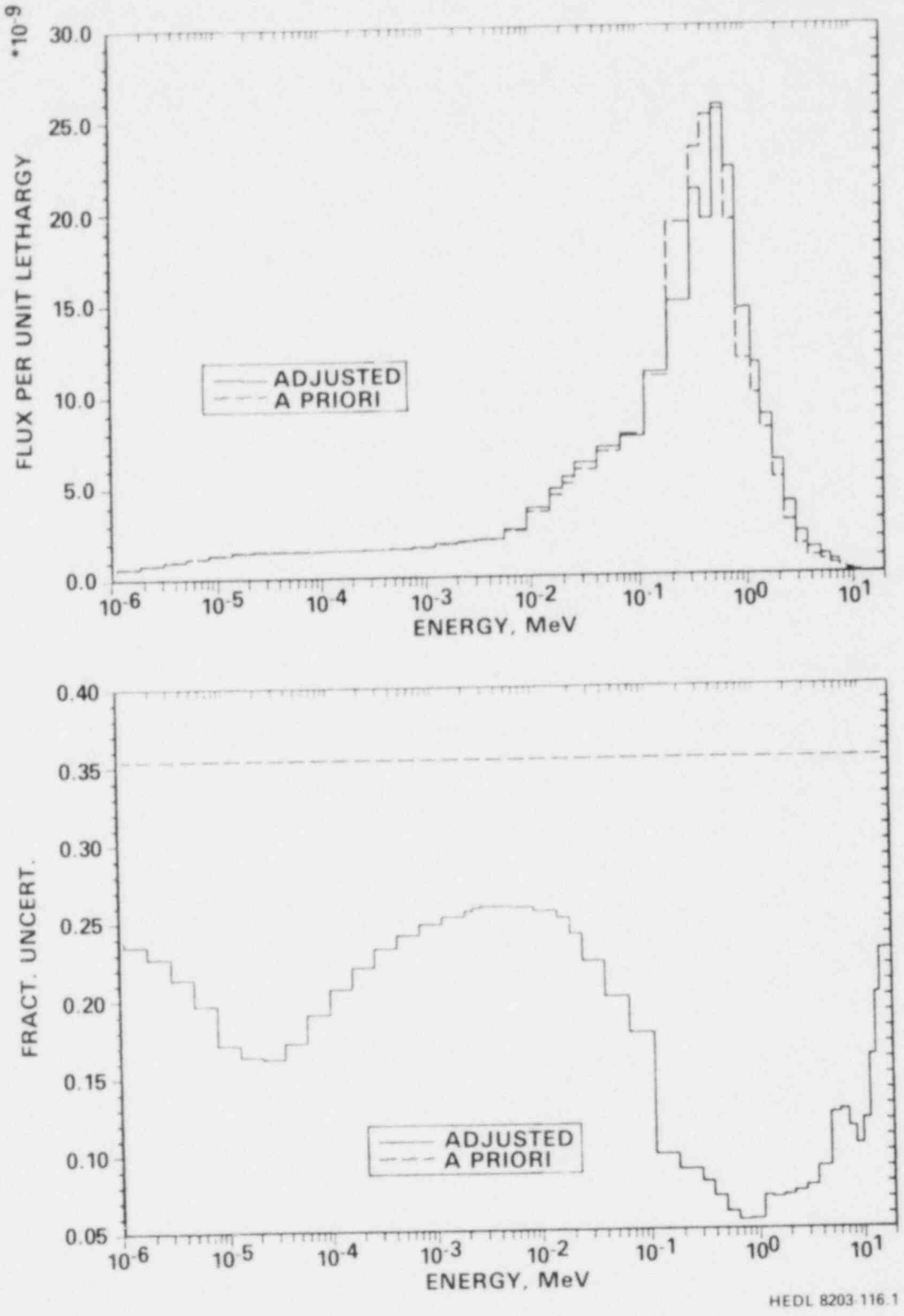

Figure 1. Adjusted and A Priori Flux and Uncertainty for PCA 12/13 Configuration at 3/4 T Position.

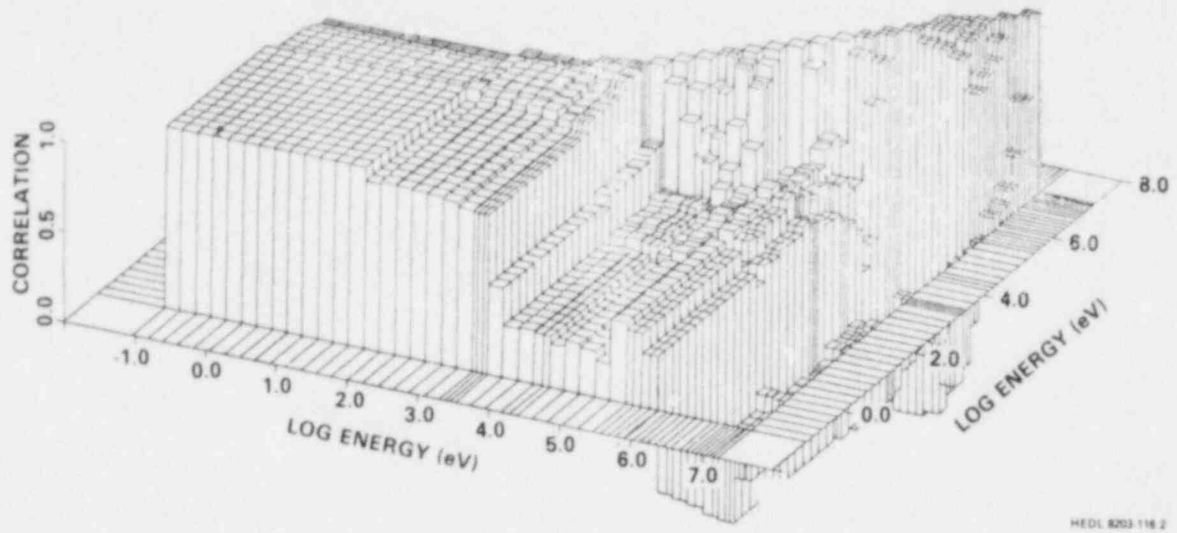

Figure 2. CFRMF Spectrum Correlation Matrix in 53 Groups.

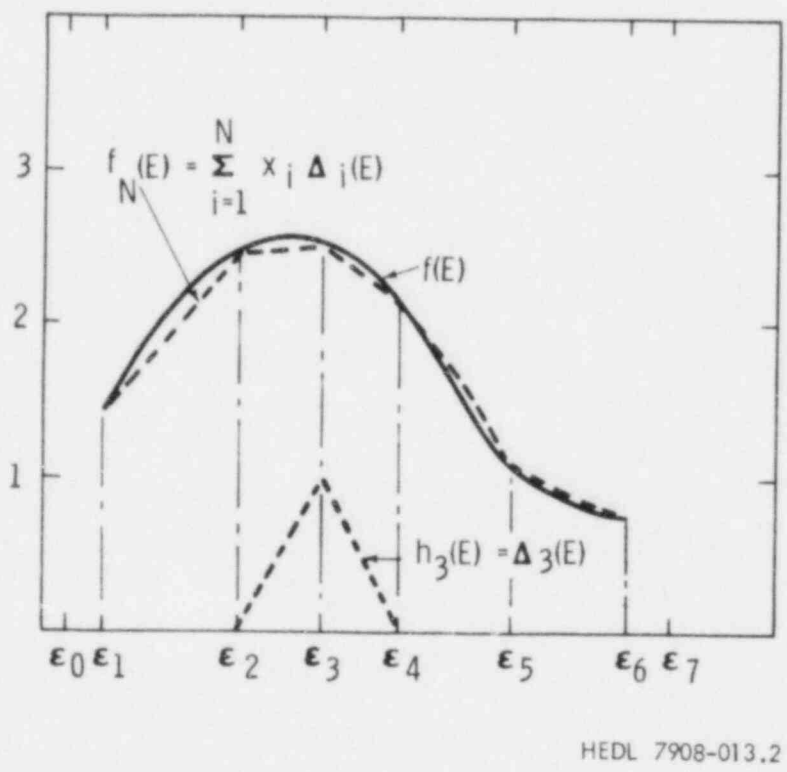

Figure 3. Representation of a Continuous Functi n f(E) by a Finite Element Basis of Triangle Functions.

EXPERIENCES WITH NEUTRON SPECTRUM UNFOLDING CODES IN DIFFERENT NEUTRON SPECTRA

É.M. Zsolnay and E.J. Szondi
Budapest Technical University, Training Nuclear Reactor,
H-1521 Budapest, Hungary

ABSTRACT

Results obtained with two different neutron spectrum unfolding codes (SANDBP[3] and RFSP-JÜL[4]) in the frame of the REAL-80 exercise are presented and discussed.

INTRODUCTION

Two special computer codes and their different versions (SAND-II[1], SANDPET[2], SANDBP[3], and RFSP-JÜL[4]) are used for neutron spectrum unfolding from foil activation data at the Training Nuclear Reactor of the Budapest Technical University. The computer codes SAND-II, SANDPET, and RFSP-JÜL are used in the form as they are known from the literature. The program SANDBP is a modified version of the code SAND-II, and it can take the uncertainties of reaction rates and cross-section values into consideration as weighting factors in the adjustment procedure. Also an uncertainty analysis can be performed with aid of this program.

In the paper results obtained with two of these neutron spectrum unfolding codes (SANDBP and RFSP-JÜL) for different (thermal and fast reactor) neutron spectra are presented and discussed. The calculations refer to the neutron spectra of the "REAL-80" exercise[5].

The investigations comprise the use of different energy group structures (100 and 620 groups) and cross-section files (ENDF/B-V and DOSCROS77[6]) in case of the same adjustment code. Their influence on the results is shown. Finally, a Monte Carlo error analysis is carried out to examine the quality of the solution spectra.

INPUT DATA

Input informations for two different neutron spectra: Oak Ridge Research Reactor (ORR) and YAYOI reactor (Tokyo) were distributed on magnetic tape in frame of the REAL-80 exercise[5].

Input neutron spectrum

The ORR neutron spectrum is a typical thermal reactor spectrum, while YAYOI is a fast reactor and the spectrum for its central region was given[5]. Both input spectra were available in 100-groups structure as calculated by transport theory codes[5,7]. In some cases this information was converted into a 620 groups spectrum using the special interpolation and extrapolation procedure of the program SAND.

Reaction rates

The input data sets contained 19 reaction rates for the ORR spectrum (7 reaction rates with and 12 ones without cadmium cover) and 12 reaction rates for the YAYOI reactor spectrum together with their uncertainties. The variances are given in table 2.

Cross-section library

Two different cross-section libraries were used in the calculations.

The ENDF/B-V reactor dosimetry file was available in 100 and 620 energy groups structure, completed with an uncertainty library[5]. In case of the ORR spectrum corrections for selfshielding and cadmium cover were given in 100 energy groups. This information was not available in 620 groups.

The DOSCROS77 reactor dosimetry file contains the cross-section data in 620 groups. This cross-section library was combined with an error library described by McElroy et al.[8]. The cross-section for the reaction W186(N,G) was taken from the ENDF/B-V dosimetry file in 620 groups.

RESULTS

The neutron spectra were unfolded under the conditions shown by table 1. The reactions TI47(N,P) for the YAYOI spectrum and FE58(N,G) in case of ORR were deleted from the analysis, showing incompatibility with respect to the other detectors. As a result, 18 and 11 reactions were used in the adjustment procedure for the ORR and YAYOI spectra, respectively.

The program SANDBP is able to take into account the uncertainties of the cross-sections and reaction rates in its adjustment procedure. However, no weighting with the uncertainties of reaction rates was possible in case of unfolding the ORR spectrum, as the uncertainty values for all the reaction rates were given to be equal (5%).

The ORR and YAYOI solution neutron spectra obtained under different conditions with the two adjustment codes are shown by figures 1 and 3.

Some characteristic integral data (together with their uncertainties), calculated with aid of these spectra, are presented in tables 1 and 2.

The convergence criterion of the solution was defined as:

$$DEV^S = \sqrt{\frac{\sum_{i=1}^{n} \left(\frac{(A_i^m - A_i^c)/A_i^m}{s_i^m} \right)^2}{n-1}} ,$$

where A_i^m = measured reaction rate;

s_i^m = uncertainty of measured reaction rate;

A_i^c = calculated reaction rate;

n = number of reaction rates involved in the adjustment procedure.

In case of the SANDBP code the standard deviation of the unfolded neutron spectra is also calculated with aid of a Monte Carlo procedure and plotted on the relevant figures. The ratio of the different solution spectra to the input spectrum is given in figures 2 and 4, furthermore the ratio of the different solutions is also presented (figure 5).
A local peak at 1 MeV appears in the YAYOI solution spectrum if weighting with the cross-section uncertainties is used in the adjustment procedure of the program SANDBP, using the ENDF/B-V cross-section library (fig.6)[10]. Detailed analysis of this effect showed that this anomaly is caused by a "jump" present in the cross-section uncertainty values of the reaction AU197G at 1 MeV. The given uncertainty value just below 1 MeV seems to be too small.
The perspective plots of the correlation matrices for the 100 groups SANDBP solution spectra show very strong correlations between the different neutron energy groups (see figure 7).

DISCUSSION

1. The solution neutron spectra supplied by the two adjustment codes show some differences (figs. 1, 3 and 5). The modification of input spectrum in case of the program RFSP-JÜL shows an overall smooth character for both the ORR and YAYOI spectra. In case of the SANDBP code much more structure (characteristic to the SAND-type codes) is present (see figs. 2 and 4).

2. The integral data derived from the SANDBP solution spectra (and calculated with aid of the ENDF/B-V cross-section data where it was necessary) show a rather good agreement for both the ORR and YAYOI spectra, independently on the cross-section library (ENDF/B-V or DOSCROS77) and energy group structure (100 or 620 groups) applied in the adjustment procedure (table 1). The RFSP-JÜL code results show in most cases somewhat lower values than the corresponding SANDBP data.

3. Differences in the speed of convergence were found in case of the YAYOI spectrum using the adjustment code SANDBP in different (100 and 620) energy group structures (see table 1). It seems the influence of the energy group structure is much stronger in this respect than that one of the cross-section library used (table 1).

4. For all the YAYOI solutions large deviations were met in the values of measured and calculated reaction rates of MN55, W186, and AU197 detectors (see table 2).

5. Discrepancies were detected in some cases using the ENDF/B-V cross-section library:
   . the cross-section structure of the reaction NA23G was always reflected in the YAYOI solution spectra (fig. 3);
   . the reactions TI47P (for YAYOI) and FE58G (for ORR) show incompatibility with respect to the other detectors.
   These effects - in combination with the relevant adjustment conditions - indicated some incorrectness in the cross-section values of these reactions[9]. This conclusion meets the findings - derived by other methods - of another laboratory[10].

6. Incorrectness in the cross-section uncertainty values of the reaction AU197G was found in the vicinity of 1 MeV. As practically two detector sets with separate response regions (one of them below 1 MeV, the other one above 1 MeV) are acting in the adjustment procedure of the YAYOI spectrum, the effect of the incorrect uncertainty value in this energy region will be emphasized. In the cross-section uncertainty library described by McElroy et al. the corresponding variances for the AU197 cross-section show a smooth character in the energy region in question. Consequently, using these data the effect observed in case of the ENDF/B-V library will not be present.

7. From the results discussed above one can conclude that the neutron spectrum adjustment codes are suitable for investigating the quality of the nuclear data applied in the adjustment procedure.

ACKNOWLEDGEMENTS

Thanks are due to Ms. E. Sipos for her assistance in the calculations.

REFERENCES

1. W.N. McElroy et al., SAND. A computer automated iterative method for neutron flux spectra determination by foil activation, AFWL-TR-67-41, Vol. I-II (September 1967).

2. W.L. Zijp and H.J. Nolthenius, Experience with neutron spectrum unfolding codes, ECN-105 (Petten, November 1981).

3. E.J. Szondi and É.M. Zsolnay, SANDBP. An iterative neutron spectrum unfolding code, BME-TR-RES-2/81 (Budapest, March 1981).

4. A. Fischer, The Petten version of the RFSP-JÜL program, Private communication (Petten, April 2nd, 1976).

5. D.E. Cullen, Summary of ORR and YAYOI data for the REAL-80 project, IAEA-NDS-33 (distributed 6 February 1981).

6. W.L. Zijp et al., Cross-section library DOSCROS77 (in the SAND-II format), ECN-25 (Petten, August 1977).

7. W.L. Zijp, C. Ertek, É.M. Zsolnay, E.J. Szondi, H.J. Nolthenius, and D.E. Cullen, First results of the REAL-80 exercise, IAEA/RL/86, BME-TR-RES-5/81, ECN-106 (September 1981).

8. W.N. McElroy and L.S. Kellogg, Fuels and materials fast-reactor dosimetry data development and testing, Nucl. Techn. 25 (1975), p. 180 (February 1975).

9. É.M. Zsolnay, Contribution to the IAEA Advisory Group Meeting on Nuclear Data for Radiation Damage Assessment and Related Safety Aspects (Vienna, 12-16 October 1981).

10. W.L. Zijp et al., Comparison of two fine group cross-section libraries resulting from the ENDF/B-V dosimetry file, ECN-97 (August 1981).

Table 1. Unfolding parameters and integral data obtained from the solution neutron spectra.

	unfolding code	cross-section file	no. of energy groups	no. of detectors	no. of iterations	DEV^s	integral parameters				
							ϕ_{total}	ϕ > 1 MeV	ϕ>0,1 MeV	reaction rate for Ni58P	dpa (ASTM)
							(in $m^{-2} . s^{-1}$)				
ORR	SANDBP	ENDF/B-V	100	18	5	0,97	$1,93\times10^{17}$	$4,06\times10^{16}$	$8,24\times10^{16}$	$5,30\times10^{-13}$	$5,67\times10^{-9}$
							*sd 3,61	sd 5,35	sd 3,86	sd 2,72	sd 3,56
	RFSP-JÜL	ENDF/B-V	100	18	2	1,35	$1,94\times10^{17}$	$3,83\times10^{16}$	$8,15\times10^{16}$	$5,11\times10^{-13}$	$5,46\times10^{-9}$
YAYOI	SANDBP	ENDF/B-V	100	11	2	1,75	$2,07\times10^{15}$	$9,08\times10^{14}$	$1,98\times10^{15}$	$1,06\times10^{-14}$	$1,26\times10^{-10}$
	SANDBP	ENDF/B-V	100	11	4	1,61	$2,08\times10^{15}$	$9,00\times10^{14}$	$1,98\times10^{15}$	$1,05\times10^{-14}$	$1,25\times10^{-10}$
							*sd 1,95	sd 3,01	sd 1,95	sd 4,03	sd 2,42
	RFSP-JÜL	ENDF/B-V	100	11	4	2,81	$1,94\times10^{15}$	$8,78\times10^{14}$	$1,86\times10^{15}$	$1,04\times10^{-14}$	$1,20\times10^{-10}$
	SANDBP	ENDF/B-V	620	11	2	3,09	$1,98\times10^{15}$	$9,04\times10^{14}$	$1,91\times10^{15}$	$1,06\times10^{-14}$	$1,21\times10^{-10}$
							*sd 2,76	sd 3,78	sd 3,14	sd 3,61	sd 3,01
	SANDBP	ENDF/B-V	620	11	4	2,96	$1,99\times10^{15}$	$9,12\times10^{14}$	$1,93\times10^{15}$	$1,06\times10^{-14}$	$1,25\times10^{-10}$
	SANDBP	DOSCROS77	620	11	2	2,89	$1,96\times10^{15}$	$9,09\times10^{14}$	$1,88\times10^{15}$	$1,05\times10^{-14}$	$1,23\times10^{-10}$
							*sd 2,38	sd 3,89	sd 2,80	sd 3,93	sd 2,52
	SANDBP	DOSCROS77	620	11	4	2,79	$1,98\times10^{15}$	$9,11\times10^{14}$	$1,91\times10^{15}$	$1,05\times10^{-14}$	$1,24\times10^{-10}$

*standard deviation (sd) is given in per cent.

Table 2. Input data and relative deviation of measured from calculated reaction rates for different solution spectra.

ORR spectrum:

reaction	input data		D*	
	measured reaction rates	uncertainties (in %)	100 groups ENDF/B-V SANDBP	100 groups R. Dos.file RFSP-JÜL
AU197(N,G)	$9,54\times10^{-10}$	5	0,06	0,48
AU197(N,G)+Cd	$5,11\times10^{-10}$	5	-0,19	-0,12
AU197(N,2N)	$1,60\times10^{-14}$	5	0,10	1,15
SC45 (N,G)	$1,14\times10^{-10}$	5	-1,07	-0,33
SC45 (N,G)+Cd	$6,29\times10^{-12}$	5	1,05	0,43
U238 (N,G)	$5,50\times10^{-11}$	5	-0,99	-1,86
U238 (N,G)+Cd	$4,40\times10^{-11}$	5	-0,26	-1,58
U238 (N,F)	$1,70\times10^{-12}$	5	-0,05	1,33
U235 (N,F)	$1,98\times10^{-9}$	5	-0,04	0,66
U235 (N,F)+Cd	$1,43\times10^{-10}$	5	-0,03	-0,97
NP237(N,F)+Cd	$3,54\times10^{-12}$	5	-0,14	0,83
CO59 (N,G)	$1,94\times10^{-10}$	5	-0,48	0,19
CO59 (N,G)+Cd	$3,67\times10^{-11}$	5	2,11	1,80
FE58 (N,G)	$5,95\times10^{-12}$	5	1,72	2,56
FE58 (N,G)+Cd	$6,47\times10^{-13}$	5	deleted	deleted
FE54 (N,P)	$4,01\times10^{-13}$	5	0,01	0,64
TI46 (N,P)	$5,02\times10^{-14}$	5	-0,16	-0,64
TI48 (N,P)	$1,34\times10^{-15}$	5	0,50	-0,14
NI60 (N,P)	$1,05\times10^{-14}$	5	-2,14	3,00

YAYOI spectrum:

reaction	input data		D*			
	measured reaction rates	uncertainties (in %)	100 groups ENDF/B-V R.Dos.file SANDBP	100 groups ENDF/B-V R.Dos.file RFSP-JÜL	620 groups ENDF/B-V R.Dos.file SANDBP	620 groups DOSCROS77 Dos.file (2 iter)
AU197(N,G)	$2,82\times10^{-14}$	3,8	2,39	5,90	4,75	4,15
TI48 (N,P)	$2,57\times10^{-17}$	3,8	-1,60	-1,56	-2,09	-1,49
CO59 (N,A)	$1,47\times10^{-17}$	2,4	0,83	1,02	-0,24	-0,46
MN55 (N,G)	$8,48\times10^{-16}$	2,8	-1,74	2,34	-6,65	-6,32
FE56 (N,P)	$1,00\times10^{-16}$	2,8	1,76	1,42	1,26	0,16
AL27 (N,P)	$3,87\times10^{-16}$	8,4	0,02	0,05	0,19	-0,03
AL27 (N,A)	$6,74\times10^{-17}$	2,9	-1,45	-0,83	-2,22	-1,95
MG27 (N,P)	$1,47\times10^{-16}$	3,1	-0,74	-0,21	-1,15	-0,88
NA23 (N,G)	$7,85\times10^{-17}$	4,1	-1,85	-0,69	0,09	-0,46
TI47 (N,P)	$1,68\times10^{-15}$	11,5	deleted	deleted	deleted	deleted
IN115(N,N')	$2,12\times10^{-14}$	3,9	-0,44	0,66	-0,74	-0,62
W 186(N,G)	$1,16\times10^{-14}$	4,9	2,16	4,86	4,01	4,34

$$^{*}D = \frac{(A_i^m - A_i^c) / A_i^m}{s_i^m}$$

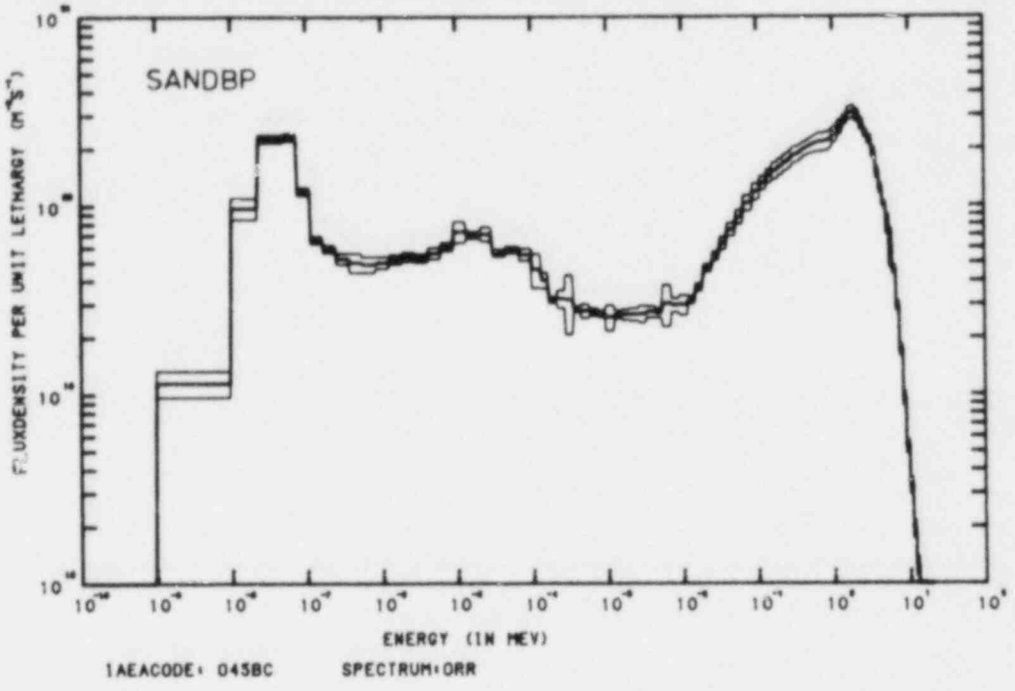

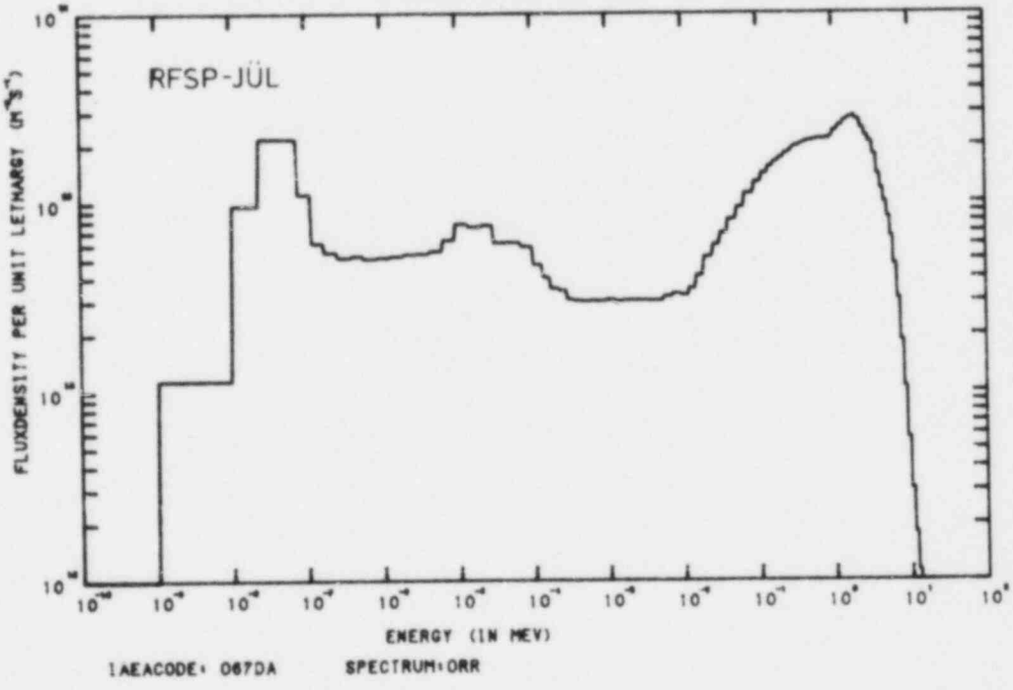

Figure 1. ORR SOLUTION SPECTRA IN 100 GROUPS.

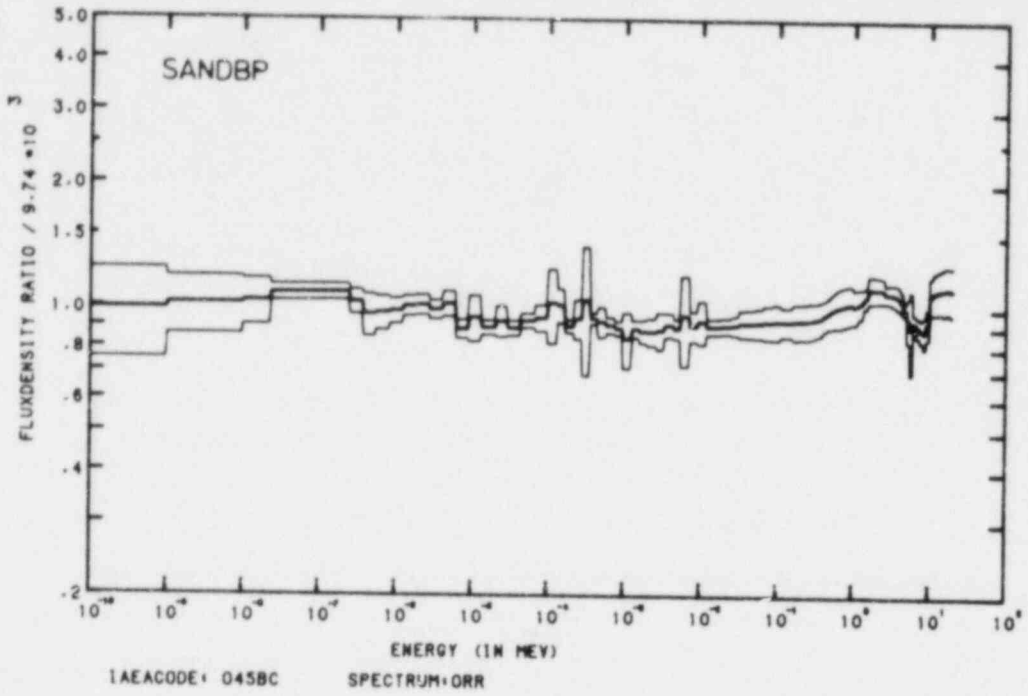

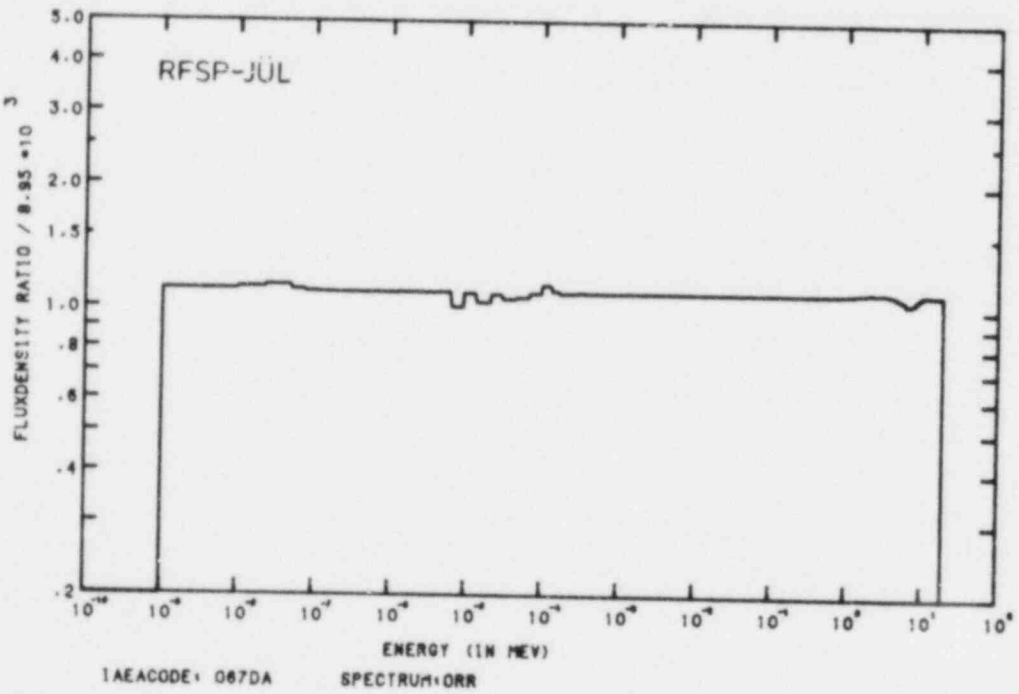

Figure 2. MODIFICATION FOR ORR (100 GROUPS).

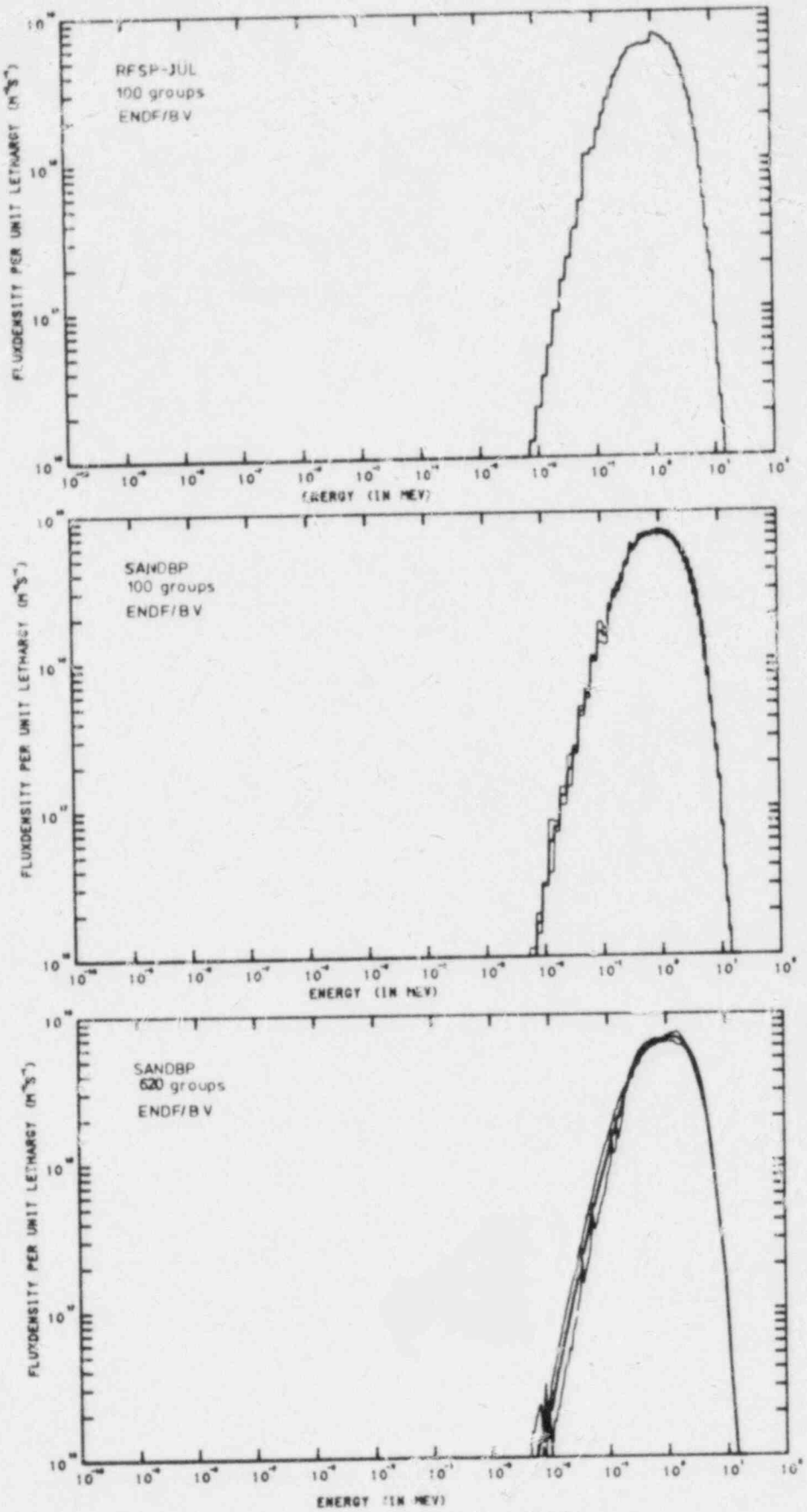

Figure 3. YAYOI SOLUTION SPECTRA.

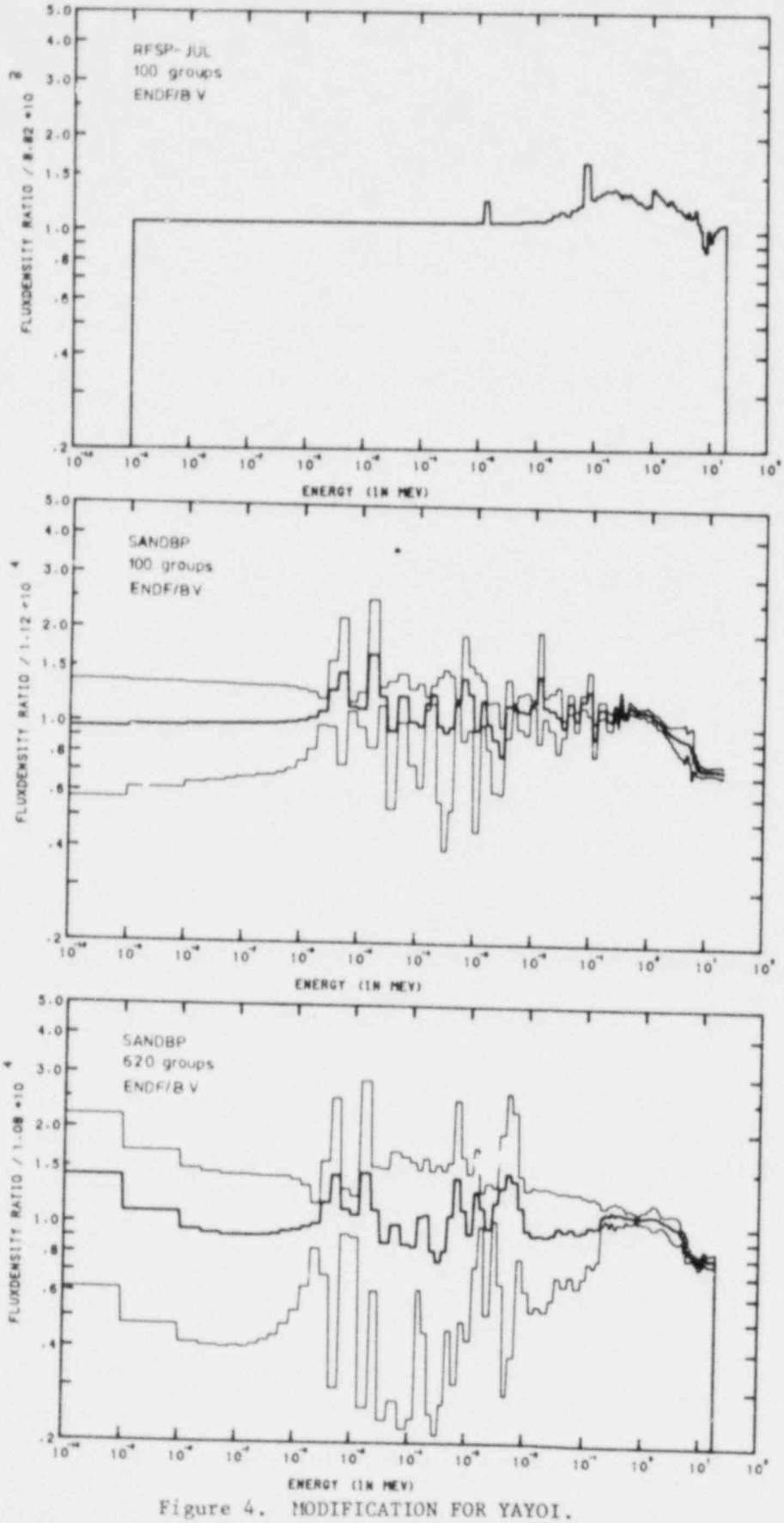

Figure 4. MODIFICATION FOR YAYOI.

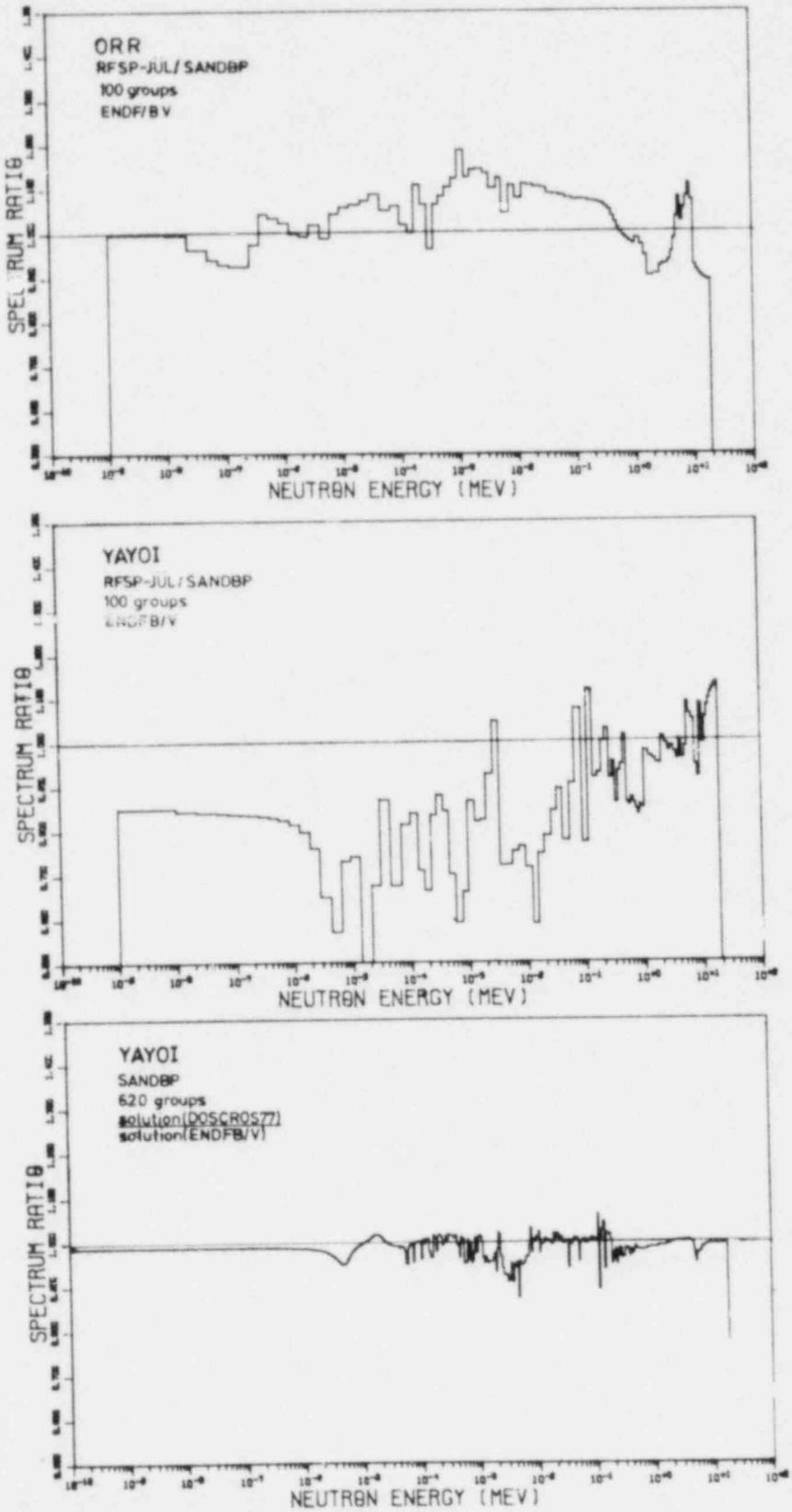

Figure 5. RATIO OF DIFFERENT SOLUTION SPECTRA.

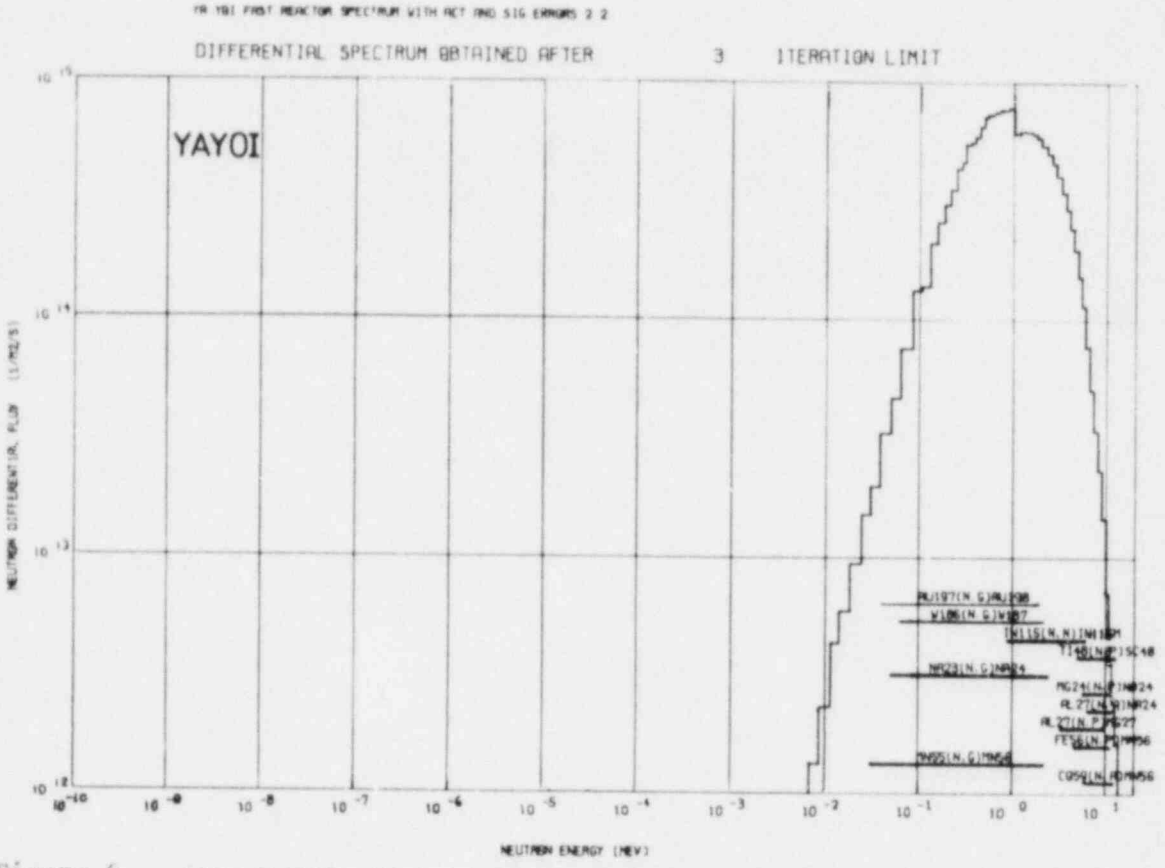

Figure 6. EFFECT OF AU197(N,G) REACTION ON THE SOLUTION SPECTRUM (100 GROUPS, ENDF/B-V).

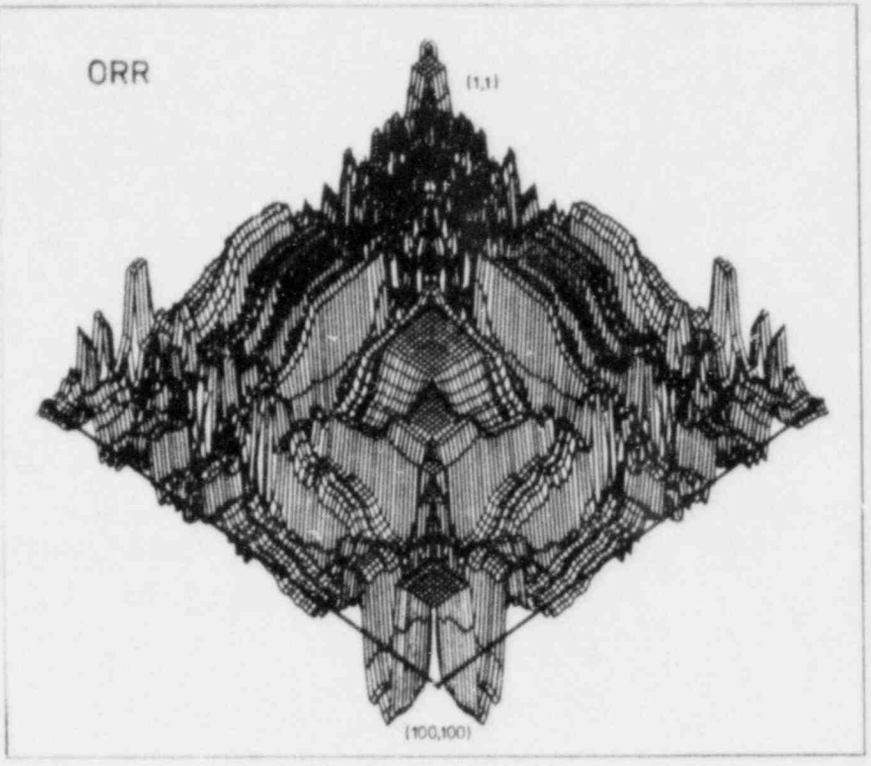

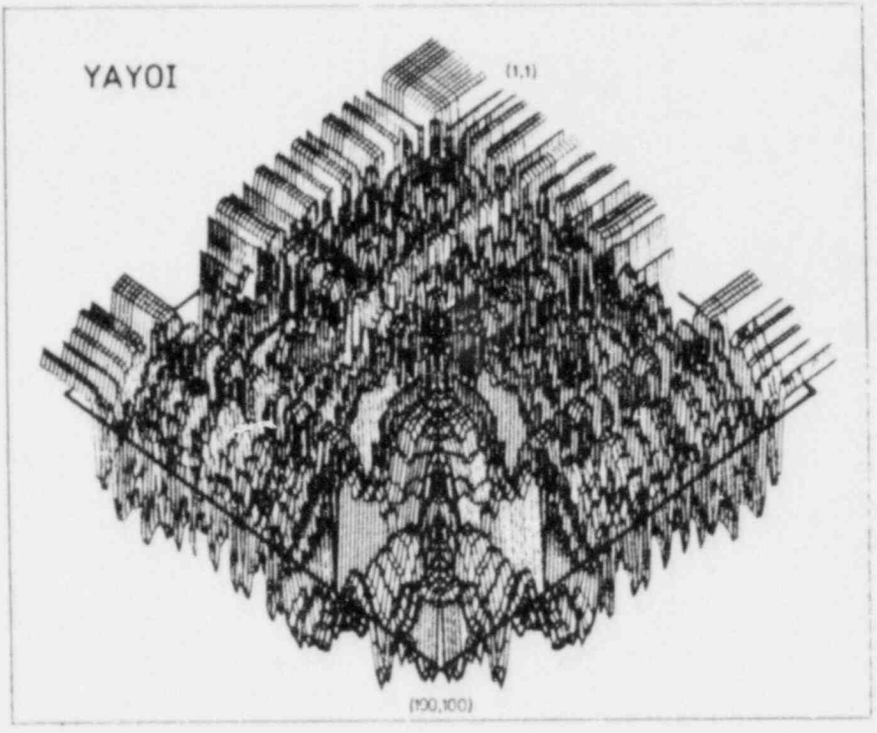

Figure 7. COVARIANCE MATRICES FOR SANDBP SOLUTIONS (100 GROUPS).

UNCERTAINTIES IN THE ESTIMATION OF RADIATION DAMAGE PARAMETERS*

F. W. Stallmann

Mathematics Department
The University of Tennessee
Knoxville, Tennessee 37916

and

Oak Ridge National Laboratory
Oak Ridge, Tennessee 37830

ABSTRACT

The evaluation of radiation embrittlement and the determination of safety limits requires the knowledge of uncertainties in the estimation of radiation exposure parameters like flux greater than 1.0 MeV or dpa of iron. Least squares adjustment methods can be used for the estimation of the exposure parameters and their uncertainties. It is of interest to determine how the uncertainties are influenced by the input data, in particular, the selection of dosimeters for the determination of exposure parameters. This investigation is simplified by the fact that in least squares methods the output uncertainties depend primarily on the input uncertainties and very little on the measured values themselves. Thus, the expected uncertainties can be determined without actually making measurements. In this paper, uncertainties for exposure parameters are calculated for a variety of foil sets. The consequences of this investigation for surveillance dosimetry are discussed.

INTRODUCTION

The determination of safe operating limits for LWR reactors pressure vessels over the operating life of the reactor requires a reliable estimation of the irradiation induced embrittlement of the pressure vessel steels. The embrittlement is assumed to be a function of chemical composition, temperature, fluence (perhaps also fluence rate), and neutron spectrum. The functional dependency between embrittlement and neutron irradiation is summarized in the form of damage exposure parameters which are weighed integrals over the fluence spectrum. The total fluence of energies greater than 1.0 MeV has been the most widely used damage exposure parameter. Irradiation induced displacement of iron atoms (dpa) is

*Research sponsored by the Division of Reactor Safety Research, U.S. Nuclear Regulatory Commission under Interagency Agreement DOE 40-551-75 with the U.S. Department of Energy under contract W-7405-eng-26 with the Union Carbide Corporation.

now considered a more reliable measure of irradiation damage and has been recommended as exposure parameter in the ASTM Standard E 693.[1] The total fluence greater than 0.1 MeV is also being considered.

The determination of damage exposure parameters in a given reactor environment is needed in two applications. The first is in materials test reactors and also for some surveillance capsules in power reactors where the measured materials damage in test specimen is correlated with exposure parameters in order to determine the functional relationship between the two. The second application is the prediction of the actual damage in reactor pressure vessels on the basis of the magnitude of exposure parameters in the pressure vessel wall. Both applications require not only reliable values of the exposure parameters but also estimates of the uncertainties in the determination of these values. Only if the uncertainties are known can a prudent but not excessive conservatism be applied.

Statistical estimates for the uncertainties of exposure parameter values in form of variances and covariances can be obtained through least squares adjustment methods. The logarithmic least squares method LSL, which is described elsewhere in these proceedings,[2] has been used to determine these uncertainties in a variety of applications. In adjustment methods calculated neutron fluence spectra are combined with the results from passive radiometric (foil) dosimetry. Estimates for the exposure parameter values can be obtained as a least squares approximation of the damage response function by a linear combination of the reaction cross sections.[3] The gaps in the approximation are then filled by the calculated spectrum.

The uncertainties in the determination of damage exposure values depend therefore on two factors:

1. the uncertainties, i.e. variances and covariances of the input data, and

2. the selection of dosimeter reactions.

In order to determine more precisely the influence of each of these factors, a number of computer experiments have been performed applying the LSL program under varying conditions. The results are reported in the following sections.

NUMERICAL EXPERIMENTS

The numerical examples in this paper are taken from our recent evaluation of the 4th BSR-HSST series, which is reported in Ref. 4. A dosimetry capsule was chosen which contained wires for the ^{63}Cu (n,α) ^{60}Co, ^{46}Ti (n,p) ^{46}Sc, ^{54}Fe (n,p) ^{54}Mn, ^{58}Ni (n,p) ^{58}Co, ^{59}Co (n,γ) ^{60}Co, ^{58}Fe (n,γ) ^{59}Fe reactions and Gadolinium covered ^{238}U and ^{237}Np for fission reactions. The neutron spectrum was obtained from a composite of three 2-dimensional DOT-calculations in 102 energy groups above 0.1 MeV which was extrapolated on both ends and reduced to 19 energy groups. The adjustment procedure consists

of free scaling and spectrum shape adjustment which means that the input variances and covariances of the spectrum are relative to the shape and not to the absolute values of the fluence spectrum.

The following input variances and correlations were chosen as a "baseline" for comparison:

1. A relative one σ standard deviation of 7.5% for calculated fluences in each of the energy groups except for the lowest group, 0-0.1 MeV which was extrapolated and allowed to be adjusted by up to a factor 10.

2. The correlation between fluences of two adjacent energy groups was assumed to be 0.247. This value was taken from the suggested flux auto correlations in the REAL 80 exercise.[5] Correlations between any two groups are calculated as the product of adjacent correlations between intervening groups.[2]

3. The reaction rate standard deviation were set to 3% for the non-fission reactions and to 6% for these fission reactions.

4. The cross section variances and covariances were calculated from the ENDF/B-V activation cross section file.

The variances 1 and 3 are rather optimistic and may not be typical particularly in reactor pressure vessel surveillance. They are, however, consistent with the differences between calculated and experimental reaction rates. This is also reflected in the values of X^2 divided by the degrees of freedom F which has the expected value of one. Experimental confirmation is lacking for the calculated fluences below 1 MeV and thus the X^2/F value changes little if the fluence standard deviations below 1 MeV are increased to 30%. The output variances for $\phi > 0.1$ MeV and dpa increase, however, substantially.

The results for a variety of input variances are listed in Table 1. The output variances increase with increasing input variances as expected. These results, and the ones in Table 2 and Table 3 are essentially independent of the fluence and reaction rate values and thus of the value of X^2/F. They represent, therefore, the expected output uncertainties for given input uncertainties and selection of dosimeters. It may be noted that the output uncertainties increase faster with increasing input uncertainties if the fission reactions are eliminated.

Tables 2 and 3 demonstrate how the selection of dosimeters affects the variances of the exposure parameters. The calculations in Table 2 are based on the input variances which are listed at the beginning of this section. These variances are so small that even pure scaling with the ^{54}Fe (n,p) reaction gives quite acceptable variances for the $\phi >$ 1.0 MeV and $\phi > 0.1$ MeV. The larger variance for dpa is caused by the response to thermal neutron fluence, which could be obtained from the calculation only by extrapolation, resulting in large uncertainties for low energies. The inclusion of either (n,γ) reactions or the ^{237}Np (n,f) reaction remedies nicely this problem.

Table 1. This table shows how the variances for the exposure parameters vary with the input variances and correlations.

Spectrum Uncertainties (% Std. Dev.)			Reaction Rate Uncertainties (% Std. Dev.)		X^2/F	Exposure Parameter Uncertainties (% Std. Dev.)		
>1 MeV	<1 MeV	Correlation Between Groups	Non-fission Dosimeters	Fission Dosimeters		ϕ>1.0 MeV	ϕ>0.1 MeV	dpa
7.5	7.5	0.247	3.0	6.0	1.04	4.7	4.7	4.2
7.5	30.0	0.247	3.0	6.0	0.99	4.7	9.5	6.3
30.0	30.0	0.247	3.0	6.0	0.52	9.0	11.7	7.6
7.5	7.5	0.247	10.0	15.0	0.63	6.8	6.6	6.2
30.0	30.0	0.247	10.0	15.0	0.45	12.5	13.9	10.2
7.5	7.5	0.0	3.0	6.0	1.10	4.5	4.2	3.9
7.5	7.5	0.835	3.0	6.0	1.02	4.5	5.7	4.6
Input uncertainties as above but the ^{238}U (n,f) and ^{237}Np (n,f) reactions were excluded.								
7.5	7.5	0.247	3.0		1.08	5.9	5.6	5.2
7.5	30.0	0.247	3.0		1.08	5.9	11.4	8.3
30.0	30.0	0.247	3.0		0.64	18.1	18.3	14.9
7.5	7.5	0.247	10.0		0.72	7.8	7.6	7.2
30.0	30.0	0.247	10.0		0.59	19.1	19.2	16.0
7.5	7.5	0.0	3.0		1.11	5.4	5.0	4.7
7.5	7.5	0.835	3.0		1.13	5.8	6.9	5.8

Table 2. This table shows how the variances of the exposure parameters vary with the selection of dosimeter reactions. Input variances: 7.5% for input spectrum, 3% and 6% respectively for non-fission and fission reactions.

^{63}Cu (n,α)	^{46}Ti (n,p)	^{54}Fe (n,p)	^{58}Ni (n,p)	^{238}U (n,f)	^{237}Np (n,f)	^{59}Co (n,γ)	^{58}Fe (n,γ)	X^2/F	Exposure Parameter Uncertainties (% Std. Dev.)		
									φ>1.0 MeV	φ>0.1 MeV	dpa
X	X	X	X	X	X	X	X	1.04	4.7	4.7	4.2
	X	X	X	X	X	X	X	0.79	4.8	5.0	4.4
		X		X	X	X	X	0.81	5.0	5.2	4.6
X	X	X	X	X		X	X	1.02	4.9	5.0	4.4
X	X	X	X			X	X	1.08	5.9	5.6	5.2
	X	X	X			X	X	0.93	6.2	6.2	5.6
		X				X	X	1.18	6.9	6.9	6.3
X	X	X	X	X	X			1.08	4.7	4.7	6.2
X	X	X	X	X				0.95	4. 9	5.0	12.2
X	X	X	X					1.06	5.6	5.4	13.4
	X		X	X				0.67	5.0	5.3	6.8
		X						--	6.9	6.9	13.6*

*Scaling through the ^{54}Fe (n,p) reaction.

Table 3. Same as Table 2 but input variances are 30% for the input spectrum, 10% and 15% respectively for non-fission and fission reactions.

^{63}Cu (n,α)	^{46}Ti (n,p)	^{54}Fe (n,p)	^{58}Ni (n,p)	^{238}U (n,f)	^{237}Np (n,f)	^{59}Co (n,γ)	^{58}Fe (n,γ)	X^2/F	Exposure Parameter Uncertainties (% Std. Dev.)		
									φ>1.0 MeV	φ>0.1 MeV	dpa
X	X	X	X	X	X	X	X	0.45	12.5	13.9	10.2
		X		X	X	X	X	0.58	12.7	14.8	10.9
X	X	X	X	X		X	X	0.48	15.0	17.2	13.3
X	X	X	X			X	X	0.59	19.1	19.2	16.0
		X				X	X	1.13	21.6	22.4	18.9
		X		X	X			0.19	12.9	15.0	12.8
X	X	X	X	X				0.17	13.2	16.4	17.4
		X						--	21.3	22.2	22.6

The input uncertainties in Table 3 are increased to more conservative values which are typical for some pressure vessel surveillance results. The influence of the dosimetry on the output variances is here much more apparent. However, it is not the sheer number of dosimeters but the inclusion of some key reactions which brings about the most substantial reduction in variances. In some cases even a slight increase in the variances of $\Phi > 1.0$ MeV and $\Phi > 0.1$ MeV is noted when the (n,γ) reaction are added. Such irregularities are probably due to linearization of the strongly nonlinear logarithmic adjustment. This points to the fact that the inclusion of irrelevant information in the adjustment procedure may lead to unexpected and sometimes undesirable results. Further investigation is needed to clear up this paradox.

DISCUSSION

The data in Table 1 show that the variances in the calculated fluences are the most crucial input uncertainties. This is compounded by the fact that, in contrast to the uncertainties for reaction rates and cross sections, uncertainties for calculated fluences are very difficult to estimate. There is, of course, always the possibility to assign very "conservative" fluence variances but the price to be paid in overestimated output variances is high. More realistic uncertainty estimates can be obtained by benchmarking the fluence calculation,[6] but it is not always obvious whether the results from the benchmark field apply to the field under study. Some indication for the accuracy of the fluence calculation can also be obtained by comparing the measured reaction rates with the calculated ones. However this information does not necessarily apply to the energies where the reaction cross section have little or no response and these are precisely the energies where accurate fluence calculations are needed most.

The most reliable, although most difficult and time consuming method for estimating the variances and covariances of calculated fluences is a complete sensitivity analysis as it was done in Ref. 7. There is some doubt that this method will be widely used in its original form. It is, however, likely that the results from one calculation can, with obvious modifications, be applied to a large number of sufficiently similar calculations.

The correlations between fluences of different energies don't seem to have a significant influence on the output uncertainties. If in doubt, experiments with different correlations can be performed to establish the extent of this variation.

A large number of potentially useful dosimeter reactions are known although only a few are used routinely. A short half life of many product isotopes eliminates many reactions from use in long term irradiation experiments. More significantly, however, only a few have cross sections which match sufficiently close the response functions of the desired exposure parameters, and all of them are far from ideal. This implies that only very few dosimetry reactions can significantly improve the variances of exposure parameters. Even if all of them are used, an accurate input spectrum calculation remains crucial.

Of the reactions investigated in Tables 2 and 3, ^{238}U (n,f) and ^{237}Np (n,f) appear to be the most useful. Neptunium in particular has a cross section which closely matches the dpa cross section and should therefore be included whenever feasible. The ^{54}Fe (n,p) reaction is easy to obtain and measure and has a very well known cross section. It is therefore routinely applied as dosimeter in almost all long term irradiations and rightly so. A suitable (n,γ) reaction may be included in the dosimeter set to determine low energy neutrons, particulatly if the ^{237}Np (n,f) reaction is absent. The other reactions did not significantly improve the output uncertainties.

Similar experiments in other neutron fields and with other dosimeter sets are in progress. Results obtained so far show the same pattern. In short term irradiations ^{103}Rh (n,n') and ^{115}In (n,n') are most useful for approximating $\phi > 1.0$ MeV. The ^{93}Nb (n,n') reaction may have the same importance as ^{237}Np for long term irradiations once cross sections and measuring procedures are better established. It should be emphasized that this discussion applies only to the determination of variances for exposure parameters through adjustment procedures. A large number of dosimetry measurements can be quite useful in verifying neutron fluence calculations and in detecting possible calculational or measuring mistakes. Adjustment procedures on the other hand work best if the number of dosimeters is small and they are independent from each other. A large number of redundant and irrelevant dosimetry measurements does not improve the output uncertainties but may lead to a system of ill-conditioned equations and numerically unreliable solutions.

CONCLUSIONS

The uncertainties in the determination of damage exposure parameter values depends crucially on the calculation of the neutron fluence spectrum and its uncertainties. Neutron dosimetry measurements can reduce the uncertainties of exposure parameters but cannot eliminate the need for good fluence calculations. Uncertainties in the fluence calculation may be determined through benchmark calculations or preferably a sensitivity analysis. There is only a small number of dosimetry reactions which is useful for the determination of exposure parameter values. Increasing the number of dosimeters beyond those which are useful does not improve the uncertainties.

REFERENCES

1. "E693 - Standard Practice for Characterizing Neutron Exposures in Ferritic Steels in Terms of Displacements per Atom (DPA)," Annual Book of ASTM Standards, Part 45.

2. F. W. Stallmann, "LSL - A Logarithmic Least Squares Adjustment Method," Proceedings of the Fourth ASTM EURATOM Symposium on Reactor Dosimetery (1982).

3. F. W. Stallmann and F. B. K. Kam, "Review of Unfolding Methods for Neutron Flux Dosimetry," Proceedings of the First ASTM-EURATOM Symposium on Reactor Dosimetry (1975).

4. F. B. K. Kam, "Characterization of the Fourth HSST Series of Neutron Spectral Metallurgical Irradiation Capsules," Proceedings of the Fourth ASTM EURATOM Symposium on Reactor Dosimetry (1982).

5. C. Ertek, et al, "Status Report on the REAL 80 Exercise," Proceedings of the Fourth ASTM-EURATOM Symposium on Reactor Dosimetry (1982).

6. M. N. McElroy, Ed., LWR Pressure Vessel Surveillance Dosimetry Improvement Program: PCA Blind Test, NUREG/CR-1861 (1981).

7. R. E. Maerker, et al, Development and Demonstration for LWR Dosimetry Applications, EPRI INP-2188 (1981).

NEUTRON SPECTRA ANALYSIS USING INFORMATION-COMPUTING SYSTEM SAIPS

H. Bondars
Latvian State University
Rīga, USSR

ABSTRACT

The present paper gives a short description of neutron spectra unfolding problem and an information-computing system SAIPS, which allows: 1) to improve methodology of unfolding, 2) to automatize calculations, to use modern cross section and spectrum libraries and unfolding programs, 3) to make calculations and use a full and qualitative information without need to go into programming problems and data processing.

The unfolding of neutron spectrum $\varphi(E)$ from measured reaction rates A_i amounts to solving with respect to $\varphi(E)$ the system of N equations

$$A_i = \int_{E_{min}}^{E_{max}} \sigma_i(E)\varphi(E)\,dE, \qquad i = 1,2,\ldots,N, \qquad (1)$$

$\sigma_i(E)$ being the dependence of the neutron cross-section on energy E for the i-th detector, N- number of used detectors. As a rule $E_{max} \leq 18$ MeV, $E_{min} \geq 10^{-10}$ MeV. To underline the physical meaning of system (1), further let us call (1) the activation equation system.

The system (1) belongs to so-called incorrectly posed problems in mathematics. For such problems it is not possible in general to prove existence, uniqueness and stability of solution. The existence of solution of the incorrectly posed problem in physics follows from its physical essence. The solving of the incorrectly posed problems is possible only using a priori information about function and methods giving stable results [1], [2]. There are developed several programs for neutron spectra unfolding from measured reaction rates [3], [4], [5], [6] and so on. These programs take in notice following peculiarities of the activation equation system: 1) number of isotopes used as detectors is limited, 2) in separated measurements usually are used from several till almost forty detectors, 3) resonance and trasolance detectors are used, 4) energy regions are wide, 5) number of used detectors in separate regions is not the same, but some parts of regions may not be crossed by them, 6) in distinction from Fredholm-type integral equation of the first kind, where the kernel is continuous function of two variables, in our case the values of kernel $\sigma_i(E)$ for different i have nothing in common, i.e. the system (1) can not be regarded as discretization of an appropriate Fredholm-type integral equation, 7) reaction rates and cross sections are known with permissible uncertainty, 8) $\sigma_i(E) \geq 0$, 9) $\varphi(E) \geq 0$, 10) spectrum unfolding have different smooth in different regions, 11) a priori information is got from different sources and is performed in tables, 12) inaccuracy of measured reaction rates may be from 1% till 20%, a priori spectra calculated reaction rates diverge from some measured detectors even some times. In modern unfolding programs a priori approximation is performed on the base of the physical conditions. System of equations can be solved performing neutron spectra in different forms and using different methods. Programs SAND II [7], [8], and MHP [5] improve a priori

approximation using given, a little bit distinctive formulas. Programm PM 3 defines a solution from condition for the minimum of functional, but programs WINDOWS 9 , RFSP JUL 10 and SPECTRA 11 add to this condition complementary demand on seeking function. Every of those mentioned programs use various neutron spectrum unfolding analytical presentations. Solution can be got with iterative process. Because methods of unfolding are approximate and a priori data have errors, iterative process stops when some coincidence of measured and calculated reaction rates is reached. Smoothest and physical most defined solution must be defined with a priori "unbinding".

Quality of solution clarifies from: 1) real form of unknown solution, 2) a priori spectra approximation, 3) unfolding methods, 4) errors in a priori data, 5) used detectors and so on. Action of these factors correlated. To find out influence of these factors on solution we must carry out number tests which are corrected with bulky calculations and routine work. Data of such researches are represented seldom and with limited volume (for example 12 , 13 , 14 , 15 , 16 and other papers). On the base of separate researches it was tried (in interlaboratories comparision unfolding programs) to present summarize conclusions. But we have not forget about its limitation. If we need more precise results researches must be repeated for each calculation version. Methods of such researches depends from its aim and demands for determination neutron spectrum unfolding trustworthiness.

Information-computing system SAIPS 3 , 17 , 18 includes neutron spectrum unfolding mathematical, information and programming software and estimations of its quality. SAIPS is adapted on ES ELVM, operating under the control of OS ES, but may be adapted on IBM 360(370). SAIPS contains: 1) modern unfolding programs SAND II, RFSP JUL, WINDOWS, PM and others 17, 2) cross section libraries of

these programs and dosimetric foiles from libraries ENDF/B-IV, ENDF/B-V, UKNDL 78, JENDL-1, BOSPOR 80 19, ZACRSS 20 and others (all together nearly 150 reactions), 3) several neutron spectrum libraries. For leading with such information is written a special programm. Using SAIPS for calculations the physicist has no need to go into programming problems. In order to achieve this purpose, we propose the operation of SAIPS should be divided into three levels: 1) adaption, generation and cheking of calculation programs and cross section and spectrum libraries, generation of software for computerized calculations, use of cross-section and spectrum libraries, updating and further development of the system, 2) operation of SAIPS, 3) performing calculations. SAIPS provides the opportunity to determine the reliability of the unfolded neutron spectrum and to plan measurement and calculation programs.

SAIPS generation and development important depends from connection with information centres. Majority programs we got from RSIC (Oak Ridge, USA), but cross-section libraries from IEAE (Vienna, Austria) and Center of Atomic Data (CJAD, Obninsk, USSR). There are no essentialy problems to adapt and aprobe in SAIPS any of cross-section and spectrum libraries and unfolding programs written in PL/1, FORTRAN and ASSEMBLER languages. Therefore we think that it would be more advisable instead of interlaboratories comparision conduct basic unfolding using SAIPS (or analogous system) in anyone of interested laboratories, but for formulating problem and analysis received results involve experts from different laboratories. Such basic unfolding should be took as a base to plan further measurements and spectrum unfolding.

The further development of SAIPS is new, more perfect system SAIPS-2. Principal changes concerns to inside structure of system, broadening users facilities for unfolding, broadening facilities to solve more different problems.

REFERENCES

1. А.Н.Тихонов, В.Я.Арсенин Методы решения некорректных задач Москва,Наука, 1974.
2. В.Ф.Турчин, В.П.Козлов, М.С.Малькевич "Использование методов математической статистики для решения некорректных задач" УФН, 1970, 102, 3.
3. К.Я.Зондарс, А.А.Лапенас "Методы расчета спектров нейтронов по измеренным скоростям реакций в SAIPS. Часть I. Обзор математических методов" Изв.АН Латв.ССР Сер.физ.тех. наук, 1980, №2.
4. W.L.Zijp "Revier of Activation Methods for the Determination of Neutron Flux Density Spectra" Reactor Centrum Nederland, Petten, R.M.G. Note 75 19 (September 1975).
5. Крамер Е.А., В.С.Трошин, Е.Г. Тихонов Активационные методы спектрометрии нейтронов Москва, Атомиздат, 1976.
6. А.А.Лапенас Измерение спектров нейтронов активационным методом, Рига, Зинатне, 1975.
7. W.N.McElroy, S.Berg, T.Crockett, R.G.Hawkins "SAND II A Computer-Automated Iterative Method for Neutron Flux Determination by Foil Activation" AFWL-TR-67-41, 1967.
8. S.Berg "Modification of SAND II" BNWL-885, 1968.
9. F.W.Stallmann, J.F.Eastham, F.B.K.Kam "WINDOWS - A program for analysis of spectral data foil activation measurements" ORNL TM - 6650, 1979.
10. A.Fischer "RFSP JUL: A programme for unfolding neutron spectra from activation data" JUL-1475, 1977(ORNL RSIC-PSR-126).
11. C.L.Greer,J.A.Halbleib,J.V.Walker "A Technique for Unfolding Neutron Spectra from Activations Measurements" SC-RR-746, 1967.

12. L.Kuijpers "Spectrum Unfolding from Activation Measurements in a CTR-Model Blanket Experiment, Comparisions and Sensitivity Analysis" KFA, JUL-1435, 1977.

I3. Г.А.Борисов и др. "Сличение результатов восстановления тестового спектра нейтронов активационными методами" Труды II Всесоюзного совещания "Метрология нейтронного излучения на реакторах и ускорителях" Москва,I974.

I4. Х.Я.Бондарс и др. "Сличение методик определения спектрального коэффициента нейтронного поля реактора ИРТ-2000" Труды II Всесоюзного совещания "Метрология нейтронного излучения на реакторах и ускорителях"М,I974,Т2.

I5. Х.Я.Бондарс и др."Применение методов SAND II и ММП для восстановления спектра быстрых нейтронов" Изв.АН Латв.ССР Сер.физ.тех.наук, I980,№4.

I6. Х.Я.Бондарс, В.А.Камнев, В.С.Трошин "Применение методов МСР,ММП и SAND II для восстановления спектра быстрых нейтронов" Вопросы дозиметрии и защиты от излучений вып.20, Москва,I98I.

I7. М.А.Берзонис,Х.Я.Бондарс"Методы расчета спектров нейтронов по измеренным скоростям реакций в SAIPS.Часть 2. Программное и информационное обеспечение"Изв.АН Латв.ССР Сер.физ.тех.наук,I98I,№I.

I8. М.А.Берзонис,Х.Я.Бондарс,Д.Я.Тайминя"Методы расчета спектров нейтронов по измеренным скоростям реакций в SAIPS. Часть 3. Библиотеки нейтронных сечений" Изв.АН Латв.ССР Сер.физ.тех.наук,I98I,№2.

I9. В.М.Бычков и др."Организация машинной библиотеки оцененных сечений пороговых реакций БОСПОР 80 и ее тестировке по интегральным экспериментам" Вопросы атомной науки и техники Сер. Ядерные константы,I979, вып.3 (72).

20. М.А.Берзонис, Х.Я.Бондарс, А.А.Лапенас"Библиотека нейтронных сечений для программы SANDII и ее обслуживающая программа" Вопросы атомной науки и техники, Сер.Ядерные константы, I978,вып.I (28).

UNFOLDING OF REAL-80 SAMPLE PROBLEMS BY ITER-3 AND STAYSL CODES

M. Najžer and B. Glumac
J. Stefan Institute, University E. Kardelj
Ljubljana, Yugoslavia

ABSTRACT

ITER-3 is a recent modification of ITER-2 unfolding code. While basic features of ITER-2 are preserved the new code is able to take into account complete covariance matrices of cross sections, reaction rates and input spectrum as well as to produce output spectrum with its associated covariance matrix. Input data from REAL-80 sample problems are unfolded by ITER-2, ITER-3 and STAYSL codes. Given are the resulting spectra as well as the integral quantities DAR, DPA, integral fluence, fluence above 0.1 and 1 MeV together with their covariance matrix or standard deviation. Results are discussed in comparison of STAYSL solution with solutions obtained by both versions of ITER code. Further, the sensitivity of the solution to the variation of correlation range in covariance matrices of the crossections is investigated.

INTRODUCTION

The REAL-80 international project gives an opportunity to compare different unfolding codes on a full size real problem. In this paper the test spectra were unfolded using ITER-2, ITER-3 and STAYSL codes. ITER-2 and STAYSL are documented in[1] and[2] respectively. ITER-3 is an extension of ITER-2 and is briefly described in the following section. Besides spectra the following integral quantities were calculated: total fluence, fluence above 0.1 MeV, DPA, DAR and 60Ni(n,p) reaction rate.

STAYSL code was applied to investigate the influence of the correlation range in covariance matrices of the crossections. The covariance matrices of the crossections were created as recommended[3].

DESCRIPTION OF ITER-3 UNFOLDING CODE

Algorithm of ITER-3 is basically similar to ITER-2 i.e. it applies the same iteration procedure. The program has been expanded so that it can take into account the covariance matrices of the reaction rates,

crossections and the input spectrum and gives an estimate of the output spectrum covariance matrix. The basic algorithm of the ITER-3 code is described in[1]. The main difference in the algorithm of ITER-3 when compared to ITER-2 is that ITER-3 takes into account the correlations between groups of a certain crossection when calculating the adjustment operator for each subsequent iterative step. The elements of the relative covariance matrix of the solution spectrum are calculated in the same way as that of STAYSL code.

RESULTS OF REAL-80

Input Data

REAL-80 input data set provides reaction rates and their covariance matrices, 100 group input spectra with the associated covariance matrices and the crossections together with their standard deviations. The covariance matrix of the crossections is calculated as recommended[3]: diagonal correlation submatrices (correlations between groups of a certain cross-section) are taken to be gaussian with FWHM = 10, the correlations between groups of different crossections is fixed to be 0.01.

Neutron Spectra

Unfolding was performed by ITER-2, ITER-3 and STAYSL unfolding codes on three sets of input data: ORR data set, YAYOI data set with 13 reaction rates and YAYOI data set with 12 reaction rates. This last set is the original YAYOI data set from which the reaction 47Ti(n,p) was omitted because it could not be properly fitted with any of the three available codes. Fig. 1 presents ratios of initial spectrum approximations towards

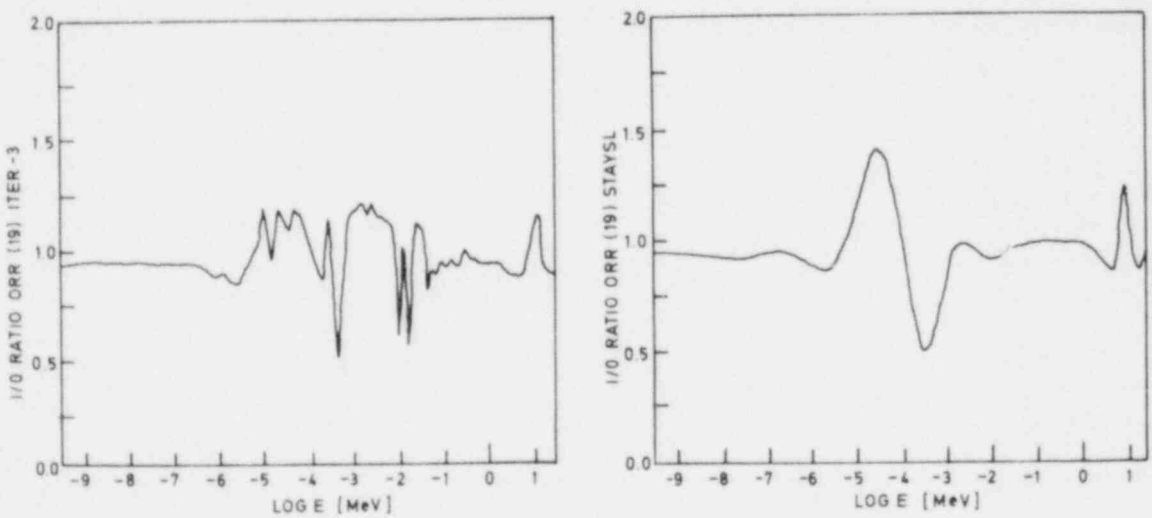

Fig 1a. Input/output ratios for ORR spectrum (19 reaction rates).

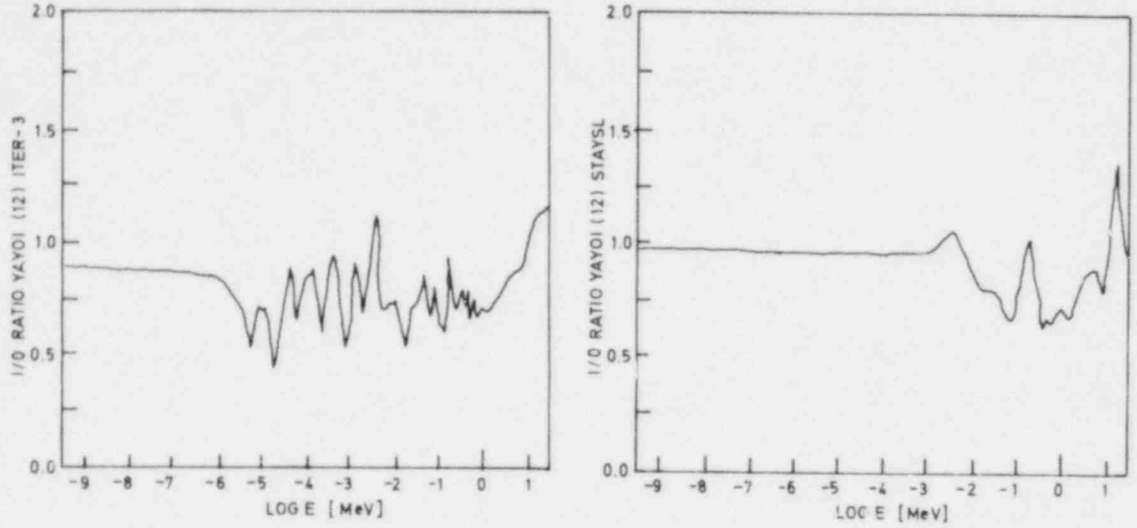

Fig 1b. Input/output ratios for YAYOI spectrum (12 reaction rates).

solution spectra for ORR and YAYOI (12 reaction rates) data sets for STAYSL and ITER-3 unfolding codes. ITER-2 gives almost exactly the same results as ITER-3. In Fig. 2 the correlation matrix of YAYOI spectrum obtained by STAYSL code is given. All unfoldings were done on our PDP 11/34 minicomputer. Computing times were some 5 hours for STAYSL and ITER-3 (the codes calculate complete crossection covariance matrices) and only approximately one minute for ITER-2.

Integral quantities

We have applied three unfolding codes on three input data sets thus obtaining nine solution spectra. For each solution spectrum we have calculated the following integral quantities together with their standard deviations: total flux, flux above 0.1 MeV, flux above 1.0 MeV, 60Ni(n,p) reaction rate, DPA and DAR.

Integral quantities have been evaluated using our program DART. This program is thoroughly documented[4,5], so we only bring here the method to estimate the standard deviation of the damage-to-activation ratio.

Let $\emptyset_n$ be the spectrum we investigate and M_{ϕ_n} its covariance matrix, let $\emptyset_f$ be a standard fission spectrum and M_{ϕ_f} its covariance matrix, let Σ_a be a certain activation crossection (60Ni(n,p)) and M_{Σ_a} its covariance matrix and let Σ_d be the damage function with its covariance matrix M_{Σ_d}. Damage-to-activation ratio is given by:

$$d = (x_n/x_f)/(y_n/y_f) \qquad (1)$$

where $x_n = \emptyset_n^t . \Sigma_d$, $x_f = \emptyset_f^t . \Sigma_d$, $y_n = \emptyset_n^t . \Sigma_a$ and $y_f = \emptyset_f^t . \Sigma_a$. We define vector $Q = (q_1, q_2, q_3, q_4) = (x_n, x_f, y_n, y_f)$. By making Taylor expansion and retaining

only the leading term we obtain:

$$|\delta d\rangle \simeq (\partial d/\partial Q)\cdot|(\delta Q)^{t}\rangle = S|(\delta Q)^{t}\rangle \qquad (2)$$

Expression (2) defines vector S as:

$$S = (\partial d/\partial x_{\mu}\ ,\ \partial d/\partial x_{\ell}, \partial d/\partial y_{\mu}, \partial d/\partial y_{\ell}) \qquad (3)$$

Standard deviation of DAR is given by:

$$\langle\delta d|(\delta d)^{t}\rangle \simeq S^{t}\cdot\langle\delta Q|(\delta Q)^{t}\rangle\cdot S = S^{t}.M.S \qquad (4)$$

where $\langle\delta Q|(\delta Q)^{t}\rangle$ is a 4 x 4 covariance matrix. Let us calculate for example matrix element M_{11}. We again apply the Taylor expansion of integral quantities defined in (1) and retain only the leading term:

$$M_{11} = \langle(\phi_{\mu}^{t}\cdot\delta\Gamma_{d}+\Gamma_{d}^{t}\delta\phi_{\mu})|(\phi_{\mu}(\delta\Gamma_{d})^{t}+\Gamma_{d}(\delta\phi_{\mu})^{t})\rangle \simeq \phi_{\mu}^{t}M_{\Gamma_{d}}\phi_{\mu}+\Gamma_{d}^{t}M_{\phi_{\mu}}\Gamma_{d} \qquad (5)$$

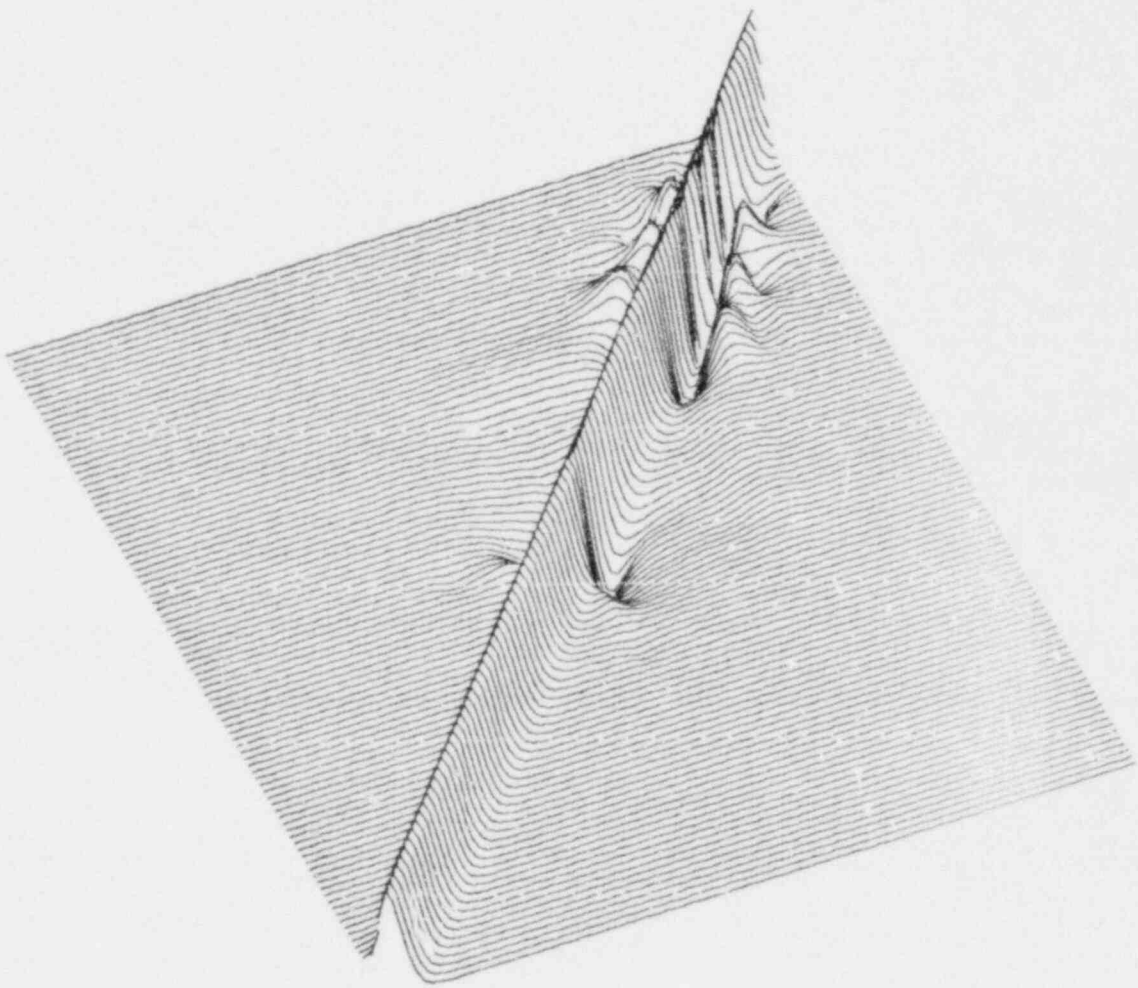

Fig. 2 Correlation matrix of the YAYOI spectrum (STAYSL).

We have assumed that no correlations exist between $\emptyset_r$ and $\emptyset_t$. Using expression (5) we can now calculate all other elements of the matrix M defined in (4). Note that the correlations of all "mixed" components $\langle q_i/q_j' \rangle$ if $i \neq j$ have beer set to zero, which is not always the case for correlations between $\emptyset_r$ and $\emptyset_t$.

We did not attempt to evaluate the correlation that might be introduced when calculating the 60Ni(n,p) reaction rate from the output spectrum when this reaction is also precent in the input data set. Therefore the standard deviation of the 60Ni(n,p) reaction rate as well as the covariance matrix of DAR are to some extent inaccurate in such cases.

COMPARISON OF ITER AND STAYSL RESULTS

Chisquare data in Table 1. show no appreciable difference in fit quality between the codes. In case of YAYOI data the same large discrepancy was found for all three codes for the 47Ti(n,p) reaction. This reaction was skipped but no large effect on solution spectra was observed. A too low chisquare value was obtained in case of ORR input data - it can indicate that the input variances may not properly reflect the actual spread in these data. Solution spectra obtained by the three codes do not deviate appreciably as it can be seen from Fig.1. In ITER spectra a fine structure can be observed which is inherent to this method. It is correlated to the detectors crossection structure and does not represent the real structure of the neutron spectrum. Most difference between codes is to be found in estimation of error bands[5]. It is interesting to note that the estimation of the output spectrum error band differs significantly for ITER-2 with respect to other two codes due to more prosaic evaluation method.

A broad and large oscillation can be observed in the input/output ratio of the STAYSL solution for the ORR spectrum. In the input/output ratio of the ITER solution this oscillation is not pronounced so much though the deviation is also rather large in the same energy region. It would be interesting to explain these discrepancies.

SENSITIVITY OF THE SOLUTION TO THE VARIATION OF THE CROSSECTION MATRIX CORRELATION RANGE

A test was performed in order to determine the influence of FWHM of the crossection correlation matrices upon the solution spectrum and its covariance matrix. For this test we supplied the STAYSL code with four different input data sets based on REAL-80 YAYOI input data set. We prepared four data sets that differed only in the FWHM of the crossections correlation matrix with FWHM being 5, 10, 20 and 30 groups respectively. As we can conclude from Fig. 3 where the ratios of output spectra with

Table 1. REAL-80 Integral Parameters

Spectrum	Unf. Code	No. Det.	Integral flux						DAR	Std Dev	DPA	Std Dev	Ni R.Rate	Std Dev
			Total	Std Dev	E 1MeV	Std Dev	E .1MeV	Std Dev						
YAYOI	STAYSL	13	1.818	.2074+12	.052	.9049+11	.085	.1978+12	.063	1.522	.108	.1246-09	.102	.1037-13	.076
YAYOI	ITER-3	13	1.726	.2070+12	.047	.8828+11	.080	.1960+12	.060	1.527	.106	.1232-09	.101	.1023-13	.078
YAYOI	ITER-2	13		.2086+12		.8877+11		.1973+12		1.528		.1239-09		.1028-13	
YAYOI	STAYSL	12	1.321	.2074+12	.051	.9082+11	.081	.1978+12	.062	1.502	.104	.1256-09	.102	.1059-13	.077
YAYOI	ITER-3	12	1.197	.2089+12	.046	.9034+11	.078	.1978+12	.059	1.502	.103	.1258-09	.101	.1061-13	.079
YAYOI	ITER-2	12		.2095+12		.9033+11		.1983+12		1.503		.1259-09		.1061-13	
ORR	STAYSL	19	.242	.1989+14	.052	.4032+13	.054	.8222+13	.082	1.361	.087	.5681-08	.100	.5290-12	.086
ORR	ITER-3	19	.266	.1999+14	.052	.4045+13	.057	.8337+13	.083	1.389	.090	.5711-08	.100	.5209-12	.085
ORR	ITER-2	19		.1992+14		.4051+13		.8314+13		1.387		.5712-08		.5220-12	

Table 2. Sensitivity of Integral Data to the Variation of FWHM of the Crossection Correlation Matrix for YAYOI Spectrum

FWHM	Integral flux						DAR	Std Dev	DPA	Std Dev	Ni R.Rate	Std Dev
	Total	Std Dev	E 1MeV	Std Dev	E .1MeV	Std Dev						
5	1.306	.20735+12	.0508	.90834+11	.0814	.19774+12	.06208	1.5027	.1048	.12558-9	.1018	.10590-13	.0774
10	1.323	.20735+12	.0507	.90813+11	.0811	.19774+12	.06199	1.5022	.1044	.12557-9	.1016	.10593-13	.0771
20	1.359	.20734+12	.0505	.90782+11	.0800	.19774+12	.0618	1.5011	.1037	.12557-9	.1013	.10600-13	.07668
30	1.385	.20736+12	.0503	.90748+11	.0792	.19776+12	.0617	1.5008	.1027	.12557-9	.1011	.10602-13	.07635

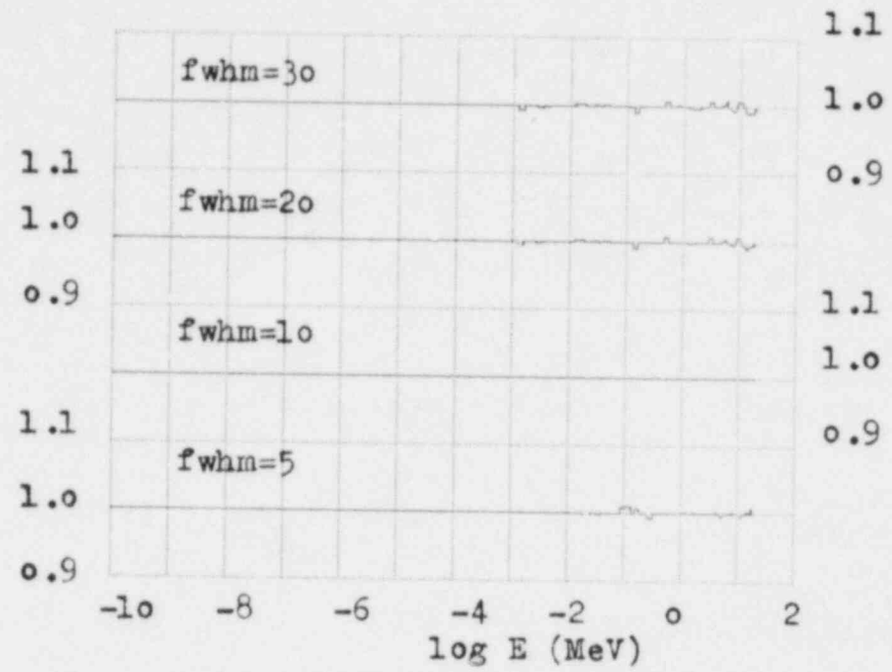

Fig. 3 Input/Output Ratios for YAYOI Data Set at Different FWHM's of the Crossections Correlation Matrix

different FWHM's of the crossections correlation matrices are depicted, the influence of the FWHM on solution spectrum is insignificant in the investigated range of FWHM. The same conclusion is reached for the output spectra covariance matrices and only negligible differences are observed in the chisquare and in the calculated integral quantities (Table 2).

DISCUSSION AND CONCLUSIONS

Results of present investigation show that ITER-2, ITER-3 and STAYSL give similar solution spectra and almost identical integral quantities in spite of the basically different algorithms. This fact supports the conclusion that the solution is mainly influenced by the quality of the input data and not so much by the investigated unfolding codes.

It is clear that STAYSL solution as well as its deviation from the input spectrum are more smooth in comparison with ITER results.

There is more difference in the error bands. It is worth to note the narrow error band[5], obtained by STAYSL and ITER-3 codes in the case of ORR spectrum. Together with the too low this gives an indication that the input data and their variances may have not been properly interrelated. A reason for this occurrence may be found in the inadequate treatment of the cross-correlations between some crossections in the

correlation matrix. We have assigned (as recommended[3]) the same arbitrarily small value to all cross-correlations. This may be, under some conditions, adequate for the cross-correlations between two entirely different crossections but it is questionalbe for treating the crossection cross-correlations between, for example, 197Au(n,gamma) detector and the same detector covered by cadmium.

STAYSL and ITER-3 require more than two orders of magnitude more computer time than ITER-2. Most of it is used on handling very large matrices. By far the largest dimension is due to group energy structure which is much finer than the actual resolving power. This is required for spectrum calculation because the fine structure of the crossections must be properly represented. It may be questionable if the same approach is needed for error and correlation analysis and if it is justified by the quality of covariance matrix data.

To speed up the computation by ITER-3 code we are investigating the possibility to split up the unfolding process into two parts. First the solution spectrum will be found in some 100 energy groups by a less demanding iterative approach. After this the covariance matrix of the output spectrum will be calculated from condensed input covariance matrices.

The analysis of the influence of the crossections covariance matrix upon the solution spectrum and its covariance matrix showed that in the case of artificially constructed crossections covariation matrices a large variation of FWHM did not exert strong influence upon the solution spectrum and its covariance matrix. This conclusion is limited to the investigated spectra and symmetrical correlations represented by a gaussian. It would be interesting to investigate also the effect of long range symmetric correlations.

REFERENCES

1. M. Najžer et al., Many Channel Spectrum Unfolding, Third ASTM Euratom Symposium, Ispra. Italy, October 1979.
2. F. Perey, STAYSL - Least Squares Dosimetry Unfolding Code, Report RSIC - PSR - 113.
3. C. Ertek, Report on REAL-80 Project, Report INDC/P(80), June 1980.
4. F. Perey, unpublished.
5. B. Glumac and M. Najžer, Unfolding of REAL-80 Sample Data by ITER and STAYSL Codes, IAEA Advisory Group Meeting on Nuclear Data for Radiation Damage Asessment and Related Safety Aspects, Vienna, Oct. 1981.

THE YAYOI BLIND INTERCOMPARISON ON MULTIPLE-FOIL REACTION RATE MEASUREMENTS

M.Nakazawa , T.Taniguchi, A.Sekiguchi
Department of Nuclear Engineering, Faculty of Engineering, University of Tokyo

K.Kobayashi
Kyoto University Reactor Institute

K.Sakurai
Japan Atomic Energy Research Institute

S.Suzuki
Power Reactor & Nuclear Fuel Development Corporation

ABSTRACT

The YAYOI blind intercomparison study meaning perfectly independent measurements of multiple-foil reaction rates in the YAYOI central neutron field by the four leading laboratories YAYOI, KUR, JAERI and PNC, in Japan have been successfully carried out and obtained the good agreements within ±2-±4%(1σ) for usual activation dosimeters. This result can be considered to show the current accuracies of the routine and daily dosimetry works of the participants because of the perfect blindness of the present intercomparison study. Basing on this intercomparison and uncertainty analysis, the reliable covariance matrix of the reaction-rates in the YAYOI core-center neutron field can be established, which is useful as the benchmark data for neutron unfolding codes of the activation spectrometry.

INTRODUCTION

The multiple-foil technique is a fundamental tool for the reactor dosimetry especially relating to the neutron flux and spectral characterization of research, material testing and power reactors. And current research activities in this field have been mainly concentrated to make clear and to improve the accuracy of the current activation technique, which is basing on the reaction-rate measurements, reaction cross section evaluations and adjustments, and unfolding procedures.

The purpose of this work is to make clear the present accuracy of reaction-rate measurements in Japan through the intercomparison study, using the YAYOI which can be considered as a complementary way to the direct uncertainty analysis of each measurements. In 1975, an interesting

intercomparison study on the reaction-rate measurements has been carried out in U.S.A. as a part of Interlaboratory LMFBR Reaction-Rate (ILRR)[6] program using the Coupled Fast Reactivity Measurements Facility (CFRMF). For reference, the final results of ILRR program have been stated consistent within ±2%(1σ) with respect to each other, and have met quite well the primary accuracy goal of ±5%(1σ) required at the beginning of the ILRR program.

One unique feature of the present YAYOI intercomparison work is the perfect blindness for the participants except for the managing group, that means the measured reaction rate data have never been obtained for this intercomparison because they did not know previously it, but their measurements were for their own purpose such as the averaged cross section measurements or Nb-dosimeter irradiations in the YAYOI. Final participants of this study have been counted four of the next laboratories, University of Tokyo(YAYOI-Group), Kyoto University Reactor Institute(KUR-Group), JMTR(Japan Material Testing Reactor) staff of JAERI and JOYO dosimetry staff of PNC, and fortunately all of them are leading and almost the same level laboratories in Japan.

Another feature of this study is the detail uncertainty analysis in the reaction-rate measurements to check and verify the standard deviations having obtained through this intercomparison study.

IRRADIATION EXPERIMENTS

Irradiation and Gamma-Ray Countings

In this intercomparison study, the activation detectors were brought from each laboratory, and they were irradiated independently by using the common rig made of 20 mm ϕ Aluminum pipe.

The activated foil set in the YAYOI was taken to each laboratory to determine their absolute gamma-ray emission rates with each laboratory's counting technique, except the KUR group who has used the same Ge(Li) detector of the YAYOI group because it was too for away to bring back their foils to the KUR.

The gamma-ray counting techniques of each laboratory are summarized in Table 1, where it should be commented that although the same detector and the same standard sources have been used between the YAYOI and the KUR groups, independent calibrations of the Ge(Li)detector and different methods of gamma-ray peak area determination have been adopted respectively between these two groups.

Main differences in their gamma-ray counting techniques have been found how to determine the peak area and also how to fit the full energy peak efficiency curves, and a little differences have been found in the correction procedures and factors relating to the gamma-ray counting technique such as the random and the real coincidence effects, finite size effect of the activation foils and the self absorption effects.

Run-To-Run Power Level Normalization

The YAYOI power-level monitoring system have been consisted with the operational chart records of the reactor power meter, which are

connected to the fission-chamber and the compensated boron ionization chamber. The reproducibility of the reactor power is in the range of 0.2 to 0.5%. Further, using the 197Au(n,γ)198Au and 56Fe(n,p)56Mn reactions, the reproducibility of these independent irradiations have been examined to make clear the uncertainties of the present reactor power normalization method and the degree of the positioning error in each irradiation. From these experiments the uncertainty due to the present independent irradiations has been concluded as low as 0.5 to 1.0%.

RESULTS

The results of the measured reaction-rate values have been summarized in Table 2, which were normalized at the YAYOI reactor operation of 500W nominal power. From these results, it can be said that the degree of the standard deviations between the participant groups can be stated within ±2 - ±4%(1σ) except the Titanium foils that show large discrepancies by about 10% and 25%. In Table 2, there have been shown the relative deviations of each laboratory data from the averaged value, that show any biased or systematic errors can not been found out for every laboratory in their measurements.

The uncertanties caused by the reaction-rate measurement procedures have been analysed by the YAYOI group as a differential approach of the uncertainty, and the results shown in the fourth column of Table 2 are found well equivalent to the third column values meaning the degree of discrepancies through this intercomparison study except the Titanium-data. That means a complementary validation of each uncertainty analysis results and some error in the Titanium reaction-rate measurements beyond the statistical deviation.

UNCERTAINTY ANALYSIS

As is stated in the previous section, in order to analyze the discrepancies between the intercompared reaction-rate values, detail uncertainty analysis has been carried out by the YAYOI group on their experimental and measurement procedures, the summary items of which has been given in Table 3. And the standard deviation matrix of the measured reaction-rate values is given in Table 4, that is defined as the root of each component of the usual relative covariance matrix.

From these analysis, it has been made clear that the main origins of uncertainty in the present reaction-rate measurements have been generally due to the uncertainty of the photopeak efficiency determination of the Ge(Li) detector that are ranging between 1.5 - 2.5% and are accounting for fifty percent or larger of the final uncertainty of the reaction-rate values. This uncertainty have been caused by the uncertainty of the standard gamma-ray source intensities and also by the fitting or interpolation error of the photopeak efficiency curve of the Ge(Li) detector. And it should be commented that the correlative errors between the standard source intensities are expected to be assigned by their suppliers if the correlative error were exist, because it is necessary

to complete the covariance matrix of the reaction-rate values which have been omitted in the present covariance matrix shown in Table 4.

Mutual Shielding Effect

There are some other problems to be discussed on the uncertainty of the reaction-rate measurements which have never been considered in Table 2, 3 and 4, they are the self- and the mutual-shielding effects due to the simultaneous multiple-foil irradiations and the perturbation effects of the dosimeter set. However, the correction factors due to this self-shielding effects have been found of no importance in the hard spectrum of the present YAYOI core-center field because there are little neutron flux in the resonance energy region.

On the second problem of the mutual shielding effect, one supplemetary experiments has been carried out using the specially arranged dosimeter package shown in Fig. 1. From the results of this experiment, some meaningful decrease effects of 58Ni(n,p) reaction have been observed by about 2.5 - 5.0% depending on the foil arrangement in the dosimeter package, while any clear differences have not been observed for the other foils of the 197Au(n,γ) and 115In(n,n') reactions. And a little larger discrepancies of the 58Ni(n,p) reaction in the present intercomparison results shown in Table 2 have been thought partly due to this mutual-shielding effect of each dosimeter package.

Although there have never been made any direct estimation on the third problem of the perturbation effect of the neutron field by the inserted dosimeter package itself, this perturbation effect could be considered of little importance in this YAYOI neutron field, because any differences have not been observed when we have applied the non-pertubing fine wire as an irradiation rig instead of the usual Aluminum pipe (20mm O.D and 18mm I.D) which had been thought to cause the severe perturbation effect.

DISCUSSIONS AND CONCLUSIONS

Through this YAYOI blind intercomparison study and the uncertainty analysis of the present reaction-rate measurements, the current accuracy of the multiple-foil reaction rate data has been made clear and it can be stated within ±2 - ±4%(1σ) for usual activation detectors which can met also the primary accuracy goal of ±5%(1σ) in the ILRR program.

Although this results of accuracy in Japan are seen a little inferior to the accuracy of ±2%(1σ) having obtained in the ILRR program, the perfect blindness of the present intercomparison is more valuable especially from the viewpoint of making clear the daily accuracies of the routine dosimetry works.

The present data of multiple-foil reaction rates with the covariance matrix in the YAYOI core-center neutron field can be also used as a benchmark problem for the unfolding calculations to evaluate the neutron flux, spectrum and some integral parameters which have been already presented for the REAL-80 project of IAEA.

The output spectrum by the NEUPAC code is shown in Fig. 2.

As a comment on the large discrepancies in the Titanium reaction-rate measurements, it would be thought possibly due to the pulse summing effect and self absorption effect, which could not be made clear at yet.

Conclusive remarks to improve the accuracy of the reaction-rate measurements basing on the present studies are stated followingly;

1) More precise determinations of the photopeak efficiency curves of the Ge(Li) detector should be made, which need more precise and more kinds of standard gamma-ray sources, and
2) the mutual shielding effect should be considered and made decreased when the multiple-foil set is irradiated simultaneously in a single package.

REFERENCES

1) R.C. Greenwood, R.G. Helmers, J.W. Rodgers, N.D. Duddy, R.J. Popek, L.S. Kellog and W.H. Zimmer, " Non-Fission Reaction Rate Measurements", Nuclear Technology Vol.25 (1975) 294
2) K. Tasaka, " Standard Spectrum Method for Analysis of a Gamma-Ray Spectrum and its Application to an Irradiated Fuel ", JAERI-M-5947 (in Japanese), 1975
3) H. Baba, " Usage of the BOB7-Series Program for the Analysis of Ge(Li) Gamma-Ray Spectra ", JAERI-M-7017, 1977
4) W.L. Zijp and J.H. Baard, " Nuclear Data Guide for Reactor Neutron Metrology ", (Part 1 : Activation reactions), ECN-70, 1979

Table 1 Gamma-ray Counting Techniques for each laboratory

	YAYOI	KUR	JAERI	PNC
Detector	∿50cc coaxial Ge(Li) detector of closed-end type Princeton Gamma-Tech.	the same detector as YAYOI	110cc Ge(Li) detector ORTEC FWHM; 0.8KeV for 122KeV and 1.8KeV for 1333KeV	ORTEC High-Purity Ge detector (HPGe), 63cc coaxial FWHM; 739eV for 22.1KeV 768eV for 88.0KeV and 1.74KeV for 1.33MeV
Source-Detector distance	usually 10cm except the surface for $^{47}Ti(n,p)^{47}Sc$	∿2cm	usually 10cm except the surface for $^{56}Fe(n,p)^{56}Mn$	10-37cm depending on the gamma-ray intensities
Peak Area Determination	Standard Peak shape method [2]	Covell's	BOB-75 Code [3]	BOB-75 code [3]
Standard Gamma-ray Source	LMRI(*) standard set of Single gamma-ray source	the same as YAYOI	^{152}Eu of LMRI (±1.5%)	^{152}Eu and others of LMRI, also calibrated by Japan radioisotope association
Fitting of the peak efficiency	$\varepsilon(E) = aE^n$	$\varepsilon(E)=aE^n$	$\ln\varepsilon(E)=\sum_{n=0}^{3} an(\ln E)^n$	$\ln\varepsilon(E)=\sum_{n=0}^{3} an(\ln E)^n$

LMRI: Laboratoire de Metrologie des Rayonnements Ionisants (France)

TABLE 2. Summary of Radioactive Capture Reaction Rates Measured for YAYOI at 500 W operation and Intercomparison of Data

Reaction	Average Reaction-rates	Standard Deviation (%)	Uncertainty YAYOI Gr. (%)	Deviation from Average Reaction Rate (%) YAYOI	KUR	JAERI	PNC
$^{59}Co(n,\alpha)^{56}Mn$	1.46-17	3.5	2.4	+0.7	+2.7	-------	-4.1
$^{55}Mn(n,\gamma)^{56}Mn$	8.28-16	2.2	2.8	+2.4	------	-0.5	-1.9
$^{56}Fe(n,p)^{56}Mn$	1.04-16	2.5	2.8	-3.9	+1.0	0	+1.9
$^{27}Al(n,p)^{27}Mg$	3.85-16	0.7	8.4	+0.5	-0.5	-------	-------
$^{27}Al(n,\alpha)^{24}Na$	6.76-17	1.6	2.9	-0.3	0	+2.2	-1.8
$^{24}Mg(n,p)^{24}Na$	1.44-16	2.7	3.1	+2.1	-2.8	-1.4	+2.8
$^{46}Ti(n,p)^{46}Sc$	1.24-15	9.7*	------	-------	-8.1	+7.3	-------
$^{47}Ti(n,p)^{47}Sc$	2.12-15	25.3*	11.5	-20.8	-6.6	+28.3	-------
$^{48}Ti(n,p)^{48}Sc$	2.78-17	9.6*	3.8	-7.6	-3.2	+10.8	-------
$^{58}Ni(n,p)^{58}Co$	1.04-14	3.4	2.4	+2.9	+2.9	-2.9	-2.9
$^{115}In(n,n')^{115}In$	2.09-14	2.6	3.9	+1.4	-2.9	+2.4	-1.9
$^{197}Au(n,\gamma)^{198}Au$	2.80-14	1.5	3.8	+0.7	-------	-2.1	+1.4

(*) The reason of this large standard deviations is being investigated.

TABLE 3 UNCERTAINTY ANALYSIS OF YAYOI DOSIMETRY SYSTEM

INVESTIGATED ITEMS	ANALYSIS METHOD	RESULTS (1-SIGMA)
1. IRRADIATION CONDITION		
• REACTOR POWER FLUCTUATION OF EACH RUN	TRACING THE POWER MONITOR CHART	< 0.2% FOR USUAL TIME CONSTANTS
• RUN TO RUN POWER NORMALIZATION	INTEGRAL ESTIMATION THROUGH REPEATED INDEPENDENT IRRADIATION EXPERIMENTS	0.4 - 1.0%
• POSITIONING ERROR IN FOIL		
• FLUX GRADIENT	DIRECT MEASUREMENTS	CONTAINED IN THE POSITIONING ERROR
• PERTURBATION EFFECTS OF IRRADIATION RIG	COMPARISONS WITH NON-PERTUBING RIG AND CALCULATIONS	~0.1%
2. GAMMA-RAY COUNTING		
• POSITIONING ERROR IN THE FOIL COUNTING	REPEATED INDEPENDENT SETTINGS AND COUNTINGS OF THE SAME SOURCE FOR EACH S-D DISTANCES	0.8 - 1% FOR LESS THAN 10CM ΔD=0.4MM FOR LARGER THAN 10CM
• RADIALLY FINITE SIZE EFFECT OF FOILS	DIRECT MEASUREMENTS OF RADIAL EFFICIENCY CHANGES	< 0.1% FOR 1CM DIA. FOIL
• SELF ABSORPTION EFFECT	TRANSMISSION COEFFICIENT MEASUREMENTS THROUGH THE SAME FOIL	0.1 - 2.0% DEPENDING ON FOIL
• COUNTING-RATE EFFECT (PILE-UP, LIVE-TIMER)	PULSER METHOD AND DIRECT MEASUREMENTS BY INCREASING THE COUNTING-RATE	< 1.0% FOR LESS THAN 2000CPS
• PEAK AREA ANALYSIS METHOD	REPEATED PEAK ANALYSES CHANGING THE B.G. COUNTING UNDER THE PEAK	CONSISTENT TO STATISTICAL ERRORS FOR THE SINGLE PEAK
• PHOTOPEAK EFFICIENCY	CONSIDERING THE UNCERTAINTY OF STANDARD SOURCES, COUNTING STATISTICS AND INTERPOLATION ERROR TO DIFFERENT GAMMA-RAY ENERGY	1.5 - 2.5% DEPENDING ON THE ENERGY
3. CONSTANTS		
NUCLEAR DECAY CONSTANTS	RE-EVALUATION & THE REFERENCE VALUES (4)	
FOIL WEIGHT MEASUREMENTS	REPEATED MEASUREMENTS	0.00035GRAMM
PURITY OF FOIL	BY THE DATA SHEETS OF EACH FOIL PRODUCTERS	< 0.1%
CLOCK	CALIBRATION TO THE STANDARD TIME	NEGLIGIBLE

TABLE 4 STANDARD RELATIVE DEVIATION MATRIX,* OF REACTION-RATES IN THE YAYOI CORE-CENTER FIELD

No.	Reaction	Reaction-Rate (1/sec.500W)	Number of Reaction 1	2	3	4	5	6	7	8	9	10	11	12	13
1	$^{59}Co(n,\alpha)^{56}Mn$	1.47-17	2.4%												
2	$^{55}Mn(n,\gamma)^{56}Mn$	8.48-16	1.7	2.8%											
3	$^{56}Fe(n,\gamma)^{56}Mn$	1.00-16	1.7	1.7	2.8%										
4	$^{27}Al(n,p)^{27}Mg$	3.87-16	1.6	1.6	1.6	8.4%									
5	$^{27}Al(n,\alpha)^{24}Na$	6.74-17	1.0	1.0	1.0	1.1	2.9%								
6	$^{24}Mg(n,p)^{24}Na$	1.47-16	1.0	1.0	1.0	1.0	2.1	3.1%							
7	$^{23}Na(n,\gamma)^{24}Na$	7.85-17	1.0	1.0	1.0	1.0	2.1	2.1	4.1%						
8	$^{47}Ti(n,p)^{47}Sc$	1.68-15	1.0	1.0	1.0	1.0	1.0	1.0	1.0	11.5%					
9	$^{48}Ti(n,p)^{48}Sc$	2.57-17	1.4	1.4	1.4	1.4	1.0	1.0	1.0	2.7	3.8%				
10	$^{58}Ni(n,p)^{58}Co$	1.07-14	1.02	1.02	1.02	1.02	1.0	1.0	1.0	1.0	1.22	2.4%			
11	$^{115}In(n,n')^{115m}In$	2.12-14	1.0	1.0	1.0	1.0	1.0	1.0	1.0	2.1	1.0	1.11	3.9%		
12	$^{186}W(n,\gamma)^{187}W$	1.16-14	1.0	1.0	1.0	1.0	1.0	1.0	1.0	1.0	1.04	1.15	1.02	4.9%	
13	$^{197}Au(n,\gamma)^{198}Au$	2.82-14	1.0	1.0	1.0	1.0	1.0	1.0	1.0	1.9	1.0	1.22	1.49	1.04	3.8%

Symmetrical Values

* It is defined as the root of each component of the relative covariance matrix.

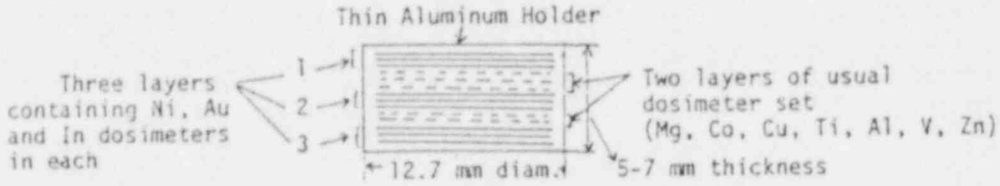

Fig. 1 Special Arranged Dosimeter Package.

(No. 1, 2, and 3 are corresponding to the upper, middle and bottom position.)

Fig. 2. OUTPUT SPECTRUM WITH 90% RESPONSE REGIONS

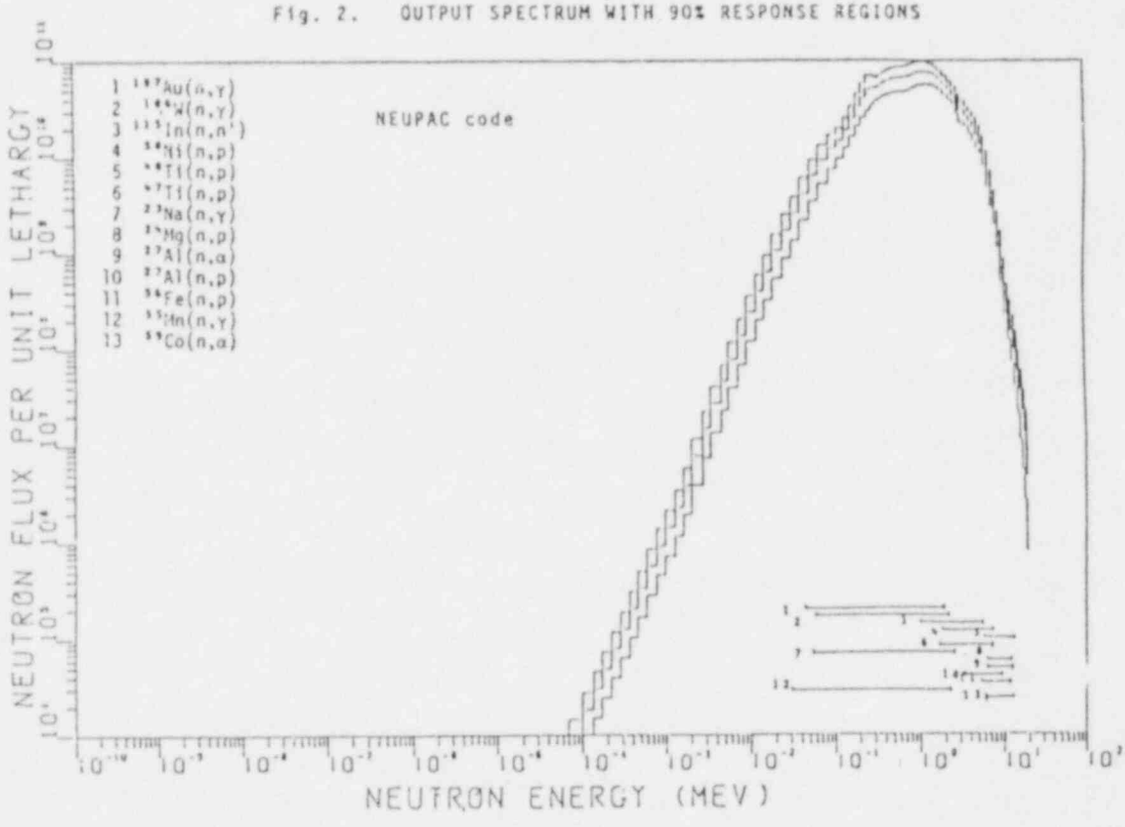

Session Highlights

HIGHLIGHTS OF SESSION A.1 — LIGHT WATER REACTORS-I

R. H. Lewis
Babcock and Wilcox
Lynchburg, VA
and
W. Schneider
Kernforschungsanlage Jülich
F. R. Germany

Of the three sessions devoted to light water reactors at this symposium, the first dealt primarily with the implementation of pressure vessel (PV) surveillance programs, including dosimetry, and with connected calculational and consistency studies.

Consistency tests between calculation and dosimetry are necessary but must not be sufficient; one way to ensure the latter demand is with the use of reference fields and standard procedures.

A remarkable improvement in the ability to predict dosimetric reaction rates has resulted from the efforts in benchmarking experiments in the United States, Europe, and Japan. The exposure uncertainties have been reduced, and the agreement shown between measured and calculated reaction rates was often excellent. For radiation damage effects to be considered as plant specific, generic data are being used to correlate neutron fluence or displacement number values with damage phenomena throughout the ASTM and Euratom communities as data reporting and tabulation has become more precise and available. In particular, progress has been reported in the developing of three-dimensional and perturbation calculation methods. Experiments at Mol, in Finland, and calculations made at HEDL show that core edge geometries greatly influence PV damage. Clever fuel management schemes can be used to slow down PV embrittlement.

The ASTM E-706 Master Matrix for LWR PV Surveillance Standards has been developed potentially as the key tool for guiding the USA program in correlating PV damage effects with dosimetry techniques. Besides the PV surveillance procedures, an overview on the standardization for LWR shielding was given.

Questions still remain, particularly on the following items in PV surveillance: the reported and reduced uncertainty figures are associated only with the characterization of the irradiation environment while the uncertainty must be seen in the context with those from metallurgy and irradiation procedures. In the reaction rate determination, there does seem to be a universal problem with the $^{237}Np(n,f)$ reaction. The relationship between the accelerated surveillance and a representative PV location should be considered. Finally the Thermal Shock problem for PWR PV has emerged as a major concern, in particular for the U.S. power reactor operators.

HIGHLIGHTS OF SESSION A.2 — FAST REACTORS

P. B. Hemmig
U.S. DOE, Washington, DC

There were several highlights in this session. The papers presented reflected not only the considerable progress made in recent years, but also a wide recognition of the importance of this work to the successful development of fast reactors. The eight papers in this session dealt with the assurance of measurement accuracy and the development of improved procedures for characterization of the irradiation environments in which reactor fuels and materials are tested.

A major development in this regard was the PNC/HEDL program for intercomparison of dosimetry measurements in JOYO and EBR-II. The results of the intercomparison in JOYO which were reported by S. Suzuki showed agreements for most reactions within ±3%. It is fair to note, however, that some iterations were required to resolve some larger differences that were first observed, and that neptunium-237 (n,f) measurements still differed by approximately 10%.

The importance of multiple foil measurements was illustrated when the reaction rates, which were based on initial calculations with the DOT 3.5 transport code, showed a difference of 66% with measured values. Differences were reduced to 4.2% using the unfolded spectrum. Dr. Lippincott reported similar agreements for HEDL and PNC measurements in EBR-II.

Interesting developments in gamma ray measurements were reported by Dr. W. Bunch of HEDL. Ion chambers, TLDs, and three types of calorimeters were used to measure gamma energy deposition within the in-reactor thimble, the vibration open test assembly, and the special characterizer assemblies. Consistent results were obtained for steel by the various methods, ranging from 0.98 for TLDs to 1.07 for calorimeter measurements.

Gamma field measurements are required to properly assess the radiation heating of test materials, since the radiation damage to these materials is temperature dependent. The close agreement between various measurement techniques is encouraging; however, it appears that there is much work to do to achieve the stated goal of plus or minus 5%.

The report by J. Bradley of AI concerned neutron field measurements using the helium accumulation from (n, α) reactions in a variety of materials. Such detectors provide good reproducibility, but are subject to sample purity problems and the need for a rather elaborate readout system. Considering the large uncertainties in the low energy cross sections for the reactions and the difficulty of predicting the spectrum shape at these low energies, the agreement of 10-30% with yields predicted

using the ENDF/B-V gas production files is a very promising sign and indicates that this technique might find wide dosimetry applications.

Measurements in the fast reactor blanket regions driven by the Tapiro reactor were reported by M. Carta. The results showed small but systematic discrepancies in the ratios of F8/F5 and C8/F5 of 10% and 6%, respectively. It is hoped that the problems with fast spectrum calculations, and the cross section data as well, can be clarified by further studies in this and similar facilities.

An interesting set of blanket pin burnup measurements in EBR-II was reported by Dr. Meneghetti of ANL. In burnup of 15,000 MWD (as measured by the La-139 yield), it was found that Pu-239 buildup was calculated to be 15% higher and Pu-240 30% lower than was measured. Such data coupled with pin to pin consistency studies can provide useful tests of the available methods and data. The burnup predictions were found to be quite sensitive to the choice of ENDF data sets, including the choice of the fission spectrum.

A wide range of measurements in the BR-2 and its zero power mockup were reported by C. de Raedt, et al. These are comprehensive studies with both destructive and nondestructive examinations after irradiation. This report provides a good summary of the state-of-the-art in these techniques.

The FFTF reactor characterization program reported by J. Rawlins covered a wide range of measurements, including a study of absolute fission rates and fission yield biases, taking into account neutron self-shielding effects. Neutron spectrum measurements were compared with multiple foil techniques and indicate that the shape is generally well represented, with goals of 5-10% accuracy in key integral parameters obtainable. This wide range of FFTF measurements from low to high power has served to advance the state of the art in many ways. We look forward to further analyses of these data, the reduction of these measurements to standard procedures, and the reports of the less conventional measurements studies, also carried out using FFTF.

The general trend indicated in this session was that progress toward better agreement between calculations and measurements has been made. One key to continued progress is the maintenance of clear distinctions between systematic and statistical errors, wherever possible. In this respect, measurements of the same quantities by different techniques and different organizations can be informative. As a final point, the calibration of the major measurement systems using standard sources and fields, maintained by organizations such as the National Bureau of Standards, will also contribute to good science and continued progress in this field.

HIGHLIGHTS FOR SESSION A.3: DATA AND TECHNIQUES

J. Grundl
National Bureau of Standards
Washington, D.C.

and

A. Fudge
U.K. Atomic Energy Authority
Harwell, U.K.

This session focused on measurement techniques and in this area emphasized the latest generation of dosimetry detection methods. (1) Measurements were presented for the sapphire detector which showed this device to be a practical damage monitor (i.e., one reflecting consistency with neutron dose in dpa units for a variety of neutron spectra and displaying manageable temperature sensitivity). (2) The niobium activation detector with its response measurement complexities was subject to an interlaboratory comparison based on niobium foil irradiations in the EBR II and BR-2 reactors. It is concluded that for routine dosimetry, accuracies of ±6 percent are achievable for the $^{93}Nb(n,n')$ reaction rate. Sustained interest in the niobium detector is further indicated by the report of a measured Cf fission-spectrum-averaged cross section for Nb(n,n'). The result, 149 mb, obtained at an accuracy of ±7 percent, represents an important integral benchmark value in view of the scarcity of cross section information of this reaction. (3) In a related area of dosimetry, a new microcalorimeter for absorbed dose rate measurements was described. Higher sensitivity, a necessary improvement goal for this technique, was reported to be a few tenths of one rad per second for accurate dose rate measurements.

Solid state track recorders for fission reaction rate measurements are beginning to find an established niche in routine reactor dosimetry. Three computer controlled systems for quantitative track counting were described that specifically aim at overcoming the present major inconvenience of manual track registration. Higher processing rates and higher track densities are to be expected. Automated instrumentation systems for proton-recoil track-scanning of nuclear-emulsions are also under advanced development and will improve accuracy and cost effectiveness. Applications of a new Compton recoil gamma-ray spectrometer designed for use in reactor radiation environments, and capable of continuous spectrometry up to 6 MeV, were outlined.

HIGHLIGHTS OF SESSION B.1 — LIGHT WATER REACTORS-II

Robert A. Shaw
Electric Power Research Institute
Palo Alto, California
and
Jürgen Ahlf
GKSS-Forschungszentrum
Germany

Austin's report on U.K. dosimetry efforts showed an increased interest in benchmark validation of calculational methods. The ASPIS facility, which has operated successfully for a few years, is being supplemented by a high flux benchmark field in the NESTOR reactor called NESSUS, and a replica of the PCA within the NESDIP program, which includes a full representation of the reactor vessel cavity.

The development of a sapphire dpa monitor seems promising. Nonetheless it must be kept in mind that earlier attempts at alternatives to activation detectors have not attained general acceptance.

Tourwe impressively demonstrated that flux perturbations in the mockup surveillance capsules in PSF can be precisely determined by 2-dimensional neutron field calculations. The variance between measured and calculated perturbations is no more than 5%.

Fabry, presenting the paper of Minsart et al., stressed the importance of reliable dosimetry for the future operation of BR3. Whereas good agreement of measured and calculated fluences can be attained at a location at the core periphery, an unresolved discrepancy exists about 10 cm into the moderator where the calculated flux is about 50% higher than the measured flux — a situation of concern for current licensing. Further evidence will be sought from samples to be taken from the core basket. A major difficulty in the estimation of RPV fluence is the complex power history of the plant.

Shaw's overview paper described in- and ex-vessel foil measurements to be conducted at ANO-2. It was stressed that although materials uncertainties are far greater than dosimetry uncertainties, reductions in the latter continue to be important. In the use of foil activities to support the accuracy of neutron transport calculational techniques, a recommendation was strongly made that the calculations include foil activities, rather than attempting to unfold foil activities to derive flux spectra.

Tsoulfanidis and Sallee in the next two papers presented the results of calculations and measurements in the cavity at ANO-1. Considerable azimuthal variation in the fluence in and near the pressure vessel was

not calculated to be present in the cavity, which potentially limits the effectiveness of foil dosimetry in cavities. Compared to measurements in the cavity, the calculations underestimated the flux for $E_n > 300$ keV and overestimated it below that energy.

Petilli described a new multiple unfolding technique which allows fluxes and cross-sections to vary using benchmark fields together with sets of results under analyses. It was suggested in the discussion that this technique was simply another form of the traditional least squares technique. The discussion did not clarify this issue.

Martin described a BWR dosimetry experiment in which foils were irradiated in the cavity of Browns Ferry-3. The results were used to agree in favor of cavity dosimetry as an alternative to in-vessel dosimetry. Members of the audience, on the other hand, stated that limitations in cavity dosimetry will require continued reliance on in-vessel dosimetry.

HIGHLIGHTS OF SESSION B.2 — BENCHMARKS AND NUCLEAR DATA

W. G. Alberts
Physikalisch-Technische Bundensanstalt
Braunschweig, Germany
and
G. Hansen
LASL
Los Alamos, New Mexico

The papers presented in this session reflect the tedious work of those who constantly work at ameliorating their benchmark neutron fields and/or the neutron cross section data base.

Special emphasis was given to the low-energy flux perturbations. New calculations were performed for the Mol and NBS Cavity Fission Fields and for the NBS ISNF benchmark. Direct recoil-proton spectrometry measurements in the Romanian and the Mol ΣΣ fields were directed toward extending the experimental spectra down to lower energies. Documenting these spectra is a continuing effort.

A second group of papers focused on cross section data testing for dosimetry cross sections as well as for neutron transport calculations. Considerable progress was noticed for data testing in the CFRMF and ^{252}Cf neutron fields. It is impressive that the introduction of variance-covariance analyses has widely found its way into the laboratories, and is a considerable improvement in the consistency of the data base. The question remains, however, whether there could be a loss — or a spurious creation — of information if energy-dependent dosimetry cross sections are adjusted using adjusted benchmark spectra.

For this reason the introduction of the ^{252}Cf fission neutron spectrum, already established as a standard field by the IAEA, into the group of CSEWG benchmark fields is strongly recommended. This field is characterized by independent measuring methods, e.g., direct spectrometry, and is less dependent on material cross sections than others are. Dosimetry cross section testing in this field, therefore, does not involve any adjustment of data and is easily reproducible.

The value of (101 ± 3) mb for the ^{235}U fission spectrum-averaged cross section of the $^{58}Ni(n,p)$ reaction which is frequently used as a reference cross section, should be checked against values measured in the ^{252}Cf fission spectrum.

HIGHLIGHTS OF SESSION B.3 – TOKAMAK RELATED PAPERS FROM THE FUSION I AND FUSION II SESSIONS

Charles E. Clifford
Princeton Plasma Physics Laboratory
Princeton, New Jersey

The Tokamak related papers in the Fusion Sessions discussed in this review are as follows:

- Proposed Neutron Diagnostic Systems for JET presented by Dr. O. N. Jarvis of the A.E.R.E., Harwell.
- The Tokamak Fusion Test Reactor, Fusion Reaction Products Diagnostics, presented by Dr. H. W. Hendel.
- Neutron Dosimetry for the Lithium Blanket Module Program, presented by Dr. Y. D. Parker of E.G.&G. Idaho, Inc.
- Fusion-Blanket Dosimetry Program at the Idaho National Engineering Laboratory (INEL) by Dr. F. Y. Tsang, E.G.&G Idaho, Inc.

The Tokamak Diagnostic Programs at both JET in Culham and TFTR in Princeton are still in the early stages of development, therefore, primarily the differences and similarities in the two machines under construction and their diagnostic philosophies are discussed.

The machine configuration for JET located in England has a D-section vacuum vessel. The major diameter of the torus is 5.9 meters and the horizontal plasma width is 2.5 meters. The vertical extent of the plasma is 4.2 meters. The TFTR located at Princeton, New Jersey has a major radius of 2.7 meters including a toroidal vacuum vessel with a one meter minor radius. With regard to the operating characteristics of the two machines, the TFTR has a pulse duration of approximately 0.5 to 1.0 seconds. JET is designed to have a five to ten second pulse width; therefore, there is considerably more time allowed for taking diagnostic measurements. The TFTR machine is attempting to achieve a break-even situation on the energy balance, which is that the energy produced in the plasma shall be equal to the energy injected by the neutral beams and the OH coils. After extensive D-T operation, it is presumed that the TFTR can achieve q=2, which requires a pulse length of up to five seconds.

JET has large mild steel magnet rings surrounding the machine to contain the magnetic field. It is anticipated that the magnetic field strength outside the rings will be on the order of 100 to 200 gauss. The TFTR is nonmagnetic and has a conducting vacuum vessel with 3 milli-ohms resistance. The stray magnetic fields around this machine are quite large.

JET has a shield design consisting of a single concrete wall which is nine feet thick and completely surrounds the square reactor hall. The TFTR has a five-foot-thick concrete wall surrounding a significantly larger machine test cell than that for the JET. In addition to the test cell wall, a three foot thick concrete igloo primary shield is installed prior to D-T operation of the TFTR.

The diagnostic configuration on TFTR is primarily vertical. Twenty large penetrations are provided through a six-foot-thick concrete shield directly underneath the machine for diagnostic measurements. The distance of the diagnostic detectors from the machine can be as small as six meters. The JET machine has primarily horizontal type diagnostics where the well-shielded diagnostics must be placed external to the reactor hall shield wall. In this instance the closest position for a well shielded detector would be approximately 18 meters.

One of the goals of the diagnostic groups is to measure the total neutron yield from each machine with the accuracy of ±15%. For these determinations, both JET and TFTR plan to use passive detectors such as foils of aluminum, nickel, copper, zirconium, and perhaps others. There is a particular interest in measuring the virgin neutron flux at or near 14.5 MeV with the foil detectors, which will probably require a better determination of the cross sections of the foil material in the energy region from 12 to 15 MeV than currently exists. There is a diagnostic requirement to determine the neutron spectrum with an energy resolution of 0.5 MeV or better. At some point it might be useful to provide the fusion community with a Foil Calibrating Facility. In addition to the foil detectors, a selection of neutron spectrometers will be used to further determine the neutron energy spectrum being emitted by the fusion reactor. These spectrometers will include (1) a ^{3}He proportional counter; (2) a ^{213}Ne scintillation detector; and (3) a proton recoil spectrometer using a thin irradiator. One of the problems which must be overcome in order to use these detectors is in designing the electronics to operate in an environment with a high level of electromagnetic interference.

The fusion community needs additional activation detector studies to help select the appropriate detectors for use in the energy range from 12 to 15 MeV and to provide more accurately evaluated cross section data sets in the same energy range.

In addition to the two papers on machine diagnostics just discussed, two others were also presented, which are on neutronic measurments related to the Lithium Blanket Module program conducted at the TFTR by EPRI. This program is directed by Dr. Dan Jassby of the Princeton University Plasma Physics Lab. The detector development work is being undertaken by Dr. Yale Harker and by Dr. F. Y. Tsang of EG&G. The Lithium Blanket Module (LBM) program is designed to provide engineering experience in the development and fabrication of realistic tritium producing blankets. A primary objective of the LBM Program is to develop an accurate calculational system for predicting neutron transport

in the tokamak machine and also in the Lithium Blanket surrounding the machine. The TFTR at Princeton provides the first usable, widely extended 14 MeV neutron-source, for this type of experiment. A simulated lithium-oxide type blanket module has been developed by General Atomic in support of this program. General Atomic will also perform the tritium production measurements by destructive examination of the lithium oxide pellets. The Lithium Blanket Module has been fully instrumented with passive detectors using typical foils again, including aluminum, copper, zirconium, nickel and also ^{238}U and ^{235}U fission foils.

HIGHLIGHTS OF SESSION C.1 — RADIATION DAMAGE CORRELATIONS AND DAMAGE ANALYSIS TECHNIQUES

L. E. Steele
Naval Research Laboratory
Washington, DC

Summary

Though diverse, this session met conference and session themes with emphasis mainly on damage resulting from pressure vessel steel exposure to energetic neutrons.

Review of Papers Presented

Two French Papers — Focus on techniques for describing damage especially preferred dosimetry procedures.

- Damage in a thermalized neutron (heavy water) environment and the contribution of lower energy neutrons.
- Tailored spectrum study with multiple dosimetry procedures to test measured vs computed neutron environment vs measured changes in properties of a steel and of tungsten.

Two papers dealt with statistical evaluation of data on irradiated steels.

- One with analysis of 144 data sets from MPC analysis to assess influence of Charpy V-notch test procedures and variations in neutron fluence determination.
- Second with analysis of unirradiated and irradiated Charpy V-notch data looking for degree of error produced by this test procedure and ways to better use C_v data.

Paper from Germany (Ahlf) — described studies of the influence of irradiation temperature (can be large) and neutron spectrum (how to evaluate the damaging contribution. Continuing study also to test flux effect and its level.

US Paper on Standardization (Hedgecock) — emphasized need for continued diligence in refining both measures of damage (mechanical, physical) and the damaging environment from perspective of ASTM.

Overview of IAEA Specialists Meeting on Irradiation Embrittlement and Surveillance of Reactor Pressure Components (Steele). Conclusions and recommendations gleened from 13 formal papers and extensive discussion were reviewed to emphasize goals of this conference.

(Cited 6 areas of emphasis)

1. Radiation Embrittlement
2. Annealing to Correct Embrittlement
3. Surveillance
4. Analysis of Fracture Potential of Vessel Steels
5. Neutron Environmental Analysis
6. Knowledge Dissemination Activities

Conclusions

1. Considering the diverse neutron spectrum conditions possible in fission and fusion systems, continued care in defining the environment is essential if adequate correlations are to be made. (And correlations are essential — explain why).

2. No single neutron threshold or dosimetry technique is adequate — so must press forward to assess physical damage along side multiple approaches to environmental determination. (For example — French study in tailored spectrum to represent PWR, showed good results with >1 MeV and DPA but not with >0.1 MeV. German study found better correlation with steel embrittlement using >1 MeV than DPA.

3. All speakers seemed to agree on need for standardization of methodology and optimization of data by standards and by statistical analysis. This implies continuing maintenance of full data banks from test reactor experiments and operating plants.

4. Results of parallel studies by specialists in damage of components is essential. Cite recommendations of IAEA specialists on Neutron Environmental Analysis.

NEUTRON ENVIRONMENTAL ANALYSIS

Based on the overview paper and other discussion, recommendations framed by IAEA specialists include the following:

1. Support goals and activities of sister international groups especially seeking improved damage function analysis for vessel steels.

2. Endorse "Caprice" committee activities and joint conference plans with OECD/NEA groups.

3. Actively support national and international dosimetry standards (through research and coordination) to systematically advance:

   A. Accuracy of pertinent nuclear constants.

   B. Methodology for long-term dosimetry.

   C. Specific surveillance studies.

   D. Damage function for steel in LWR environment.

   E. Definition of environment in most appropriate terms.

   F. Means for projection of damaging environment – capsule to wall or to point in vessel as 1/4 T.

HIGHLIGHTS OF SESSION C.2 — NUCLEAR DATA NEEDS AND PROBLEMS

John Lewellen
U.S. DOE
Washington, D.C.

Dr. Kocherov gave highlights of an IAEA Advisory Group Meeting on Nuclear Data for Radiation Damage and Related Safety Aspects which was held in Vienna in October 1981. Requirements for nuclear data used for estimating radiation damage were reviewed and recommendtions concerning future activities of the IAEA nuclear data section were developed. One recommendation was to establish for international reference a new Reactor Radiation Damage Nuclear Data File within the next three years. Other conclusions and recommendations can be found in the report INDC (NDS)-128/GR.

Furthr IAEA action is described in the paper by Cullen, Kocherov, and McLaughlin on the present IAEA reactor dosimetry file, IRDF-82. This file was released in February, 1982 and is now available through the Agency. It provides a comprehensive set of dosimetry reaction cross sections and uncertainties in multigroup form. Multigroup spectra are also provided. Listings of file contents and comparisons of average cross sections for CF-252 and U-235 fission spectra with integral experiments were reported.

A paper presented by Dr. Fu of ORNL on experience using covariances of ENDF/B-V dosimetry cross sections attracted much interest. Ratio data with covariances were combined with eleven ENDF/B-V dosimetry cross sections using a generalized least-squares method. Some problems encountered in this work, which is continuing and is still developmental in nature, were traced to several deficiencies in the covariances. The character of the input data and an example illustrating the problems were discussed in detail. It now appears that use of this approach enables assignment of more credible covariance matrices to the input data and significant improvement in the results.

Other generalized least-squares analyses are being done at HEDL by R. E. Schenter and others, and a summary was presented. The FERRET code was used, in a pointwise energy sense, to obtain cross section evaluations with uncertainty values. Two important reactions, FE-58 (n,α) FE-59, and FE-54 (n,p) Mn-54 have been released as part of the Version V dosimetry file.

Work of R. L. Simons and his associates at HEDL includes reevaluation of neutron dosimeters from forty-one PWR surveillance capsules. The ratio of new to old exposure values for fluence greater than 1 MeV averaged 1.3. Factors which were analzyed and found to be significant in at least some cases include:

- capsule geometry corrections
- fissile impurity atoms
- burn-in of Pu-239
- differences in fuel loading for each fuel cycle.

The fission reactions for U-238 and Np-237 were found to be important in achieving uncertainties of 15% or better in exposure values. Without these indicators, uncertainty increased to about 30%. Several improved practices for dosimetry analyses were tested, and specified practices will be recommended through ASTM standards.

Interlaboratory dosimetry comparisons using the ORR-PSF facility have been conducted by Kellogg. Considerable experience has been gained in correctly interpreting the results obtained from the cooperating organizations. Accordingly, general radiometric procedures for use by ASTM are being prepared. One approach now being studied is a way to provide fission fluxes equivalent to the fields pertaining to the actual measurements. The results indicate, as noted before, that accuracy is improved by inclusion of fissionable dosimeters, and in general, the goal of 15% uncertainty or better in fluence is becoming achievable.

Measurements of integral helium generation in Li-6 and B-10 were reported by B. M. Oliver at AI and others. Numerous small samples of boron, enriched boron and enriched LiF were irradiated in the sigma-sigma and fission cavity standard fields at Mol, Belgium. Reports on similar measurements in the BIG 10 and CFRMF fields have been given earlier.

The measured reaction rates have been compared with theoretical values and values calculated from the Version V cross sections, and spectrum-unfolded neutron spectral shapes. It appears that the Li-6 results can be understood if interpreted carefully. However, the relative B-10 cross section inferred from the measurements remains roughly 10% higher than predicted. Study of this discrepancy is continuing.

The status of ENDF/B fission yield files and their development was summarized in an abstract of a paper by R. E. Schenter of HEDL and others. At present, extensive yields and their uncertainties for fission in 11 nuclides, in some cases for more than one incident neutron energy, exist in ENDF/B. Emphasis in this paper will be on the detailed status of yields important for dosimetry applications.

Generally, the papers given in Session C.2 indicate considerable progress. A large data base is becoming available and understanding of evaluation techniques for data and uncertainties is improving.

HIGHLIGHTS FOR SESSION C.3 – FUSION II, INTENSE NEUTRON SOURCES FOR FUSION RADIATION DAMAGE STUDIES

R. Dierckx
Joint Research Centre
Ispra, Italy
and
L. Greenwood
Argonne National Laboratory
Argonne, Illinois

The most important development focused on the Fusion Materials Irradiation Test Facility, FMIT, a special-purpose neutron source still in the project phase. Other countries are interested in principle, but have no direct plans to build this type of source. The Rotating Target Neutron Source, RTNSII, is now fully operating and used intensively for Fusion related damage studies.

In the absence of available special purpose high-energy intense neutron sources, the use of existing spallation sources is being forwarded. The Argonne (USA) Intense Pulsed Neutron Source, IPNS, is now operating. At SIN (Switzerland) a similar source is being built, and in Germany, such a source is projected. All these sources provide a relatively high neutron flux ($0 = 6 \times 10^{13}$ n/cm^2 per ma) in quite a large volume (1 liter).

The targets of these spallation sources are made of a high Z-material (uranium or lead) leading to a neutron spectrum with two components; a fission-like part and a high-energy neutron tail (up to 100 MeV).

At Los Alamos, the LAMPF's beam stop, a copper block, can also be used for fusion related radiation damage experiments (JRC/ISPRA/Europe has an irradiation in progress). A copper target gives harder neutron spectra than a high Z target, but a lower flux level.

Dosimetry techniques including helium accumulation detectors are being developed. Dosimetry cross sections and displacement cross sections, as well as tests at higher energies (up to 40 MeV) are needed.

In conclusion, special purpose neutron sources (RTNS, FMIT) are preferred, but in the absence of such intense neutron sources, spallation sources can provide useful information.

RAPPORT SUR LA SESSION D 1 - RÉACTEUR À EAU LÉGÈRE III

PAR P. MAS
Centre D'Etudes Nucleaires
de Grenoble
Grenoble, France

J'ai beaucoup de chances de rapporter cette troisième session sur les réacteurs à eau légère car c'est celle qui m'a le plus intéressé. Je trouve en effet que les sujets traités dans cette session éclairent particulièrement la finalité de notre travail.

Je dois dire ici que toutes les communications de cette session étaient de grande qualité et si j'insiste plus particulièrement sur certains sujets, ce n'est pas par dédain pour les autres, mais c'est parce que personnellement les premiers me posent plus de questions.

Pour en revenir à notre objet, l'éclairage particulier sur nos travaux a été donné par des métallurgistes, des exploitants de réacteurs et enfin par des représentants de la sûreté. En ce qui concerne les premiers, vous avouerais-je que je n'ai pu toujours saisir vraiment à fond les subtilités savantes qui nous étaient exposées. Cependant, j'ai été très impressionné par la qualité des travaux qui se poursuivent et notamment, sur les effets du choc thermique, d'autant plus qu'en EUROPE, les travaux sur ce sujet sont encore très peu développés.

Les communications des exploitants de réacteurs ont eu l'immense avantage de nous montrer concrètement la nature des problèmes qui se posent et la difficulté pratique de les résoudre. L'exposé de M. SANDRELLI était à cet égard fort instructif. Le nombre de détecteurs perdus, les difficultés pour accéder au réacteur en sont une illustration pertinente et les résultats intéressants. Quant aux problèmes de surveillance qui ont fait par ailleurs l'objet d'un atelier l'après-midi, j'ai été très impressionné par l'ingéniosité qui est mise dans l'élaboration des programmes, ce qui ressort particulièrement bien de l'exposé de M. LOWE. Ingéniosité également dans la détermination de la sensibilité de l'exposition aux distributions de puissance. On a pu mesurer, à travers la communication de M. ANDERSON, tout le parti que l'on peut tirer de telles considérations.

Enfin, l'exposé fait par M. NEIL RANDALL m'a réellement très intéressé. Il me semble en effet que l'on trouve là l'application et la

.../...

justification du travail qui est fait dans les laboratoires de dosimétrie, tant en ce qui concerne l'amélioration des données nucléaires, que la validation générale des méthodes de calcul neutroniques ou de détermination expérimentale et théorique des dommages que l'irradiation neutronique cause aux aciers des cuves de pression. Je dois dire, ici, que je suis content de constater qu'il y a eu une certaine évolution dans la désignation des fluences responsables des dommages. L'unité d.p.a., qui est maintenant recommandée depuis quelques années tant par l'A.S.T.M. que par l'EURATOM, semble avoir maintenant franchi la porte des organismes de sûreté. Mais peut-être faut-il se presser lentement. Il paraît à peu près admis maintenant par la majorité que la fluence supérieure à 1 MeV ne rend pas compte des dommages -ce qui n'empêche pas les courbes de référence d'être toujours dans cette unité. Le d.p.a. étant plus sévère pourrait être choisi facilement mais pourquoi pas la fluence supérieure à 0,1 MeV. La poursuite des études dans ce domaine me semble nécessaire, même si des détecteurs de dommages tels que le saphir et le tungstène apportent une réponse globale.

Enfin, je voudrais faire une petite remarque : j'ai très peu vu, avec les chiffres qui nous étaient montrés, les barres d'erreur correspondantes. Il y a là un oubli regrettable. Il y a 15 ans, ai-je lu dans une communication, les fluences étaient déterminées avec un facteur 2 d'incertitude. Qu'en est-il maintenant ? et qu'en est-il des déterminations du déplacement de la température de transition ? Il y a sûrement là un champ de réflexion important. Je souhaite qu'à notre prochain symposium quelques exposés soient en relation avec ce sujet et que d'ici là des analyses de sensibilité soient faites.

HIGHLIGHTS OF SESSION D.2 -- ADJUSTMENT CODES AND UNCERTAINTIES

M. Petilli
CNEN
Rome, Italy
and
F. Schmittroth
Westinghouse Hanford
Richland, Washington

Uncertainties, correlations and their mathematical representation as covariance matrices were a central feature of this session as well as an important part of the general symposium. The first paper discussed the REAL-80 exercise, an international comparison of widely used unfolding codes. An important goal in this study was to assess state of the art methods in deriving values and uncertainties for integral quantities such as dpa. It was concluded that the predicted displacements in steel varied by about 6% or less among the various participants.

A clear secondary achievement of this exercise was to provide much thought about covariance matrices and their use and evaluation. This paper as well as others at the session and the associated poster sessions stressed the need for using and understanding the data correlations and uncertainties that affect derived integral quantities.

A paper discussing dosimetry measurements in the Japanese reactor JOYO also emphasized a proper treatment of uncertainties and correlations as used in the recently developed Japanese code NEUPAC. A careful treatment of experimental uncertainties in the JOYO analysis was also presented.

Other developments included a further extension of the generalized least-squares codes LSL and FERRET which utilize lognormal distributions. An extreme example of adjustment was presented for a FERRET analysis that included adjustments of several hundred percent. Studies with LSL explored the sensitivity of derived dpa uncertainties on different assumptions for input uncertainties and correlations. Discussion of highly refined analyses with the ORNL LEPRICON code should also be mentioned. Finally, a detailed discussion of RFSP unfolding calculations emphasized the importance of having proper cross section covariance matrices available.

Throughout the session, lively discussions reflected the vitality that presently exists in the development and application of data adjustment methods in reactor dosimetry.

Workshops

WORKSHOP ON ADJUSTMENT CODES AND UNCERTAINTIES

F. W. Stallmann
Oak Ridge National Laboratory
Oak Ridge, TN

HIGHLIGHTS

Adjustment procedures have come a long way since this topic was discussed at the First ASTM-EURATOM Symposium on Reactor Dosimetry in 1975. At that time the determination of neutron spectra was done with a variety of unfolding methods whose assumptions and goals were rather vaguely defined and unrealistic. Today it is generally accepted that only a well defined statistical procedure such as least squares should be used and that the only legitimate goal is to reduce the uncertainties for the output spectra through a suitable combination of input information. This implies that the uncertainties of all input data, i.e., reaction rates, cross sections, and input spectra must be available as well defined variances and covariances. It also implies that inconsistencies which are outside the uncertainty bounds cannot by tolerated and have to be resolved before an adjustment procedure can be applied. Ideas and problems concerning the assignment of variance and covariances to input data and the treatment of inconsistencies have already surfaced on several occasions in other sessions and were focussed more clearly at the workshop.

This workshop began with an overview by W. L. Zijp, "Workshop on Spectrum Adjustment Procedures," and was followed by a presentation by R. A. Maerker of the covariance matrix for the calculated PCA spectrum at simulated surveillance position. This covariance matrix was obtained through the methodology described in "Development and Demonstration of an Advanced Methodology for LWR Dosimetry Applications" (EPRI NP-2188), R. A. Maerker, et al. Notable is the high correlation between fluence rates at different energy groups which indicates that the fluence spectrum shape can much more accurately be calculated than the absolute fluence rates. It is hoped that these results will provide a model for determining fluence covariances for other calculated fluence spectra.

Discussions during the workshop were concerned with the determination of covariances for reaction cross section data. Presently available data in the ENDF/B-V format are rather unrealistic in that total correlation is assumed within given energy groups making adjustments inflexible within groups and discontinuous between groups. The covariance data also tend to become more and more unwieldly if the cross section data are corrected using benchmark irradiations. No consensus was reached but the need was felt for further standardization of covariance data and for procedures of assigning covariance in expanded or condensed group structues.

Further discussions concerned the use of total or partial X^2 tests for the determination of inconsistencies in the input data. Again no consensus was reached.

One object of the workshop was to provide input for the ASTM EIV.05.01 Task Group on Uncertainty Analysis. Within this context participants were encouraged to comment on the new ASTM Standard on Adjustment Methods. The most recent version will be sent to interested participants of the workshop.

WORKSHOP ON SPECTRUM ADJUSTMENT PROCEDURES

W. L. Zijp
Netherlands Energy Research Foundation
Petten, Netherlands
and
F. W. Stallmann
Oak Ridge National Laboratory
Oak Ridge, TN

1. Scope of adjustment

Adjustment codes are designed to modify input data in such a way that the resulting modified (i.e. output) data are more consistent with the measured "integral" values given in the input. The set of input data comprises three categories of data:
- a set of n reaction rates, preferably accompanied with information on their uncertainties and correlations;
- a set of m group values for the fluence rate, preferably accompanied with information on their uncertainties and correlations;
- cross-section data for these n reactions in k groups, preferably accompanied with information on their uncertainties and their correlations (primarily for each reaction separately, but maybe also between the various reactions involved).

The uncertainties and correlations are normally transformed into a covariance matrix, or into a correlation matrix.

2. Importance of adjustment

Neutron spectrum adjustment procedures are important for application to determine among others
- in-core spectra in fission reactors;
- reactor pressure vessel spectra;
- first wall fusion reactor spectra;
- neutron spectra for the purpose of accident dosimetry;
- accelerator produced neutron spectra;
- which spectra are a means to derive integral parameters (such as reaction rates) and their uncertainties.

Such adjustment procedures are especially useful in situations where other detection methods (like time-of-flight and proton recoil methods) cannot be applied, because of space limitations and/or high background gamma radiation levels. On the other hand, active spectrometer methods like proton recoil do not necessarily render superfluous the spectrum adjustment methods, nor can adjustment methods replace high resolution spectral measurements.

A particular type of adjustment met in practice is the normalization of an available spectrum representation on the basis of one, two, or three activation detector responses. Sometimes an adjustment procedure is started with the special aim to check the numerical values of the input data by comparing the experimental reaction rates with the calculated reaction rates, derived from input cross-sections and input spectrum.

3. Practical characteristics of codes

Assuming that a valid mathematical procedure is used, the following characteristics are of practical importance for the selection of a code:
- requirements for specifying input values for uncertainties in reaction rates, group fluence rates, and group cross-section values;
- requirements for specifying input values for correlations between reaction rates, between fluence rates, and between group cross-section values;
- the convergence criterion (in cases that an iteration procedure is involved);
- the number of groups involved (in routine use, or its maximum value);
- possibility for calculating uncertainty information for the output spectrum;
- compatibility with computers (programming language; memory capacity required; processing time).

4. Input requirements

It is difficult to present a list of codes frequently used or to recommend particular codes for application. As an indication of the applicability of adjustment codes we list here the codes used in the REAL-80 exercise, together with a scheme* of some important requirements.

adjustment code	input requirements						output feature
	s(A)	s(σ)	s(φ)	cov(A)	cov(σ)	cov(φ)	s(φ)
CRYSTAL BALL	+	–	–	–	–	–	–
FERRET							
GERDMO2							
ITER							
LOUHI-78							
LSL	+	+	+	+	+	+	+
NEUPAC	+	+	+	+	+	+	+
SAND-II	–	–	–	–	–	–	–
SANDBP	+	+	–	–	–	–	+
SANDMX	?	?	–	–	–	–	+
SANDPET	+	+	+	–	*	–	+
SENSAK							
STAY'SL	+	+	+	+	+	+	+
WINDOWS	+	–	**	–	–	–	–

* two very simple correlation matrices (with values 0 and 1) can be used.
**not applicable.

*Not yet completed.

5. Input spectrum

All adjustment codes listed above require an input spectrum. After normalization the input spectrum should not deviate too much from the actual neutron spectrum. More quantitatively, the (normalized) input spectrum should be able to predict the measured reaction rates within say 25 per cent. Normally reactor spectra based on reactor physics calculations have a good quality to prepare an input spectrum.
Remark: Sometimes the calculated spectra have to be extrapolated to lower and/or to higher energy regions, in order to meet the requirements with respect to the number of groups used in the adjustment code. Sometimes also conversions have to be performed, e.g. from point values to group values or vice versa, or from one group structure to another.

6. Input reaction rates

The input reaction rates should preferably have an uncertainty (in terms of standard deviation for reproducibility) of less than 5 per cent, or, if possible, less than 3 per cent.
Remarks: 1. These values refer to the routinely used activation detectors. For special applications less routine reactions may be applied with somewhat larger uncertainties. 2. The mentioned values of 5 and 3 per cent are goal quantities which maybe contain an unknown systematic deviation (e.g. related to an inaccurate value of the gamma-ray emission probability, or an inaccurate half-life).

7. Input cross-sections

The input cross-section data should, where possible, be based on a recently evaluated nuclear data file, e.g. the ENDF/B-V dosimetry file, or the more extended International Reactor Dosimetry File (IRDF), to be released early 1982, or on fine group cross-section data libraries derived from these files (e.g. the DOSCROS81 file).

8. Number of groups

The number of groups normally used in the adjustment procedures depends on the features of the code, the capabilities of the computer, the structure of available cross-section data, and the desired smoothness of the output spectrum. If the code permits, it may sometimes be advantageous to choose a group structure which is also applied in the transport theory calculation of the input spectrum. There does not exist a single recommended group structure, which should be preferably applied for general application in all laboratories. When one can only apply a limited number of groups, the group structure should primarily be governed by the type of spectrum under investigation (thermal, fast, CTR). For many activation reactions evaluated cross-section data are available in a 640 group structure (e.g. in the DAMSIG81 and the DOSCROS81 libraries).

However, experimental information on covariance data for the cross-sections is at present rather rare, and this does not require so many groups for a good representation. The covariance information for cross-sections, which is available in the ENDF/B-V dosimetry file, is available in a rather coarse block structure (typically less than 30 blocks). Within each block the cross-section values are completely correlated, i.e. the shape of the cross-section curve is maintained within each energy interval of the block.

If the consistency of the input data is guaranteed, then the number of fine groups used in the adjustment procedure has no major effect on the predicted values for reaction rates. If consistencies may occur, then these may sometimes become apparent when a group structure, which is fine enough, is used. In such cases one may notice a large number of iterations and/or the occurrence of local peaks and valleys in the output spectrum. However, these "local peaks and vallyes" are not exclusively caused by inconsistent input data.

9. Number of detectors

The number of detection reactions should not be chosen too small. As a general rule the improvement obtained in an adjustment procedure will increase with the number of detectors, but one should realize that the energy response of a detector determines largely its actual contribution to an improvement. One may therefore state that the number of detection reactions is less important than their individual responses which determines the coverage and the resolution of the output spectrum in the energy range of interest.
An extended set of detectors which supplies a very welcome overlap of response regions might be helpful to arrive at a guaranteed reliability of the output group fluence rate. For any particular application there exists in practice only a limited number of useful reactions (rarely more than 15 to 20) with clearly different energy response which can be used. An approach of merely increasing the number of reactions without careful consideration of their energy response may not lead to an appreciably better adjustment result (i.e. a spectrum with significantly smaller output uncertainties).

The number of detectors has also some relation with the quality of the calculated input spectrum. Under favourable conditions the adjustment involves only normalization and some minor modifications. In such cases a limited number of detectors is acceptable and justified. Relevant reactions should be included even with a good quality input spectrum. If, however, no good quality input spectrum can be supplied and major modifications cannot be excluded, then the adjustment should preferably be based on a somewhat larger detector set. General rule: In each case the detector set should be chosen carefully and with a view to the detector response in the energy range of interest.

10. Differential performance

The output spectra obtained by the codes used in the REAL-80 exercise show the largest differences in the intermediate region of the thermal ORR spectrum, where the response of the activation detectors is rather poor. Remark: This conclusion was reached for this calculational exercise, and may not be valid for other cases met in practice (e.g. for reactor pressure vessel spectra), where it is difficult to obtain good quality input data. The differential shape of output spectra with a very fine group structure in regions where the activation detector gives poor response, is not a good indicator for the performance of adjustment methods. The corresponding uncertainties remain necessarily large, so that large differences among different codes may be well within uncertainty bounds.

11. Integral performance

The REAL-80 exercise has shown that the adjustment codes listed above yield spectra by means of which, under the specified conditions, one can predict quite well spectrum-averaged reaction rates, such as activation rate in nickel and the displacement rate in steel. Also the quantities like $\phi > 1$ MeV and $\phi > 0{,}1$ MeV can be calculated quite well by this approach.

12. Choice of codes

One should always try to perform adjustments with those types of codes, which can take into account the uncertainties in the reaction rates, the fluence rates, and the cross-sections. This approach assumes that these data are available or can be reasonably estimated. If those uncertainty data are absent, and cannot be produced with reasonable effort, one has to rely on codes, which do not require these uncertainties. For those cases the SAND-II types of codes have found wide application. It is noted that the SAND-II code has some user-friendly attractive features. When adjustment codes are used for critical applications, it it necessary to provide estimates for the uncertainties. The output uncertainties cannot be determined without some reasonable estimates for the input uncertainties. This requirement cannot be circumvented by using codes which do not require input uncertainties.

13. Least squares principle

Many adjustment codes are based on a least squares principle. It has been recognized that even the SAND-II algorithm involves implicitly a least squares approach: in each iteration step the adjustment minimizes the deviation for the logarithms of the physical quantities involved. The LSL code, recently developed at ORNL, uses also the least squares adjustment of the logarithms of the physical quantities. Such an approach gives the guarantee that the output fluence rates and cross-se - tions are always positive.

14. Chi-square consistency tests

If one assumes that the joint density functions of the input variables have a normal character, one has the possibility to perform two statistical tests to check the distribution of the input data:

a. The well known chi-square test to check the internal consistency of input data, taking into account the covariance matrix;
b. The same chi-square test to check the randomness of the components constituting the chi-square value.

Let $\underline{A}$ = vector of n input reaction rates α_i;

$\underline{\phi}$ = vector of m input fluence rates ϕ_j;

$\underline{S}$ = vector for all group cross-section values σ_{ij}, in series for all reactions involved;

$\underline{\underline{V}}_{\alpha}$ = covariance matrix for the reaction rates;

$\underline{\underline{V}}_{\phi}$ = covariance matrix for the fluence rates;

$\underline{\underline{V}}_{S}$ = covariance matrix for the cross-section.

Let subscript 0 denote the initial estimate (input value);

superscript $\hat{}$ denote the adjusted value (output value).

Then one has the following generalized least-squares expression:

$$\chi^2 = (\underline{\phi}_o - \hat{\underline{\phi}})^T \cdot \underline{\underline{V}}_{\phi_o}^{-1} \cdot (\underline{\phi}_o - \hat{\underline{\phi}})$$

$$+ (\underline{S}_o - \hat{\underline{S}})^T \cdot \underline{\underline{V}}_{S_o}^{-1} \cdot (\underline{S}_o - \hat{\underline{S}})$$

$$+ (\underline{A}_o - \hat{\underline{A}})^T \cdot \underline{\underline{V}}_{A_o}^{-1} \cdot (\underline{A}_o - \hat{\underline{A}})$$

It is assumed that the three parameter vectors are independent. This generalized least squares expression can conveniently be written in matrix notation:

$$\chi^2 = \begin{pmatrix} \underline{\phi}_o - \hat{\underline{\phi}} \\ \underline{S}_o - \hat{\underline{S}} \\ \underline{A}_o - \underline{A} \end{pmatrix}^T \cdot \begin{pmatrix} \underline{\underline{V}}_{\phi_o} & 0 & 0 \\ 0 & \underline{\underline{V}}_{S_o} & 0 \\ 0 & 0 & \underline{\underline{V}}_{A_o} \end{pmatrix}^{-1} \cdot \begin{pmatrix} \underline{\phi}_o - \hat{\underline{\phi}} \\ \underline{S}_o - \hat{\underline{S}} \\ \underline{A}_o - \hat{\underline{A}} \end{pmatrix}$$

Let $\underline{\underline{V}}_{A_o}$ denote the covariance matrix for input (experimental) reaction rates, and

$\underline{\underline{V}}_{A'}$ denote the covariance matrix for expected (calculated) reaction rates A', based on values for $\underline{S}_o$ and $\underline{\phi}_o$.

It can be shown that the minimum value of chi-square can be calculated easily from the input data, using the relation

$$\chi^2 = (\underline{A}_o - \underline{A}')^T \cdot (\underline{\underline{V}}_{A_o} + \underline{\underline{V}}_{\underline{A}'})^{-1} \cdot (\underline{A}_o - \underline{A}')$$

It is noted that the consistency test can be performed before the solution is calculated, if at least all input data are accompanied with covariance information.

Since one may expect that each of the n reaction rates contributes on the average 1/n-th part of the minimum chi-square value, one may test for the presence of one or a few outlying reaction rates. A (too) large contribution to χ^2_{min} from a particular reaction rate should be investigated carefully. However, a large contribution to the chi-square value arising from any piece of bad data may be cancelled by contributions from data which have better than expected agreement with each other. Too small contributions to χ^2_{min} may occur when the uncertainty estimates involved are too large.

15. Role of chi-square

The interpretation of the quality of the output spectrum depends on the extent with which the uncertainty information is taken into account. One should realize that the consistency of all data involved in an adjustment procedure plays an essential role.

If the adjustment procedure leads to an unlikely large value of the chi-square parameter, the set of input data is inconsistent, and the results of the adjustment algorithm are questionable, or even unreliable. In this case the whole set of input data should be carefully examined in an attempt to improve its consistency. If an unlikely small value of the chi-square occurs, the data under consideration are "too good"; this is an indication for a too conservative estimation of the variances involved.

Any changes in the input data for a new adjustment (which changes need not be equal for the different parameters) should be based on a good knowledge of the physics aspects of the adjustment problem. One should never automatically use the approach, to modify all uncertainties involved with the same constant factor, in order to arrive at a chi-square value of unity.

General rules:

1. Unlikely large values of chi-square indicate inconsistencies in the input data set;
2. Unlikely small values of chi-square may indicate too large values of the variances involved;
3. Discrepant or outlying values for one chi-square component (related to a cross-section, or a reaction rate) do not automatically lead to unlikely large values of χ^2.

16. Internal consistency

The most practical way to determine inconsistencies is to look at the chi-square value defined above, which is based on the comparison between measured and calculated reaction rates. In general the internal consistency of the input data is considered to be more important than the particular algorithm of the adjustment code. If the internal consistency cannot be judged by the chi-square value (as is the case for SAND-II types of codes), the quality of the input data and the behaviour of the adjustment code can sometimes be judged from other characteristics, such as

- the number of iterations required to reach acceptable convergence;
- the smoothness of the output spectrum (taking into account the chosen group structure).

17. Role of covariance information

If covariance information is used in the adjustment algorithm, the adjustment essentially modifies the input data in such a way that the output uncertainties are smaller than the corresponding input uncertainties. Mathematically the adjustment implies then a minimization of the generalized least-squares expression. If an adjustment code does not require explicit input values for the covariance matrix, the algorithm involved has to use, instead of a specified covariance matrix, some empirical rules, for which not always an explicit expression is present or known.
In a very simple case dealing with two activation reactions it has been shown that the output spectra obtained with some codes which do not require a covariance matrix, can be approximated by the output spectra of STAY'SL (which requires full covariance matrix information) with a specially chosen structure of the input spectrum covariance matrix.

18. Objectivity, uniqueness

If the required covariance input information is not readily available, and has to be estimated partly, the output spectrum will be dependent on this estimation procedure. Consequently the output spectrum will be influenced by the experience and skill of the scientist performing the adjustment. An objective and unique result can only be obtained, if least-squares procedures are used, and if all required input information is available. For a given set of input data, comprising full covariance matrix information, each code which is based on a generalized least-squares principle will give an objective and well-defined solution. This means that the adjustment problem is completely defined by the set of input data, and that any change in the input data defines a new problem. A well defined output spectrum, however without uncertainty information, can be obtained with the CRYSTAL BALL code, for which the required input uncertainties refer only to the reaction rates.

19. Absence of covariance information

At present it is rather difficult to find or to construct all uncertainty and correlation information required for adjustment codes like STAY'SL, which use a weight matrix corresponding to the inverse of the covariance matrix. The practice has arisen to introduce rough estimates for missing values for matrix elements, and to make changes - by trial and error - in the values of some matrix elements, in order to arrive at an output spectrum which seems acceptable from a physics point of view. It is emphasized that such an approach is very subjective. The problem of lacking covariance information is most heavy for the group fluence rate values. Maybe it is worthwhile to establish guidelines for deriving input values for fluence rate correlations. It seems convenient to have the same histogram structure both for the cross-section uncertainty and the spectrum correlation. Further the overall pattern of the correlation function should be dependent on the representative energy/lethargy value of the group, and not by the serial number of the group. However, if one cannot make estimates, but instead makes some rough guesses, which are not physically justified, then one should not be surprised when the output of an adjustment procedure yields unrealistic data. Therefore one should be very careful in creating covariance information.

20. Estimation of covariance information

It should be noted that variances and covariances need not to be known in an accurate way, in order to be applied in adjustment procedures. Rough and subjective estimates (accurate within say 30 per cent) will be sufficient for many applications. This means that the variances and covariances need not always be derived from elaborate sensitivity calculations or similar tools. Frequently any simple but sufficiently conservative estimate may legitimately be used. Such simplifications will of course lead to an increase in the output uncertainties, but such an increase may not be large enough to justify the effort for a more elaborative uncertainty analysis.

21. Future needs

a. An annual or biannual status report on the precision and accuracy of cross-section data for neutron metrology reactions.
b. Smaller uncertainties for some of these reactions, apparent from such a status report.
c. Rules for deriving values needed in covariance matrices, based on a knowledge of the physics aspects of the adjustment problem, in cases where the required numerical values for one or more matrix elements are lacking.
d. A detailed study of the effect of neutron self-shielding in activation detectors.
e. A better approach for the treatment of the influence of detector covers, made of cadmium, gadolinium, or boron.

22. Some conclusions

1. The occurrence of unlikely values of the chi-square parameter is a sufficient, but not a necessary condition in order to arrive at the conclusion that inconsistencies are present.
2. From a methodology point of view the use of adjustment codes which can provide output uncertainties for the output spectrum should be encouraged.
3. The lack of sufficient data and/or the presence of too inaccurate data on variances and covariances should not directly exclude the use of adjustment procedures which require input uncertainties and provide output uncertainties.
4. There is an urgent need for good covariance information for spectra of practical interest.

WORKSHOP ON NUCLEAR DATA AND BENCHMARKS

A. Fabry
CEN/SCK
Mol, Belgium

B. Magurno
Brookhaven National Laboratory
Upton, NY

W. N. McElroy
Westinghouse Hanford Company
Richland, WA

and

E. P. Lippincott
Westinghouse Hanford Company
Richland, WA

The current status of dosimetry benchmark fields was introduced by W. N. McElroy. At present there are three CSEWG benchmarks (CFRMF, BIG-10, and ^{235}U fission), only one of which has an accepted set of uncertainties. There are also two proposed benchmarks (^{252}Cf and ISNF). It was proposed that additional benchmarks be established for use in ASTM standards but that these not be required to meet the CSEWG specifications and acceptance. These benchmark fields would be of four types: LWR surveillance, fast reactor fission, and fusion neutronic benchmarks, and gamma benchmarks. Examples include NESDIP, VENUS, YAYOI, PCA/PSF, EE, EBR-11, FFTF, and accelerator spectra.

Considerable discussion ensued on the proper use of benchmarks and uncertainty requirements. It is likely that benchmark data will be used not only for data testing, but also for data adjustment. Of great concern when this is done is the proper handling of correlations between the cross sections, spectra, and integral data that are introduced. This can be avoided if a small number of groups can be used and simultaneous adjustment of unknown plus benchmark spectra, cross sections, and reaction rates are carried out. It is unlikely that this will be done routinely, but the effects of correlations introduced into cross section evaluations must be investigated. If these effects can be neglected or approximated for classes of problems, considerable simplification will result. It is apparent, however, that cross section files and covariance matrices already contain hidden correlations with integral data.

Discussion of the benchmark uncertainty specification requirements led to two conclusions:

1. Detailed uncertainty information on benchmarks such as BIG-10 will not be available in the near future. This will severely limit the application of benchmarks and vigorous cross section consistency tests can only be made if this uncertainty data is available.

2. J. J. Wagschal suggested that specifications of benchmarks should be in two parts. First would be a detailed description of all dimensions, compositions, densities, etc. necessary for input to physics calculations. It should be noted that this has not been done for all cases, e.g. there are many ^{252}Cf fields in use each of which needs to be completely described. The second part is a reference calculated spectrum. Thus laboratories would be free to calculate improved spectral representations.

The current, reported status of the ^{252}Cf fission neutron spectrum was not reviewed at this meeting but some discussion was prompted by recent preliminary high-energy threshold measurements in the PTB ^{252}Cf field and by HEDL analyses of emulsions irradiated in the NBS ^{252}Cf field.

Additional discussion then commenced on nuclear data. Data from CFRMF was exhibited to demonstrate the consistency of the ENDF/B-V cross sections, to show the spectral sensitivities in the three CSEWG benchmark fields, and to illustrate least squares cross section adjustments as made by FERRET on the CFRMF spectrum. All cross sections except five were found to be consistent with the calibrated spectrum and after adjustment only $^{10}B(n,\alpha)$ was found to be inconsistent.

Data on a preliminary adjustment of the $^{56}Fe(n,\gamma)$ cross section using five EBR-11 spectra was shown to quantitatively agree with the CFRMF analysis and inferences from BIG-10. Adjustments based on EBR-11 data is expected to improve cross section consistency for several dosimetry reactions appropriate for high fluence measurements.

WORKSHOP ON LWR SURVEILLANCE AND DOSIMETRY

Art Lowe
Babcock and Wilcox
Lynchburg, VA
and
H. Tourwé
SCK/CEN
Mol, Belgium

The following represent the highlights of the LWR Surveillance and Dosimetry workshop:

1. The scrap technique for producing dosimetry material has been proven to be both a practical and reliable method for determining fluence values. The method can be used to supply fluence values on the reactor vessel and, when used for comparison with capsule dosimetry, yield more accurate lead factors.

2. The uncertainty of specific activities at the surveillance capsule locations is largely due to the uncertainties of the dimensional relationship of the capsule dosimeters relative to the various core and internal components.

3. The current uncertainty in fluence determination is adequate now but must be improved because future analysis of reactor vessel integrity will demand it. Also, the present uncertainty of fluence analysis is better than the uncertainty in the metallurgical (materials) data; however, as metallurgical analysis techniques improve, a need will probably develop for greater accuracy in fluence analysis.

4. Researchers developing sophisticated analytical techniques to predict fluences in surveillance capsules or vessels should not forget that the ultimate user is looking for a simple and efficient procedure.

5. Problems experienced in the analysis of dosimetry by various laboratories demonstrated a need for a standard to address the design of dosimeters used in surveillance capsules, especially in the design of fission dosimeters.

6. The continuous improvement in measuring techniques and analytical data demonstrate a need to be able to retrieve raw dosimeter data for re-evaluation so that detailed documentation of the actual dosimetry methods and dosimetry to be used in the evaluation of dosimeters will be included.

WORKSHOP ON NEUTRON AND GAMMA-RAY TRANSPORT METHODS

R. E. Maerker
Oak Ridge National Laboratory
Oak Ridge, TN
and
M. Austin
Rolls-Royce and Associates, Ltd.
Derby, England

SCOPE

The original intention of the Chairmen, which was to provide a balanced input to the discussion by U.S. and European participants, was frustrated because several well-known European calculators were unable to attend the Conference. A program of informal presentations involving mainly U.S. contributors was arranged, with the intention of stimulating a general discussion. This formula was successful and resulted in a comprehensive session. The theme of the Workshop was to be the application of transport techniques to the analysis of design situations or benchmark experiments. In addition, informal update information was presented on the current status of DOT-IV development, the availability of the Vitamin-E transmission data library, and the status of ENDF/B-V dosimetry cross sections.

CONTRIBUTIONS

Transport Code Development and Data

A further example of state-of-the-art application of transport analysis was provided by the Maerker and Williams calculation of the PSF Startup Experiment. The treatment (DOT IV, Vitamin-C, flux synthesis) was essentially similar to that described by Maerker in analyzing the Westinghouse perturbation experiment in the same facility. Given the general agreement (to within 10%) on the absolute reaction rate reported for the latter work, it was somewhat surprising to observe a discrepancy of roughly twice that value in the startup analysis.

The synthesis technique appeared to account adequately for the SSC perturbation, but the 20-25% underestimate held throughout the PSF configuration. Since one objective of the ORNL work was to provide reference data for the interpretation of the long-term PSF irradiation measurements, it appears that the current techniques will underestimate the experimental fluences unless an explanation is found for this discrepancy.

In a general discussion on further developments of the Sn method it was concluded that in its present manifestation, DOT-IV, the technique had probably reached an optimum status within the limits imposed by two-dimensional treatment. The significant, remaining development was the extension of the method to the third space dimension. In this context the paper by Takeuchi on the Japanese 3D code, PALLAS-XYZ, was viewed with interest. However, it was noted that at this early stage, the code was restricted in its application, particularly to cylindrical problems. Maerker completed this section with a brief summary of features of Version IV of the DOT code (not yet generally available outside the USA). They were mainly concerned with increased flexibility of problem treatment, including ability to vary spatial mesh and facilities for varying angular quadrature and scatter order with spatial location.

A brief discussion on data for transport calculations was initiated by a statement on the main differences between the new Vitamin-E compilation and the earlier Vitamin-C (ENDF/B-IV based) library, given by Trubey of ORNL. The discussion also covered the status of self-shielding treatment, spectrum-weighting in fine group condensation and the now familiar inadequacy in the inelastic cross-section data for iron.

Design Application of Treatment Calculations

Addressing the subject of Monte-Carlo code development in the U.K., Heffer of the Berkeley Nuclear Laboratories described his work with the SPARTAN code in evaluating radiation energy deposition in the graphite moderator of the AGR core. The complexity of the problem required three-dimensional treatment, and the prohibitive cost of Monte-Carlo thermal calculations in such a system led to attempts to link the Monte Carlo with discrete ordinates and collision probability codes, which has been only partially successful. The problems involved in calculating gamma-heating for comparison with calorimetry results necessitated the linking of neutron, gamma-ray and electron transport calculations. A current preoccupation was the acquisition and implementation of an adequate nuclear data base.

The session was completed with two informal presentations by representatives of the U.S. vendors, Whitmarsh (Babcock and Wilcox), and Anderson (Westinghouse), who described their use of transport methods to produce vessel fluences, including the analysis and use of surveillance capsule results. Both employed discrete ordinates (DOT) but while B&W used CASK library data, Westinghouse used a library which, although based on ENDF/BII, had been developed in-house over a considerable period of time. The point was made that the analyst had to be capable of defining the radiation environment at any critical component position, and with the current preoccupation with problems such as pressurized thermal shock, the relatively simple situation of computing damage rates at the center line T/4 location might change. The dual purpose of calculations was to calibrate the dosimeter reaction-rates

in the surveillance capsules and perform a longer-term extrapolation of vessel wall fluence to obtain plant lifetime estimates. Although the same problem treatment (r, θ calculations at the core midplane with r, z assessment of the vessel-wall profile outside the belt-line region) was used by the two vendors, there was a distinct difference in approach between the two. While the B&W technique was to "normalize" the calculation to the measured reaction-rate values within the capsule, the Westinghouse approach was to use the results of calculations as long as calculated reaction-rates lay within 20% of the appropriate measured surveillance values.

The B&W treatment of the source distribution (using PDQ calculations) included a detailed assessment of in-cycle and cycle-to-cycle variation; the Westinghouse distributions used for calculations employed PDQ calculations together with measured in-core distributions. Whitmarsh assessed the uncertainty associated with his predictions to be in the range of 14% (capsule) — 32% (vessel welds outside the beltline). Detailed discussion of plans to modify fuel-load patterns was deferred until the presentation of Anderson's paper later in the conference. Looking ahead to potential changes to current methods of assessment, Anderson warned of the problems in analyzing cavity reaction-rate measurements. These results could be very dependent on the cavity size; early calculations showed that although in narrow cavity plants (18 cm) the azimuthal peaking of vessel flux was maintained over the core height, in wide cavity plants (90 cm) neutron streaming ensured that the peaks were smoothed out and that the axial profile was flat. Both representatives commented on the probable cost of implementing the newly-developed least squares adjustment approach to the estimation of vessel damage-rate, at least at the current stage of its development, but agreed that a much clearer view of its potential would become apparent after ORNL had completed the analysis of the Arkansas reactor system.

FOURTH ASTM-EURATOM SYMPOSIUM ON REACTOR DOSIMETRY

National Bureau of Standards
Gaithersburg, Maryland

March 22-26, 1982

ATTENDEES

Jürgen Ahlf
GKSS-Forschungszentrum
Geesthacht GmbH
F. R. Germany

Ralf John Ahlstrand
Imatra Power Company
Helsinki, Finland

Alain Alberman
Commissariat A L'Energie Atomique
CEN, Saclay S.P.S.
France

Wolfgang G. Alberts
Physikalisch-Technische
Bundesanstalt (PTB)
F. R. Germany

R. A. Anderl
EG&G Idaho, Inc.
Idaho Falls, ID 83415

Stan Anderson
Westinghouse Electric Corp.
Pittsburgh, PA 15239

Melvyn Austin
Rolls-Royce & Associates, Ltd.
Derby, England

Bruno Bars
Technical Research Centre of
Finland
Espoo 15, Finland

Dieter Bellmann
GKSS-Forschungszentrum
Geesthacht GmbH
F. R. Germany

Larry W. Brackenbush
Battelle-Pacific Northwest
Laboratories
Richland, WA 99352

James G. Bradley
Rockwell International
Canoga Park, CA 91107

William E. Brandon
University of Arkansas
Fayetteville, AR 72701

Bryan L. Broadhead
Oak Ridge National Laboratory
Oak Ridge, TN 37830

Wilbur L. Bunch
Westinghouse Hanford Co.
Richland, WA 99352

A. Capgras
CEN, Saclay S.P.S
France

Charles E. Clifford
Princeton University
Plasma Physics Laboratory
Princeton, NJ 08544

C. O. Cogburn
University of Arkansas
Fayetteville, AR 72701

R. D. Cheverton
Oak Ridge National Laboratory
Oak Ridge, TN 37830

Anna De Carli
C.S.N. Casaccia, CNEN
Rome, Italy 00060

Ronald Dierckx
Commission of the European Communities
Joint Research Centre
EURATOM
Ispra, Italy

Charles Eisenhauer
National Bureau of Standards
Washington, DC 20234

A. Fabry
CEN/SCK B-2400
Mol, Belgium

Harry Farrar IV
Rockwell International Corporation
Canoga Park, CA 91304

Armando Foglio-Para
Politecnico DiMilano
Via Ponzio 3413
Milan, Italy 20133

C. Y. Fu
Oak Ridge National Laboratory
Oak Ridge, TN 37830

Alan J. Fudge
United Kingdom Atomic Energy Authority
A.E.R.E., Harwell
United Kingdom

Jean-Pierre Genthon
CEN, Saclay S.P.S.
France

D. Gillam
National Bureau of Standards
Washington, DC 20234

Omer F. Goktepe
NSWC
Silver Spring, MD 20910

Raymond Gold
Westinghouse Hanford Co.
Richland, WA 99352

Lawrence R. Greenwood
Argonne National Laboratory
Argonne, IL 60439

James Grundl
National Bureau of Standards
Washington, DC 20234

G. L. Guthrie
Westinghouse Hanford Co.
Richland, WA 99352

Gordon E. Hansen
Los Alamos Scientific Laboratory
Los Alamos, NM 87545

Yale D. Harker
EG&G Idaho, Inc.
Idaho Falls, ID 83415

Peter J. H. Heffer
Central Electricity Generating Board
Berkeley Nuclear Laboratories
Berkeley, Glos., England

F. Hegedus
Swiss Federal Institute for Reactor Research, EIR
Switzerland

Craig Heimbach
Aberdeen Proving Grounds
Aberdeen, MD 21005

Philip B. Hemmig
U.S. DOE
Washington, DC 20585

Hans W. Hendel
Princeton University
Princeton, NJ 08540

W. C. Hopkins
Bechtel Power Corp.
Gaithersburg, MD 20877

O. N. Jarvis
A.E.R.E., Harwell
United Kingdom

Stuart Mark Jefferies
University of London Reactor Centre
Ascot, Berkshire
United Kingdom

F. B. K. Kam
Oak Ridge National Laboratory
Oak Ridge, TN 37830

L. S. Kellogg
Westinghouse Hanford Co.
Richland, WA 99352

D. W. Kneff
Rockwell International
Canoga Park, CA 91304

Nikolai Kocherov
International Atomic Energy Agency
Vienna, Austria

G. Lamaze
National Bureau of Standards
Washington, DC 20234

John W. Lewellen
U.S. DOE
Washington, DC 20545

Robert H. Lewis
Babcock & Wilcox
Lynchburg, VA 24505

Li Linpei
National Bureau of Standards
Washington, DC 20234

E. P. Lippincott
Westinghouse Hanford Co., HEDL
Richland, WA 99352

Li Lishing
Brown Boveri Reaktor GmbH
Mannheim, West Germany 6800

Raoul Lloret
Commissariat A L'Energie, Atomique
CEN, Grenoble
France

A. Lowe
Babcock & Wilcox
Lynchburg, VA 24505

W. N. McElroy
Westinghouse Hanford Co.
Richland, WA 99352

E. D. McGarry
National Bureau of Standards
Washington, DC 20234

Richard E. Maerker
Oak Ridge National Laboratory
Oak Ridge, TN 37830

Benjamin Magurno
Brookhaven National Laboratory
Upton, NY 11973

Wolf Mannhart
Physikalisch-Technische
Bundesanstalt (PTB)
F. R. Germany

Gerald C. Martin
General Electric Company
Vallecitos Nuclear Center
Pleasanton, CA 94566

Pierre Mas
Commissariat A L'Energie, Atomique
CEN, Grenoble
France

John A. Mason
Imperial College
University of London Reactor Centre
Ascot, Berkshire
England

David Meneghetti
Argonne National Laboratory
Argonne, IL 60439

Pierre Menessier
Commissariat à l'Energie Atomique
CEN, Cadarache
France

L. F. Miller
Oak Ridge National Laboratory
Oak Ridge, TN 37830

D. W. Muir
Los Alamos National Laboratory
Los Alamos, NM 87544

Masaharu Nakazawa
University of Tokyo
Japan

Masakuni Narita
Hokkaido University
Sapporo 060, Japan

Randall R. Nason
Sandia National Laboratories
Albuquerque, NM 87185

David W. Nigg
EG&G Idaho, Inc.
Idaho Falls, ID 83401

Henk J. Nolthenius
Netherlands Energy Research Foundation
ECN, Petten
The Netherlands

E. B. Norris
Southwest Research Institute
San Antonio, TX 78284

B. M. Oliver
Rockwell International
Canoga Park, CA 91304

Maria Petilli
CNEN
C.S.N. Casaccia
Rome, Italy

Eckhard Polke
Kraftwerk Union A. G.
F. R. Germany

Neil Randall
U.S. Nuclear Regulatory Commission
Washington, DC

John A. Rawlins
Westinghouse Hanford Co.
Richland, WA 99352

Peter Robertson
Battelle Pacific Northwest Labs.
Richland, WA 99352

J. W. Rogers
EG&G Idaho, Inc.
Idaho Falls, ID 83402

H. Rottger
Commission European Communities — JRC, Petten
The Netherlands

Frank H. Ruddy
Westinghouse Hanford Co.
Richland, WA 99352

Bert W. Rust
National Bureau of Standards
Washington, DC 20234

Wesley W. Sallee
University of Arkansas
Fayetteville, AR 72701

Daniel Sam
Naval Surface Weapons Center
Silver Spring, MD 20910

Giancarlo G. Sandrelli
ENEL-Thermal and Nuclear Res. Center
Milano, Italy 20133

V. Sangiust
Politecnico Di Milano
Instituto Ingegneria Nucleare
CESNEF
Milano, Italy 20133

F. A. Schmittroth
Westinghouse Hanford Co.
Richland, WA 99352

Jack K. Schmotzer
Babcock & Wilcox
Alliance, OH 44601

Wolfdietrich Schneider
Kernforschungsanlage, ZBB
Julich, F. R. Germany

Robert B. Schwartz
National Bureau of Standards
Washington, DC 20234

Akira Sekiguchi
University of Tokyo
Tokyo, Japan 113

Charles Serpan
U.S. Nuclear Regulatory Commission
Washington, DC

R. A. Shaw
Electric Power Research Institute
Palo Alto, CA 94303

Bryce Shriver
University of Virginia
Charlottesville, VA 22901

R. L. Simons
Westinghouse Hanford Co.
Richland, WA 99352

Robert K. Smither
Argonne National Laboratory
Argonne, IL 60439

Valentiw Spiegel
National Bureau of Standards
Washington, DC 20234

F. W. Stallmann
Oak Ridge National Laboratory
Oak Ridge, TN 37830

L. E. Steele
Naval Research Laboratory
Washington, DC

Soju Suzuki
Power Reactor and Nuclear Fuel Development Corp.
Ibaraki-ken, Japan

Egon J. Szondi
Budapest Technical University
Budapest, Hungary H-1521

Taketoshi Taniguchi
University of Tokyo
Tokyo, Japan 113

Kari Torronen
Technical Res. Centre of Finland
Espoo 15, Finland 02150

Hugo Tourwe
SCK/CEN
Mol, Belgium

Francis Y. Tsang
EG&G Idaho, Inc.
Idaho Falls, ID 83415

Nicholaus Tsoulfanidis
University of Missouri-Rolla
Rolla, MO 65401

Matti Valo
Technical Res. Centre of Finland
Espoo 15, Finland SF-02150

Jerome D. Varsik
Combustion Engineering
Windsor, CT 06095

Peter Von Der Hardt
Commission of the European
Communities
Joint Res. Centre (EURATOM)
ZG Petten (NH), Netherlands 1755

J. J. Wagschal
Racah Institute of Physics
Hebrew University
Jerusalem, Israel

Leon West
University of Arkansas
Fayetteville, AR 72701

Charles L. Whitmarsh
Babcock & Wilcox
Lynchburg, VA 24502

John G. Williams
University of London Reactor
Centre
Ascot, Berkshire
United Kingdom

M. L. Williams
Oak Ridge National Laboratory
Oak Ridge, TN 37830

Willem L. Zijp
Netherlands Energy Res.
Foundation, ECN
Petten, The Netherlands

William H. Zimmer
EG&G Ortec
Oak Ridge, TN 37830

E. M. Zsolnay
Nuclear Reactor of the Technical
University
Budapest, Hungary

D. K. Trubey
Oak Ridge National Laboratory
Oak Ridge, TN 37830

★U.S. GOVERNMENT PRINTING OFFICE: 1982-546-067/93